

PHOSPHINE-SUPPORTED ORGANOMANGANESE COMPLEXES

CHEMISTRY OF MANGANESE COMPLEXES CONTAINING METAL–CARBON,
METAL–SILICON, AND METAL–HYDRIDE LINKAGES

By

JEFFREY S. PRICE, H.B.Sc.

A Thesis Submitted to the School of Graduate Studies in Partial Fulfillment of the
Requirements for the Degree Doctor of Philosophy

McMaster University

© Copyright by Jeffrey S. Price, January 2020

DOCTOR OF PHILOSOPHY (2020)

McMaster University

(Department of Chemistry and Chemical Biology)

Hamilton, Ontario

TITLE: Chemistry of Manganese Complexes Containing Metal–Carbon, Metal–Silicon,
and Metal–Hydride Linkages

AUTHOR: Jeffrey S. Price

SUPERVISOR: Prof. David J. H. Emslie

NUMBER OF PAGES: lxix, 477

Lay Abstract

The focus of this work is the synthesis and investigation of manganese-containing complexes with Mn–P, Mn–C, Mn–H, and/or Mn–Si linkages. Many of these complexes feature unusual bonding motifs, including the first group 7 complexes bearing an unstabilized silylene ($:\text{SiR}_2$) ligand and the first 1st row transition metal complexes bearing an unstabilized silene ($\text{R}_2\text{Si}=\text{CR}_2$) ligand. Variable temperature Nuclear Magnetic Resonance (NMR) spectroscopy and X-ray crystallography were employed to investigate the structures of these complexes, while Density Functional Theory (DFT) calculations and trapping experiments were employed to understand the mechanisms for various unusual chemical transformations. Some of the complexes were evaluated for activity towards catalytic hydrosilylation of ethylene. This work provides valuable insights to unusual metal–ligand bonding motifs and reactions, and as such contributes to the fundamental understanding of organometallic chemistry.

Abstract

The solid state structures and the physical, solution magnetic, solid state magnetic, and spectroscopic (NMR and UV/Vis) properties of a range of oxygen- and nitrogen-free dialkylmanganese(II) complexes are reported, and the solution reactivity of these complexes towards H_2 and $ZnEt_2$ is described. The dialkyl compounds investigated are $[\{Mn(\mu-CH_2SiMe_3)_2\}_\infty]$ (**1**), $[\{Mn(CH_2CMe_3)(\mu-CH_2CMe_3)_2\}_2\{Mn(\mu-CH_2CMe_3)_2Mn\}]$ (**2**), $[Mn(CH_2SiMe_3)_2(dmpe)]$ (**3**) (dmpe = 1,2-bis(dimethylphosphino)ethane), $[\{Mn(CH_2CMe_3)_2(\mu-dmpe)\}_2]$ (**4**), $[\{Mn(CH_2SiMe_3)(\mu-CH_2SiMe_3)\}_2(\mu-dmpe)]$ (**5**), $[\{Mn(CH_2CMe_3)(\mu-CH_2CMe_3)\}_2(\mu-dmpe)]$ (**6**), $[\{Mn(CH_2SiMe_3)(\mu-CH_2SiMe_3)\}_2(\mu-dmpm)]$ (**7**) (dmpm = bis(dimethylphosphino)methane), and $[\{Mn(CH_2CMe_3)(\mu-CH_2CMe_3)\}_2(\mu-dmpm)]$ (**8**). Syntheses for **1-4** have previously been published, but the solid state structures and most properties of **2-4** had not been described. Compounds **5** and **6**, with a 1:2 dmpe:Mn ratio, were prepared by reaction of **3** and **4** with base-free **1** and **2**, respectively. Compounds **7** and **8** were accessed by reaction of **1** and **2** with 0.5 or more equivalents of dmpm per manganese atom. An X-ray structure of **2** revealed a tetrametallic structure with two terminal and six bridging alkyl groups. In the solid state, bis(phosphine)-coordinated **3-8** adopted three distinct structural types: (a) monometallic $[LMnR_2]$, (b) dimetallic $[R_2Mn(\mu-L)_2MnR_2]$, and (c) dimetallic $[\{RMn(\mu-R)\}_2(\mu-L)]$ (L = dmpe or dmpm). Compound **3** exhibited particularly desirable properties for an ALD or CVD precursor, melting at 62-63 °C, subliming at 60 °C (5 mTorr), and showing negligible decomposition after 24 h at 120 °C. Comparison of variable temperature solution and solid state magnetic data provided insight into the solution structures of **2-8**. Solution reactions of **1-8** with H_2 yielded manganese metal, demonstrating the thermodynamic feasibility of the key reaction steps required for manganese(II) dialkyl complexes to serve, in combination with H_2 , as precursors for metal ALD or pulsed-CVD. By contrast, the solution reactions of **1-8** with $ZnEt_2$ yielded a zinc-manganese alloy with an approximate 1:1 Zn:Mn ratio.

Wilkinson's manganese(I) ethylene hydride complex *trans*-[(dmpe)₂MnH(C₂H₄)] (**10**) can react as a source of a low-coordinate manganese(I) ethyl complex. This is illustrated in the reactivity of **10** towards a variety of reagents in this work (*vide infra*). The proposed low-coordinate intermediate, [(dmpe)₂MnEt] (**13**), was not observed spectroscopically, but could be trapped using isonitrile ligands; reaction of **10** with CNR (R = ^tBu, *o*-xylyl) afforded the manganese(I) ethyl complexes [(dmpe)₂MnEt(CNR)] (**14a**: R = ^tBu, **14b**: R = *o*-xylyl). Ethyl complex **14a** did not react further with CN^tBu at 80 °C. By contrast, complex **14b** reacted with excess *o*-xylyl isonitrile to form 1,1 insertion products, including the iminoacyl complex [(dmpe)Mn(CNXyl)₃{C(=NXyl)CEt(=NXyl)}] (**15**, Xyl = *o*-xylyl). Complexes **14a-b** and **15**, as well as previously reported **10**, were crystallographically characterized, and DFT calculations were employed to probe the accessibility of *cis* ethylene hydride and ethyl isomers of **10**.

Reaction of the ethylene hydride complex *trans*-[(dmpe)₂MnH(C₂H₄)] (**10**) with H₂SiEt₂ at 20 °C afforded the silylene hydride [(dmpe)₂MnH(=SiEt₂)] (**16^{Et2}**) as the *trans* isomer. By contrast, reaction of **10** with H₂SiPh₂ at 60 °C afforded [(dmpe)₂MnH(=SiPh₂)] (**16^{Ph2}**) as a mixture of the *cis* (major) and *trans* (minor) isomers, featuring a Mn–H–Si interaction in the former. The reaction to form **16^{Ph2}** also yielded [(dmpe)₂MnH₂(SiHPh₂)] (**18^{Ph2}**); [(dmpe)₂MnH₂(SiHR₂)] {R = Et (**18^{Et2}**) and Ph (**18^{Ph2}**)} were accessed cleanly by reaction of **16^{R2}** with H₂. Both **16^{Et2}** and **16^{Ph2}** engaged in unique reactivity with ethylene, generating the silene hydride complexes *cis*-[(dmpe)₂MnH(R₂Si=CHMe)] {R = Et (**19^{Et2}**) and Ph (**19^{Ph2}**)}. Compounds *trans*-**16^{Et2}**, *cis*-**16^{Ph2}**, and **19^{Ph2}** were crystallographically characterized, and bonding in **16^{Et2}** and **19^{Et2}** was probed computationally.

trans-[(dmpe)₂MnH(C₂H₄)] (**10**) reacted with primary hydrosilanes H₃SiR (R = Ph, ⁿBu) at 60 °C to afford ethane and the manganese disilyl hydride complexes [(dmpe)₂MnH(SiH₂R)₂] (**20^{Ph}**: R = Ph, **20^{Bu}**: R = ⁿBu). **20^R** reacted with ethylene to form silene hydride complexes [(dmpe)₂MnH(RHSi=CHMe)] (**19^{Ph,H}**: R = Ph, **19^{Bu,H}**: R =

ⁿBu). Compounds **19**^{R,H} reacted with a second equivalent of ethylene to generate [(dmpe)₂MnH(REtSi=CHMe)] (**19**^{Ph,Et}: R = Ph, **19**^{Bu,Et}: R = ⁿBu), resulting from apparent ethylene insertion into the silene Si–H bond. Furthermore, in the absence of ethylene, silene complex **19**^{Bu,H} slowly isomerized to the silylene hydride complex [(dmpe)₂MnH(=SiEtⁿBu)] (**16**^{Bu,Et}). Reactions of **20**^R with ethylene likely proceed via low-coordinate silyl {[dmpe)₂Mn(SiH₂R)] (**17**^{Ph}: R = Ph, **17**^{Bu}: R = ⁿBu)} or silylene-hydride {[dmpe)₂MnH(=SiHR)] (**16**^{Ph,H}: R = Ph, **16**^{Bu,H}: R = ⁿBu)} intermediates accessed from **20**^R by H₃SiR elimination. DFT calculations and high temperature NMR spectra support the accessibility of these intermediates, and reactions of **20**^R with isonitriles or *N*-heterocyclic carbenes yielded the silyl isonitrile complexes [(dmpe)₂Mn(SiH₂R)(CNR')] (**21a-d**: R = Ph or ⁿBu; R' = *o*-xylyl or ^tBu), and NHC-stabilized silylene-hydride complexes [(dmpe)₂MnH{=SiHR(NHC)}] (**22a-d**: R = Ph or ⁿBu; NHC = 1,3-diisopropylimidazolin-2-ylidene or 1,3,4,5-tetramethyl-4-imidazolin-2-ylidene), respectively, all of which were crystallographically characterized.

Manganese silyl dihydride complexes [(dmpe)₂MnH₂(SiHR₂)] {R = Ph (**18**^{Ph2}) or Et (**18**^{Et2})} and [(dmpe)₂MnH₂(SiH₂R)] {R = Ph (**18**^{Ph}) or ⁿBu (**18**^{Bu})} were generated by exposure of silylene hydride complexes, [(dmpe)₂MnH(=SiR₂)] (**16**^{R2}), and disilyl hydride complexes, [(dmpe)₂MnH(SiH₂R)₂] (**20**^R), respectively, to H₂ at room temperature. In solution, **18**^R and **18**^{R2} exist as an equilibrium mixture of a *central* isomer with a meridional H–Si–H arrangement of the silyl and hydride ligands {this isomer may be considered to contain an η³-coordinated silicate (H₂SiR₃[−]) anion}, and a *transHSi* isomer with *trans*-disposed hydride and nonclassical hydrosilane ligands (the latter is the result of significant but incomplete hydrosilane oxidative addition). Additionally, DFT calculations indicate the thermodynamic accessibility of *lateral*H₂ and *trans*H₂ isomers with *cis*- and *trans*-disposed silyl and dihydrogen ligands, respectively. Compounds **18**^{Ph2} and **18**^{Ph} crystallized as the *central* isomer, whereas **18**^{Bu} crystallized as the *transHSi* isomer. Bonding in the *central* and *transHSi* isomers of **18**^R and **18**^{R2} was further investigated through ²⁹Si-edited ¹H–¹H COSY solution NMR experiments to determine both the sign and magnitude of *J*_{29Si,1H} coupling (negative and positive values of *J*_{29Si,1H}

are indicative of dominant 1-bond and 2-bond coupling, respectively). These experiments afforded $J_{29\text{Si},1\text{H}}$ coupling constants of -47 Hz for $\eta^3\text{-(H}_2\text{SiR}_3)$ in the central isomer of $\mathbf{18}^{\text{Et}2}$ (calcd. -40 to -47 for $\mathbf{18}^{\text{R}}$ and $\mathbf{18}^{\text{R}2}$), -38 to -54 Hz for $\eta^2\text{-(R}_3\text{Si-H)}$ in the *transHSi* isomer of $\mathbf{18}^{\text{R}}$ and $\mathbf{18}^{\text{R}2}$ (calcd. -26 to -47 Hz), and 5 to 9 Hz for the terminal manganese hydride ligand in the *transHSi* isomer of $\mathbf{18}^{\text{Et}2}$, $\mathbf{18}^{\text{Ph}}$, and $\mathbf{18}^{\text{Bu}}$ (calcd. 12 to 14 Hz for $\mathbf{18}^{\text{R}}$ and $\mathbf{18}^{\text{R}2}$), experimentally supporting the nonclassical nature of bonding in the *central* and *transHSi* isomers.

Exposure of disilyl hydride complexes $\mathbf{20}^{\text{R}}$ to diisopropylcarbodiimide $\{\text{C}(\text{N}^i\text{Pr})_2\}$ afforded manganese(I) amidinylsilyl complexes $[(\text{dmpe})_2\text{Mn}\{\kappa^2\text{-SiHR}(\text{N}^i\text{PrCHN}^i\text{Pr})\}]$ $\{\text{R} = \text{Ph} (\mathbf{25}^{\text{Ph,H}})$ or $n\text{Bu} (\mathbf{25}^{\text{Bu,H}})\}$. DFT calculations and analysis of XRD bond metrics suggest that the structure of $\mathbf{25}^{\text{R,H}}$ involves a contribution from a resonance structure featuring a neutral base-stabilized silylene and an anionic amido donor on manganese. Reactions of $\mathbf{20}^{\text{R}}$, as well as the silylene hydride complex $\mathbf{16}^{\text{Et}2}$, with CO_2 yielded the manganese(I) formate complex *trans*- $[(\text{dmpe})_2\text{Mn}(\text{CO})(\kappa^1\text{-O}_2\text{CH})]$ ($\mathbf{26}$), with a polysiloxane byproduct. Compound $\mathbf{26}$ was found to undergo reversible CO_2 elimination at room temperature, and was only stable under an atmosphere of CO_2 . Complexes $\mathbf{25}^{\text{R,H}}$ and $\mathbf{26}$ were crystallographically characterized.

Silyl, silylene, and silene complexes in this work were accessed via reactions of $[(\text{dmpe})_2\text{MnH}(\text{C}_2\text{H}_4)]$ ($\mathbf{10}$) with hydrosilanes, in some cases followed by ethylene. Therefore, ethylene (C_2H_4 and C_2D_4) hydrosilylation was investigated using $[(\text{dmpe})_2\text{MnH}(\text{C}_2\text{H}_4)]$ ($\mathbf{10}$) as a pre-catalyst, resulting in stepwise conversion of primary to secondary to tertiary hydrosilanes. Various catalytically active manganese-containing species were observed during catalysis, including silylene and silene complexes, and a catalytic cycle is proposed. The proposed catalytic cycle is unusual due to the involvement of silylene hydride and silene hydride complexes, potentially as on-cycle species.

The reaction of $[(\text{dmpe})_2\text{MnH}(\text{C}_2\text{H}_4)]$ ($\mathbf{10}$) with H_2 at 60 °C afforded ethane and the dihydrogen hydride complex $[(\text{dmpe})_2\text{MnH}(\text{H}_2)]$ ($\mathbf{11}$), which has previously been

prepared by an alternative route. Complex **10** reacted with hydroborane reagents 9-BBN or HBMe₂ at 60 °C to afford EtBR₂ and Mn(I) borohydride complexes [(dmpe)₂Mn(μ-H)₂BR₂] (**29**: R₂ = C₈H₁₄, **30**: R = Mes); two intermediates were observed in each of these reactions. Deuterium labelling experiments using the deuterated hydroborane DBMe₂ suggest that this reaction proceeds via the 5-coordinate ethyl isomer of **10**; [(dmpe)₂MnEt] (**13**). By contrast, exposure of **10** to BH₃·NMe₃ required a higher temperature (90 °C) to yield [(dmpe)₂Mn(μ-H)₂BH₂] (**28**), and ethylene was formed as the reaction byproduct; this reaction presumably proceeded by ethylene substitution. Deuterium incorporation into both the MnH and BH environments of **28** was observed under an atmosphere of D₂ at 90 °C. Reactions of **10** with free dmpe yielded ethylene and a mixture of [{(dmpe)₂MnH}₂(μ-dmpe)] (**31**) and [(dmpe)₂MnH(κ¹-dmpe)] (**32**), which could be isolated by washing/recrystallization or sublimation, respectively. Similar reactivity was observed between **10** and HPPh₂, which afforded ethylene and [(dmpe)₂MnH(HPPh₂)] (**33**) at 90 °C. Exposure of **10** to HSnPh₃ yielded the manganese(II) stannyl hydride complex [(dmpe)₂MnH(SnPh₃)] (**34**) along with ethylene and, presumably, additional unidentified products. However, the mechanism for formation of **34** is unclear, it could not be isolated in pure form due to decomposition to form various species including SnPh₄, and the mechanism of the decomposition process remains obscure. Previously reported complex **11**, along with new complexes **28-31** and **33-34**, were crystallographically characterized.

This work provides valuable insights to unusual metal–ligand bonding motifs and reactions, and as such contributes to the fundamental understanding of organometallic chemistry.

Acknowledgements

First and foremost I would like to thank my supervisor, Dr. David J. H. Emslie, for all the help and encouragement he has offered me throughout my time in his research group. It has truly been a privilege to work with him, and I appreciate all the understanding and time he has given me over the years. As a guide to the world of chemistry, there is nobody better.

I would also like to thank all the members of the Emslie group, both current and past; Dr. Nick Andreychuck, Dr. Preeti Chadha, Dr. Brad Cowie, Kris Kolpin, Dr. Kelly Motolko, Dr. Todd Whitehorne, Dr. Edwin Wong, Dr. Bala Vidjayacoumar, Dr. Kevin Yu, Majeda Al Hareri, Declan DeJordy, Novan Gray, Nick Hoffman, Katarina Paskaruk, Sunny (Aathith) Vasanthakumar, and Kasuni Wedisinghe. Both inside and outside the lab, you have all worked hard to make graduate life in the Emslie group a wonderful experience. Regardless of where our futures take us, the friendships we have made will last a lifetime. I would not have been able to complete my thesis without the support of all of you, and I am particularly indebted towards Brad and Nick A., who showed me the ropes when I first entered the group, and whose love of chemistry was infectious to all around them.

I am also deeply grateful to all those at McMaster you have offered their time and expertise over the years. This includes Karen Neumann, Paul Dube, Dr. Hilary Jenkins, Dr. Steve Kornic, Megan Fair, Dr. Kirk Green, Dr. Fan Fei, and Victoria Jarvis. I would like to particularly thank Dr. Bob Berno and Dr. James Britten for the vast amounts of time they have taken to help me using the NMR and X-ray diffraction facilities, respectively. I truly appreciate all the rapid and helpful responses to all my panicked midnight e-mails!

I would also like to express my appreciation to the staff at the Department of Chemistry and Chemical Biology for their assistance with administrative issues over the years; Jane Garneau, Linda Spruce, Christine Cosgrove, Connie Carrabs, Sara Warner,

Salina Jaffer, and Leah Allen. I would also like to thank the librarians at Thode library, led by Hope Li, for all the help they have offered me over the years in searching for books or journal articles.

I am deeply indebted to the members of my Ph.D. committee, Dr. Yuriy Mozharivskyj and Dr. Ignacio Vargas-Baca, for all their support over the years. In addition to their work on my committee, I am grateful to Dr. Mozharivskyj for his assistance in analyzing magnetic data, and to Dr. Vargas-Baca for his assistance in DFT calculations. Your generosity with your time and expertise is truly appreciated.

I would also like to thank the Department of Chemistry and Chemical Biology, Intel Corporation (though the Semiconductor Research Corporation), and the governments of Ontario (through OGS) and Canada (though Dr. Emslie's NSERC discovery grant) for providing funding either for my research or stipend over the years.

Finally, I would like to thank my family and friends for all their encouragement and support over the years; none of this would have been possible without you. This work would not have been possible without the continuing support of my brother Benji and parents Maxine and Steve. I am also profoundly grateful for all the close friendships I have developed at McMaster, including those from the Emslie lab and the Mother Liquors. To Dr. Lucia Lee, I am so thankful for our continuing friendship, which has helped me through the best and worst of times. Lastly, I am particularly grateful to have had the opportunity to know Dr. Greg Bahun, the most generous person I have ever known.

Let me Rephrase That – C. Montgomery Burns

Table of Contents

LAY ABSTRACT.....	iii
ABSTRACT.....	iv
ACKNOWLEDGEMENTS.....	ix
TABLE OF CONTENTS.....	xii
LIST OF FIGURES.....	xxi
LIST OF SCHEMES.....	xliii
LIST OF TABLES.....	xlix
LIST OF COMPOUNDS (OBSERVED)	liii
KEY INTERMEDIATES CALCULATED BY DFT.....	lvii
LIST OF ABBREVIATIONS, ACRONYMS, AND SYMBOLS	lviii
DECLARATION OF ACADEMIC ACHIEVEMENT.....	lxix
CHAPTER 1: INTRODUCTION	
1.1 – Introductory Remarks	1
1.2 – CVD and ALD Using Manganese Precursors	1
1.2.1 – Scope of Section.....	2
1.2.2 – Introductory Remarks on CVD and ALD	2

1.2.3 – Introduction to Chemical Vapour Deposition (CVD).....	3
1.2.4 – Introduction to Atomic Layer Deposition (ALD)	4
1.2.5 – Requirements for CVD and/or ALD Precursors	6
1.2.6 – A Brief Introduction to Deposition of Elemental Metals by ALD or Pulsed-CVD	7
1.2.7 – Chemical Vapour Deposition Using Mn-containing Precursors.....	11
1.2.8 – Atomic Layer Deposition (ALD) of Manganese-containing Films	15
1.3 – Manganese Alkyl Complexes	19
1.3.1 – Scope of Section.....	19
1.3.2 – Alkyl Complexes for Transition Metal ALD	19
1.3.3 – Homoleptic Neutral Dialkylmanganese(II) Complexes.....	20
1.3.4 – Lewis Base Adducts of Neutral Dialkylmanganese(II) Complexes.....	24
1.3.5 – Selected Reactions of Neutral Dialkylmanganese(II) Complexes (Homoleptic and Lewis Base Adducts).....	30
1.3.6 – Homoleptic Neutral Tri- and Tetra- Alkylmanganese Complexes and their Lewis Base Adducts.....	31
1.4 – Manganese Hydride Complexes	33
1.4.1 – Scope of Section.....	33
1.4.2 – Manganese(I) Hydride Carbonyl Complexes.....	33
1.4.3 – CO-Free Manganese Hydride Complexes.....	36
1.4.4 – Selected Characterization Methods for Manganese Hydride Complexes.....	39
1.4.5 – Selected Stoichiometric Reactions of Manganese Hydride Complexes	40
1.4.6 – σ -H ₂ Complexes of Mn	43
1.5 – Manganese Silyl Complexes.....	46
1.5.1 – Scope of Section.....	46
1.5.2 – Early Manganese Silyl Complexes	46
1.5.3 – Structurally Characterized Hydride-free Mn(I) Silyl Complexes	47
1.5.4 – Structurally Characterized Mn(II) and Mn(III) Hydride-free Silyl Complexes	50

1.5.5 – Introduction to ‘Nonclassical’ Hydrosilane Complexes of Transition Metals..	51
1.5.6 – Silyl Hydride/hydrosilane Complexes of Manganese.....	55
1.6 – Silylene Complexes of Transition Metals.....	63
1.6.1 – Scope of Subsection	63
1.6.2 – Introduction to Silylene Complexes.....	63
1.6.3 – Electronic Structure of Silylene Complexes	64
1.6.4 – Characterization of Base-free non-Electronically Stabilized Silylene Complexes.....	66
1.6.5 – Silylene Hydride Complexes.....	68
1.6.6 – Silylene Complexes with Terminal SiH Substituents	71
1.6.7 – NHC-Stabilized Silylene Complexes of Transition Metals	72
1.6.8 – Silylene Complexes of Early/Mid Transition Metal Centres	76
1.6.9 – Reactions of silylene complexes with alkenes and alkynes	80
1.6.10 – Complexes related to silylene complexes	84
1.7 – Silene Complexes of Transition Metals.....	89
1.7.1 – Scope of Section.....	89
1.7.2 – Introduction to Silene Complexes.....	89
1.7.3 – Electronic Structure of Silene Complexes	91
1.7.4 – Synthesis of Silene Complexes	93
1.7.5 – Solid State Structural Characterization of Silene Complexes.....	99
1.7.6 – Spectroscopic Characterization of Silene Complexes.....	100
1.7.7 – Silene Hydride Complexes; Interligand Si–H Interactions	101
1.7.8 – Complexes of Ligands Containing a π -system for which a Resonance Structure can be Drawn which Includes a Si=C Bond.....	102

**CHAPTER 2: DIALKYL MANGANESE(II) COMPLEXES; SYNTHESIS,
CHARACTERIZATION, AND SOLUTION-STATE REACTIVITY FOR
DEPOSITION OF ELEMENTAL MANGANESE**

2.1 – Introduction to Chapter 2	107
2.2 – Synthesis and X-ray Crystal Structures	109
2.3 – NMR Spectroscopy and Magnetic Measurements.....	120
2.4 – Physical Properties of 1-8	126
2.5 – Reactions with Hydrogen and Diethyl Zinc.....	127
2.6 – Summary and Conclusions for Chapter 2	132

**CHAPTER 3: ANALYSIS OF WILKINSON AND GIROLAMI'S
trans-[(dmpe)₂MnH(C₂H₄)]**

3.1 – Introduction to Chapter 3	134
3.2 – X-ray Crystal Structure of <i>trans</i> -[(dmpe) ₂ MnH(C ₂ H ₄)]	135
3.3 – Potential Pathways for Reactions of [(dmpe) ₂ MnH(C ₂ H ₄)] with Hydrides.....	138
3.4 – DFT calculations for isomerization of <i>trans</i> -[(dmpe) ₂ MnH(C ₂ H ₄)] to [(dmpe) ₂ MnEt].....	141
3.5 – Trapping of the Putative [(dmpe) ₂ MnEt] Intermediate.....	147
3.6 – Summary and Conclusions for Chapter 3	154

CHAPTER 4: SYNTHESIS OF SILYLENE HYDRIDE COMPLEXES AND REACTIVITY WITH ETHYLENE TO AFFORD SILENE HYDRIDE COMPLEXES

4.1 – Introduction to Chapter 4	156
4.2 – Synthesis and Characterization of Manganese Silylene Hydride Complexes	156
4.3 – DFT Fragment Interaction Analysis of Silylene Hydride Complexes.....	162
4.4 – Synthesis and Characterization of Silene Hydride Complexes.....	164
4.5 – Fragment Interaction Analysis of Silene Hydride Complex [(dmpe) ₂ MnH(Et ₂ Si=CHMe)].....	166
4.6 – Potential Mechanisms for Silene Hydride Synthesis	167
4.7 – Summary and Conclusions for Chapter 4	169

CHAPTER 5: SYNTHESIS OF MANGANESE DISILYL HYDRIDE COMPLEXES AND REACTIVITY WITH ETHYLENE TO AFFORD SILENE HYDRIDE COMPLEXES

5.1 – Introduction to Chapter 5	170
5.2 – Synthesis and Characterization of Manganese Disilyl Hydride Complexes	172
5.3 – Reactions of Manganese Disilyl Hydride Complexes with Ethylene.....	176
5.3 – DFT Calculations on Low-Coordinate Silyl and Silylene Hydride Intermediates Derived from 20^R	185
5.4 – High Temperature NMR Spectra of 20^R : <i>in situ</i> Generation of <i>trans</i> -Silylene Hydride (<i>trans</i> - 16^{R,H}) Species	188

5.5 – Trapping Experiments with Isonitriles and <i>N</i> -Heterocyclic Carbenes	190
5.6 – Pathways for Reactions of 20^R with Ethylene	199
5.7 – Summary and Conclusions for Chapter 5	202

CHAPTER 6: MANGANESE SILYL DIHYDRIDE COMPLEXES: A SPECTROSCOPIC, CRYSTALLOGRAPHIC AND COMPUTATIONAL STUDY OF NONCLASSICAL SILICATE AND HYDROSILANE HYDRIDE ISOMERS

6.1 – Introduction to Chapter 6	203
6.2 – Synthesis of Silyl Dihydride Complexes	204
6.3 – 1D NMR Characterization of Silyl Dihydride Complexes	205
6.4 – X-ray Crystal Structures of Silyl Dihydride Complexes	208
6.5 – DFT Calculations on Silyl Dihydride Complexes	212
6.6 – Determination of Sign and Magnitude of $J_{\text{Si,H}}$	219
6.7 – Summary and Conclusions for Chapter 6	224

CHAPTER 7: REACTIONS OF MANGANESE DISILYL HYDRIDE COMPLEXES WITH REAGENTS CONTAINING UNSATURATED POLAR BONDS

7.1 – Introduction to Chapter 7	227
7.2 – Synthesis and Characterization of $[(\text{dmpe})_2\text{Mn}\{\kappa^2\text{-SiHR}(\text{N}^i\text{PrCHN}^i\text{Pr})\}]$	227
7.3 – Synthesis and Characterization of <i>trans</i> - $[(\text{dmpe})_2\text{Mn}(\text{CO})(\kappa^1\text{-O}_2\text{CH})]$ (26)	231

7.4 – Potential Pathways for Reactions of Disilyl Hydride Complexes with {C(N ^t Pr) ₂ } or CO ₂	233
7.5 – Summary and Conclusions for Chapter 7	238
CHAPTER 8: CATALYTIC HYDROSILYLATION OF ETHYLENE	
8.1 – Introduction of Chapter 8.....	239
8.2 – Catalytic Hydrosilylation of Ethylene	240
8.3 – Monitoring Ethylene Hydrosilylation by H ₃ Si ⁿ Bu Over Time	242
8.4 – Proposed Catalytic Cycles of Ethylene Hydrosilylation.....	246
8.5 – Summary and Conclusions for Chapter 8	250
CHAPTER 9: SYNTHESIS OF MANGANESE HYDRIDE COMPLEXES WITH VARIOUS CO-LIGANDS (NOT INCLUDING Si-BASED CO-LIGANDS)	
9.1 – Introduction to Chapter 9	251
9.2 – Reaction of <i>trans</i> -[(dmpe) ₂ MnH(C ₂ H ₄)] with H ₂	251
9.3 – Reactions of <i>trans</i> -[(dmpe) ₂ MnH(C ₂ H ₄)] with Hydroboranes; Synthesis and Characterization of Borohydride Complexes of Manganese(I)	253
9.4 – Synthesis and Characterization of κ ¹ -dmpe Hydride Complexes of Manganese	265
9.5 – Reaction of <i>trans</i> -[(dmpe) ₂ MnH(C ₂ H ₄)] with HPPPh ₂	270
9.6 – Reactions of <i>trans</i> -[(dmpe) ₂ MnH(C ₂ H ₄)] (10) with Hydrotin Reagents	275
9.7 – Summary and Conclusions for Chapter 9	277

CHAPTER 10: FUTURE DIRECTIONS

10.1 – Future Directions Pertaining to Vapour-phase Deposition of Mn-containing Thin Films	279
10.2 – Future Directions Pertaining to Dialkylmanganese(II) Chemistry	281
10.3 – Future Directions Pertaining to the Structure of [(dmpe) ₂ MnH(C ₂ H ₄)] (10)	282
10.4 – Future Directions Pertaining to DFT Calculations	284
10.5 – Future Directions Pertaining to Manganese Silylene Hydride Complexes	284
10.6 – Future Directions Pertaining to Manganese Silene Hydride Complexes.....	287
10.7 – Future Directions Pertaining to Silyl Dihydride Complexes	289
10.8 – Future Directions Pertaining to Reactions of Disilyl Hydride Complexes with CO ₂ and C(N ^{<i>i</i>} Pr) ₂	290
10.9 – Future Directions Pertaining to Catalytic Hydrosilylation	292
10.10 – Future Directions Pertaining to Manganese Hydride Complexes with non-Si Co-ligands	293

CHAPTER 11: EXPERIMENTAL METHODS

11.1 – General Details.....	294
11.1.1: Laboratory Equipment and Apparatus	294
11.1.2: Solvents	294
11.1.3: Starting Materials	295
11.1.4: Instrumentation and Analysis.....	295
11.1.5: DFT Calculations	299

11.1.6: Additional Notes	301
11.2 – Synthetic Procedures and Characterization Pertaining to the Work of Chapter 2.....	301
11.3 – Synthetic Procedures and Characterization Pertaining to the Work of Chapter 3.....	305
11.4 – Synthetic Procedures and Characterization Pertaining to the Work of Chapter 4.....	309
11.5 – Synthetic Procedures and Characterization Pertaining to the Work of Chapter 5.....	316
11.6 – Synthetic Procedures and Characterization Pertaining to the Work of Chapter 6.....	341
11.7 – Synthetic Procedures and Characterization Pertaining to the Work of Chapter 7.....	345
11.8 – Synthetic Procedures and Characterization Pertaining to the Work of Chapter 8.....	349
11.9 – Synthetic Procedures and Characterization Pertaining to the Work of Chapter 9.....	354
APPENDIX 1	363
APPENDIX 2.....	389
REFERENCES.....	394

List of Figures

Figure 1.1: Periodic table, not including hydrogen, halogens and noble gases, highlighting metals that have been deposited by thermal ALD or pulsed-CVD (only reports in peer-reviewed literature are included). Metals that have been deposited by ALD are enclosed by solid black boxes. Metals (or alloys) that have been deposited only by pulsed-CVD are enclosed by dashed black boxes. Atomic numbers are shown above the atom symbols and Pauling electronegativities are shown below (for values with two decimal places, the oxidation state is: I for groups 1 and 11, II for groups 2, 4-10 and 12, III for groups 3 and 13, and IV for group 14). Non-metals (including semi-metals) and elements without significant natural abundance are shown in white. The remaining elements are shaded.	8
Figure 1.2: Single-source precursors used for CVD of Mn-containing thin films (not including elemental manganese).....	12
Figure 1.3: Precursors used for CVD of Mn-containing thin films (not including oxides or elemental manganese) by simultaneous decomposition of multiple precursors or decomposition of Mn-containing precursors in the presence of a reactive gas.	13
Figure 1.4: Mn-containing precursors used for CVD of manganese oxides (pink box; oxides and silicates) in the presence of oxygen or water.....	14
Figure 1.5: Precursors used for CVD of elemental manganese.....	15
Figure 1.6: Mn-containing reagents used for ALD of manganese oxide.....	16
Figure 1.7: Mn-containing precursors used for ALD of Mn-containing thin films (aside from oxides).....	17
Figure 1.8: Neutral homoleptic dialkylmanganese(II) complexes for which an X-ray crystal structure has been obtained.	21
Figure 1.9: Lewis base adducts of $\text{Mn}(\text{CH}_2\text{EMe}_3)_2$ (E = C, Si) for which X-ray crystal structures were obtained.	26

Figure 1.10: Structurally characterized dmpe adducts of neutral MnR ₂ complexes.	29
Figure 1.11: Structurally characterized neutral bis(η^1 -allyl)manganese(II) complexes..	30
Figure 1.12: Reported neutral homoleptic tri- and tetra- alkylmanganese complexes....	32
Figure 1.13: CO-free terminal manganese hydride complexes.	37
Figure 1.14: σ -H ₂ complexes of Mn.	45
Figure 1.15: Early manganese silyl complexes.	47
Figure 1.16: Structurally characterized Mn(I) silyl complexes lacking hydride co-ligands.	48
Figure 1.17: Structurally characterized hydride-free Mn(II) and Mn(III) silyl complexes.	51
Figure 1.18: Top; From left to right, structures of classical hydrosilane, nonclassical hydrosilane, and classical silyl hydride complexes. Bottom; Dewar-Chatt-Duncanson model of σ donation and π backdonation from/to a hydrosilane ligand.	52
Figure 1.19: Early examples of complexes reported to involve multiple Si–H interactions to the same silicon centre.	55
Figure 1.20: Silyl hydride/hydrosilane complexes characterized by X-ray or neutron crystallography. For clarity, all structures are shown as nonclassical hydrosilane complexes.	59
Figure 1.21: Early examples of isolated silylene complexes.	64
Figure 1.22: Electronic structure of Fischer-type silylene complexes. For clarity, in the diagram for σ -donation, only one lobe is shown for each orbital (from a variety of potential orbitals on the transition metal, and an sp ² orbital on the Si centre).	65
Figure 1.23: <i>N</i> -heterocyclic silylene complexes (NHSi ligands).	65
Figure 1.24: Early examples of silylene hydride complexes.	68
Figure 1.25: Early examples of silylene complexes with a terminal SiH substituent.	72

Figure 1.26: Glossary of NHCs.	73
Figure 1.27: The first reported NHC-silylene adducts and NHC-stabilized silylene complexes. The M–Si bond is shown as a double bond for clarity, and does not reflect the bond strength.....	73
Figure 1.28: Electronic structure of NHC-stabilized silylene complexes. Dashed line in the Chemdraw figure indicates a single or double bond. For clarity, in the diagram for σ -donation, only one lobe is shown for each orbital.	74
Figure 1.29: NHC-stabilized silylene hydride complexes. The M–Si bond is shown as a double bond for clarity, and does not reflect bond strength.	76
Figure 1.30: Base-free silylene complexes of gr. 3-5.....	77
Figure 1.31: Donor-stabilized silylene complexes of gr. 4-5.	78
Figure 1.32: Reported silylene complexes of rhenium.	78
Figure 1.33: Silylene complexes of manganese.....	80
Figure 1.34: Common mechanisms for olefin hydrosilylation. Key alkene insertion steps are highlighted in grey.	82
Figure 1.35: η^3 -H ₂ SiR ₂ complexes of transition metals. For clarity, all structures have been drawn with single bonds between Si and the metal, and between each of those and the bridging hydride ligands.	85
Figure 1.36: Structures used to describe η^3 -H ₂ SiR ₂ complexes of transition metals.....	85
Figure 1.37: Selected silylyne complexes of transition metals. Base-stabilized structures are drawn with a triple bond between Si and the metal for clarity, and this does not reflect the bond strength.....	88
Figure 1.38: Alternative bonding descriptions of NHC-stabilized silylyne complexes. .	88
Figure 1.39: Early examples of observed free silenes and silene transition metal complexes.	90

Figure 1.40: Dewar-Chatt-Duncanson model of σ donation and π backdonation from/to a silene ligand.	92
Figure 1.41: Canonical resonance structures of (top) metallasilacyclopropane/silene complexes and (bottom) metallacyclopropane/alkene complexes.....	93
Figure 1.42: Resonance structures used to describe silene hydride complexes with an interligand Si–H interaction.....	102
Figure 1.43: Transition metal η^2 -silaallene, η^3 -silaallyl, or η^3 -silapropargyl complexes.	103
Figure 1.44: Resonance structures of η^3 -silaallyl and η^3 -silapropargyl complexes.	104
Figure 1.45: Complexes containing non-aromatic ligands featuring extended π -systems that include a “Si=C” moiety (not including η^2 -silaallene, η^3 -silaallyl, or η^3 -silapropargyl complexes; see Figure 1.43).	105
Figure 2.1: X-ray crystal structure for $[\{\text{Mn}(\text{CH}_2\text{CMe}_3)(\mu\text{-CH}_2\text{CMe}_3)_2\}_2\{\text{Mn}(\mu\text{-CH}_2\text{CMe}_3)_2\text{Mn}\}]$ (2). Hydrogen atoms are omitted for clarity, and ellipsoids are set to 50 % probability.....	112
Figure 2.2: X-ray crystal structures for (left) $[(\text{dmpe})\text{Mn}(\text{CH}_2\text{SiMe}_3)_2]$ (3) and (right) $[\{(\mu\text{-dmpe})\text{Mn}(\text{CH}_2\text{CMe}_3)_2\}_2]$ (4). Hydrogen atoms are omitted for clarity, and ellipsoids are set to 50 %. For 3 , all carbon atoms in the dmpe ligand are disordered over two positions, and only the dominant conformation (69 %) is shown above.	114
Figure 2.3: X-ray crystal structures for $[(\mu\text{-dmpe})\{\text{Mn}(\text{CH}_2\text{SiMe}_3)(\mu\text{-CH}_2\text{SiMe}_3)\}_2]$ (5) obtained by crystallization from toluene (left) or hexanes (middle), and (right) the X-ray crystal structure for $[(\mu\text{-dmpe})\{\text{Mn}(\text{CH}_2\text{CMe}_3)(\mu\text{-CH}_2\text{CMe}_3)\}_2]$ (6). Hydrogen atoms are omitted for clarity, and ellipsoids are set to 50 %. For 5 (obtained from toluene), the unit cell contains three independent and essentially isostructural molecules, and only one is shown. For 6 , positions of all carbon atoms in three of the four neopentyl groups (C(1)-C(15)) are disordered over two positions. The figure shows only one position for each of	

the disordered groups (occupancy: 50 % for C1-C5, 82 % for C6-C10, and 87 % for C11-C15)..... 116

Figure 2.4: X-ray crystal structures for (left) $[(\mu\text{-dmpm})\{\text{Mn}(\text{CH}_2\text{SiMe}_3)(\mu\text{-CH}_2\text{SiMe}_3)\}_2]$ (7) and (right) $[(\mu\text{-dmpm})\{\text{Mn}(\text{CH}_2\text{CMe}_3)(\mu\text{-CH}_2\text{CMe}_3)\}_2]$ (8). Hydrogen atoms are omitted for clarity, and ellipsoids are set to 50 %. For 8, poor quality of data means that the structure is only suitable to establish connectivity. The unit cell contains five independent and essentially isostructural molecules, and only one is shown..... 118

Figure 2.5: X-ray crystal structure for $[\{(\text{Et}_3\text{P})\text{Mn}(\text{CH}_2\text{SiMe}_3)(\mu\text{-CH}_2\text{SiMe}_3)\}_2]$ (9). Hydrogen atoms are omitted for clarity, and ellipsoids are set to 50 %. 119

Figure 2.6: Left: Room temperature ^1H NMR spectra for 2-8 (500 MHz, C_6D_6). Black tick marks indicate broad peaks associated with organomanganese(II) complexes, while the sharp signals are due to residual $\text{C}_6\text{D}_5\text{H}$ in the NMR solvent and trace hexanes. Middle: low frequency portion of the ^1H NMR spectra for $[(\mu\text{-dmpe})\{\text{Mn}(\text{CH}_2\text{CMe}_3)(\mu\text{-CH}_2\text{CMe}_3)\}_2]$ (6) from 186 to 298 K (500 MHz, d_8 -toluene). Broad signals (|) are due to 6, while sharp signals are due to residual d_7 -toluene solvent impurity (\neq) and hexanes (*). Right: Region of the ^1H NMR spectra used for Evans measurements for 6 between 186 and 298 K (500 MHz, 40:1 d_8 -toluene:toluene); the methyl group from external toluene (\dagger) is calibrated to 2.11 ppm, and the methyl group of internal toluene (\ddagger) is observed to shift with temperature. Shoulders to the right of the two toluene (C_7H_8) signals are the residual solvent signals due to d_7 -toluene, $\text{C}_6\text{D}_5(\text{CHD}_2)$.120

Figure 2.7: SQUID magnetic susceptibility data from 5 to 300 K. Left: $\chi_{\text{M}(\text{corr})}$ vs. T (solid lines) and $(1/\chi_{\text{M}(\text{corr})})$ vs. T (dashed lines) for paramagnetic 3 (red) and 4 (blue). Right: $\chi_{\text{M}(\text{corr})}$ vs. T (solid lines) and $\chi_{\text{M}(\text{corr})} \cdot \text{T}$ vs. T (dashed lines) for 2 (red), 5 (blue), 6 (purple), 7 (orange), and 8 (green), which feature antiferromagnetic interactions..... 123

Figure 2.8: Solution magnetic susceptibilities per mole of Mn calculated from Evans measurements at various temperatures for $[\{\text{Mn}(\text{CH}_2\text{CMe}_3)(\mu\text{-CH}_2\text{CMe}_3)\}_2\{\text{Mn}(\mu\text{-CH}_2\text{CMe}_3)_2\text{Mn}\}]$ (2) (blue diamonds),

$[(\mu\text{-dmpe})\{\text{Mn}(\text{CH}_2\text{SiMe}_3)(\mu\text{-CH}_2\text{SiMe}_3)\}_2]$ (5) (green triangles),
 $[(\mu\text{-dmpe})\{\text{Mn}(\text{CH}_2\text{CMe}_3)(\mu\text{-CH}_2\text{CMe}_3)\}_2]$ (6) (red squares), and
 $[(\mu\text{-dmpm})\{\text{Mn}(\text{CH}_2\text{SiMe}_3)(\mu\text{-CH}_2\text{SiMe}_3)\}_2]$ (7) (purple 'x' symbols)..... 125

Figure 3.1: Left: X-ray crystal structure of *trans*- $[(\text{dmpe})_2\text{MnH}(\text{C}_2\text{H}_4)]$ (***trans*-10**) with ellipsoids drawn at 50% probability. Hydrogen atoms on the metal centre and ethylene ligand were located from the difference map and refined isotropically. Most hydrogen atoms have been omitted for clarity. Right: geometry optimized (DFT calcd.) structure of *trans*- $[(\text{dmpe})_2\text{MnH}(\text{C}_2\text{H}_4)]$ (***trans*-10**). Most hydrogen atoms have been omitted for clarity. 136

Figure 3.2: ETS-NOCV analysis of bonding between $[(\text{dmpe})_2\text{MnH}]$ (equatorial dmpe geometry) and ethylene in *trans*- $[(\text{dmpe})_2\text{MnH}(\text{C}_2\text{H}_4)]$ (***trans*-10**). Inset: SCF deformation density isosurface from a fragment interaction calculation using neutral $[(\text{dmpe})_2\text{MnH}]$ (equatorial dmpe geometry) and ethylene fragments for *trans*- $[(\text{dmpe})_2\text{MnH}(\text{C}_2\text{H}_4)]$ (***trans*-10**). 137

Figure 3.3: First-row transition metal (Fe,^{485,486} Ni,⁴⁸⁷ Co,^{488,489} or Mn¹²⁰) alkene hydride complexes (not including complex **10**)..... 140

Figure 3.4: First row transition metal ethyl complexes reported to feature a β -agostic interaction.^{490,491,492,493,494,495,496,497} 140

Figure 3.5: Potential energies (E ; kJ mol^{-1}) relative to ***trans*-10**, calculated for structures (left to right) i. *trans*- $[(\text{dmpe})_2\text{MnH}(\text{C}_2\text{H}_4)]$ (***trans*-10**), ii. an isomer of *cis*- $[(\text{dmpe})_2\text{MnH}(\text{C}_2\text{H}_4)]$ in which the ethylene ligand is oriented perpendicular to the plane formed by manganese, the hydride, and the ethylene centroid (***cis*-10^L**), iii. the transition state for isomerization of ***cis*-10^L** to ***cis*-10^I** $\{(\text{cis-10}^{\text{L/I}})^\ddagger\}$, iv. an isomer of *cis*- $[(\text{dmpe})_2\text{MnH}(\text{C}_2\text{H}_4)]$ in which the ethylene carbon atoms lie within the plane formed by manganese, the hydride, and the ethylene centroid (***cis*-10^I**), v. the transition state for isomerization of ***cis*-10^I** to **13 ^{β -agostic}** $\{(\text{10/13})^\ddagger\}$, vi. $[(\text{dmpe})_2\text{MnEt}]$ with a β -agostic interaction (**13 ^{β -agostic}**), vii. $[(\text{dmpe})_2\text{MnEt}]$ without an agostic interaction where the Mn–C $_{\alpha}$ –C $_{\beta}$ angle was restrained to 109.5° (**13^{109.5}**), viii. the transition state for isomerization

of $13^{\beta\text{-agostic}}$ to $13^{\alpha\text{-agostic}}$ $\{(13^{\beta/\alpha})^\ddagger\}$, and ix. $[(\text{dmpe})_2\text{MnEt}]$ with an α -agostic interaction ($13^{\alpha\text{-agostic}}$). All structures except $13^{109.5}$ correspond to an energy minimum. The geometry optimized cores are depicted above each Chemdraw structure, showing Mn in blue, C in dark grey, and H in light grey, accompanied by stick bonds to the phosphorus donor atoms. Relative energies are those before zero-point energy (ZPE) correction. 142

Figure 3.6: Potential energies (E ; kJ mol^{-1}) relative to *trans*- 10_{PH_3} , calculated for structures (left to right) i. *trans*- $[(\text{PH}_3)_4\text{MnH}(\text{C}_2\text{H}_4)]$ (*trans*- 10_{PH_3}), ii. an isomer of *cis*- $[(\text{PH}_3)_4\text{MnH}(\text{C}_2\text{H}_4)]$ in which the ethylene ligand is oriented perpendicular to the plane formed by manganese, the hydride, and the ethylene centroid (*cis*- $10_{\text{PH}_3}^\perp$), and iii. an isomer of *cis*- $[(\text{PH}_3)_4\text{MnH}(\text{C}_2\text{H}_4)]$ in which the ethylene carbon atoms lie within the plane formed by manganese, the hydride, and the ethylene centroid (*cis*- $10_{\text{PH}_3}^\parallel$). Geometry optimized cores are depicted above each Chemdraw structure, showing Mn in blue, C in dark grey, and H in light grey, accompanied by stick bonds to the phosphorus donor atoms. Relative energies are those before zero-point energy (ZPE) correction. 145

Figure 3.7: Regions of the $^1\text{H}\{^{31}\text{P}\}$ (above) and ^1H (below) NMR spectra for the MnCH_2 environments in a) *cis*- $[(\text{dmpe})_2\text{MnEt}(\text{CN}^t\text{Bu})]$ (*cis*- 14a) and b) *trans*- $[(\text{dmpe})_2\text{MnEt}(\text{CN}^t\text{Bu})]$ (*trans*- 14a)..... 150

Figure 3.8: X-ray crystal structures of a) *trans*- $[(\text{dmpe})_2\text{MnEt}(\text{CN}^t\text{Bu})]$ (*trans*- 14a) and b) *trans*- $[(\text{dmpe})_2\text{MnEt}(\text{CNXyl})]$ (*trans*- 14b) with ellipsoids drawn at 50% probability. Hydrogen atoms have been omitted for clarity. In the case of *trans*- 14a , all atoms except P and Mn are disordered over two positions, and only one conformation {50.1(2)% and 52.8(2)% for the two dmpe ligands, 50.5(2)% for the isonitrile ligand, and 56.0(3)% for the ethyl ligand} is shown. In the case of *trans*- 14b , one dmpe ligand and the N atom are both disordered over two positions, and only one conformation {51.4(3)% for the dmpe ligand and 55(2)% for N} is shown. 151

Figure 3.9: X-ray crystal structure of $[(\text{dmpe})\text{Mn}(\text{CNXyl})_3\{\text{C}(=\text{NXyl})\text{CEt}(=\text{NXyl})\}]$ (15), with ellipsoids drawn at 50% probability. Methyl groups on the *o*-xylyl ligands and all hydrogen atoms have been omitted for clarity. The phenyl group of one isonitrile

ligand is disordered over two positions and only the dominant conformation {51.4(6)%} is shown. 153

Figure 4.1: X-ray crystal structure of *trans*-[(dmpe)₂MnH(=SiEt₂)] (*trans*-**16**^{Et₂}) with ellipsoids drawn at 50% probability. Most hydrogen atoms have been omitted for clarity and the hydrogen atom on Mn was located from the difference map and refined isotropically. The unit cell contained four independent and essentially isostructural molecules, and only one is shown..... 158

Figure 4.2: Left: X-ray crystal structure of *cis*-[(dmpe)₂MnH(=SiPh₂)] (*cis*-**16**^{Ph₂}). *cis*-**16**^{Ph₂} co-crystallized with the *central* isomer of [(dmpe)₂MnH₂(SiHPh₂)] (**18**^{Ph₂}), with superimposed (dmpe)₂Mn and phenyl groups, and only the structure of *cis*-**16**^{Ph₂} is shown. Hydrogen atoms have been omitted for clarity (and the bridging metal hydride environment was not located from the difference map). The unit cell contains two independent and essentially isostructural molecules, and only one is shown. Right: geometry optimized (DFT calcd.) structure of *cis*-[(dmpe)₂MnH(=SiPh₂)] (*cis*-**16**^{Ph₂}). Most hydrogen atoms have been omitted for clarity. 161

Figure 4.3: Deformation density contributions $\Delta\rho_1$, $\Delta\rho_2$, and $\Delta\rho_3$ to bonding between the SiEt₂ and (dmpe)₂MnH fragments in a) *trans*-[(dmpe)₂MnH(=SiEt₂)] (*trans*-**16**^{Et₂}), b) *cis*-[(dmpe)₂MnH(=SiEt₂)] (*cis*-**16**^{Et₂}), and c) [(dmpe)₂MnH(Et₂Si=CHMe)] (**19**^{Et₂}). Increased (green) and decreased (yellow) electron density is presented relative to the fragments; isosurfaces are set to 0.003. 163

Figure 4.4: Key fragment orbitals contributing to $\Delta\rho_1$ and $\Delta\rho_1$ in a) *cis*-[(dmpe)₂MnH(=SiEt₂)] (*cis*-**16**^{Et₂}) and b) [(dmpe)₂MnH(Et₂Si=CHMe)] (**19**^{Et₂}); isosurfaces are set to 0.04. 164

Figure 4.5: X-ray crystal structure of [(dmpe)₂MnH(Ph₂Si=CHMe)] (**19**^{Ph₂}) with ellipsoids drawn at 50 % probability. Most hydrogen atoms have been eliminated for clarity, and hydrogen atoms on Mn(1) and C(1) (H(1) and H(2)) were located from the difference map and refined isotropically. Inset shows the metal, silene, and hydride core,

with most H atoms, the dmpe ligands, and the most of the phenyl substituents on Si (aside from the *ipso* carbons) removed for clarity..... 166

Figure 5.1: X-ray crystal structure of $[(\text{dmpe})_2\text{MnH}(\text{SiH}_2\text{Ph})_2]$ ($\mathbf{20}^{\text{Ph}}$) with ellipsoids drawn at 50% probability. Most hydrogen atoms have been omitted for clarity. Hydrogen atoms on Mn and Si were located from the difference map and refined isotropically. Dmpe ligands are disordered over two positions and only the dominant conformation {94.7(8)%} is shown..... 175

Figure 5.2: Disilyl hydride and silyl hydrosilane complexes reported by Tobita et al.. 175

Figure 5.3: ^1H NMR spectra (298 K, C_6D_6 , 600 MHz) for the reaction of $[(\text{dmpe})_2\text{MnH}(\text{SiH}_2\text{Ph})_2]$ ($\mathbf{20}^{\text{Ph}}$) with ethylene over time (initial, $n_{\text{C}_2\text{H}_4} \approx n_{\text{silane}}$). The x-axis corresponds to the bottom spectrum, and for clarity, each spectrum above that is shifted by 0.15 ppm to lower frequency. The inset shows the relative concentration of hydride-containing species versus time; reactant $[(\text{dmpe})_2\text{MnH}(\text{SiH}_2\text{Ph})_2]$ ($\mathbf{20}^{\text{Ph}}$; light blue *), silene hydride $[(\text{dmpe})_2\text{MnH}(\text{PhHSi}=\text{CHMe})]$ ($\mathbf{19}^{\text{Ph,H}}$; purple x), silene hydride $[(\text{dmpe})_2\text{MnH}(\text{PhEtSi}=\text{CHMe})]$ ($\mathbf{19}^{\text{Ph,Et}}$; red ■), and $[(\text{dmpe})_2\text{MnH}(\text{C}_2\text{H}_4)]$ ($\mathbf{10}$; dark blue ♦). 178

Figure 5.4: Calculated isomers (i-iv) of silene hydride complexes $[(\text{dmpe})_2\text{MnH}(\text{RR}'\text{Si}=\text{CHMe})]$ ($\mathbf{19}^{\text{Ph,H}}$: R = Ph, R' = H; $\mathbf{19}^{\text{Bu,H}}$: R = ⁿBu, R' = H; $\mathbf{19}^{\text{Ph,Et}}$: R = Ph, R' = Et; $\mathbf{19}^{\text{Bu,Et}}$: R = ⁿBu, R' = Et) featuring Si–H interligand interactions. 183

Figure 5.5: Calculated structure (ball and stick diagram) for the lowest energy isomer of silene hydride complex $[(\text{dmpe})_2\text{Mn}(\text{}^n\text{BuHSi}=\text{CHMe})]$ ($\mathbf{19}^{\text{Bu,H}}$). All hydrogen atoms have been omitted for clarity except those on Mn or the Si=C unit. The inset shows a top-down view of the Mn silene hydride core, with selected bond distances. 184

Figure 5.6: DFT calculated Gibbs free energies at 298.15 K ($\Delta G^{298.15\text{K}}$; kJ mol^{-1}) to access reactive intermediates (and the H_3SiR byproduct) from disilyl hydride complexes $[(\text{dmpe})_2\text{MnH}(\text{SiH}_2\text{R})_2]$ ($\mathbf{20}^{\text{Ph}}$: R = Ph, blue dotted lines; $\mathbf{20}^{\text{Bu}}$: R = ⁿBu, red dashed lines). Calculated intermediates (left to right) are: (i) an isomer of $[(\text{dmpe})_2\text{Mn}(\text{SiH}_2\text{R})]$ with an equatorial dmpe arrangement (*trans-17*^{Ph}: R = Ph, *trans-17*^{Bu}: R = ⁿBu), (ii) an isomer of

$[(\text{dmpe})_2\text{Mn}(\text{SiH}_2\text{R})]$ with a disphenoidal dmpe arrangement and a hydrocarbyl substituent on silicon oriented towards the vacant coordination site {rotamer 1 of *cis*-**17^R**: R = Ph (*cis*-**17^{Ph}**), ⁿBu (*cis*-**17^{Bu}**)}, (iii) an isomer of $[(\text{dmpe})_2\text{Mn}(\text{SiH}_2\text{R})]$ with a disphenoidal dmpe arrangement and an SiH substituent oriented towards the vacant coordination site {rotamer 2 of *cis*-**17^R**: R = Ph (*cis*-**17^{Ph}**); a minimum was not located for R = ⁿBu}, (iv) an isomer of $[(\text{dmpe})_2\text{MnH}(\text{=SiHR})]$ with interacting *cis*-disposed silylene and hydride ligands (*cis*-**16^{Ph,H}**: R = Ph, *cis*-**16^{Bu,H}**: R = ⁿBu), and (v) *trans*- $[(\text{dmpe})_2\text{MnH}(\text{=SiHR})]$ (*trans*-**16^{Ph,H}**: R = Ph, *trans*-**16^{Bu,H}**: R = ⁿBu). Geometry optimized cores of the phenyl analogues of reactive intermediates are depicted below each energy level, showing Mn in red, Si in pink, C in dark grey, and H in light grey, accompanied by stick bonds to the phosphorus donor atoms. 186

Figure 5.7: 1D NOESY/EXSY NMR spectrum of a solution of $[(\text{dmpe})_2\text{MnH}(\text{SiH}_2^{\text{nBu}})_2]$ (**20^{Bu}**) at 335 K with excitation at the SiH signal of **20^{Bu}**, showing chemical exchange between the SiH and MnH environments of $[(\text{dmpe})_2\text{MnH}(\text{SiH}_2^{\text{nBu}})_2]$ (**20^{Bu}**) and *trans*- $[(\text{dmpe})_2\text{MnH}(\text{=SiH}^{\text{nBu}})]$ (*trans*-**16^{Bu,H}**), and the SiH environment of free $\text{H}_3\text{Si}^{\text{nBu}}$. Positive (EXSY) peaks are indicative of chemical exchange and negative (NOESY) peaks are indicative of through-space coupling (500 MHz, C_6D_6). 190

Figure 5.8: X-ray crystal structures of (top left) *cis*- $[(\text{dmpe})_2\text{Mn}(\text{SiH}_2\text{Ph})(\text{CNxylyl})]$ (*cis*-**21a**), (top right) *cis*- $[(\text{dmpe})_2\text{Mn}(\text{SiH}_2^{\text{nBu}})(\text{CNxylyl})]$ (*cis*-**21b**), (bottom left) *cis*- $[(\text{dmpe})_2\text{Mn}(\text{SiH}_2\text{Ph})(\text{CN}^t\text{Bu})]$ (*cis*-**21c**), and (bottom right) *cis*- $[(\text{dmpe})_2\text{Mn}(\text{SiH}_2^{\text{nBu}})(\text{CN}^t\text{Bu})]$ (*cis*-**21d**), with ellipsoids drawn at 50% probability. Hydrogen atoms on Si were located from the difference map and refined isotropically, and all other hydrogen atoms have been omitted for clarity. In the case of *cis*-**21a**, the dmpe ligands are disordered over two positions, and only the dominant (95%) are shown. In the case of *cis*-**21b**, the dmpe ligands and N atom are disordered (one dmpe and the N atom over two positions and the other dmpe over three), and only the dominant conformation (66% for the dmpe ligands, and 72% for N) is shown. In the case of *cis*-**21c**, the unit cell contains two independent and essentially isostructural molecules (one of

which has shown) both of which have one dmpe ligand disordered over two positions and the other over three, and only the dominant conformation (96% and 81%) is shown. In the case of **cis-21d**, the unit cell contains two independent and essentially isostructural molecules both of which have one dmpe ligand disordered over two positions and the other over three, and one has both butyl groups disordered and only the structure without butyl disorder is shown with the dominant (62%) dmpe configuration..... 193

Figure 5.9: X-ray crystal structures of (top left) *cis*-[(dmpe)₂MnH{=SiHPh(ⁱPrNHC)}] (**cis-22a**), (top right) *cis*-[(dmpe)₂MnH{=SiHⁿBu(ⁱPrNHC)}] (**cis-22b**), (bottom left) *cis*-[(dmpe)₂MnH{=SiHPh(^McNHC)}] (**cis-22c**), and (bottom right) *trans*-[(dmpe)₂MnH{=SiHⁿBu(^McNHC)}] (**trans-22d**) with ellipsoids drawn at 50% probability. Hydrogen atoms on Mn and Si were located from the difference map and refined isotropically, and all others have been omitted for clarity. In the case of **cis-22a**, the dmpe ligands are disordered over 3 positions, the dominant (51%) of which is shown. In the case of **cis-22b**, the dmpe ligands are disordered over 2 positions, the dominant (95%) of which is shown..... 198

Figure 6.1: Selected regions of the room temperature and low temperature NMR spectra for (top) [(dmpe)₂MnH₂(SiH₂Ph)] (**18^{Ph}**) and (bottom) [(dmpe)₂MnH₂(SiH₂ⁿBu)] (**18^{Bu}**) showing, from left to right, the silicon hydride and metal hydride regions of the ¹H NMR spectra, the ³¹P{¹H} NMR spectra, and ²⁹Si{¹H} NMR spectra. Signals in the low temperature spectra are assigned to low symmetry (†; *central*) and high symmetry (*; *transHSi*) isomers..... 205

Figure 6.2: X-ray crystal structures of (a) the *central* isomer of [(dmpe)₂MnH₂(SiHPh₂)] (**central-18^{Ph2}**), and (b) the *central* isomer of [(dmpe)₂MnH₂(SiH₂Ph)] (**central-18^{Ph}**). Ellipsoids are drawn at 50% probability. Hydrogen atoms on Mn and Si were located from the difference map and refined isotropically. All other hydrogen atoms have been omitted for clarity. 209

Figure 6.3: a) X-ray crystal structure of the *transHSi* isomer of [(dmpe)₂MnH₂(SiH₂ⁿBu)] (**transHSi-18^{Bu}**) with ellipsoids drawn at 50% probability. The terminal metal hydride

atom was located from the difference map and refined isotropically. All other hydrogen atoms have been omitted for clarity. The Si atom is disordered over 4 positions (2 sets of 2 related by symmetry), the butyl group is disordered over 2 positions (related by symmetry), and the dmpe ligands are disordered over 8 positions (4 sets of 2 related by symmetry). Only one conformation is shown for clarity, with occupancies of 36.8(3)% and 16.0(1)% for silicon and the dmpe ligands, respectively. b) Overlay of the X-ray crystal structure (blue) of *transHSi*-[(dmpe)₂MnH₂(SiH₂ⁿBu)] (**transHSi-18^{Bu}**) and DFT calculated structure (red) of *transHSi*-[(dmpe)₂MnH₂(SiH₂Et)] (**transHSi-18^{Et}**), with selected H atoms in the calculated structure depicted as spheres. Methyl groups on the dmpe ligands, and most hydrogen atoms, have been omitted for clarity..... 211

Figure 6.4: Structures of experimentally unobserved *transH₂*, *lateralH₂*, and *lateralHSi* isomers of [(dmpe)₂MnH₂(SiHRR')] (**18^{Ph2}**: R = R' = Ph; **18^{Et2}**: R = R' = Et; **18^{Ph}**: R = Ph, R' = H; **18^{Et}**: R = Et, R' = H). Of these, energy minima were only located for the *transH₂* and *lateralH₂* isomers by DFT calculations. For structures of the experimentally observed *central* and *transHSi* isomers (for which energy minima were also located via DFT), see Scheme 6.2..... 212

Figure 6.5: Relative total bonding energies (kJ mol⁻¹) of the *central*, *transHSi*, *transH₂*, and *lateralH₂* isomers of [(dmpe)₂MnH₂(SiHPh₂)] (**18^{Ph2}**; blue ♦), [(dmpe)₂MnH₂(SiHEt₂)] (**18^{Et2}**; red ■), [(dmpe)₂MnH₂(SiH₂Ph)] (**18^{Ph}**; green ▲), and [(dmpe)₂MnH₂(SiH₂Et)] (**18^{Et}**; purple ●). 213

Figure 6.6: Geometry optimized structures of the isomers of [(dmpe)₂MnH₂(SiHEt₂)] (**18^{Et2}**) determined by DFT calculations. Spheres represent Mn (red), Si (pink), P (orange), and H (white), whereas carbon atoms are represented by grey vertices. *P*-methyl groups and most H atoms have been omitted for clarity. 215

Figure 6.7: Relative total bonding energies (kJ mol⁻¹) of the *central*, *transHSi*, *transH₂*, *lateralH₂*, and *lateralHSi* isomers of silyl dihydride complexes where the two dmpe ligands have been replaced with four PH₃ ligands; [(PH₃)₄MnH₂(SiHPh₂)] (**18^{Ph2:PH3}**; blue

◆, [(PH₃)₄MnH₂(SiHEt₂)] (**18**^{Et₂;PH₃}; red ■), [(PH₃)₄MnH₂(SiH₂Ph)] (**18**^{Ph;PH₃}; green ▲), and [(PH₃)₄MnH₂(SiH₂Et)] (**18**^{Bu;PH₃}; purple ●). 219

Figure 6.8: Comparisons of ¹H–¹H COSY spectra (500 MHz, *d*₈-toluene) of [(dmpe)₂MnH₂(SiHEt₂)] (**18**^{Et₂}) at 229 K showing cross-peaks (with ²⁹Si satellites) used to measure the sign and magnitude of *J*_{Si,H} via coupling between (top row) *central* isomer H_{Si} and H_{MnSi} environments, (middle row) *transHSi* isomer H_{Si} and H_{MnSi} environments, and (bottom row) *transHSi* isomer H_{MnSi} and H_{Mn} environments. From left to right within a row, the same spectral regions are shown with equivalent acquisition parameters (e.g. ns, tdl eff) in the standard ¹H–¹H dqf COSY spectrum (black), the ¹H–¹H{³¹P} dqf COSY spectrum (red), and the ²⁹Si_{edited} ¹H–¹H COSY spectrum (blue). Peak labels match those in Figure 6.6. In the structures to the left of each row, the blue arrow indicates the two ¹H environments whose active coupling gives rise to the cross-peak shown, the red arrow indicates the passive ¹H–²⁹Si coupling used as an internal reference in the measurement, and the green arrow indicates the passive ¹H–²⁹Si coupling being measured. The lines on the cross-peaks in the ²⁹Si_{edited} ¹H–¹H COSY spectra represent the vector between the ²⁹Si satellites (black line; used to determine relative sign), the magnitude of the coupling used as the internal reference (red line), and the magnitude of *J*_{Si,H} for which the sign is being determined (green line). 222

Figure 7.1: X-ray crystal structure of [(dmpe)₂Mn{κ²-SiHPh(N^{*i*}PrCHN^{*i*}Pr)}]} (**25**^{Ph,H}) with ellipsoids at 50% probability. Most hydrogen atoms have been omitted for clarity. H(1) and H(7) were located from the difference map and refined isotropically. Two independent and essentially isostructural molecules were observed in the unit cell, only one of which is shown. 230

Figure 7.2: X-ray crystal structure of *trans*-[(dmpe)₂Mn(CO)(κ¹-O₂CH)] (**26**), with ellipsoids drawn at 50% probability. H(1) was located from the difference map and refined isotropically. Most hydrogen atoms have been omitted for clarity. Two independent and essentially isostructural molecules are observed in the unit cell, one of which is shown.).. 233

Figure 8.1: *SiH* (left) and *MnH* (middle) regions of the ^1H NMR spectra (298 K, 500 or 600 MHz) for the hydrosilylation of ethylene by $\text{H}_3\text{Si}^n\text{Bu}$ using $[(\text{dmpe})_2\text{MnH}(\text{C}_2\text{H}_4)]$ (**10**) pre-catalyst (7 mol% relative to the hydrosilane) under ~ 1.7 atm of ethylene (initial, $n_{\text{C}_2\text{H}_4} \approx 40 \times n_{\text{silane}}$) in C_6D_6 and after various time intervals at 60°C . The x-axis corresponds to the bottom ^1H NMR spectrum, and for clarity, each spectrum above that is shifted by 0.3 (*SiH* region) or 0.4 (*MnH* region) ppm to lower frequency. Right: graphs showing the ratio of (top) hydrosilanes (dark blue $\blacklozenge = \text{H}_3\text{Si}^n\text{Bu}$; red $\blacksquare = \text{H}_2\text{SiEt}^n\text{Bu}$; green $\blacktriangle = \text{HSiEt}_2^n\text{Bu}$; purple $\times = \text{HSiViEt}^n\text{Bu}$; light blue $*$ = unidentified *SiH*-containing silane) and (bottom) *MnH*-containing species {dark blue $\blacklozenge = [(\text{dmpe})_2\text{MnH}(\text{C}_2\text{H}_4)]$ (**10**); light blue $*$ = $[(\text{dmpe})_2\text{MnH}(\text{SiH}_2^n\text{Bu})_2]$ (**20^{Bu}**); green $\blacktriangle = [(\text{dmpe})_2\text{MnH}_2(\text{SiHEt}^n\text{Bu})]$ (**18^{Bu,Et}**); purple $\times = [(\text{dmpe})_2\text{MnH}(^n\text{BuHSi}=\text{CHMe})]$ (**19^{Bu,H}**); red $\blacksquare = [(\text{dmpe})_2\text{MnH}(^n\text{BuEtSi}=\text{CHMe})]$ (**19^{Bu,Et}**)} in these reactions, as measured by ^1H NMR spectroscopy..... 244

Figure 8.2: Graphs showing the ratio of (top) hydrosilanes (dark blue $\blacklozenge = \text{H}_3\text{Si}^n\text{Bu}$; red $\blacksquare = \text{H}_2\text{SiEt}^n\text{Bu}$; green $\blacktriangle = \text{HSiEt}_2^n\text{Bu}$; purple $\times = \text{HSiViEt}^n\text{Bu}$; light blue $*$ = unidentified *SiH*-containing silane) and (bottom) *MnH*-containing species {dark blue $\blacklozenge = [(\text{dmpe})_2\text{MnH}(\text{C}_2\text{H}_4)]$ (**10**); red $\blacksquare = [(\text{dmpe})_2\text{MnH}(^n\text{BuEtSi}=\text{CHMe})]$ (**19^{Bu,Et}**); green $\blacktriangle = [(\text{dmpe})_2\text{MnH}_2(\text{SiHEt}^n\text{Bu})]$ (**18^{Bu,Et}**); purple $\times = [(\text{dmpe})_2\text{MnH}(^n\text{BuEtSi}=\text{CHMe})]$ (**19^{Bu,Et}**)} measured over time by ^1H NMR spectroscopy (in C_6D_6 at 56°C) for the hydrosilylation of ethylene (initial, $n_{\text{C}_2\text{H}_4} \approx n_{\text{silane}}$) by a mixture of hydrosilanes corresponding to the 13 h mark in Figure 8.1..... 245

Figure 9.1: Left: X-ray crystal structure of $[(\text{dmpe})_2\text{MnH}(\text{H}_2)]$ (**11**) with ellipsoids drawn at 50% probability. Hydrogen atoms have been omitted for clarity. H and H_2 ligands were not located from the difference map, and Mn is disordered over two positions, with only one conformation {51.5(1)%} shown. Right: geometry optimized (DFT calcd.) structure of $[(\text{dmpe})_2\text{MnH}(\text{H}_2)]$ (**11**)..... 253

Figure 9.2: Regions of the ^nH NMR spectra ($n = 1$; 500 or 600 MHz, $n = 2$; 77 MHz) in C_6D_6 at 298 K containing the *EtBMe* $_2$ (left) and metal hydride/borohydride (right)

environments for, from bottom to top, ^1H NMR for the reaction of 2 DBMes₂ with **10** after heating overnight at 60 °C, ^2H NMR for the reaction of 2 DBMes₂ with **10** after heating overnight at 60 °C, ^1H NMR for the reaction of 2 HBMes₂ with **10** after heating overnight at 60 °C, and ^1H NMR for EtBMes₂. * is from an impurity in the C₆D₆ used.
 256

Figure 9.3: Left: (boro)hydride region of the ^1H NMR spectra, and right: $^{31}\text{P}\{^1\text{H}\}$ NMR spectra, for reactions of *trans*-[(dmpe)₂MnH(C₂H₄)] (**10**) with (bottom) 9-BBN or (top) HBMes₂ before completion. * = peaks attributed to the dominant intermediate isomer, and † = peaks attributed to the minor intermediate isomer. C₆D₆, 600 MHz, 298 K. 257

Figure 9.4: Potential structures of intermediates in the reaction of *trans*-[(dmpe)₂MnH(C₂H₄)] (**10**) with 9-BBN or HBMes₂. 258

Figure 9.5: NMR spectra for borohydride complexes [(dmpe)₂Mn(μ-H)₂BR₂] (**28**: R = H, **29**: R₂ = C₈H₁₄, **30**: R = Mes) in *d*₈-toluene (**28**, **30**) or C₆D₆ (**29**) at 298 K. From left to right, the MnH₂BR₂ region of the ^1H NMR spectra (600 MHz), the $^{11}\text{B}\{^1\text{H}\}$ NMR spectra (192 MHz), and the $^{31}\text{P}\{^1\text{H}\}$ NMR spectra (243 MHz). 259

Figure 9.6: Variable temperature (174-339 K) ^1H NMR spectra of [(dmpe)₂Mn(μ-H)₂BH₂] (**28**) zoomed into the (left) terminal MnH₂BH₂ and (right) bridging MnH₂BH₂ regions in *d*₈-toluene at 500 MHz. Chemical shift scale refers to the spectrum at c. 178 K, and each additional spectrum above that is shifted to lower frequency by 0.1 ppm (MnH₂BH₂ region) or 0.4 ppm (MnH₂BH₂ region) for clarity. ... 260

Figure 9.7: X-ray crystal structures of [(dmpe)₂Mn(μ-H)₂BR₂] (**28**: R = H, **29**: R₂ = C₈H₁₄, **30**: R = Mes) with ellipsoids drawn at 50% probability. Most hydrogen atoms have been omitted for clarity. Hydrogen atoms on Mn and B were located from the difference map and refined isotropically. 261

Figure 9.8: Structurally characterized borohydride complexes of Mn(I). 264

Figure 9.9: Alkyl (left) and hydride (middle) regions of the ^1H NMR spectrum, and the full $^{31}\text{P}\{^1\text{H}\}$ NMR spectrum (right) of (top) [(dmpe)₂MnH(κ¹-dmpe)] (**32**) and (bottom)

$[(\text{dmpe})_2\text{MnH}]_2(\mu\text{-dmpe})$ (**31**) in C_6D_6 at 298 K (600 MHz). * and † represent PCH_3 environments from the κ^1 - and chelating dmpe ligands, respectively. 267

Figure 9.10: X-ray crystal structures of (left) *trans,trans*- $[(\text{dmpe})_2\text{MnH}]_2(\mu\text{-dmpe})$ (*trans,trans*-**31**) and (right) *cis,cis*- $[(\text{dmpe})_2\text{MnH}]_2(\mu\text{-dmpe})$ (*cis,cis*-**31**) with ellipsoids drawn at 50% probability. Most hydrogen atoms have been omitted for clarity. Hydrogen atoms on Mn(1) were located from the difference map and refined isotropically {the hydride on Mn(2) in the *cis,cis* isomer was not located from the difference map and is not included in the figure or CIF}. For *cis,cis*-**31**, all dmpe ligands were disordered over two positions, and only the major conformation (84.3(2)%) is shown. Due to poor quality data, bond metrics are not discussed. 270

Figure 9.11: NMR spectra (C_6D_6) of $[(\text{dmpe})_2\text{MnH}(\text{PPh}_2)]$ (**33**) at 298 K; aromatic (left) and hydride (middle) regions of the ^1H (bottom) and $^1\text{H}\{^{31}\text{P}\}$ (top) NMR spectra (600 MHz), and $^{31}\text{P}\{^1\text{H}\}$ (top right) and ^{31}P (bottom right) NMR spectra (243 MHz).. 272

Figure 9.12: NMR spectra (d_8 -toluene, 500 MHz) of $[(\text{dmpe})_2\text{MnH}(\text{PPh}_2)]$ (**33**) at 207 K; aromatic region of the ^1H (bottom left) and $^1\text{H}\{^{31}\text{P}\}$ (top left) NMR spectra, and (right) the region of the $^{31}\text{P}\text{-}^1\text{H}$ HMBC spectrum showing the cross-peak between the terminal *PH* signal and the major ^{31}P environment. 272

Figure 9.13: X-ray crystal structure of $[(\text{dmpe})_2\text{MnH}(\text{PPh}_2)]$ (**33**) with ellipsoids drawn at 50% probability. Most hydrogen atoms have been omitted for clarity. Hydrogen atoms on Mn(1) and P(1) were located from the difference map and refined isotropically. The HPPH_2 ligand was disordered over two positions, and only the major conformer {86.8(2)%} is shown. 274

Figure 9.14: X-ray crystal structure of $[(\text{dmpe})_2\text{MnH}(\text{SnPh}_3)]$ (**34**) with ellipsoids drawn at 50% probability. Most hydrogen atoms have been omitted for clarity. The hydrogen atom on Mn(1) was located from the difference map and refined isotropically. 276

Figure 11.1: $[(\text{dmpe})_2\text{Mn}(\mu\text{-H})_2\text{BC}_8\text{H}_{14}]$ (**29**) with C atom labels used in the NMR list. 356

- Figure A.1:** Calculated structures of, from left to right, two isomers of $[(\text{dmpe})_2\text{Mn}\{\kappa^2\text{-SiHPh}(\text{N}^i\text{PrCHN}^i\text{Pr})\}]$ (**25^{Ph,H}**) and two isomers of $[(\text{dmpe})_2\text{Mn}\{\kappa^2\text{-SiHEt}(\text{N}^i\text{PrCHN}^i\text{Pr})\}]$ (**25^{Et,H}**)..... 364
- Figure A.2:** Calculated structures of, from left to right, *trans*- $[(\text{dmpe})_2\text{Mn}(\text{CO})(\kappa^1\text{-O}_2\text{CH})]$ (**26**) and *trans*- $[(\text{dmpe})_2\text{MnH}(\text{CO})]$ (**27**). 364
- Figure A.3:** Superimposed calculated (red) and X-ray (blue and green) structures of, from left to right, $[(\text{dmpe})_2\text{Mn}\{\kappa^2\text{-SiHPh}(\text{N}^i\text{PrCHN}^i\text{Pr})\}]$ (**25^{Ph,H}**) and *trans*- $[(\text{dmpe})_2\text{Mn}(\text{CO})(\kappa^1\text{-O}_2\text{CH})]$ (**26**). The two X-ray structures in each figure are from two independent and essentially isostructural molecules in the unit cell. 365
- Figure A.4:** ^1H NMR spectrum of $[(\text{dmpe})_2\text{Mn}\{\kappa^2\text{-SiHPh}(\text{N}^i\text{PrCHN}^i\text{Pr})\}]$ (**25^{Ph,H}**) in C_6D_6 (600 MHz, 298 K)..... 370
- Figure A.5:** Expanded aromatic region of the ^1H NMR spectrum of $[(\text{dmpe})_2\text{Mn}\{\kappa^2\text{-SiHPh}(\text{N}^i\text{PrCHN}^i\text{Pr})\}]$ (**25^{Ph,H}**) in C_6D_6 (600 MHz, 298 K). A and B represent peaks from the dominant and minor isomers, respectively. 370
- Figure A.6:** Expanded SiH region of the ^1H NMR spectrum of $[(\text{dmpe})_2\text{Mn}\{\kappa^2\text{-SiHPh}(\text{N}^i\text{PrCHN}^i\text{Pr})\}]$ (**25^{Ph,H}**) in C_6D_6 (600 MHz, 298 K). A and B represent peaks from the dominant and minor isomers, respectively. 371
- Figure A.7:** Expanded SiH region of the $^1\text{H}\{^{31}\text{P}\}$ NMR spectrum of $[(\text{dmpe})_2\text{Mn}\{\kappa^2\text{-SiHPh}(\text{N}^i\text{PrCHN}^i\text{Pr})\}]$ (**25^{Ph,H}**) in C_6D_6 (600 MHz, 298 K). A and B represent peaks from the dominant and minor isomers, respectively. 371
- Figure A.8:** Expanded N(CHMe₂) region of the ^1H NMR spectrum of $[(\text{dmpe})_2\text{Mn}\{\kappa^2\text{-SiHPh}(\text{N}^i\text{PrCHN}^i\text{Pr})\}]$ (**25^{Ph,H}**) in C_6D_6 (600 MHz, 298 K). A and B represent peaks from the dominant and minor isomers, respectively. 372
- Figure A.9:** Expanded high frequency alkyl region of the ^1H NMR spectrum of $[(\text{dmpe})_2\text{Mn}\{\kappa^2\text{-SiHPh}(\text{N}^i\text{PrCHN}^i\text{Pr})\}]$ (**25^{Ph,H}**) in C_6D_6 (600 MHz, 298 K). A and B represent peaks from the dominant and minor isomers, respectively. 372

Figure A.10: Expanded low frequency alkyl region of the ^1H NMR spectrum of $[(\text{dmpe})_2\text{Mn}\{\kappa^2\text{-SiHPh}(\text{N}^i\text{PrCHN}^i\text{Pr})\}]$ ($25^{\text{Ph,H}}$) in C_6D_6 (600 MHz, 298 K). A and B represent peaks from the dominant and minor isomers, respectively.....	373
Figure A.11: $^{13}\text{C}\{^1\text{H}\}$ NMR spectrum of $[(\text{dmpe})_2\text{Mn}\{\kappa^2\text{-SiHPh}(\text{N}^i\text{PrCHN}^i\text{Pr})\}]$ ($25^{\text{Ph,H}}$) in C_6D_6 (151 MHz, 298 K).	373
Figure A.12: Expanded aromatic region of the $^{13}\text{C}\{^1\text{H}\}$ NMR spectrum of $[(\text{dmpe})_2\text{Mn}\{\kappa^2\text{-SiHPh}(\text{N}^i\text{PrCHN}^i\text{Pr})\}]$ ($25^{\text{Ph,H}}$) in C_6D_6 (151 MHz, 298 K). A and B represent peaks from the dominant and minor isomers, respectively.....	374
Figure A.13: Expanded N(CHMe ₂) region of the $^{13}\text{C}\{^1\text{H}\}$ NMR spectrum of $[(\text{dmpe})_2\text{Mn}\{\kappa^2\text{-SiHPh}(\text{N}^i\text{PrCHN}^i\text{Pr})\}]$ ($25^{\text{Ph,H}}$) in C_6D_6 (151 MHz, 298 K). A and B represent peaks from the dominant and minor isomers, respectively.....	374
Figure A.14: Expanded high frequency alkyl region of the $^{13}\text{C}\{^1\text{H}\}$ NMR spectrum of $[(\text{dmpe})_2\text{Mn}\{\kappa^2\text{-SiHPh}(\text{N}^i\text{PrCHN}^i\text{Pr})\}]$ ($25^{\text{Ph,H}}$) in C_6D_6 (151 MHz, 298 K). A and B represent peaks from the dominant and minor isomers, respectively.....	375
Figure A.15: Expanded low frequency alkyl region of the $^{13}\text{C}\{^1\text{H}\}$ NMR spectrum of $[(\text{dmpe})_2\text{Mn}\{\kappa^2\text{-SiHPh}(\text{N}^i\text{PrCHN}^i\text{Pr})\}]$ ($25^{\text{Ph,H}}$) in C_6D_6 (151 MHz, 298 K). A and B represent peaks from the dominant and minor isomers, respectively.....	375
Figure A.16: $^{29}\text{Si}\{^1\text{H}\}$ NMR spectrum of $[(\text{dmpe})_2\text{Mn}\{\kappa^2\text{-SiHPh}(\text{N}^i\text{PrCHN}^i\text{Pr})\}]$ ($25^{\text{Ph,H}}$) in C_6D_6 (119 MHz, 298 K). A and B represent peaks from the dominant and minor isomers, respectively.....	376
Figure A.17: $^{29}\text{Si}\text{-}^1\text{H}$ HMBC NMR spectrum of $[(\text{dmpe})_2\text{Mn}\{\kappa^2\text{-SiHPh}(\text{N}^i\text{PrCHN}^i\text{Pr})\}]$ ($25^{\text{Ph,H}}$) in C_6D_6 (119 MHz, 298 K). A and B represent peaks from the dominant and minor isomers, respectively.	376
Figure A.18: Expanded aromatic region of the $^{29}\text{Si}\text{-}^1\text{H}$ HMBC NMR spectrum of $[(\text{dmpe})_2\text{Mn}\{\kappa^2\text{-SiHPh}(\text{N}^i\text{PrCHN}^i\text{Pr})\}]$ ($25^{\text{Ph,H}}$) in C_6D_6 (119 MHz, 298 K). A and B represent peaks from the dominant and minor isomers, respectively.....	377

Figure A.19: $^{31}\text{P}\{^1\text{H}\}$ NMR spectrum of $[(\text{dmpe})_2\text{Mn}\{\kappa^2\text{-SiHPh}(\text{N}^i\text{PrCHN}^i\text{Pr})\}]$ ($25^{\text{Ph,H}}$) in C_6D_6 (243 MHz, 298 K). A and B represent peaks from the dominant and minor isomers, respectively.....	377
Figure A.20: ^1H NMR spectrum of $[(\text{dmpe})_2\text{Mn}\{\kappa^2\text{-SiH}^n\text{Bu}(\text{N}^i\text{PrCHN}^i\text{Pr})\}]$ ($25^{\text{Bu,H}}$) in C_6D_6 (600 MHz, 298 K).....	378
Figure A.21: Expanded NC(H)N region of the ^1H NMR spectrum of $[(\text{dmpe})_2\text{Mn}\{\kappa^2\text{-SiH}^n\text{Bu}(\text{N}^i\text{PrCHN}^i\text{Pr})\}]$ ($25^{\text{Bu,H}}$) in C_6D_6 (600 MHz, 298 K). A and B represent peaks from the dominant and minor isomers, respectively.....	378
Figure A.22: Expanded SiH region of the ^1H NMR spectrum of $[(\text{dmpe})_2\text{Mn}\{\kappa^2\text{-SiH}^n\text{Bu}(\text{N}^i\text{PrCHN}^i\text{Pr})\}]$ ($25^{\text{Bu,H}}$) in C_6D_6 (600 MHz, 298 K). A and B represent peaks from the dominant and minor isomers, respectively.....	379
Figure A.23: Expanded SiH region of the $^1\text{H}\{^{31}\text{P}\}$ NMR spectrum of $[(\text{dmpe})_2\text{Mn}\{\kappa^2\text{-SiH}^n\text{Bu}(\text{N}^i\text{PrCHN}^i\text{Pr})\}]$ ($25^{\text{Bu,H}}$) in C_6D_6 (600 MHz, 298 K). A and B represent peaks from the dominant and minor isomers, respectively.....	379
Figure A.24: Expanded N(CHMe ₂) region of the ^1H NMR spectrum of $[(\text{dmpe})_2\text{Mn}\{\kappa^2\text{-SiH}^n\text{Bu}(\text{N}^i\text{PrCHN}^i\text{Pr})\}]$ ($25^{\text{Bu,H}}$) in C_6D_6 (600 MHz, 298 K). A and B represent peaks from the dominant and minor isomers, respectively.....	380
Figure A.25: Expanded high frequency alkyl region of the ^1H NMR spectrum of $[(\text{dmpe})_2\text{Mn}\{\kappa^2\text{-SiH}^n\text{Bu}(\text{N}^i\text{PrCHN}^i\text{Pr})\}]$ ($25^{\text{Bu,H}}$) in C_6D_6 (600 MHz, 298 K). A and B represent peaks from the dominant and minor isomers, respectively.....	380
Figure A.26: Expanded low frequency region of the ^1H NMR spectrum of $[(\text{dmpe})_2\text{Mn}\{\kappa^2\text{-SiH}^n\text{Bu}(\text{N}^i\text{PrCHN}^i\text{Pr})\}]$ ($25^{\text{Bu,H}}$) in C_6D_6 (600 MHz, 298 K). A and B represent peaks from the dominant and minor isomers, respectively.....	381
Figure A.27: $^{13}\text{C}\{^1\text{H}\}$ NMR spectrum of $[(\text{dmpe})_2\text{Mn}\{\kappa^2\text{-SiH}^n\text{Bu}(\text{N}^i\text{PrCHN}^i\text{Pr})\}]$ ($25^{\text{Bu,H}}$) in C_6D_6 (151 MHz, 298 K).....	381

- Figure A.28:** Expanded high frequency alkyl region of the $^{13}\text{C}\{^1\text{H}\}$ NMR spectrum of $[(\text{dmpe})_2\text{Mn}\{\kappa^2\text{-SiH}^n\text{Bu}(\text{N}^i\text{PrCHN}^i\text{Pr})\}]$ ($25^{\text{Bu,H}}$) in C_6D_6 (151 MHz, 298 K). A and B represent peaks from the dominant and minor isomers, respectively. 382
- Figure A.29:** Expanded middle frequency alkyl region of the $^{13}\text{C}\{^1\text{H}\}$ NMR spectrum of $[(\text{dmpe})_2\text{Mn}\{\kappa^2\text{-SiH}^n\text{Bu}(\text{N}^i\text{PrCHN}^i\text{Pr})\}]$ ($25^{\text{Bu,H}}$) in C_6D_6 (151 MHz, 298 K). A and B represent peaks from the dominant and minor isomers, respectively. 382
- Figure A.30:** Expanded low frequency alkyl region of the $^{13}\text{C}\{^1\text{H}\}$ NMR spectrum of $[(\text{dmpe})_2\text{Mn}\{\kappa^2\text{-SiH}^n\text{Bu}(\text{N}^i\text{PrCHN}^i\text{Pr})\}]$ ($25^{\text{Bu,H}}$) in C_6D_6 (151 MHz, 298 K). A and B represent peaks from the dominant and minor isomers, respectively. 383
- Figure A.31:** $^{29}\text{Si}\{^1\text{H}\}$ NMR spectrum of $[(\text{dmpe})_2\text{Mn}\{\kappa^2\text{-SiH}^n\text{Bu}(\text{N}^i\text{PrCHN}^i\text{Pr})\}]$ ($25^{\text{Bu,H}}$) in C_6D_6 (119 MHz, 298 K). 383
- Figure A.32:** $^{29}\text{Si}\text{-}^1\text{H}$ HSQC NMR spectrum of $[(\text{dmpe})_2\text{Mn}\{\kappa^2\text{-SiH}^n\text{Bu}(\text{N}^i\text{PrCHN}^i\text{Pr})\}]$ ($25^{\text{Bu,H}}$) in C_6D_6 (119 MHz, 298 K). 384
- Figure A.33:** Expanded SiH region of the $^{29}\text{Si}\text{-}^1\text{H}$ HSQC NMR spectrum of $[(\text{dmpe})_2\text{Mn}\{\kappa^2\text{-SiH}^n\text{Bu}(\text{N}^i\text{PrCHN}^i\text{Pr})\}]$ ($25^{\text{Bu,H}}$) in C_6D_6 (119 MHz, 298 K). A and B represent peaks from the dominant and minor isomers, respectively. 384
- Figure A.34:** $^{31}\text{P}\{^1\text{H}\}$ NMR spectrum of $[(\text{dmpe})_2\text{Mn}\{\kappa^2\text{-SiH}^n\text{Bu}(\text{N}^i\text{PrCHN}^i\text{Pr})\}]$ ($25^{\text{Bu,H}}$) in C_6D_6 (243 MHz, 298 K). A and B represent peaks from the dominant and minor isomers, respectively. 385
- Figure A.35:** ^1H NMR spectrum of *trans*- $[(\text{dmpe})_2\text{Mn}(\text{CO})(\kappa^1\text{-O}_2\text{CH})]$ (**26**) in C_6D_6 (600 MHz, 298 K). 385
- Figure A.36:** Expanded formyl region of the ^1H NMR spectrum of *trans*- $[(\text{dmpe})_2\text{Mn}(\text{CO})(\kappa^1\text{-O}_2\text{CH})]$ (**26**) in C_6D_6 (600 MHz, 298 K). 386
- Figure A.37:** Expanded alkyl region of the ^1H NMR spectrum of *trans*- $[(\text{dmpe})_2\text{Mn}(\text{CO})(\kappa^1\text{-O}_2\text{CH})]$ (**26**) in C_6D_6 (600 MHz, 298 K). 386
- Figure A.38:** $^{13}\text{C}\{^1\text{H}\}$ NMR spectrum of *trans*- $[(\text{dmpe})_2\text{Mn}(\text{CO})(\kappa^1\text{-O}_2\text{CH})]$ (**26**) in C_6D_6 (151 MHz, 298 K). 387

Figure A.39: Expanded formyl region of the $^{13}\text{C}\{^1\text{H}\}$ NMR spectrum of <i>trans</i> - $[(\text{dmpe})_2\text{Mn}(\text{CO})(\kappa^1\text{-O}_2\text{CH})]$ (26) in C_6D_6 (151 MHz, 298 K).	387
Figure A.40: Expanded alkyl region of the $^{13}\text{C}\{^1\text{H}\}$ NMR spectrum of <i>trans</i> - $[(\text{dmpe})_2\text{Mn}(\text{CO})(\kappa^1\text{-O}_2\text{CH})]$ (26) in C_6D_6 (151 MHz, 298 K).	388
Figure A.41: $^{31}\text{P}\{^1\text{H}\}$ NMR spectrum of <i>trans</i> - $[(\text{dmpe})_2\text{Mn}(\text{CO})(\kappa^1\text{-O}_2\text{CH})]$ (26) in C_6D_6 (243 MHz, 298 K).	388
Figure B.1: NMR spectra {298 K, C_6D_6 , 600 (^1H), 77 (^2H), 151 ($^{13}\text{C}\{^1\text{H}\}$), or 175 ($^{13}\text{C}\{^1\text{H}\}$ -uDEFT and DEPTq) MHz} for reaction mixtures from catalytic hydrosilylation of H_2SiEt_2 by ethylene or <i>d</i> ₄ -ethylene using $[(\text{dmpe})_2\text{MnH}(\text{C}_2\text{H}_4)]$ (10) as a precatalyst (7 mol% catalyst load, 4 days at 60 °C, $n_{\text{ethylene}} \approx 40 \times n_{\text{H}_2\text{SiEt}_2}$, initial pressure of C_2H_4 and C_2D_4 are c. 1.7 and 1.0 atm, respectively). Left: various regions of, from bottom to top, the ^2H , $^2\text{H}\{^1\text{H}\}$, and ^1H NMR spectra of the reaction involving <i>d</i> ₄ -ethylene, and the ^1H NMR spectrum of the reaction involving protonated ethylene (unknown hydrosilane byproduct not shown). Right: the ethyl region of, from bottom to top, the uDEFT $^{13}\text{C}\{^1\text{H}\}$, DEPTq $^{13}\text{C}\{^1\text{H}\}$, and $^{13}\text{C}\{^1\text{H}\}$ NMR spectra of the reaction involving <i>d</i> ₄ -ethylene, and the $^{13}\text{C}\{^1\text{H}\}$ NMR spectrum of the reaction involving protonated ethylene. * represents peaks tentatively assigned to the ethyl environments of HSiViEt_2 . In all cases (except the $^{13}\text{C}\{^1\text{H}\}$ NMR spectrum of the reaction involving protonated ethylene), NMR spectra were collected after vacuum distillation to remove manganese-containing species. Top: hydrosilane product distribution from hydrosilylation of ethylene (1 st row) or <i>d</i> ₄ -ethylene (2 nd row) by H_2SiEt_2	389
Figure B.2: NMR spectra {298 K, C_6D_6 , 600 (^1H), 77 (^2H), 151 ($^{13}\text{C}\{^1\text{H}\}$), or 175 ($^{13}\text{C}\{^1\text{H}\}$ -uDEFT and DEPTq) MHz} for reaction mixtures from catalytic hydrosilylation of $\text{H}_3\text{Si}^n\text{Bu}$ by ethylene or <i>d</i> ₄ -ethylene using $[(\text{dmpe})_2\text{MnH}(\text{C}_2\text{H}_4)]$ (10) as a precatalyst (7 mol% catalyst load, 4 days at 60 °C, $n_{\text{ethylene}} \approx 40 \times n_{\text{H}_3\text{Si}^n\text{Bu}}$, initial pressure of C_2H_4 and C_2D_4 are c. 1.7 and 1.0 atm, respectively). Left: various regions of, from bottom to top, the ^2H , $^2\text{H}\{^1\text{H}\}$, and ^1H NMR spectra of the reaction involving <i>d</i> ₄ -ethylene, and ^1H NMR spectrum of the reaction involving ethylene (unknown hydrosilane byproduct not	

shown). Right: the ethyl region of, from bottom to top, the uDEFT $^{13}\text{C}\{^1\text{H}\}$, DEPTq $^{13}\text{C}\{^1\text{H}\}$, and $^{13}\text{C}\{^1\text{H}\}$ NMR spectra of the reaction involving d_4 -ethylene, and the $^{13}\text{C}\{^1\text{H}\}$ NMR spectrum of the reaction involving protonated ethylene. * indicate peaks tentatively assigned to the ethyl environments of $\text{HSiViEt}^n\text{Bu}$. NMR spectra were collected after Vacuum distillation removed manganese-containing species. Top: hydrosilane product distribution from hydrosilylation of ethylene (1st row) or d_4 -ethylene (2nd row) by $\text{H}_3\text{Si}^n\text{Bu}$. The $^{13}\text{C}\{^1\text{H}\}$ NMR spectrum of the reaction involving protonated ethylene was from a reaction mixture allowed to react for 8 days. 391

List of Schemes

Scheme 1.1: Potential ALD processes for elemental manganese deposition proposed by the (a) Winter and (b) Zaera groups, based on preliminary results ($Mn_{(s)}$ was not observed in either case).	18
Scheme 1.2: Decomposition pathways via β -hydride elimination from homoleptic transition metal alkyl complexes. For clarity, the simplest β -hydride-containing ligand (Et) is used in place of a generic alkyl ligand.	20
Scheme 1.3: Synthetic routes for neutral dialkylmanganese(II) complexes.	22
Scheme 1.4: Selected synthetic pathways (not involving H_2 as a reagent) for the preparation of Mn(I) hydride carbonyl complexes.	35
Scheme 1.5: Synthesis of CO-containing manganese(I) hydride complexes using H_2	36
Scheme 1.6: Acid/base reactivity of manganese hydride complexes.	41
Scheme 1.7: Insertion reactivity of manganese hydride complexes.	42
Scheme 1.8: Halogenation of manganese hydride complexes. X = halogen.	42
Scheme 1.9: Bimolecular reductive elimination reactivity of manganese hydride complexes. R = alkyl or acyl.	43
Scheme 1.10: Selected synthetic routes to hydride-free manganese(I) silyl complexes.	49
Scheme 1.11: Synthetic routes to silyl hydride/hydrosilane complexes. For clarity, all these complexes are drawn as nonclassical hydrosilane complexes.	62
Scheme 1.12: Equilibrium between silylene hydride and silyl complexes.	69
Scheme 1.13: Synthetic routes used to prepare isolated silene complexes. In some cases where the silene was generated by a mechanism that resulted in a hydride ligand, the silene complex underwent subsequent H–H or C–H bond-forming reductive elimination involving the hydride and another co-ligand to generate a hydride-free silene complex,	

and this subsequent reactivity is not shown in the scheme. For generality, charge is not included (both neutral and cationic species have been observed).	94
Scheme 1.14: Equilibrium between $[\text{Cp}^*(\text{Me}_3\text{P})\text{IrH}(\text{Me}_2\text{Si}=\text{CH}_2)]^+$ and $[\text{Cp}^*(\text{Me}_3\text{P})\text{IrMe}\{\text{SiMe}_2(\text{OEt}_2)\}]^+$, and trapping experiments.	97
Scheme 2.1: Possible pathways for $\text{Mn}_{(s)}$ deposition using dialkylmanganese(II) complexes in combination with H_2 or ZnEt_2 co-reactants.	108
Scheme 2.2: Synthesis of complexes 1-8	110
Scheme 2.3: Reactions of 1-8 with H_2 in benzene or toluene.	129
Scheme 2.4: Reactions of dmpe complexes 3-6 with ZnEt_2 ($\text{R} = \text{CH}_2\text{EMe}_3$; $\text{X} = \text{Et}$ or R ; $\text{E} = \text{C}$ or Si) in benzene.	131
Scheme 3.1: Reported synthetic routes to $[(\text{dmpe})_2\text{MnH}(\text{C}_2\text{H}_4)]$ (10).....	134
Scheme 3.2: Potential pathways (A and B) for the reaction of <i>trans</i> - $[(\text{dmpe})_2\text{MnH}(\text{C}_2\text{H}_4)]$ (10) with various reagents. Only one isomer of all complexes except 10 is shown. $\text{E} = \text{SiR}_3, \text{SnR}_3, \text{BR}_2, \text{H}$	138
Scheme 3.3: Reactions of <i>trans</i> - $[(\text{dmpe})_2\text{MnH}(\text{C}_2\text{H}_4)]$ (10) with isonitriles to afford ethyl complexes $[(\text{dmpe})_2\text{MnEt}(\text{CNR})]$ (14a : $\text{R} = \textit{i}-Bu, 14b: \text{R} = \textit{o}-xylyl) and further insertion products, including [(\text{dmpe})\text{Mn}(\text{CNXyl})_3\{\text{C}(=\text{NXyl})\text{CEt}(=\text{NXyl})\}] (15).$	149
Scheme 4.1: Reactions of $[(\text{dmpe})_2\text{MnH}(\text{C}_2\text{H}_4)]$ (10) with H_2SiR_2 to form (when $\text{R} = \text{Et}$) <i>trans</i> - $[(\text{dmpe})_2\text{MnH}(=\text{SiEt}_2)]$ (<i>trans</i> - 16^{Et2}), or (when $\text{R} = \text{Ph}$) a mixture of <i>cis</i> - and <i>trans</i> - $[(\text{dmpe})_2\text{MnH}(=\text{SiPh}_2)]$ (<i>cis</i> - 16^{Ph2} and <i>trans</i> - 16^{Ph2}) along with $[(\text{dmpe})_2\text{MnH}_2(\text{SiHPh}_2)]$ (18^{Ph2}). Subsequent reactions of the silylene hydride complexes (<i>trans</i> - 16^{Et2} or <i>cis</i> - and <i>trans</i> - 16^{Ph2}) with H_2 to form $[(\text{dmpe})_2\text{MnH}_2(\text{SiHR}_2)]$ (18^{Et2} : $\text{R} = \text{Et}$, 18^{Ph2} : $\text{R} = \text{Ph}$) are also included. Only one isomer of 18^{R2} is shown.	157
Scheme 4.2: Reaction of silylene hydride complexes $[(\text{dmpe})_2\text{MnH}(=\text{SiR}_2)]$ $\{\text{R} = \text{Et}$ (16^{Et2}) or Ph (16^{Ph2}) $\}$ with ethylene to form $[(\text{dmpe})_2\text{MnH}(\text{R}_2\text{Si}=\text{CHMe})]$ $\{\text{R} = \text{Et}$ (19^{Et2}) or Ph (19^{Ph2}) $\}$	165

Scheme 4.3: Two potential pathways for the formation of [(dmpe)₂MnH(R₂Si=CHMe)] (**19**^{Et2}: R = Et, **19**^{Ph2}: R = Ph) via reaction of [(dmpe)₂MnH(=SiR₂)] (**16**^{Et2}: R = Et, **16**^{Ph2}: R = Ph) with ethylene. Key: [Mn] = (dmpe)₂Mn, [MnH] = (dmpe)₂MnH. 168

Scheme 5.1: Reactions of [(dmpe)₂MnH(C₂H₄)] (**10**) with R₂SiH₂ (R = Et, Ph) to afford silylene hydride compounds **16**^{R2} and silyl dihydride complex **18**^{Ph2}, and subsequent reactivity with ethylene to afford silene hydride complexes **19**^{R2}. *cis*-**10**, **13**, **17**^{R2}, and **12** are hypothesized intermediates, for which DFT calculations have located energy minima. Only one isomer is shown for all complexes, except **10** and **16**^{R2}. 171

Scheme 5.2: Reactions of [(dmpe)₂MnH(C₂H₄)] (**10**) with primary hydrosilanes to afford disilyl hydride complexes [(dmpe)₂MnH(SiH₂R)₂] (**20**^{Ph}: R = Ph, **20**^{Bu}: R = ⁿBu). Only one isomer of all complexes is shown. 173

Scheme 5.3: Reactions of disilyl hydride complexes [(dmpe)₂MnH(SiH₂R)₂] (**20**^{Ph}: R = Ph, **20**^{Bu}: R = ⁿBu) with one, two, or three equivalents of ethylene to afford SiH-containing silene hydride complexes [(dmpe)₂MnH(RHSi=CHMe)] (**19**^{Ph,H}: R = Ph, **19**^{Bu,H}: R = ⁿBu), silene hydride complexes with two hydrocarbyl groups on Si [(dmpe)₂MnH(REtSi=CHMe)] (**19**^{Ph,Et}: R = Ph, **19**^{Bu,Et}: R = ⁿBu), and ethylene hydride complex [(dmpe)₂MnH(C₂H₄)] (**10**), respectively. Only one isomer is shown for each silene hydride complex. 177

Scheme 5.4: Solution decomposition of [(dmpe)₂MnH(ⁿBuHSi=CHMe)] (**19**^{Bu,H}) to form silylene complex *trans*-[(dmpe)₂MnH(=SiEtⁿBu)] (*trans*-**16**^{Bu,Et}) as the major product. 181

Scheme 5.5: Trapping of putative silyl (**17**^R) and silylene hydride (**16**^{R,H}) intermediates: synthesis of silyl isonitrile complexes [(dmpe)₂Mn(SiH₂R)(CNR')] (**21a**: R = Ph, R' = *o*-xylyl; **21b**: R = ⁿBu, R' = *o*-xylyl; **21c**: R = Ph, R' = ^tBu; **21d**: R = ⁿBu, R' = ^tBu) and NHC-stabilized silylene hydride complexes [(dmpe)₂MnH{=SiHR(NHC)}] (**22a**: NHC = ^{iPr}NHC, R = Ph; **22b**: NHC = ^{iPr}NHC, R = ⁿBu; **22c**: NHC = ^{Me}NHC, R = Ph; **22d**: NHC = ^{Me}NHC, R = ⁿBu. 191

Scheme 5.6: Proposed pathways for reactions of disilyl hydride complexes $[(\text{dmpe})_2\text{MnH}(\text{SiH}_2\text{R})_2]$ ($\mathbf{20}^{\text{Ph}}$: R = Ph, $\mathbf{20}^{\text{Bu}}$: R = ^nBu) with ethylene to form silene hydride complexes $[(\text{dmpe})_2\text{MnH}(\text{RHSi}=\text{CHMe})]$ ($\mathbf{19}^{\text{Ph,H}}$; R = Ph, $\mathbf{19}^{\text{Bu,H}}$: R = ^nBu). $[\text{Mn}] = \text{Mn}(\text{dmpe})_2$. Only one isomer of $\mathbf{16}^{\text{R,H}}$ is shown. Boxes indicate complexes which have been isolated or spectroscopically observed. 200

Scheme 5.7: Initial steps in the pathway proposed for reactions of silene hydride complexes $[(\text{dmpe})_2\text{MnH}(\text{RHSi}=\text{CHMe})]$ ($\mathbf{19}^{\text{Ph,H}}$; R = Ph, $\mathbf{19}^{\text{Bu,H}}$: R = ^nBu) with ethylene to afford $[(\text{dmpe})_2\text{MnH}(\text{REtSi}=\text{CHMe})]$ ($\mathbf{19}^{\text{Ph,Et}}$; R = Ph, $\mathbf{19}^{\text{Bu,Et}}$: R = ^nBu). $[\text{Mn}] = \text{Mn}(\text{dmpe})_2$. Intermediates $\mathbf{A}^{\text{R,Et}}$ and $\mathbf{B}^{\text{R,Et}}$ are analogous to intermediates \mathbf{A}^{R} and \mathbf{B}^{R} in Scheme 5.6, but with an ethyl group in place of one hydrogen atom on silicon. Only one isomer of $\mathbf{16}^{\text{R,Et}}$ is shown. Boxes indicate complexes which have been isolated or spectroscopically observed. 201

Scheme 6.1: Syntheses of $[(\text{dmpe})_2\text{MnH}_2(\text{SiHR}_2)]$ {R = Ph ($\mathbf{18}^{\text{Ph}_2}$), R = Et ($\mathbf{18}^{\text{Et}_2}$)} and $[(\text{dmpe})_2\text{MnH}_2(\text{SiH}_2\text{R})]$ {R = Ph ($\mathbf{18}^{\text{Ph}}$), R = ^nBu ($\mathbf{18}^{\text{Bu}}$)} 204

Scheme 6.2: Isomers of $[(\text{dmpe})_2\text{MnH}_2(\text{SiHR}_2)]$ {R = Ph ($\mathbf{18}^{\text{Ph}_2}$), R = Et ($\mathbf{18}^{\text{Et}_2}$)} and $[(\text{dmpe})_2\text{MnH}_2(\text{SiH}_2\text{R})]$ {R = Ph ($\mathbf{18}^{\text{Ph}}$), R = ^nBu ($\mathbf{18}^{\text{Bu}}$)} observed in solution. 206

Scheme 7.1: Reactions of disilyl hydride complexes $[(\text{dmpe})_2\text{MnH}(\text{SiH}_2\text{R})_2]$ ($\mathbf{20}^{\text{Ph}}$: R = Ph, $\mathbf{20}^{\text{Bu}}$: R = ^nBu) with diisopropylcarbodiimide to afford the amidinylsilyl complexes $[(\text{dmpe})_2\text{Mn}\{\kappa^2\text{-SiHR}(\text{N}^i\text{PrCHN}^i\text{Pr})\}]$ ($\mathbf{25}^{\text{Ph,H}}$: R = Ph, $\mathbf{25}^{\text{Bu,H}}$: R = ^nBu). Only one diastereomer of $\mathbf{25}^{\text{R,H}}$ is shown, as two canonical structures..... 228

Scheme 7.2: Reaction of disilyl hydride complexes $[(\text{dmpe})_2\text{MnH}(\text{SiH}_2\text{R})_2]$ ($\mathbf{20}^{\text{Ph}}$: R = Ph, $\mathbf{20}^{\text{Bu}}$: R = ^nBu) with carbon dioxide to afford the formate complex *trans*- $[(\text{dmpe})_2\text{Mn}(\text{CO})(\kappa^1\text{-O}_2\text{CH})]$ ($\mathbf{26}$). 231

Scheme 7.3: Potential pathways for the reactions of $[(\text{dmpe})_2\text{MnH}(\text{SiH}_2\text{R})_2]$ ($\mathbf{20}^{\text{Ph}}$: R = Ph, $\mathbf{20}^{\text{Bu}}$: R = ^nBu) with $\text{E}=\text{C}=\text{E}$ (E = N^iPr , O). $[\text{Mn}] = \text{Mn}(\text{dmpe})_2$. For some compounds, more than one isomer is likely to be accessible (e.g. *cis* vs *trans*, the presence/absence of an interaction between silicon and an adjacent hydride ligand, or coordination/lack of

coordination of lone pairs on E to the metal center), but for clarity, only one isomer is shown. Solid boxes indicate known complexes and intermediates.	235
Scheme 8.1: Proposed catalytic cycle for ethylene hydrosilylation by primary and secondary hydrosilanes. [Mn] = Mn(dmpe) ₂ . Only one isomer is shown for complexes 16 and 18 . Boxes represent complexes observed by NMR spectroscopy during catalysis.	247
Scheme 9.1: Synthesis of [(dmpe) ₂ MnH(H ₂)] (11).....	252
Scheme 9.2: Synthesis of borohydride Mn(I) complexes [(dmpe) ₂ Mn(μ-H) ₂ BR ₂] (28 : R = H, 29 : R ₂ = C ₈ H ₁₄ , 30 : R = Mes).	254
Scheme 9.3: Reaction of <i>trans</i> -[(dmpe) ₂ MnH(C ₂ H ₄)] (10) with DBMes ₂ . Only one potential isomer of 13 and <i>d</i> - 12 is shown.	256
Scheme 9.4: Potential mechanism for deuterium incorporation into [(dmpe) ₂ Mn(μ-H) ₂ BH ₂] (28) by D ₂ . Only one isomer of 12_d_n is shown.	265
Scheme 9.5: Synthesis {under inert atmosphere (red reaction arrow) or an atmosphere of H ₂ (blue reaction arrows)} and purification of [{(dmpe) ₂ MnH} ₂ (μ-dmpe)] (31) and [(dmpe) ₂ MnH(κ ¹ -dmpe)] (32) from <i>trans</i> -[(dmpe) ₂ MnH(C ₂ H ₄)] (10). Only one isomer of 31 and 32 is shown.....	266
Scheme 9.6: Synthesis of [(dmpe) ₂ MnH(PHPh ₂)] (33).	271
Scheme 9.7: Reaction of <i>trans</i> -[(dmpe) ₂ MnH(C ₂ H ₄)] (10) with HSnPh ₃	275
Scheme 10.1: Potential deposition of Mn-containing films using proton-source co-reactants. For example, E = O, S, N, or F, and x = 1 or 0.5.....	280
Scheme 10.2: Potential CVD reactivity to obtain thin films of elemental manganese from manganese(I) hydride precursors. L represents a neutral, volatile ligand (e.g. HBR ₂ , PR ₃). Only one isomer of all complexes are shown.	281
Scheme 10.3: Potential routes (a-c) to the synthesis of derivatives of [(dmpe) ₂ MnH(C ₂ H ₄)] (10) with different alkene ligands. Only one isomer of each complex is shown, R≠H.	283

Scheme 10.4: Potential routes (a-b) to the synthesis of [(dmpe) ₂ MnH(alkyne)] complexes. For route b, R' = H.	284
Scheme 10.5: Potential routes to isolation of manganese complexes bearing electronically unstabilized terminal silylene ligands with a terminal SiH substituent; [(dmpe) ₂ MnH(=SiHR)] (16^{R,H}). Only one isomer is shown for all complexes.....	286
Scheme 10.6: Potential routes for accessing a silene hydride complex or an NHC-stabilized silylene hydride complex with two terminal SiH substituents. Only one isomer is shown for all complexes.....	289
Scheme 10.7: Potential catalytic cycle for hydrosilylation of CO ₂ using <i>trans</i> -[(dmpe) ₂ Mn(CO)(κ ¹ -O ₂ CH)] (26). For clarity, a tertiary hydrosilane is shown as feedstock, though this chemistry could also potentially apply to other hydrosilanes.....	292

List of Tables

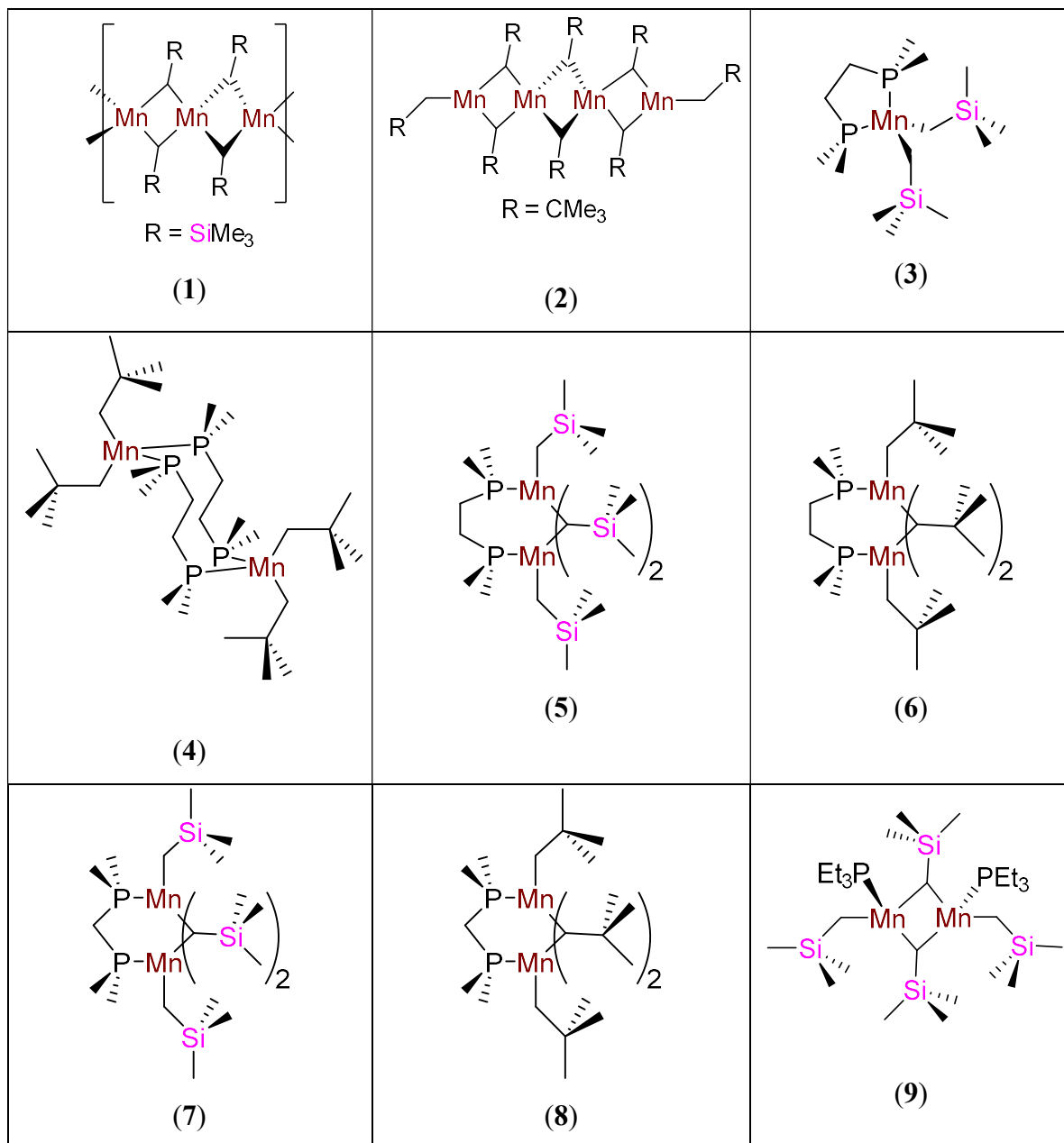
Table 1.1: Selected Mn–Mn and Mn–C distances (Å) for neutral dialkylmanganese(II) complexes obtained by X-ray crystallography (br = bridging, term = terminal). Letters are those in Figure 1.8.....	23
Table 1.2: Selected distances (Å) for adducts of $\text{Mn}(\text{CH}_2\text{SiMe}_3)_2$ obtained by X-ray crystallography. L indicates the neutral ligand. n_L and n_{Mn} are the number of neutral ligands and metal centres in one molecule. Letters correspond to structures in Figure 1.9.	28
Table 1.3: Selected distances (Å) for adducts of $\text{Mn}(\text{CH}_2\text{CMe}_3)_2$ obtained by X-ray crystallography. L indicates the neutral ligand. n_L and n_{Mn} are the number of neutral ligands and metal centres in one molecule. Letters correspond to structures in Figure 1.9.	29
Table 1.4: ^{29}Si NMR chemical shifts and solid-state Mn–Si distances for hydride-free Mn(I) silyl complexes for which X-ray crystal structures have been reported. Reference column refers to the report where a crystal structure was obtained (not where the complex was first synthesized). Letters correspond to those in Figure 1.16.....	50
Table 1.5: Selected NMR data for silyl hydride/hydrosilane complexes of Mn. References refer to the first reported synthesis, and when NMR data was obtained following the initial report, references for that are in the pertinent box. For clarity, all chemical formulae are given as the classical silyl hydride isomer. If no sign is explicitly given, $J_{\text{Si,H}}$ values are magnitudes. NMR values are from the first report (in some cases, later publications included slightly different data, often due to use of an alternative solvent). Empty boxes indicate that no data was reported.....	57
Table 1.6: Selected structural parameters determined by X-ray (or, if indicated, neutron) crystallography for silyl hydride/hydrosilane complexes of Mn. For clarity, all chemical formulae are given as the classical silyl hydride isomer. Letters correspond to Figure 1.20, and the references refer to the report of the structure (not the synthesis).....	61

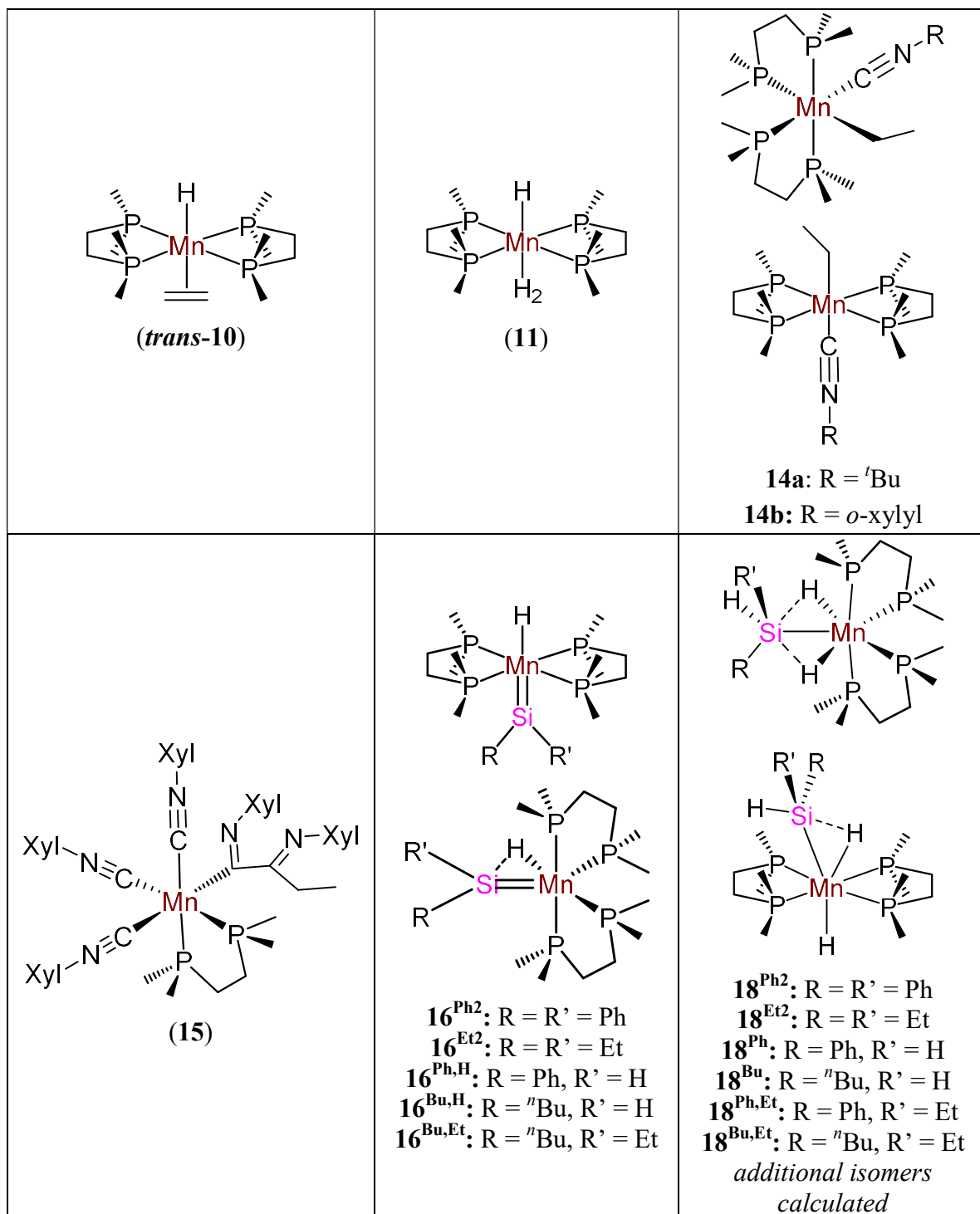
Table 1.7: M–Si distances for base-free, non-electronically stabilized silylene complexes (Å), as determined by X-ray or neutron crystal structures. Only metals for which solid state structures of such complexes have been obtained are included. Values are accurate as of 2016, and given to two decimal places.	67
Table 1.8: Structural and spectroscopic data for silylene hydride complexes for which solid state structures have been reported and the metal hydride was located from the difference map. Unless otherwise noted, values were obtained by X-ray diffraction.	70
Table 1.9: Structurally characterized NHC-stabilized silylene complexes. NHC names relate to those in Figure 1.26.....	75
Table 1.10: Structural and spectroscopic parameters for $\eta^3\text{-H}_2\text{SiR}_2$ complexes. Complexes are identified by the letter in Figure 1.35. H_{br} is a hydride interacting with Si and the metal.	86
Table 1.11: Isolated silene complexes. n.o. = not observed, X = any non-metal.	95
Table 1.12: Spectroscopically observed non-isolated silene complexes. n.o. indicates not observed. Complexes reported as metallasilacyclopropane complexes are shown as silene complexes for consistency.	98
Table 2.1: Room temperature solution and solid state magnetic data for 2-8 . $\chi_{\text{M(corr)}}$ = corrected molar magnetic susceptibility; μ_{B} = effective magnetic moment; θ = Weiss temperature.	122
Table 2.2: Magnetic parameters determined by fitting an exchange expression to the SQUID magnetic susceptibility data for compounds 2 and 5-8 . J = exchange coupling constant; ρ = fraction paramagnetic impurity; θ = Weiss-like temperature correction; $R = [(\sum\chi_{\text{obs}} - \chi_{\text{calc}})^2 / (\sum\chi_{\text{obs}})^2]^{1/2}$	124
Table 2.3: Physical properties of complexes 1-8	127
Table 2.4: Reaction conditions and by-products for: (i) the solution reactions of 1-8 with H_2 yielding Mn metal (determined by PXRD), and (ii) solution reactions of 1-8 with ZnEt_2 to deposit a 1:1 Mn/Zn alloy (determined by PXRD, and in some cases XPS;	

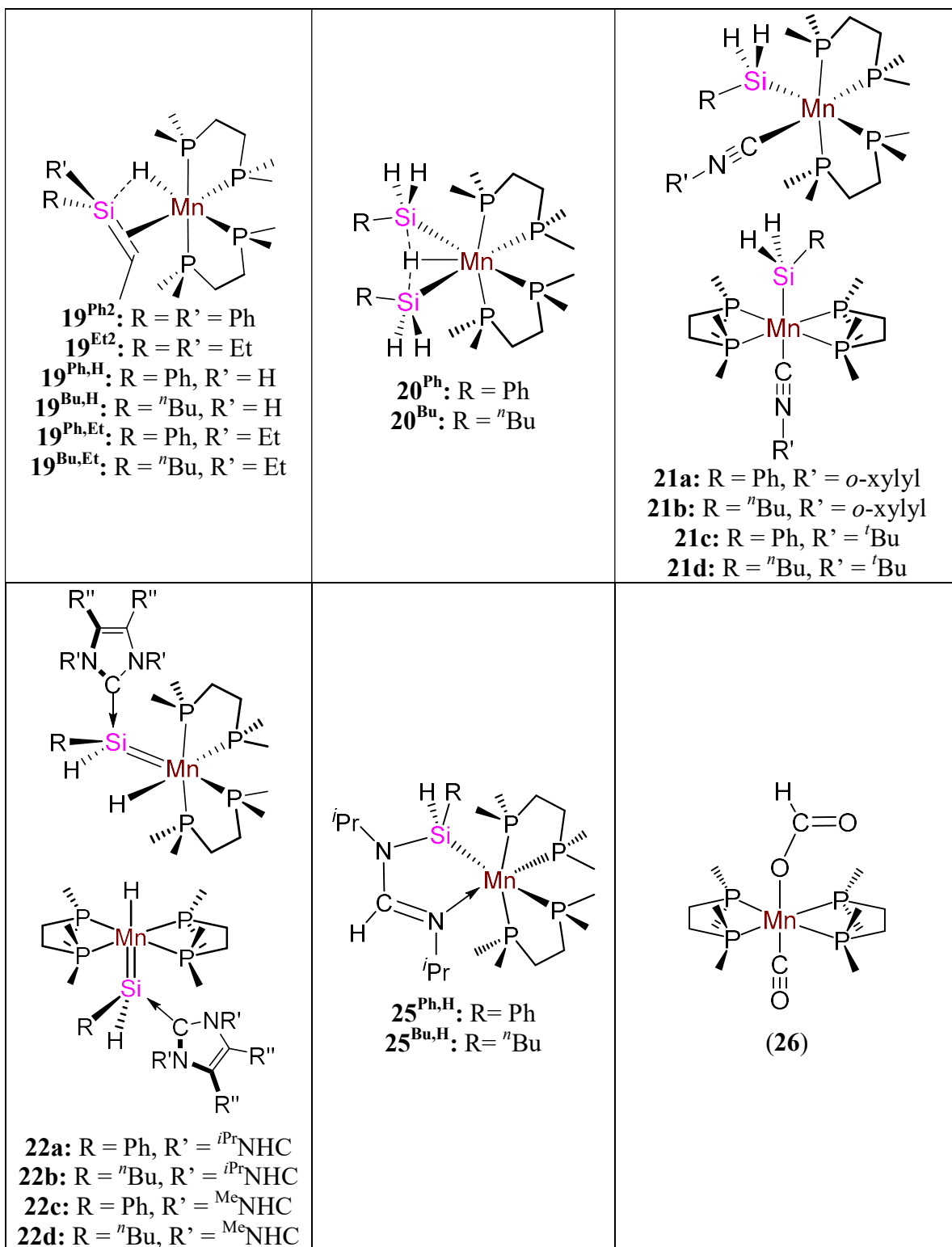
accompanied by Zn metal deposition in the reaction of 2 with ZnEt ₂). Complex 10 is <i>trans</i> -[(dmpe) ₂ MnH(C ₂ H ₄)].	128
Table 3.1: Selected angles (deg), distances (Å) (and Mayer bond orders) for DFT calculated structures in Figure 3.5.	143
Table 3.2: Activation Parameters for Transformations a-f in Figure 3.5; ΔE [‡] (calculated before ZPE correction), ΔH [‡] , and ΔG [‡] (kJ mol ⁻¹ at 298.15 K), ΔZPE [‡] (kJ mol ⁻¹ at 0 K), and ΔS [‡] (J mol ⁻¹ K ⁻¹ at 298.15 K).	144
Table 3.3: Selected angles (deg), distances (Å) (and Mayer bond orders) for DFT calculated PH ₃ analogues of ethylene hydride complexes.	145
Table 5.1: Selected ¹ H, ¹³ C, ²⁹ Si and ³¹ P NMR chemical shifts (ppm) and coupling constants (Hz) for silene hydride complexes [(dmpe) ₂ MnH(RR'Si=CHMe)] (19 ^{Ph2} : R = R' = Ph; 19 ^{Et2} : R = R' = Et; 19 ^{Ph,H} : R = Ph, R' = H; 19 ^{Bu,H} : R = ⁿ Bu, R' = H; 19 ^{Ph,Et} : R = Ph, R' = Et; 19 ^{Bu,Et} : R = ⁿ Bu, R' = Et); in C ₆ D ₆ (19 ^{R2} and 19 ^{Ph,Et}) or <i>d</i> ₈ -toluene (19 ^{R,H} and 19 ^{Bu,Et}). Unless otherwise noted, values are from NMR spectra at 298 K. For 19 ^{R,H} , NMR environments are reported for both observed isomers.	180
Table 5.2: Thermodynamic parameters calculated by DFT for the formation of intermediates in Figure 5.6 from disilyl hydride complexes [(dmpe) ₂ MnH(SiH ₂ R) ₂] { 20 ^{Ph} (R = Ph) / 20 ^{Bu} (R = ⁿ Bu)}; ΔE (calculated before ZPE correction), ΔH, ΔG ^{298.15K} , ΔG ^{335K} (kJ mol ⁻¹ at 298.15 K or, for ΔG ^{335K} , 335 K), and ΔS (J mol ⁻¹ K ⁻¹ at 298.15 K).	185
Table 6.1: Selected angles (deg) and distances (Å) (and Mayer bond orders) for experimentally observed <i>central</i> and <i>transHSi</i> isomers from calculated {or X-ray} structures of 18 . Atom labels correspond to those for 18 ^{Et2} in Figure 6.6.	214
Table 6.2: Selected angles (deg) and distances (Å) (and Mayer bond orders) for experimentally unobserved <i>transH₂</i> and <i>lateralH₂</i> isomers from calculated structures of 18 . Atom labels correspond to those for 18 ^{Et2} in Figure 6.6.	216
Table 6.3: ²⁹ Si–H coupling constants (<i>J</i> _{Si,H}) measured by ²⁹ Si ₋ edited ¹ H– ¹ H COSY NMR spectroscopy (and calculated by DFT) for silyl dihydride complexes 18 (Hz).	223

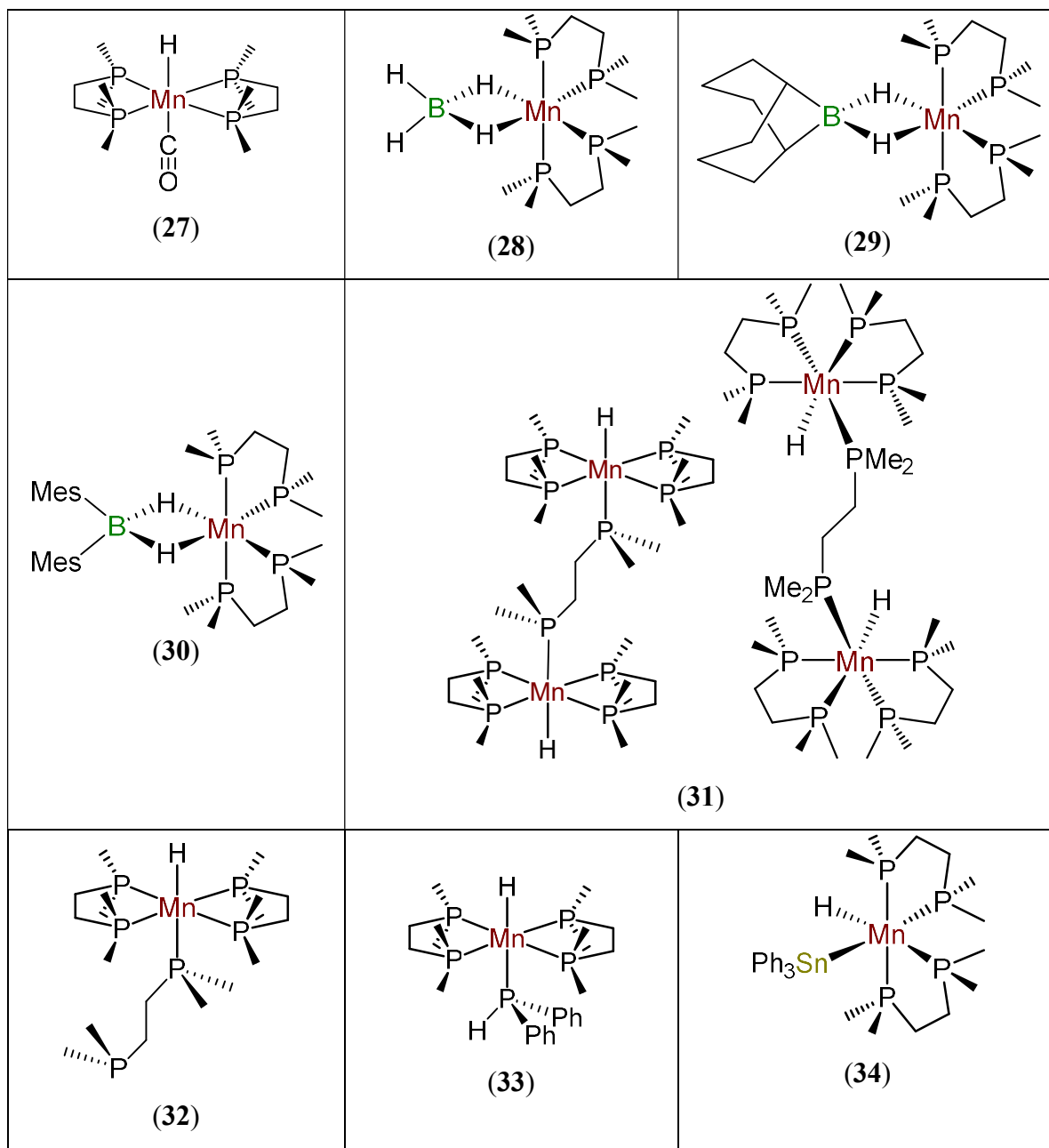
Table 8.1: Ratio of hydrosilane products (assigning the tertiary hydrosilane product a value of 100) observed by ^1H NMR spectroscopy after hydrosilylation of ethylene catalysed by $[(\text{dmpe})_2\text{MnH}(\text{C}_2\text{H}_4)]$ (10) pre-catalyst (7 mol%) with 1.7 atm ethylene (initially $n_{\text{silane}} \approx n_{\text{ethylene}}$; for reactions with H_3SiR , the headspace was re-filled with ethylene after 1 week) at 60 °C in C_6D_6 after 50 days (H_3SiPh), 25 days ($\text{H}_3\text{Si}^i\text{Bu}$) or 6 days (H_2SiR_2).....	241
Table A.1: Selected Distances (Å) (and Mayer Bond Orders) for DFT Calculated or XRD Structures of κ^2 -amidinylsilyl Complexes 25^{R,H}	365
Table A.2: Selected Angles (°) for DFT Calculated or XRD Structures of κ^2 -amidinylsilyl Complexes 25^{R,H}	366
Table A.3: Selected Angles (°) and Distances (Å) (and Mayer Bond Orders) for DFT Calculated {or XRD} Structures of Formate Complex 26	366
Table A.4: Total bonding energy (E), Enthalpy (H), Entropy (S), and Gibbs Free Energy (G) at 298 K for DFT Calculated Structures of κ^2 -amidinylsilyl Complexes 25^{R,H}	366
Table A.5: Total bonding energy (E), Enthalpy (H), Entropy (S), and Gibbs Free Energy (G) at 298 K for DFT Calculated Structures of Formate Complex 26 , and Products of CO_2 Abstraction from 26	367
Table A.6: Hirshfeld Charges for DFT Calculated Structures of κ^2 -amidinylsilyl Complexes 25	367
Table A.7: Hirshfeld Charges for DFT Calculated Structure of Formate Complex 26	367
Table A.8: Crystal and structure refinement data for $[(\text{dmpe})_2\text{Mn}\{\kappa^2\text{-SiHPh}(\text{N}^i\text{PrCHN}^i\text{Pr})\}]$ (25^{Ph,H}).....	368
Table A.9: Crystal and structure refinement data for <i>trans</i> - $[(\text{dmpe})_2\text{Mn}(\text{CO})(\kappa^1\text{-O}_2\text{CH})]$ (26).....	369

List of Compounds (Observed)

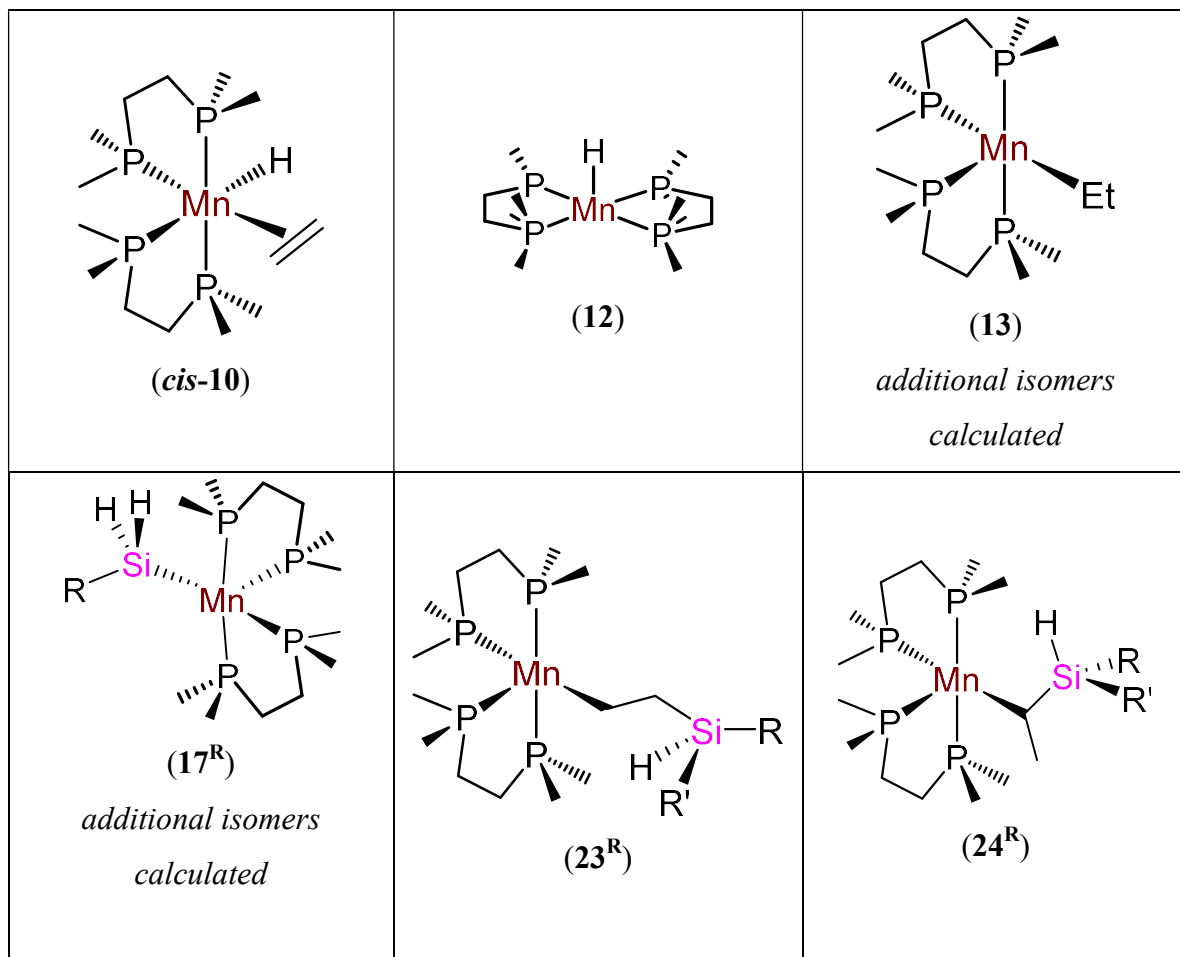








Key Intermediates Calculated by DFT



List of Abbreviations, Acronyms, and Symbols

General (acronyms)

CIF – Crystallographic Information File

CMOS – complementary metal-oxide semiconductor

CSD – Cambridge Structural Database

DRAM – dynamic random-access memory

ESI – electronic supporting information

HOMO – highest occupied molecular orbital

LPV – low pressure/vacuum

LUMO – lowest unoccupied molecular orbital

MIM – metal-insulator-metal

MOS – metal-oxide-semiconductor

m.p. – melting point

NIR – near-infrared

n.o. – not observed

OA – oxidative addition

o.d. – outer diameter

RE – reductive elimination

SG – special glass

T – temperature

TFEL – thin-film electroluminescent

TIP – temperature independent paramagnetism

UHAR – ultrahigh aspect ratio

UHV – ultra-high vacuum

UV – ultraviolet (radiation)

u. p. – unidentified product

General (symbols)^a

μ_n – bridging ligand

κ^n – denticity

Δ – difference or change

E – energy

H – enthalpy

S – entropy

G – Gibbs free energy

η^n – hapticity

n – moles

\parallel – parallel

\perp – perpendicular

% – percent

^a Symbols related to DFT, IR spectroscopy, NMR spectroscopy, UV/Vis spectroscopy, and magnetism are listed below (the latter is listed under ‘SQUID’).

‡ – transition state

Units

Å – angstrom

A (mA) – ampere (milliampere)

atm – standard atmosphere

BM – Bohr magneton

°C – degrees Celsius

deg or ° – degree

g (mg) – gram (milligram)

h – hour

Hz (MHz) – hertz (megahertz)

J (kJ) – Joule (kilojoule)

K – Kelvin

L (mL) – litre (millilitre)

m (nm, µm, mm, cm) – metre (nanometre, micrometre, millimetre, centimetre)

mol (mmol) – mole (millimole)

mol% – mole percent

M (µM, mM) – molarity (micromolarity, millimolarity)

Oe – oersted

ppm – parts per million

s (ms) – second (millisecond)

Torr (mTorr) – torr (millitorr)

V (kV) – volts (kilovolts)

W (kW) – Watts (kilowatts)

Equipment and Techniques (abbreviations, acronyms, and symbols)

ALD – Atomic Layer Deposition

Anal. – combustion elemental analysis results

CVD – Chemical Vapour Deposition

DFT – Density Functional Theory

$\Delta\rho_n$ – deformation density

ψ_n – wavefunction

ADF – Amsterdam Density Functional

BSSE – basis set superposition error

D3-BJ – Grimme's D3 dispersion correction method with Becke-Johnson damping

DZP – double- ζ basis set with one polarization function

ETS-NOCV – extended transition state method for energy decomposition analysis with natural orbitals for chemical valence

GUI – graphical user interphase

NBO – natural bond order

NOCV – natural orbitals for chemical valence

PBE – Perdew-Burke-Ernzerhof exchange and correlation functional

PBE0 – hybrid Perdew-Burke-Ernzerhof exchange and correlation functional

SCF – self-consistent field

TZ2P – triple- ζ basis set with two polarization functions

TZ2P-J – triple- ζ basis set with two polarization functions with additional steep basis functions

ZORA – scalar zeroth-order regular approximation for relativistic effects

ZPE – zero point energy

EPR – electron paramagnetic resonance (spectroscopy)

FT-IR – Fourier-transform infrared (spectroscopy)

IR – infrared (spectroscopy)

$\nu(\text{XY})$ – frequency of the stretch vibration arising from atoms X and Y

NMR – nuclear magnetic resonance (spectroscopy)

app. – apparent

br. – broad

d – doublet

m – multiplet

p – pentet

q – quartet

s – singlet

sat. – satellite

t – triplet

v. – very

δ – chemical shift

$J_{x,y}$ – coupling constant between nuclei x and y, where the number of bonds is not specified

${}^nJ_{x,y}$ – n-bond coupling constant between nuclei x and y

1D – one dimensional

2D – two dimensional

COSY – correlation spectroscopy

uDEFT – uniform driven equilibrium Fourier transform

DEPTq – distortionless enhancement by polarization transfer including the detection of quaternary nuclei

DOSY – diffusion ordered spectroscopy

dqf – double quantum filter

EXSY – exchange spectroscopy

FID – free induction decay

HMBC – heteronuclear multiple bond correlation

HMQC – heteronuclear multiple quantum coherence

HSQC – heteronuclear single quantum coherence

INEPT – insensitive nuclei enhanced by polarization transfer

NOE – nuclear Overhauser effect

NOESY – nuclear Overhauser effect spectroscopy

ns – number of scans

T_1 relaxation – spin-lattice relaxation

td1 eff – size of FID utilized for the 2nd dimension in a 2D NMR experiment

td2 eff – size of FID utilized for the 1st dimension in a 2D NMR experiment

TOCSY – total correlation spectroscopy

PEALD – plasma enhanced atomic layer deposition

PVD – physical vapour deposition

PXRD – powder X-ray diffraction

SQUID – superconducting quantum interference device

MPMS: Magnetic Properties Measurement System

μ_B – effective magnetic moment

J – exchange coupling constant (for antiferromagnetic coupling)

ρ – fraction paramagnetic impurity

χ – magnetic susceptibility

100R – Measure of goodness of fit ($R = [(\sum \chi_{obs} - \chi_{calc})^2 / (\sum \chi_{obs})^2]^{1/2}$)

θ – Weiss temperature or Weiss-like temperature correction

UV/Vis – ultraviolet and visible (Spectroscopy)

λ_{\max} – wavelength of maximum intensity

Vis – visible spectroscopy

XPS – X-ray photoelectron spectroscopy

XRD – X-ray diffraction

CCD – charge coupled device

Chemical species (compounds, ligands, and substituents)

acac – acetylacetonate

Ad – adamantyl

AMD – amidinate

Ar – aryl

Dipp – 2,6-diisopropylphenyl

Dur – duryl (2,3,5,6-tetramethylphenyl)

i – ipso

m – meta

Mes – mesityl

Naph – naphthyl

o – ortho

p – para

Ph – phenyl

tol – tolyl (methylphenyl)

Trip – 2,4,6-triisopropylphenyl

xyl – xylyl

9-BBN – borabicyclo(3.3.1)nonane

bipy – 2,2' bipyridine

Bis(phosphines)

depe – 1,2-bis(diethylphosphino)ethane

dfepe – 1,2-bis(ferrocenylphosphino)ethane

dmpe – 1,2-bis(dimethylphosphino)ethane

dmpm – 1,2-bis(dimethylphosphino)methane

dmpp – 1,2-bis(dimethylphosphino)propane

dppe – 1,2-bis(diphenylphosphino)ethane

dppm – 1,2-bis(diphenylphosphino)methane

dtbpm – 1,2-bis(di-*tert*-butylphosphino)methane

Butyl groups

ⁿBu – *n*-butyl (*n* = normal)

^tBu – *tert*-butyl

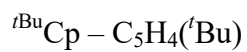
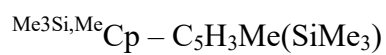
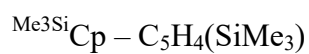
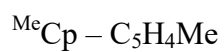
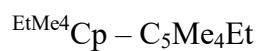
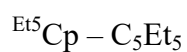
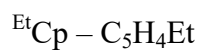
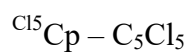
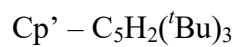
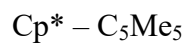
C_x – specific carbon label

C_{br} – carbon bridging between two metal atoms

C_{term} – carbon bound to a single metal atom

COD – 1,5-cyclooctadiene

Cp – cyclopentadienyl



Cy – cyclohexyl

DIBAL – diisobutylaluminum hydride

DME – 1,2-dimethoxyethane

dpm – dipivaloylmethanate

Et – ethyl

hex – 1-hexyl

hfac – hexafluoroacetylacetonate

L – general neutral ligand

LA – Lewis acid

Me – methyl

NHC – *N*-heterocyclic carbene

^{*i*}PrNHC – 1,3-diisopropylimidazolin-2-ylidene

^{Me}NHC – 1,3,4,5-tetramethyl-4-imidazolin-2-ylidene

NHSi– *N*-heterocyclic silylene

pmdeta – pentamethyldiethylenetriamine

Propyl groups

^{*i*}Pr – *iso*-propyl

^{*n*}Pr – *n*-propyl (*n* = normal)

Py – pyridinyl

R – general anionic organic substituent (typically an H, CR₃ or SiR₃ group)

tfac – trifluoroacetylacetonate

THF – tetrahydrofuran

TMEDA – N,N,N',N'-tetramethylethylenediamine

Tp – hydrotris(pyrazolyl)borate, {HB(pz)₃}⁻

Xyl – *o*-xylyl, 2,6-dimethylphenyl

Declaration of Academic Achievement

Dr. David J. H. Emslie was responsible for the synthesis and obtaining an X-ray crystal structure of dineopentylmanganese(II) (**2**). Dr. Preeti Chadha, as postdoctoral fellow in the Emslie group, was responsible for the synthesis and obtaining X-ray crystal structures of complexes $[\{(\mu\text{-dmpe})\text{Mn}(\text{CH}_2\text{CMe}_3)_2\}_2]$ (**4**), $[(\mu\text{-dmpe})\{\text{Mn}(\text{CH}_2\text{CMe}_3)(\mu\text{-CH}_2\text{CMe}_3)\}_2]$ (**6**), and $[(\mu\text{-dmpm})\{\text{Mn}(\text{CH}_2\text{CMe}_3)(\mu\text{-CH}_2\text{CMe}_3)\}_2]$ (**8**) (for complex **8**, one of two different structures was obtained by Dr. Chadha, and the other by the author). Dr. Hilary Jenkins (of the McMaster Analytical X-ray Diffraction Facility) was responsible for XRD crystal mounting, data acquisition, refinement, and structure solution for $[(\mu\text{-dmpe})\{\text{Mn}(\text{CH}_2\text{SiMe}_3)(\mu\text{-CH}_2\text{SiMe}_3)\}_2]$ (**5**) and $[(\mu\text{-dmpm})\{\text{Mn}(\text{CH}_2\text{SiMe}_3)(\mu\text{-CH}_2\text{SiMe}_3)\}_2]$ (**7**), Dr. James Britten (of the McMaster Analytical X-ray Diffraction Facility) was responsible for XRD refinement and structure solution for $[(\text{dmpe})\text{Mn}(\text{CNXyl})_3\{\text{C}(=\text{NXyl})\text{CEt}(=\text{NXyl})\}]$ (**15**), and Fang Yuan (a graduate student in the Mozharivskij group at McMaster University) was responsible for XRD crystal mounting and data acquisition for $[(\text{dmpe})_2\text{MnEt}(\text{CNXyl})]$ (**14b**), $[(\text{dmpe})\text{Mn}(\text{CNXyl})_3\{\text{C}(=\text{NXyl})\text{CEt}(=\text{NXyl})\}]$ (**15**), $[(\text{dmpe})_2\text{MnH}\{\text{=SiH}^n\text{Bu}(^i\text{PrNHC})\}]$ (**22b**), and $[(\text{dmpe})_2\text{MnH}\{\text{=SiHPh}(^{\text{Me}}\text{NHC})\}]$ (**22c**). Dr. Paul Dube was responsible, in combination with the author, for obtaining SQUID data on complexes **2-8**. Megan Fair was responsible for running combustion elemental analysis when carried out in-house. Dr. Allen Pauric was responsible for obtaining T_1 relaxation times and attempting DOSY NMR measurements for $[\{(\mu\text{-dmpe})\text{Mn}(\text{CH}_2\text{CMe}_3)_2\}_2]$ (**4**). Dr. Rana Sodhi (of Surface Interface Ontario) was responsible for obtaining XPS. Dr. Bob Berno created the pulse program for ^{29}Si _edited ^1H - ^1H COSY NMR spectroscopy. All other results were obtained by Jeffrey S. Price.

Chapter 1:

Introduction

1.1 – Introductory Remarks

This thesis includes the synthesis of volatile manganese alkyl complexes as potential Atomic Layer Deposition (ALD) precursors, the synthesis and reactivity of manganese alkyl, hydride and silyl complexes (which could be potential Chemical Vapour Deposition (CVD) precursors), the synthesis of silylene and silene complexes, and manganese-catalyzed ethylene hydrosilylation. Therefore, the introduction is divided into the following topics:

1.2 – CVD and ALD Using Manganese Precursors

1.3 – Manganese Alkyl Complexes

1.4 – Manganese Hydride Complexes

1.5 – Manganese Silyl Complexes

1.6 – Silylene Complexes of Transition Metals

1.7 – Silene Complexes of Transition Metals

1.2 – CVD and ALD Using Manganese Precursors

Portions of this section have been reprinted (adapted) with permission from Emslie, D. J. H.; Chadha, P.; Price, J. S. Metal ALD and Pulsed CVD: Fundamental Reactions and Links with Solution Chemistry, *Coord. Chem. Rev.* **2013**, *257*, 3282-3296 (Copyright 2013 Elsevier B.V.), and Price, J. S.; Chadha, P.; Emslie, D. J. H. Base-Free and Bisphosphine Ligand Dialkylmanganese(II) Complexes as Precursors for Manganese Metal Deposition, *Organometallics* **2016**, *35*, 168-180 (Copyright 2016 American Chemical Society).

1.2.1 – Scope of Section

This section provides an introduction to the thin film deposition techniques of Chemical Vapour Deposition (CVD) and Atomic Layer Deposition (ALD), with a particular focus on deposition of elemental manganese. A review of thermal CVD and ALD using manganese-containing precursors is provided. Plasma enhanced CVD and ALD are beyond the scope. Nucleation issues are an important consideration in developing CVD or ALD reaction chemistry, but are also beyond the scope.

1.2.2 – Introductory Remarks on CVD and ALD

Deposition of thin films is an important area in materials science. Many different types of materials can be deposited as thin films including nitrides, carbides, oxides, and pure metals. Research in this field is often focused on applications related to microelectronics, and being able to prepare high quality thin films with a specific thickness is important as advances in this area are often driven by shrinking the size of the critical features (e.g. transistors and memory cells) in technological devices (e.g. microprocessors and memory). The breadth of research involved in thin film deposition is highlighted by the existence of dedicated peer-reviewed journals such as *Thin Solid Films* and *Chemical Vapor Deposition*.

While a variety of methods exist for depositing thin films (including wet chemical deposition, electrochemical deposition, and physical vapour deposition), the processes of Chemical Vapour Deposition (CVD) and Atomic Layer Deposition (ALD) are of particular interest in materials chemistry as methods to deposit films with predictable thicknesses and composition. Introductions to these techniques are provided in sections 1.2.3 and 1.2.4, respectively.

In CVD and ALD, particularly challenging targets are thin films of pure, elemental metals {which are often required for diffusion barriers, electronic contacts, resistors, interconnects, electrodes, reflective coatings, or protective coatings (those resistant to oxidation, corrosion, or abrasion)}.^{1,2} For many metals, thermal CVD and ALD

processes have yet to be conceived. Furthermore, many of the existing methods for metal CVD or ALD suffer from limitations which preclude industrial applications, including poor physical properties and significant contamination (especially by carbon).¹ Therefore, it is incumbent upon synthetic chemists to develop chemistry to enable new approaches in metal CVD and/or ALD.³

1.2.3 – Introduction to Chemical Vapour Deposition (CVD)

Chemical Vapour Deposition (CVD) is a method for depositing thin films by decomposition of vapours of a volatile precursor at the surface of a heated substrate, where all by-products are volatile. CVD normally requires a carrier gas (usually inert, but sometimes a reactive gas) both to bring the precursor into the reactor, and to remove the volatile by-products from the reactor. Normally, a large excess of precursor is continuously allowed to flow over the substrate, and as time passes the deposited film becomes thicker (thus, the duration of precursor exposure, and the amount of precursor that reaches each point on the substrate surface, controls the film thickness). A variety of texts have been written which provide excellent overviews of the CVD process and its applications.⁴ While a variety of modifications of CVD exist, this introduction is focused exclusively on thermal CVD. This technique is generally utilized for deposition of thin films 0.1-10 μm in thickness, with thickness controlled by the vapour pressure, gas-flow rate, and deposition temperature, in addition to the duration of deposition (*vide supra*). Some advantages of CVD are the potential to produce films of high density, purity, uniformity, reproducibility of thickness, and conformality (relative to non-vapour phase deposition techniques, but not relative to ALD; *vide infra*). Other advantages are relatively low temperatures required for deposition, an easily adjustable deposition rate, good adhesion to a substrate, and high deposition rates.⁵

Metal hydride complexes are one class of CVD precursor that has been investigated for deposition of elemental metals.⁶ The driving force for metal reduction in these complexes is often reductive elimination (sometimes bimolecular) of H_2 . A significant amount of work has been reported on $\text{Al}_{(s)}$ deposition⁷ from various amine

adducts of alane ($R_3N \cdot AlH_3$)⁸ or aluminaborane $\{R_3N \cdot AlH_2(BH_4)\}$.⁹ $Al_{(s)}$ deposition by CVD has also been reported from alkyl hydride compounds such as Me_2AlH , though only under an atmosphere of H_2 .¹⁰ Similarly, $W_{(s)}$ deposition has been reported from mixed hydrocarbyl-hydride complexes $[Cp_2WH_2]$ ¹¹ and $[^{Me}Cp_2WH_2]$ ¹² under an atmosphere of H_2 .

1.2.4 – Introduction to Atomic Layer Deposition (ALD)

For many years, Physical Vapour Deposition (PVD) and CVD (*vide supra*) have been central techniques for the deposition of thin metal films with a broad range of applications. However, the directional nature of these methods can lead to difficulties in: (a) obtaining ultra-thin films of uniform thickness, and (b) deposition of conformal films within nano-scale high aspect ratio features (e.g. trenches or vias), and these difficulties are becoming increasingly significant in the microelectronics industry as a result of rapidly decreasing device (e.g. transistor or memory cell) dimensions. Furthermore, CVD suffers from: (a) the potential for particle formation due to reactions occurring in the vapour phase rather than on the substrate surface, (b) in the case of solid precursors, dependence of film growth rate on precursor particle size, and (c) unavailability of precursors for deposition of certain materials, including many of the transition metals.^{13,14}

Atomic Layer Deposition (ALD), sometimes referred to as Atomic Layer Epitaxy (ALE), is a technique related to CVD which largely overcomes the limitations outlined above, although the overall deposition rate is generally much lower than that of CVD. In ALD, a volatile metal precursor is employed, as in CVD, but in this case, the substrate temperature and precursor thermal stability are such that the precursor does not undergo thermal decomposition upon contact with the substrate. Instead, deposition is achieved by repeated alternating self-terminating surface-based reactions between a metal precursor and a co-reactant, at least one of which is adsorbed (through chemisorption or physisorption) on the substrate surface.¹³⁻¹⁷ In thermal ALD, the co-reactant is a ‘stable’ entity (e.g. H_2 , H_2O , O_2 or O_3), while in plasma-enhanced ALD (PEALD), the co-reactant is plasma-generated (e.g. H, O or N atoms). Potential drawbacks of PEALD are that it

introduces additional complexity to an ALD reactor, exposure to plasma-generated ions and UV-radiation can cause damage to the substrate and/or the growing film, and conformal deposition inside high aspect ratio features is difficult; this is especially the case for metal deposition using hydrogen plasma, since hydrogen radicals have particularly high recombination rates on most metal surfaces.¹⁸ On the other hand, a major advantage of PEALD is that it can be used to deposit a range of materials at low temperature, due to the high reactivity of species such as atomic hydrogen, oxygen and nitrogen. In this thesis, only thermal ALD will be discussed, and from herein the term ALD is used to mean thermal ALD unless otherwise specified.

The reactions in ALD are designed to yield only volatile byproducts, and these byproducts, as well as excess metal precursor / co-reactant, are removed in inert gas purge steps between metal precursor and co-reactant pulses. The defining characteristic of ALD is that the metal precursor and the co-reactant are adsorbed and/or react with the surface in a *self-limiting* fashion. Therefore, so long as sufficient vapour doses of the metal precursor and co-reactant are delivered to ensure maximum surface coverage and complete reaction, the thickness of the deposited film will depend only on the number of precursor/purge/co-reactant/purge cycles, and the film will grow conformally on all exposed surfaces on which nucleation can occur, including the surfaces of high aspect-ratio features. If self-limiting behaviour cannot be achieved, the overall process is termed pulsed-CVD.¹³⁻¹⁷

Although ALD offers advantages not conferred by pulsed-CVD, in both cases, the use of a metal precursor *and* a co-reactant provides access to a broader range of deposition chemistries than CVD involving thermal decomposition of a single metal precursor. Consequently, both ALD and pulsed-CVD provide the potential for deposition of materials that are inaccessible using single precursor CVD, as well as enhanced potential for the development of deposition reactions capable of operating at low temperature.

1.2.5 – Requirements for CVD and/or ALD Precursors

Both CVD and ALD rely upon delivery of a metal-containing precursor molecule to the surface of a substrate in the vapour phase, followed by reactivity (thermal decomposition or reaction with a co-reactant) to generate the desired material and volatile byproducts which are readily eliminated from the growing film. Consequently, ALD and CVD place strict requirements on the physical and chemical properties of metal precursors and co-reactants. In particular, metal precursors and (for ALD) co-reactants should exhibit:

- Volatility such that the precursor can be delivered below the temperature required for film deposition (for solid precursors used with an ALD reactor operating under non-UHV conditions, typical vapour pressures at the delivery temperature are in the 0.01 to 10 Torr range, preferably at least 0.1 Torr).¹³ It is also preferable that the precursor (and, for ALD, co-reactant) are sufficiently volatile to allow low-temperature ALD/CVD if the reactivity between the precursor, the co-reactant (for ALD), and the substrate is such that this can be achieved.
- For ALD, sufficiently high thermal stability and reactivity to ensure that ALD can be achieved at temperatures below the onset of CVD (the larger the ALD window, the better). A similar criterion will in some cases apply to pulsed-CVD.
- Long-term thermal stability at the temperature of the delivery bubbler.
- ALD/CVD reactivity that yields only volatile byproducts.
- Surface reactivity which allows adsorption and film growth on both the substrate material (in initial stages of film deposition) and the growing film material.
- Scaleable syntheses with reasonable overall yields.
- Low melting points are also desirable, since the use of liquid precursors helps to avoid particle incorporation, and to ensure uniformity in the amount of precursor and co-reactant delivered in each pulse (for solids, the amount of precursor or co-

reactant delivered in each pulse can depend on average particle size, which can vary significantly as precursor / co-reactant is consumed). With respect to the latter point, use of liquid precursors and co-reactants is less critical for ALD than for CVD, since film thickness will depend only on the number of reaction cycles, providing that sufficiently long precursor and co-reactant pulses are employed.

These requirements unavoidably curtail the complexity of ALD and CVD precursors and (for ALD) co-reactants. However, by the same token, the development of new ALD reactivity that is compatible with precursors and co-reactants that meet the above criteria presents a substantial and interesting challenge. This is especially the case for more difficult targets (e.g. metals currently inaccessible by ALD or low temperature ALD reactivities), and in many cases the development of new ALD or CVD reactivity must go hand in hand with the design of new precursors able to meet the requirements of the target reactivity.

1.2.6 – A Brief Introduction to Deposition of Elemental Metals by ALD or Pulsed-CVD

Relative to metal oxide and metal nitride ALD, examples of thermal ALD for metal deposition are far less common. In fact, as illustrated graphically in Figure 1.1, thermal ALD of metals has thus far mainly been achieved for the least electropositive transition metals: the noble metals, 1st row congeners of the noble metals, rhenium, the group 6 elements molybdenum and tungsten. The only group 3-5 transition metal to have been deposited by ALD is titanium.

3 Li 0.98	4 Be 1.57											5 B 2.04	6 C 2.55	7 N 3.04	8 O 3.44
11 Na 0.93	12 Mg 1.31											13 Al 1.61	14 Si 1.90	15 P 2.19	16 S 2.58
19 K 0.82	20 Ca 1.00	21 Sc 1.36	22 Ti 1.54	23 V 1.63	24 Cr 1.66	25 Mn 1.55	26 Fe 1.83	27 Co 1.88	28 Ni 1.91	29 Cu 1.90	30 Zn 1.65	31 Ga 1.81	32 Ge 2.01	33 As 2.18	34 Se 2.55
37 Rb 0.82	38 Sr 0.95	39 Y 1.22	40 Zr 1.33	41 Nb 1.6	42 Mo 2.16	43 Tc 1.9	44 Ru 2.2	45 Rh 2.28	46 Pd 2.20	47 Ag 1.93	48 Cd 1.69	49 In 1.78	50 Sn 1.96	51 Sb 2.05	52 Te 2.1
55 Cs 0.79	56 Ba 0.89	71 Lu 1.27	72 Hf 1.3	73 Ta 1.5	74 W 2.36	75 Re 1.9	76 Os 2.2	77 Ir 2.20	78 Pt 2.28	79 Au 2.54	80 Hg 2.00	81 Tl 2.04	82 Pb 2.33	83 Bi 2.02	84 Po 2.0
87 Fr 0.7	88 Ra 0.9	103 Lr --													

<i>Ln</i>	57 La 1.10	58 Ce 1.12	59 Pr 1.13	60 Nd 1.14	61 Pm --	62 Sm 1.17	63 Eu --	64 Gd 1.20	65 Tb --	66 Dy 1.22	67 Ho 1.23	68 Er 1.24	69 Tm 1.25	70 Yb --
<i>An</i>	89 Ac 1.1	90 Th 1.3	91 Pa 1.5	92 U 1.38	93 Np 1.36	94 Pu 1.28	95 Am 1.3	96 Cm 1.3	97 Bk 1.3	98 Cf 1.3	99 Es 1.3	100 Fm 1.3	101 Md 1.3	102 No 1.3

Figure 1.1: Periodic table, not including hydrogen, halogens and noble gases, highlighting metals that have been deposited by thermal ALD or pulsed-CVD (only reports in peer-reviewed literature are included). Metals that have been deposited by ALD are enclosed by solid black boxes.^b Metals (or alloys) that have been deposited only by pulsed-CVD are enclosed by dashed black boxes. Atomic numbers are shown above the atom symbols and Pauling electronegativities are shown below (for values with two decimal places, the oxidation state is: I for groups 1 and 11, II for groups 2, 4-10 and 12, III for groups 3 and 13, and IV for group 14).²¹ Non-metals (including semi-metals) and elements without significant natural abundance are shown in white. The remaining elements are shaded.

^b References for elemental metal ALD of most of the elementals highlighted in Figure 1.1 can be found in ref. 19a. Since the publication of this review (in 2013), ALD processes have been reported for deposition of Al_(s),^{19b} Ti_(s),^{19c} Re_(s),^{19d} Ag_(s),^{19e} Au_(s),^{19f} and Sn_(s).^{19g} In addition, Winter et al. has reported ALD-like deposition of elemental Cr_(s) and Mn_(s), though this process only proceeded on Ru substrates and stopped after the substrate was completely covered.²⁰

From the above discussion, it follows that a major challenge in ALD is the development of suitable reaction chemistry for deposition of metals not yet accessed by ALD. However, even for metals that have previously been accessed by ALD, various features of the precursors, the deposition process, and/or the resulting films may prevent commercial application. These include: (a) difficulties in precursor scale-up, (b) insufficient precursor or co-reactant thermal stability, (c) an ALD temperature that is too high to be compatible with the desired substrate (temperatures of 200-400 °C are common), (d) an ALD temperature that causes agglomeration of thin metal films,²² (e) deposition of metal films containing impurities at levels that are unacceptable for the target application, (f) impractical or complex and costly deposition conditions (e.g. those involving extremely long pulse or purge durations, an unacceptably low growth rate, a very narrow ALD temperature window, injection of the precursor or co-reactant as a solution, or UHV deposition conditions), (g) an unacceptably long induction period prior to the onset of self-limiting film growth,¹⁵ (h) film growth that does not lead to continuous films at low film thicknesses (island growth),^{15,17} (i) film morphologies that do not provide the desired physical properties and performance, (j) poor adhesion between the deposited film and the underlying substrate, and (k) deposition of films that do not have the desired crystalline phase, crystal orientation, or level of crystallinity. Which of these potential limitations are relevant will depend on the metal being deposited and the target application.

Limitations (b)-(e) above can be related fairly directly to precursor, co-reactant and reaction byproduct volatility/thermal stability, and the reaction pathways occurring at the surface. By contrast, limitations (g-k) will be substrate specific and are less directly linked to the fundamental classes of chemical reaction involved in metal deposition. The development of new ALD methods that overcome limitations such as those outlined above is clearly an important goal, although in the case of substrate-specific behaviour, the development of multiple fundamentally different reaction chemistries, each with a different substrate scope, may be required. New ALD reaction chemistries that allow for straightforward and controlled addition of specific impurities *via* an ALD mechanism

may also be of interest. Furthermore, substrate-selective ALD/pulsed-CVD of metals (e.g. deposition on Pd and/or Pt rather than an glass, silica or a metal oxide surface,^{23,24} on H-terminated Si rather than OH-terminated SiO₂,²⁵ or on substrates patterned with self-assembled polymer monolayers)^{26,27,28} is an active field of research with its own deposition chemistry requirements.

Metals deposited by ALD have a broad range of potential applications in the fields of microelectronics (microprocessors, memory devices etc.), flat panel displays, fuel-cells, solar cells, and catalysis.^{13,17} In the area of microelectronics, various potential applications of ALD metal films have been cited in the literature. These include:¹⁷ rear electrode materials for inverted TFEL devices or plugs for the UHAR contacts of advanced DRAM (Mo, W),²⁹ positive channel MOS gate electrodes (Re, Ru, Rh, Ir, Pd, Pt),²⁷ electrode materials in MIM capacitors for future DRAM (Ru, Ir),^{14,30} nanocrystals for non-volatile nanocrystal memory (W, Ru, Pd, Au),¹⁷ diffusion barriers, adhesion layers or seed layers for copper deposition (Ru, Os, Rh and others),^{30,31} precursors to CoSi₂, NiSi or PtSi source and drain materials to replace TiSi₂ in MOS devices (generated by annealing Co, Ni or Pt metal films on silicon substrates),^{25,32,33} gate materials for CMOS devices (Pt),³³ and interconnect wiring (Cu or Ag).³⁴

Elemental metals with low electronegativity pose a particular challenge, in that metal precursors usually contain the metal in a positive oxidation state, and reduction to the zero oxidation state becomes increasingly difficult as the metal becomes more electropositive (i.e. the potential for $M^{x+} \rightarrow M^0$ reduction becomes increasingly negative). In this regard, manganese is an interesting target for elemental ALD, given that it has an electronegativity of 1.55 (Pauling scale), which is higher than that of gr. 3-4 metals, but lower than that of gr. 8-11 metals. Manganese is also the only gr. 7-11 metal (not including radioactive Tc) for which thin film deposition of the elemental metal by ALD has not been reported (*vide supra*). One of the most discussed applications of manganese in metal thin film deposition chemistry is formation of a diffusion barrier between silica and copper in microelectronics.³⁵ These barriers (composed of manganese oxide, silicide,

and/or silicate) can be ‘self-formed’ by migration of Mn(0) from a deposited Cu/Mn alloy into the silica substrate,³⁶ or from initial Mn(0) deposition onto a silica surface.³⁷ While CVD of elemental manganese has been reported to form films of varying quality from a number of precursors (see section 1.2.7), no ALD method has yet been reported to produce high quality films of Mn(0); section 1.2.8.

Neutral homoleptic metal alkyl complexes are intriguing potential precursors for electropositive metal ALD because (a) the high reactivity of polar metal–alkyl bonds may provide access to low temperature reaction pathways for elemental metal deposition,^c (b) the metal-nitrogen and metal-oxygen bonds typically encountered in coordination complexes can be avoided, precluding metal oxide or nitride formation, and (c) the expected byproducts in reactions with hydride sources (alkanes; see Chapter 2) are highly unreactive and volatile (and therefore should be easily eliminated from the growing film).

Transition metal alkyl complexes have rarely been used as precursors for pulsed-CVD or ALD, although notable exceptions are [PtMe₂(COD)],³⁹ and [MeCpPtMe₃].⁴⁰ Chapter 2 of this thesis will investigate the potential for neutral homoleptic alkylmanganese complexes, and Lewis base adducts thereof, to act as precursors in Mn_(s) deposition.

1.2.7 – Chemical Vapour Deposition Using Mn-containing Precursors

To our knowledge the first report of CVD using a manganese-containing precursor involved the deposition of Mn silicides MnSi and Mn₅Si₃ (the deposited film contained a mixture of both) by Aylett and Colquhoun in 1977 from the volatile precursor [(CO)₅Mn(SiH₃)] (a in Figure 1.2).⁴¹ Manganese silicide (with varying Mn : Si stoichiometries) could also be deposited from CVD of [{(OC)₅Mn} ₂ (μ-SiH₂)] (b in Figure 1.2)⁴² or [(OC)₅Mn(SiCl₃)] (c in Figure 1.2)^{43,44} at temperatures ranging from 300-700 °C. Thin films of other manganese-containing species have been prepared from CVD using single-source precursors, including MnGe_{x(s)} (from

^c Alkyl complexes of more electropositive metals are typically more reactivity towards σ -bond metathesis reactions; see ref. 38.

$[\{(OC)_5Mn\}_2Ge\{\kappa^2-CH_2(CMe)(CMe)CH_2\}]$; d in Figure 1.2),⁴⁵ $MnGa_{(s)}$ (from $[(OC)_5MnGaH_2(NMe_3)]$; e in Figure 1.2),⁴⁶ $MnIn_{(s)}$ (from $[(OC)_5MnIn\{\kappa^2-(CH_2)_3NMe_2\}_2]$; f in Figure 1.2),⁴⁶ and $MnF_{2(s)}$ {from $[(TMEDA)Mn(hfac)_2]$; g in Figure 1.2}.⁴⁷

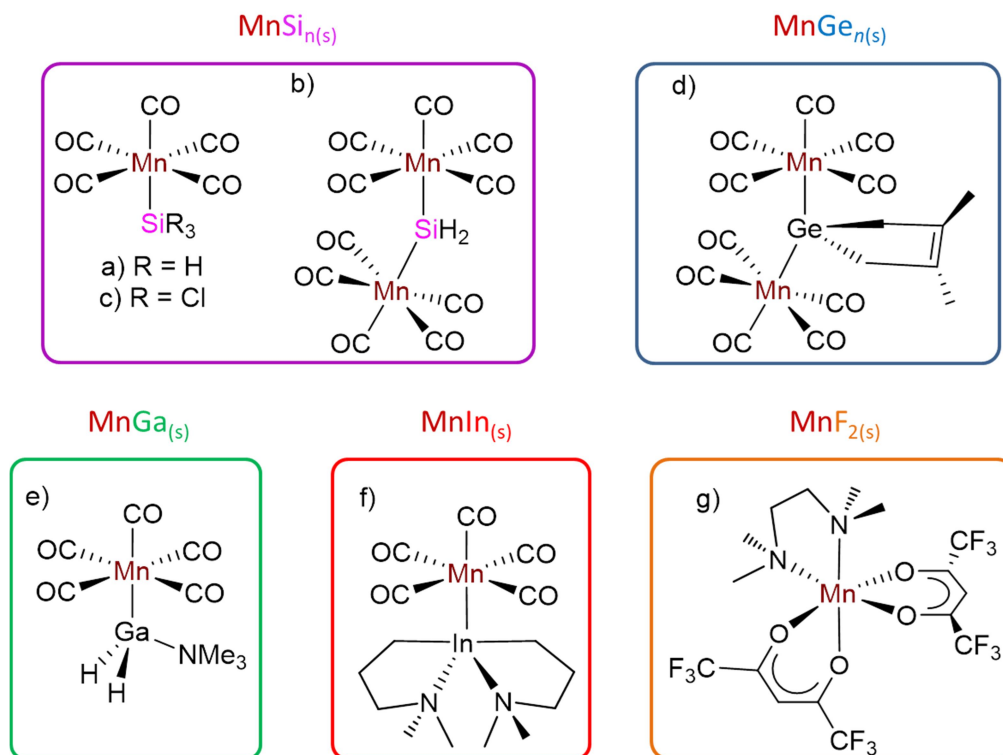


Figure 1.2: Single-source precursors used for CVD of Mn-containing thin films (not including elemental manganese).

In addition to using single-source precursors, Mn-containing thin films have also been deposited by simultaneous decomposition of multiple precursors, one of which is a volatile Mn-containing complex. Complexes used as Mn sources include $[MeMn(CO)_5]$ (for $MnSe_{(s)}$,⁴⁸ $Cd_{(1-x)}Mn_xTe_{(s)}$,⁴⁹ $Hf_{1-x-y}Cd_xMn_yTe_{(s)}$,⁵⁰ or $MnAs_{(s)}$,⁵¹ a in Figure 1.3), $[CpMn(CO)_3]$ (for $MnS_{(s)}$; b in Figure 1.3),⁵² $[^{Me}CpMn(CO)_3]$ (for $Cd_{(1-x)}Mn_xTe_{(s)}$; c in Figure 1.3),⁴⁹ $[Mn(acac)_2]$ (for $Mn_xZn_{(1-x)}Fe_2O_{4(s)}$; d in Figure 1.3),⁵³ $[Mn(dpm)_3]$ (for $LaMnO_{3(s)}$ or $PrMnO_{3(s)}$; e in Figure 1.3),⁵⁴ and $[Mn\{(\textit{i}PrN)_2C^nBu\}_2]$ (for Mn_4N or $MnCu_x$; f in Figure 1.3).⁵⁵ CVD using Mn-containing precursors has also been used to

dope various films with Mn, including $\text{ZnE}_{(s)}$ ($E = \text{S, Se}$) {using $[\text{M}^{\text{e}}\text{CpMn}(\text{CO})_3]$ (d in Figure 1.3)⁵⁶ or $[\text{Cp}_2\text{Mn}]$ (g in Figure 1.3)}⁵⁷ or $\text{AlN}_{(s)}$ {using $[\text{M}^{\text{e}}\text{Cp}_2\text{Mn}]$ (h in Figure 1.3)}.⁵⁸

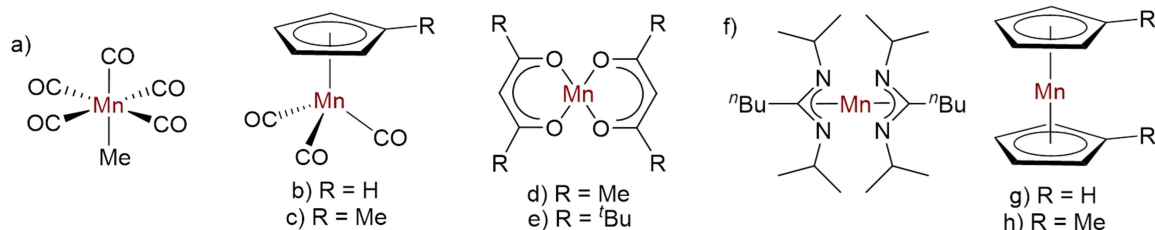


Figure 1.3: Precursors used for CVD of Mn-containing thin films (not including oxides or elemental manganese) by simultaneous decomposition of multiple precursors or decomposition of Mn-containing precursors in the presence of a reactive gas.

However, the most common manganese-containing thin film to have been deposited by CVD are oxides, usually formed by decomposition of a Mn-containing species in the presence of O_2 (either reagent-grade or air) or water. Examples of Mn-sources for these processes include $[\{\text{Mn}(\text{CO})_5\}_2]$ (a in Figure 1.4),⁵⁹ $[\text{ArMn}(\text{CO})_3]$ ($\text{Ar} = t\text{BuCp}$, Cp^* ; b and c in Figure 1.4),⁶⁰ $[(\eta^5\text{-C}_6\text{H}_7)\text{Mn}(\text{CO})_3]$ (d in Figure 1.4), $[\text{Mn}(\text{acac})_3]$ (e in Figure 1.4),⁶¹ $[\text{Mn}(\text{dpm})_3]$ (f in Figure 1.4),^{62,63} $[(\text{TMEDA})\text{Mn}(\text{hfac})_2]$ {g in Figure 1.4; in the absence of O_2 , $\text{MnF}_{2(s)}$ deposition was observed: *vide supra*},^{64,65} and $[(\text{TMEDA})\text{Mn}(\text{tfac})_2]$ (h in Figure 1.4).^{65,66} As well, CVD using Si-containing precursors $[\text{M}^{\text{e}3\text{Si}}\text{CpMn}(\text{CO})_3]$ (i in Figure 1.4), $[\text{M}^{\text{e}3\text{Si},\text{Me}}\text{CpMn}(\text{CO})_3]$ (j in Figure 1.4),⁶⁰ or $[(\text{Mn}\{\text{N}(2\text{-Py})(\text{SiMe}_3)_2\}_2)_2]$; k in Figure 1.4]⁶⁷ in the presence of O_2 has been shown to produce thin films composed of both manganese silicate and oxide. Manganese oxide is also commonly observed during deposition of $\text{Mn}(0)$ on silica substrates in the absence of O_2 (*vide infra*).

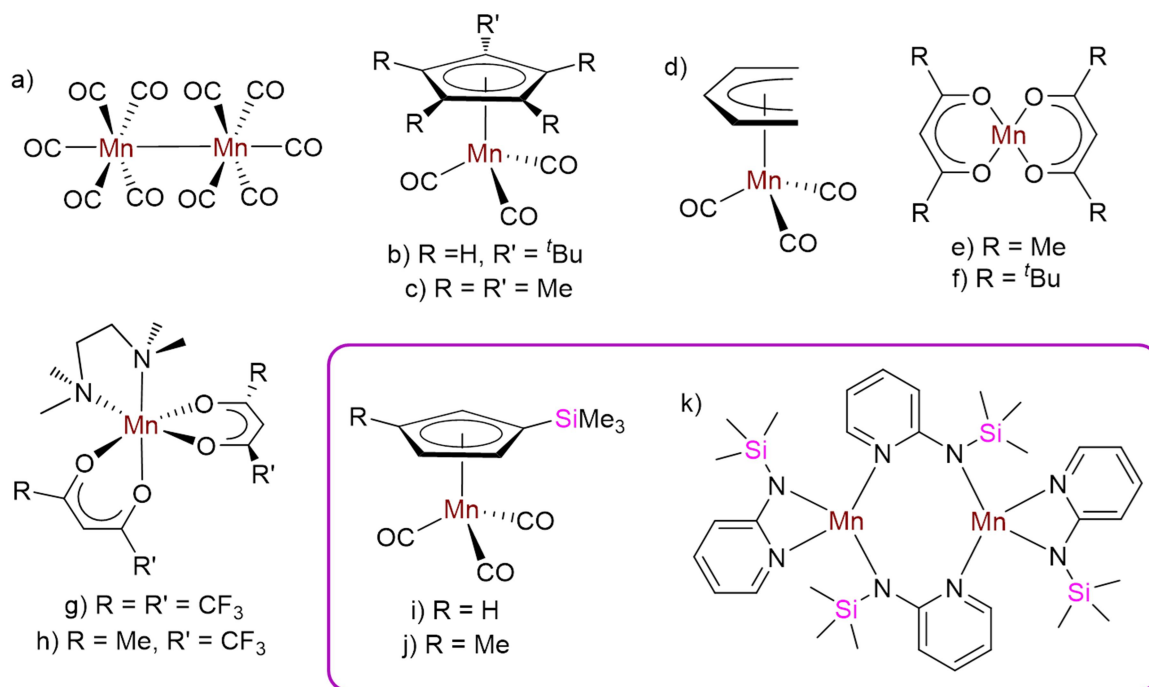


Figure 1.4: Mn-containing precursors used for CVD of manganese oxides (pink box; oxides and silicates) in the presence of oxygen or water.

In 1997, decades after it was used as a source of Mn dopants by CVD (*vide supra*), $[\text{}^{\text{Me}}\text{CpMn}(\text{CO})_3]$ (a in Figure 1.5) was shown to deposit films (in the presence or absence of H_2) of elemental $\text{Mn}_{(\text{s})}$ by CVD.^{68,69} In the last ten years, elemental $\text{Mn}_{(\text{s})}$ has been deposited by CVD using $[\text{Mn}\{(\text{}^t\text{PrN})_2\text{C}^n\text{Bu}\}_2]$ (b in Figure 1.5),⁷⁰ bis[1-(*tert*-butylamide)-2-dimethylaminoethane-*N,N'*]manganese (c in Figure 1.5),⁷¹ or $[\text{}^{\text{Et}}\text{Cp}_2\text{Mn}]$ (d in Figure 1.5),³⁵ in each case in the presence of H_2 (deposition using $[\text{Mn}\{(\text{RN})_2\text{CR}'\}_2]$ was also successful in the absence of H_2).⁶⁹ When deposited on silica, a layer of oxide, silicide, and/or silicate was observed between the substrate and $\text{Mn}_{(\text{s})}$ film, due to diffusion of Mn atoms into the silica; this layer blocked further migration of Mn atoms into the bulk silica.⁶⁹ Attempts to deposit $\text{Mn}_{(\text{s})}$ by CVD using $[\{\text{Mn}(\text{CO})_5\}_2]$ yielded films composed only of oxide, though it is unclear if the oxygen content is residual from the precursor, substrate, or incidental oxidation of $\text{Mn}(0)$.⁷² It is also notable that exposure of $[\text{}^{\text{Et}}\text{Cp}_2\text{Mn}]$ to a silica substrate at temperatures lower than the onset of $\text{Mn}_{(\text{s})}$ CVD ($<500\text{ }^\circ\text{C}$) yielded manganese oxide, potentially due to reactions with the silica

substrate as opposed to decomposition.⁷³ It is worth noting that in 1994, Dossi et al. reported a process which was described as CVD of elemental manganese using $[\{\text{Mn}(\text{CO})_5\}_2]$, but didn't involve decomposition at the solid/vapour interphase. Instead, it involved initial sublimation of intact precursors, which were then heated to cause decomposition (with no Mn-containing vapour remaining). In addition, the presence of $\text{Mn}_{(s)}$ was inferred from H_2 evolution (from the putative reaction of $\text{Mn}(0)$ with residual water), and the films were not directly characterized.⁷⁴

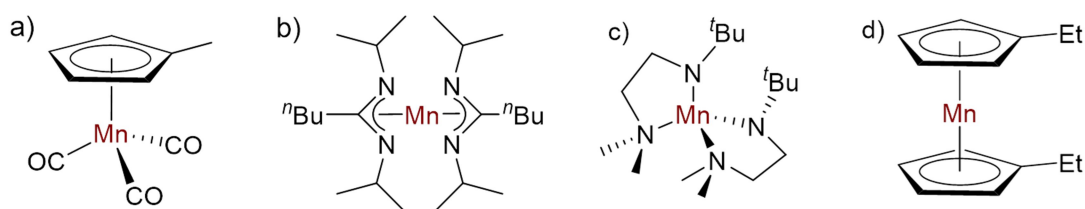


Figure 1.5: Precursors used for CVD of elemental manganese.

1.2.8 – Atomic Layer Deposition (ALD) of Manganese-containing Films

To our knowledge, the first report of ALD of a manganese-containing film was the deposition of manganese oxide from $[\text{Mn}(\text{dpm})_3]$ (a in Figure 1.6) and ozone in 2003 by Kjakshus et al.⁷⁵ Interestingly, different oxides were observed at different temperature ranges; $\text{MnO}_{2(s)}$ for deposition between 140 and 230 °C, with $\text{Mn}_3\text{O}_{4(s)}$ deposition at higher temperatures. Reports on ALD of manganese oxides (of varying stoichiometries) have dominated the literature of Mn-containing films formed from ALD. The majority of these reports involve the same precursor combination as Kjakshus' initial report ($[\text{Mn}(\text{dpm})_3]$ with ozone).^{75,76} Ozone is also used as a co-reactant for ALD of manganese oxide using $[\{\text{Mn}(\text{CO})_5\}_2]$ (b in Figure 1.6)⁷⁷ or $[\text{Mn}^{\text{Me}}\text{CpMn}(\text{CO})_3]$ (c in Figure 1.6).⁷⁸ Manganese oxide ALD has also been reported with water as the co-reactant and either $[(\text{EtCp})_2\text{Mn}]$ (d in Figure 1.6)⁷⁹ or $[\text{Mn}(\text{tBu-MeAMD})_2]$ (e in Figure 1.6)⁸⁰ as the Mn-containing precursor. In addition, Qin and Zaera have reported ALD of manganese oxide using $[\text{Mn}^{\text{Me}}\text{CpMn}(\text{CO})_3]$ (c in Figure 1.6) and N_2O , though with only three ALD cycles.⁸¹ Thin films of polymetallic oxides (where one of the metals is Mn) have also been

deposited by ALD, using cycles of three reagents; (a) a Mn-containing species, (b) another metal-containing precursor, and (c) and oxygen-containing co-reactant. These films include $M'MnO_3$ ($M' = Y,^{82} La, Sm, Tb, Yb, Lu$),⁸³ $(Mn,Co)_3O_4$,⁸⁴ $Li_xMn_2O_4$,⁸⁵ and Ti_xMn_yO .⁸⁶ Mn-containing precursors and oxygen-containing co-reactants used in these reports are the same as those used for manganese oxide deposition.

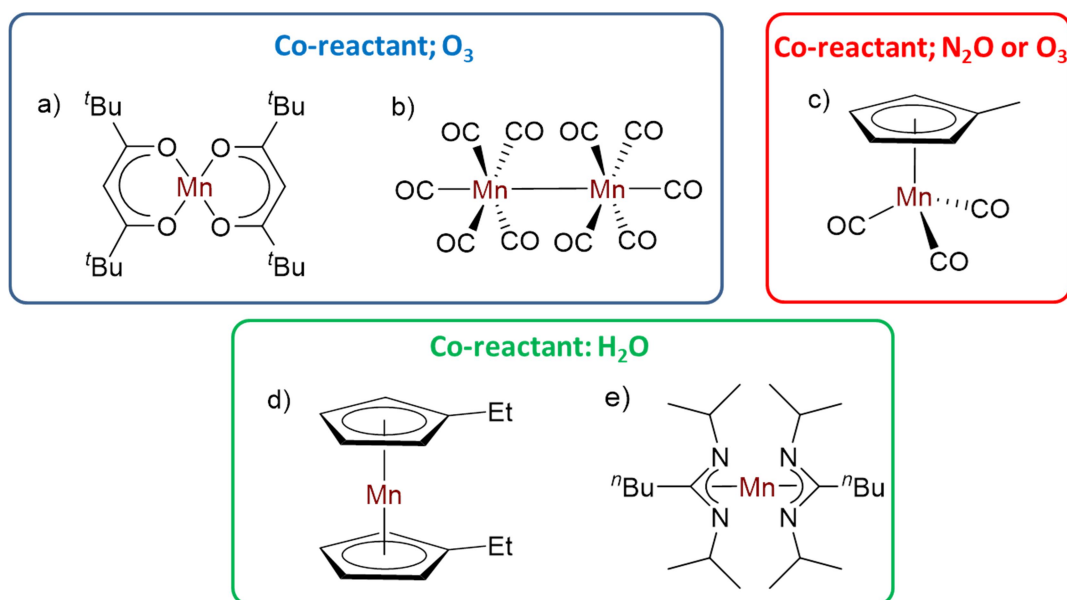


Figure 1.6: Mn-containing reagents used for ALD of manganese oxide.

Only a handful of ALD processes have been reported for manganese-containing films that aren't oxides. For example, in 2014 the Winter group reported deposition of a Mn/Cu alloy using $[Mn_2(tBuNCHC(tBu)(Me)O)_4]$ (a in Figure 1.7) as the Mn-containing precursor, with $[Cu(OCHMeCH_2NMe_2)_2]$ and $BH_3(NHMe_2)$ as co-reactants.⁸⁷ In 2016, Ahvenniemi and Karppinen reported the deposition of a 'hybrid' film with Mn ions separated by rigid organic backbones {using $[Mn(dpm)_3]$ (b in Figure 1.7) as the manganese-containing precursor and terephthalic acid as the co-reactant}.⁸⁸ The same year, the Winter group reported ALD of a manganese borate $\{Mn_3(BO_3)_2\}$ using $[MnTp_2]$ (c in Figure 1.7) and ozone,⁸⁹ and the Georgy group reported ALD of MnF_2 using $[^{Et}Cp_2Mn]$ (d in Figure 1.7) and HF .⁹⁰

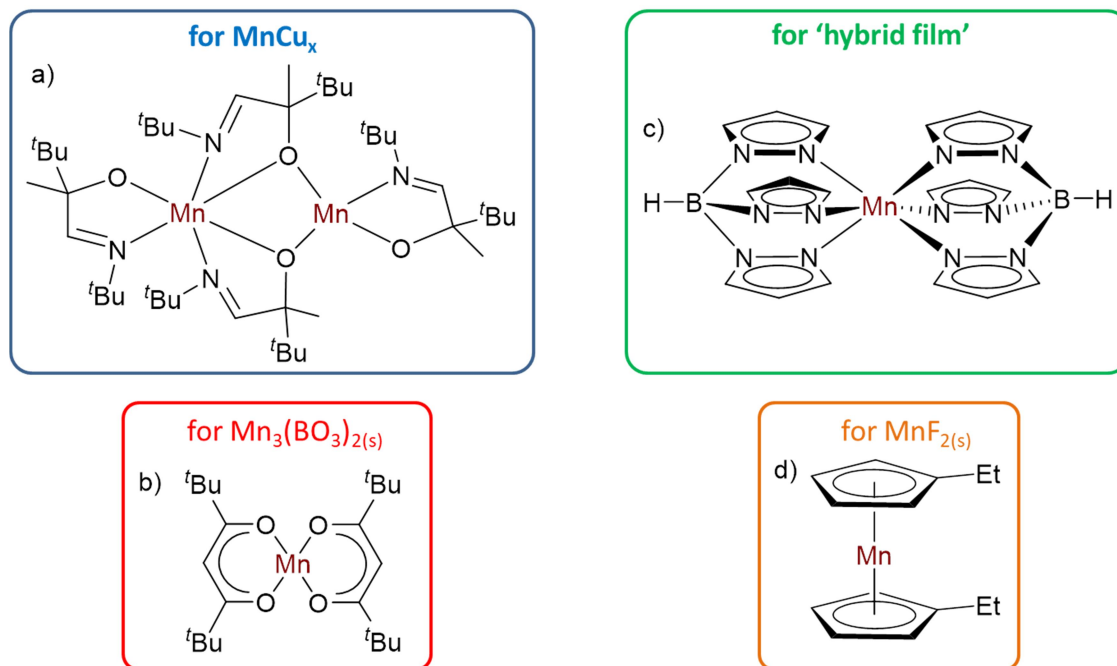
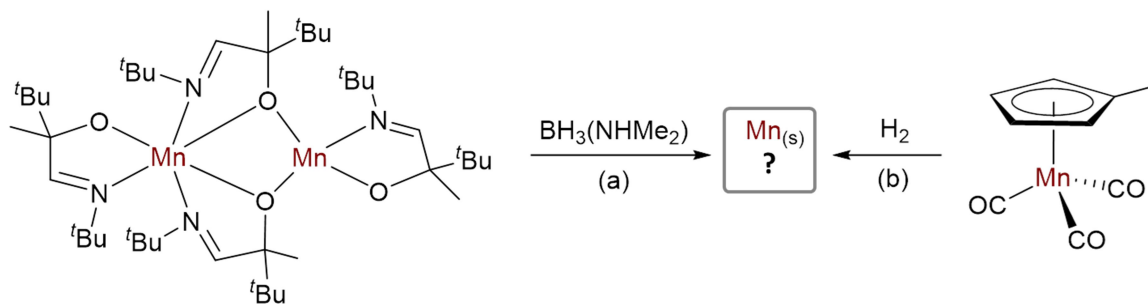


Figure 1.7: Mn-containing precursors used for ALD of Mn-containing thin films (aside from oxides).

No successful methods for $Mn_{(s)}$ ALD have yet been reported. However, the Winter and Zaera groups have reported preliminary results suggesting potential routes for ALD of elemental manganese (Scheme 1.1). First, the Winter group reported ALD using the Mn(II) α -imino alkoxide dimer [$\{Mn(Me^tBuCOCN^tBu)(\mu-Me^tBuCOCN^tBu)\}_2$] as a Mn-containing precursor and $BH_3(NHMe_2)$ as a reducing co-reactant, which produced a manganese oxide film (presumably due to initial deposition of $Mn_{(s)}$ followed by oxidation upon exposure to air).²⁰ However, this deposition was only observed on Ru substrates, and following complete coverage of the substrate, film growth ceased. This was hypothesized to be due to Ru-catalyzed conversion of the borane co-reactant to a more reactive species. Second, the Zaera group conducted an ALD experiment with [$^{Me}CpMn(CO)_3$] and H_2 , though only 3 ALD cycles were carried out and Si/SiO₂ was used as a substrate (which leads to Mn(0) conversion to manganese silicide and manganese oxide; *vide supra*). While this experiment did not afford Mn metal, the

authors suggested that elemental manganese deposition should be possible on an alternative substrate, or using an alternative reducing agent.⁸¹



Scheme 1.1: Potential ALD processes for elemental manganese deposition proposed by the (a) Winter and (b) Zaera groups, based on preliminary results ($\text{Mn}_{(s)}$ was not observed in either case).

1.3 – Manganese Alkyl Complexes

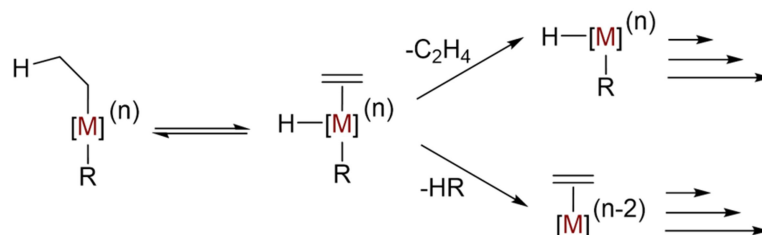
Portions of this section have been reprinted (adapted) with permission from Price, J. S.; Chadha, P.; Emslie, D. J. H. Base-Free and Bisphosphine Ligand Dialkylmanganese(II) Complexes as Precursors for Manganese Metal Deposition, *Organometallics* **2016**, *35*, 168-180. Copyright 2016 American Chemical Society.

1.3.1 – Scope of Section

The aim of this section is to provide an overview of the synthesis and structure of neutral homoleptic base-free dialkylmanganese(II) complexes, and their adducts with Lewis bases. A particular focus is given to adducts of $\text{Mn}(\text{CH}_2\text{EMe}_3)_2$ ($\text{E} = \text{C}, \text{Si}$) and complexes of dmpe. An overview of dialkylmanganese(II) complex reactivity is also provided. Spectroscopic and magnetic characterization of these complexes is beyond the scope of this section. A brief overview is also given of neutral homoleptic polyalkyl manganese complexes of manganese(III) and (IV), and their Lewis base adducts.

1.3.2 – Alkyl Complexes for Transition Metal ALD

Alkyl complexes, which feature the simplest hydrocarbyl ligands, are among the most studied species in organometallic chemistry. Homoleptic alkyl complexes, where all ligands are identical, are of particular interest in that their reactivity is completely dependent on reactions of alkyl ligands. While homoleptic metal alkyl complexes have been known since the discovery of ZnEt_2 in 1849, the development of stable transition metal examples only began in the 1970s with the introduction of bulky ligands which lack β -hydrogen atoms.⁹¹ Employment of such ligands imparts stability by preventing β -hydride elimination (Scheme 1.2), one of the most common decomposition pathways for transition metal alkyl complexes.⁹² Despite the reversibility of this process, the resulting alkene and hydride ligands are prone to further, irreversible reactions. For example, C–H bond-forming reductive elimination from mixed alkyl hydride products is kinetically much more favourable than C–C bond-forming reductive elimination from homoleptic precursors.⁹³



Scheme 1.2: Decomposition pathways via β -hydride elimination from homoleptic transition metal alkyl complexes. For clarity, the simplest β -hydride-containing ligand (Et) is used in place of a generic alkyl ligand.

1.3.3 – Homoleptic Neutral Dialkylmanganese(II) Complexes

The first neutral homoleptic dialkylmanganese(II) complex, MnMe_2 , was reported by Clauss and von Beermann over a half century ago. However, the structure of this compound, which explodes under the influence of shock or friction, remains unknown.⁹⁴ In the 1970s, Wilkinson et al. prepared homoleptic trimethylsilylmethyl ($-\text{CH}_2\text{SiMe}_3$), neopentyl ($-\text{CH}_2\text{CMe}_3$), neophyl ($-\text{CH}_2\text{CMe}_2\text{Ph}$),^{95,96} and 1-adamantylmethyl⁹⁷ manganese(II) complexes, which all displayed much greater thermal stability than MnMe_2 due to increased steric bulk. X-ray crystal structures were reported for the trimethylsilylmethyl and neophyl complexes, which are polymeric and dimeric, respectively (a and c in Figure 1.8).^{96,98} However, only limited structural data, and no CIF files, were reported; X-ray crystal structures of both complexes were later reported by the Mulvey⁹⁹ and Cámpora¹⁰⁰ groups {the original CIF files were later submitted to the CSD as a communication, though the data quality was poor}.¹⁰¹ As well, Wilkinson noted that $\text{Mn}(\text{CH}_2\text{CMe}_3)_2$ is a tetramer in the solid state, citing a personal communication from M. B. Hursthouse and P. Raithby⁹⁸ (the CIF was also later submitted to the CSD as a communication, though the quality is also poor; b in Figure 1.8).¹⁰¹ In addition, gas-phase electron diffraction has determined that $\text{Mn}(\text{CH}_2\text{CMe}_3)_2$ is monomeric in the gas-phase.¹⁰²

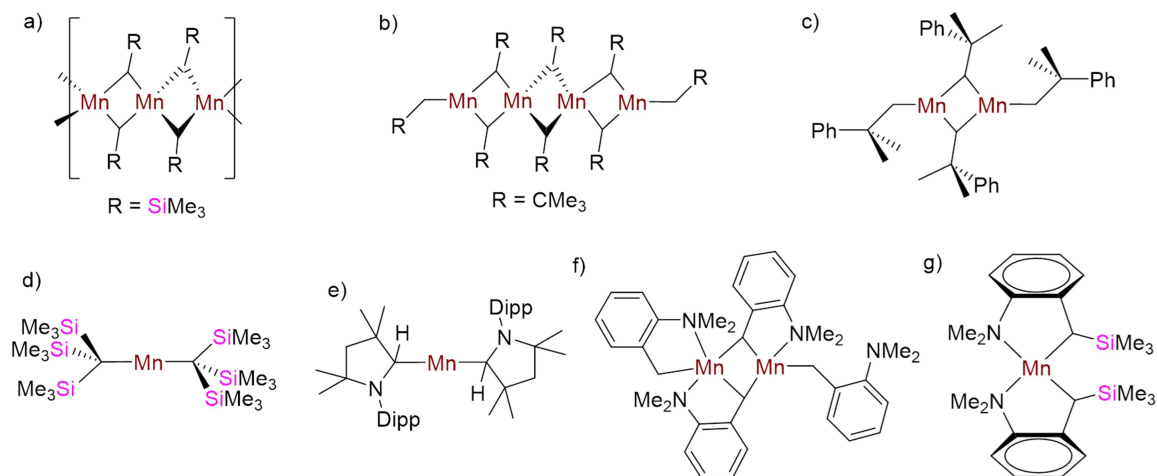


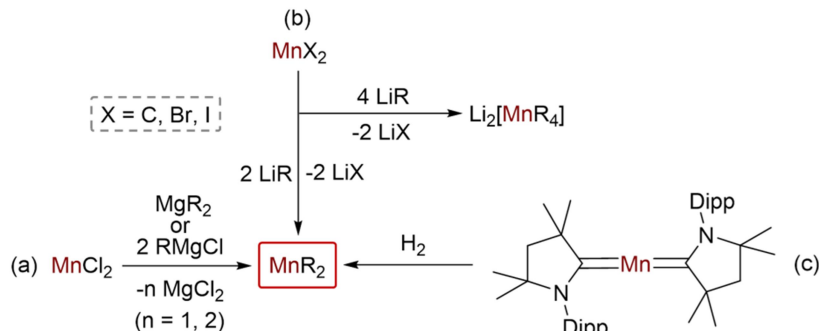
Figure 1.8: Neutral homoleptic dialkylmanganese(II) complexes for which an X-ray crystal structure has been obtained.

More recently, neutral homoleptic dialkylmanganese(II) complexes with tris(trimethylsilyl)methyl¹⁰³ or 2-pyrrolidinyl ligands¹⁰⁴ have also been crystallographically characterized (d and e, respectively, in Figure 1.8), and a gas-phase electron diffraction structure was obtained for $[\text{Mn}\{\text{CH}(\text{SiMe}_3)_2\}_2]$.¹⁰⁵ These three examples (with extremely bulky alkyl groups) are isostructural monomers with *trans* disposed alkyl ligands ($\text{C-Mn-C} = 180^\circ$).^{103,105} Additionally, it should be noted that homoleptic dialkylmanganese(II) complexes with benzyl¹⁰⁰ or $-\text{C}(\text{SiMe}_3)_2(\text{SiMe}_2\text{NMe}_2)$ ¹⁰⁶ ligands have been prepared, but not structurally characterized (though the former was inferred to be polymeric based on low solubility). All stable examples of base-free neutral dialkylmanganese(II) complexes lack β -hydrides, so are not susceptible to the common alkyl decomposition pathway of β -hydride elimination.

Two neutral homoleptic dialkylmanganese(II) complexes with pendent amine groups have also been reported; $[\text{Mn}(o\text{-CH}_2\text{C}_6\text{H}_4\text{NMe}_2)_2]$ (f in Figure 1.8)¹⁰⁷ and $[\text{Mn}(o\text{-CH}(\text{SiMe}_3)\text{C}_6\text{H}_4\text{NMe}_2)_2]$ (g in Figure 1.8).¹⁰⁸ These complexes feature coordination of the pendent amine donors to the metal centres. While the first of these complexes is a dimer in the solid state, with three of the four amine donors coordinated to

the metal centres, the bulkier analogue is monometallic, with coordination of both amine donors to the metal centre.

Many neutral dialkylmanganese(II) complexes were prepared by the reaction of MnCl_2 with Grignard reagents or dialkylmagnesium species (a in Scheme 1.3). By contrast, reactions of MnCl_2 with alkyllithium reagents often resulted in tetraalkylmanganese(II) dianions; several of these have been isolated, even with ligands for which the neutral MnR_2 complexes are unstable.⁹⁶ However, for some very bulky ligands, $\{o\text{-CH}_2\text{C}_6\text{H}_4\text{NMe}_2, o\text{-CH}(\text{SiMe}_3)\text{C}_6\text{H}_4\text{NMe}_2, 1\text{-adamantylmethyl}, \text{-CH}(\text{SiMe}_3)_2, \text{and } \text{-C}(\text{SiMe}_3)_2(\text{SiMe}_2\text{NMe}_2)\}$ neutral MnR_2 species could also be prepared from the reaction of an alkyllithium precursor with MnX_2 ($\text{X} = \text{Cl}, \text{Br}, \text{I}$); presumably steric congestion limits further alkylation (b in Scheme 1.3).^{97,105-108} In addition, one example (e in Figure 1.8) was prepared by the reaction of H_2 with a bis(carbene) complex (c in Scheme 1.3).¹⁰⁴



Scheme 1.3: Synthetic routes for neutral dialkylmanganese(II) complexes.

X-ray crystallography is a mainstay characterization technique in organometallic chemistry, and is commonly used to investigate the structures of dialkylmanganese(II) complexes in the solid state (Table 1.1).^d The monometallic complexes feature Mn–C distances of 2.102(4)-2.136(4) Å. However, the polymetallic examples feature two (polymeric complexes) or three (dimeric complexes) sets of Mn–C distances. For dimeric

^d In the following discussion, the original structures of neophyl, neosilyl, and neopentyl complexes, and $[\text{Mn}(o\text{-CH}_2\text{C}_6\text{H}_4\text{NMe}_2)_2]$, are excluded due to low data quality.

complexes, the shortest Mn–C distance involves the terminal alkyl ligand (2.118(2) Å), and is consistent with the distances observed in monometallic species. The metal centres in polymetallic complexes are bridged by two alkyl ligands, and each metal is involved in one shorter (2.2023(17)-2.255(2) Å) and one longer (2.327(2)-2.4358(17) Å) Mn–C distance, both of which are longer than the Mn–C_{terminal} distance in mono- and di-metallic complexes. Furthermore, short Mn–Mn distances (< 2.9 Å) are observed in the polymetallic species, potentially allowing for metal–metal interactions.

Table 1.1: Selected Mn–Mn and Mn–C distances (Å) for neutral dialkylmanganese(II) complexes obtained by X-ray crystallography (br = bridging, term = terminal). Letters are those in Figure 1.8.

Complex	d(Mn–Mn)	d(Mn–C _{br}) (shorter)	d(Mn–C _{br}) (longer)	d(Mn–C _{term})	Structure	Ref.
a	2.682(2)- 3.149(2)	2.116(6)- 2.265(8)	2.365(7)- 2.480(9)	–	polymer	Wilkinson (1976/2012) ^a
a	2.8874(5)- 2.8897(5)	2.2023(17)- 2.2039(17)	2.4203(17)- 2.4358(17)	–	polymer	Mulvey (2009) ⁹⁹
b	2.706(6)- 2.733(6)	2.21(1)- 2.26(1)	2.34(1)- 2.44(1)	2.10(1)	tetramer	Wilkinson (1976/2012) ^a
c	2.718(3)	2.257(9)	2.331(9)	2.15(1)	dimer	Wilkinson (1976/2012) ^a
c	2.7286(6)	2.255(2)	2.327(2)	2.118(2)	dimer	Cámpora (2010) ¹⁰⁰
d	–	–	–	2.102(4)	monomer	Sullivan (1985) ¹⁰³
e	–	–	–	2.106(2)	monomer	Dittrich (2013) ¹⁰⁴
f	2.810(3)	2.30-2.31	2.30-2.38	2.14-2.18	dimer	Manzer (1977) ¹⁰⁷
g	–	–	–	2.131(4)-2.136(4)	monomer	Liu (2008) ¹⁰⁸

a. Wilkinson first reported these complexes in 1976,⁹⁵ but only provided limited structural data. The CIF was deposited in the Cambridge Structural Database in 2012.¹⁰¹

By contrast, NMR spectroscopy, which is one of the most utilized methods for investigating the structures of organometallic complexes in the solution state, is not normally used for dialkylmanganese(II) complexes, which are paramagnetic (high spin d^5), and therefore produce spectra with extremely broad peaks and widely dispersed chemical shifts.¹⁰⁹ However, given the presence of unpaired electrons, EPR spectroscopy and magnetic measurements are commonly used characterization tools. Additional tools which are sometimes used to characterize dialkylmanganese(II) complexes include IR spectroscopy, photoelectron spectroscopy, and mass spectrometry.

1.3.4 – Lewis Base Adducts of Neutral Dialkylmanganese(II) Complexes

Dialkylmanganese(II) complexes have been coordinated to a wide variety of Lewis bases including PMe_3 ,^{110,111} PEt_3 , PMe_2Ph , PMePh_2 , PCy_3 ,¹¹² dmpe ,^{111,113,114} pyridine,^{99,100} 2,2'-bipyridine (bipy),¹⁰⁰ TMEDA (*N,N,N',N'*-tetramethylethylenediamine),^{95,96} a bidentate diimine ligand {*N,N'*-bis(mesitylmethylene)-1,2-cyclohexanediamine},¹¹⁵ sparteine,¹¹⁶ THF,^{100,114,117} $i\text{-Pr}_2\text{NC(O)CH}_2\text{Ph}$,¹¹⁸ 1,4-dioxane,⁹⁹ and a carbene {1,3-bis(2,6-diisopropylphenyl)imidazole-2-ylidene},¹¹⁹ although many of these complexes have not yet been structurally characterized. Additionally, dialkylmanganese(II) complexes with *o*-phenylenedimethylene {*o*- $\text{C}_6\text{H}_4(\text{CH}_2)_2^{2-}$ },¹¹¹ cyclohexyl, *tert*-butyl,¹²⁰ and methyl^{121,122} groups have been structurally characterized, but only with neutral supporting co-ligands. In general, these adducts are prepared by exposure of base-free dialkylmanganese(II) complexes to free Lewis bases, generation of the base-free dialkylmanganese(II) complexes in the presence of free Lewis bases, or substitution of another neutral ligand in a dialkylmanganese(II) complex.

Given the focus on neopentyl ($-\text{CH}_2\text{CMe}_3$) and neosilyl ($-\text{CH}_2\text{SiMe}_3$) complexes in this work (see Chapter 2), a comprehensive overview of their adducts with Lewis bases is included here. In Wilkinson's report of the first stable dialkylmanganese(II) complexes, it was suggested that Lewis base coordination should break up the oligomeric nature of the base-free complexes (the earliest examples were polymeric, tetrameric, or

dimeric in the solid state; *vide supra*). This has a significant effect on the physical properties; for example, the first reported adduct of $\text{Mn}(\text{CH}_2\text{SiMe}_3)_2$ (with TMEDA) sublimed at a temperature 70 °C lower than the base-free complex and is significantly more soluble in non-coordinating solvents.⁹⁶

Concurrent with the first reports of stable base-free dialkylmanganese(II) complexes (*vide supra*), the Wilkinson group also reported adducts of $\text{Mn}(\text{CH}_2\text{EMe}_3)_2$ (E = C, Si) with monodentate (pyridine) or bidentate (N,N'-dimethylpiperazine or TMEDA) amines.^{95,96} It was observed that these adducts contain either 2 equivalents of a monodentate amine, or 1 equivalent of a bidentate amine. However, no crystal structures were obtained at that time. A few years later, the same group reported adducts of various dialkylmanganese(II) complexes with a series of monodentate phosphines (PR_3 ; $\text{R}_3 = \text{Me}_2\text{Ph}$, MePh_2 , Ph_3 , $(\text{OMe})_3$, $(\text{SiMe}_3)_3$, Cy_3 , Me_3 , Et_3),^{110,112} as well as a bidentate phosphine (dmpe).¹¹¹ In all cases, 1:1 adducts were formed, though EPR studies have shown that in solution, 1:1 PMe_3 adducts are in an equilibrium with a small amount of the 1:2 $\text{MnR}_2\text{:PMe}_3$ adduct, formed by ligand redistribution (addition of excess free phosphine allowed *in-situ* characterization of pure 1:2 adducts).¹¹² While the monodentate phosphine adducts proved to be susceptible to phosphine loss, adducts of bidentate phosphines were significantly more stable under vacuum.¹¹¹

X-ray crystal structures have been obtained for a series of Lewis base adducts of $\text{Mn}(\text{CH}_2\text{SiMe}_3)_2$ (Figure 1.9). In the solid state, the 1:1 adducts of $\text{Mn}(\text{CH}_2\text{SiMe}_3)_2$ with PMe_3 ,¹¹⁰ PMePh_2 ,^{110,112} THF (two isostructural structures have been reported),^{100,117} or pyridine⁹⁹ form dimers with two terminal and two bridging alkyl groups, and one neutral donor located on each metal centre (a-c and f in Figure 1.9). A similar dimetallic core was observed in the adduct containing half an equivalent of 1,4-dioxane per Mn centre (i in Figure 1.9).⁹⁹ In each case, the Mn–Mn distances (2.7715(8)-2.828(1) Å; Table 1.2) are shorter than those in base-free $[\{\text{Mn}(\text{CH}_2\text{SiMe}_3)_2\}_\infty]$ (2.8874(5)-2.8897(5) Å). Furthermore, these polymetallic adducts contain three significantly different Mn–C distances involving each metal; short (2.111(3)-2.128(3) Å) Mn–C_{terminal} distances,

slightly longer (2.193(5)-2.218(3) Å) bridging Mn–C distances, and significantly longer (2.346(2)-2.389(5) Å) bridging Mn–C distances (Table 1.2). Relative to the two sets of bridging Mn–C distances in base-free $[\{\text{Mn}(\text{CH}_2\text{SiMe}_3)_2\}_\infty]$, the shorter set in these adducts is similar (2.2023(17)-2.2039(17) Å), but the longer set is significantly shorter (2.4203(17)-2.4358(17) Å).

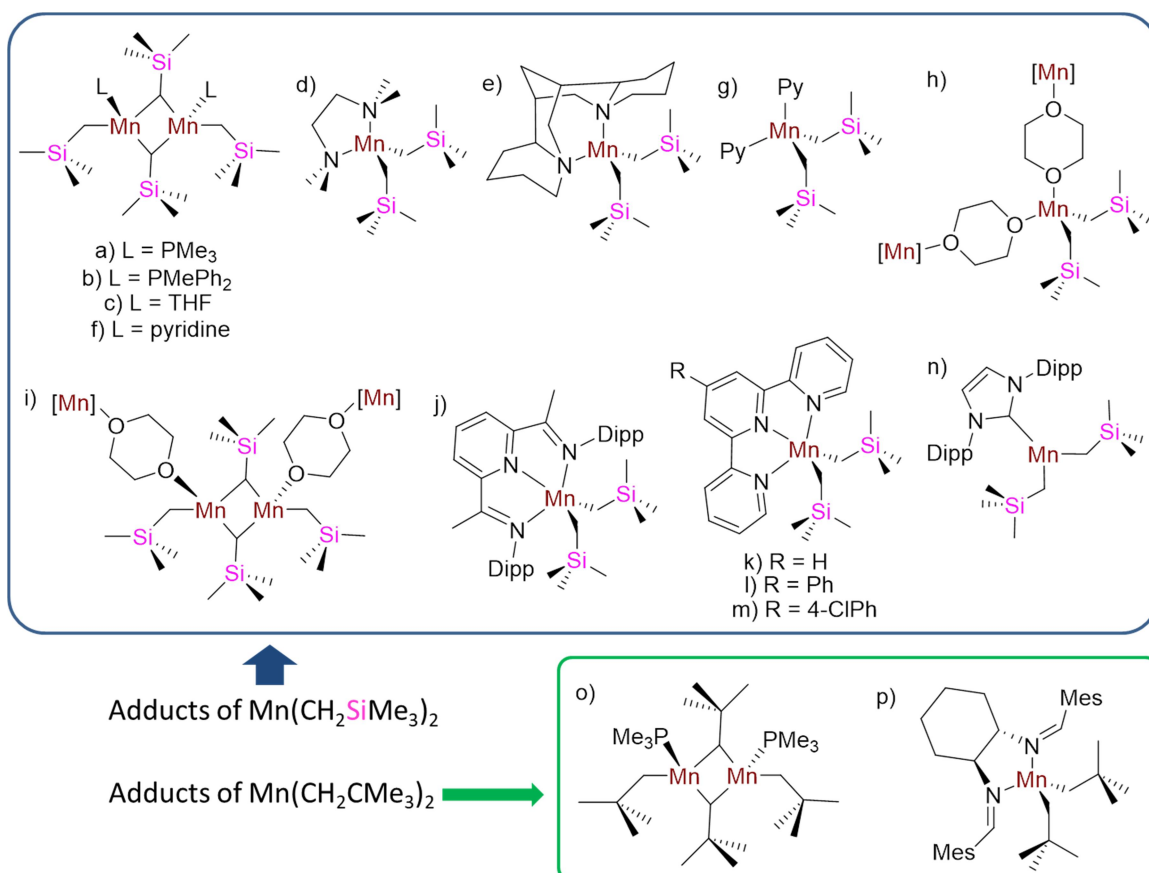


Figure 1.9: Lewis base adducts of $\text{Mn}(\text{CH}_2\text{EMe}_3)_2$ (E = C, Si) for which X-ray crystal structures were obtained.

The other adducts of $\text{Mn}(\text{CH}_2\text{SiMe}_3)_2$ involve monometallic environments at Mn. These include 1:1 adducts with bidentate TMEDA,⁹⁹ sparteine,¹¹⁶ or 1,4-dioxane (in this structure, the two donors are attached to different well-separated Mn atoms) moieties⁹⁹ (d, e, or h in Figure 1.9), and the adduct with two equivalents of pyridine (g in Figure 1.9),¹⁰⁰ which all feature tetrahedral donor coordination at manganese. The 5-coordinate

1:1 adducts with tridentate bis(imine) pyridine¹²³ or tris(pyridine)¹²⁴ moieties (j-m in Figure 1.9) adopted a related edge-capped tetrahedral environment at manganese, with coordination of all three N donors. Finally, a solid-state structure was obtained for an NHC adduct (1,3-bis(2,6-diisopropylphenyl)imidazol-2-ylidene; n in Figure 1.9), which is unique (for complexes in Figure 1.9) in that it yields a 3-coordinate trigonal planar environment at Mn, presumably due to the extreme steric bulk of the neutral donor.¹¹⁹ In all these monometallic structures, the Mn–C distances range from 2.129(1)-2.220(7) Å (Table 1.2); the fact that many of these are longer than the Mn–C_{terminal} distances in dimetallic adducts could be due to the presence of extremely bulky neutral ligands.

In contrast to the neosilyl complexes, only two crystal structures have been obtained for Lewis base adducts of Mn(CH₂CMe₃)₂ (Figure 1.9, Table 1.3). One of these was a PMe₃ adduct (o in Figure 1.9) isostructural to the neosilyl PMe₃ analogue (a in Figure 1.9).¹¹² The Mn–Mn distance in the PMe₃ adduct of Mn(CH₂CMe₃)₂ (2.772(1) Å) is significantly longer than in the neosilyl analogue (2.718(3) Å), due to the reduced steric profile of CH₂SiMe₃ vs. CH₂CMe₃ ligands (resulting from longer C–Si vs. C–C bonds). In addition, an adduct was obtained with a bidentate diimine ligand (p in Figure 1.9), for which the crystal structure revealed a monometallic species.¹¹⁵ The Mn–C bonds in this structure (2.141(6)-2.165(6) Å) are consistent with those observed in monometallic adducts of Mn(CH₂SiMe₃)₂ (*vide supra*).

Table 1.2: Selected distances (Å) for adducts of $\text{Mn}(\text{CH}_2\text{SiMe}_3)_2$ obtained by X-ray crystallography. L indicates the neutral ligand. n_L and n_{Mn} are the number of neutral ligands and metal centres in one molecule. Letters correspond to structures in Figure 1.9.

L (complex)	n_L/n_{Mn}	Mn-Mn	Mn-C _{br1}	Mn-C _{br2}	Mn-C _{term}	Mn-L	Ref.
PMe_3 (a)	2/2	2.772(1)	2.208(3)	2.369(5)	2.111(3)	2.650(1)	Wilkinson (1982) ¹¹⁰
PMePh_2 (b)	2/2	2.828(1)	2.193(5)	2.389(5)	2.117(5)	2.684(1)	Wilkinson (1983) ¹¹²
THF (c) ^a	2/2	2.790(2)	2.214(3)	2.376(3)	2.128(3)	2.188(4)	Gambarotta/ Thompson (2003) ¹¹⁷
THF (c)	2/2	2.7792(11)	2.203(4)	2.352(4)	2.127(4)	2.184(4)	Cámpora (2010) ¹⁰⁰
TMEDA (d)	1/1	–	–	–	2.1379(15)	2.3284(12)	Mulvey (2009) ⁹⁹
Sparteine (e)	1/1	–	–	–	2.158(2)- 2.165(2)	2.297(2)- 2.329(2)	Chirik (2004) ¹¹⁶
Pyridine (f)	2/2	2.7927(5)	2.1991(18)	2.3711(7)	2.124(2)	2.2251(14)	Cámpora (2010) ¹⁰⁰
Pyridine (g)	2/1	–	–	–	2.143(3)- 2.150(4)	2.260(3)- 2.263(3)	Mulvey (2009) ⁹⁹
1,4-dioxane (h)	1:1 ^b	7.296 ^c	–	–	2.1385(12)	2.2611(9)	Mulvey (2009) ⁹⁹
1,4-dioxane (i)	1:2 ^b	2.7715(8)- 2.7747(8), 7.296(1)- 7.297(1) ^c	2.202(2)- 2.218(3)	2.346(2)- 2.365(3)	2.120(3)- 2.126(4)	2.2419(15)- 2.2515(15)	Mulvey (2009) ⁹⁹
Bis(imine)- pyridine (j)	1/1	–	–	–	2.133(2)- 2.169(2)	2.2279(17)- 2.4181(12)	Cámpora (2010) ¹²³
Tris(py) i (k)	1/1	–	–	–	2.172(3)- 2.177(3)	2.279(3)- 2.341(2)	Zhang/Zheng (2016) ¹²⁴
Tris(py) ii (l)	1/1	–	–	–	2.161(3)- 2.220(7)	2.270(2)- 2.318(3)	Zhang/Zheng (2016) ¹²⁴
Tris(py) iii (m)	1/1	–	–	–	2.166(2)- 2.173(2)	2.274(2)- 2.319(2)	Zhang/Zheng (2016) ¹²⁴
IPr (n)	1/1	–	–	–	2.129(1)	2.236(2)	Mulvey/ Robertson (2011) ¹¹⁹

a. Bond metrics in the paper and CIF are slightly different, though within the margin of error; values in Table 1.2 are from the CIF.

b. A ratio is provided because these complexes are polymeric.

c. This range corresponds to Mn centres separated by a bridging ligand, with no Mn–Mn interaction.

Table 1.3: Selected distances (Å) for adducts of $\text{Mn}(\text{CH}_2\text{CMe}_3)_2$ obtained by X-ray crystallography. L indicates the neutral ligand. n_L and n_{Mn} are the number of neutral ligands and metal centres in one molecule. Letters correspond to structures in Figure 1.9.

L (complex)	n_L/n_{Mn}	Mn-Mn	Mn-C _{br1}	Mn-C _{br2}	Mn-C _{term}	Mn-L	Ref.
PMe_3 (o)	2/2	2.718(3)	2.23(2), 2.31(2)	2.44(2), 2.45(2)	2.14(3), 2.19(3)	2.67(1)	Wilkinson (1983) ¹¹²
Diimine (p)	1/1	–	–	–	2.141(6)- 2.165(6)	2.279(4)- 2.344(4)	Copéret (2002) ¹¹⁵

While no bis(phosphine) adducts of $\text{Mn}(\text{CH}_2\text{EMe}_3)_2$ (E = C, Si) have been structurally characterized, X-ray crystal structures have been obtained for dmpe adducts of MnR_2 ($\text{R}_2 = \{o\text{-(CH}_2)_2\text{C}_6\text{H}_4\}$, Cy_2 , or $\{\text{CH}(\text{SiMe}_3)_2\}_2$; Figure 1.10).^{111,114,120} In each case, a different number of dmpe equivalents were observed in the adduct. $[(\text{dmpe})_2\text{Mn}\{o\text{-(CH}_2)_2\text{C}_6\text{H}_4\}]$ (a in Figure 1.10) is a monomer with two chelating dmpe ligands; the ability of Mn to assume an octahedral environment is presumably due to the small steric footprint of the single chelating dialkyl ligand ($\text{C-Mn-C} = 84.7(2)^\circ$).¹¹¹ By contrast, $[\{\text{Mn}(\text{Cy})(\mu\text{-Cy})\}_2(\mu\text{-dmpe})]$ (b in Figure 1.10), contains half an equivalent of dmpe per metal centre, and a structure similar to dimetallic monodentate phosphine complexes (a-b in Figure 1.9), but where the two P donors are tethered together by an ethylene bridge.¹²⁰ The final example, $[(\text{dmpe})\text{Mn}\{\text{CH}(\text{SiMe}_3)_2\}_2]$ (c in Figure 1.10), is a 1:1 adduct where the environment about Mn is distorted tetrahedral, and a very obtuse C-Mn-C angle of $141.4(7)^\circ$ is presumably due to the presence of extremely bulky alkyl ligands.¹¹⁴

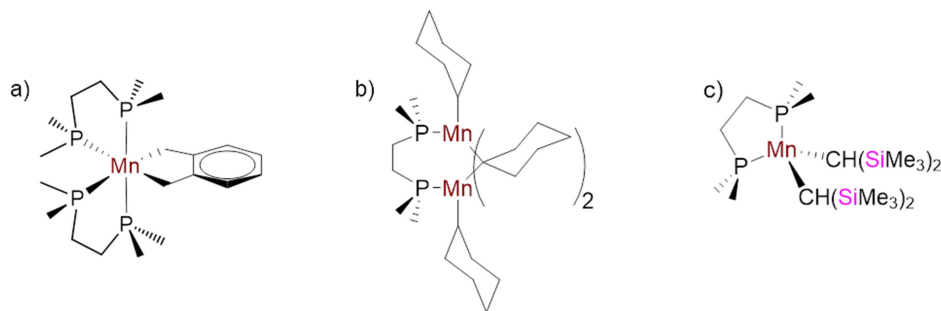


Figure 1.10: Structurally characterized dmpe adducts of neutral MnR_2 complexes.

While allyl ligands normally interact in an η^3 -fashion, η^1 -coordinated allyl ligands can be considered as alkyl groups with a pendent alkene moiety.⁹³ In 2012, the Hanusa group reported the synthesis and X-ray crystal structures for a pair of Lewis base adducts of neutral bis(η^1 -allyl)manganese(II) complexes where the hydrocarbyl substituents are, like alkyl ligands, σ -donors; [(TMEDA)Mn{C(H)(SiMe₃)C(H)=C(SiMe₃)₂}₂] and [(THF)₂Mn{C(H)(SiMe₃)C(H)=C(H)(SiMe₃)₂}₂] (a and b, respectively, in Figure 1.11).¹²⁵ Both adducts are monomers with a tetrahedral environment at Mn, and feature Mn–C distances (2.174(2)-2.189(3) Å) similar to those of monometallic neutral dialkylmanganese(II) adducts listed in Tables 1.2-1.3 (2.129(1)-2.220(7) Å).

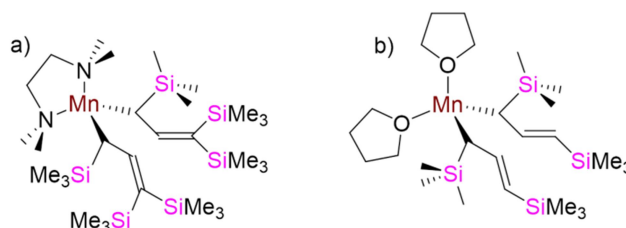


Figure 1.11: Structurally characterized neutral bis(η^1 -allyl)manganese(II) complexes.

1.3.5 – Selected Reactions of Neutral Dialkylmanganese(II) Complexes (Homoleptic and Lewis Base Adducts)

Dialkylmanganese(II) complexes are prone to decomposition, even in the absence of β -hydrides. As well, they are highly air- and moisture sensitive. In some cases, the products of thermal decomposition or exposure to H₂O or O₂ have been identified. For example, dineophylmanganese(II) decomposes via *C_{ortho}*-H bond oxidative addition (followed by *C_α*-H bond-forming reductive elimination involving an intact alkyl ligand).⁹⁶ Wilkinson suggested that exposure of dialkylmanganese(II) complexes to small amount of O₂ results in oxidation to neutral tetraalkylmanganese(IV) complexes.⁹⁶ However, an excess of O₂ yields insoluble manganese oxides.¹¹² Cámpora et al. has reported the products of the reaction of a 1:1 bipy adduct of Mn(CH₂SiMe₃)₂ (which was not structurally characterized) with a quarter equivalent of oxygen to form a tetrametallic

mixed valence manganese(II/III) complex with two oxo ligands, each bridging between three Mn atoms (two with two alkyl groups, and two with one alkyl group and bipy).¹⁰⁰

Surprisingly, exposure of the phosphine adducts [$\{(Me_3P)Mn(CH_2SiEMe_3)_2\}_2$] (E = C, Si) to dihydrogen did not result in any reaction at room temperature.¹¹² However, proton sources such as alcohols and pyrroles have been shown to cleanly protonate off alkyl groups from dialkylmanganese(II) complexes, with concurrent installation of new anionic ligands.^{114,117} As well, alkyl ligands have been shown to be prone to 1,2-insertion across the C=N bonds in imine¹¹⁵ or isocyanide¹²⁶ adducts of dineopentylmanganese(II). Furthermore, a series of tris(pyridine) adducts of $Mn(CH_2SiMe_3)_2$ have displayed activity towards catalytic hydroboration, presumably via initial σ -bond metathesis (or oxidative addition followed by reductive elimination) to form a manganese(II) hydride or boryl complex.¹²⁴

1.3.6 – Homoleptic Neutral Tri- and Tetra- Alkylmanganese Complexes and their Lewis Base Adducts

While the majority of reported neutral homoleptic alkylmanganese complexes are divalent, a small number of stable tetraalkylmanganese(IV) analogues have also been prepared. In 1972, Bower and Tennent reported $Mn(1\text{-norbornyl})_4$ (a in Figure 1.12),¹²⁷ which is stable to β -hydride elimination because, as Bredt's rule states, generation of double bonds at the bridgehead position of a small ring system is disfavoured.¹²⁸ This complex is prepared from the reaction of $MnCl_2$ and excess alkylolithium, and presumably involves disproportionation of a transient dialkylmanganese(II) species. Then, in 1983, Wilkinson et al. reported the stable base-free tetraalkylmanganese(IV) complexes $[MnR_4]$ (R = CH_2SiMe_3 , CH_2CMe_3) (b-c in Figure 1.12) and phosphine adducts of $[MnMe_4]$ (d-e in Figure 1.12) via disproportionation of a transient Mn(III) intermediate; an X-ray crystal structure was obtained for the dmpe adduct revealing octahedral coordination of the four alkyl and two phosphine donors.¹²⁹

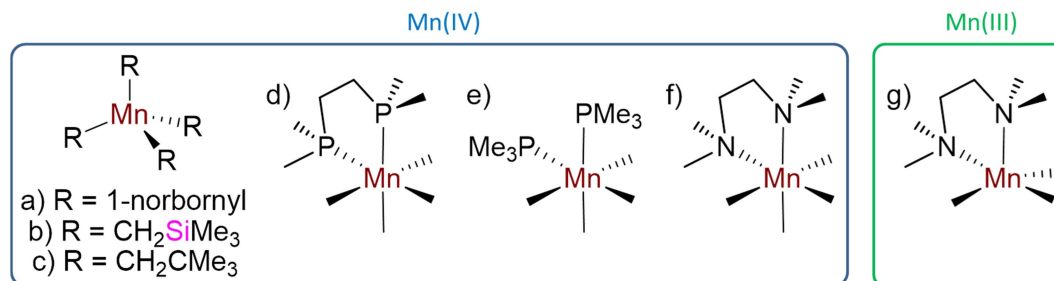


Figure 1.12: Reported neutral homoleptic tri- and tetra- alkylmanganese complexes.

The Marks group has recently reported an X-ray crystal structure of [(TMEDA)MnMe₃] (g in Figure 1.12), the single known Lewis base adduct of a neutral homoleptic trialkylmanganese(III) complex.¹²² However, this complex was unstable and underwent spontaneous disproportionation to Mn(II) and Mn(IV) complexes over hours (in solution) or days (in the solid state). The resulting TMEDA adduct of MnMe₄ (f in Figure 1.12) was unstable, but was characterized by Evans magnetic measurements.

1.4 – Manganese Hydride Complexes

1.4.1 – Scope of Section

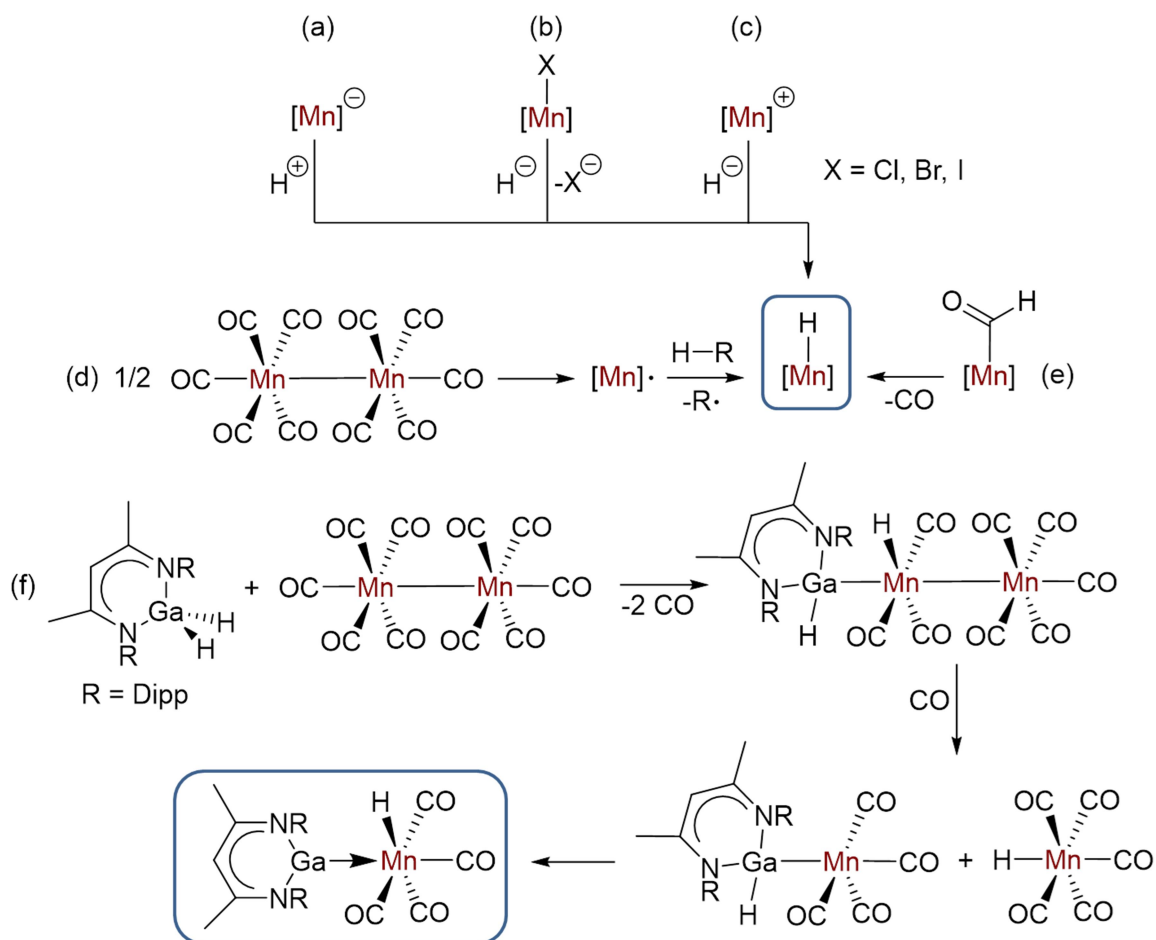
The aim of this section is to provide an overview of the synthesis, structure, characterization, and reactivity of manganese hydride complexes, and σ -H₂ complexes of manganese are also discussed. Given the vast size of this field, this review is not comprehensive. While many bi- and tri- metallic complexes have been reported with bridging hydrides, this review will cover *only* complexes with terminal hydride ligands. As well, manganese hydride complexes with silyl, silylene, or silene co-ligands are covered separately in sections 1.5, 1.6, and 1.7, respectively, and Mn(I) borohydride complexes are discussed in Chapter 3. Complexes where the hydride interacts with co-ligands (for example, boryl groups) are also beyond the scope of this section.

1.4.2 – Manganese(I) Hydride Carbonyl Complexes

While the earliest reports on manganese hydrides involved ill-defined homoleptic species,¹³⁰ the first stable molecular manganese hydride complex, [(OC)₅MnH] (synthesized by protonation of the [(OC)₅Mn]⁻ anion), was reported by Hieber and Wagner in 1957.¹³¹ Though initial characterization was limited, subsequent X-ray and neutron crystal structures determined that this species features an octahedral environment with the hydride ligand occupying one of the six coordination sites.^{132,133} Over the past half century, the chemistry of manganese hydride complexes has been dominated by complexes which, like [(OC)₅MnH], are (a) monovalent, (b) octahedral at the metal centre, (c) feature carbonyl co-ligands, and (d) neutral. Structurally characterized examples of these complexes feature a wide variety of co-ligands, including monodentate phosphines,¹³⁴⁻¹³⁷ bidentate bis(phosphine) ligands,¹³⁸⁻¹⁴⁴ isonitriles,¹⁴⁵ a Ga carbenoid,¹⁴⁶ a bidentate P-C_{NHC} ligand,¹⁴⁷ tridentate neutral P-N-P pincer ligands,¹⁴⁸⁻¹⁵¹ a tridentate neutral P-N-N pincer ligand,¹⁵² and η^6 -hexamethylbenzene.^{153,154} To date, all CO-containing manganese hydride complexes to be structurally characterized (either neutral or ionic) have been monovalent.

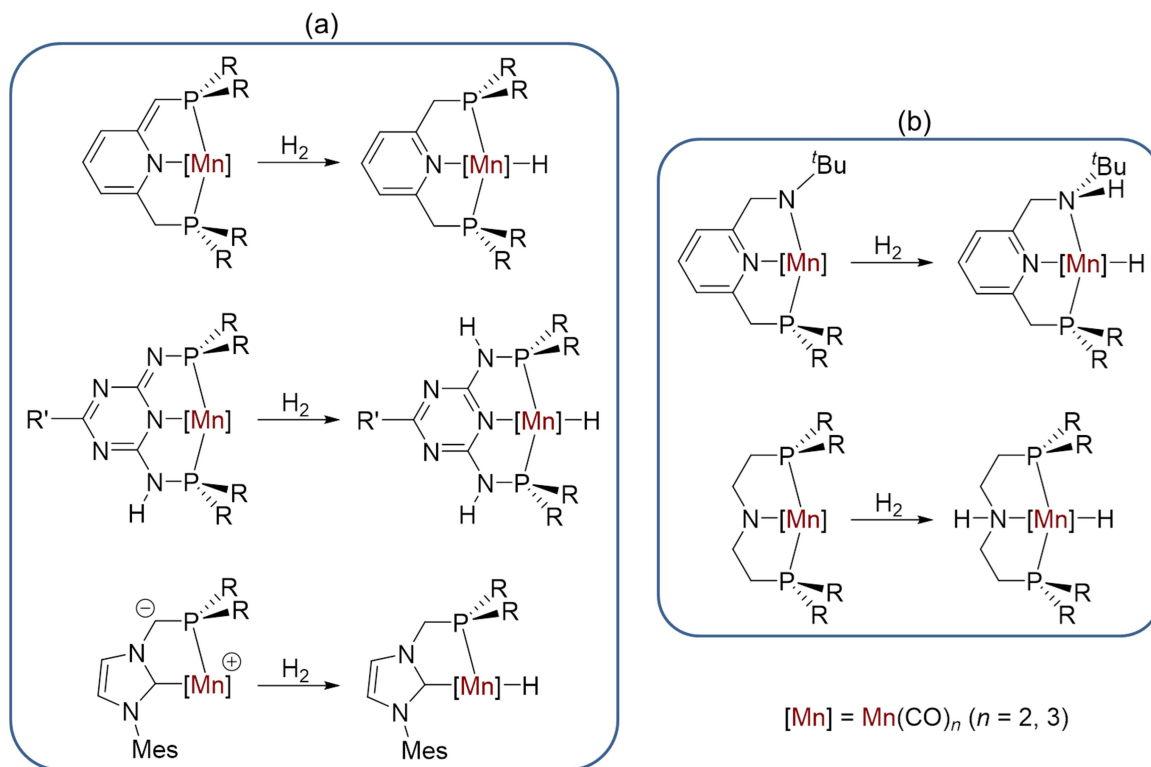
Ph.D. Thesis — Jeffrey S. Price; McMaster University – Chemistry

Many Mn(I) carbonyl complexes have been prepared in a similar manner to $[(OC)_5MnH]$ (exposure of the conjugate base to an acid; a in Scheme 1.4).^{145,155} Other pathways include addition of a hydride (e.g. NaH, LiAlH₄, or NaBEt₃H) to a Mn(I) halide complex (b in Scheme 1.4)^{141,149,153} or Mn(I) cation (c in Scheme 1.4),¹⁴² homolysis of $[{Mn(CO)_5}]_2$ in the presence of a source of hydrogen atoms (d in Scheme 1.4; the hydrogen source is sometimes the solvent),^{135,138,156-158} and thermal decomposition of a Mn formyl complex (e in Scheme 1.4; the eliminated CO ligand may be incorporated into the resulting manganese hydride complex).¹³⁷ As well, α -hydride elimination from a gallyl ligand has been observed to yield a manganese hydride with a gallylene ligand (f in Scheme 1.4).¹⁴⁶ Of course, manganese hydride complexes can also be prepared by manipulation of other manganese hydride complexes (where the hydride ligand is not directly involved in the reactions). Examples of this include co-ligand substitution¹⁴⁰ and deprotonation of a co-ligand.¹⁴³



Scheme 1.4: Selected synthetic pathways (not involving H_2 as a reagent) for the preparation of Mn(I) hydride carbonyl complexes.

Additional synthetic pathways for forming Mn(I) hydride complexes with carbonyl co-ligands involve H_2 addition to complexes with multidentate ligands (Scheme 1.5). These reactions involve protonation either at a site on the multidentate ligand distant from the metal centre (a in Scheme 1.5; these reactions were often driven by aromatization within the multidentate ligand)^{144,147,148} or at an amido anion to generate an amine donor (b in Scheme 1.5).^{152,159} In some cases, primary alcohols substituted for H_2 as the hydride source (with production of an aldehyde byproduct).



Scheme 1.5: Synthesis of CO-containing manganese(I) hydride complexes using H₂.

In 2004, McGrady et al. reported an X-ray crystal structure of [^{M_e}Cp(OC)₂MnH][−], which is (to date) the only example of an anionic Mn(I) hydride complex to have been structurally characterized in the solid state¹⁶⁰ (this complex was first observed spectroscopically a decade earlier by Schubert,¹⁶¹ and a very similar complex, [Cp(OC)₂MnH][−], was isolated by Cooper et al. as early as 1988).¹⁶² As well, X-ray crystal structures have been reported for a pair of cationic Mn(I) hydride complexes prepared by heterolytic H₂ cleavage; these complexes are octahedral with two bis(phosphine) ligands (one of which contains a pendent ammonium group) forming an equatorial plane, and *trans*-disposed carbonyl and hydride ligands..^{143,163}

1.4.3 – CO-Free Manganese Hydride Complexes

The first CO-free manganese complex to be reported was [(F₃P)₅MnH] (a in Figure 1.13) in 1968, which is electronically similar to [(OC)₅MnH]¹⁶⁴ (subsequent

reports provided detailed spectroscopic analysis for this complex).¹⁶⁵ In 1970, Das and Rao reported a series of anionic Mn(IV) complexes with halide and pyridine-based ligands, though with limited characterization (b in Figure 1.13).¹⁶⁶ Starting in the 1980s, a series of examples featuring monodentate phosphine co-ligands were reported; [^{Me}Cp(ON)(PPh₃)MnH] (c in Figure 1.13),¹⁶⁷ [(Me₃P)₂MnH(η⁶-C₆H₆)] (d in Figure 1.13),¹⁶⁸ and [(R₃P)₂(ON)₂MnH] (e in Figure 1.13; an X-ray crystal structure was obtained for R = Me).^{169,170} As well, in 2004 Roddick et al. observed the Mn(III) dihydride complex [Cp(dfepc)MnH₂] (f in Figure 1.13) in an equilibrium with the σ-dihydrogen species.¹⁷¹

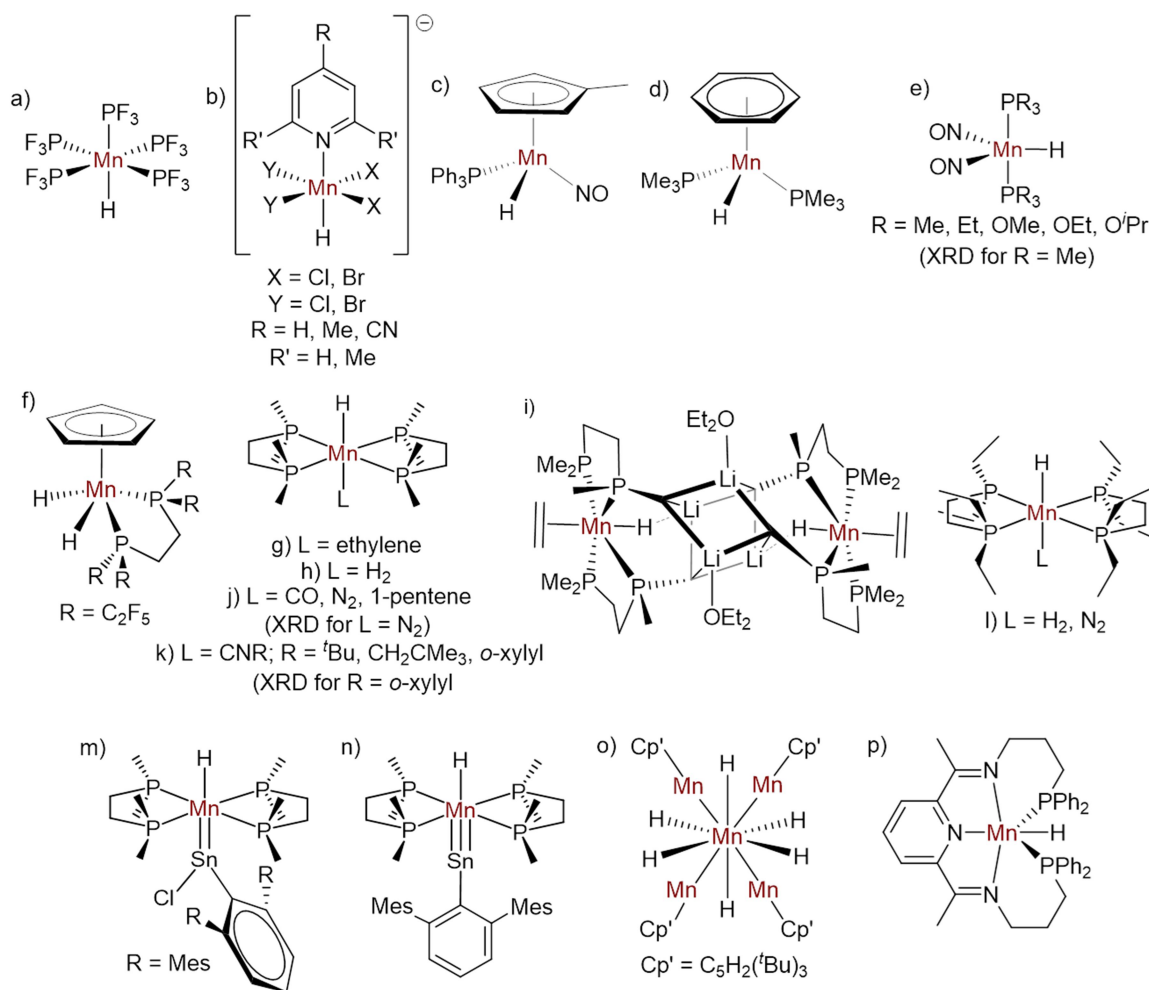


Figure 1.13: CO-free terminal manganese hydride complexes.

In the early 1980s, Girolami and Wilkinson reported the synthesis of a pair of dmpe Mn(I) complexes; [(dmpe)₂MnHL] (L = ethylene, H₂; g and h in Figure 1.13).^{120,172} Lithiation of the ethylene complex resulted in abstraction of hydrogen atoms on the bis(phosphine) co-ligands to form [{(Me₂PCH₂CH₂PMeCH₂)₂MnH(C₂H₄)}₂Li₄(OEt)₂] (i in Figure 1.14), which was the first CO-free manganese hydride complex to be structurally characterized.¹²⁰ In 1992, the Jones group investigated the reactions of Wilkinson's [(dmpe)₂MnH(H₂)] with a variety of nucleophiles (CO, N₂, ethylene, 1-pentene and isonitriles), and observed substitution of the dihydrogen ligand in each case (g, j, and k in Figure 1.13); crystal structures were obtained for the *o*-xylyl isonitrile and η¹-dinitrogen analogues.¹⁷³ To provide additional insight into the bonding environment of the H₂ and N₂ adducts, Jones also prepared the depe analogues [(depe)₂MnHL] (L = H₂, N₂; l in Figure 1.13).¹⁷³ More recently, H₂ substitution from [(dmpe)₂MnH(H₂)] has also been employed in the synthesis of the chlorostannylidene-hydride complex [(dmpe)₂MnH{=SnCl(2,6-Mes₂C₆H₃)}], and abstraction of the halide produced the stannylidyne-hydride anion [(dmpe)₂MnH{≡Sn(2,6-Mes₂C₆H₃)}]⁻; X-ray crystal structures were reported for both complexes (m and n, respectively, in Figure 1.13).¹⁷⁴ Only a couple of additional carbonyl-free Mn complexes with terminal hydride ligands have been structurally characterized; in 2012, a Mn cluster containing a MnH₆ core (o in Figure 1.13) was reported by Neese and Walter et al.,¹⁷⁵ and in 2017, Baik and Trovitch et al. reported the crystal structure of a Mn(I) hydride complex with a pentadentate P–N–N–N–P ligand (p in Figure 1.13).¹⁷⁶

Seven synthetic pathways have been used to prepare the complexes outlined in Figure 1.13. Most commonly, CO-free manganese hydride complexes were prepared by the reaction of other manganese hydride complexes, where the hydride ligand was not directly involved in the reactions {used for the synthesis of a, g, i, j, k, l (where L = N₂), m, and n in Figure 1.13}. Other pathways involve i) protonation (by a solvent) of a transient Mn(IV) complex generated by halogenation of pyridine-based adducts of Mn(II) dihalides (used for the synthesis of b in Figure 1.13), ii) exposure of a manganese halide to a hydride-source (used for the syntheses of c, e, o, and p in Figure 1.13), iii) co-

condensation of elemental manganese with benzene and phosphines (used for the synthesis of d in Figure 1.13; the source of the hydride atom is unclear), iv) substitution of a neutral ligand with H₂ followed by oxidative addition of the H–H bond across the metal centre (used for the synthesis of f in Figure 1.13), v) β-hydride elimination from a transient manganese ethyl complex (used for the synthesis of g in Figure 1.13), and vi) reaction of a Mn(I) aluminate complex with water {used for the syntheses of h and l (where L = H₂) in Figure 1.13},

1.4.4 – Selected Characterization Methods for Manganese Hydride Complexes

Given that carbonyl groups are common co-ligands in manganese hydride complexes (*vide supra*), IR spectroscopy is commonly utilized to measure C≡O frequencies (which provides insight about the electronic environment at the metal centre). In complexes with nitrosyl co-ligands, the N=O stretch in the IR spectrum is also normally reported. Notably, the M–H stretch is not normally reported.

The majority of manganese hydride complexes, unlike homoleptic alkyl complexes (see section 1.3), are diamagnetic. Mn(I) is d⁶, so a low-spin octahedral structure (most manganese hydride complexes are monovalent and octahedral; *vide supra*) would have only paired d electrons. Because of this, NMR spectroscopy is generally used to characterize these complexes. The hydride ligand gives rise to a diagnostically low frequency (negative) signal in ¹H NMR spectroscopy, providing a key handle for characterizing such complexes.¹⁷⁷ Furthermore, many hydride complexes feature phosphine co-ligands, so ³¹P NMR spectroscopy is a common characterization tool (³¹P is 100% naturally abundant and has a spin of ½). It is notable that NMR signals for spin ½ nuclei (e.g. ¹H or ³¹P) close to a quadrupolar metal centre may be broadened due to very short T₂ relaxation times. However, for octahedral manganese complexes (⁵⁵Mn = 100% abundance, I = 5/2, Q = 4.0×10⁻²⁹ m²), substantial signal broadening is not typically observed, presumably due to a small electric field gradient at the metal nucleus.¹⁰⁹

Like most organometallic species, analysis of the solid state structure is of great interest in that it provides an unambiguous description of the bonding environment. However, X-ray crystallography suffers from some limitations in the analysis of hydride complexes. Specifically, given the low electron density around a hydride ligand, the hydrogen atoms are often not located, and when they are located the M–H distances are inaccurate. It is important to note that even when the hydride ligand is not directly located from the difference map, its location can often be inferred from the arrangement of co-ligands on the metal centre. To get around these problems, neutron crystal structures are sometimes obtained, where hydrogen atoms could be accurately located.¹⁷⁸ However, use of neutron crystallography is often limited by expense, access, and requirement for large crystal sizes. Neutron structures have been obtained for $[(OC)_5MnH]$ ¹³³ and $[(OC)_4(Ph_3P)MnH]$,¹⁷⁹ and reveal Mn–H distances of 1.573(2)-1.601(16) Å.

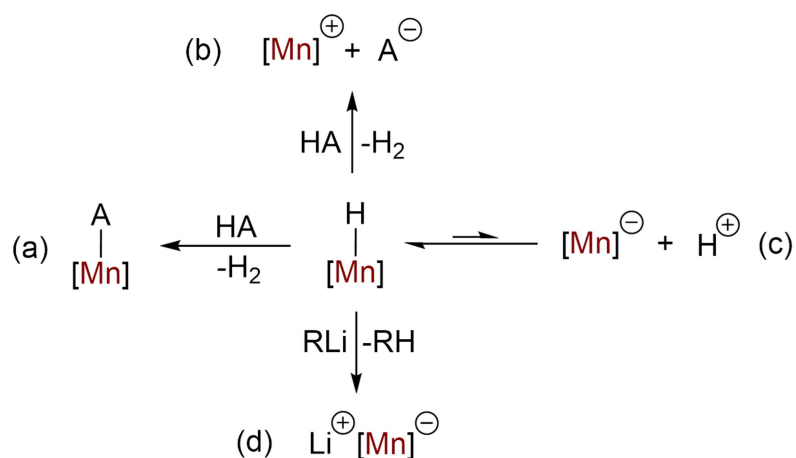
1.4.5 – Selected Stoichiometric Reactions of Manganese Hydride Complexes

A vast number of reactions of manganese hydride complexes have been reported, so a complete list of their reactions is beyond the scope of this review. However, we will briefly provide an overview of some key classes of reported stoichiometric reactions (focusing only on those for which the hydride ligand is directly involved).^e Reactions where such species are implicated in catalytic cycles have been reported, including dehydrogenative coupling of alcohols with amines,¹⁴⁸ and hydrogenation of CO₂.¹⁵⁰ However, further discussion of catalytic reactions is beyond the scope of this review.

Many manganese hydride reactions can be described in terms of acid/base chemistry. Most transition metal ‘hydride’ complexes are amphoteric, where the *MH* moiety could act either as a acid (proton) or base (hydride).¹⁸⁰ Neutral manganese hydride complexes react with weak acids to produce H₂, and the resulting Mn-containing species either obtains a new anionic ligand or becomes cationic (a and b, respectively, in Scheme 1.6). Examples the former are the reaction of $[(OC)_5MnH]$ with CF₃SO₃H to yield $[(OC)_5Mn(O_3SCF_3)]$,¹⁸¹ and the reactions of $[(Et_3P)_2(ON)_2MnH]$ with alcohols to form

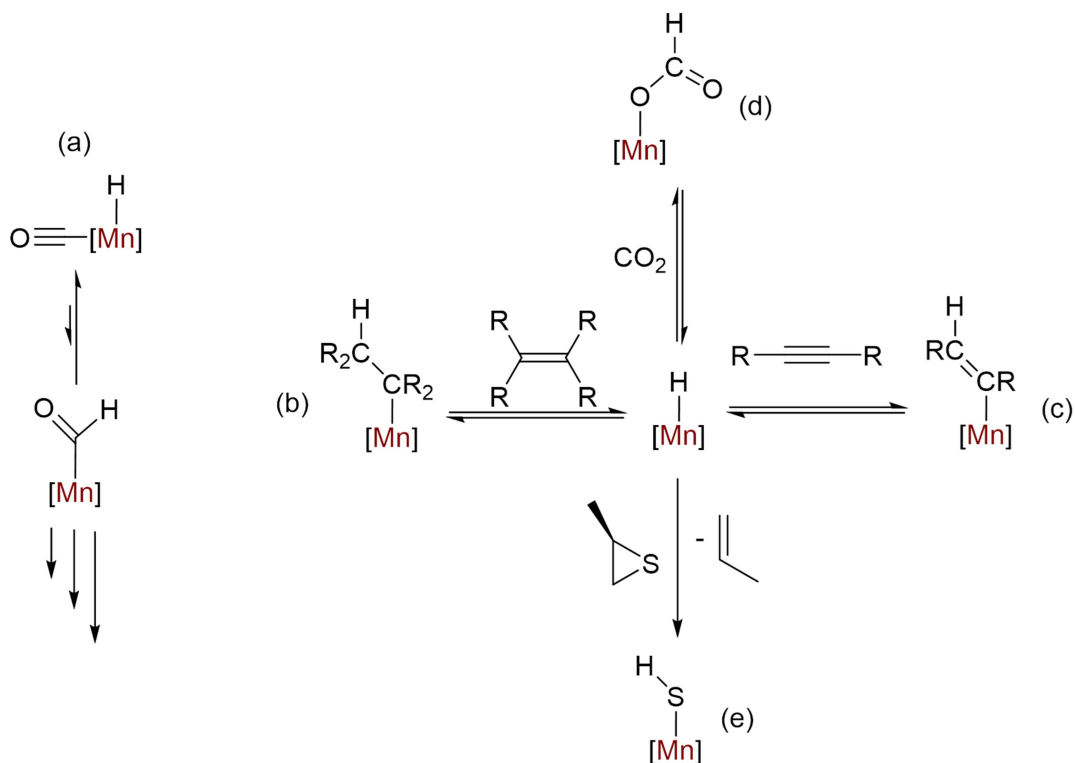
^e References in section 1.4.5 provide examples for each reaction.

$[(Et_3P)_2(ON)_2Mn(OR)]$.¹⁷⁰ An example of the latter is the reaction of $[(OC)_3(R_3P)_2MnH]$ with HPF_6 in acetonitrile (to generate $[(OC)_3(R_3P)_2Mn(NCMe)][PF_6]$ with concomitant H_2 elimination).¹⁵⁷ Manganese hydride complexes have been observed to act as weak Brønsted-Lowry acids (c in Scheme 1.6). For example, $[(OC)_5MnH]$ has a pK_a of 7.1 in water¹⁸² or 15.1 in acetonitrile.¹⁸³ In fact, exposure of Mn(I) hydride complexes to alkyllithium reagents can abstract the hydride ligand as a proton (forming a Mn-containing anion and an alkane byproduct; d in Scheme 1.6).¹⁸⁴



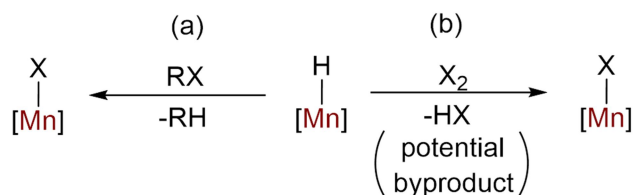
Scheme 1.6: Acid/base reactivity of manganese hydride complexes.

Much of the chemistry involving hydride ligands involves insertion into the Mn–H bond to yield new anionic σ -donor ligands. For example, many reactions of carbonyl-containing manganese hydride complexes proceed by initial 1,1-insertion of CO into the Mn–H ligand to form a transient formyl intermediate (a in Scheme 1.7).¹⁸⁵ As well, 1,2-insertion reactivity has been observed between manganese hydride complexes and alkenes (to generate alkyl complexes¹⁸⁶ or result in H/D exchange with deuterated alkenes,¹⁸⁷ via irreversible or reversible 1,2-insertion of an alkene into the Mn–H bond, respectively), alkynes,¹⁷⁰ or CO_2 (b-d in Scheme 1.7).^{150,152,170} Insertion of heteroatoms such as S (from a propylene sulfide reagent) into the Mn–H bond has also been observed (e in Scheme 1.7).¹⁸⁸



Scheme 1.7: Insertion reactivity of manganese hydride complexes.

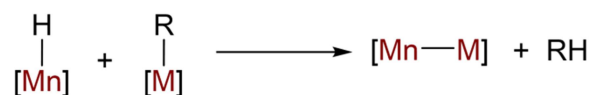
Another set of reactions observed in manganese hydride complexes involve hydrogen/halogen exchange. For example, $[(OC)_{5-n}(R_3P)_nMnH]$ ($n = 0, 1$) reacts with CCl_4 or $XP(CF_3)_2$ ($X = Cl, Br, \text{ or } I$) to form $[(OC)_5MnX]$ and $CHCl_3$ or $HP(CF_3)_2$ (a in Scheme 1.8).^{134,189} Also, $[(OC)_3(R_3P)_2MnH]$ undergoes H/X exchange with X_2 ($X = Br, I$) (b in Scheme 1.8).¹⁵⁶



Scheme 1.8: Halogenation of manganese hydride complexes. X = halogen.

In aromatic or donating solvents, reactions of the manganese(I) hydride complex $[(OC)_5MnH]$ with various metal alkyl or acyl complexes (of Mn, Re, Co, or Fe) have

resulted in bimolecular C–H bond-forming reductive elimination, usually yielding a bimetallic Mn–M complex (in some cases, subsequent decomposition resulted in a different complex being observed); Scheme 1.9.¹⁹⁰ The byproducts of this reaction were normally the expected protonated ‘R’ groups (alkanes or aldehydes, respectively), though in some cases reactions involving alkyl complexes yielded an aldehyde byproduct (the expected product if there is initial 1,1-insertion of a carbonyl co-ligand into the Mn–C_{alkyl} bond to form an acyl group prior to reductive elimination). As well, reactions involving manganese alkyl or aryl complexes with [(OC)₅MnH] in alkane solvents yielded bimetallic η^1 -aldehyde complexes (where the aldehyde byproduct does not dissociate from the transition metal coordination sphere).¹⁸⁵



Scheme 1.9: Bimolecular reductive elimination reactivity of manganese hydride complexes. R = alkyl or acyl.

1.4.6 – σ -H₂ Complexes of Mn

σ -H₂ complexes feature neutral ligands formed upon side-on coordination of dihydrogen to a transition metal centre.^{191,192} If this ligand then undergoes oxidative addition, the result would be a dihydride complex. The first examples of σ -dihydrogen complexes were reported by Kubas in 1984.¹⁹³ Structurally, these complexes can be differentiated from dihydride species by short H–H distances (≤ 1.2 Å).¹⁹¹ Spectroscopically, the H–H distance can be estimated by measuring the ¹H–²H NMR coupling constant of a partially deuterated analogue,⁹³ solid-state NMR spectroscopy (based on large dipolar coupling between the two H atoms in dihydrogen ligands),¹⁹⁴ and T₁ solution-state NMR measurements.¹⁹⁵ Also, determination of the oxidation state (for example, by electrochemical methods), has been used to infer whether the ‘H₂’ moiety is a single neutral H₂ ligand or two anionic hydride ligands.¹⁷³ It is notable that the NMR

chemical shifts of the H₂ environments in σ -H₂ complexes are in the same low-frequency range as the *MH* environment in hydride complexes.¹⁹¹

In 1985, Girolami and Wilkinson reported the ‘Mn(III) trihydride complex’ [(dmpe)₂MnH₃].¹²⁰ However, Jones has subsequently shown (by T₁ NMR measurement and electrochemistry) that this complex, as well as its *depe* analogue, is better described as a *trans*-Mn(I) dihydrogen-hydride complex (with rapid exchange between the dihydrogen and MnH environments); a and b in Figure 1.14.¹⁷³ A similar series of reports has involved [Cp(OC)₂Mn(H₂)], which was first prepared in 1988¹⁶² but not recognized as a σ -H₂ complex until the next year (c in Figure 1.14).¹⁹⁶ However, [Cp(OC)₂Mn(H₂)], as well as Cp* and ^{Et5}Cp analogues of this complex (d and e in Figure 1.14),¹⁹⁷ were only characterized by IR spectroscopy and were thermally unstable. [(OC)₄Mn(H₂)X] (X = Cl, Br; f and g in Figure 1.14) complexes have been observed in Ar matrices.¹⁹⁸ As well, in 2004 Roddick et al. observed the σ -H₂ complex [Cp(*dfepe*)Mn(H₂)] (h in Figure 1.14) in equilibrium with the Mn(III) dihydride complex [Cp(*dfepe*)MnH₂] (*vide supra*).¹⁷¹ Various stable cationic H₂ Mn complexes have been spectroscopically observed, including [(R₃P)_{5-n}(OC)_nMn(H₂)]⁺ {R₃ = OEt₃, Ph(OEt)₂, Ph₂(OEt), Cy₃, (OCH₂C)₃Me, n = 3, 2, 1; i-o in Figure 1.14, not all combinations were observed}^{199,200} and [(OC)(PP₁)(PP₂)Mn(H₂)]⁺ (PP = *dppe*, *dppm*, PN^{M^cP}, PN^{PhP}, PN^{nBuP}, P₂^{PhN₂^{Bn}}; p-t in Figure 1.14).¹⁴¹ The only two examples of manganese σ -H₂ complexes for which an X-ray crystal structure has been obtained are [(L)₂(OC)Mn(H₂)]⁺ (L = *dppe*, *depe*; u and v in Figure 1.14), though the dihydrogen atom locations proved unstable to refinement.²⁰¹ All reported Mn σ -H₂ complexes are monovalent, and have been prepared by i) the reaction of a manganese aluminate complex with water, ii) protonation of a hydride complex, iii) substitution of a neutral ligand by H₂, or iv) coordination of H₂ to a vacant coordination site.

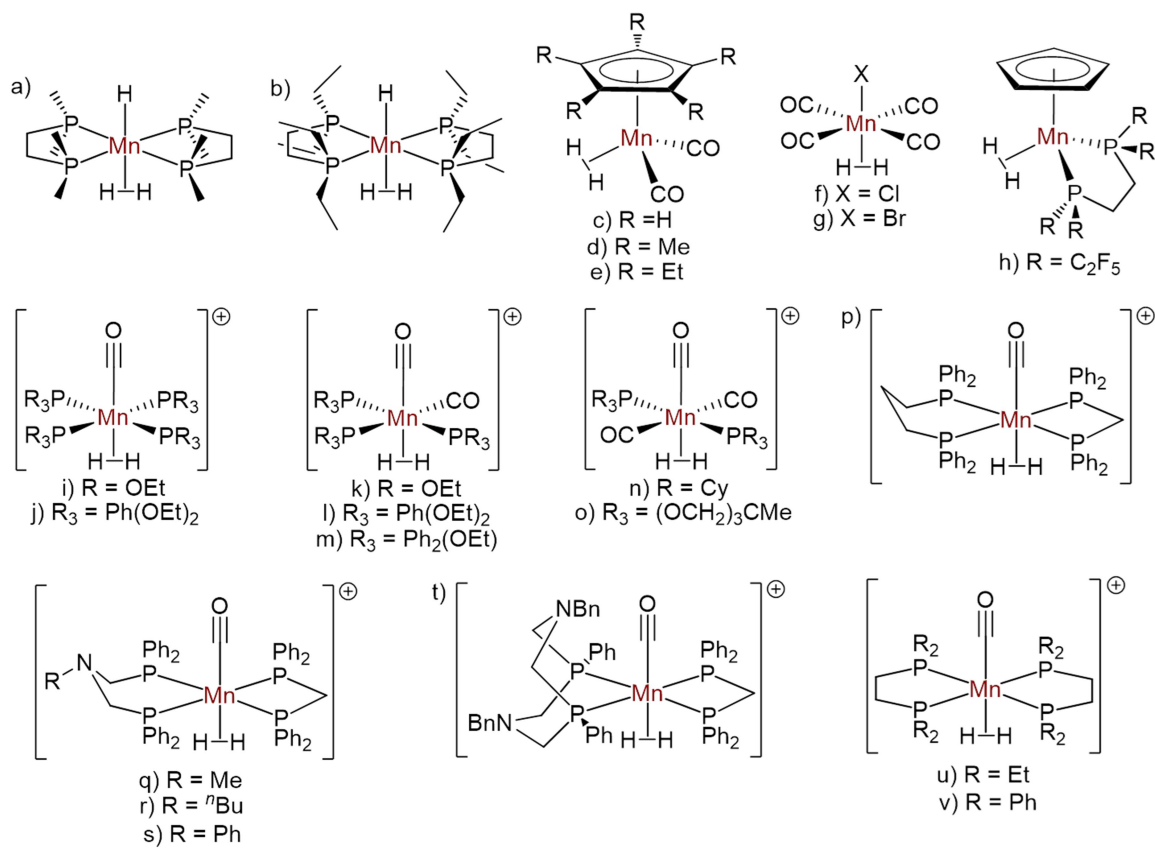


Figure 1.14: $\sigma\text{-H}_2$ complexes of Mn.

1.5 – Manganese Silyl Complexes

Portions of this section have been reprinted (adapted) with permission from Price, J. S.; Emslie, D. J. H.; Berno, B. Manganese Silyl Dihydride Complexes: A Spectroscopic, Crystallographic, and Computational Study of Nonclassical Silicate and Hydrosilane Hydride Isomers, *Organometallics* **2019**, *38*, 2347-2362. Copyright 2019 American Chemical Society.

1.5.1 – Scope of Section

The aim of this section of to provide an overview of monometallic manganese silyl complexes, with a particular focus on complexes with hydride co-ligands (including classical silyl hydride, nonclassical hydrosilane, and classical hydrosilane complexes). Also included is a brief introduction to ‘nonclassical’ hydrosilane complexes, where silyl and hydride ligands feature significant Si–H interligand interactions. This section will focus on synthesis, structures, and characterization; reactivity is beyond the scope. For silyl complexes lacking hydride co-ligands, only those with structural characterization are included (for silyl hydride/hydrosilane complexes, a comprehensive review is provided).

1.5.2 – Early Manganese Silyl Complexes

Transition metal complexes with silyl ligands are extremely common in organometallic chemistry. As expected for heavy analogues of alkyl ligands, bonding involving silyl groups is dominated by σ -donation from a formally anionic SiR_3 group (although σ -donation is weaker than in alkyl ligands with identical substituents). However, unlike alkyl ligands, significant π -backdonation (into a Si–R σ^* -orbital) is also pertinent.²⁰²

The first manganese silyl complex $\{[(\text{OC})_5\text{Mn}(\text{SiPh}_3)]$ (a in Figure 1.15)}, reported in 1966 by Graham et al., was prepared by the reaction of HSiPh_3 and half an equivalent of $[(\text{OC})_5\text{MnMn}(\text{CO})_5]$ with concurrent H_2 elimination.²⁰³ While initially this complex was characterized only by IR spectroscopy and elemental analysis, an X-ray

crystal structure was later reported.²⁰⁴ The first manganese silyl complex to be crystallographically characterized, $[(OC)_5Mn(SiMe_3)]$ (b in Figure 1.15), was reported two years later by Hamilton and Corey.²⁰⁵ Another set of milestones were reached in 1971 with the syntheses of the first manganese silyl hydride complexes $[Cp(OC)_2MnH(SiCl_3)]$, $[^{Me}Cp(OC)_2MnH(SiPh_3)]$,²⁰⁶ and $[Cp(OC)_2MnH(SiPh_3)]$ ²⁰⁷ (c-e in Figure 1.15) by the Graham group, followed 10 years later by the first reported X-ray crystal structure ($[^{Me}Cp(OC)_2MnH(SiFPh_2)]$; f in Figure 1.15) by Schubert et al.^{f,208} Despite the fact that manganese is the third most abundant transition metal in the Earth's crust,²¹⁰ only 22 monometallic manganese silyl complexes have been structurally characterized (a tiny fraction of the total number of transition metal silyl complexes).²¹¹

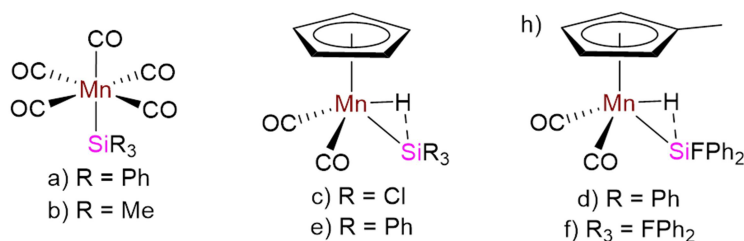


Figure 1.15: Early manganese silyl complexes.

1.5.3 – Structurally Characterized Hydride-free Mn(I) Silyl Complexes

A handful of manganese(I) silyl complexes which lack hydride co-ligands have been structurally characterized (Figure 1.16). In all of these cases, the environment about the metal centre is octahedral, and at least three of the co-ligands are carbonyls. When a phosphine co-ligand is also present, the PR_3 ligand is located *trans* to the silyl group (c and h in Figure 1.16). By contrast, in $[(OC)_3(CNAr^{Dipp2})_2Mn(SiCl_2Me)]$ (f in Figure 1.16), the extreme steric bulk of the two isonitrile co-ligands forces those to be *trans* to each other (and, by extension, the silyl ligand is *trans* to a CO ligand).

^f In 1971,²⁰⁷ Graham cites a manuscript in preparation as having determined the structure of $[Cp(OC)_2MnH(SiPh_3)]$ by X-ray crystallography. However, no such structure has been deposited in the CSD, or to our knowledge published. Various bonding metrics were later published by Corriu et al.,²⁰⁹ citing a PhD thesis.

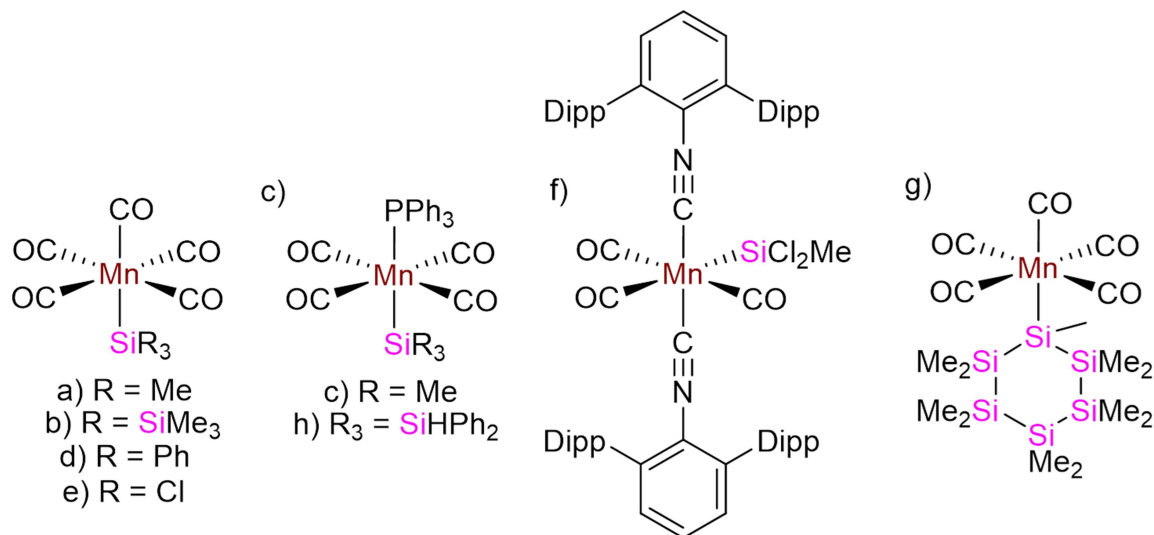
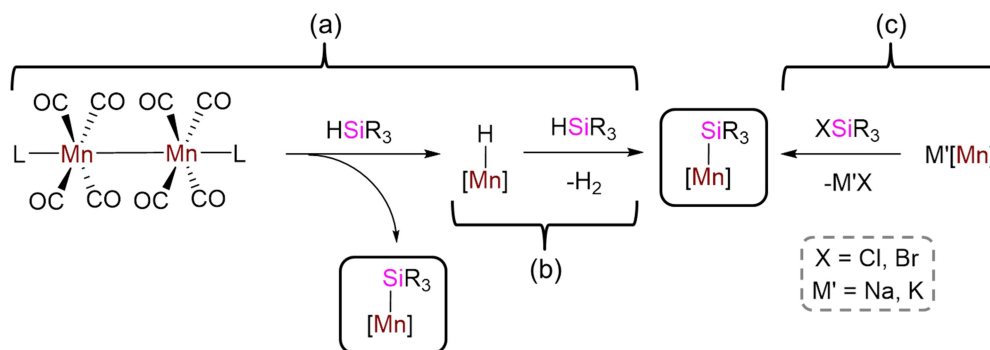


Figure 1.16: Structurally characterized Mn(I) silyl complexes lacking hydride co-ligands.

Common routes for accessing hydride-free manganese(I) silyl complexes are summarized in Scheme 1.10.^g These include the pathway used in the seminal synthesis of [(OC)₅Mn(SiPh₃)] (*vide supra*); the reaction of bimetallic Mn(0) complexes with two equivalents of a hydrosilane (a in Scheme 1.10).^{43,203,212-215} This reaction was proposed to proceed via oxidative addition of the H–Si bond across the Mn–Mn bond, initially yielding a single equivalent of the manganese (I) silyl product and a manganese(I) hydride byproduct; a second equivalent of HSiR₃ could then react with the hydride byproduct to generate a second equivalent of the Mn(I) silyl complex with H₂ elimination. In fact, the second half of this mechanism (reaction of a hydrosilane with a Mn(I) hydride complex; b in Scheme 1.10) is another commonly used pathway to access Mn(I) silyl complexes.^{203,212} The final commonly used synthetic route to Mn(I) silyl complexes involves the reaction of a halosilane with an alkali metal salt of a manganese(I) anion (c in Scheme 1.10).^{145,212,216-218}

^g References in the following paragraph are for syntheses of complexes in Figure 1.16 via the identified route.



Scheme 1.10: Selected synthetic routes to hydride-free manganese(I) silyl complexes.

Given that all examples of hydride-free Mn(I) silyl complexes feature carbonyl co-ligands (*vide supra*), IR spectroscopy is a commonly utilized characterization tool because the carbonyl C≡O bond vibrations are highly dependent on the electronic environment at the metal centre. As well, the diamagnetic nature of these complexes has allowed them to be characterized in the solution state by NMR spectroscopy. In particular, ^{29}Si NMR spectroscopy (^{29}Si is 4.70% abundant, with $I = \frac{1}{2}$) provides a diagnostic NMR handle; for the hydride-free silyl complexes in Figure 1.16 for which ^{29}Si NMR chemical shifts have been located, the MnSi environments range from -43.2 to 59.13 ppm (Table 1.4). This extremely wide range appears to be highly dependent on the nature of the substituents on Si. Of course, X-ray crystallography is another commonly employed method for investigating the structure of silyl complexes, and Mn–Si distances for hydride-free Mn(I) silyl complexes range from $2.342(2)$ – $2.564(6)$ Å (Table 1.4).

Table 1.4: ^{29}Si NMR chemical shifts and solid-state Mn–Si distances for hydride-free Mn(I) silyl complexes for which X-ray crystal structures have been reported. Reference column refers to the report where a crystal structure was obtained (not where the complex was first synthesized). Letters correspond to those in Figure 1.16.

Complex	^{29}Si NMR (MnSi) δ (ppm)	d(Mn–Si) (Å)	Reference
$[(\text{OC})_5\text{Mn}(\text{SiMe}_3)]$ (a)	10.98 ²¹⁹	2.498(5)	Hamilton and Corey (1968) ²⁰⁵
$[(\text{OC})_5\text{Mn}\{\text{Si}(\text{SiMe}_3)_3\}]$ (b)	–	2.564(6)	Simpson (1973) ²²⁰
$[(\text{OC})_4(\text{Ph}_3\text{P})\text{Mn}(\text{SiMe}_3)]$ (c)	–	2.453(4)	Simpson (1976) ²¹⁴
$[(\text{OC})_5\text{Mn}(\text{SiPh}_3)]$ (d)	17.9 ²²¹	2.504(6)	Butler (1997) ²⁰⁴
$[(\text{OC})_5\text{Mn}(\text{SiCl}_3)]$ (e)	59.13 ⁴⁴	2.352(2)	Jin (2008) ⁴³
$[(\text{OC})_3(\text{CNAr}^{\text{Dipp}2})_2\text{Mn}(\text{SiCl}_2\text{Me})]$ (f)	–	2.342(2)-2.346(2)	Figueroa (2011) ¹⁴⁵
$[(\text{OC})_5\text{Mn}(\text{SiMe}\{\kappa^2\text{-(SiMe}_2)_5\})]$ (g)	–21.5, ²¹⁷ –43.2 ²¹⁸	2.537(1)	Roewer (2017) ²¹⁸
$[(\text{OC})_4(\text{Ph}_3\text{P})\text{Mn}(\text{SiHPh}_2)]$ (h)	–24.5 ²¹⁵	2.410(1)	Wang (2018) ²¹⁵

1.5.4 – Structurally Characterized Mn(II) and Mn(III) Hydride-free Silyl Complexes

Relative to Mn(I) silyl complexes, even fewer hydride-free manganese silyl complexes have been reported for other oxidation states. In fact, X-ray crystal structures have only been reported for two Mn(II) examples (both Lewis base adducts of $[\text{Mn}\{\text{Si}(\text{SiMe}_3)_3\}_2]$; a and b in Figure 1.17) and one Mn(III) example ($[\text{Cp}^{\text{Me}}(\text{OC})_2\text{Mn}(\text{SiCl}_3)_2]$; c in Figure 1.17). The divalent complexes were both prepared by THF substitution from $[(\text{THF})_2\text{Mn}\{\text{Si}(\text{SiMe}_3)_3\}_2]$ (which was itself characterized by IR spectroscopy, elemental analysis, and magnetic measurements).²²² Both of these divalent complexes are tetrahedral at the Mn centre, and contain Mn–Si distances of 2.642(3)-2.662(6) Å which are significantly longer than those for Mn(I) analogues (*vide supra*).²²² By contrast, the trivalent example (formed as a byproduct in the synthesis of $[\text{Cp}^{\text{Me}}(\text{OC})_2\text{MnH}(\text{SiCl}_3)]$) features a Mn–Si distance of 2.320(2) Å, which is shorter than those observed in Mn(I) complexes (*vide supra*).²²³ Mn(II) complexes are paramagnetic,

and therefore NMR spectra are not generally obtained for these complexes. In addition, no NMR data was reported for $[\text{M}^{\text{e}}\text{Cp}(\text{OC})_2\text{Mn}(\text{SiCl}_3)_2]$.

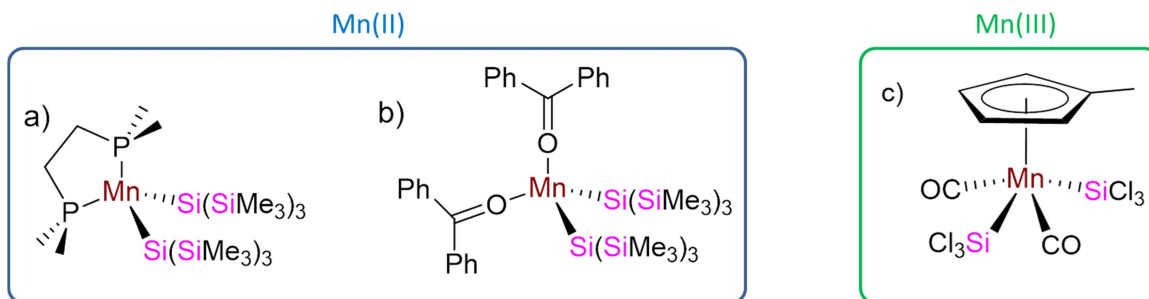


Figure 1.17: Structurally characterized hydride-free Mn(II) and Mn(III) silyl complexes.

1.5.5 Introduction to ‘Nonclassical’ Hydrosilane Complexes of Transition Metals

Transition metal hydrosilane complexes are a class of sigma complex important in many chemical transformations, especially those involving formation of Si–C bonds.^{208,224-230} Isolated examples of hydrosilane complexes are far less common than related dihydrogen complexes, despite the fact that the first hydrosilane complex was reported by Graham et al. in 1969,²³¹ 15 years before Kubas’ report of the first H_2 complex.¹⁹³ Upon oxidative addition of the Si–H bond, classical silyl hydride complexes (with two separate 2c-2e bonds, as opposed to a single 3c-2e bond) are formed. However, as early as 1971, Graham reported a monometallic silyl hydride complex with significant interligand Si–H bonding.²⁰⁷ These “nonclassical” hydrosilane complexes have been the subject of a number of reviews,²³²⁻²³⁴ and from a molecular orbital perspective, they are typically described using a modification of the Dewar-Chatt-Duncanson bonding model, with concomitant σ donation and π backdonation to/from the metal (Figure 1.18). A

variety of terms have been employed to describe these intermediate complexes,^{h,235} and comprehensive studies by a number of groups, including those of Nikonov,^{236,237,242-248} Sabo-Etienne,^{234,249-254} and Scherer,^{239-241,255,256} have shown that a continuum exists between classical hydrosilane and classical silyl hydride complexes along the oxidative addition/reductive elimination reaction coordinate, with progressively weakening Si–H interactions indicative of a greater degree of oxidative addition. Nonclassical hydrosilane complexes therefore provide snapshots along the oxidative addition pathway, which is one of the most important classes of organometallic reaction.

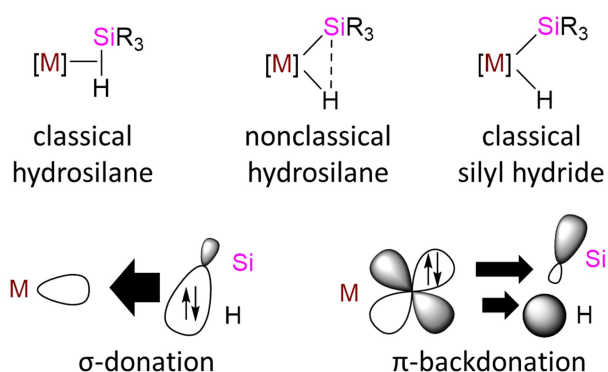


Figure 1.18: Top; From left to right, structures of classical hydrosilane, nonclassical hydrosilane, and classical silyl hydride complexes. Bottom; Dewar-Chatt-Duncanson model of σ donation and π backdonation from/to a hydrosilane ligand.

Analyses of nonclassical hydrosilane complexes have naturally focused on the strength of the Si–H interaction, from which the degree of oxidative addition can be

^h A variety of terms have been used to describe Si–H interactions in nonclassical hydrosilane complexes, including stretched σ -bonding or Si–H bonding (ref 226), interligand hypervalent interactions (IHI; refs. 236 and 237), secondary Interactions between silicon and hydrogen atoms (SISHA; ref. 234), and α -agostic interactions (ref. 235). Complexes featuring interligand Si–H interactions are sometimes referred to as hybrids between σ -hydrosilane and silyl hydride complexes (ref. 238), or complexes featuring incomplete (or arrested) oxidative addition. The latter are sometimes divided further into asymmetric oxidative addition products (ASOAPs, typically featuring significant Si–H interactions and negative $J_{\text{Si,H}}$ coupling constant), and symmetric oxidative addition products (SOAPs, featuring weak residual Si–H interactions and positive $J_{\text{Si,H}}$ coupling constants); refs. 239-241.

inferred. These strengths have often been determined computationally,^{237,239-241,245,246,250,255,257-260} while experimental studies have primarily involved solid-state structural determination of the Si–H distance. However, care must be taken when discussing Si–H distances determined by X-ray crystallography, due to difficulties associated with accurately locating hydrogen atoms from the difference map. More importantly, it has been observed that significant changes in the degree of oxidative addition (based on $J_{\text{Si,H}}$ coupling constants; *vide infra*) may only yield very small changes in the Si–H distance, and Si–H distances below the sum of the van der Waals radii may be steric in origin, so do not necessarily imply Si–H bonding.²³³ Furthermore, there is no intuitive boundary to define nonclassical hydrosilane complexes with respect to either classical hydrosilane or classical silyl hydride complexes, and different Si–H distance ranges have been suggested to correspond to these intermediate complexes. The lower end of this range is often considered to be 1.8 Å, while distances of 2.1 and 2.4 Å have been proposed by Nikonov²³³ and Sabo-Etienne²³⁴ respectively to correspond to the upper limit.

Spectroscopically, ^1H and ^{29}Si NMR chemical shifts are not especially useful to evaluate the extent of hydrosilane oxidative addition, given that similar ranges of values are observed for classical hydrosilane, classical silyl hydride, and nonclassical hydrosilane complexes.²³⁴ By contrast, ^{29}Si – ^1H NMR coupling constants ($J_{\text{Si,H}}$) can be used as a sensitive tool to measure the nature of interligand Si–H interactions.²⁶¹ However, it is important to recognize that 1-bond Si–H coupling has a negative sign, whereas 2-bond Si–H coupling has a positive sign, so $J_{\text{Si,H}}$ passes through zero on the continuum from a classical hydrosilane to a classical silyl hydride complex, and proper placement of a complex along this continuum requires knowledge both of the magnitude and sign of $J_{\text{Si,H}}$.^{209,241,256,260,262}

The magnitude of $J_{\text{Si,H}}$ can typically be obtained via 1D ^1H or ^{29}Si NMR spectroscopy, but measurement of the sign is more difficult. One method used in the literature is spin tickling,²⁶⁰ but individual multiplet signals must be well-resolved, and its

analysis is not conceptually straightforward.²⁶³ Recently, Scherer reported an alternative spectroscopic method for determining the sign (and magnitude) of $J_{\text{Si,H}}$ in silyl hydride/hydrosilane complexes where the silicon centre also features a terminal Si–H bond. This method relies upon 2D ^1H – ^1H COSY data, using the negative coupling constants of the terminal Si–H bond²⁶⁴ as an internal reference to definitely determine the sign of $J_{\text{Si,H}}$ from the orientation of ^{29}Si satellites associated with a cross-peak of interest.^{241,256} While there is still some debate, $J_{\text{Si,H}}$ values ranging from 0 to –70 Hz are commonly considered to indicate activated Si–H bonds in nonclassical silyl hydride complexes (with values more negative than –70 Hz indicative of classical hydrosilane complexes and positive values indicative of classical silyl hydride complexes).^{224,241,260}

A range of transition metal complexes have also been isolated containing a silyl group accompanied by more than one hydride ligand. The generic term ‘silyl dihydride’ is frequently used to describe complexes with one SiR_3 and two hydride moieties interacting with a metal centre, regardless of the extent of any interligand Si–H interaction(s). Within this class of complexes, a variety of examples have been observed where a single silyl ligand simultaneously interacts with multiple hydride ligands.^{245,265,266} In 1989, Crabtree et al. first proposed such a complex as a potential intermediate in the dynamic exchange between the terminal metal hydride and bridging hydrosilyl environments in $[(\text{Ph}_3\text{P})_2\text{IrH}_2(\eta^2\text{-HSiEt}_3)]^+$.²⁶⁷ Then, in 1990, the same group reported the first examples of transition metal (Re) complexes featuring multiple (four or two) hydride ligands interacting with a single silyl ligand (Figure 1.19, a and b), though the hydride atoms were not crystallographically located.²⁶⁸ Five years later, Klabunde and Radonovich et al. reported X-ray crystal structures for a pair of chromium disilyl dihydride complexes with short distances between one of the silyl ligands and two neighboring hydride ligands (1.75(7) and 1.60(6) Å for one, 1.66(4) and 1.87(4) Å for the other; c in Figure 1.19), though the authors stopped short of stating that two Si–H interactions were present due to significant errors in the bond distances and potential involvement of the second silyl ligand in the bonding scheme.²⁶⁹ Then, in 1999, Sabo- Etienne and Chaudret reported a Ru complex featuring a silyl ligand with two adjacent

hydride co-ligands (d in Figure 1.19), with short Si–H distances of 1.72(3) and 1.83(3) Å determined by X-ray diffraction.²⁷⁰ Over the past two decades, approximately a dozen crystallographically characterized monometallic transition metal silyl dihydride complexes have been reported to feature interactions between a silyl ligand and two hydride ligands, and are often referred to as silicate (H_2SiR_3^-) complexes.^{244,247,248,251,269-275} However, no examples involving manganese have yet been reported. These complexes highlight the potential for silicon hypervalency in transition metal complexes, and are of interest as models in the heterolytic splitting of hydrosilanes on metal centres.²³²

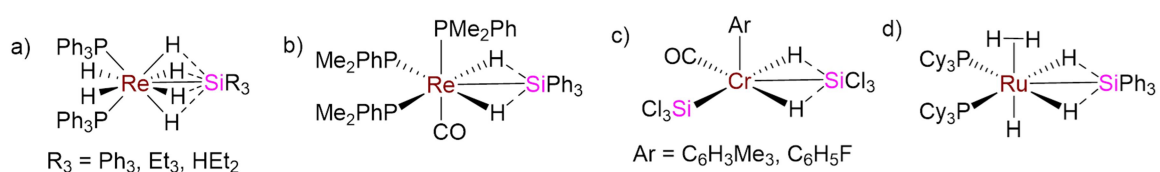


Figure 1.19: Early examples of complexes reported to involve multiple Si–H interactions to the same silicon centre.²⁶⁸⁻²⁷⁰

1.5.6 – Silyl Hydride/hydrosilane Complexes of Manganese

A wide variety of classical silyl hydride, nonclassical hydrosilane, and classical hydrosilane complexes (collectively referred to herein as silyl hydride/hydrosilane complexes) have been reported for manganese. To our knowledge, all reported examples involve varying degrees of oxidative addition to a Mn(I) centre, to the extent that classical silyl hydride examples could be considered complexes of Mn(III). Photoelectron spectroscopy is sometimes employed to determine if the metal centre could be best described as mono- or tri- valent.^{276,277} However, it is of note that the overall electron count is unaffected by the extent of oxidative addition (i.e. both 6-coordinate Mn(I) and 7-coordinate Mn(III) complexes are 18-electron species). As well, DFT calculations have often been employed to gain a greater understanding of the bonding environment at the metal centre.^{239-241,258,259,278} It is also notable that the vast majority of Mn silyl hydride/hydrosilane complexes are neutral, with the exception of anionic $[(\text{OC})_4\text{MnH}(\text{SiPh}_3)]^-$ and cationic $[(\text{OC})_3\{\text{MeC}(\text{CH}_2\text{O})_3\text{P}\}_2\text{MnH}(\text{SiR}_3)]^+$.^{200,279}

The vast majority of reported silyl hydride/hydrosilane complexes of Mn contain carbonyl co-ligands and are diamagnetic. Because of this, IR and NMR spectroscopy are commonly used characterization tools. Nearly all reported examples have been characterized by IR spectroscopy because the electronic environment at the metal centre has a significant effect on the C≡O vibration. In fact, many manganese silyl hydride/hydrosilane complexes have been analyzed by IR spectroscopy with no corroborating spectroscopic or structural data; [(OC)₄MnH(SiPh₃)]⁻,²⁷⁹ [Cp(OC)₂MnH(SiRPh₂)] (R = Ph²⁰⁷ or H²⁷⁷), [^{Me}Cp(OC)₂MnH(SiRPh₂)] (R = Cl, Br, I,²⁸⁰ or Me²⁸¹), and [Tp(OC)₂MnH(SiEt₃)].²⁸²

NMR analysis of manganese silyl hydride/hydrosilane complexes has mainly focused on three parameters. The most common NMR handle to be reported is the MnH environment in the ¹H NMR spectrum, which gives rise to a low frequency environment (-5.21 to -16.81 ppm; Table 1.5) characteristic of a metal hydride. In a significant subset of examples, the ²⁹Si NMR chemical shift was also reported, and these values (-2.62 to 60.7 ppm; Table 1.5) are consistent with hydride-free Mn(I) silyl complexes (*vide supra*). ²⁹Si-¹H coupling constants involving the adjacent MnSi and MnH moieties (which are important for identifying classical silyl hydride vs. nonclassical hydrosilane vs. classical hydrosilane complexes; *vide supra*) have been reported to range in magnitude from 20 to 69 Hz (aside from [^{Me}Cp(OC)(Me₃P)MnH(SiCl₃)], all *J*_{Si,H} have a magnitude greater than 40 Hz; Table 1.5). For a handful of cases, the signs of these coupling constants were measured or calculated to be negative (in no cases were positive coupling constants measured or calculated). These coupling constants are consistent with (or indicative of, for complexes where the sign of *J*_{Si,H} has been determined) significant Si...H interactions associated with nonclassical hydrosilane ligands (*vide supra*).

Table 1.5: Selected NMR data for silyl hydride/hydrosilane complexes of Mn. References refer to the first reported synthesis, and when NMR data was obtained following the initial report, references for that are in the pertinent box. For clarity, all chemical formulae are given as the classical silyl hydride isomer. If no sign is explicitly given, $J_{\text{Si,H}}$ values are magnitudes. NMR values are from the first report (in some cases, later publications included slightly different data, often due to use of an alternative solvent). Empty boxes indicate that no data was reported.

Complex	^1H NMR (MnH) δ (ppm)	^{29}Si NMR (MnSi) δ (ppm)	$J_{\text{Si,H}}$ (Hz) expt. {calcd.}	Ref.
[Cp(OC) ₂ MnH(SiCl ₃)]	-9.70	–	–	Graham (1971) ²⁰⁶
[^{Me} Cp(OC) ₂ MnH(SiPh ₃)]	-11.50	18.5 ²⁰⁹	64.7 ²⁰⁹	Graham (1971) ²⁰⁶
[^{Me} Cp(OC) ₂ MnH{SiHPh(α -Naph)}]	-11.23, -11.46 ²⁰⁹	7.5 ²⁰⁹	69 ²⁰⁹	Corriu (1979) ²⁸³
[^{Me} Cp(OC) ₂ MnH{SiClPh(α -Naph)}]	-10.68 ²⁰⁹	58.3 ²⁰⁹	–	Corriu (1979) ²⁸³
[^{Me} Cp(OC) ₂ MnH{SiFPh(α -Naph)}]	-11.70 ²⁰⁹	57.3 ²⁰⁹	–	Corriu (1979) ²⁸³
[^{Me} Cp(OC) ₂ MnH{Si(OMe)Ph(α -Naph)}]	-12.03 ²⁰⁹	–	–	Corriu (1979) ²⁸³
[^{Me} Cp(OC) ₂ MnH(SiHPh ₂)]	– ^a	13.5 ²⁸⁴	64 ²⁸⁴ {-63, -68} ²⁴¹	Schubert (1981) ²⁸⁰
[^{Me} Cp(OC) ₂ MnH(SiFPh ₂)]	-12.03 ²⁴¹	60.7 ²⁴¹	57 ²⁴¹ {-52} ²⁴¹	Schubert (1981) ²⁸⁰
[^{Me} Cp(OC) ₂ MnH{SiMePh(α -Naph)}]	-11.97, -12.00 ²⁰⁹	–	–	Corriu (1977) ²⁸⁵
[^{Me} Cp(OC){(PhO) ₃ P}MnH(SiHPh ₂)]	– ^a	21.0	48	Schubert (1984) ²⁸⁴
[^{Me} Cp(OC){(EtO) ₃ P}MnH(SiHPh ₂)]	– ^a	–	–	Schubert (1984) ²⁸⁴
[^{Me} Cp(OC)(Ph ₃ P)MnH(SiHPh ₂)]	-11.1 ²⁸⁶	23.8	62	Schubert (1984) ²⁸⁴
[^{Me} Cp(OC)(ⁿ Bu ₃ P)MnH(SiHPh ₂)]	-11.8 ²⁸⁶	24.8	37	Schubert (1984) ²⁸⁴
[^{Me} Cp(OC)(Me ₃ P)MnH(SiHPh ₂)]	-12.0 ²⁸⁶	26.0 ²⁸⁷	38 \pm 2 ²⁸⁷	Schubert (1984) ²⁸⁴
[^{Me} Cp(OC){(<i>p</i> -ClPh) ₃ P}MnH(SiHPh ₂)]	-11.4	22.0 ²⁸⁷	46.5 \pm 1.5 ²⁸⁷	Schubert (1985) ²⁸⁶
[^{Me} Cp(OC){(<i>p</i> -tol) ₃ P}MnH(SiHPh ₂)]	-10.9	23.6 ²⁸⁷	44.5 \pm 1.5 ²⁸⁷	Schubert (1985) ²⁸⁶
[^{Me} Cp(OC)(PhMe ₂ P)MnH(SiHPh ₂)]	-11.7	24.9 ²⁸⁷	39.7 \pm 0.6 ²⁸⁷	Schubert (1985) ²⁸⁶
[^{Me} Cp(OC)(ⁿ Bu ₃ P)MnH(SiHEt ₂)]	-12.6	–	–	Schubert (1985) ²⁸⁶
[^{Me} Cp(OC)(Ph ₃ P)MnH(SiHEt ₂)]	-11.8	–	–	Schubert (1985) ²⁸⁶
[^{Me} Cp(OC) ₂ MnH(SiCl ₃)]	–	54.9	54.8 \pm 0.6, {-38} ²⁵⁸	Schubert (1986) ²⁸⁷
[^{Me} Cp(OC)(ⁿ BuNC)MnH(SiHPh ₂)]	–	22.6	57.5 \pm 0.6	Schubert (1986) ²⁸⁷
[^{Me} Cp(OC)(^t PrNC)MnH(SiHPh ₂)]	–	22.8	58 \pm 2	Schubert (1986) ²⁸⁷

Ph.D. Thesis — Jeffrey S. Price; McMaster University – Chemistry

$[\text{MeCp}(\text{OC})(\text{Me}_3\text{P})\text{MnH}(\text{SiCl}_3)]$	–	59.5	$20 \pm 2, -22^{258}$	Schubert (1986) ²⁸⁷
$[\text{Cp}^*(\text{OC})_2\text{MnH}(\text{SiHPh}_2)]$	–	18.2	65.4 ± 0.6	Schubert (1986) ²⁸⁷
$[\text{Cp}(\text{OC})_2\text{MnH}(\text{SiEt}_3)]$	–13.8	–	–	Wrighton (1987) ²⁸⁸
$[\text{Cp}(\text{OC})_2\text{MnH}(\text{SiMe}_2\text{Et})]$	–10.8	–	–	Wrighton (1987) ²⁸⁸
$[\text{Cp}(\text{OC})_2\text{MnH}(\text{Si}^i\text{Pr}_3)]$	–15.1	–	–	Wrighton (1987) ²⁸⁸
$[\text{Cp}(\text{OC})_2\text{MnH}(\text{Si}^n\text{Pr}_3)]$	–13.2	–	–	Wrighton (1987) ²⁸⁸
$[\text{Cp}^*(\text{OC})_2\text{MnH}(\text{SiEt}_3)]$	–13.7	–	–	Wrighton (1987) ²⁸⁸
$[\text{MeCp}(\text{OC})\text{MnH}(\kappa^2\text{-P}(\text{Ph})_2\text{CH}_2\text{CH}_2\text{SiMe}_2)]$	–12.8	47.2	–	Schubert (1987) ²⁸⁹
$[\text{MeCp}(\text{OC})\text{MnH}(\kappa^2\text{-P}(\text{Ph})_2\text{CH}_2\text{CH}_2\text{SiPh}_2)]$	–14.0	33.1	–	Schubert (1987) ²⁸⁹
$[\text{C}^{15}\text{Cp}(\text{OC})_2\text{MnH}(\text{SiEt}_3)]$	–12.2	–	–	Wrighton (1989) ²⁹⁰
$[\text{Cp}(\text{dmpe})\text{MnH}(\text{SiH}_2\text{Ph})]$	–14.14	–	–	Sun (1994) ²⁹¹
$[\text{Cp}(\text{dmpe})\text{MnH}(\text{SiHPh}_2)]$	–14.42	–	–	Sun (1994) ²⁹¹
$[\text{Cp}(\text{dmpe})\text{MnH}(\text{SiPh}_3)]$	–14.13	–	–	Sun (1994) ²⁹¹
$[\text{Cp}(\text{dmpp})\text{MnH}(\text{SiH}_2\text{Ph})]$	–14.58	–	–	Sun (1994) ²⁹¹
$[\text{Cp}(\text{dmpp})\text{MnH}(\text{SiHPh}_2)]$	–14.47	–	–	Sun (1994) ²⁹¹
$[\text{Cp}(\text{dmpp})\text{MnH}(\text{SiPh}_3)]$	–14.41	–	–	Sun (1994) ²⁹¹
$[\text{Cp}(\text{dmpm})\text{MnH}(\text{SiHPh}_2)]$	–9.59	–	–	Sun (1994) ²⁹¹
$[\text{Cp}(\text{Me}_3\text{P})_2\text{MnH}(\text{SiHPh}_2)]$	–14.23	–	–	Sun (1994) ²⁹¹
$[\text{Cp}(\text{dmpe})\text{MnH}(\text{SiClPh}_2)]$	–14.54	–	–	Sun (1994) ²⁹¹
$[\text{MeCp}(\text{OC})_2\text{MnH}(\text{SiEt}_3)]$	–13.50	–	–	Hill (1996) ²⁹²
$[\text{MeCp}(\text{OC})_2\text{MnH}(\text{SiMeEt}_2)]$	–13.27	–	–	Hill (1996) ²⁹²
$[\text{MeCp}(\text{OC})_2\text{MnH}(\text{SiMe}_2\text{Et})]$	–13.09	–	–	Hill (1996) ²⁹²
$[\text{MeCp}(\text{OC})_2\text{MnH}(\text{SiHEt}_2)]$	–12.63	–	–	Hill (1996) ²⁹²
$[\text{Cp}(\text{OC})_2\text{MnH}(\text{SiMeEt}_2)]$	–13.50	–	–	Hill (1996) ²⁹²
$[\text{Cp}^*(\text{OC})_2\text{MnH}(\text{SiMeEt}_2)]$	–13.33	–	–	Hill (1996) ²⁹²
$[\text{Cp}^*(\text{OC})_2\text{MnH}(\text{SiMe}_2\text{Et})]$	–13.01	–	–	Hill (1996) ²⁹²
$[\text{MeCp}(\text{OC})_2\text{MnH}\{\text{SiPh}_2(\text{SiHPh}_2)\}]$	–10.71	–2.62	57	Schubert (1997) ²⁹³
$[\text{MeCp}(\text{OC})_2\text{MnH}\{\text{SiMe}_2(o\text{-}(\text{SiMe}_2\text{H})\text{Ph})\}]$	–12.3	–	–	Schubert (1998) ²⁹⁴
$[\text{MeCp}(\text{OC})(\text{Me}_3\text{P})\text{MnH}\{\text{SiMe}_2(o\text{-}(\text{SiMe}_2\text{H})\text{Ph})\}]$	–11.71	26.1	–	Schubert (1998) ²⁹⁴
$[\text{MeCp}(\text{OC})(\text{Me}_3\text{P})\text{MnH}\{\text{SiMe}_2(\text{CH}_2\text{CH}_2\text{SiMe}_2\text{H})\}]$	–12.9	33.7	–	Schubert (1998) ²⁹⁴
$[\text{MeCp}(\text{OC})(\text{Me}_3\text{P})\text{MnH}\{\text{SiMe}_2(\text{OSiMe}_2\text{H})\}]$	–12.7	52.4	–	Schubert (1998) ²⁹⁴
$[(\text{OC})_3\{\text{MeC}(\text{CH}_2\text{O})_3\text{P}\}_2\text{MnH}(\text{SiEt}_3)]^+$	–16.81	–	–	Kubas (2000) ²⁰⁰
$[(\text{OC})_3\{\text{MeC}(\text{CH}_2\text{O})_3\text{P}\}_2\text{MnH}(\text{SiH}_2\text{Ph})]^+$	–15.3	–	–	Kubas (2000) ²⁰⁰
$[(\text{OC})_3\text{MnH}(\kappa_3\text{-Si}_2\text{-xanthene})]$	–5.21	23.1	49	Tobita (2012) ²⁹⁵
$[(\eta^5\text{-C}_5\text{H}_4\text{CH}_2^{\text{Mes}}\text{NHC})(\text{OC})\text{MnH}(\text{SiHPh}_2)]$	–10.48	18.0	47.6	Valyev (2016) ²⁹⁶
$[(\eta^5\text{-C}_5\text{H}_4\text{CH}_2\text{CH}_2^{\text{Mes}}\text{NHC})(\text{OC})\text{MnH}(\text{SiHPh}_2)]$	–10.49	16.8	47.4	Valyev (2016) ²⁹⁶
$[\text{MeCp}(\text{OC})_2\text{MnH}(\text{SiMe}_3)]^b$	–	–	{–66}	Scherer (2017) ²⁴¹
$[\text{MeCp}(\text{OC})_2\text{MnH}(\text{SiMe}_2\text{Cl})]^b$	–	–	{–36}	Scherer (2017) ²⁴¹

$[\text{M}^{\text{c}}\text{Cp}(\text{OC})_2\text{MnH}(\text{SiMeCl}_2)]^{\text{b}}$	–	–	{-47}	Scherer (2017) ²⁴¹
$[\text{M}^{\text{e}}\text{Cp}(\text{OC})_2\text{MnH}(\text{SiCl}_3)]^{\text{b}}$	–	–	{-59}	Scherer (2017) ²⁴¹

- a. No specific MnH chemical shift was reported, but it was noted that it lies between -11.1 and -12.0 ppm.²⁸⁴
 b. These complexes were not synthesized, but used as models for DFT calculations.

Solid state structures have only been obtained for a relatively small subset of silyl hydride/hydrosilane complexes (Figure 1.20). Nearly every example contains a Cp donor; the only exceptions are a pair of complexes reported by the Tobita group (j and k in Figure 1.20), which contain chelating silicon-based donors.²⁹⁵

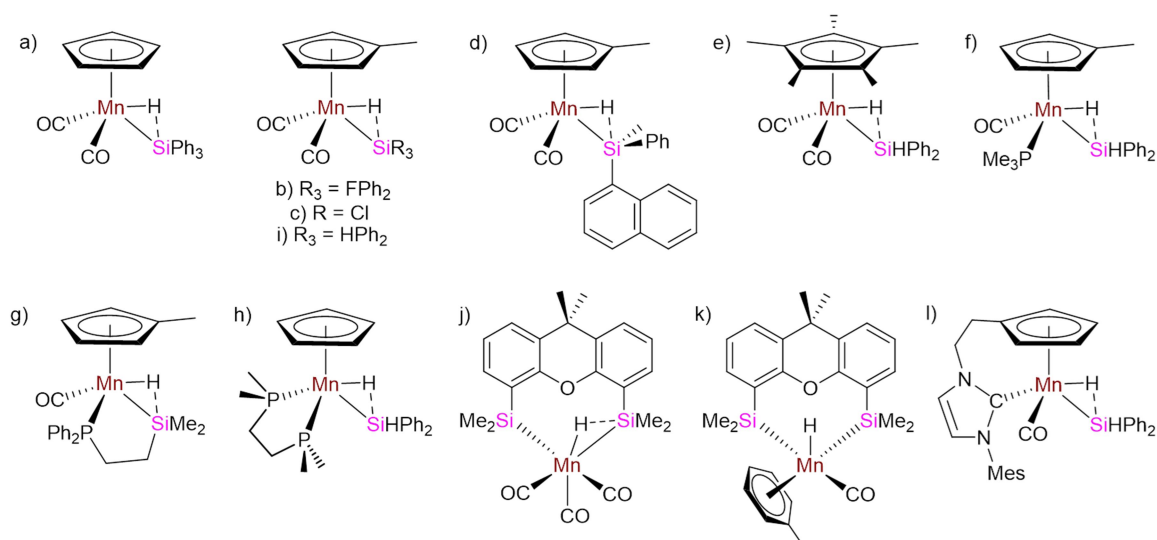


Figure 1.20: Silyl hydride/hydrosilane complexes characterized by X-ray or neutron crystallography. For clarity, all structures are shown as nonclassical hydrosilane complexes.

Discussions of the solid state structures of manganese silyl hydride complexes normally involve four parameters; the Mn–Si, Mn–H, and Si–H distances, as well as the Si–Mn–H angle (Table 1.6). However, three of these parameters involve hydrogen atoms, which are not accurately located from the difference map by X-ray crystallography. To obtain accurate values, authors often turn to DFT calculations or neutron crystallography.

Of particular interest are Si–H distances (1.60(2)-2.60(4) Å)ⁱ and Si–Mn–H angles (35.1(9)-74(1)°)^j, in that higher values are directly associated with a silyl hydride/hydrosilane complex lying further along the oxidative addition continuum. Si–H_{Mn} distances observed in the two silyl hydride/hydrosilane complexes for which neutron structures were obtained (1.802(5)-1.806(14) Å) are within the range associated with nonclassical hydrosilane complexes (*vide supra*). The range of Mn–Si distances observed in manganese silyl hydride/hydrosilane complexes (2.254(1)-2.6174(5) Å)^k encompasses the range observed for hydride-free Mn(I) and Mn(III) silyl complexes (2.320(2)-2.564(6) Å; *vide supra*), while the Mn–H distances in these complexes (1.45(3)-1.61(2) Å; if only values from neutron structures are included this range is 1.569(4)-1.575(14) Å) are similar to those in silyl-free Mn(I) hydride complexes (see section 1.4.4).

ⁱ If the Si–H distance of 2.60(4) Å in the disilyl hydride complex [(OC)₃MnH(κ₃-Si₂-xanthene)] (j in Figure 1.20) is excluded as an outlier, the upper limit of this range becomes 1.97(3) Å.

^j If the Si–Mn–H angle of 74(1)° in the disilyl hydride complex [(OC)₃MnH(κ₃-Si₂-xanthene)] (j in Figure 1.20) is excluded as an outlier, the upper limit of this range becomes 55(1)°.

^k If the Mn–Si distance of 2.6174(5) Å in the disilyl hydride complex [(OC)₃MnH(κ₃-Si₂-xanthene)] (j in Figure 1.20) is excluded as an outlier, the upper limit of this range becomes 2.461(7) Å.

Table 1.6: Selected structural parameters determined by X-ray (or, if indicated, neutron) crystallography for silyl hydride/hydrosilane complexes of Mn. For clarity, all chemical formulae are given as the classical silyl hydride isomer. Letters correspond to Figure 1.20, and the references refer to the report of the structure (not the synthesis).

Complex	d(Mn–Si) (Å)	d(Mn–H) (Å)	d(Si–H) (Å)	∠(Si–Mn–H)	Ref.
[Cp(OC) ₂ MnH(SiPh ₃)] (a) ^a	2.424(2)	1.55(4)	1.76(4)	–	Corriu (1982) ²⁰⁹
[^{Me} Cp(OC) ₂ MnH(SiPh ₂ F)] (b) {neutron structure}	2.352(4)	1.569(4)	1.802(5)	50.0(2)	Schubert (1982) ²⁰⁸
[^{Me} Cp(OC) ₂ MnH(SiPh ₂ F)] (b) ^b	2.3509(2)	–	–	–	Scherer (2006) ²³⁹
[^{Me} Cp(OC) ₂ MnH(SiCl ₃)] (c)	2.254(1)	1.47(3)	1.79(4)	52.26	Schubert (1983) ²²³
[^{Me} Cp(OC) ₂ MnH{SiMePh(α-Naph)}] (d) ^c	2.461(7)	–	–	–	Corriu (1984) ²⁹⁷
[Cp*(OC) ₂ MnH(SiHPh ₂)] (e) ^d	2.395(1)	1.52(3)	1.77(3)	48(1)	Schubert (1986) ²⁸⁷
[^{Me} Cp(OC)(Me ₃ P)MnH(SiHPh ₂)] (f)	2.327(1)	1.49(4)	1.78(4)	50(2)	Schubert (1986) ²⁸⁷
[^{Me} Cp(OC)MnH(κ ² -P(Ph) ₂ CH ₂ CH ₂ SiMe ₂)] (g)	2.457(2)	1.53(4)	1.75(4)	44.8(15)	Schubert (1987) ²⁸⁹
[Cp(dmpe)MnH(SiHPh ₂)] (h) ^c	2.319(4)	–	–	–	Sun (1994) ²⁹¹
[^{Me} Cp(OC) ₂ MnH(SiHPh ₂)] (i) {neutron structure}	2.391(12)	1.575(14)	1.806(14)	49.1(5)	Scherer (2009) ²⁵⁹
[(OC) ₃ MnH(κ ₃ -Si ₂ -xanthene)] (j)	2.3942(5), ^e 2.6174(5) ^f	1.61(2)	2.60(4), ^e 1.60(2) ^f	74(1), ^e 35.1(9) ^f	Tobita (2012) ²⁹⁵
[(η ⁶ -Toluene)(OC)MnH(κ ₂ -Si ₂ -xanthene)] (k)	2.4026(7), 2.4069(7)	1.45(3)	1.88(3), 1.97(3)	51(1), 55(1)	Tobita (2012) ²⁹⁵
[(η ⁵ -C ₅ H ₄ CH ₂ CH ₂ ^{Mes} NHC)(OC)MnH(SiHPh ₂)] (l)	2.3456(6)	1.47(3)	1.74(3)	48(1)	Valyaev (2016) ²⁹⁶

a. Selected bond metrics were provided with citation of a PhD thesis (ref. 7 in ref. 209). No structure has been submitted to the CSD, and ∠(Si–Mn–H) was not included in the text, so is not included here.

b. Hydride ligand was fixed based on neutron diffraction data, so this data is not included.

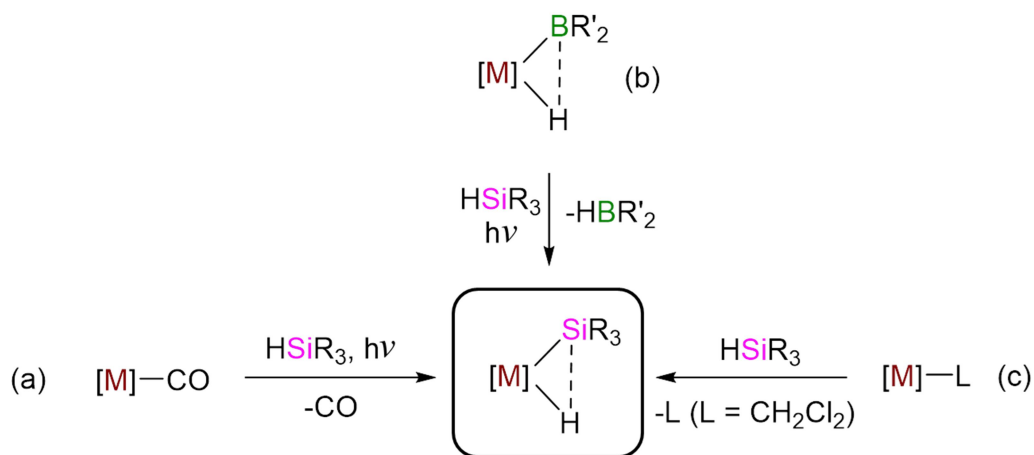
c. Hydride ligand was not located from the difference map.

d. Another unpublished crystal structure of this complexes was also reported in a dissertation (ref. 22 in ref. 297).

e. Involving the Si atom not adjacent to a hydride moiety.

f. Involving the Si atom interacting with an adjacent hydride moiety.

The original, and by far most common, synthetic route for accessing silyl hydride/hydrosilane complex is substitution of CO by a free hydrosilane under photochemical conditions (a in Scheme 1.11), followed by (for nonclassical hydrosilane complexes) partial or (for classical silyl hydride complexes) complete oxidative addition. In rare situations, such complexes have been formed by photochemically-induced substitution of a σ -hydroborane ligand (b in Scheme 1.11)²⁹⁸ or thermal substitution of a very weak ligand (c in Scheme 1.11).²⁰⁰ As well, different silyl hydride/hydrosilane complexes have been prepared by modification of the silyl group on an already existing silyl hydride/hydrosilane complex.²⁸³



Scheme 1.11: Synthetic routes to silyl hydride/hydrosilane complexes. For clarity, all these complexes are drawn as nonclassical hydrosilane complexes.

1.6 – Silylene Complexes of Transition Metals

1.6.1 – Scope of Subsection

The aim of this section is to provide an overview of known silylene transition metal complexes, with a focus on crystallographic and spectroscopic characterization. Comprehensive overviews are provided only for certain subsets of silylene complexes of particular relevance to this thesis; (a) base-free, non-electronically stabilized silylene complexes with hydride co-ligands, (b) base-free, non-electronically stabilized silylene complexes with terminal hydrogen substituents on Si, (c) NHC-stabilized silylene complexes, (d) silylene complexes of groups 3-5 and 7, and (e) reactions of silylene complexes with alkenes or alkynes. With the exception of Mn examples, only species with terminal (i.e. non-bridging) silylene ligands are discussed. In addition, a brief discussion of related species (with similar M–Si bond distances to silylene complexes) is included; η^3 -H₂SiR₂ complexes and base-stabilized silylyne complexes. For the most part, synthetic methods and reactivity are beyond the scope of this review.

1.6.2 – Introduction to Silylene Complexes

Silylenes (:SiR₂), as heavy analogues of carbenes, are of great interest as extremely reactive moieties.^{299,300} While accessing non-transient free silylenes normally requires substantial electronic or steric stabilization,³⁰¹ highly unstable simple silylenes can be observed by transition metal coordination.³⁰²⁻³⁰⁴

The accessibility of transition metal silylene complexes has been postulated since the early 1970s, when Kumada et al. proposed a transient Pt dimethyl silylene complex as an intermediate in the catalytic disproportionation of RMe₂SiSiMe₂H (R = Me, H).³⁰⁵ A few years later, in 1977, Schmid and Welz isolated the first example of a silylene complex, [(OC)₄Fe{=SiMe₂(NHEt₂)}] (a in Figure 1.21).³⁰⁶ However, it took another decade before the Tilley³⁰⁷ and Zybail³⁰⁸ groups independently reported the first solid-state structural characterization of such complexes (b and c, respectively, in Figure 1.21). All these early isolated silylene complexes feature base-stabilization of the silicon centre.

Development of base-free silylene complexes started in the early 1990s when the Tilley group reported the first isolated (1990)³⁰⁹ and crystallographically characterized (1993)³¹⁰ silylene complexes (d and e, respectively, in Figure 1.21). Over the past three decades, a wide range of terminal silylene complexes have been reported, mainly with late transition metals. In addition to interesting catalytic and stoichiometric reactivity, base-free terminal silylene complexes have been observed to feature short M–Si distances and highly electrophilic Si centres relative to ubiquitous silyl (–SiR₃) complexes.^{302-304,311}

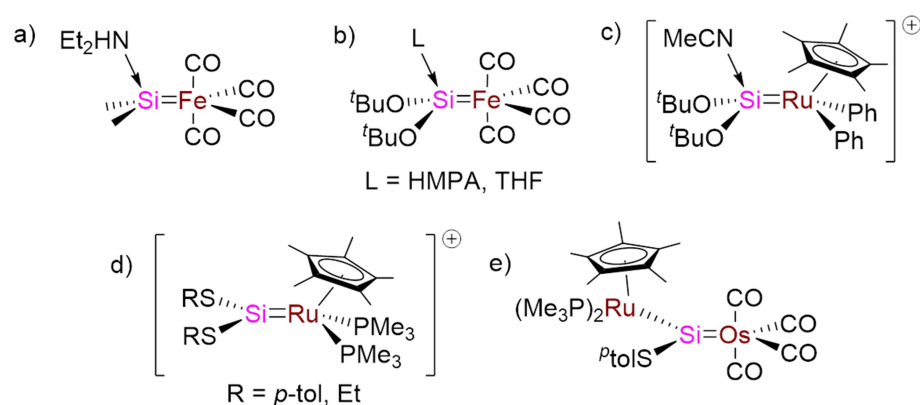


Figure 1.21: Early examples of isolated silylene complexes.

1.6.3 – Electronic Structure of Silylene Complexes

Bonding between a silylene ligand and a transition metal centre parallels that of carbene complexes, with a formal double bond between the Si and M atoms. The vast majority of reported examples are electrophilic at silicon, and are therefore analogous to Fischer-type carbene complexes. The electronic structure of these complexes has been discussed in a number of reports,³¹² and can be described most simply as involving σ -donation from a filled sp^2 orbital of the silylene fragment to a vacant metal d-orbital (the singlet form of simple free silylenes is more stable than the triplet form),³¹³ with concurrent π -backdonation from a metal d-orbital to the empty p-orbital of the silylene (which is orthogonal to the plane formed by Si and the two substituents); Figure 1.22.³⁰² Compared to Fischer carbene complexes with equivalent substituents, the degree of π -backdonation is typically less, resulting in the M–Si bond being polarized towards the

metal, making the Si centre highly electrophilic and reducing the extent of M=Si double bond character.³⁰²

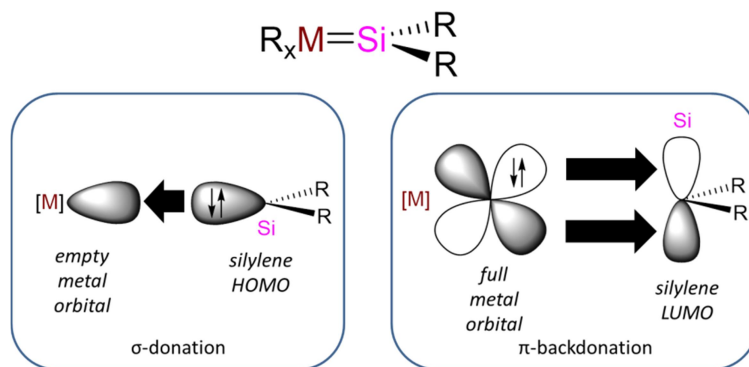


Figure 1.22: Electronic structure of Fischer-type silylene complexes. For clarity, in the diagram for σ -donation, only one lobe is shown for each orbital (from a variety of potential orbitals on the transition metal, and an sp^2 orbital on the Si centre).

A significant subset of Fischer-type silylene complexes involves *N*-heterocyclic silylene (NHSi) ligands. One class of NHSi (Figure 1.23; left) involves two N substituents on the Si centre forming part of a Si-containing ring (analogous to *N*-heterocyclic carbenes). These NHSi ligands are electronically stabilized because filled p orbitals on N donate some electron density to the empty p-orbital on silicon, and their complexes feature less electropositive Si centres than complexes with non-electronically stabilized silylene ligands.³¹⁴ Silylene groups where one of the substituents on Si is a bidentate amidinate ligand are also commonly referred to as NHSi ligands, though could alternatively be considered a type of base-stabilized silylene (Figure 1.23; right).^{315,316} Free NHSi moieties are often stable in the absence of a transition metal centre.^{315,316}

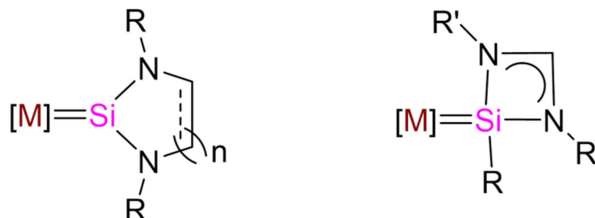


Figure 1.23: *N*-heterocyclic silylene complexes (NHSi ligands).

1.6.4 – Characterization of Base-free non-Electronically Stabilized Silylene Complexes

X-ray crystallography is an important technique in the characterization of silylene complexes. Relative to other silicon-based ligands, silylene complexes display two diagnostic structural features. First, they feature a planar environment about the sp^2 Si centre (in which lies both substituents of Si, the Si centre, and the metal); the sum of angles about the Si centre is normally statistically equivalent to 360° . Second, these complexes usually feature shorter M–Si distance than in silyl complexes of the same metal, but longer than in silylyne complexes (a summary of M–Si distances in structurally characterized silylene complexes is provided in Table 1.7).²²⁹ In general, the only complexes with shorter M–Si bonds are silylyne complexes. However, it should be noted that exceptions to this have been reported, including the first structurally characterized silylene complex where the Os–Si distance matches that of a single bond (in this complex, alternative resonance structures could be envisaged where the silylene-character is removed).³¹⁰ As well, chromium and nickel complexes with *N*-heterocyclic silylene complexes have been reported with shorter M–Si distances than non-electronically stabilized examples.^{314,317} In addition, the shortest Fe–Si bond is found in a complex with an η^3 -H₂SiR₂ ligand (*vide infra*),³¹⁸ and the shortest Pd–Si bonds are found in complexes with pincer ligands containing central silyl donors.³¹⁹ Therefore, it is clear that bond lengths can be influenced by factors other than intrinsic bond strength, especially when Si is part of a multidentate or η^n -coordinated ($n > 1$) ligand.

Table 1.7: M–Si distances for base-free, non-electronically stabilized silylene complexes (Å), as determined by X-ray or neutron crystal structures. Only metals for which solid state structures of such complexes have been obtained are included. Values are accurate as of 2016, and given to two decimal places.

M	d(M–Si) {# of complexes} ²¹¹	M	d(M–Si) {# of complexes} ²¹¹
Hf	2.65 {1}	Os	2.22-2.42 {4} ^d
Cr	2.36-2.48 {4}	Co	2.12 {1} ^e
Mo	2.29-2.39 {8} ^a	Ir	2.21-2.26 {3}
W	2.33-2.64 {14} ^b	Ni	2.09-2.13 {2}
Fe	2.15 {1}	Pd	2.24 {1}
Ru	2.18-2.28 {9} ^c	Pt	2.21-2.27 {5}

- a. This range includes two structures of $[\text{Cp}^*(\text{dmpe})\text{MoH}(=\text{SiEt}_2)]$, obtained by neutron and X-ray diffraction.
- b. If $[(\text{OC})_5\text{W}\{\text{SiPh}(\text{C}_6\text{H}_2\text{-}2,6\text{-}\{\text{PO}(\text{O}^i\text{Pr})_2\}_2\text{-}4\text{-}^i\text{Bu})\}]$, with an extremely bulky substituent on Si, is excluded as an outlier, this range becomes 2.33-2.44 Å. Also, this range includes two structures of $[\text{EtMe}_4\text{Cp}(\text{OC})_2\text{WH}(=\text{SiH}\{\text{C}(\text{SiMe}_3)_3\})]$, obtained by neutron and X-ray diffraction.
- c. This does not include $[(\text{OC})_4\text{Os}(=\text{Si}\{S^p\text{tol}\}\{\text{RuCp}^*(\text{PMe}_3)_2\})]$, for which there is a contribution from a zwitterionic resonance structure with a Ru=Si bond (2.286(2) Å).³¹⁰
- d. If $[(\text{OC})_4\text{Os}(=\text{Si}\{S^p\text{tol}\}\{\text{RuCp}^*(\text{PMe}_3)_2\})]$, for which are various resonance structures which dilute the silylene character of the Os–Si bond, is treated as an outlier then this range becomes 2.22-2.26 Å.
- e. No Co examples of base-free, non-electronically stabilized silylene complexes had been reported prior to 2016, so the single reported example (from 2018) is included here.³²⁰

NMR spectroscopy is also commonly used to definitively identify silylene complexes of transition metals. In particular, the high frequency ²⁹Si NMR chemical shift (>200 ppm) of the sp² Si centre in base-free, non-electronically stabilized silylene complexes is very diagnostic.³⁰⁴ This mirrors ¹³C NMR chemical shifts for carbene donors in transition metal complexes, which generally lie between 240 and 370 ppm.³²¹ By contrast, the vast majority of ²⁹Si NMR chemical shifts for *N*-heterocyclic silylene complexes lie in the 40-190 ppm range.³¹⁶ In certain classes of base-free, non-electronically stabilized silylene complexes, complementary NMR information can also be diagnostic. For example, hydrogen substituents on silylene ligands give rise to unusually high frequency ¹H NMR chemical shifts (6.34-12.1 ppm,¹ in contrast to H-substituted silyl ligands which normally give rise to ¹H NMR chemical shifts from 4 to 5.5 ppm).²²⁷ As well, for transition metals which are NMR active, the M–Si coupling

¹ See section 1.6.6 for references used to obtain ¹H NMR chemical shifts of silylene complexes with terminal hydride substituents.

constants involving silylene ligands are significantly higher than those involving silyl ligands (for example, in $[\text{Cp}^*(\text{OC})_2\text{W}(\text{SiMe}_3)(=\text{SiMe}_2)]$, which contains a silyl and a silylene ligand, the coupling constant between ^{183}W and ^{29}Si is 30.5 Hz for the former and 154.9 Hz for the latter).³²²

1.6.5 – Silylene Hydride Complexes

In 1993, shortly after they reported the first X-ray crystal structure of a silylene complex (*vide supra*), the Tilley group reported the synthesis and X-ray crystal structure of *trans*- $[(\text{C}_3\text{H}_5)_3\text{P}]_2\text{PtH}\{\text{=Si}(\text{SEt})_2\}^+$, the first silylene complex with a hydride co-ligand (as in Figure 1.24).³²³ One of the reasons that silylene hydride complexes are of great interest is that they can potentially be observed as a variety of isomers.³²⁴ Also, they often exist in equilibrium with silyl complexes (the product of 1,1-insertion of the hydride across the $\text{M}=\text{Si}$ double bond; Scheme 1.12). This equilibrium is often implicated both in the synthesis of silylene hydride complexes (by initial generation of an α -hydride containing silyl ligand)²²⁷⁻²²⁹ and reactions of silylene hydride complexes (the vacant coordination site generated in the isomerization of a silylene hydride to a silyl complex permits various reagents to coordinate to the metal centre prior to intramolecular reactivity involving the silyl ligand). As well, the presence of a hydride ligand offers an additional NMR handle for monitoring reactions involving silylene hydride complexes.

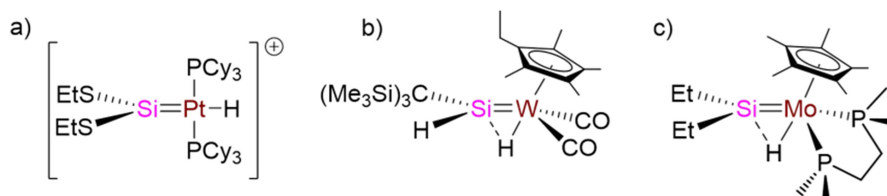
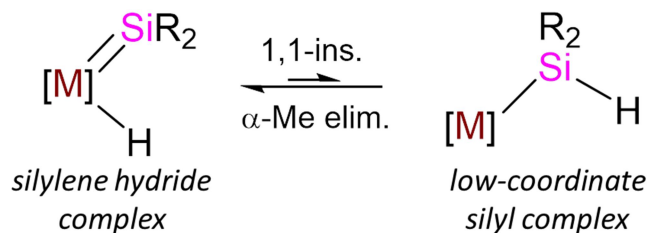


Figure 1.24: Early examples of silylene hydride complexes.



Scheme 1.12: Equilibrium between silylene hydride and silyl complexes.

In many silylene-hydride complexes, significant Si–H interligand interactions have been observed. Silylene hydride complexes with interligand Si–H interactions were first reported in 2004 independently by the Tobita³²⁵ (b in Figure 1.24; [^{EtMe4}Cp(OC)₂WH(=SiH{C(SiMe₃)₃})]) and Tilley³²⁶ (c in Figure 1.24; [Cp*(dmpe)MoH(=SiEt₂)]^m groups, and since that time solid-state structures of a variety of such complexes have been reported for W,^{327,328} Fe,³²⁹ Ru,³³⁰⁻³³² and Ni.³³³ Structurally, the interacting metal hydride ligands are generally oriented so that they could interact with the vacant p orbital on Si (i.e. out of the plane formed by Si and its terminal substituents). These interligand interactions are apparent from short Si–H distances. While the range of Si–H distances from all crystallographically characterized examples of these complexes is 1.17(5)-1.94(6) Å (Table 1.8), this is misleading both because of the difficulty in accurately locating hydrogen atoms by X-ray diffraction, and the presence of outliers at both ends of this range. For a pair of these complexes (the first two reported; b and c in Figure 1.24), neutron structures were also obtained to allow for accurate determination of the Si_{sp2}–H_M distances (1.68(1)-1.720(10) Å; Table 1.8), which are longer than a single bond (in base-free silylene complexes with a terminal hydride substituent, the Si_{sp2}–H_{Si} distances range from 1.33-1.56 Å),²¹¹ though are close enough to suggest some degree of interligand interaction.²³³ Spectroscopically, interligand Si–H interactions are apparent in the magnitudes of ²⁹Si–¹H coupling constants (28-62 Hz; Table 1.8), which are intermediate between those expected for 1-bond (~200 Hz) and 2-

^m A variety of other Mo silylene hydride complexes have been reported to feature Si–H interligand interactions, but for these complexes an X-ray crystal structure was not obtained, or the bridging hydride was not located from the difference map.

bond (< 10 Hz) coupling²⁶¹ (as discussed in section 1.5.5, determining the sign of $J_{\text{Si,H}}$ is necessary for accurate interpretation of this data, especially at low magnitudes; however this has not been normally done in the literature for silylene hydride complexes).

Table 1.8: Structural and spectroscopic data for silylene hydride complexes for which solid state structures have been reported and the metal hydride was located from the difference map. Unless otherwise noted, values were obtained by X-ray diffraction.

	Complex	d(M–Si) (Å)	$\Sigma(X\text{–Si–}Y),$ X, Y ≠ H _M (°)	d(H _M –Si) (Å)	$J_{\text{H,Si}}$ (Hz)	Ref.
Mo	[Cp*(dmpe)MoH(=SiEt ₂)]	2.34(1), ^a	358.9(5), ^a	1.68(1), ^a	44	Tilley (2004) ³²⁶
		2.344(7) ^b	359.1(1) ^b	1.74(2) ^b		
W	[^{EtMe₄} Cp(OC) ₂ WH(=SiH{C(SiMe ₃) ₃ })] ^c	2.359(8), ^a	359.4(5), ^a	1.72(1), ^a	28.3	Tobita (2004, ³¹⁴ 2012) ³²⁷
		2.370(1) ^b	357(3) ^b	1.71(6) ^b		
	[Ar(OC) ₂ WH(=Si{O ⁱ Pr}{C(SiMe ₃) ₃ })] ^d Ar = ^{EtMe₄} Cp	2.3760(9)	360.0(2)	1.94(6)	34.3	Tobita (2012) ³²⁷
Fe	[Cp*(^t Pr ₂ MeP)FeH{=SiH(Trip)}]	2.129(1)	357(2)	1.67(5)	–	Tilley (2018) ³²⁹
Ru	[Cp*(^t Pr ₃ P)RuH ₂ (=SiHMes)] ⁺	2.246(1)	360.0(5)	1.74(6) ^e	62.3	Tilley (2013) ³³⁰
	[(RNC){PhB(CH ₂ PPh ₂) ₃ }RuH(=SiMes ₂)] R = <i>o</i> -xylyl	2.299(2)	359.9(2)	1.17(5) ^f	43	Tilley (2014) ³³¹
	[Cp*(IXy)RuH{=SiH(Trip)}·AgOTf] ^g	2.264(1)	355(2)	1.77(5)	36.6	Tilley (2014) ³³²
Ni	[(dtbpe)NiH(=SiMes ₂)] ⁺	2.147(2)	360.0(2)	1.64(7)	43.4	Hillhouse (2010) ³³³

- From neutron structure data.
- From X-ray structure data.
- The neutron structure was obtained from an analogue where the hydride substituents on W and Si were replaced with ²H.
- It is possible that the solid state structure does not accurately reflect the solution state structure; the large $J_{\text{Si,H}}$ is indicative of a strong interligand Si–H interaction in solution while the long Si–H crystallographically determined distance (and the position of the interacting hydride close to the plane formed by Si and its terminal substituents) is indicative of a negligible interligand interaction.
- The position of one of the hydride ligands (not included in Table 1.8) was unstable under refinement.
- The author noted that this value is unrealistically short.
- This structure involves the Ag ion also interacting with the Ru=Si bond.

Surprisingly, no apparent weakening of the M–Si bond is observed relative to complexes without these interligand interactions (in stark contrast to Lewis base coordination to Si in silylene complexes, which result in significant weakening of this bond; *vide infra*); the M–Si distances (Table 1.8) are well within the range of base-free silylene complexes (Table 1.7).ⁿ As well, this interaction does not appear to impart significant pyramidalization to the Si centre (sum of angles around Si, not including H_M, is $\geq 355^\circ$; Table 1.8), suggesting that the character of the Si atom remains sp² (again in contrast to Lewis base coordination to Si in silylene complexes; *vide infra*). Finally, the ¹⁸³W–²⁹Si coupling constants for the two W complexes in Table 1.8 (109.9 and 132 Hz) are comparable to those in related hydride-free silylene complexes.

1.6.6 – Silylene Complexes with Terminal SiH Substituents

Silylene complexes with a terminal SiH substituent are relatively rare; such a complex, [(Et₃P)₃IrH₂{=SiH(C₆H₃-Mes₂-2,6)}][B(C₆F₅)₄], was first reported by Tessier and Youngs in 2002 (a in Figure 1.25).³³⁴ The same year, Tilley et al. suggested [{PhB(CH₂PPh₂)₃}IrH₂{=SiH(Trip)}] (b in Figure 1.25) as an intermediate in the synthesis of a disubstituted silylene hydride complex,³³⁵ and two years later, the Tobita³²⁵ and Tilley³²⁶ groups independently reported the first structurally characterized examples, [^{EtMe₄}Cp(OC)₂WH(=SiH{C(SiMe₃)₃})] (c in Figure 1.25; the same complex as b in Figure 1.24) and [Cp*(dmpe)MoH(=SiHPh)] (d in Figure 1.25), respectively. Aside from Ir examples,³³⁴⁻³³⁶ these types of complexes have only been reported for groups 6^{325,326,328,337-339} and 8^{329,330,332,340-343}, and group 7 examples are notably absent. Extensive studies by the Tilley and Tobita groups have demonstrated that hydride substituents on the sp² Si centres permit these silylene complexes to demonstrate unusual reactivity, including alkene insertion into that Si–H bond (*vide infra*)^{330,335,336,340} and accessing silylyne (M≡SiR) complexes.^{328,339}

ⁿ As well, the iron complex [Cp*(ⁱPr₂MeP)FeH{=SiH(Trip)}], which was reported in 2018, features a shorter Fe–Si distance than the single iron silylene complex in Table 1.7, which only includes species reported prior to 2017.

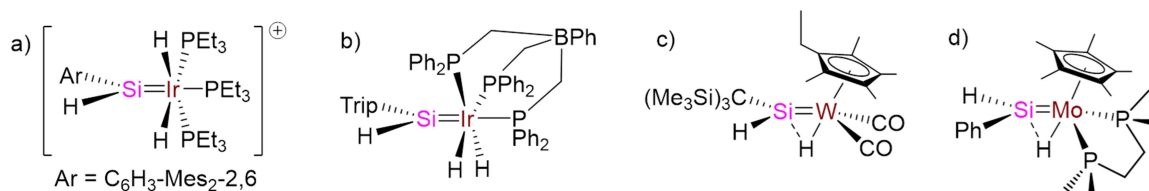


Figure 1.25: Early examples of silylene complexes with a terminal SiH substituent.

1.6.7 – NHC-Stabilized Silylene Complexes of Transition Metals

The first reported examples of transition metal silylene complexes were stabilized by Lewis base coordination to the silicon centre (*vide supra*). Of the various base-stabilized silylene complexes that have since been reported, one of the common classes involves *N*-heterocyclic carbenes (NHCs; various examples are outlined in Figure 1.26) as the Lewis base. One of the reasons for this is the accessibility of stable NHC-silylene adducts which can act as precursors in the synthesis of such complexes. While the first reported NHC-silylene adduct involved an otherwise stable parent free silylene,³⁴⁴ in 2009, the Roesky³⁴⁵ and Filippau³⁴⁶ groups simultaneously reported the synthesis of stable NHC-silylene adducts X₂Si-IPr (X = Cl or Br; a and b, respectively, in Figure 1.27) which involve stabilization of unstable parent free dihalosilylenes. These adducts contain a lone pair and were proposed to be able to act as Lewis bases. The following year, both groups investigated the reactions of these adducts with transition metal precursors to prepare NHC-stabilized silylene transition metal complexes (Roesky group; c and d in Figure 1.27)^{347,348} or an NHC-stabilized silylyne transition metal complex (Filippau group).³⁴⁹ In the past decade, many NHC-stabilized silylene transition metal complexes have been reported for V, Cr, W, Fe, Co, Rh, and Ni (Table 1.9; *vide infra*),^{347,348,350-362} and the most common method for their synthesis is substitution of neutral ligands by an intact silylene-NHC adduct. However, there are a handful of examples which were formed by addition of a free carbene to a base-free silylene complex³⁵³ or a pyridine-stabilized silylene complex (via substitution of pyridine).³⁵⁶ As well, carbene association to a transient (unobserved) base-free silylene complex is presumably the final step in the syntheses of a pair of NHC-stabilized iron silylene complexes.^{359,360}

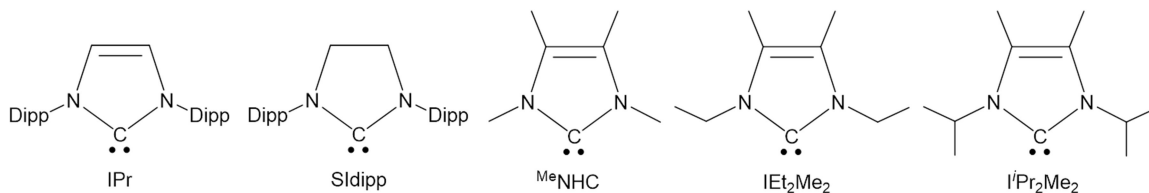


Figure 1.26: Glossary of NHCs.

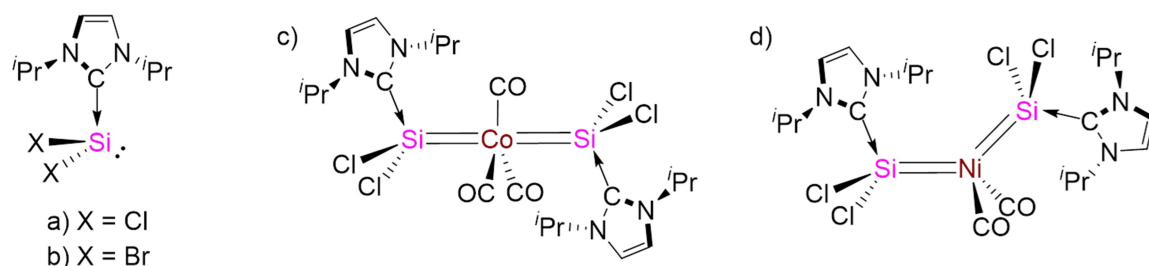


Figure 1.27: The first reported NHC-silylene adducts and NHC-stabilized silylene complexes. The M–Si bond is shown as a double bond for clarity, and does not reflect the bond strength.

Coordination of a Lewis base such as an NHC to the sp^2 Si centre of a silylene complex significantly affects the M–Si bond (Figure 1.28). First, the degree of π -backdonation is significantly reduced because of much poorer overlap of the pertinent orbitals and build up of electron density in the accepting Si-based orbital (a Si–C_{NHC} σ antibonding orbital). Second, the formerly vacant p orbital on Si has been hybridized, leading to pyramidalization. Because of these effects, the M–Si bond is significantly weaker than in base-free silylene complexes, though usually stronger than in silyl complexes.³⁰²

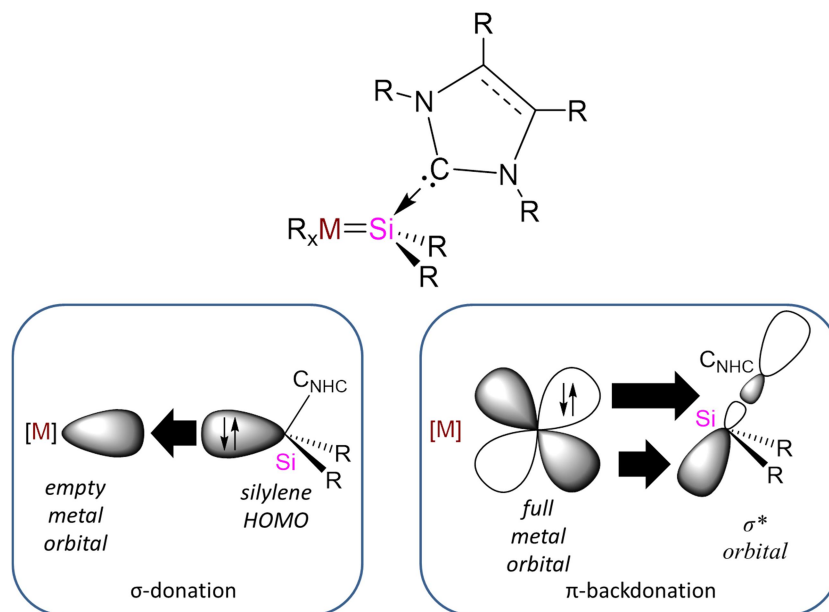
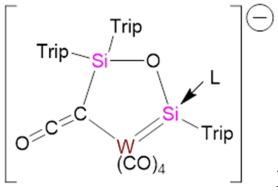


Figure 1.28: Electronic structure of NHC-stabilized silylene complexes. Dashed line in the Chemdraw figure indicates a single or double bond. For clarity, in the diagram for σ -donation, only one lobe is shown for each orbital.

Weaker bonding in base-stabilized silylene complexes is reflected in significantly longer M–Si bond lengths than in base-free silylenes (Table 1.9), though they remain on the shorter end of the range normally observed in silyl complexes. This reflects that the bond strength is intermediate between that in base-free silylene (sp^2 -hybridized Si) and silyl (sp^3 -hybridized Si) complexes. For most NHC-stabilized silylene complexes, this is also reflected by NMR spectroscopy; their ^{29}Si NMR chemical shifts typically fall within the 25-100 ppm range (Table 1.9; shifted to higher frequency of silyl complexes, but not nearly to the extent observed for silylene complexes). However, in a number of NHC-stabilized silylene complexes, very low frequency ^{29}Si chemical shifts have been observed (Table 1.9). This has been rationalized by adoption of a zwitterionic bonding motif which results in limited π -backdonation to the Si centre from the metal.³⁵⁷ As well, terminal H substituents on NHC-stabilized silylene ligands give rise to ^1H NMR environments in the range associated with silyl complexes or free hydrosilanes (4.16-7.27 ppm).

Table 1.9: Structurally characterized NHC-stabilized silylene complexes. NHC names relate to those in Figure 1.26.

	Complex	d(M–Si) (Å)	$\delta^{29\text{Si}}$ (ppm)	Reference
V	[Cp(OC) ₃ V{=SiCl ₂ (IPr)}]	2.4043(7)	88.7	Roesky (2011) ³⁵⁰
	[Cp*(OC) ₃ Cr{=Si(OH) ₂ (Sidipp)}]	2.4128(7)	39.6	Filippau (2014) ³⁵¹
Cr	[(OC) ₄ Cr{=SiCl ₂ (IPr)} ₂]	2.3113(12), 2.3118(12)	64.57	Ghadwal and Frenking (2017) ³⁵²
	[(OC) ₅ W{=SiH ₂ (IPr)}]	2.573(4)	-71.6	Rivard (2012) ³⁵⁴
W	 L = ^{M^e} NHC	2.6342(7)	31.12	Scheschkewitz (2015) ³⁵³
	[Cp*(OC) ₂ WH(=SiH{C(SiMe ₃) ₃ }{ ^{M^e} NHC})]	2.5206(8)	-16.7	Tobita (2015) ³⁵⁶
	[(OC) ₄ W{=SiCl ₂ (IPr)} ₂]	2.464(2), 2.4707(19)	24.84	Ghadwal and Frenking (2017) ³⁵²
	[(OC) ₅ W{=SiH(Si ^t Bu ₃)(^{M^e} NHC)}]	2.668(2)	-94.2	Inoue (2017) ³⁵⁵
	[(OC) ₄ Fe{=SiCl ₂ (IPr)}]	2.229(11)	59.2	Roesky (2011) ³⁵⁰
	[L ₂ FeH ₂ (η ² -HSiPh ₂){=SiHPh(L)}] (L = IEt ₂ Me ₂)	2.170(1)	27.55	Deng (2014) ³⁵⁹
	[(OC) ₄ Fe{=SiHAr(^{M^e} NHC)}] (Ar = 2,6-bis(2,4,6-triisopropylphenyl)phenyl)	2.3268(6)	-11.1	Müller (2016) ³⁵⁷
	[(OC) ₃ Fe{=SiHCl(IPr)} ₂]	2.189(3), 2.213(3)	44.02, 44.32	Robinson (2016) ³⁵⁸
Fe	[(OC) ₄ Fe{=SiH(Si ^t Bu ₃)(^{M^e} NHC)}]	2.3717(16)	-48.3	Inoue (2017) ³⁵⁵
	[(OC) ₄ Fe{=SiCl ₂ (^{M^e} NHC)}]	2.242(3)	63	Inoue (2017) ³⁵⁵
	[(OC) ₄ Fe{=SiH ₂ (^{M^e} NHC)}]	2.295(3)	-25.5	Inoue (2017) ³⁵⁵
	[(OC) ₄ Fe{=SiMe ₂ (^{M^e} NHC)}]	2.3273(5)	29.4	Inoue (2017) ³⁵⁵
	[(IPr) ₂ Fe(η ³ -H ₃ SiHPh ₂){=SiH ₂ (IPr)}]	2.2227(10)	–	Radius (2017) ³⁶⁰
	[(OC) ₄ Fe{=SiMe ₂ (IPr ₂ Me ₂)}]	2.3323(4)	26.3	Scheschkewitz and Jana (2019) ³⁶¹
Co	[(OC) ₃ Co{=SiCl ₂ (IPr)} ₂] ⁺	2.2276(12), 2.2278(13)	44.11	Roesky (2010) ³⁴⁷
	[(Cp(OC)Co{=SiCl ₂ (IPr)}]	2.1349(4)	31.86	Roesky (2011) ³⁵⁰
Rh	[(OC) ₂ Rh{=SiCl ₂ (IPr)} ₂]	2.3605(8)	27.9	Rivard (2012) ³⁵⁴
Ni	[(OC) ₂ Ni{=SiCl ₂ (IPr)} ₂]	2.1854(7), 2.1955(9)	43.19	Roesky (2010) ³⁴⁸
	[{(Me ₃ Si) ₃ Si}Ni{=SiMe ₂ (IPr)}]	2.223(5)	–	Tilley (2019) ³⁶²

Two NHC-stabilized silylene complexes with hydride co-ligands have been reported (not considering complexes where all hydride co-ligands are involved in interligand interactions with other co-ligands);³⁶⁰ the iron complex $[(\text{IEt}_2\text{Me}_2)_2\text{FeH}_2(\eta^2\text{-HSiPh}_2)\{\text{=SiHPh}(\text{IEt}_2\text{Me}_2)\}]$ (a in Figure 1.29)³⁵⁹ and the tungsten complex $[\text{Cp}^*(\text{OC})_2\text{WH}(\text{=SiH}\{\text{C}(\text{SiMe}_3)_3\}\{\text{M}^c\text{NHC}\})]$ (b In Figure 1.29).³⁵⁶ While significant Si–H interactions were observed in the iron system, the tungsten complex only features a weak interligand Si–H interaction ($J_{\text{Si,H}} = 27.0$ Hz). A base-free silylene analogue of this complex, $[\text{Cp}^*(\text{OC})_2\text{WH}(\text{=SiH}\{\text{C}(\text{SiMe}_3)_3\})]$, was not included in Table 1.8 because no X-ray crystal structure was obtained. However, this complex features a much higher $J_{\text{Si,H}}$ coupling of 109.9 Hz,³²⁵ suggesting that NHC coordination to a silylene hydride complex significantly weakens any interligand Si–H interactions.

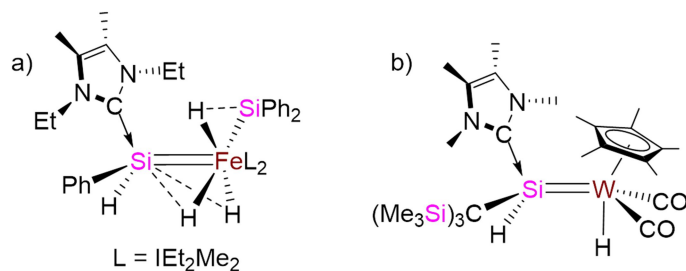


Figure 1.29: NHC-stabilized silylene hydride complexes. The M–Si bond is shown as a double bond for clarity, and does not reflect bond strength.

1.6.8 – Silylene Complexes of Early/Mid Transition Metal Centres

The majority of reported silylene complexes involve late transition metal centres, and of silylene complexes involving gr. 3-7, the vast majority are group 6 complexes. Only a handful of base-free silylene complexes have been reported for gr. 3-5 metals (Figure 1.30). To date, the only group 3 example involves an *N*-heterocyclic silylene ligand (a in Figure 1.30).³⁶³ Meanwhile, the only group 4 examples are a series of related *N*-heterocyclic silylene titanium(II) complexes (b-d in Figure 1.30),³⁶⁴ a series of titanium silylene complexes with a chelating κ^2 -disilyl substituent on the sp^2 Si centre ($[\text{Cp}_2\text{LTi}(\text{=Si}\{\kappa^2\text{-Si}(\text{SiMe}^t\text{Bu}_2)\text{C}(\text{SiMe}^t\text{Bu}_2)_2\text{Si}(\text{SiMe}^t\text{Bu}_2)\})]$; L = THF, PMe_3 , *o*-xylylNC:

e-g in Figure 1.30),³⁶⁵ and the hafnium complexes [^{Et}Cp(Me₃P)_nHf{=Si(SiMe^tBu₂)₂}] (n = 0 or 1; h and i in Figure 1.30)³⁶⁶ and [Cp₂Hf(=Si{κ²-C(SiMe₃)C(Ph)C(Ph)C(SiMe₃)})] (j in Figure 1.30; decomposes above -70 °C).³⁶⁷ The only vanadium example to have been structurally characterized involves an *N*-heterocyclic silylene (k in Figure 1.30).³⁶⁸ In addition, a pair of base-free vanadium silylene complexes with non-electronically stabilized silylene ligands have also been reported with limited characterization; in 2005 Egorov et al. reported [Cp*₂V(=SiMe₂)] based on EPR spectroscopic observation (l in Figure 1.30),³⁶⁹ and in 2008 the Tilley group reported [Cp(dmpe)V(=SiPh₂)]⁺ on the basis of elemental analysis (m in Figure 1.30).³⁷⁰ These early transition metal silylene complexes have generally been proposed to be nucleophilic at Si (akin to Schrock-type carbene complexes), on the basis of reactions with various nucleophiles which result in reactivity which does not involve nucleophile coordination to the Si centre, in contrast to the bulk of reported silylene complexes which are electrophilic at silicon (*vide supra*).

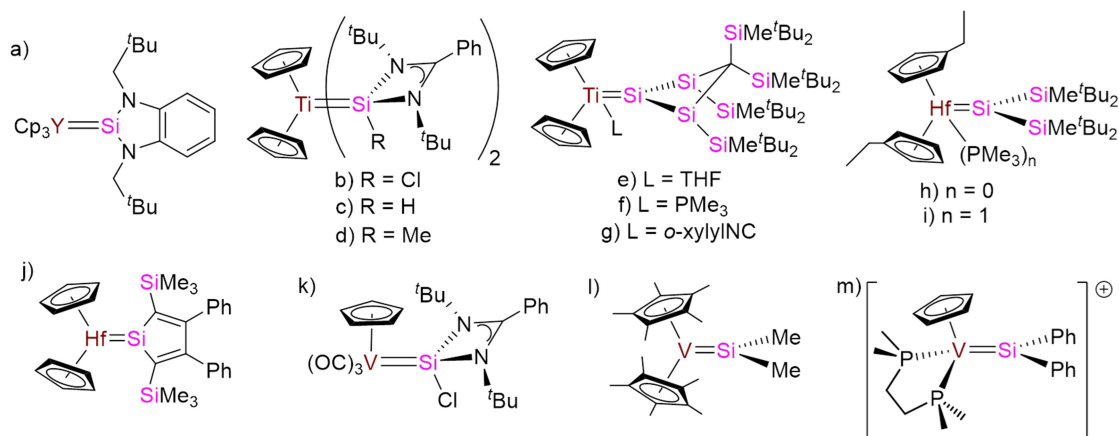


Figure 1.30: Base-free silylene complexes of gr. 3-5.

In addition, a pair of donor-stabilized silylene complexes of gr. 5 transition metals have been reported. In 2005, the Tobita group reported the tantalum complex [Cp₂Ta{κ₂-Me₂Si(OMe)SiMe₂}], which features a bidentate alkoxy-bridged bis(silylene) ligand (a in Figure 1.31).³⁷¹ Six years later, the NHC-stabilized vanadium silylene complex [Cp(OC)₃V{=SiCl₂(IPr)}] was reported by Dittrich and Roesky et al. (b in Figure 1.31).³⁵⁰

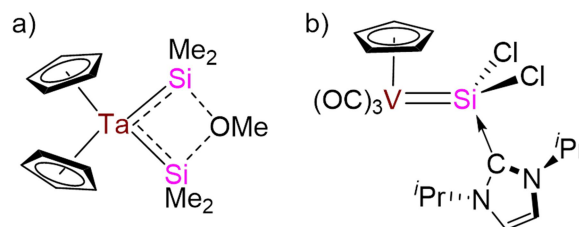


Figure 1.31: Donor-stabilized silylene complexes of gr. 4-5.

Despite the numerous examples of gr. 6 and 8 silylene complexes, no base-free, monometallic, non-electronically stabilized group 7 silylene complexes have been isolated. No Tc silylene complexes of any nature have been reported (as expected due to its radioactivity), and the only structurally characterized Re examples involve *N*-heterocyclic silylene ligands which would be stable even in the absence of transition metal coordination (a and b in Figure 1.32).³⁷² Additionally, in 1991 the Gladysz group reported the base-stabilized silylene complex $[\text{Cp}(\text{ON})(\text{Ph}_3\text{P})\text{Re}\{\text{=SiMe}_2(\text{NC}_5\text{H}_5)\}]^+$ (c in Figure 1.32), and suggested the involvement of a base-free rhenium silylene intermediate ($[\text{Cp}(\text{ON})(\text{Ph}_3\text{P})\text{Re}(\text{=SiMe}_2)]^+$) in a number of chemical transformations.³⁷³ As well, a pair of radical silylene complexes have been observed by EPR spectroscopy (d and e in Figure 1.32).³⁷⁴

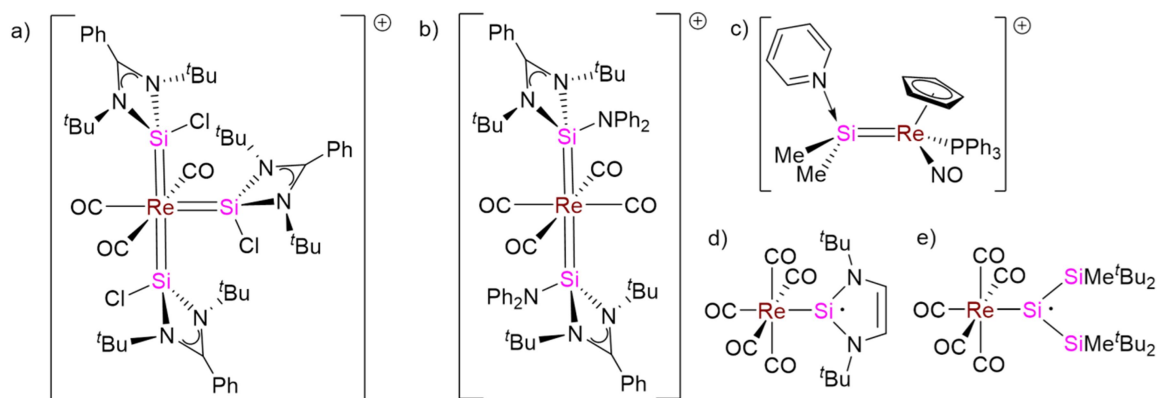


Figure 1.32: Reported silylene complexes of rhenium.

A handful of manganese complexes involving bridging or electronically stabilized silylene ligands have been reported. As early as 1973, Simon and Dahl reported the

dinuclear complex $[(OC)_4Mn]_2(\mu_2-SiPh_2)_2$, for which an X-ray crystal structure was obtained that showed two silylene ligands, each bridging between the two Mn atoms (a in Figure 1.33).³⁷⁵ A decade later, Herrmann et al. reported the dimetallic complex $[\{Cp^*(OC)_2MnH\}_2(\mu-SiH_2)]$ and trimetallic complex $[\{Cp(OC)_2Mn\}_3(\mu_2-SiH_2)]$ (b and c, respectively, in Figure 1.33),³⁷⁶ and an X-ray crystal structure was later obtained for the former.³⁷⁷ Herrmann's complexes (like the earlier 1973 example) each contain a silylene ligand bridging between two Mn atoms. The Mn–Si distances in these bridging complexes (2.402(2)-2.434(3) Å) are nearly equivalent to the average over all structurally characterized manganese silyl complexes (2.45 Å),²¹¹ suggestive of negligible double bond character.

In 1991, the Corriu and Ogino groups independently reported the first monometallic manganese silylene complexes, which in both cases featured base-stabilization. The Corriu example (for which a crystal structure was not obtained) featured coordination to the sp^2 Si centre by a pendant amine ($[^{Me}Cp(OC)_2Mn\{=SiPh(C_{12}H_{14}N)\}]$; d in Figure 1.33), and the electronically-stabilized nature of the silylene ligand is apparent by the stability of the free silylene in the absence of a transition metal centre.³⁷⁸ Ogino's report ($[(OC)_4Mn\{\kappa^2-Me_2Si(OMe)SiMe_2\}]$) involved a delocalized bis(silylene)ligand where the Si centres were bridged by an oxymethyl group (e in Figure 1.33), and a base-free manganese silylene complex ($[(OC)_4Mn(SiMe_2OMe)(=SiMe_2)]$) was proposed as an intermediate in its synthesis.³⁷⁹ Twenty years later, the Roesky group reported a pair of complexes featuring *N*-heterocyclic silylene ligands, where the free ligand is stable in the absence of a transition metal centre (f and g in Figure 1.33).³⁷² The Mn–Si distances of 2.2789(8)-2.3571(7) Å in these reports are at the very low end of known metal silyl complexes (the shortest Mn–Si bond in a silyl complex is 2.254(1) Å in $[^{Me}Cp(OC)_2MnH(SiCl_3)]$),²²³ and the ^{29}Si NMR chemical shifts of 61.11-124.0 ppm are consistent with a limited degree of silylene character (as expected for base-stabilized or *N*-heterocyclic silylene complexes; *vide supra*). Very recently (following publication of the base-free silylene hydride complexes discussed in Chapter 4), the Driess group reported X-ray crystal structures for a series of

N-heterocyclic silylene manganese(II) complexes (h-j in Figure 1.33).³⁸⁰ However, the Mn–Si distances in these divalent manganese complexes of 2.5923(5)-2.6347(7) Å are significantly longer than those in Roesky’s monovalent examples (*vide supra*).

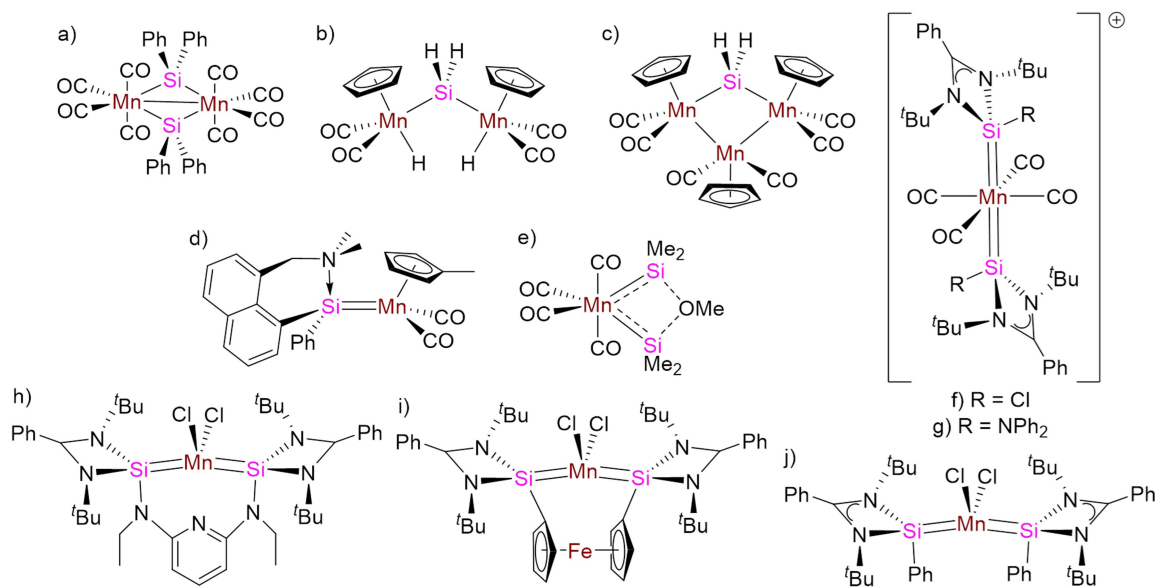


Figure 1.33: Silylene complexes of manganese.

1.6.9 – Reactions of silylene complexes with alkenes and alkynes

Given that reactions of transition metal silylene complexes with various reagents have been reviewed elsewhere,³⁰³ we herein provide a comprehensive review only of reactions with alkene and alkyne reagents, as this pertains directly to a significant portion of the work presented in this thesis.

Alkene hydrosilylation, the addition of a H–Si bond across an unsaturated C=C bond, is an industrially important chemical transformation.^{381,382-385} In 2003, the Tilley group reported a new mechanism for hydrosilylation mediated by transition metal silylene complexes with a terminal hydrogen substituent, which has subsequently become known as the Glaser-Tilley mechanism (Figure 1.34 bottom).³⁴⁰ This mechanism is unusual in that it selectively converts primary hydrosilanes (H₃SiR, R = Ph, Hex, Mes, Cy) to secondary hydrosilanes.^{385,386} A key step in this mechanism is the direct insertion

of an alkene into the Si–H bond of a terminal silylene ligand with a terminal SiH substituent. This stoichiometric reaction was first observed in the reaction of $[\{\text{PhB}(\text{CH}_2\text{PPh}_2)_3\}\text{IrH}_2\{=\text{SiH}(\text{Trip})\}]$ (b in Figure 1.25; *vide supra*) with cyclooctene,³³⁵ and subsequently demonstrated in the stoichiometric reactions of $[\text{Cp}^*(^i\text{Pr}_3\text{P})\text{RuH}_2\{=\text{SiHPh}(\text{Et}_2\text{O})\}]^+$ (the catalyst in the initial report on the Glaser-Tilley mechanism) with 1-hexene³⁴⁰ and the base-free analogue $[\text{Cp}^*(^i\text{Pr}_3\text{P})\text{RuH}_2(=\text{SiHMes})]^+$ with various alkenes in the absence of free hydrosilanes.³⁸⁷ Calculations have shown that this mechanism is lower in energy than the conventional Chalk-Harrod or modified Chalk-Harrod mechanisms (Figure 1.34 top left and top right, respectively) for model cationic Ru systems.³⁸⁸ Cationic Ru^{330,340} and Ir³³⁶ catalysts have been shown to be active towards hydrosilylation of a variety of terminal linear (ethylene, 1-hexene, 1-octene, vinyltrimethylsilane, *tert*-butylethylene, styrene, and *p*-chlorostyrene) and internal cyclic (1-methylcyclohexene, cyclopentene, cyclohexene, and *cis*-cyclooctene) olefins. Unlike other hydrosilylation mechanisms, no vinylsilane byproducts were observed in these reactions.

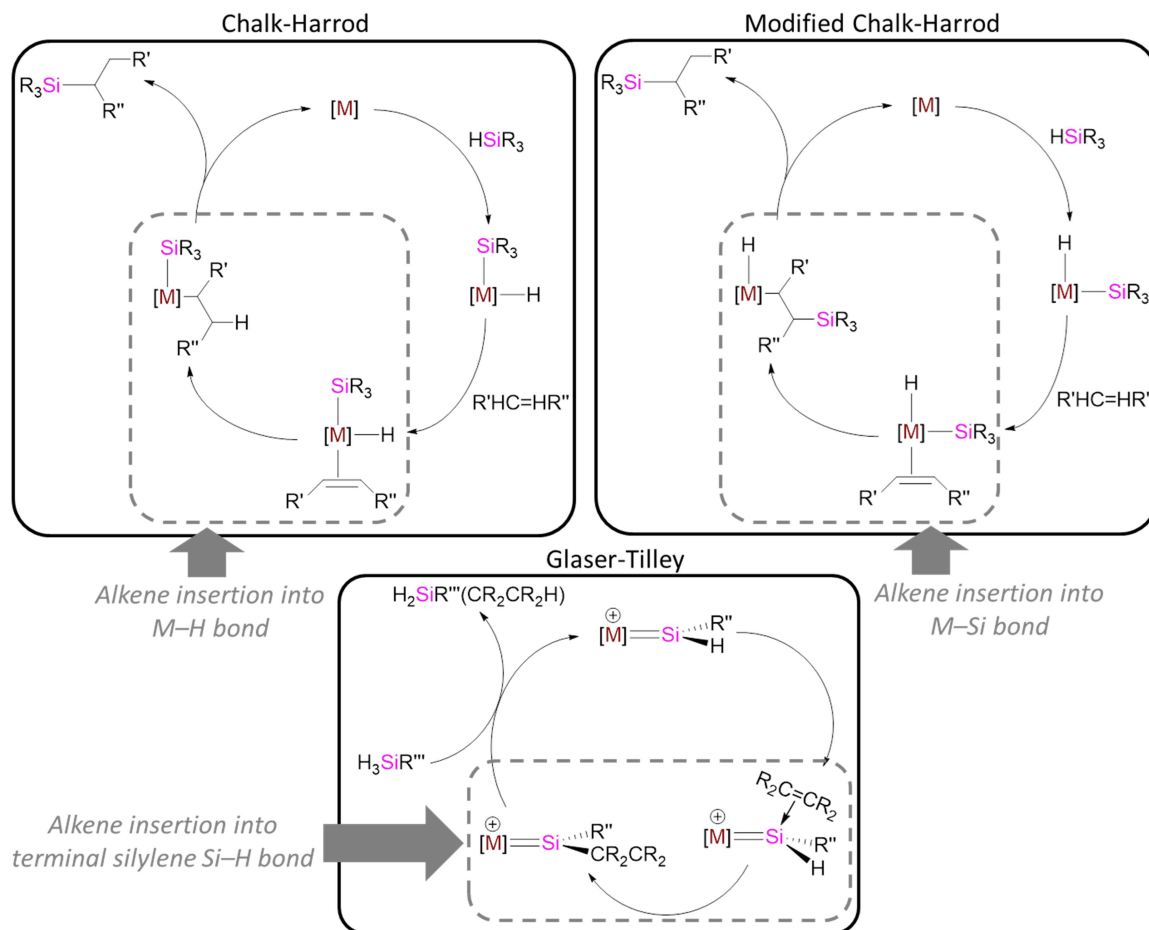


Figure 1.34: Common mechanisms for olefin hydrosilylation.³⁴⁰ Key alkene insertion steps are highlighted in grey.

It appears that a very electropositive Si centre is required for the Glaser-Tilley mechanism to proceed. Aside from the initial (stoichiometric) report of alkene insertion into the terminal Si-H bond of $[\{\text{PhB}(\text{CH}_2\text{PPh}_2)_3\}\text{IrH}_2\{=\text{SiH}(\text{Trip})\}]$ (which can be considered to be zwitterionic with a positive charge on Ir), all such reactions have involved cationic systems. Furthermore, in the reaction of neutral $[\{\text{PhB}(\text{CH}_2\text{PPh}_2)_3\}\text{IrH}_2\{=\text{SiH}(\text{Trip})\}]$ with cyclooctene, various alternative mechanisms for alkene insertion (i.e. not direct insertion into the Si-H bond, as in the Glaser-Tilley mechanism) were proposed.³³⁵

While the cationic osmium complex $[\text{Cp}^*(^i\text{Pr}_3\text{P})\text{OsH}_2\{=\text{SiH}(\text{Trip})\}]^+$ was observed to react rapidly with alkenes even at low temperatures (though it proved to be inactive towards catalytic hydrosilylation),³⁴⁰ the neutral complex $[\text{Cp}^*(^i\text{Pr}_3\text{P})\text{OsH}\{=\text{SiH}(\text{Trip})\}]$ was unreactive towards either alkenes or alkynes. As well, calculations have shown that the ΔG barrier for ethylene insertion into the terminal Si–H bond (including ethylene coordination to the Si centre) for models of these Os complexes indicated that the activation barrier is 77 kJ mol⁻¹ lower for the cationic system.³⁴²

Reactions of silylene complexes with alkynes are uncommon. In 2002, Tilley et al. reported the reaction of the cationic iridium complex $[\text{Cp}^*(\text{Me}_3\text{P})\text{IrH}(=\text{SiPh}_2)]^+$ with 4-ethynyltoluene (the reactions of the same complex with 2-butyne or 1,2-propadiene yielded a mixture of products) to form the η^3 -silaallyl complex $[\text{Cp}^*(\text{Me}_3\text{P})\text{Ir}\{\eta^3\text{-Ph}_2\text{SiCHCH}(p\text{-tol})\}]^+$ (f in Figure 1.43; see section 1.7.8). This reaction was proposed to proceed either by initial 2+2 cycloaddition of the C≡C and Ir=Si bonds, or 1,2-insertion of the triple bond into the Ir–Si bond of a silyl isomer.³⁸⁹ The former of these two proposed mechanisms (2+2 cycloaddition) was observed directly in the reactions of the titanium silylene complexes $[\text{Cp}_2\text{LTi}(=\text{Si}\{\mu\text{-SiSi}(\text{SiMe}^t\text{Bu}_2)\}_2\{\text{Si}(\text{SiMe}^t\text{Bu}_2)_2\})]$ (L = THF, PMe₃, *o*-xylylNC; e-g in Figure 1.30) with terminal alkynes RC≡CH (R = SiMe₃, ^{*t*}Bu, or Ph) to generate silatitanacyclobutane complexes.^{365,390} In addition, the latter of these two proposed mechanisms (1,2-insertion of the alkyne into a metal-silyl bond) was also proposed for the reaction of $[\text{Cp}^*(\text{dmpe})\text{MoH}(=\text{SiMe}_2)]$ with Me₃SiC≡CH to form the vinylidene complex $[\text{Cp}^*(\text{dmpe})\text{MoH}\{=\text{C}=\text{C}(\text{SiHMe}_2)(\text{SiMe}_3)\}]$ (the product of silylene isomerization to a silyl complex followed by 1,2-insertion of the alkyne into the Mo–Si bond to form a vinyl complex, and subsequent α -hydride elimination).³²⁶ Very recently, Driess et al. reported that (NHSi)₂MnCl₂ complexes (and MnCl₂ or [(OC)₅MnBr] in the presence of free *N*-heterocyclic silylenes) catalyze hydrogenation of alkynes to alkenes.³⁸⁰ A Glaser-Tilley mechanism for catalytic alkyne hydrosilylation has not been reported, but various alkynes have been observed to insert into the terminal Si–H bond of

cationic $[\text{Cp}^*(\text{Pr}_3\text{P})\text{RuH}(=\text{SiHMes})][\text{B}(\text{C}_6\text{F}_5)_4]^{387}$ and a neutral *N*-heterocyclic silylene complex of Ni,³⁹¹ forming silylene complexes with a vinyl substituent on Si.

Reactions of silylene complexes with alkenes and alkynes can also result in simple substitution of the silylene ligand. For example, in the reactions of $[(\text{Cy}_3\text{P})_2\text{Pt}(=\text{SiMes}_2)]$ with ethylene, propyne, and 2-butyne all resulted in substitution of the silylene ligand, affording a variety of Si-containing byproducts, which likely arise from decomposition of the extruded silylene.³⁹²

1.6.10 – Complexes related to silylene complexes

Any discussion of silylene complexes would be incomplete without discussion of species which feature a similar M–Si environment. For example, $\eta^3\text{-H}_2\text{SiR}_2$ complexes are isomers of silylene dihydride complexes and bear significant similarities. The first structurally characterized complexes which can be described in this manner were a pair of dimetallic species, each with a bridging SiH_4 ligand reported by Sabo-Etienne et al. in 2000 (a-b in Figure 1.35).³⁹³ Six years later, the Peters group reported a pair of monometallic iron examples, which they described as adducts of H_2SiR_2 (c-d in Figure 1.35).³¹⁸ Over the past decade, the Tilley group has reported a series of Ru $\eta^3\text{-H}_2\text{SiR}_2$ complexes (e-n in Figure 1.35).³⁹⁴ These complexes can often be described with a bonding scheme along the continuum from a silylene dihydride complex to an H_2SiR_2 adduct. A detailed description of the nature of bonding in these complexes is beyond the scope of this chapter, though various bonding descriptions used in the literature are shown in Figure 1.36 (some of these were reported as a resonance structure).

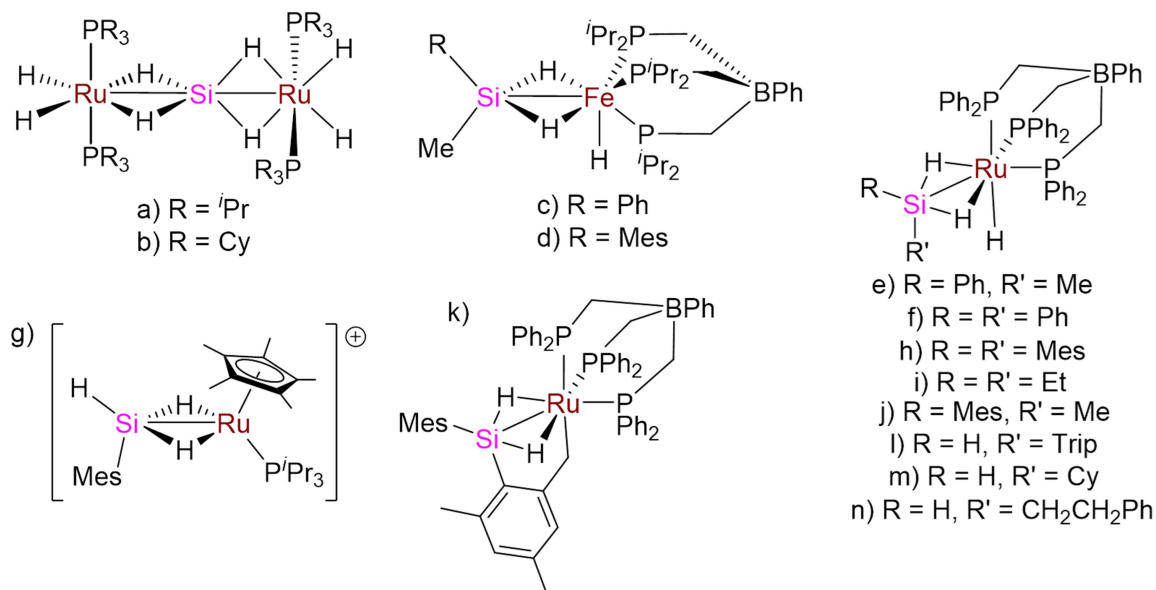


Figure 1.35: $\eta^3\text{-H}_2\text{SiR}_2$ complexes of transition metals. For clarity, all structures have been drawn with single bonds between Si and the metal, and between each of those and the bridging hydride ligands.

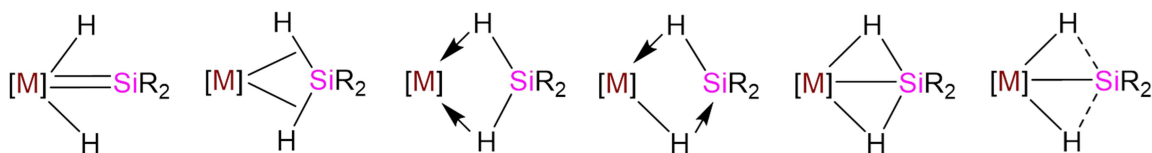


Figure 1.36: Structures used to describe $\eta^3\text{-H}_2\text{SiR}_2$ complexes of transition metals.

Many similarities exist between $\eta^3\text{-H}_2\text{SiR}_2$ complexes and silylene complexes. Of structurally characterized examples, with one exception, the M–Si distances in $\eta^3\text{-H}_2\text{SiR}_2$ complexes (Table 1.10) are either within or below the range of silylene complexes involving their respective metal (Table 1.7). Also similar to base-free silylene complexes, the environment about the Si atom (excluding the ‘bridging’ hydride moieties) is planar; $\Sigma(\text{X–Si–Y})$ ($\text{X}, \text{Y} \neq \text{H}_{\text{br}}$) $\geq 359.5^\circ$ (Table 1.10). The two ‘bridging’ hydride moieties are located in a plane (with Si) significantly angled from the plane of Si and its terminal substituents, in most cases close to 90° (Table 1.10), and like some silylene hydride complexes (*vide supra*), short Si–H_{bridging} distances were observed (Table 1.10). Further

illustrating the silylene-like character of $\eta^3\text{-H}_2\text{SiR}_2$ complexes, some examples have displayed similar hydrosilylation activity.³⁸⁵

Table 1.10: Structural and spectroscopic parameters for $\eta^3\text{-H}_2\text{SiR}_2$ complexes. Complexes are identified by the letter in Figure 1.35. H_{br} is a hydride interacting with Si and the metal.

Complex	d(M–Si) (Å)	$\Sigma(\text{X–Si–Y})$, X,Y $\neq\text{H}_{\text{br}}$ (°)	d($\text{H}_{\text{M}}\text{–Si}$) (Å)	$\angle(\text{X–Si–Y})\text{–}$ ($\text{H}_{\text{br}}\text{–Si–H}_{\text{br}}$) X,Y $\neq\text{H}_{\text{br}}$ (°)	$\delta^{29}\text{Si}$ in ppm ($J_{\text{IH},29\text{Si}}$ in Hz)	Ref.
a	2.1875(4)	359.5	1.69(3), 1.73(3)	69	–	Sabo-Etienne (2000) ³⁹³
b	–	–	–	–	290.2 (36) ^a	Sabo-Etienne (2000) ³⁹³
c	2.1280(7)	360.0(1)	1.464(1)- 1.552(2)	83	162 (68) ^a	Peters (2006) ³¹⁸
d	2.131(1)- 2.141(1)	360.0(2)- 360.1(2)	1.56(4)- 1.74(4)	88-89	160 (70) ^a	Peters (2006) ³¹⁸
e	2.263(1)	359.9(2)	1.61(4)- 1.66(7)	88	154 (65) ^a	Tilley (2011) ³⁹⁴
f	–	–	–	–	141 (68) ^a	Tilley (2011) ³⁹⁴
g ^b	2.246(1)	360.0(5)	1.74(6)	–	228.7 (62.3)	Tilley (2013) ³³⁰
h	–	–	–	–	131 (65) ^a	Tilley (2014) ³³¹
I	–	–	–	–	175 (64) ^a	Tilley (2014) ³³¹
J	–	–	–	–	145 (69) ^a	Tilley (2014) ³³¹
k	2.3046(8)	360.0(1)	1.72(3)- 1.73(2)	85	138 (105)	Tilley (2014) ³³¹
l	–	–	–	–	123 (68) ^a	Tilley (2018) ³⁹⁵
m and n	–	–	–	–	–	Tilley (2018) ³⁹⁵

- a. The bridging hydride ligands are in rapid exchange with the terminal hydride ligand(s), so this is an average over both environments.
 b. One of the H atoms on Ru was not accurately located crystallographically (it was unstable under refinement).

NMR spectroscopy, however, highlights a significant electronic difference between $\eta^3\text{-H}_2\text{SiR}_2$ and base-free silylene complexes (including silylene hydride complexes with Si–H interactions; *vide supra*). With two exceptions, the ^{29}Si NMR chemical shifts of $\eta^3\text{-H}_2\text{SiR}_2$ complexes (Table 1.10; 123-175 ppm) lie intermediate between silyl and silylene complexes. $\eta^3\text{-H}_2\text{SiR}_2$ complexes with higher frequency

chemical shifts can be considered to have greater silylene dihydride-like character. The magnitudes of the ^{29}Si - ^1H coupling constant involving the ‘bridging’ hydride ligands also could potentially provide insight into the nature of the bonding. If the two complexes with silylene-like ^{29}Si chemical shifts are excluded, it appears at first glance that the majority of $J_{\text{Si,H}}$ (Table 1.10) are only slightly higher than those observed in silylene hydride complexes with Si-H interligand interactions (28-62 Hz; *vide supra*). However, this is misleading because (with one exception) the ‘bridging’ hydride ligands are in rapid chemical exchange with terminal metal hydride ligands, so the ^{29}Si - $^1\text{H}_{\text{Br}}$ and ^{29}Si - $^1\text{H}_{\text{M}}$ coupling constants are averaged. Given that the 2-bond coupling constants involving the non-interacting metal hydrides would be around 10 Hz, the ^{29}Si - ^1H coupling constants involving the ‘bridging’ hydrides could be estimated to be around 90-100 Hz. This range is close to the single example where there are no additional metal hydride ligands present to exchange with the ‘bridging’ hydride (105 Hz), and suggests that in general, higher (non-averaged) $J_{\text{Si,H}}$ couplings are indicative of less silylene character in $\eta^3\text{-H}_2\text{SiR}_2$ complexes.

Another class of complexes related to silylene complexes are silylyne complexes (Si analogues of carbyne complexes, with a formal $\text{M}\equiv\text{Si}$ triple bond). The first base-free silylyne complex was reported by the Tilley group in 2003 ($[\text{Cp}^*(\text{dmpe})\text{MoH}(\equiv\text{SiMe}_3)]^+$; a in Figure 1.37).³⁹⁶ Since that time, base-free silylyne complexes have been reported for Nb, Cr, Os, and W, in addition to Mo, and the triple-bond character is apparent from M-Si distances shorter than in silylene complexes involving the same metal (where a comparable is available).³⁹⁷ As base coordination to the sp^2 Si environment in silylene complexes results in significant weakening of the M-Si bond (*vide supra*), base coordination to the sp Si centre in silylyne complexes likewise weakens the M-Si bond. Thus, base-coordinated silylyne complexes have a bonding situation very similar to base-free silylene complexes.

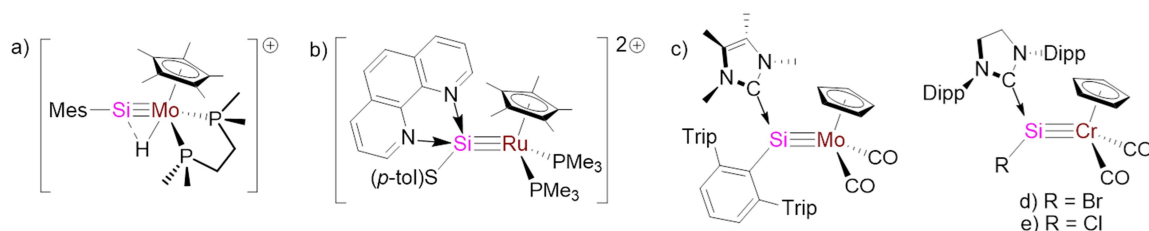


Figure 1.37: Selected silylyne complexes of transition metals. Base-stabilized structures are drawn with a triple bond between Si and the metal for clarity, and this does not reflect the bond strength.

The first base-stabilized silylyne complex was actually reported over a decade prior to the first base-free example; in 1992 the Tilley group reported a Ru dicationic silylyne structure with 2,2'-bipyridine coordination to the Si centre (b in Figure 1.37). The Ru–Si distance of 2.269(5) Å in this species is within the range associated with ruthenium silylene complexes (2.18–2.28 Å; Table 1.7).³⁹⁸ Two decades later, the Fillipou group reported NHC-stabilized silylyne complexes of Mo (c in Figure 1.37)³⁴⁹ and Cr (d and e in Figure 1.37),³⁹⁹ which feature M–Si bonds {d(Mo–Si) of 2.3474(6) Å and d(Cr–Si) of 2.160–2.162(1) Å} only slightly shorter than those in structurally characterized silylene complexes of Mo or Cr, respectively (Table 1.7). As well, the environment about Si (including the NHC substituent) in these complexes is nearly planar ($\Sigma X-Si-Y \geq 357^\circ$). Emphasizing the silylene-like nature of these complexes, Fillipou describes NHC-stabilized silylyne complexes as having a zwitterionic silylene structure (Figure 1.38). Though not directly related to silylene complexes, a pair of doubly NHC-coordinated silylyne complexes (with two NHCs bound to the Si centre) have been reported for Cr³⁹⁹ and W,³⁵⁶ and feature M–Si bonding consistent with a single bond.

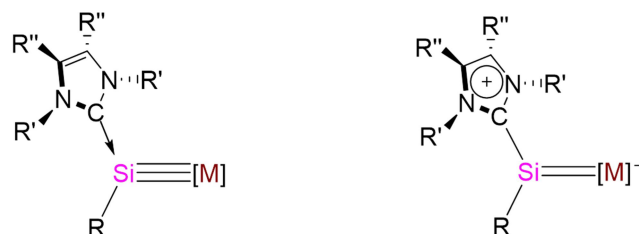


Figure 1.38: Alternative bonding descriptions of NHC-stabilized silylyne complexes.

1.7 – Silene Complexes of Transition Metals

1.7.1 – Scope of Section

The aim of this section is to provide an overview of the synthesis and characterization of transition metal silene complexes, with a focus on those which have been directly observed. Special emphasis is given to silene hydride complexes with an Si–H interligand interaction. Also included are complexes with non-aromatic ligands in which a silene moiety is incorporated into a larger π -system (i.e. where a resonance structure can be drawn with a Si=C double bond). Not included in this review are reactions of silene complexes or reports of silene complexes as un-observed intermediates in chemical transformations.

1.7.2 – Introduction to Silene Complexes

Silenes ($R_2Si=CR_2$) are compounds with a double bond between sp^2 Si and C atoms; i.e. heavier analogues of alkenes where one of the carbon atoms has been replaced with a silicon. Evidence for the existence of a transient silene ($Me_2Si=CH_2$) was first provided in 1967 by Gusel'nikov and Flowers.⁴⁰⁰ The transient nature of many silenes is due to their propensity to spontaneously decompose by dimerization. By employing bulky substituents, Brook et al. were able to prepare, in 1979, the first spectroscopically observed silene (in equilibrium with the dimer cyclization product; a in Figure 1.39)⁴⁰¹ and two years later reported the first isolable, stable (in the solid state) silene (b in Figure 1.39).^{402,403} When in solution, these silenes decomposed over weeks or days, respectively, to form acylsilanes. Over the past forty years, a variety of stable silenes have been prepared by similarly employing steric bulk to impart kinetic stabilization (i.e. prevent dimerization).⁴⁰⁴ Silenes are far more reactive than alkenes due to a significantly weaker π -bond. Silicon forms weaker π bonds than C in general,⁴⁰⁵ and this is reflected in the low π bond strengths of silenes (estimated from bond rotation barriers to be 119-192 kJ mol^{-1} for a variety of free silenes, which is about half as strong as in olefins).⁴⁰⁶ This weakness is due in part to the poor size match between C and Si orbitals, leading to poor orbital

overlap.³⁰⁰ Furthermore, the greater Si–C bond length in silenes (relative to the C–C bond lengths in olefins) caused by the greater atomic radius of Si ensures that silenes are sterically more susceptible to nucleophilic attack.³⁰⁰ As a result, free silenes are generally air-sensitive. The synthesis, reactivity, and structures of free silenes have been reviewed elsewhere.^{300,407,408}

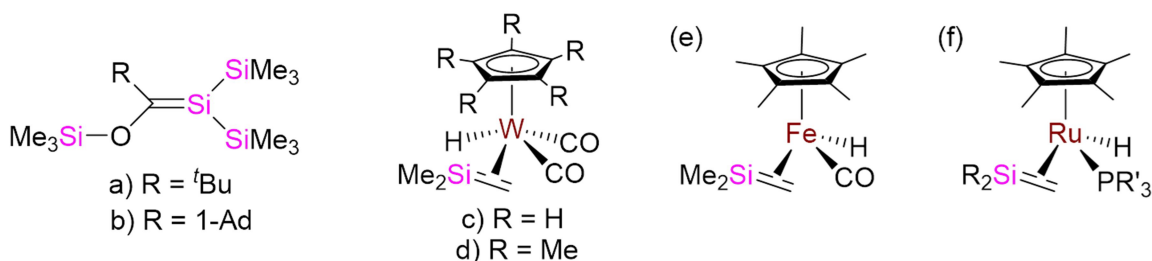


Figure 1.39: Early examples of observed free silenes and silene transition metal complexes.

Otherwise unstable silene moieties (those lacking bulky substituents) have been stabilized by being brought within the coordination sphere of a transition metal.⁴⁰⁷ Pannell first proposed a transition metal silene complex as an intermediate in the isomerization of $[\text{Cp}(\text{OC})_2\text{Fe}(\text{CH}_2\text{SiHMe}_2)]$ to $[\text{Cp}(\text{OC})_2\text{Fe}(\text{SiMe}_3)]$ in 1970.⁴⁰⁹ Just over a decade later, Wrighton et al. reported the first spectroscopically observed silene complexes $\{[(\eta^5\text{-C}_5\text{R}_5)(\text{OC})_n\text{MH}(\text{Me}_2\text{Si}=\text{CH}_2)]$; $n = 2$ ($\text{M} = \text{W}$, $\text{R} = \text{H}$ or Me , c-d in Figure 1.39)⁴²⁰ or 1 ($\text{M} = \text{Fe}$, $\text{R} = \text{Me}$, e in Figure 1.39)⁴²¹, which were described as metallasilacyclopropane species (assignment of these species as metallasilacyclopropane complexes by the authors, as opposed to silene complexes, was somewhat arbitrary; *vide infra*). Wrighton's complexes were observed only at low temperature, and formed by β -hydride elimination from a $-\text{CH}_2\text{SiHMe}_2$ ligand. The Fe complex (which differs from Pannell's proposed intermediate by replacement of a Cp with a Cp* group) decomposed above 225 K in the presence of CO to form the silyl complex $[\text{Cp}^*(\text{OC})_2\text{Fe}(\text{SiMe}_3)]$, thus supporting Pannell's initial mechanistic proposal.

In 1988, the Tilley group reported the first isolable, thermally stable, and (for one analogue) crystallographically characterized silene complexes; $[\text{Cp}^*(\text{R}_3\text{P})\text{RuH}(\text{R}'_2\text{Si}=\text{CH}_2)]$ (f in Figure 1.39). Since that time, less than two dozen silene complexes of transition metals have been observed. The relatively small size of this field makes this a particularly exciting area of chemical exploration. Reviews of transition metal silene complexes can be found as sub-headings in more general silene reviews.^{300,407,410}

1.7.3 – Electronic Structure of Silene Complexes

Bonding between silene ligands and transition metals can be described in a similar manner to alkene complexes, based on the Dewar-Chatt-Duncanson model. This model describes bonding as involving both σ donation and π backdonation (Figure 1.40). Backdonation into the π^* antibonding orbital centred around the Si=C bond leads to elongation (weakening) of the Si=C bond upon silene coordination to the metal, as does σ donation (which involves removal of electron density from the Si-C π bonding orbital). Unlike alkene complexes (and disilene $\text{R}_2\text{Si}=\text{SiR}_2$ complexes), the bonding environment is necessarily unsymmetrical in silene complexes. The π -bond of a free silene is polarized towards carbon, leading to a HOMO with a higher contribution from the carbon 2p atomic orbital relative to the silicon 3p atomic orbital, and the opposite is the case for the LUMO. Because of this, the σ -donor interaction is dominated by the C atom in the silene fragment (in contrast, π -backdonation involves both the Si and C silene atoms). Therefore, when the silene ligand is oriented *trans* to a co-ligand, the carbon atom (as opposed to the C-Si centroid) occupies the position directly *trans* to the co-ligand. Detailed descriptions of the electronic structure of silene-transition metal bonding are scarce, though a couple of reports have been published involving Pt silene complexes.^{411,412}

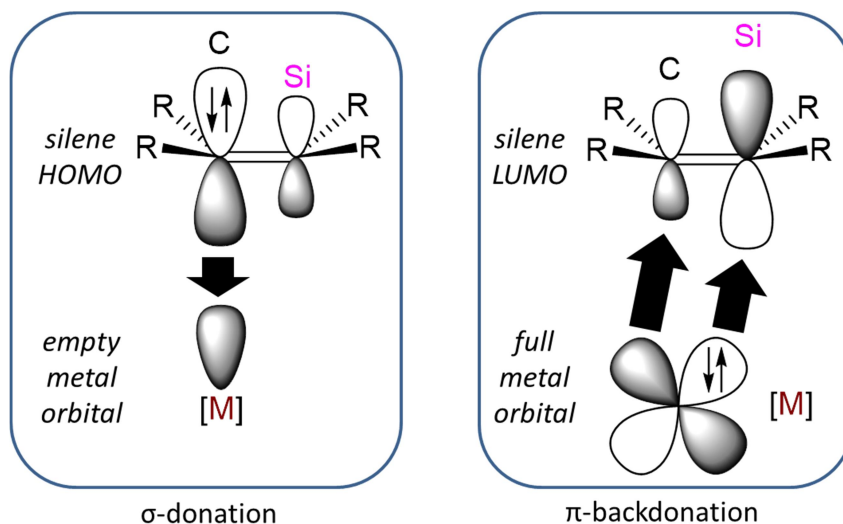


Figure 1.40: Dewar-Chatt-Duncanson model of σ donation and π backdonation from/to a silene ligand.

In situations where π backdonation is significant, silene complexes can be alternatively described as metallasilacyclopropane complexes (just as alkene complexes in similar situations can be described as metallacyclopropane complexes), which are the products of oxidative addition of the π bond across the metal centre. For both silene and alkene complexes, an accurate bonding picture involves resonance structures of the two extremes (Figure 1.41). Both terms are sometimes used interchangeably in the literature, though often one term is used to indicate the dominant resonance structure.

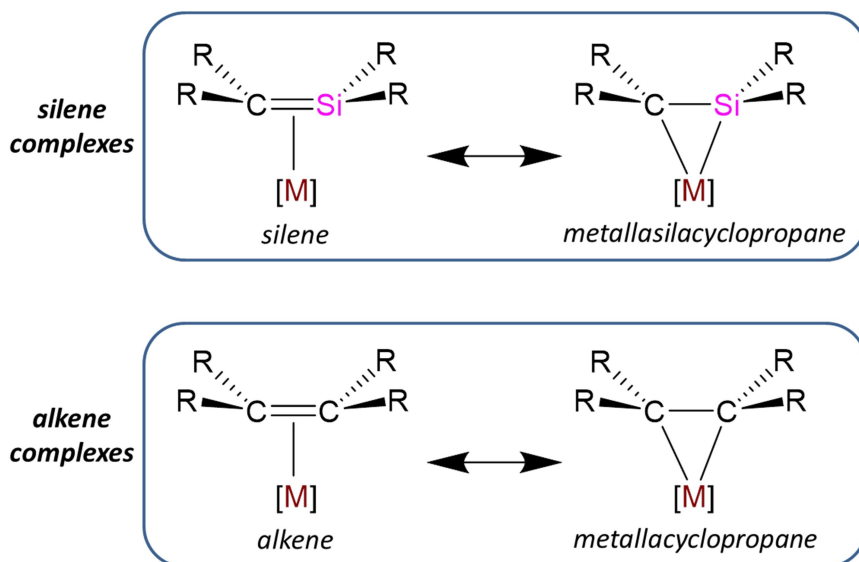
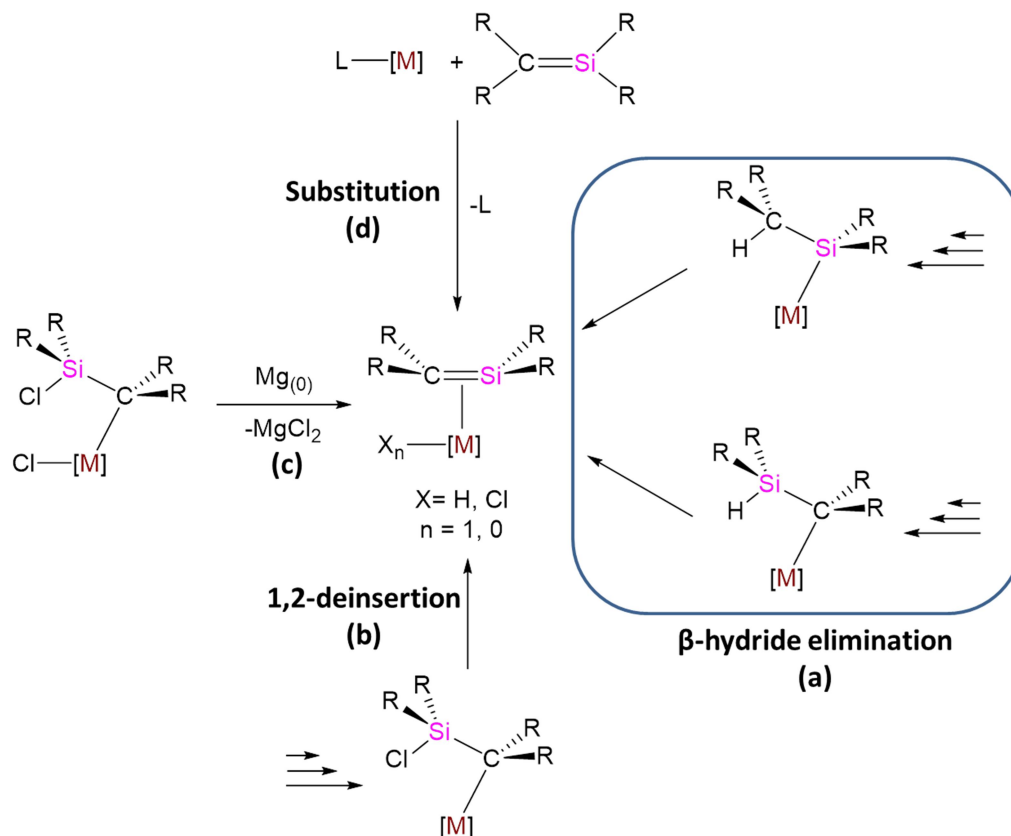


Figure 1.41: Canonical resonance structures of (top) metallasilacyclopropane/silene complexes and (bottom) metallacyclopropane/alkene complexes.

1.7.4 – Synthesis of Silene Complexes

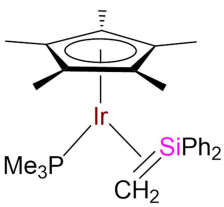
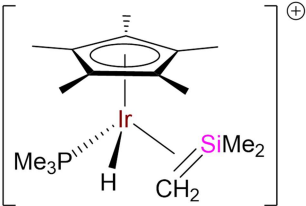
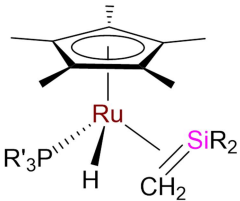
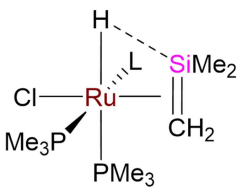
Only a handful of silene complexes of transition metals have been isolated (Table 1.11), and examples are currently limited to complexes of Ir, Ru, W, Ni, and Pt. In solution, Tilley's $[\text{Cp}^*(\text{PMe}_3)\text{IrH}(\text{Me}_2\text{Si}=\text{CH}_2)][\text{B}(\text{C}_6\text{F}_5)_4]$ was observed to exist in equilibrium with another species (an Et_2O -coordinated silylene complex, presumably formed via a silyl intermediate; *vide infra*). However it was isolated in the solid state, so it is included in Table 1.11. The plurality of these complexes were prepared by initial installation of a β -hydride containing ligand ($-\text{CH}_2\text{SiR}_2\text{H}$ or $-\text{SiR}_2\text{Me}$) followed by β -hydride elimination (a in Scheme 1.13). Installation of β -hydride containing ligand has been achieved via a variety of methods, including addition of Grignard reagents to metal halides and isomerization of a silylene complex. Other pathways to silene complexes have involved initial installation of a β -chloride containing ligand, followed by 1,2-deinsertion (for $[(\text{Me}_3\text{P})_3\text{RuHCl}(\text{Me}_2\text{Si}=\text{CH}_2)]$; b in Scheme 1.13), reduction of an alkyl halide complex by $\text{Mg}_{(0)}$ {for $[\text{Cp}_2\text{W}(\text{Me}_2\text{Si}=\text{CH}_2)]$; c in Scheme 1.13 (this may proceed via initial formation of a Grignard reagent followed by intramolecular reaction involving

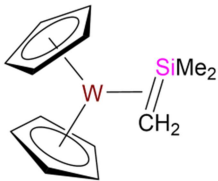
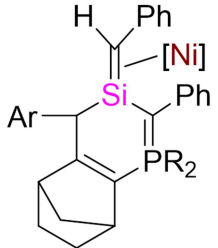
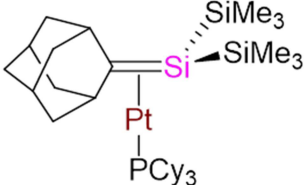
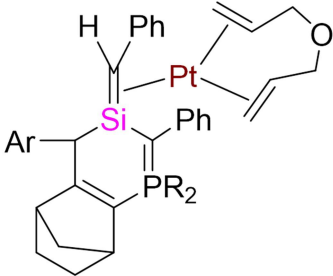
a chloride ligand}}, and phosphine or alkene substitution by an isolated or *in-situ* generated free silene {for group 10 complexes; d in Scheme 1.13 (this mechanism requires large substituents on the silene, and the limited number of silene complexes prepared by this method is presumably due to the dearth of isolable free silenes)}.



Scheme 1.13: Synthetic routes used to prepare isolated silene complexes. In some cases where the silene was generated by a mechanism that resulted in a hydride ligand, the silene complex underwent subsequent H–H or C–H bond-forming reductive elimination involving the hydride and another co-ligand to generate a hydride-free silene complex, and this subsequent reactivity is not shown in the scheme. For generality, charge is not included (both neutral and cationic species have been observed).

Table 1.11: Isolated silene complexes. n.o. = not observed, X = any non-metal.

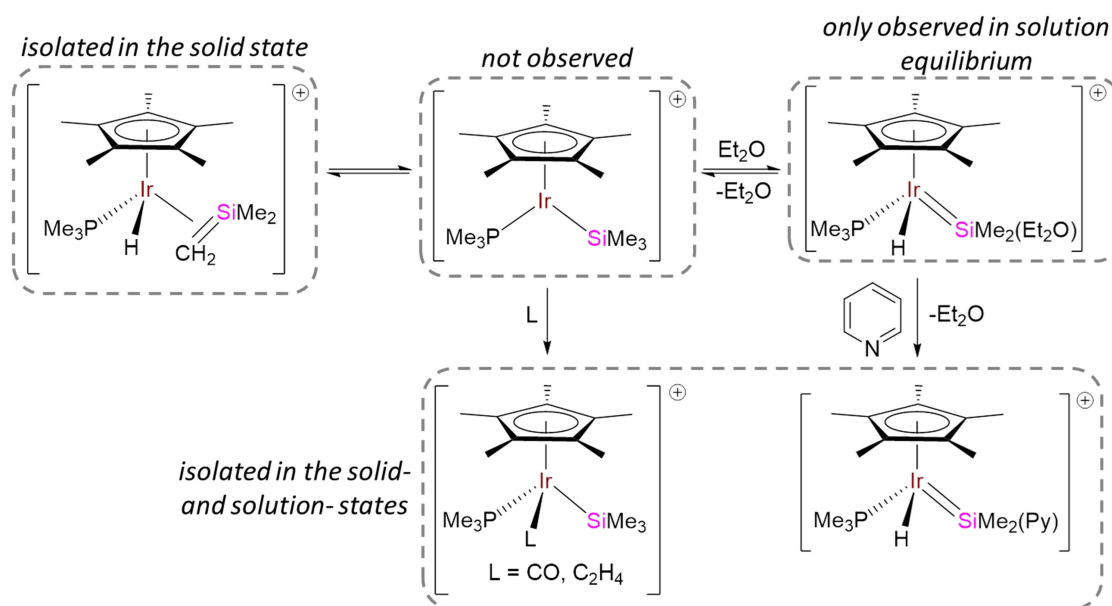
M	Complex	NMR: δ (ppm) $\{^1J_{C,H} \text{ (Hz)}\}$	XRD (\AA , $^\circ$)	Ref.
Ir		^{13}C : -33.37 {142} ^{29}Si : -20.77	Si=C: 1.810(6) Ir-Si: 2.317(2) Ir-C: 2.189(8) $\Sigma(\text{X-Si-X})$: 341	Tilley (1990) ⁴¹³
		^{13}C : -16.8 {147.5} ^{29}Si : 2.1	Si=C: 1.84(2) Ir-Si: 2.439(8) Ir-C: 2.22(2) $\Sigma(\text{X-Si-X})$: 353	Tilley ^a (2001) ⁴¹⁴
	 a) R = Ph, R' = ⁱ Pr b) R = Ph, R' = Cy c) R = Me, R' = Cy d) R = Me, R' = ⁱ Pr	^{13}C : -29.04 {143} (a), -29.68 (b), n.o. (c), -22.42 (d) ^{29}Si : 6.14 (a), n.o. (b), n.o. (c), n.o. (d)	(a only) Si=C: 1.78(2)-1.79(2) Ru-Si: 2.365(5)-2.382(4) Ru-C: 2.25(2)-2.26(1) $\Sigma(\text{X-Si-X})$: 343	Tilley (1988, 1993) ⁴¹⁵
Ru	 L = PMe ₃ (multiple isomers)	^{13}C : -11.2, -29.7 ^{29}Si : -19.4, -19.8	Si=C: 1.788(11)-1.790(6) Ru-Si: 2.526(2)-2.468(2) Ru-C: 2.307(7)-2.200(6) $\Sigma(\text{X-Si-X})$: 344	Berry (2003) ⁴¹⁶

			Si=C: 1.800(8)	
W		^{13}C : -41.09 {137} ^{29}Si : -15.66	W-Si: 2.534(2) W-C: 2.329(7) $\Sigma(\text{X-Si-X})$: 340	Berry (1990) ⁴¹⁷
Ni		^{13}C : n.o. ^{29}Si : 23.7	Si=C: 1.825(3) Ni-Si: 2.181(1) Ni-C: 2.000(3) $\Sigma(\text{X-Si-X})$: 344	Baceiredo and Kato (2013) ⁴¹⁸
		^{13}C : 137.8 ^{29}Si : 6.8	Si=C: 1.838(12) Pt-Si: 2.298(3) Pt-C: 2.161(11) $\Sigma(\text{X-Si-X})$: 354	Apeloig (2004) ⁴¹¹
Pt		^{13}C : n.o. ^{29}Si : n.o.	Si=C: 1.802(3) Pt-Si: 2.440(1) Pt-C: 2.236(3) $\Sigma(\text{X-Si-X})$: 351	Baceiredo and Kato (2013) ⁴¹⁸

a. This complex was only isolated in the solid state.

Tilley's silene complex $[\text{Cp}^*(\text{Me}_3\text{P})\text{IrH}(\text{Me}_2\text{Si}=\text{CH}_2)]^+$ is of particular interest because, although it was isolated in the solid state, it was observed to exist in equilibrium with the base-stabilized silylene complex $[\text{Cp}^*(\text{Me}_3\text{P})\text{IrMe}\{\text{SiMe}_2(\text{OEt}_2)\}]^+$, formed via an unobserved silyl intermediate $[\text{Cp}^*(\text{Me}_3\text{P})\text{Ir}(\text{SiMe}_3)]^+$ (Scheme 1.14).⁴¹⁴ The silylene and silyl intermediate species in this equilibrium were trapped by reaction with nucleophiles (pyridine coordination to the Si centre of the silylene, or CO or ethylene coordination to the Ir centre in the silyl isomer; Scheme 1.14), and the 'trapped' species

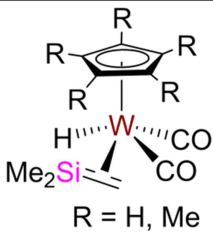
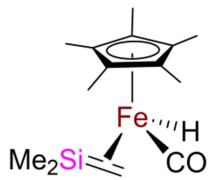
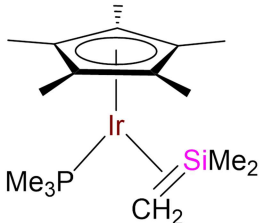
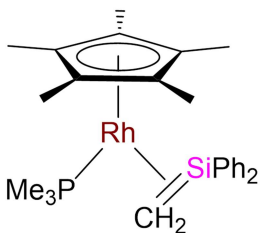
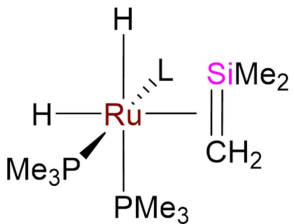
were isolated.^{389,414} This equilibrium highlights the reversibility of the final step in the synthesis of many silene complexes (β -hydride elimination from a silyl complex; *vide supra*).



Scheme 1.14: Equilibrium between $[\text{Cp}^*(\text{Me}_3\text{P})\text{IrH}(\text{Me}_2\text{Si}=\text{CH}_2)]^+$ and $[\text{Cp}^*(\text{Me}_3\text{P})\text{IrMe}\{\text{=SiMe}_2(\text{OEt}_2)\}]^+$, and trapping experiments.^{389,414}

Wrighton's seminal synthesis of the first silene complexes (*vide supra*) involved spectroscopic observation of W and Fe species (c-e in Figure 1.39), which could not be isolated due to instability at room temperature. Since that time, a handful of silene complexes of transition metals have been spectroscopically observed but not isolated (Table 1.12). For example, in 1999 Berry observed the ruthenium silene complex $[(\text{Me}_3\text{P})_3\text{RuH}_2(\text{Me}_2\text{Si}=\text{CH}_2)]$, which was thermally stable but existed in a solution equilibrium with the silyl complex $[(\text{Me}_3\text{P})_3\text{RuH}(\text{SiMe}_3)]$.⁴¹⁹

Table 1.12: Spectroscopically observed non-isolated silene complexes. n.o. indicates not observed. Complexes reported as metallasilacyclopropane complexes are shown as silene complexes for consistency.

M	Complex	NMR: δ (ppm) { $^1J_{C,H}$ (Hz)}	Reason not Isolated	Author
W	 <p>R = H, Me</p>	^{13}C : -27.6 (R = Me) ^{29}Si : n.o.	Unstable at room temperature	Wrighton (1983) ⁴²⁰
Fe		^{13}C : -20.39 ^{29}Si : n.o.	Decomposition above 225 K	Wrighton (1987) ⁴²¹
Ir		n.o.	Unable to purify from byproducts	Tilley (1990) ⁴¹³
Rh		^{13}C : 66.07 {145.6} ^{29}Si : -17.63	Unable to purify from byproducts	Tilley (1990) ⁴¹³
Ru	 <p>L = PMe_3</p>	^{13}C : -20.75 ^{29}Si : -12.93	Exists in equilibrium with silyl complex.	Berry (1999) ⁴¹⁹

1.7.5 – Solid State Structural Characterization of Silene Complexes

X-ray crystal structures of silene complexes are relatively rare. To our knowledge, only 8 such complexes have been reported. The four key structural parameters generally analyzed are the Si–C, M–Si, and M–C distances, as well as the sum of non-M bond angles centred on the Si centre.

The bonding metric most directly descriptive of the nature of silene complexes is the Si–C distance. Reported values range from 1.78(2)-1.84(2) Å (Table 1.11) which, though shorter than the characteristic Si–C single bond length (1.87 Å),⁴²² is significantly longer than in structurally characterized examples of electronically un-stabilized free silenes, despite the presence of very bulky substituents in the latter {for example, the Si–C distances in $\text{Me}_2\text{Si}=\text{C}(\text{SiMe}_3)(\text{SiMe}^t\text{Bu}_2)$, $(\text{Me}_3\text{Si})_2\text{Si}=\text{C}(1\text{-Ad})(\text{OSiMe}_3)$ and $(\text{Me}_3\text{Si})(\text{Me}_2^t\text{BuSi})\text{Si}=\text{Ad}$ (Ad = 2-adamantyl) range from 1.702(5) to 1.764(3) Å}.^{403,423} The Si–C distance is a good measure of the nature of silene-metal bonding, as both ligand donation and metal backdonation result in elongation of the Si–C bond. Greater elongation of the Si–C bond is associated with greater contribution from a metallasilacyclopropane resonance structure.

Free silenes, like alkenes, feature sp^2 hybridization of the silene C and Si atoms, and are therefore planar at both positions. Upon coordination to a transition metal, pyramidalization can be expected at both positions (again, analogous to alkene complexes). However, because one or both substituents on C are normally hydrogen atoms, which are not accurately located by X-ray diffraction, only the sum of the angles around Si is normally discussed. As expected, X-ray crystal structures show significant pyramidalization; the sum of bond angles centred on the Si atom (not including bonds to the metal) have been shown to range from 340-354° (360° would correspond to a planar sp^2 environment, while 328.5° would correspond to an sp^3 environment). Greater degrees of pyramidalization are associated with greater contribution of a metallasilacyclopropane resonance structure.

The final sets of bond metrics commonly analyzed in silene complexes are the M–Si and M–C distances. In all cases, the bond between the metal and silicon is 0.11–0.27 Å (5–12 %) longer than bond between the metal and carbon, reflecting both the greater atomic radius of silicon (the covalent radius of Si is 0.39 Å larger than C)⁴²⁴ and asymmetric orbital overlap (Figure 1.40). For nearly all silene complexes, the distances from the metal to Si are on the shorter side relative to those in silyl complexes, and distances to C are on the longer side relative to those in alkyl complexes (in both cases, of the same metal).

1.7.6 – Spectroscopic Characterization of Silene Complexes

NMR spectroscopy is commonly used for the characterization of silene complexes. Unfortunately, there is no single diagnostic environment indicative of a silene complex. Reported ²⁹Si NMR (Si=C) chemical shifts range from –20.77 to 23.7 ppm, falling within the range for transition metal silyl complexes. Similarly, ¹³C NMR (Si=C) chemical shifts normally range from –11.2 to –41.09 ppm, similar to that observed for M–CH₂SiR₃ environments in β-Si-containing alkyl ligands (the reported values of 66.07 and 137.8 ppm for [(Me₃P)Cp*Rh(Ph₂Si=CH₂)] and [(C₃H₅)Pt(Ad=Si(SiMe₃)₂), respectively, are clearly outliers). In complexes with an H substituent on the Si=C environment, the C–H coupling constant can also be used to probe the degree to which the sp² environment in a hypothetical free silene has been pyramidalized (for example, ethylene has a ¹J_{C,H} of 156.2 Hz and methane has a ¹J_{C,H} of 125.0 Hz).⁴²⁵ Silene complexes with Si=CH substituents feature ¹J_{C,H} values of 137–143 Hz, indicative of a structure intermediate between the canonical silene and metallasilacyclopropane complexes (Figure 1.41); lower ¹J_{C,H} values are associated with a greater contribution from a metallasilacyclopropane resonance structure. This parameter offers a relatively diagnostic signal to differentiate from a –CH₂SiR₃ alkyl group, which could potentially have similar ¹³C and ²⁹Si chemical shifts, but where the ¹J_{C,H} for the methylene bridge would be expected to range from 120–130 Hz (lower in the presence of an agostic interaction), which is lower than that expected for a silene complex.⁴²⁶

For $[\text{Cp}_2\text{WH}(\text{Me}_2\text{Si}=\text{CH}_2)]$, where the transition metal contains an NMR-active (spin $\frac{1}{2}$) ^{183}W nucleus (NA = 14.28 %), coupling to ^{183}W from the ^{13}C or ^{29}Si environments in the silene core was found to be 28.5 and 57.1 Hz, respectively.⁴¹⁷ These values are much smaller than is normal for alkyl (43-89 Hz)⁴²⁷ or silyl (e.g. 83.0-117.6 Hz for a series of tungsten silyl complexes reported by the Berry group)⁴¹⁷ complexes, respectively, and the latter is similar to the tungsten disilene complexes $[\text{Cp}_2\text{WH}(\text{Me}_2\text{Si}=\text{SiMe}_2)]$ (50.7 Hz).⁴²⁸ As well, comparable ^{183}W - ^{29}Si coupling constants (54-55 Hz) were reported for Wrighton's $[(\eta^5\text{-C}_5\text{R}_5)(\text{OC})_2\text{WH}(\text{Me}_2\text{Si}=\text{CH}_2)]$.⁴²⁰ This offers an additional diagnostic NMR handle for differentiating silene and β -Si-containing alkyl ligands for species with suitable NMR-active metal nuclei.

For some silene complexes where extensive NMR data could not be obtained (usually due to instability) identification has been based on mass spectrometry.⁴¹³ Diagnostic MS peaks include the molecular ion, and the molecular ion minus the free silene moiety. In addition, iron and cobalt silene complexes have been generated in the gas phase and observed exclusively by MS.⁴²⁹ As well, Mori et al. reported observing the Zr silene complex $[\text{Cp}_2\text{Zr}(\text{PhMeSi}=\text{CH}_2)]$ in solution based on the observation of a transient Cp environment in the ^1H NMR spectrum, without any other diagnostic data (though this complex was the expected intermediate in a variety of reported transformations).⁴³⁰

1.7.7 – Silene Hydride Complexes; Interligand Si–H Interactions

Given that the most common method for preparing isolated silene complexes involves β -hydride elimination (*vide supra*), hydrides are common co-ligands in silene complexes. While in most instances, no apparent interaction was observed between the silene and hydride ligands, $[(\text{Me}_3\text{P})_3\text{RuH}_2(\text{Me}_2\text{Si}=\text{CH}_2)]$ featured a significant interligand interaction between the hydride and the Si centre of the silene ligand.⁴¹⁶ This was apparent from short Si–H_{Ru} distances of 1.557-1.664 Å, and a large scalar ^{29}Si - ^1H coupling constant of 75 Hz (these parameters are similar to those observed for σ -hydrosilane complexes; see section 1.5.5).^{224,233,241} Furthermore, unlike other structurally

characterized silene complexes, $[(\text{Me}_3\text{P})_3\text{RuH}_2(\text{Me}_2\text{Si}=\text{CH}_2)]$ displayed a M–Si distance (2.468(2)-2.526(2) Å) which is on the longer edge of the range of Ru–Si bond lengths found in silyl complexes. Given these observations, a proper description of the bonding environment of these complexes requires employment of an additional resonance structure involving an alkyl ligand with a β -Si–H metal interaction (Figure 1.42). In fact, Sabo-Etienne et al. has described a pair of Ru complexes with similar bonding metrics to this as alkyl complexes with β -Si–H metal interactions, though they could alternatively have been described as silene hydride complexes with interligand interactions.⁴³¹

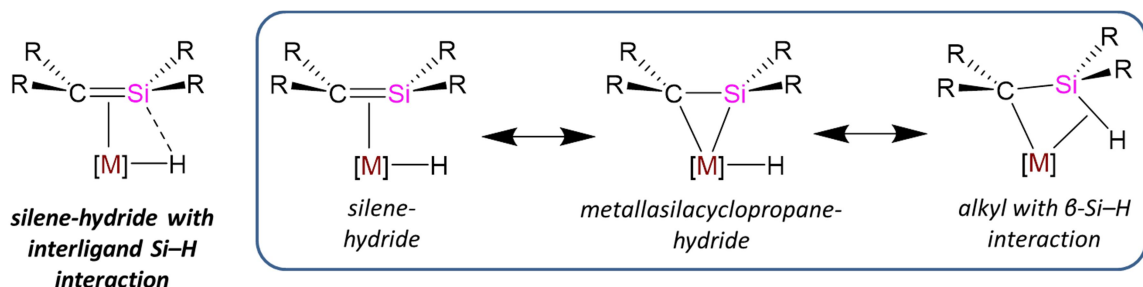


Figure 1.42: Resonance structures used to describe silene hydride complexes with an interligand Si–H interaction

1.7.8 – Complexes of Ligands Containing a π -system for which a Resonance Structure can be Drawn which Includes a Si=C Bond

A variety of complexes have been structurally characterized where a silene moiety is incorporated into a ligand where the π system is delocalized over additional (usually carbon, sometimes also germanium) atoms. In these situations, a resonance structure can be envisaged involving a silene ‘Si=C’ donor. While many such complexes have been reported for aromatic systems where one or more Si atoms have been incorporated into an η^4 -cyclobutadiene,⁴³² η^5 -cyclopentadienyl⁴³³ or η^6 -benzene⁴³⁴ ligand, the number of non-aromatic systems is relatively scarce. The simplest of these, and first to be reported, are heavy analogues of allene complexes where one of the terminal carbon atoms is replaced by a silicon; 1-silaallenes. In 1995, Jones et al. reported the Ru silaallene complexes $[\text{Cp}^*(\text{R}_3\text{P})\text{RuH}(\eta^2\text{-Me}_2\text{Si}=\text{C}=\text{CPh}_2)]$ $\{\text{R}_3 = \text{Cy}_3$ (for which an X-ray

crystal structure was obtained) or Me₂Ph; a and b, respectively, in Figure 1.43), in which the ‘Si=C’ portion of the silaallene is the bonding site (the ‘C=C’ portion does not interact with the metal) and which contains a significant interligand Si–H interaction {d(Si–H) = 1.70(3) Å, *J*_{Si,H} = 57-66 Hz}.⁴³⁵ Thus, the bonding scheme involved is very similar to that in the silene hydride complex [(Me₃P)₃RuH₂(Me₂Si=CH₂)] reported by Berry (*vide supra*),⁴¹⁶ and the Si–C bond length of 1.805(6) Å is within the range observed for transition metal silene complexes.

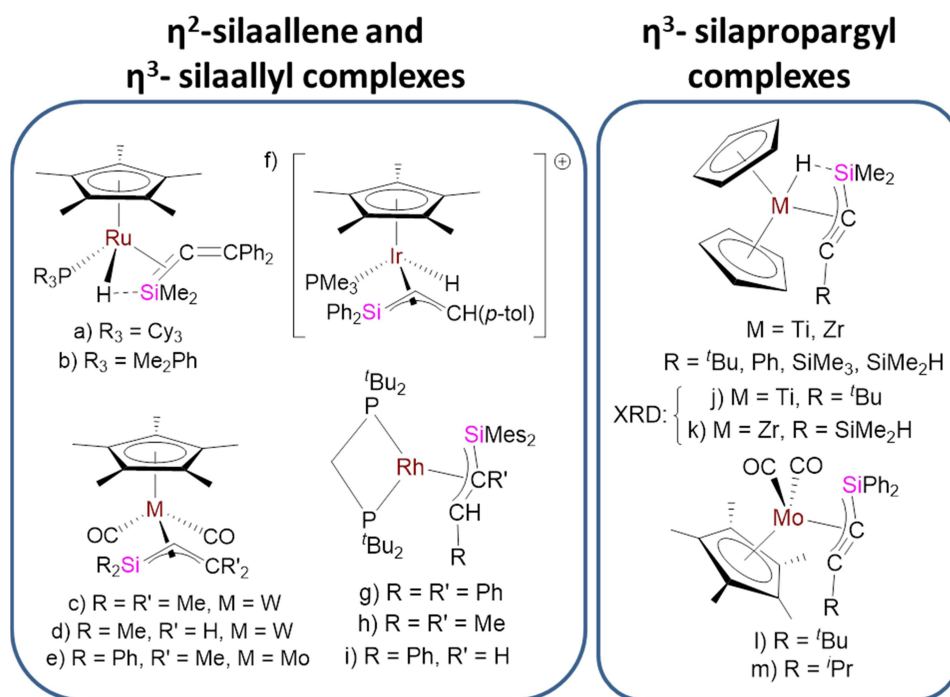


Figure 1.43: Transition metal η²-silaallene, η³-silaallyl, or η³-silapropargyl complexes.

Related to this, Sakaba et al. has reported crystal structures for η³-silaallyl complexes, which feature ligands that are heavy analogues of η³-allyl ligands where one terminal carbon atom was supplanted by Si; [Cp*(OC)₂W(η³-Me₂SiCHCMe₂)] and [Cp*(OC)₂Mo(η³-Ph₂SiCHCMe₂)] (c and e, respectively, in Figure 1.43).⁴³⁶ Despite the fact that these complexes involve η³ coordination of all three atoms in the π system, the Si–C distances of 1.800(4)-1.817(3) are very similar to that in the η²-silaallene complex reported by Jones, indicative of some double bond character. Additional examples of η³-

silaallyl complexes have been reported by the Sakaba $\{[(OC)_2Cp^*W(\eta^3-Me_2SiCHCH_2)]\}$; d in Figure 1.43)⁴³⁶ and the Tilley $\{[Cp^*(Me_3P)Ir\{\eta^3-Ph_2SiCHCH(p-tol)\}]^+\}$ and $[(dtbpm)Rh(\eta^3-Mes_2SiCR'CHR)]$; f-i in Figure 1.43)^{273,389} groups without solid-state characterization. Calculations by Sakaki et al. have suggested that the bonding in these systems can best be described with resonance contributions from canonical η^3 -silaallene and κ^2 -alkene-silyl structures (Figure 1.44; left).⁴³⁷

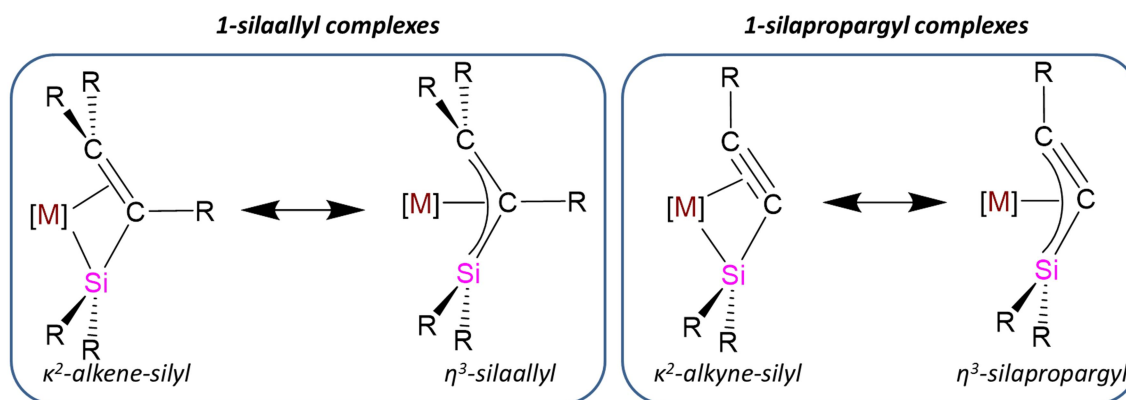


Figure 1.44: Resonance structures of η^3 -silaallyl and η^3 -silapropargyl complexes.

In 1995 and 1998, Rosenthal et al. reported a series of Ti and Zr κ^2 -alkyne-silyl complexes $[Cp_2MH(\eta^3-SiMe_2CCR)]$.⁴³⁸ The structurally characterized examples $[Cp_2TiH(\eta^3-Me_2SiCC^tBu)]$ and $[Cp_2ZrH\{\eta^3-Me_2SiCC(SiMe_2H)\}]$ (j and k, respectively, in Figure 1.43) feature very short Si–C distances of 1.766(7) and 1.787(3) Å, which are statistically equivalent to the shortest values reported for a silene transition metal complex (*vide supra*), suggestive of appreciable double-bond character. Subsequent reports by the Sakaki group (which proposed such complexes based on DFT calculations)⁴³⁷ and Sakaba (who reported similar complexes in 2009)⁴³⁹ have described these complexes utilizing contributions of κ^2 -alkyne-silyl and η^3 -silapropargyl resonance structures, analogous to the bonding description of η^3 -silaallyl complexes (Figure 1.44; right). Sakaba's $[Cp^*(OC)_2Mo(\eta^3-Ph_2SiCCR)]$ (l and m in Figure 1.43) displayed Si–C lengths of 1.795(3)-1.806(3) Å, which though marginally longer than in Rosenthal's group 4 complexes, are also within the range expected for silene complexes (*vide supra*).

A number of other non-aromatic complexes featuring ‘delocalized’ silene moieties have been reported. First, in 1998, a Co complex with a 1,3-dibora-5-silapenta-1,4-diene ligand was serendipitously prepared by Berndt and Siebert et al. (a in Figure 1.45), which is structurally similar to an η^5 -pentadienyl ligand with some carbon atoms substituted by B and Si.⁴⁴⁰ The internal Si–C distance of 1.809(3) Å is within the range associated with silene complexes. Second, in 2010 the Tokitoh group reported a silacyclohexadienyl chromium complex with the Si atom in the π -system (b in Figure 1.45).⁴⁴¹ The π -system Si–C distance of 1.822(4) Å, though slightly longer than expected for silene complexes, is shorter than the Si–C distance of 1.853(5) Å involving the sp^3 carbon atom in the same ligand, suggesting some degree of double bond character in the former. Lastly, in 2013, Tobita et al. reported η^3 - α -silabenzyl complexes of W⁴⁴² and Mo⁴⁴³ ($[(OC)_2Cp^*M(\eta^3-R_2SiAr)]$; c-e in Figure 1.45), which each contain an analogue of an η^3 benzyl ligand where the exo-cyclic donor carbon atom has been replaced with a silicon atom. While the Si–C distances of the bonding moiety are significantly elongated relative to known silene complexes (1.834(5)-1.850(3) Å), some double-bond character is apparent because they are slightly shorter than the Si–C distances for the terminal Si substituents in the same complexes (1.867(5)-1.873(3) Å).

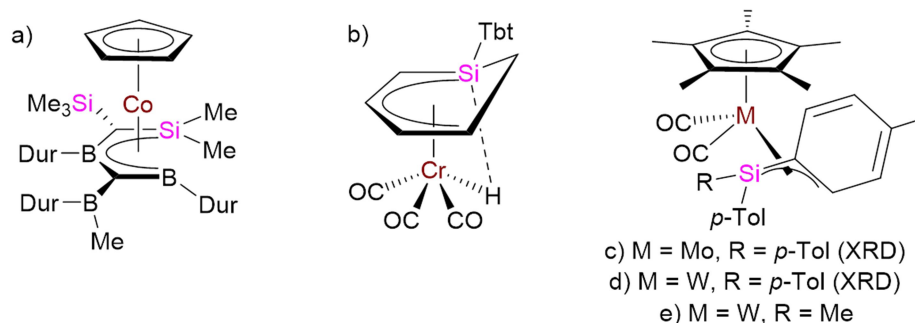


Figure 1.45: Complexes containing non-aromatic ligands featuring extended π -systems that include a “Si=C” moiety (not including η^2 -silaallene, η^3 -silaallyl, or η^3 -silaproparyl complexes; see Figure 1.43).

In addition, DFT calculations have been used to discard silene-containing resonance structures as contributors to the description for the bridging moieties in a pair

Ph.D. Thesis — Jeffrey S. Price; McMaster University – Chemistry

of dinuclear complexes reported by Sakaki and Sakaba et al. in 2011 ($[\text{Cp}^*(\text{CO})_2\text{M}(\text{Ph}_2\text{SiCCSiPh}_2)\text{M}(\text{CO})_2\text{Cp}^*]$; $\text{M} = \text{W}, \text{Mo}$)⁴⁴⁴ and a disilacyclopent-3-ynyl zirconium complex reported by Rosenthal et al. in 2010.⁴⁴⁵ Also, in 2014 the Tokitoh group reported the X-ray crystal structure of a chromium complex with a 9-silaphenanthrene ligand where the bonding mode appears to be an η^2 -silene donor, with very short Si–C distances of 1.782(9)-1.790(9) Å.⁴⁴⁶ However, while the X-ray crystal structure was submitted to the Cambridge Structural Database and appears in the electronic supporting information of the publication, the text of the report does not discuss the structure at all, and surprisingly indicates that they were unable to prepare this complex.

Chapter 2

Dialkylmanganese(II) Complexes; Synthesis, Characterization, and Solution-state Reactivity for Deposition of Elemental Manganese

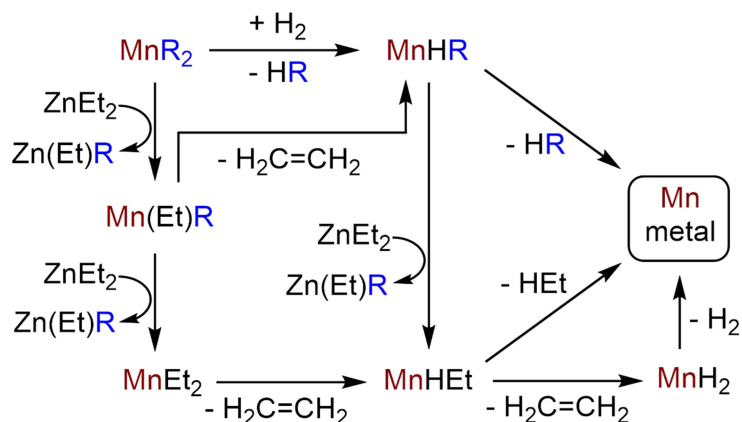
Portions of this section have been reprinted (adapted) with permission from Price, J. S.; Chadha, P.; Emslie, D. J. H. Base-Free and Bisphosphine Ligand Dialkylmanganese(II) Complexes as Precursors for Manganese Metal Deposition, *Organometallics* **2016**, *35*, 168-180. Copyright 2016 American Chemical Society.

2.1 – Introduction to Chapter 2

The Emslie group has previously investigated the use of metal alkyl complexes (*e.g.* ZnEt_2) as co-reactants for copper metal ALD,⁴⁴⁷ and in this work we set out to determine whether highly reactive electropositive transition metal alkyl complexes could exhibit the reactivity, volatility, and thermal stability suitable to effect electropositive metal deposition in combination with reagents such as H_2 or ZnEt_2 (hydrogen gas has previously been used as a co-reactant for ALD of Fe,⁴⁴⁸ Ru,⁴⁴⁹ Co,⁴⁴⁸ Ir,⁴⁵⁰ Ni,^{448,451} Pd,⁴⁵² and Cu;^{23,448,453} ZnEt_2 has been used as a co-reactant for ALD of Cu²⁸).

Reactivity envisaged between a dialkylmanganese precursor and H_2 or ZnEt_2 is shown in Scheme 2.1. With H_2 , a mixed alkyl hydride complex (MnHR) should be accessible by σ -bond metathesis, or oxidative addition of H_2 followed by reductive elimination of HR. This mixed alkyl hydride complex can be expected to be particularly susceptible to HR reductive elimination for both thermodynamic and kinetic reasons,⁹³ leading to manganese metal deposition. With ZnEt_2 , stepwise alkyl exchange with MnR_2 would provide $\text{Mn}(\text{Et})\text{R}$ and then MnEt_2 , which can be expected to undergo rapid β -hydride elimination to form either MnHR or MnHEt respectively. MnHR is the same intermediate targeted in reactions with H_2 , and MnHEt will decompose via either HET reductive elimination to form manganese metal, or β -hydride elimination to form MnH_2 ; an unstable species observed only in low temperature matrices.⁴⁵⁴ While HR ($\text{R} =$

CH_2EMe_3 , $\text{E} = \text{C}, \text{Si}$) is the only byproduct expected in reactions with H_2 , byproducts in the reactions with ZnEt_2 can include ZnEtR (or ZnR_2 ; not shown in Scheme 1), ethylene, HR , HEt , and H_2 .



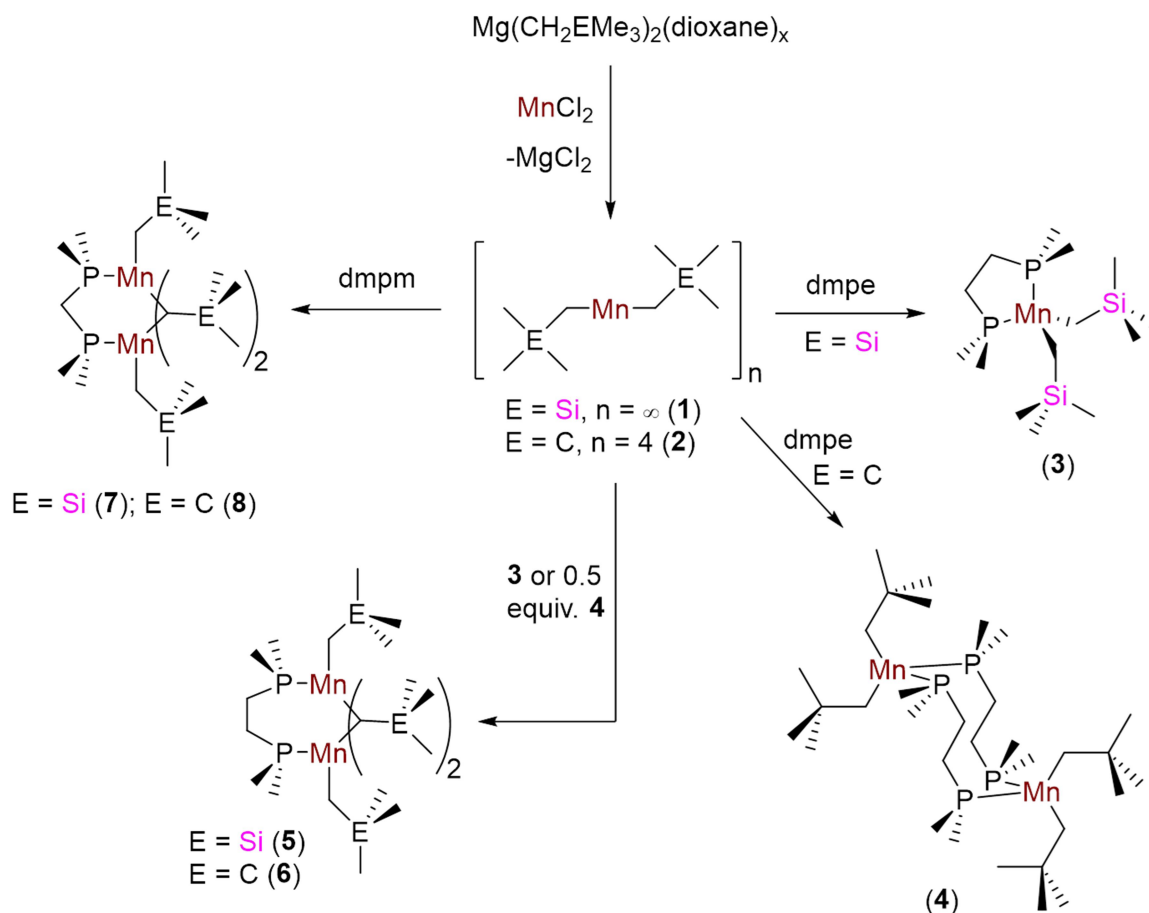
Scheme 2.1: Possible pathways for $\text{Mn}_{(s)}$ deposition using dialkylmanganese(II) complexes in combination with H_2 or ZnEt_2 co-reactants.

The aforementioned reactivity can only be utilized for manganese ALD if a dialkylmanganese(II) precursor with an appropriate balance of thermal stability, volatility, and reactivity can be identified. A review of known dialkylmanganese(II) complexes, and their Lewis base adducts, is provided in section 1.3. Herein we describe the synthesis of both new and previously reported dialkylmanganese(II) complexes (8 in total), detailed solution and solid state characterization, including single crystal X-ray diffraction, PXRD, NMR, and UV-Visible spectroscopy, and variable temperature solution state (Evans) and solid state (SQUID) magnetic measurements, evaluation of thermal stability and volatility, and solution reactivity studies with H_2 and ZnEt_2 leading to manganese metal and manganese-zinc alloy electroless deposition. This work targets base-free as well as dmpe - {bis(dimethylphosphino)ethane-} and dmpm - {bis(dimethylphosphino)methane-} coordinated bis(trimethylsilylmethyl)- and dineopentyl- manganese(II) complexes, since (a) they have fairly low molecular weights and do not contain aromatic groups, maximizing the potential for appreciable volatility, (b) they do not contain β -hydrogen atoms, imparting thermal stability, (c) they are free

from oxygen or nitrogen donors, precluding manganese oxide or nitride deposition, and (d) the chelate effect will help to prevent phosphine ligand dissociation during sublimation. The base-free compounds^{95,96} and the 1:1 MnR₂:dmpe adducts¹¹¹ have previously been reported, but a high quality X-ray crystal structure has only been reported for [$\{\text{Mn}(\mu\text{-CH}_2\text{SiMe}_3)_2\}_\infty$].

2.2 – Synthesis and X-ray Crystal Structures

Base-free bis(trimethylsilylmethyl)manganese(II) (**1**) and dineopentylmanganese(II) (**2**) were prepared via the reactions of MnCl₂ with MgR₂(dioxane)_x (R = CH₂SiMe₃ or CH₂CMe₃; x = 0.25-0.8), following modifications of the literature procedures (Scheme 2.2).⁹⁶ The 1:1 Mn:dmpe (dmpe = 1,2-bis(dimethylphosphino)ethane) complexes, [(dmpe)Mn(CH₂SiMe₃)₂] (**3**) and [$\{(\mu\text{-dmpe})\text{Mn}(\text{CH}_2\text{CMe}_3)_2\}_2$] (**4**), were also prepared as previously reported (Scheme 2.2),¹¹¹ while the 2:1 Mn:dmpe complexes, [$(\mu\text{-dmpe})\{\text{Mn}(\text{CH}_2\text{SiMe}_3)(\mu\text{-CH}_2\text{SiMe}_3)\}_2$] (**5**) and [$(\mu\text{-dmpe})\{\text{Mn}(\text{CH}_2\text{CMe}_3)(\mu\text{-CH}_2\text{CMe}_3)\}_2$] (**6**), were synthesized by addition of 1 equivalent of the corresponding base-free dialkylmanganese(II) precursor to **3** and **4**, respectively (Scheme 2.2). Compounds **1** and **2** reacted with bis(dimethylphosphino)methane (dmpm) to form exclusively [$(\mu\text{-dmpm})\{\text{Mn}(\text{CH}_2\text{SiMe}_3)(\mu\text{-CH}_2\text{SiMe}_3)\}_2$] (**7**) and [$(\mu\text{-dmpm})\{\text{Mn}(\text{CH}_2\text{CMe}_3)(\mu\text{-CH}_2\text{CMe}_3)\}_2$] (**8**), even when an excess of dmpm was added (Scheme 2.2).



Scheme 2.2: Synthesis of complexes 1-8.

Compound 4 is colourless, 3 is yellow, and 2 is dark brown, whereas 1 and 5-8 are red or black when crystalline, and pale pink when powdered. All eight compounds display high oxygen sensitivity, and were characterized by combustion elemental analysis, single crystal X-ray diffraction (except 1),^o PXRD on the bulk sample, ¹H NMR spectroscopy (except nearly insoluble 1), UV/Vis spectroscopy (except nearly insoluble 1 and colourless 4), and both SQUID and Evans solution magnetic measurements (except 1); *vide infra*. Additionally, melting points and sublimation temperatures were determined, and thermal stability was assessed.

^o Complex 1 has previously been characterized by X-ray diffraction and SQUID; ref. 96 and 99.

A good quality X-ray structure has not previously been reported for base-free dineopentylmanganese(II) (**2**). However, Wilkinson et al. noted in 1976 that **2** is a tetramer in the solid state,⁹⁶ citing a personal communication from M. B. Hursthouse and P. Raithby (and a poor quality crystal structure was later submitted to the CSD).¹⁰¹ Additionally, an electron diffraction study was reported for **2**, revealing a monometallic structure in the vapor phase.¹⁰² In this work, dark brown X-ray quality crystals of **2** were obtained from hexanes at $-30\text{ }^{\circ}\text{C}$, confirming a tetrametallic structure (Figure 2.1), with the two outer manganese atoms in a distorted trigonal planar geometry ($\Sigma(\text{C}-\text{Mn}(1)-\text{C}) = 359.82(6)^{\circ}$; $\text{C}-\text{Mn}(1)-\text{C} = 105.16(3), 122.62(3)$ and $132.04(4)^{\circ}$) and the inner manganese atoms in a distorted tetrahedral geometry ($\text{C}-\text{Mn}(2)-\text{C} = 100.06(3)-122.50(3)^{\circ}$). The only other neutral dialkylmanganese(II) complex known to contain a trigonal planar manganese centre is $[\{\text{Mn}(\text{CH}_2\text{CMe}_2\text{Ph})(\mu\text{-CH}_2\text{CMe}_2\text{Ph})\}_2]$,^{96,98,100} though it deviates more from planarity ($\Sigma(\text{C}-\text{Mn}-\text{C}) = 354.7(1)^{\circ}$) than complex **2**, likely due to an η^2 interaction between each manganese atom and the phenyl ring of a bridging $\text{CH}_2\text{CMe}_2\text{Ph}$ group. The tetrametallic structure of **2** presumably differs from the polymeric structure of **1**⁹⁶ due to the increased steric demands of neopentyl versus trimethylsilylmethyl ligands.

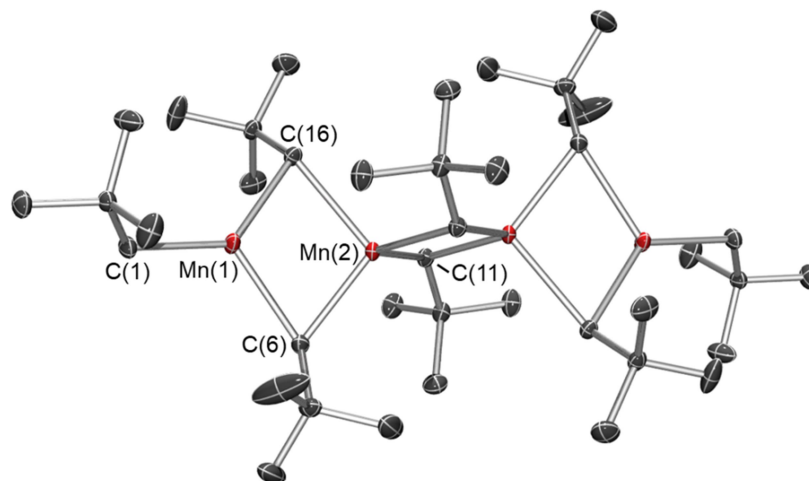


Figure 2.1: X-ray crystal structure for $[\{\text{Mn}(\text{CH}_2\text{CMe}_3)(\mu\text{-CH}_2\text{CMe}_3)_2\}_2\{\text{Mn}(\mu\text{-CH}_2\text{CMe}_3)_2\text{Mn}\}]$ (**2**). Hydrogen atoms are omitted for clarity, and ellipsoids are set to 50 % probability. Bond distances (Å) and angles (°): Mn(1)⋯Mn(2) 2.7022(4), Mn(2)⋯Mn(2') 2.7165(4), Mn(1)–C(1) 2.1211(9), Mn(1)–C(6) 2.2322(9), Mn(2)–C(16) 2.232(1), Mn(2)–C(11) 2.213(1), Mn(1)–C(16) 2.3265(7), Mn(2)–C(6) 2.3939(7), Mn(2)–C(11') 2.4092(9), Mn(1)–C(6)–Mn(2) 71.38(3), Mn(1)–C(16)–Mn(2) 72.67(3), Mn(2)–C(11)–Mn(2') 71.85(3), C(1)–Mn(1)–C(6) 132.04(4), C(1)–Mn(1)–C(16) 122.62(3), C(6)–Mn(1)–C(16) 105.16(3).

Compound **2** has an inversion centre between the central manganese atoms, and the terminal Mn(1)–C(1) bond distance of 2.1211(9) Å is significantly shorter than the Mn–C bonds to the bridging neopentyl ligands. For each bridging neopentyl group, one Mn–C bond is approximately 0.1–0.2 Å shorter than the other, with the short Mn–C distances ranging from 2.213(1) to 2.232(1) Å, and long Mn–C distances of 2.3265(7) to 3-coordinate Mn(1), and 2.3939(7) and 2.4092(9) Å to 4-coordinate Mn(2). Bridging alkyl groups in multimetallic manganese alkyl complexes in the literature also exhibit one short and one long Mn–C bond (see Section 1.3),⁴⁵⁵ as do all μ -alkyl manganese complexes in this work (*vide infra*). The Mn(1)–Mn(2) and Mn(2)–Mn(2') distances in **2** are 2.7022(4) and 2.7165(4) Å, which are almost 0.2 Å shorter than the Mn–Mn distances previously reported for $[\{\text{Mn}(\text{CH}_2\text{SiMe}_3)_2\}_\infty]$ (**1**). Furthermore, the Mn–C–Mn angles in

2 (71.38(3)-72.67(3)°) are approximately 5° more acute than those in **1**, while the Mn–C distances are comparable.¹⁰⁰ The Mn–Mn distances in **2** lie between the sum of ionic (2.58 Å) and Van der Waals radii (4.10 Å),⁴⁵⁶ and are within the range previously reported (2.5-3.2 Å) for single Mn–Mn bonds in the vast majority of coordination and organometallic complexes.⁴⁵⁵ However, they are longer than the shortest Mn–Mn distances in elemental manganese (2.26, 2.37 and 2.47 Å for α -, β - and γ -Mn, respectively).⁴⁵⁷

X-ray quality crystals of the 1:1 Mn:dmpe complexes, [(dmpe)Mn(CH₂SiMe₃)₂] (**3**) and [{(μ-dmpe)Mn(CH₂CMe₃)₂}₂] (**4**), were obtained from hexanes at –30 °C. Compound **3** (Figure 2.2; left) is monometallic with a tetrahedral geometry that is distorted due to the small bite angle of dmpe (78.76(2)° in **3**). By contrast, **4** (Figure 2.3; right) is dimetallic with bridging dmpe ligands and a Mn–Mn distance of 6.756(2) Å, which is far greater than the sum of the van der Waals radii. Compound **4** features tetrahedral manganese centres (X–Mn–X = 94.79(2)-122.20(9)°; X = C or P) and a central 10-membered ring with a boat-chair-boat conformation, which is the dominant conformation of cyclodecane.⁴⁵⁸ An organometallic complex featuring a similar M₂(μ-dppe)₂ core (dppe = bis(diphenylphosphino)ethane) has been structurally characterized for Mo.⁴⁵⁹ The Mn–P and Mn–C distances in **3** and **4** are unremarkable, ranging from 2.6241(9) to 2.6541(5) Å (Mn–P) and 2.1320(14) to 2.160(2) Å (Mn–C), similar to the Mn–P and Mn–C_{terminal} bond lengths in **1**, **2**, [(PMe₃)₂Mn(CH₂Ph)₂],¹¹¹ and [(TMEDA)Mn(CH₂SiMe₃)₂] (TMEDA = *N,N,N',N'*-tetramethyl-ethylenediamine).⁹⁹ By contrast, significantly longer Mn–P and Mn–C distances were reported for [(dmpe)Mn{CH(SiMe₃)₂}₂],¹¹⁴ presumably due to greatly increased steric hindrance at the metal centre.

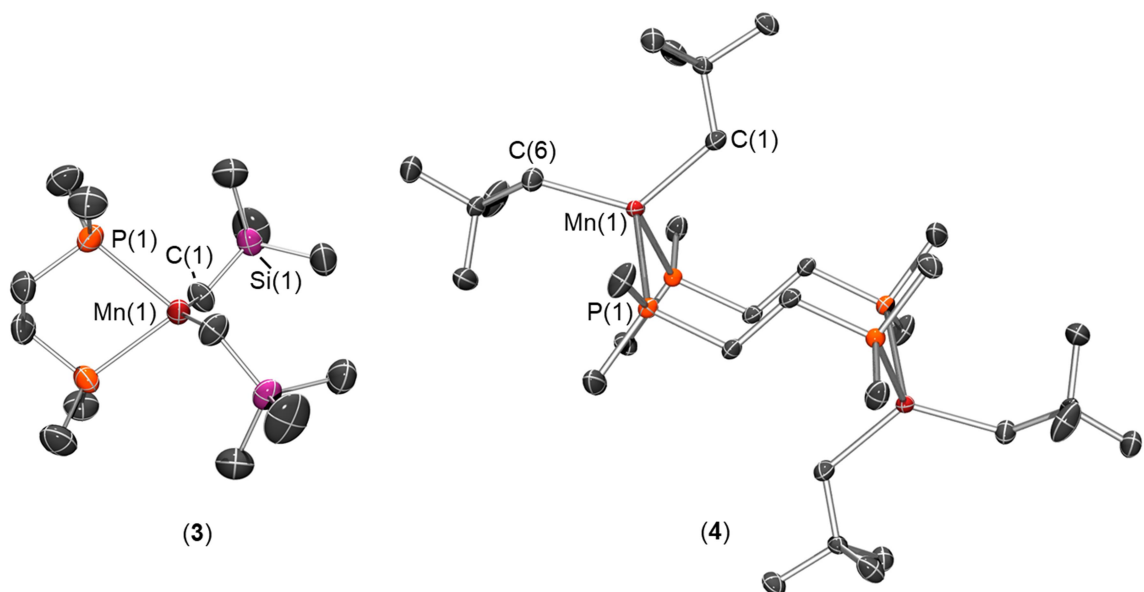


Figure 2.2: X-ray crystal structures for (left) [(dmpe)Mn(CH₂SiMe₃)₂] (**3**) and (right) [{(μ-dmpe)Mn(CH₂CMe₃)₂}₂] (**4**). Hydrogen atoms are omitted for clarity, and ellipsoids are set to 50 %. For **3**, all carbon atoms in the dmpe ligand are disordered over two positions, and only the dominant conformation (69 %) is shown above. Bond distances (Å) and angles (°): Mn–C 2.1320(14), Mn–P 2.6541(5), P–Mn–P 78.76(2), C–Mn–C 144.34(9), P(1)–Mn–C(1) 108.59(5), P(1)–Mn–C(1′) 98.89(4). For **4**, bond distances (Å) and angles (°): Mn···Mn 6.756(2), Mn(1)–P(1) 2.6241(9), Mn(1)–P(2′) 2.643(1), Mn(1)–C(1) 2.160(2), Mn(1)–C(6) 2.160(2), P(1)–Mn(1)–P(2) 94.79(2), C(1)–Mn(1)–C(6) 122.20(9), C(1)–Mn(1)–P(1) 104.25(7), C(6)–Mn(1)–P(1) 106.94(7), C(1)–Mn(1)–P(2) 119.20(7), C(6)–Mn–P(2) 105.25(7).

Bright red X-ray quality crystals of [(μ-dmpe){Mn(CH₂SiMe₃)(μ-CH₂SiMe₃)₂}₂] (**5**) were obtained at –30 °C from both toluene and hexanes. The unit cell for the structure obtained from toluene (Figure 2.3; left) contains three independent molecules, while the structure obtained from hexanes (Figure 2.3; middle) has only one independent molecule in the unit cell. Black X-ray quality crystals of the neopentyl analogue, [(μ-dmpe){Mn(CH₂CMe₃)(μ-CH₂CMe₃)₂}₂] (**6**) (Figure 2.3; right) were obtained from toluene at –30 °C. Both **5** and **6** are dimetallic with tetrahedral manganese centres (C–

Mn–X = 94.4(1)-131.4(4)°; X = C or P) coordinated to one terminal alkyl group, two bridging alkyl groups, and one phosphorus atom of a bridging dmpe ligand. The terminal Mn–C distances in **5** and **6** (2.123(2)-2.141(5) Å in **5**; 2.160(6) and 2.18(1) Å in **6**) are shorter than the bridging Mn–C distances, and as in base-free **1** and **2**, each of the bridging alkyl groups is closer to one manganese atom than the other; the short Mn–C_{bridging} distances range from 2.183(2) to 2.211(4) Å in **5** and 2.252(5) to 2.27(1) Å in **6**, whereas the long Mn–C_{bridging} distances range from 2.362(2) to 2.379(4) Å in **5** and 2.300(9) to 2.342(6) Å in **6**.

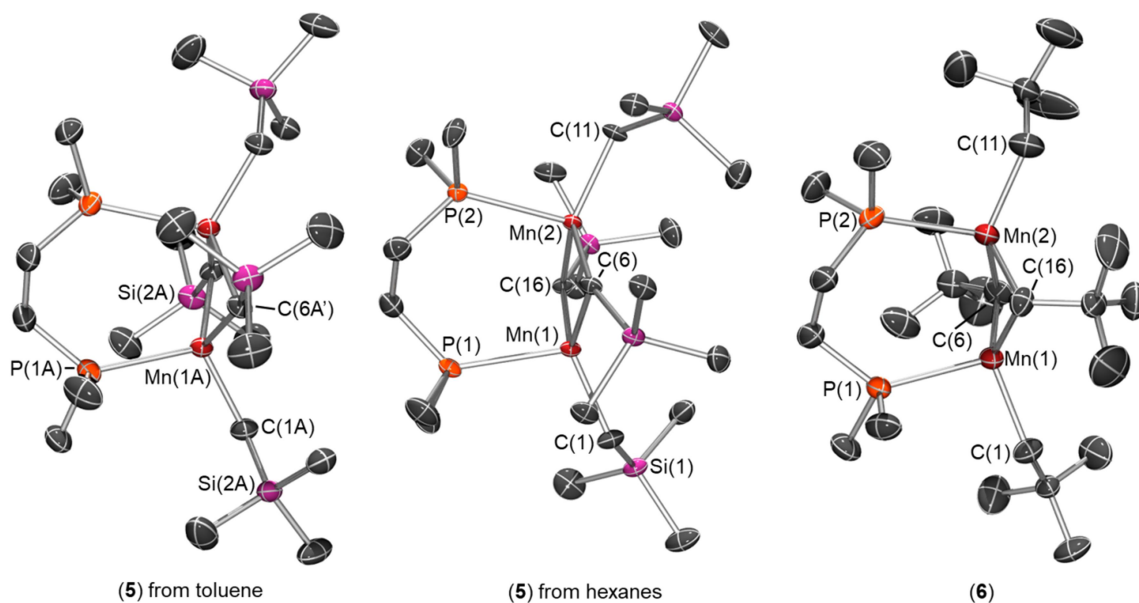


Figure 2.3: X-ray crystal structures for $[(\mu\text{-dmpe})\{\text{Mn}(\text{CH}_2\text{SiMe}_3)(\mu\text{-CH}_2\text{SiMe}_3)\}_2]$ (**5**) obtained by crystallization from toluene (left) or hexanes (middle), and (right) the X-ray crystal structure for $[(\mu\text{-dmpe})\{\text{Mn}(\text{CH}_2\text{CMe}_3)(\mu\text{-CH}_2\text{CMe}_3)\}_2]$ (**6**). Hydrogen atoms are omitted for clarity, and ellipsoids are set to 50 %. For **5** (obtained from toluene), the unit cell contains three independent and essentially isostructural molecules, and only one is shown. Atoms below with a ‘B’ or ‘C’ suffix are the atoms related to those with the same identifying number and the suffix ‘A’, but in the structures not shown in the figure. Bond distances (Å) and angles (°): Mn(1A)⋯Mn(1A') 2.7202(6), Mn(1B)⋯Mn(1B') 2.7177(6), Mn(1C)⋯Mn(1C') 2.7322(6), Mn(1A)–P(1A) 2.6007(9), Mn(1B)–P(1B) 2.5909(9), Mn(1C)–P(1C) 2.6020(9), Mn(1A)–C(1A) 2.123(2), Mn(1B)–C(1B) 2.137(2), Mn(1C)–C(1C) 2.136(2), Mn(1A)–C(6A) 2.183(2), Mn(1B)–C(6B) 2.200(2), Mn(1C)–C(6C) 2.208(2), Mn(1A)–C(6A') 2.366(2), Mn(1B)–C(6B') 2.370(2), Mn(1C)–C(6C') 2.362(2), Mn(1A)–C(6A)–Mn(1A') 73.34(7), Mn(1B)–C(6B)–Mn(1B') 72.88(7), Mn(1C)–C(6C)–Mn(1C') 73.35(8). For **5** (obtained from hexanes), bond distances (Å) and angles (deg): Mn(1)⋯Mn(2) 2.7255(9), Mn(1)–P(1) 2.581(1), Mn(2)–P(2) 2.603(2), Mn(1)–C(1) 2.133(4), Mn(2)–C(11) 2.141(5), Mn(1)–C(6) 2.211(4), Mn(2)–C(16) 2.210(4), Mn(1)–C(16) 2.379(4), Mn(2)–C(6) 2.372(4), Mn(1)–C(6)–Mn(2) 72.9(1), Mn(1)–C(16)–Mn(2) 72.8(1). For **6**, positions of all carbon atoms in three of the four

neopentyl groups (C(1)-C(15)) are disordered over two positions. The figure shows only one position for each of the disordered groups (occupancy: 50 % for C1-C5, 82 % for C6-C10, and 87 % for C11-C15). Bond distances (Å) and angles (°): Mn(1)···Mn(2) 2.685(1), Mn(1)–P(1) 2.605(1), Mn(2)–P(2) 2.641(1), Mn(1)–C(1) 2.160(6), Mn(2)–C(11) 2.18(1), Mn(1)–C(16) 2.252(5), Mn(2)–C(6) 2.27(1), Mn(1)–C(6) 2.300(9), Mn(2)–C(16) 2.342(6), Mn(1)–C(6)–Mn(2) 72.0(3), Mn(1)–C(16)–Mn(2) 71.5(2).

The Mn–P distances in **5** and **6** are similar and unexceptional. However, the Mn–Mn distances of 2.7177(6)-2.7322(6) Å in **5** are shorter than those in base-free **1** by over 0.15 Å, likely due to the tethering influence of the bridging bis(phosphine) ligand. The Mn–C–Mn angles in **5** (72.88(7)-73.35(8)°) are also more acute than those in base-free **1** (76.82(4) and 77.19(5)°), consistent with the shorter Mn–Mn distance in the former compound. The Mn–Mn distance of 2.685(1) Å in **6** is less than 0.05 Å shorter than the corresponding distance in base-free **2**, but it is significantly shorter than the Mn–Mn distance in **5**. The Mn–C_{terminal} and average Mn–C_{bridging} distances (*vide supra*) are slightly longer in **6** than in **5**, and the Mn–C–Mn angles in **6** (71.5(2)-72.0(3)°) are slightly more acute than those in **5** (*vide supra*). These geometric trends mirror those observed for base-free **1** and **2**. An even shorter Mn–Mn distance of 2.616(5) Å, and a particularly acute Mn–C–Mn angle of 69.6(4)°, were previously reported for isostructural [(μ-dmpe){MnCy(μ-Cy)}₂] (Cy = cyclohexyl),¹²⁰ which features more sterically demanding and electron donating secondary alkyl groups.

Bright red X-ray quality crystals of [(μ-dmpm){Mn(CH₂SiMe₃)(μ-CH₂SiMe₃)}₂] (**7**) were obtained from hexanes at –30 °C (Figure 2.4 left), revealing a dimetallic structure analogous to the structures of the 2:1 MnR₂:dmpe complexes, **5** and **6**. The Mn–Mn, Mn–C and Mn–P distances and Mn–C–Mn angles in **7** are very similar to those in **5**, although the dmpm ligand in **7** is bound less symmetrically than the dmpe ligand in **5** (the Mn–P distances in **7** differ by approx. 0.06 Å in **7**, compared with approx. 0.02 Å in **5**). The solid state structure of [(μ-dmpm){Mn(CH₂CMe₃)(μ-CH₂CMe₃)}₂] (**8**) was also determined using crystals obtained (a) from hexanes at –30 °C (not shown), and (b) by

slow evaporation of a hexanes solution at 20 °C (Figure 2.4 right). However, the quality of the both data sets was only suitable to establish connectivity, which is analogous to that of **7**.

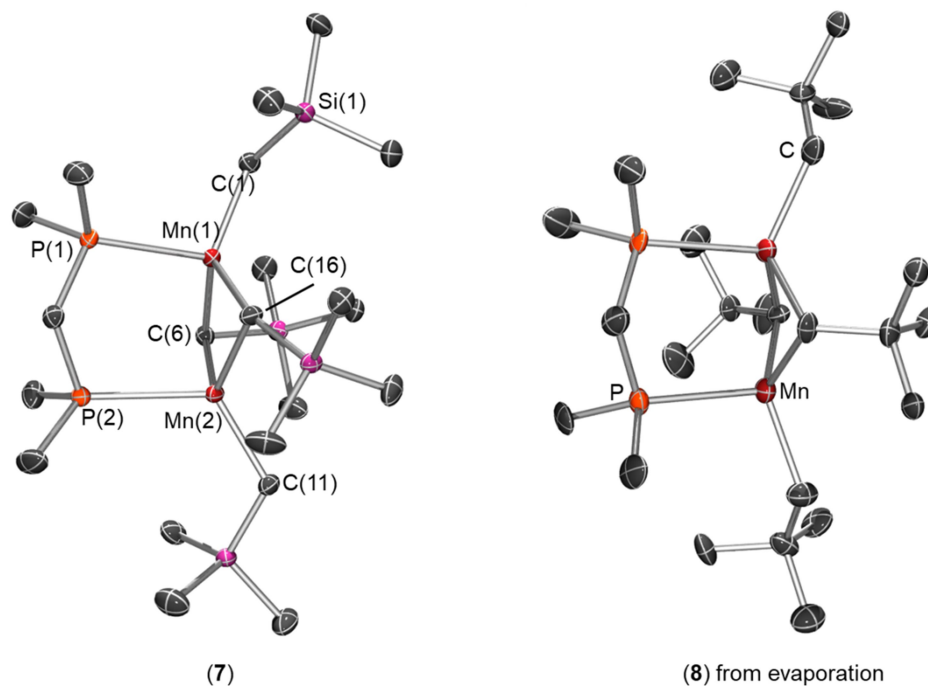


Figure 2.4: X-ray crystal structures for (left) $[(\mu\text{-dmpm})\{\text{Mn}(\text{CH}_2\text{SiMe}_3)(\mu\text{-CH}_2\text{SiMe}_3)\}_2]$ (**7**) and (right) $[(\mu\text{-dmpm})\{\text{Mn}(\text{CH}_2\text{CMe}_3)(\mu\text{-CH}_2\text{CMe}_3)\}_2]$ (**8**). Hydrogen atoms are omitted for clarity, and ellipsoids are set to 50 %. For **7**, bond distances (Å) and angles (°): Mn(1)⋯Mn(2) 2.7243(5), Mn(1)–P(1) 2.6584(5), Mn(2)–P(2) 2.6016(6), Mn(1)–C(1) 2.134(1), Mn(2)–C(11) 2.121(1), Mn(1)–C(6) 2.220(2), Mn(2)–C(16) 2.233(1), Mn(1)–C(16) 2.340(1), Mn(2)–C(6) 2.337(1), Mn(1)–C(6)–Mn(2) 73.38(5), Mn(1)–C(16)–Mn(2) 73.08(4). For **8**, poor quality of data means that the structure is only suitable to establish connectivity. The unit cell contains five independent and essentially isostructural molecules, and only one is shown.

The structures of **5** and **7** can also be compared with $[(\text{PMe}_3)\text{Mn}(\text{CH}_2\text{SiMe}_3)(\mu\text{-CH}_2\text{SiMe}_3)]_2$ (for which an X-ray crystal structure has

previously been reported),¹¹⁰ and an isostructural PEt_3 complex, $[\{(\text{PEt}_3)\text{Mn}(\text{CH}_2\text{SiMe}_3)(\mu\text{-CH}_2\text{SiMe}_3)\}_2]$ (**9**),¹¹² for which we have obtained an X-ray crystal structure (Figure 2.5). Key differences are that the phosphine ligands in the PR_3 ($\text{R} = \text{Me}$ or Et) complexes are *trans* to one another across the Mn–Mn axis, and the Mn–Mn distances (2.772(1) Å ($\text{R} = \text{Me}$) and 2.7937(3) Å ($\text{R} = \text{Et}$)) are 0.05 to 0.07 Å longer than those in **5** and **7**. Furthermore, the Mn–C–Mn angles in the monophosphine complexes (74.5(1)° for $\text{R} = \text{Me}$ and 75.21(3)° for $\text{R} = \text{Et}$) are marginally less acute than those in **5** and **7** ($\sim 73^\circ$), while Mn–P and Mn–C distances are comparable. These data highlight the substantial influence of the bidentate dmpe ligand on the relative orientation of the phosphorus donors, the Mn–Mn distance, and the Mn–C–Mn angle. The neopentyl complex, $[\{(\text{PMe}_3)\text{Mn}(\text{CH}_2\text{CMe}_3)(\mu\text{-CH}_2\text{CMe}_3)\}_2]$,¹¹² has also been reported, featuring an elongated Mn–Mn distance (2.718(3) Å) and statistically equivalent Mn–C–Mn angles (69.6(6)° and 71.0(6)°) relative to **6**.

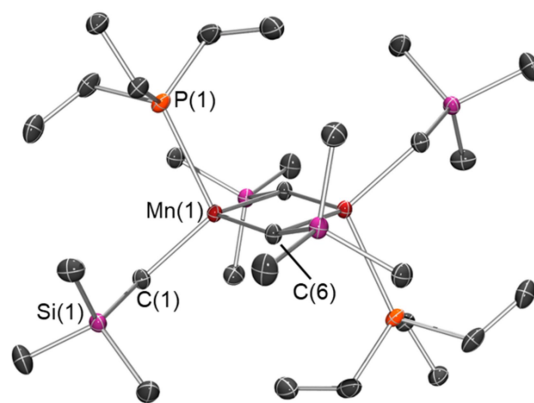


Figure 2.5: X-ray crystal structure for $[\{(\text{Et}_3\text{P})\text{Mn}(\text{CH}_2\text{SiMe}_3)(\mu\text{-CH}_2\text{SiMe}_3)\}_2]$ (**9**). Hydrogen atoms are omitted for clarity, and ellipsoids are set to 50 %. Bond distances (Å) and angles (°): Mn–Mn 2.7937(3), Mn–P 2.6473(4), Mn–C(1) 2.136(1), Mn–C(8) 2.215(1), Mn–C(6') 2.3588(9), Mn–C(6)–Mn 75.21(3).

2.3 – NMR Spectroscopy and Magnetic Measurements

The ^1H NMR spectra of complexes **2-8** (Figure 2.6 left; C_6D_6 , 500 MHz) show paramagnetically broadened and shifted peaks, between 5 and 60 ppm, with full width at half maximum values from 1150 to 8200 Hz. Further spectra were collected in d_8 -toluene between 186 K and room temperature {Figure 2.6 (middle) for **6**}. A spectrum was not collected for **1** due to insolubility in non-coordinating solvents.

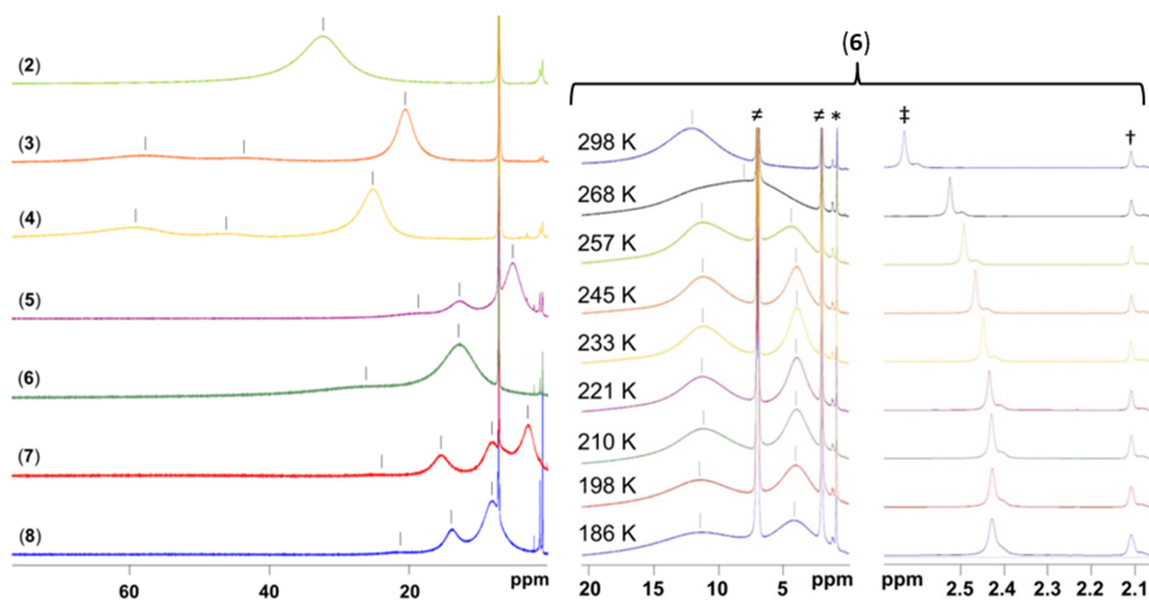


Figure 2.6: Left: Room temperature ^1H NMR spectra for **2-8** (500 MHz, C_6D_6). Black tick marks indicate broad peaks associated with organomanganese(II) complexes, while the sharp signals are due to residual $\text{C}_6\text{D}_5\text{H}$ in the NMR solvent and trace hexanes. Middle: low frequency portion of the ^1H NMR spectra for $[(\mu\text{-dmpe})\{\text{Mn}(\text{CH}_2\text{CMe}_3)(\mu\text{-CH}_2\text{CMe}_3)\}_2]$ (**6**) from 186 to 298 K (500 MHz, d_8 -toluene). Broad signals (\parallel) are due to **6**, while sharp signals are due to residual d_7 -toluene solvent impurity (\neq) and hexanes (*). Right: Region of the ^1H NMR spectra used for Evans measurements for **6** between 186 and 298 K (500 MHz, 40:1 d_8 -toluene:toluene); the methyl group from external toluene (\dagger) is calibrated to 2.11 ppm, and the methyl group of internal toluene (\ddagger) is observed to shift with temperature. Shoulders to the right of the two toluene (C_7H_8) signals are the residual solvent signals due to d_7 -toluene, $\text{C}_6\text{D}_5(\text{CHD}_2)$.

Based on the solid-state structure of phosphine-free **2**, six ^1H NMR signals are predicted with integrations of 36H, 18H, 18H, 8H, 4H and 4H. However, it is not unreasonable to expect that the MnCH_2 signals would be broadened to the point at which they cannot be located, due to their proximity to the high spin d^5 metal centres; in this case, a total of three ^1H NMR signals would be observed. At room temperature, the ^1H NMR spectrum of **2** shows only a single broad ^1H NMR resonance, but at $-32\text{ }^\circ\text{C}$ this peak splits into the expected three signals.

The ^1H NMR spectra for dmpe complexes **3** and **4**,^p which do not contain bridging alkyl groups, would be expected to give rise to three signals (18H, 12H and 4H, not including MnCH_2 signals), whereas the ^1H NMR spectra for **5-8** should give rise to four signals (18H, 18H, 12H, and either 4H or 2H, not including MnCH_2 signals). The expected number of signals was observed for **3**, **4** and **7** at $25\text{ }^\circ\text{C}$, below $10\text{ }^\circ\text{C}$ for **5**, and below $-28\text{ }^\circ\text{C}$ for **8**. For compound **6**, just two ^1H NMR signals were observed at room temperature, and at $-15\text{ }^\circ\text{C}$ the largest of these signals split into two, yielding three broad peaks; the observation of just three signals (-15 to $-80\text{ }^\circ\text{C}$) in the spectrum for **6** is likely due to coincidental overlap of two signals (Figure 2.6; middle). The increased number of signals in the low temperature ^1H NMR spectra of **2**, **5**, **6** and **8** may be attributed to (a) different temperature dependencies for overlapping paramagnetically shifted signals, or (b) decoalescence of signals that are averaged at room temperature due to exchange processes. For compound **8**, explanation ‘a’ is most likely on the basis of solution magnetic measurements (*vide infra*). By contrast, for compounds **2**, **5** and **6**, explanation ‘b’ seems likely, given that solution magnetic measurements indicate that these tetrametallic or dimetallic complexes exist in equilibrium with other manganese-containing species in solution (*vide infra*).

^p Attempts to determine whether the dimeric structure of complex **4** (Figure 2.2 right) remained intact in solution or dissociated into monometallic species using DOSY NMR spectroscopy failed due to very short T_1 relaxation times (the average for the three signals in complex **4** is 0.282 ms at 0.03 gmL^{-1}).

Solid state and solution magnetic measurements were carried out on complexes **2-8** (Table 2.1). SQUID magnetic measurements have previously been reported for **1**, and show antiferromagnetic coupling/exchange between the manganese atoms.⁹⁹ SQUID magnetic measurements on **3**, which is monometallic, and **4**, which is a dimer with spatially separated manganese centres, show that both complexes obey the Curie-Weiss law (Figure 2.7; 300 to 5 K), leading to effective magnetic moments (μ_B) of 5.8 ± 0.2 and 5.83 ± 0.03 BM, respectively, and magnetic susceptibilities ($\chi_{M(\text{corr})}$) of $14.0 \times 10^{-3} \pm 1.2 \times 10^{-3}$ and $14.08 \times 10^{-3} \pm 0.13 \times 10^{-3}$ cm³/mol of Mn at room temperature (for a high spin d⁵ metal centre, the ideal values for μ_B and $\chi_{M(\text{corr})}$ are 5.92 BM and 14.6×10^{-3} cm³/mol, respectively). Compounds **3** and **4** are therefore paramagnetic with no antiferromagnetic exchange.

Table 2.1: Room temperature solution and solid state magnetic data for **2-8**. $\chi_{M(\text{corr})}$ = corrected molar magnetic susceptibility; μ_B = effective magnetic moment; θ = Weiss temperature.

Complex	$\chi_{M(\text{corr})}$ per Mn centre (10^{-3} cm ³ /mol)	
	in C ₆ D ₆ at 298 K	in the solid state at 300 K
2	4.2 ± 0.1^c	2.82 ± 0.03
3	13.6 ± 0.5 ($\mu_B = 5.71$ BM ± 0.11) ^d	14.0 ± 1.2 ($\mu_B = 5.8$ BM ± 0.2) ^a
4	14.4 ± 0.5 ($\mu_B = 5.87$ BM ± 0.10)	14.1 ± 0.1 ($\mu_B = 5.83$ BM ± 0.03) ^b
5	3.5 ± 0.3	3.48 ± 0.04
6	6.5 ± 0.3	3.30 ± 0.03
7	3.0 ± 0.2	3.24 ± 0.03
8	3.4 ± 0.1	3.35 ± 0.03

a. $\theta = -0.6 \pm 0.1$ K for **3**.
 b. $\theta = 0.04 \pm 0.06$ K for **4**.
 c. Lit: 3.9 BM.⁹⁶
 d. Lit: 5.6 BM.¹¹¹

By contrast, the SQUID magnetic data (Figure 2.7) for complexes **2** and **5-8**, which feature Mn–Mn distances between 2.685(1) and 2.7322(6) Å, do not obey the Curie law, and are indicative of significant antiferromagnetic exchange/coupling between neighboring manganese centres (with paramagnetic impurity tails at low temperature). At room temperature, the magnetic susceptibility per manganese centre is 2.82×10^{-3} cm³/mol

for tetrametallic **2**, and ranges from 3.24×10^{-3} to 3.48×10^{-3} cm³/mol for bimetallic **5-8**; these values are far lower than that expected for a paramagnetic metal centre with five unpaired d-electrons (14.6×10^{-3} cm³/mol). The variable temperature magnetic behaviour of **2** and **5-8** is qualitatively similar to that reported for polymeric **1**⁹⁹ and dimetallic $[\{(THF)Mn(CH_2SiMe_3)_2\}_2]$,¹¹⁷ and for the latter compound, Gambarotta and Thompson et al. concluded that the significant magnetism observed at low temperatures indicates an absence of Mn–Mn bonding, despite the short Mn–Mn distance of 2.7878(9) Å.¹¹⁷

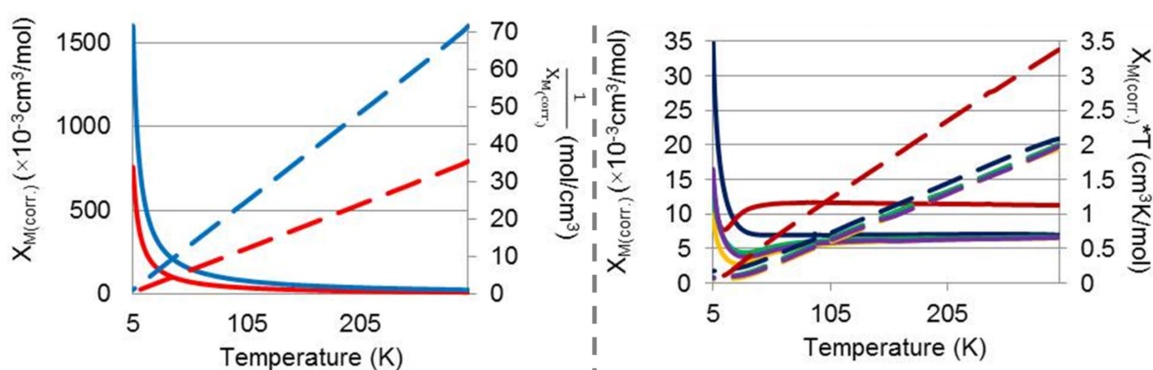


Figure 2.7: SQUID magnetic susceptibility data from 5 to 300 K. Left: $\chi_{M(\text{corr})}$ vs. T (solid lines) and $1/\chi_{M(\text{corr})}$ vs. T (dashed lines) for paramagnetic **3** (red) and **4** (blue). Right: $\chi_{M(\text{corr})}$ vs. T (solid lines) and $\chi_{M(\text{corr})} * T$ vs. T (dashed lines) for **2** (red), **5** (blue), **6** (purple), **7** (orange), and **8** (green), which feature antiferromagnetic interactions.

The SQUID magnetic susceptibility data for dinuclear **5-8** and tetranuclear **2** was fitted to an exchange expression for simple high spin Mn(II) systems using MAGMUN-4.1,⁴⁶⁰ and the resulting fits (Table 2.2) are in good agreement with the experimental data. The resulting calculated g factors are close to 2.0, as expected for high spin organomanganese(II) complexes which lack an orbital contribution to the magnetic moment, and the exchange coupling constants (J) for **2** and **5-8** range from -107 to -117 cm⁻¹, indicative of strong antiferromagnetic coupling (J is an averaged value for compound **2**).

Table 2.2: Magnetic parameters determined by fitting an exchange expression to the SQUID magnetic susceptibility data for compounds **2** and **5-8**. J = exchange coupling constant; ρ = fraction paramagnetic impurity; θ = Weiss-like temperature correction; $R = [(\sum\chi_{obs} - \chi_{calc})^2 / (\sum\chi_{obs})^2]^{1/2}$.

Compound ^a	Mean g-value	Intradimer J (cm ⁻¹)	ρ	θ (K)	100R
2 ^b	2.07 ± 0.01	-117 ± 1	0.005	2.4	0.71
5	2.12 ± 0.02	-112 ± 2	0.02	4.9	1.47
6	2.10 ± 0.02	-112 ± 2	0.01	1.1	1.03
7	2.07 ± 0.01	-109 ± 1	0.007	3.4	0.82
8	2.04 ± 0.03	-107 ± 2	0.011	5.1	1.06

a. The calculated temperature independent paramagnetism (TIP) is 0 cm³/mol for **2**, **6** and **7**, 4×10^{-5} cm³/mol for **5**, and 3×10^{-5} cm³/mol for **8**.

b. For **2**, J is average over the three Mn–Mn interactions present.

Solution state magnetic measurements were conducted using the Evans NMR method.⁴⁶¹ Measurements were taken at room temperature for all complexes (in a 40:1 mixture of C₆D₆:C₆H₆; Table 2.1), and between 298 and 186 K for **2** and **5-7** {in a 40:1 mixture of *d*₈-toluene:toluene; for **6** see Figure 2.6 (right)}. Complexes **3** and **4**, which are monometallic or feature well-separated manganese centres, have room temperature solution effective magnetic moments of 5.71 BM and 5.87 BM, respectively, which are very close to the theoretical value of 5.92 BM, and are statistically equivalent to the solid state effective magnetic moments. Dmpm complexes **7** and **8** gave rise to statistically identical solution and solid state magnetic susceptibilities at room temperature, indicating that the solid state structures of **7** and **8** remain intact in solution. Additionally, variable temperature Evans magnetic measurements on compound **7** (Figure 2.8; 298 to 186 K) yielded magnetic susceptibility values that are statistically equivalent to those from SQUID measurements over the same temperature range.

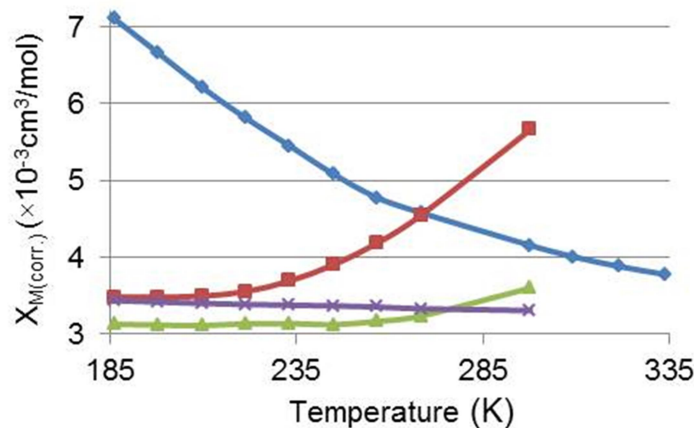


Figure 2.8: Solution magnetic susceptibilities per mole of Mn calculated from Evans measurements at various temperatures for $[\{\text{Mn}(\text{CH}_2\text{CMe}_3)(\mu\text{-CH}_2\text{CMe}_3)_2\}_2\{\text{Mn}(\mu\text{-CH}_2\text{CMe}_3)_2\text{Mn}\}]$ (**2**) (blue diamonds), $[(\mu\text{-dmpe})\{\text{Mn}(\text{CH}_2\text{SiMe}_3)(\mu\text{-CH}_2\text{SiMe}_3)\}_2]$ (**5**) (green triangles), $[(\mu\text{-dmpe})\{\text{Mn}(\text{CH}_2\text{CMe}_3)(\mu\text{-CH}_2\text{CMe}_3)\}_2]$ (**6**) (red squares), and $[(\mu\text{-dmpm})\{\text{Mn}(\text{CH}_2\text{SiMe}_3)(\mu\text{-CH}_2\text{SiMe}_3)\}_2]$ (**7**) (purple ‘x’ symbols).

By contrast, the solution magnetic susceptibilities for base-free **2** and dimetallic **6** are significantly higher than the solid state values (although they are still much lower than those expected in the absence of antiferromagnetic exchange). For dimetallic **6**, the solution magnetic susceptibility values decreased as the temperature was lowered, until an asymptote was reached at a value corresponding to that from solid state SQUID measurements; compound **5** showed analogous behavior, but with a much less pronounced change in magnetic susceptibility (Figures 2.7 and 2.8). This behavior is consistent with a solution equilibrium (significant above 245 K for **5**, and above 210 K for **6**) between the dimetallic solid state structures and entropically favored paramagnetic species; most likely mononuclear $[(\text{dmpe})\text{Mn}(\text{CH}_2\text{EMe}_3)_2]$ [E = Si (**3**) or C (**4**)] and base-free “ $\text{Mn}(\text{CH}_2\text{EMe}_3)_2$ ”. Our inability to directly observe the proposed minor solution species by variable temperature ^1H NMR spectroscopy is consistent with both the low concentrations of these species in solution, the broadness of the observed ^1H NMR

signals, and the likelihood of rapid exchange between these species and **5** and **6**, especially at the upper end of the temperature range.

Unlike the solution magnetic susceptibility data for complexes **5** and **6**, the solution magnetic susceptibility of base-free **2** increased as the temperature was reduced and did not reach a plateau (Figure 2.8), moving increasingly further from the solid state magnetic susceptibility value of $2.82 \times 10^{-3} \text{ cm}^3/\text{mol}$ of Mn. This increase in magnetic susceptibility is indicative of an equilibrium that shifts at lower temperature towards species with weaker antiferromagnetic coupling than is observed in tetrametallic **2**. Above room temperature, the magnetic susceptibility of the solution (per manganese atom) continued to decrease towards the solid state value, but magnetic measurements were not accessible above $60 \text{ }^\circ\text{C}$ ($\chi_{M(\text{corr})} = 3.8 \times 10^{-3} \text{ cm}^3/\text{mol}$) due to slow decomposition of solutions of **2** above this temperature.

2.4 – Physical Properties of 1-8

Melting points ranging from 62 to $176 \text{ }^\circ\text{C}$ were measured for **1-8** in a flame sealed glass capillary under an atmosphere of argon (Table 2.3). All complexes were found to melt without noticeable decomposition (determined visually and by ^1H NMR spectroscopy and/or PXRD after cooling to room temperature) if the temperature was reached quickly ($5 \text{ }^\circ\text{C}/\text{min.}$), with the exception of **6** which showed minor decomposition. Importantly, the melting points of **3** and **4** match those reported by Wilkinson et al.,¹¹¹ confirming that the originally reported complexes were 1:1 Mn:dmpe complexes as proposed, rather than 2:1 complexes.

Table 2.3: Physical properties of complexes **1-8**.

Complex	m.p. (°C)	Sublimation Temp. at 5 mTorr (°C)	Thermal Decomp. Data (°C)
1	151-153 (lit. 98) ⁹⁶	150-160 (lit. 150) ⁹⁹	195 (rapid decomp.)
2	99-102	90 (lit. 100) ⁹⁶	110 (> 50 % after 24 h)
3	62-63 (lit. 62-64) ¹¹¹	60	120 (v. little over 24 h)
4	132 (lit. 132-133) ¹¹¹	80	120 (complete after 5-6 hours)
5	145-146	115-135 (decomp. products sublime)	120 (complete after 5-6 hours)
6	149-151.5 (part. decomp.)	110	110 (visible after 2-3 hours)
7	176	100	120 (v. little over 24 h)
8	161.5-165	100-120	110 (v. little over 24 h)

a. Amount of decomposition assessed visually and by ¹H NMR spectroscopy and/or PXRD after cooling to room temperature.

Base-free [$\{\text{Mn}(\mu\text{-CH}_2\text{SiMe}_3)_2\}_\infty$] (**1**), though very thermally stable (rapid decomp. 195 °C), is not especially volatile (sublim. at 150-160 °C; 5 mTorr). This low volatility can be explained by the polymeric nature of **1** in the solid state. By contrast, [$\{\text{Mn}(\text{CH}_2\text{CMe}_3)(\mu\text{-CH}_2\text{CMe}_3)_2\}_2\{\text{Mn}(\mu\text{-CH}_2\text{CMe}_3)_2\text{Mn}\}$] (**2**), which exists as a monomer in the vapor phase,¹⁰² sublimed at 90 °C (5 mTorr), but was more than 50 % decomposed after 24 h at 110 °C. The remaining complexes, **3-8**, sublimed between 60 and 135 °C at 5 mTorr, although **5** underwent extensive decomposition during sublimation, and **6** and **8** decomposed slowly at the sublimation temperature (Table 2.3). The 1:1 MnR₂:dmpe complexes, monometallic **3** and dimetallic **4**, exhibited the most promising volatility/thermal stability characteristics for possible applications in ALD or CVD, subliming at 60 and 80 °C, respectively, with negligible decomposition after 24 h at 120 and 110 °C, respectively. Furthermore, **3** has a melting point of 62-63 °C, so would be a liquid at the delivery temperature in a typical ALD or CVD experiment.

2.5 – Reactions with Hydrogen and Diethyl Zinc

Solutions of complexes **2-8**, or a slurry of **1**, were placed under 2 atm. of H₂ in an aromatic solvent, the reactions were monitored by ¹H NMR spectroscopy, and insoluble products were characterized using PXRD. Reactions took place between 25 and 120 °C (Table 2.4), and in each case, a clear colourless or very pale beige solution was formed with a metallic-looking silver-grey mirror on the walls of the NMR tube (Scheme 2.3), or

in one case (complex **1**) a precipitate of black powder. The diamagnetic reaction byproducts were tetramethylsilane or neopentane, accompanied by dmpe or dmpm in the case of compounds **3-8** (Scheme 2.3). The deposited solid was identified as manganese metal by PXRD. Additionally, conducting the reactions of **3** and **5** with H₂ in the presence of hexaethylbenzene as an internal NMR standard yielded exactly two and four equivalents of SiMe₄, respectively,^q illustrating complete removal of the alkyl groups from manganese. The appearance of the deposited films is also consistent with metallic manganese.

Table 2.4: Reaction conditions and by-products for: (i) the solution reactions of **1-8** with H₂ yielding Mn metal (determined by PXRD), and (ii) solution reactions of **1-8** with ZnEt₂ to deposit a 1:1 Mn/Zn alloy (determined by PXRD, and in some cases XPS; accompanied by Zn metal deposition in the reaction of **2** with ZnEt₂). Complex **10** is *trans*-[(dmpe)₂MnH(C₂H₄)].

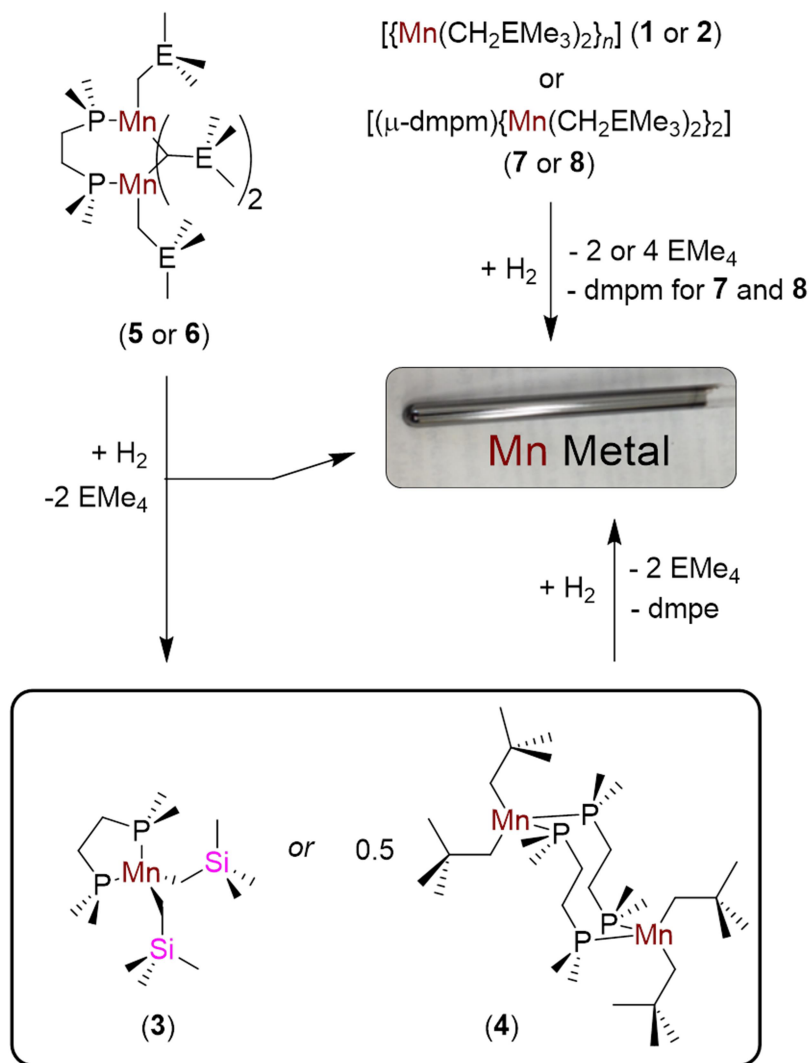
Complex	T _{reaction} with H ₂ (°C) / time (h)	H ₂ reaction by-products ^a	T _{reaction} with ZnEt ₂ (°C) / time (h)	ZnEt ₂ reaction by-products ^{a,b}
1	120 / 48	SiMe ₄	25 / 12	C ₂ H ₆ , C ₂ H ₄ , SiMe ₄ , ZnRX
2	25 / 72	CMe ₄	25 / 12	C ₂ H ₆ , C ₂ H ₄ , CMe ₄ , ZnRX
3	120 / 24	SiMe ₄ , dmpe	60 / 1	C ₂ H ₆ , C ₂ H ₄ , 10 , SiMe ₄ , u.p. ^c
4	70 / 216 (or 100 / 24)	CMe ₄ , dmpe	25 / 72	C ₂ H ₆ , C ₂ H ₄ , 10 , ZnRX
5	120 / 4	SiMe ₄ , 3	25 / 48	C ₂ H ₆ , C ₂ H ₄ , 10 , SiMe ₄ , ZnRX,
6	25 / 168 (or 60 / 1)	CMe ₄ , 4	25 / 12	C ₂ H ₆ , C ₂ H ₄ , 10 , ZnRX, u.p. ^c
7	120 / 4	SiMe ₄ , dmpm, u.p. ^c	90 / 0.5	C ₂ H ₆ , C ₂ H ₄ , ZnRX, dmpm
8	100 / 4	CMe ₄ , dmpm	95 / 1	C ₂ H ₆ , C ₂ H ₄ , ZnRX, dmpm

a. By-products identified by ¹H NMR spectroscopy.

b. R = CH₂EMe₃; X = Et or R; E = C or Si.

c. u.p. = unidentified phosphorus-containing product.

^q For **5**, 4 equivalents of SiMe₄ was observed after the intermediate (**3**) had reacted with excess H₂ at 120 °C for 12 h.



Scheme 2.3: Reactions of **1-8** with H_2 in benzene or toluene.

Polymeric complex **1** was the least reactive towards hydrogen, requiring several days at $120\text{ }^\circ\text{C}$ to react completely, most likely due to very low solubility. By contrast, highly soluble tetrametallic **2** reacted to completion within three days at room temperature; **2** is far more reactive than **1** and **3-8**, likely due to the presence of 3-coordinate manganese centres. Complexes **3** and **4**, which contain one equivalent of dmpe per manganese centre, showed low reactivity towards H_2 ; the reaction with **3** was only complete after 12 hours at $120\text{ }^\circ\text{C}$, and the reaction with **4** was complete after 24 hours at $100\text{ }^\circ\text{C}$. Dimetallic **5** and **6**, which contain half an equivalent of dmpe per manganese

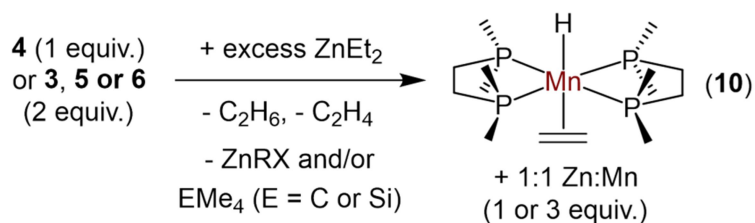
centre, reacted with H₂ to form **3** or **4**, accompanied by tetramethylsilane or neopentane and manganese metal. Complete consumption of **5** required 4.5 hours at 120 °C,^r and the analogous reaction with **6** proceeded over a week at room temperature. The similarity in the reaction conditions required for consumption of **6** and **2** supports the proposal (*vide supra*) that in solution, **6** exists in equilibrium with **2** and **4** (*i.e.* H₂ likely reacts with **2** that is in equilibrium with **6** in solution, leaving unreacted **4**). Compounds **7** and **8** reacted with H₂ over the course of 4 hours at 120 °C and 100 °C, respectively. However, unlike the dmpe analogues (**5** and **6**), compounds **7** and **8** reacted with H₂ to provide manganese metal without formation of an observable monometallic intermediate. A general trend for **1-8** is the greater reactivity of the neopentyl complexes towards H₂.

Overall, the reactions of the dialkylmanganese(II) complexes and their bis(phosphine) adducts with H₂ highlight the utility of metal alkyl complexes for electropositive metal deposition, demonstrating the thermodynamic feasibility of key reaction steps en route to manganese deposition. In solution, base-free **2** and dmpe complex **6** displayed the highest reactivity. However, solution reaction temperatures may not be of direct relevance to thermal ALD, given that adsorption to the surface of the growing thin film during ALD is likely to result in phosphine dissociation and/or formation of surface-bound species with coordination geometries and steric environments which differ significantly from those in the intact precursor complex.

Complexes **1-8** were also reacted with 1-3 equivalents of ZnEt₂ (per Mn) in C₆D₆ (**2-8**) or *d*₈-toluene (**1**) in a sealed NMR tube, the reactions were monitored by ¹H and/or ³¹P NMR spectroscopy, and precipitated solids were characterized by PXRD and in some cases XPS. Complexes **1-2** and **4-6** reacted completely over 12-72 hours at room temperature, whereas **3** required heating for 1 hour at 60 °C, and dmpm complexes **7** and **8** required heating at 90-95 °C for 30-60 minutes. In each of these reactions, a silver-coloured mirror was deposited onto the walls of the NMR tube, and ethane, ethylene and

^r Complex **5** slowly decomposed to **3** at 120 °C in solution. However, this decomposition proceeded much more slowly than the reaction to form **3** in the presence of H₂.

ZnX(CH₂EMe₃) (X = Et or CH₂EMe₃; E = Si or C) were released, accompanied in some cases by a small amount of EMe₄ (E = Si or C); H₂ formation was not observed. Compounds **7** and **8** released free dmpm,^s whereas dmpe compounds **3-6** formed *trans*-[(dmpe)₂MnH(C₂H₄)] (**10**) (0.5 equiv. per Mn in **3-4** and 0.25 equiv. per Mn in **5-6**; Scheme 2.4), and free dmpe was not liberated.^t



Scheme 2.4: Reactions of dmpe complexes **3-6** with ZnEt₂ (R = CH₂EMe₃; X = Et or R; E = C or Si) in benzene.

The reactivity of **5** and **6** with ZnEt₂ is greater than that of **3** and **4**, respectively, implying that **3** and **4** are not formed as intermediates in the reactions of **5** and **6** with ZnEt₂, in contrast to the analogous reactions with H₂ (*vide supra*). The aforementioned manganese(I) hydride compound, diamagnetic *trans*-[(dmpe)₂MnH(C₂H₄)] (**10**), was first prepared by Wilkinson et al. via the reactions of manganese dihalides with MgEt₂,^{120,172} and may be formed in this work by i) initial generation of a Mn(II) ethyl intermediate followed by β-hydride elimination and bi-molecular HR reductive elimination, ii) bi-molecular HR reductive elimination from manganese dihydride and manganese hydrido/alkyl centres, or iii) comproportionation between a manganese dihydride species and elemental manganese (or an unobserved zero-valent manganese species formed en route to manganese metal).

^s NMR signals for free dmpm were shifted by 0.05-0.1 ppm (¹H NMR) and 1-3 ppm (³¹P NMR) relative to a reference sample.

^t A small amount of an unidentified phosphorus-containing product was observed in the reaction of **3** with ZnEt₂ at 60 °C. This product was not observed in the reaction of **5** with ZnEt₂, most likely due to milder reaction conditions.

By PXRD, the insoluble product from the reactions of **1-8** with ZnEt_2 was an approximate 1:1 manganese-zinc alloy,⁴⁶² accompanied by zinc metal in the case of **2**. The presence of both zinc and manganese was further confirmed by XPS on representative samples ($\text{Zn:Mn} = 0.68 : 1$ for **2** and $1.32 : 1$ for **7**). Elemental zinc deposition could potentially occur via hydride transfer from a manganese hydride intermediate to a dialkyl zinc compound, leading to a zinc hydrido/alkyl species with very limited thermal stability; the only isolated zinc hydrido hydrocarbyl compounds (not counting heterobimetallic species or those with pendent amine coordination to the metal) contain extremely large aryl groups {e.g. $\text{R} = (\text{C}_6\text{H}_3\text{-2,6-(C}_6\text{H}_3\text{-2,6-}^i\text{Pr}_2)_2$,⁴⁶³ $\text{C}_6\text{H}_3\text{-2,6-(C}_6\text{H}_2\text{-2,4,6-}^i\text{Pr}_3)_2$, and $\text{C}_6\text{H}_2\text{-2,6-(C}_6\text{H}_2\text{-2,4,6-}^i\text{Pr}_3)_2\text{-4-SiMe}_3$ }⁴⁶⁴, although ZnHMe has been observed in an argon matrix⁴⁶⁵ and spectroscopically in the gas phase.⁴⁶⁶ In addition, ZnH_2 is reported to decompose to Zn and H_2 at 90°C .⁴⁶⁷

2.6 – Summary and Conclusions for Chapter 2

In the solid state, dineopentylmanganese(II) (**2**) is tetrametallic with two terminal alkyl groups and six bridging alkyl groups. The outer manganese centres are trigonal planar, whereas the inner manganese centres are tetrahedral. Dmpe complexes of bis(trimethylsilylmethyl)manganese(II) and dineopentylmanganese(II) adopt three distinct structural types: monometallic $[\text{LMnR}_2]$ (**3**), dimetallic $[\text{R}_2\text{Mn}(\mu\text{-L})_2\text{MnR}_2]$ (**4**), and dimetallic $[(\mu\text{-L})\{\text{RMn}(\mu\text{-R})\}_2]$ (**5-6**). By contrast, dmpm only yielded $[(\mu\text{-L})\{\text{RMn}(\mu\text{-R})\}_2]$ complexes (**7-8**). All polymetallic complexes feature doubly bridging alkyl groups with one long and one short Mn–C bond, and the neopentyl complexes exhibit more acute Mn–C–Mn angles and shorter Mn–Mn distances than trimethylsilylmethyl analogues.

All complexes have non-zero magnetic susceptibilities between 300 and 5 K. Both $[(\text{dmpe})\text{Mn}(\text{CH}_2\text{SiMe}_3)_2]$ (**3**) and $[(\mu\text{-dmpe})\text{Mn}(\text{CH}_2\text{CMe}_3)_2]_2$ (**4**) obey the Curie-Weiss law, whereas tetrametallic dineopentylmanganese(II) (**2**) and $[(\mu\text{-L})\{\text{RMn}(\mu\text{-R})\}_2]$ ($\text{L} = \text{dmpe}$ (**5-6**) or dmpm (**7-8**)) engage in strong antiferromagnetic

coupling with J values from -107 to -117 cm^{-1} . Comparison of solution and solid state magnetic data indicates that the structures of the dmpm complexes (**7** and **8**) are maintained in solution, whereas the $[(\mu\text{-dmpe})\{\text{RMn}(\mu\text{-R})\}_2]$ complexes (**5** and **6**) exist in equilibrium at 25 $^\circ\text{C}$ with species with a higher average magnetic susceptibility; most likely $[(\text{dmpe})\text{MnR}_2]$ and “ MnR_2 ”. However, the solution magnetic susceptibilities of **5** and **6** decreased with decreasing temperature until an asymptote was reached, consistent with the presence of only **5** or **6** in solution at low temperature. In contrast, the solution state magnetic susceptibility (per Mn) of dineopentylmanganese(II) (**2**) almost doubled as the temperature was reduced from 335 to 185 K, implying that the tetrametallic solid state structure is in equilibrium with species which exhibit less effective antiferromagnetic coupling and are favored at lower temperatures.

The two compounds without bridging alkyl groups (**3** and **4**) exhibited the most desirable thermal stability and volatility for ALD or CVD applications, and all CH_2SiMe_3 derivatives exhibited slightly increased thermal stability relative to CH_2CMe_3 analogues; monometallic **3** was the most promising, melting at $62\text{-}63$ $^\circ\text{C}$, subliming at 60 $^\circ\text{C}$ (5 mTorr), and undergoing negligible decomposition after 24 h at 120 $^\circ\text{C}$.

Solution reactions of **1-8** with H_2 yielded manganese metal with elimination of 2 equiv. of HR ($\text{R} = \text{CH}_2\text{EMe}_3$; in all cases, neopentyl complexes displayed higher reactivity towards H_2 than trimethylsilylmethyl analogues), demonstrating the thermodynamic feasibility of the key reaction steps required for manganese(II) dialkyl complexes to serve, in combination with H_2 , as precursors for metal ALD or pulsed-CVD. By contrast, the solution reactions of **1-8** with ZnEt_2 yielded a zinc-manganese alloy with an approximate $1:1$ Zn:Mn ratio, eliminating ethane and ethylene, accompanied by dmpm, *trans*- $[(\text{dmpe})_2\text{MnH}(\text{C}_2\text{H}_4)]$ (**10**), EMe_4 and/or ZnXR ($\text{R} = \text{CH}_2\text{EMe}_3$; $\text{X} = \text{Et}$ or R).

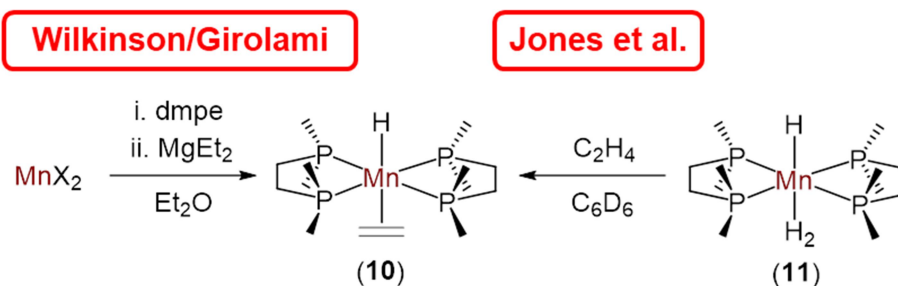
Chapter 3

Analysis of Wilkinson and Girolami's *trans*-[(dmpe)₂MnH(C₂H₄)]

Portions of this chapter have been adapted with permission from Price, J. S.; Emslie, D. J. H.; Vargas-Baca, I.; Britten, J. F. [(dmpe)₂MnH(C₂H₄)] as a Source of a Low-Coordinate Ethyl Manganese(I) Species: Reactions with Primary Silanes, H₂, and Isonitriles, *Organometallics* **2018**, *37*, 3010-3023.

3.1 – Introduction to Chapter 3

trans-[(dmpe)₂MnH(C₂H₄)] (**10**) was first reported by Girolami and Wilkinson et al. in 1983. This complex was originally prepared by the reaction of MnBr₂(dmpe)₂ and MgEt₂, and two years later, they reported an analogous synthesis using MnCl₂ and free dmpe (Scheme 3.1).^{120,172} The authors proposed a potential reaction mechanism involving initial formation of MnEtX(dmpe)₂, followed by bi-molecular C–C bond-forming reductive elimination to generate MnX(dmpe)₂ (X = Cl, Br) from which alkylation and β-hydride elimination would generate the observed product. Based on NMR spectroscopy, an octahedral environment with *trans*-disposed hydride and rapidly rotating ethylene ligands was proposed. A decade later, Jones et al. reported the synthesis of **10** from an alternative route; substitution by ethylene of a H₂ ligand in [(dmpe)₂MnH(H₂)] (**11**); Scheme 3.1.¹⁷³ However, neither Wilkinson nor Jones reported an X-ray crystal structure of **10**.



Scheme 3.1: Reported synthetic routes to [(dmpe)₂MnH(C₂H₄)] (**10**). X = Cl, Br.^{120,172,173}

In 1985, Girolami and Wilkinson reported the lithiation of **10** to form $[\{(Me_2PCH_2CH_2PMeCH_2)_2MnH(C_2H_5)\}_2Li_4(OEt_2)_2]$. To our knowledge, this is the only report regarding the potential reactivity of complex **10**. Complex **10** is a rare example of a first row transition metal ethylene hydride complex. As well, it is stable indefinitely under an inert atmosphere at room temperature and is diamagnetic.

3.2 – X-ray Crystal Structure of *trans*-[(dmpe)₂MnH(C₂H₄)]

X-ray quality crystal of *trans*-[(dmpe)₂MnH(C₂H₄)] (*trans*-**10**) were grown from a dilute solution in hexanes at $-30\text{ }^\circ\text{C}$ (Figure 3.1 left), and confirmed that the *trans* octahedral structure proposed by Wilkinson in solution by analysis of the NMR spectra¹²⁰ is maintained in the solid state, with the equatorial girdle of phosphine donors displaced toward the smaller hydride ligand. Complex *trans*-**10** shows significant metallacyclopropane character, which is apparent from the elongated C–C distance of 1.420(2) Å (compared to 1.329 Å in ethylene and 1.535 Å in ethane).⁴⁶⁸ The C–C distance is similar to those in previously characterized $[\{(Me_2PCH_2CH_2PMeCH_2)_2MnH(C_2H_4)\}_2Li_4(OEt_2)_2]$ (bottom right in Figure 3.3) and $[Na(pmdeta)]_2-[(\kappa^2-C_4H_8)Mn(C_2H_4)_2]$ (pmdeta = pentamethyldiethylenetriamine) of 1.41(1)-1.444(4) Å.^{120,469}

Substantial metallacyclopropane character in *trans*-**10** is also supported by DFT calculations (ADF, gas phase, all-electron, PBE, D3-BJ, TZ2P, ZORA); Figure 3.1 right. In particular, the C–C Mayer bond order is 1.03 (compared to 1.85 for free ethylene and 0.91 for free ethane) and in a fragment $\{(dmpe)_2MnH$ and $C_2H_4\}$ interaction calculation, a substantially negative Hirschfield charge of -0.273 was observed for the ethylene fragment. Furthermore, ETS-NOCV (extended transition state method for energy decomposition analysis with natural orbitals for chemical valence; Figure 3.2) calculations on *trans*-**10** partitioned the ethylene-manganese interaction into σ donation and π -backdonation contributions of 103.9 and 300.1 kJ mol⁻¹ respectively.

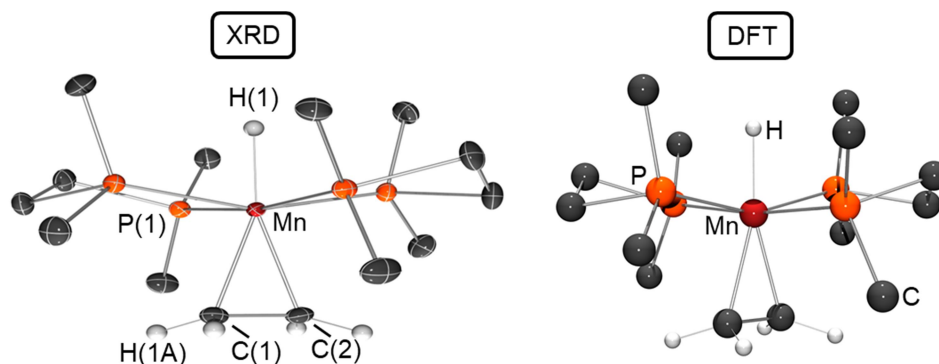


Figure 3.1: Left: X-ray crystal structure of *trans*-[(dmpe)₂MnH(C₂H₄)] (*trans*-**10**) with ellipsoids drawn at 50% probability. Hydrogen atoms on the metal centre and ethylene ligand were located from the difference map and refined isotropically. Most hydrogen atoms have been omitted for clarity. Bond distances (Å) and angles (deg): Mn–H(1) 1.56(4), Mn–C(1) 2.123(2), Mn–C(2) 2.121(2), C(1)–C(2) 1.420(2), Σ(H–C(1)–X) (X = C, H) 349(3), Σ(H–C(2)–X) (X = C, H) 349(3), Σ(P–Mn–P) (*cis*) 356.44(4). Right: geometry optimized (DFT calcd.) structure of *trans*-[(dmpe)₂MnH(C₂H₄)] (*trans*-**10**). Most hydrogen atoms have been omitted for clarity.

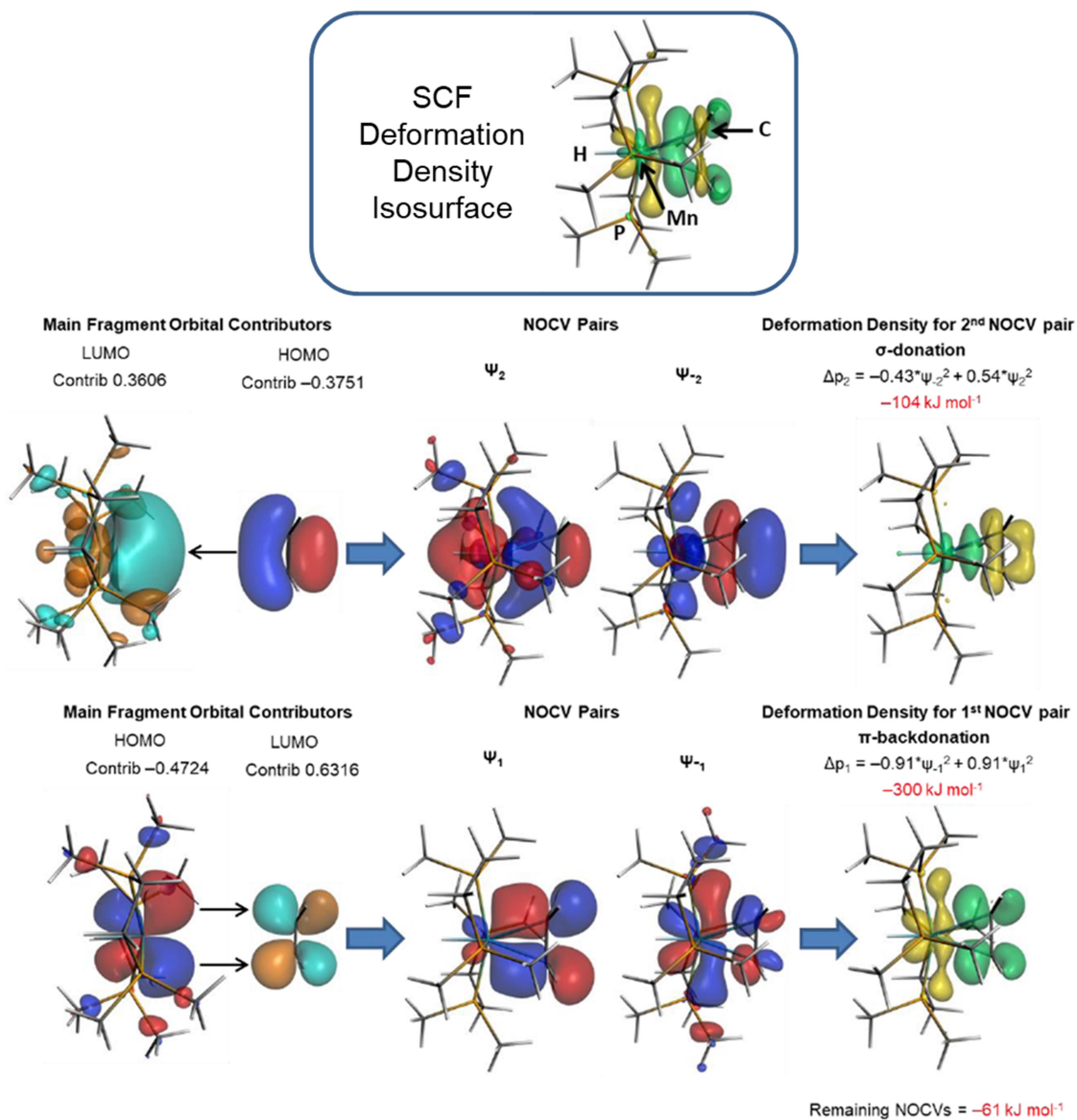
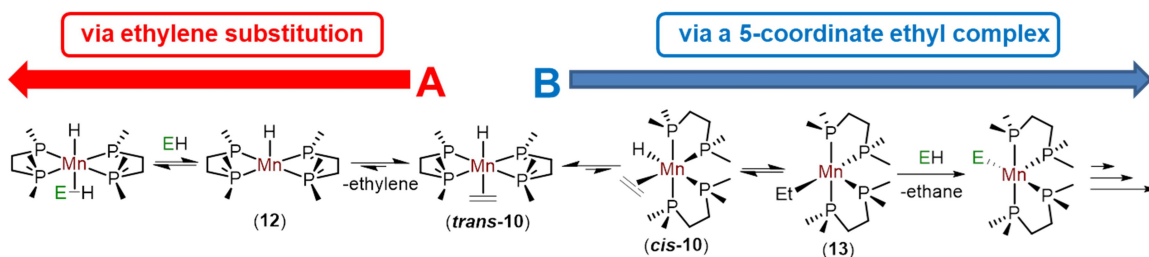


Figure 3.2: ETS-NOCV analysis of bonding between $[(dmpe)_2MnH]$ (equatorial dmpe geometry) and ethylene in $trans-[(dmpe)_2MnH(C_2H_4)]$ (*trans*-10). Inset: SCF deformation density isosurface from a fragment interaction calculation using neutral $[(dmpe)_2MnH]$ (equatorial dmpe geometry) and ethylene fragments for *trans*- $[(dmpe)_2MnH(C_2H_4)]$ (*trans*-10).

3.3 – Potential Pathways for Reactions of $[(\text{dmpe})_2\text{MnH}(\text{C}_2\text{H}_4)]$ with Hydrides

trans- $[(\text{dmpe})_2\text{MnH}(\text{C}_2\text{H}_4)]$ (**trans-10**) could potentially react with reagents such as hydrosilanes, hydrostannanes, hydroboranes, and H_2 through two different pathways (A and B; Scheme 3.2). The simplest of these pathways would be ethylene substitution, labelled pathway A in Scheme 3.2. The combined bonding energies of ethylene and a $[(\text{dmpe})_2\text{MnH}]$ (**12**) fragment with an equatorial dmpe arrangement (i.e. the products of ethylene dissociation from **trans-10**) are 182 kJ mol^{-1} higher in energy than **trans-10**. This, in combination with an entropic driving force, suggests that dissociation of ethylene (the rate determining step in dissociative substitution, assuming the simplest possible mechanism not involving partial dmpe dissociation) may be possible at elevated temperature.^u Pathway A would yield ethylene and $[(\text{dmpe})_2\text{MnH}_2\text{R}]$ (where R is an anionic ligand). An analogous mechanism could also be envisaged for the reactions of **10** with non-hydride Lewis bases (e.g. PR_3 ; see Chapter 9), which would yield $[(\text{dmpe})_2\text{MnHL}]$ (where L is a neutral ligand), again with ethylene elimination.



Scheme 3.2: Potential pathways (A and B) for the reaction of *trans*- $[(\text{dmpe})_2\text{MnH}(\text{C}_2\text{H}_4)]$ (**10**) with various reagents. Only one isomer of all complexes except **10** is shown. E = SiR_3 , SnR_3 , BR_2 , H.

An alternative reaction pathway could involve initial isomerization of the alkene hydride complex *trans*-**10** to a 5-coordinate ethyl complex $[(\text{dmpe})_2\text{MnEt}]$ (**13**); pathway B in Scheme 3.2. This putative intermediate would be formed by initial isomerization of *trans*-**10** to *cis*- $[(\text{dmpe})_2\text{MnH}(\text{C}_2\text{H}_4)]$ (**cis-10**), which could generate **13** by 1,2 insertion

^u Complex **10** displays significant thermal stability, decomposing slowly at $140 \text{ }^\circ\text{C}$.

of the ethylene into the Mn–H bond. Intermediate **13** could then react with an E–H reagent (e.g. hydrosilanes, hydroboranes, H₂) via either σ -bond metathesis or oxidative addition followed by reductive elimination to install a new anionic ligand in place of the ethyl group (with ethane as the byproduct); Scheme 3.2. Thus, *trans*-**10** could act as a masked form of a highly reactive low-coordinate Mn(I) alkyl species.

Equilibria between alkene hydride and coordinatively unsaturated alkyl complexes (as envisaged in pathway B) have been observed for a range of 2nd and 3rd row transition metal complexes. For example, the NMR spectra of isolable ethylene hydride complexes typically indicate exchange between the protons of the alkene and the hydride ligands, and in some cases (e.g. in complexes of Nb,^{470,471} Ta,^{471,472} W,⁴⁷³ Re,⁴⁷⁴ Os,⁴⁷⁵ Ru,⁴⁷⁵ Rh,⁴⁷⁶ Ir,⁴⁷⁷ Pd,⁴⁷⁸ and Pt⁴⁷⁹), reaction with a neutral donor has been shown to trap the alkyl isomer. However, in several cases, there is experimental evidence to suggest that exchange between the hydride and alkene protons occurs via a β -agostic alkyl complex, with "in-place" exchange of the bridging hydrogen atom rather than via a true low-coordinate (i.e. non-agostic) species.⁴⁷⁹⁻⁴⁸³ This is indicated by dynamic NMR studies, including pairwise coalescence of the four ³¹P NMR resonances observed for [(*cis*-Ph₂PCH=CHPh₂)₂MoH(C₂H₄)₂]⁺ at low temperature,⁴⁸⁰ exchange of the hydride and C₂H₄ environments in [κ^1, η^6 -Cy₂P(*o*-C₆H₄)(*o*-C₆H₄NMe₂)}RuH(C₂H₄)]⁺ without epimerization,⁴⁸¹ and exchange of the hydride and C₂H₄ environments in [(κ^3 -POCOP)MH(C₂H₄)]⁺ {M = Rh or Ir; POCOP = *o*-C₆H₃(OP^{*t*}Bu₂)₂} while maintaining top-bottom asymmetry.⁴⁸²

In contrast to ethylene hydride complexes of 2nd and 3rd row transition metals, 1st row transition metal examples are scarce (Figure 3.3),^{120,484-488} and their isomerization to afford alkyl complexes has rarely been investigated. In fact, for the complexes in Figure 3.3, an equilibrium with an ethyl isomer has only been reported for the cobalt complex [(Me₃P)₃CoH(C₂H₄)] (though in this case calculations suggested very similar energies for the non-agostic and β -agostic cobalt ethyl structures)^{487,488} and the iron cyclopentadienyl complex [Cp*FeH(C₂H₄)(PMe₃)].⁴⁸⁴ However, from the reverse perspective, the 1st row

transition metal (Sc ,⁴⁸⁹ Ti ,^{490,491} Ni ,^{492,493,494} and Co ^{495,496}) ethyl complexes in Figure 3.4 all feature a β -agostic C–H–M interaction, and the cobalt,⁴⁹⁵ nickel α -diimine⁴⁹⁴, and nickel β -diketiminate⁴⁹³ complexes undergo NMR-observable exchange of the ethyl group CH_2 and CH_3 protons and/or carbon atoms, presumably via an undetected ethylene hydride complex.

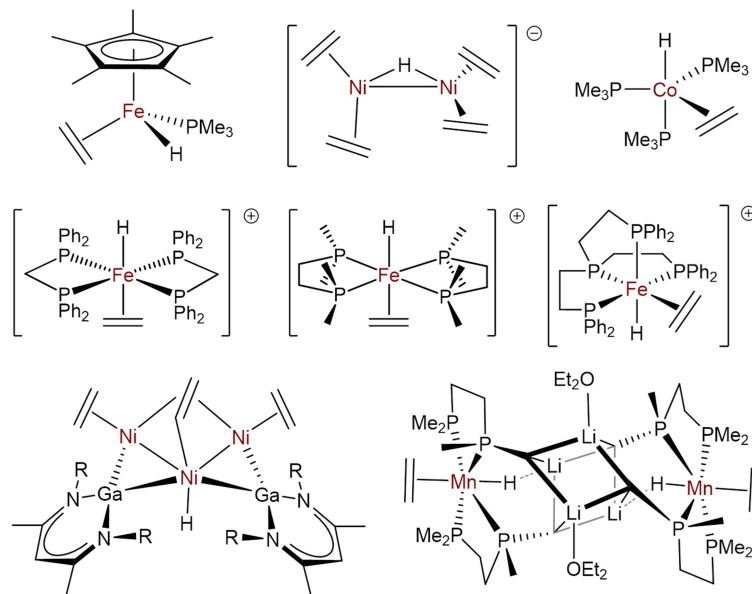


Figure 3.3: First-row transition metal (Fe ,^{484,485} Ni ,⁴⁸⁶ Co ,^{487,488} or Mn ¹²⁰) alkene hydride complexes (not including complex **10**).

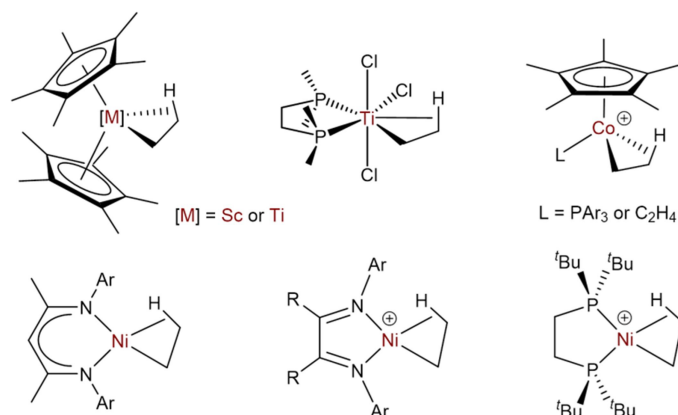


Figure 3.4: First row transition metal ethyl complexes reported to feature a β -agostic interaction.⁴⁸⁹⁻⁴⁹⁶

In contrast to pathway A (which generates ethylene and $[(\text{dmpe})_2\text{MnH}_2\text{R}]$; *vide supra*), reactions proceeding by pathway B would initially yield ethane and $[(\text{dmpe})_2\text{MnR}]$ (where R is an anionic ligand). As the initially generated complex $[(\text{dmpe})_2\text{MnR}]$ is coordinately unsaturated, it is susceptible to further inter- or intramolecular reactivity to generate a coordinately saturated complex. Furthermore, unlike the substitution mechanism A (which involves generation of a potentially highly-reactive byproduct in ethylene), the putative ethane byproduct in pathway B would not react further with the generated complex. Furthermore, pathway B features a significant driving force in effectively irreversible C–H bond formation when eliminating ethane, in contrast to pathway A where the product and reactant may be in equilibrium if ethylene is not removed.

3.4 – DFT calculations for isomerization of *trans*- $[(\text{dmpe})_2\text{MnH}(\text{C}_2\text{H}_4)]$ to $[(\text{dmpe})_2\text{MnEt}]$

Reactions of *trans*- $[(\text{dmpe})_2\text{MnH}(\text{C}_2\text{H}_4)]$ (***trans*-10**) with a variety of hydridic reagents are, in many cases (i.e. those which proceed via pathway B in Scheme 3.2), predicated on the thermodynamic accessibility of the Mn(I) ethyl complex $[(\text{dmpe})_2\text{MnEt}]$ (**13**). However, in all the reactions for which this mechanism is proposed (Chapters 4, 5, and 9), neither $[(\text{dmpe})_2\text{MnEt}]$ (**13**) nor putative intermediate *cis*- $[(\text{dmpe})_2\text{MnH}(\text{C}_2\text{H}_4)]$ (***cis*-10**) were detected spectroscopically. Therefore, to investigate the accessibility of these complexes we turned to DFT calculations (ADF, gas phase, all-electron, PBE, D3-BJ, TZ2P, ZORA; Figure 3.5 and Table 3.1).

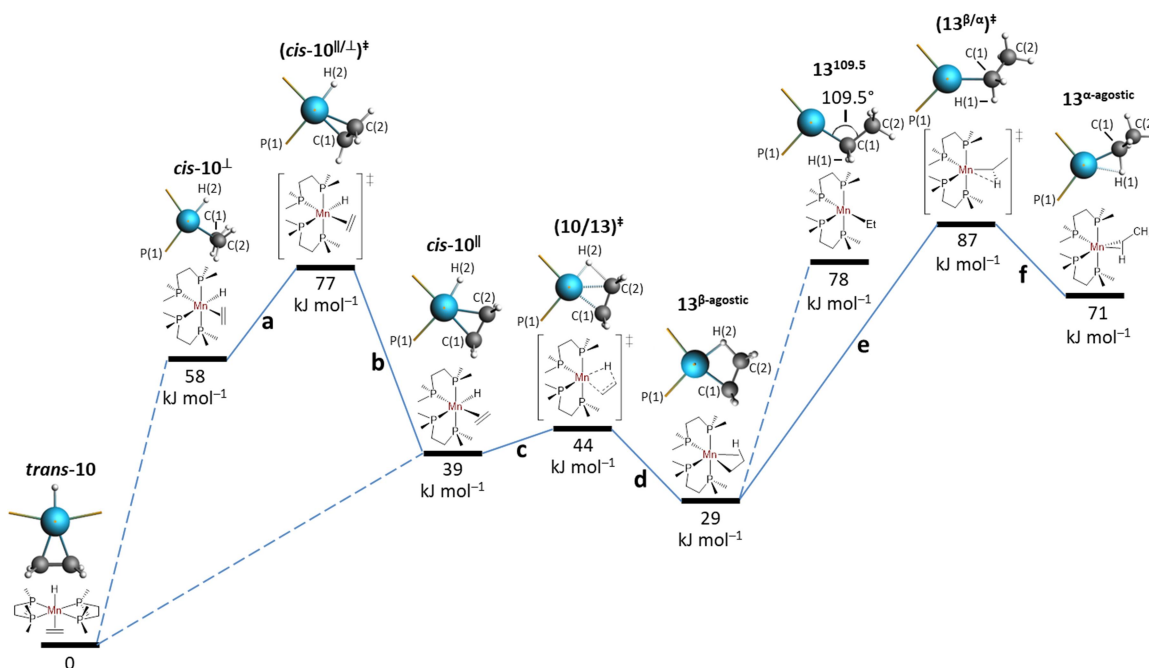


Figure 3.5: Potential energies (E ; kJ mol⁻¹) relative to *trans*-10, calculated for structures (left to right) i. *trans*-[(dmpe)₂MnH(C₂H₄)] (*trans*-10), ii. an isomer of *cis*-[(dmpe)₂MnH(C₂H₄)] in which the ethylene ligand is oriented perpendicular to the plane formed by manganese, the hydride, and the ethylene centroid (*cis*-10[⊥]), iii. the transition state for isomerization of *cis*-10[⊥] to *cis*-10[⊥] $\{(cis-10^{\perp})^{\ddagger}\}$, iv. an isomer of *cis*-[(dmpe)₂MnH(C₂H₄)] in which the ethylene carbon atoms lie within the plane formed by manganese, the hydride, and the ethylene centroid (*cis*-10[⊥]), v. the transition state for isomerization of *cis*-10[⊥] to 13^{β-agostic} $\{(10/13)^{\ddagger}\}$, vi. [(dmpe)₂MnEt] with a β-agostic interaction (13^{β-agostic}), vii. [(dmpe)₂MnEt] without an agostic interaction where the Mn–C_α–C_β angle was restrained to 109.5° (13^{109.5}), viii. the transition state for isomerization of 13^{β-agostic} to 13^{α-agostic} $\{(13^{\beta/\alpha})^{\ddagger}\}$, and ix. [(dmpe)₂MnEt] with an α-agostic interaction (13^{α-agostic}). All structures except 13^{109.5} correspond to an energy minimum. The geometry optimized cores are depicted above each Chemdraw structure, showing Mn in blue, C in dark grey, and H in light grey, accompanied by stick bonds to the phosphorus donor atoms. Relative energies are those before zero-point energy (ZPE) correction.

Table 3.1: Selected angles (deg), distances (Å) (and Mayer bond orders) for DFT calculated structures in Figure 3.5.^a

Parameter	<i>cis</i> - 10 [⊥]	(<i>cis</i> - 10 [⊥]) [‡]	<i>cis</i> - 10	(10 / 13) [‡]	13 ^β -agostic	(13 ^{β/α}) [‡]	13 ^α -agostic	13 ^{109.5}
Mn–C(1)	2.14 (0.57)	2.18 (0.53)	2.13 (0.60)	2.11 (0.66)	2.06 (0.73)	2.09 (0.75)	1.96 (0.87)	2.09 (0.83)
Mn–C(2)	2.15 (0.54)	2.16 (0.48)	2.11 (0.56)	2.12 (0.45)	2.21 (0.23)	3.17 (<0.05)	3.19 (<0.05)	2.98 (<0.05)
C(1)–C(2)	1.41 (1.05)	1.41 (1.09)	1.42 (1.06)	1.44 (1.01)	1.48 (0.95)	1.53 (0.88)	1.52 (0.89)	1.54 (0.85)
Mn–H(2)	1.58 (0.83)	1.58 (0.82)	1.56 (0.82)	1.57 (0.68)	1.71 (0.34)	3.38 (<0.05)	3.39 (<0.05)	3.14 (<0.05)
Mn–H(1)	–	–	–	2.77 (<0.05)	2.76 (<0.05)	2.50 (<0.05)	1.95 (0.20)	2.72 (<0.05)
C(2)–H(2)	2.48 (<0.05)	2.36 (0.06)	2.12 (0.13)	1.62 (0.32)	1.22 (0.68)	1.10 (0.96)	1.10 (0.96)	1.10 (0.97)
C(1)–H(1) ^b	–	–	–	1.09 (1.03)	1.09 (1.02)	1.11 (0.99)	1.16 (0.87)	1.11 (1.01)
Mn–C(1)–C(2) ^c	71.1	70.5	69.8	70.7	75.2	121.6	132.4	109.5
Mn–H(2)–C(2)	–	–	–	83.1	96.8	69.9	70.4	71.4
Mn–C(1)–H(1)	–	–	–	116.1	118.5	97.8	72.3	112.8
P(1)–Mn–C(1)	–	–	–	91.9	97.1	133.1	151.0	100.4
P(1)–Mn–C(1)–C(2)	–95.6	–133.3	174.9	173.5	171.1	136.4	98.4	171.1
Mn–C(1)–C(2)–H(2)	–41.4	–34.5	–2.8	1.0	–2.2	–54.7	–34.9	–58.4

^a Atom labels correspond to those in Figure 3.5. For alkyl isomers ((**10**/**13**)[‡], **13**^β-agostic, (**13**^{β/α})[‡], **13**^α-agostic, and **13**^{109.5}), C(1) is C_α, C(2) is C_β, H(1) is the closest H on C_α to the Mn centre, and H(2) is the closest H on C_β to the Mn centre. For alkene hydride isomers (*cis*-**10**[⊥], (*cis*-**10**[⊥])[‡], and *cis*-**10**^{||}), H(2) is the metal hydride, while C(1) and C(2) are ethylene carbon atoms.

^b For *cis*-**10**[⊥], (*cis*-**10**[⊥])[‡], and *cis*-**10**^{||}, all carbon–H_{ethylene} distances were calculated to be 1.09 Å with Mayer bond orders ranging from 1.01 to 1.04.

^c Mn–C(2)–C(1) angles for *cis*-**10**[⊥], (*cis*-**10**[⊥])[‡], and *cis*-**10**^{||} are similar to the Mn–C(1)–C(2) angles: 70.3°, 71.8°, and 71.2° respectively.

Geometry optimization of *cis*-[(dmp_e)₂MnH(C₂H₄)] (*cis*-**10**) yielded two local minima; an isomer of lower energy, *cis*-**10**^{||}, where the ethylene carbon atoms lie within the plane formed by manganese, the hydride, and the ethylene centroid, and an isomer of higher energy, *cis*-**10**[⊥], in which the ethylene ligand is perpendicular to the aforementioned plane. Isomers *cis*-**10**^{||} and *cis*-**10**[⊥] are interconverted by an approximate 90° rotation of the ethylene ligand {via transition state (*cis*-**10**^{⊥/||})[‡] with activation barriers of 19 or 38 kJ mol⁻¹; Table 3.2}, and are 39 and 58 kJ mol⁻¹ higher in energy than the *trans* isomer (*trans*-**10**) respectively (Figure 3.5).

Table 3.2: Activation Parameters for Transformations a-f in Figure 3.5; ΔE^\ddagger (calculated before ZPE correction), ΔH^\ddagger , and ΔG^\ddagger (kJ mol^{-1} at 298.15 K), $\Delta \text{ZPE}^\ddagger$ (kJ mol^{-1} at 0 K), and ΔS^\ddagger ($\text{J mol}^{-1} \text{K}^{-1}$ at 298.15 K).

	ΔE^\ddagger	$\Delta \text{ZPE}^\ddagger$	ΔH^\ddagger	ΔS^\ddagger	ΔG^\ddagger
<i>cis</i> -10 [⊥] → <i>cis</i> -10 [⊥] (a)	19	-0.7	17	-18	22
<i>cis</i> -10 [⊥] → <i>cis</i> -10 [⊥] (b)	38	0.8	37	-21	44
<i>cis</i> -10 [⊥] → 13 ^β -agostic (c)	5	-3.1	2	-9	4
13 ^β -agostic → <i>cis</i> -10 [⊥] (d)	15	-6.0	8	-9	11
13 ^β -agostic → 13 ^α -agostic (e)	58	-4.4	56	29	47
13 ^α -agostic → 13 ^β -agostic (f)	16	-1.9	14	12	11

To probe the origin of the greater stability of *trans*-**10** versus *cis*-**10**[⊥] and *cis*-**10**[⊥], geometry optimizations were carried out on *cis*- and *trans*-[(PH₃)₄MnH(C₂H₄)] (**10**_{PH3}), in which steric hindrance between phosphine groups is minimized (Figure 3.6, Table 3.3). In this case, *cis*-**10**_{PH3}[⊥] (the *cis* isomer isostructural to *cis*-**10**[⊥]) is lower in energy than the *trans* isomer, *trans*-**10**_{PH3}, by 5 kJ mol^{-1} , whereas *cis*-**10**_{PH3}[⊥] (the *cis* isomer isostructural to *cis*-**10**[⊥]) is higher in energy than *trans*-**10**_{PH3} by 22 kJ mol^{-1} . These data imply that unfavorable steric interactions between the dmpe ligands in *cis*-**10**[⊥] and *cis*-**10**[⊥] are responsible for their diminished stability relative to *trans*-**10**. This steric penalty for adoption of a disphenoidal arrangement of the dmpe ligands also explains why *trans*-**10** is isolated as a *trans* alkene hydride rather than as an ethyl isomer (despite the fact that the latter are usually lower in energy for 1st row transition metal complexes; *vide supra*), since the latter would require a disphenoidal arrangement of the dmpe ligands if an agostic interaction is to be accommodated to saturate the metal's coordination sphere (*vide infra*).

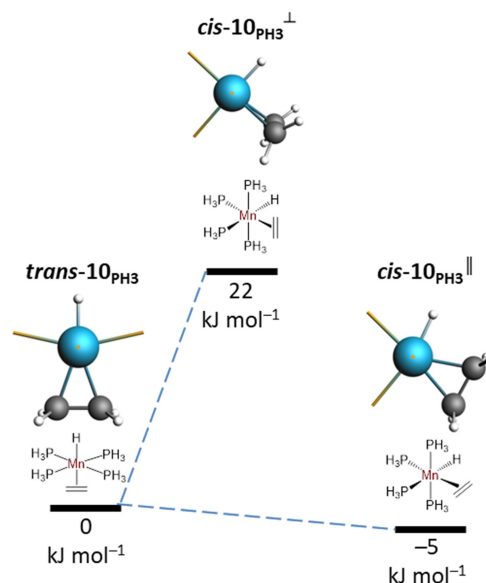


Figure 3.6: Potential energies (E ; kJ mol^{-1}) relative to *trans*- 10_{PH_3} , calculated for structures (left to right) i. *trans*- $[(\text{PH}_3)_4\text{MnH}(\text{C}_2\text{H}_4)]$ (*trans*- 10_{PH_3}), ii. an isomer of *cis*- $[(\text{PH}_3)_4\text{MnH}(\text{C}_2\text{H}_4)]$ in which the ethylene ligand is oriented perpendicular to the plane formed by manganese, the hydride, and the ethylene centroid (*cis*- $10_{\text{PH}_3}^\perp$), and iii. an isomer of *cis*- $[(\text{PH}_3)_4\text{MnH}(\text{C}_2\text{H}_4)]$ in which the ethylene carbon atoms lie within the plane formed by manganese, the hydride, and the ethylene centroid (*cis*- $10_{\text{PH}_3}^\parallel$). Geometry optimized cores are depicted above each Chemdraw structure, showing Mn in blue, C in dark grey, and H in light grey, accompanied by stick bonds to the phosphorus donor atoms. Relative energies are those before zero-point energy (ZPE) correction.

Table 3.3: Selected angles (deg), distances (\AA) (and Mayer bond orders) for DFT calculated PH_3 analogues of ethylene hydride complexes.

Parameter	<i>trans</i> - 10_{PH_3}	<i>cis</i> - $10_{\text{PH}_3}^\perp$	<i>cis</i> - $10_{\text{PH}_3}^\parallel$
Mn–C	2.11 (0.59)	2.15 (0.48-0.49)	2.10-2.14 (0.57-0.58)
Mn–H	1.56 (0.90)	1.57 (0.83)	1.57 (0.80)
Mn–P	2.18 (0.98-1.02)	2.17-2.19 (0.98-1.10)	2.16-2.18 (1.00-1.11)
C–C (ethylene)	1.42 (1.03)	1.41 (1.08)	1.42 (1.04)
C–H (ethylene)	1.09 (1.03)	1.09 (1.03-1.04)	1.09 (1.03)
C–H _{hydride}	–	–	2.27 (0.09)
$\Sigma(\text{H–Mn–Y})$ (X,Y = C,H)	350.4	351.1-351.2	351.5
$\Sigma(\text{P–Mn–P})$ (<i>cis</i>)	359.2	–	–

Geometry optimization of $[(dmpe)_2MnEt]$ (**13**) led to an energy minimum ($\mathbf{13}^{\beta\text{-agostic}}$) featuring a β -agostic interaction to the otherwise vacant coordination site. This structure exhibits an acute $Mn-C_{\alpha}-C_{\beta}$ angle of 75.2° , a short $Mn-H_{\beta}$ distance of 1.71 \AA , an elongated $C_{\beta}-H$ distance of 1.22 \AA , and an acute (relative to a complex with an agostic interaction) $Mn-H-C_{\beta}$ angle of 96.8° , collectively indicative of a β -agostic interaction.⁴⁹⁷ $\mathbf{13}^{\beta\text{-agostic}}$ is 29 kJ mol^{-1} higher in energy than the *trans* ethylene hydride isomer (*trans-10*), but lies 10 kJ mol^{-1} below the most stable *cis* ethylene hydride isomer (*cis-10*^l). Structure $\mathbf{13}^{\beta\text{-agostic}}$ is accessed via 1,2-insertion with a transition state $\{(\mathbf{10}/\mathbf{13})^\ddagger\}$ only 5 kJ mol^{-1} higher in energy than starting complex *cis-10*^l (Table 3.2). This energy barrier is quite low, but lies within the range reported for related first row transition metal complexes. For example, ΔE^\ddagger was calculated to be 82 kJ mol^{-1} for $[(PMe_3)_3CoH(C_2H_4)]$ and less than 2 kJ mol^{-1} for $[CpCoH(C_2H_4)(PMe_3)]^+$.^{488,498}

With respect to the reactivity of an ethyl isomer of *trans-10* with various hydridic reagents, a *cis* vacant coordination site is presumably required on the metal centre, necessitating dissociation of the β -agostic interaction in $\mathbf{13}^{\beta\text{-agostic}}$. However, no such energy minimum could be located; the energy of such a species was estimated by restraining the $Mn-C_{\alpha}-C_{\beta}$ angle to 109.5° , yielding a structure ($\mathbf{13}^{109.5}$) 49 kJ mol^{-1} higher in energy than $\mathbf{13}^{\beta\text{-agostic}}$. This energy difference is consistent with the typical strength of a first row transition metal β -agostic interaction.^{491,498} However, it differs significantly from that calculated for the ethyl isomer of $[(PMe_3)_3CoH(C_2H_4)]$,⁴⁸⁸ where the non-agostic structure was reported to be 4 kJ mol^{-1} lower in energy than the β -agostic isomer.

A second energy minimum ($\mathbf{13}^{\alpha\text{-agostic}}$) was located for $[(dmpe)_2MnEt]$ (**13**) with an obtuse $Mn-C_{\alpha}-C_{\beta}$ angle of 132.4° , featuring an agostic interaction between one of the α C-H bonds and the metal centre. This structure features a very acute $Mn-C_{\alpha}-H$ angle of 72.3° , as well as a short $Mn-H_{\alpha}$ distance of 1.95 \AA , and a slightly elongated $C_{\alpha}-H_{\alpha}$ distance of 1.16 \AA . Conversion of $\mathbf{13}^{\beta\text{-agostic}}$ to $\mathbf{13}^{\alpha\text{-agostic}}$ not only involves cleavage of the β -agostic interaction and establishment of an α -agostic interaction, but also migration of

the Mn–C bond into the position previously occupied by the β -agostic interaction, with concomitant Mn–C $_{\alpha}$ –C $_{\beta}$ angle expansion and rotation about the Mn–C $_{\alpha}$ and C $_{\alpha}$ –C $_{\beta}$ bonds (Table 3.1). $\mathbf{13}^{\alpha\text{-agostic}}$ is 42 kJ mol $^{-1}$ higher in energy than $\mathbf{13}^{\beta\text{-agostic}}$, and is accessed via a transition state $\{(\mathbf{13}^{\beta/\alpha})^{\ddagger}\}$ located 58 kJ mol $^{-1}$ higher in energy than $\mathbf{13}^{\beta\text{-agostic}}$ (Table 3.2), so could conceivably play a role in the reactivity of *trans*-**10** with hydridic reagents such as hydrosilanes (Chapters 4-5), H $_2$, or hydroboranes (Chapter 9). This energy barrier lies within the 44–85 kJ mol $^{-1}$ range calculated for this type of isomerization in a series of Co(III) ethyl cations derived from $\{[(C_5R'_5)CoH(C_2H_4)(PR_3)]^+\}$; R = Me, P(OMe) $_3$, R' = H, Me}.⁴⁹⁹

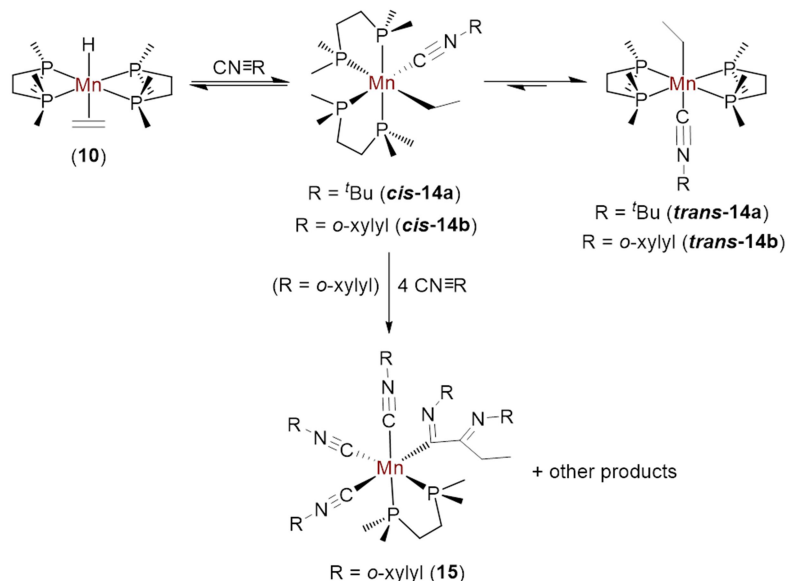
An energy minimum was also located for an ethyl isomer with the vacant coordination site *trans* to the ethyl ligand and no agostic interaction ($\mathbf{13}^{trans}$). However, this minimum featured 2 unpaired electrons and is 85 kJ mol $^{-1}$ higher in energy than $\mathbf{13}^{\beta\text{-agostic}}$. The restricted calculation (modelling a diamagnetic structure) afforded a minimum 5 kJ mol $^{-1}$ higher in energy than the paramagnetic minimum, with a HOMO-LUMO gap of just 69 kJ mol $^{-1}$ {cf. 250, 160, 115, and 116 kJ mol $^{-1}$ for $\mathbf{13}^{\beta\text{-agostic}}$, $\mathbf{13}^{\alpha\text{-agostic}}$, $\mathbf{13}^{109.5}$, and $(\mathbf{13}^{\beta/\alpha})^{\ddagger}$ respectively; none of these species geometry optimized to a lower energy paramagnetic isomer}. Therefore, $\mathbf{13}^{trans}$ presumably does not play an important role in the reactivity of *trans*-**10**.

The largest activation energy associated with conversion of *trans*-**10** to $\mathbf{13}^{\beta\text{-agostic}}$ or $\mathbf{13}^{\alpha\text{-agostic}}$ is presumably associated with *trans* to *cis* isomerization of **10** (likely via a 5-coordinate intermediate formed by phosphine or ethylene dissociation), rather than 1,2-insertion to convert *cis*-**10**^l to $\mathbf{13}^{\beta\text{-agostic}}$ or isomerization of $\mathbf{13}^{\beta\text{-agostic}}$ to $\mathbf{13}^{\alpha\text{-agostic}}$, since the activation barriers for the latter two transformations are only 5 and 58 kJ mol $^{-1}$ respectively (Figure 3.5, Table 3.2).

3.5 – Trapping of the Putative [(dmpe) $_2$ MnEt] Intermediate

In pursuit of experimental corroboration for the accessibility of [(dmpe) $_2$ MnEt] (**13**) from *trans*-[(dmpe) $_2$ MnH(C $_2$ H $_4$)] (*trans*-**10**), a trapping experiment was conducted

with *tert*-butyl isonitrile (CN^tBu) at 50 °C, affording [(dmpe)₂MnEt(CN^tBu)] (**14a**) (Scheme 3.3). This reaction initially formed a low-symmetry species identified by NMR spectroscopy as the *cis* isomer of **14a**, featuring ¹H NMR resonances for two diastereotopic MnCH₂ protons (−0.12 and 0.22 ppm; Figure 3.7) and three broad ³¹P NMR signals (61.6, 74.4, and 81 ppm; broadening is presumably due to reversible isonitrile or phosphine donor dissociation in solution). Upon cooling to 207 K, the ³¹P signals sharpened and one signal split into two, giving the expected four ³¹P environments. At the temperature of synthesis (50 °C), *cis*-**14a** slowly converted into *trans*-**14a** (Scheme 3.3), which gave rise to a single sharp ³¹P NMR signal at 74.7 ppm and an apparent octet in the ¹H NMR spectrum due to the MnCH₂ protons (0.47 ppm; apparent octet due to very similar ³J_{H,H} and ³J_{H,P} coupling to the adjacent CH₃ group and 4 equivalent phosphines; Figure 3.7). This *cis-trans* isomerization did not proceed to completion, but an equilibrium was established (over many days at 50 °C, or a few hours at 80 °C), dominated by *trans*-**14a**. The reaction to form complex **14a** is, to the best of our knowledge, only the second example where an ethyl complex could be trapped by Lewis base addition to an isolable 1st row transition metal ethylene hydride complex.⁴⁸⁴ Complex **14a** shows surprising thermal stability for a β-hydrogen containing alkyl complex; in solution, negligible decomposition was observed after 12 hours at 80 °C.



Scheme 3.3: Reactions of *trans*-[(dmpe)₂MnH(C₂H₄)] (**10**) with isocyanides to afford ethyl complexes [(dmpe)₂MnEt(CNR)] (**14a**: R = *t*Bu, **14b**: R = *o*-xylyl) and further insertion products, including [(dmpe)Mn(CNXyl)₃{C(=NXyl)CEt(=NXyl)}] (**15**).

Assignment of the two species produced in the reaction of **10** with CN^{*t*}Bu as isomers of **14a**, as opposed to iminoacyl complexes, was corroborated by the observation of NMR coupling between the α ethyl protons and the ³¹P nuclei, indicating the close (in this case, 3 bond) proximity of these nuclei. Upon ³¹P decoupling of the ¹H NMR spectrum, the multiplets associated with the MnCH₂ environments collapsed to signals with the expected ¹H–¹H coupling; doublets (²J_{H,H} = 11 Hz) of quartets (³J_{H,H} = 7 Hz) for the diastereotopic MnCH₂ protons of *cis*-**14a**, and a quartet (³J_{H,H} = 8 Hz) for the MnCH₂ protons of *trans*-**14a** (Figure 3.7).

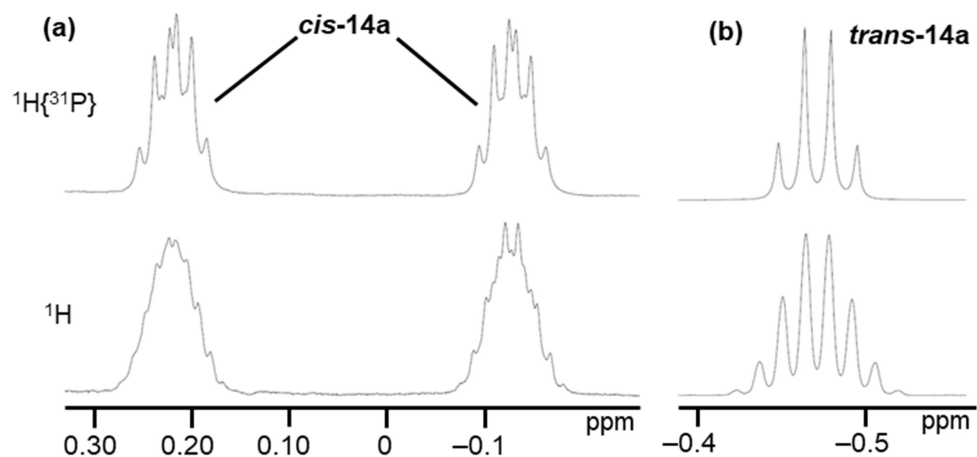


Figure 3.7: Regions of the $^1\text{H}\{^{31}\text{P}\}$ (above) and ^1H (below) NMR spectra for the MnCH_2 environments in a) *cis*- $[(\text{dmpe})_2\text{MnEt}(\text{CN}^t\text{Bu})]$ (*cis*-**14a**) and b) *trans*- $[(\text{dmpe})_2\text{MnEt}(\text{CN}^t\text{Bu})]$ (*trans*-**14a**).

In contrast to the clean reactivity of **10** with CN^tBu , the reaction of **10** with *o*-xylyl isonitrile (CNXyl , $\text{Xyl} = o\text{-xylyl}$) produced a mixture of products (Scheme 3.3), including a minor product identified by X-ray crystallography and NMR spectroscopy as *trans*- $[(\text{dmpe})_2\text{MnEt}(\text{CNXyl})]$ (*trans*-**14b**; b in Figure 3.8). A low concentration of a short lived, low symmetry, species was also observed, and is presumed to be the *cis* isomer of $[(\text{dmpe})_2\text{MnEt}(\text{CNXyl})]$ (*cis*-**14b**), with two ^1H signals for the diastereotopic MnCH_2 environments at 0.03 and 0.27 ppm, and an apparent triplet for the MnCH_2CH_3 environment (1.92 ppm, $^3J_{\text{H,H}} = 8$ Hz). DFT calculations support the thermodynamic accessibility of both *cis*- and *trans*- isomers of ethyl complexes **14a,b** in solution, given that the former are only 12-18 kJ mol^{-1} higher in energy than the latter.

Both *trans*-**14a,b** were characterized by X-ray diffraction (Figure 3.8), and are the first crystallographically characterized examples of terminal manganese ethyl complexes, although $[\text{Mn}(\mu\text{-Et})_4\{\text{Li}(\text{TMEDA})\}_2]$, which features ethyl ligands bridging between Mn and Li centres, has been reported.⁵⁰⁰ In the solid state, these manganese(I) ethyl complexes feature an octahedral environment around the manganese centre, with the ethyl ligand *trans* to the isonitrile ligand. X-ray crystal structures of *trans*-**14a,b** also

feature notably acute C–N–C angles {**14a**: 146.0(5)°-148.3(5)°; **14b**: 159(1)°}, long N–C_{terminal} distances {**14a**: 1.207(5)-1.214(4) Å; **14b**: 1.22(1) Å}, and short Mn–C_{CNR} bonds {**14a**: 1.803(4)-1.813(3) Å; **14b**: 1.793(3) Å}, consistent with strong π -backdonation from the electron rich “(dmpe)₂MnEt” fragment to the isonitrile ligand.⁵⁰¹

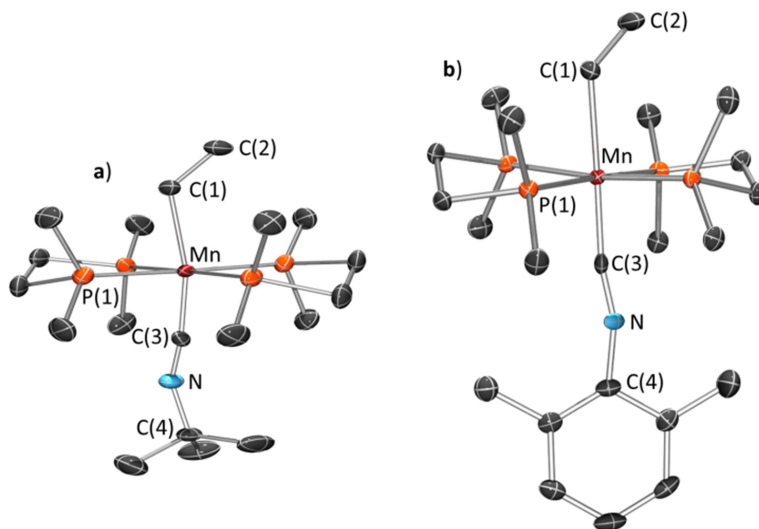


Figure 3.8: X-ray crystal structures of a) *trans*-[(dmpe)₂MnEt(CN^tBu)] (*trans*-**14a**) and b) *trans*-[(dmpe)₂MnEt(CNXyl)] (*trans*-**14b**) with ellipsoids drawn at 50% probability. Hydrogen atoms have been omitted for clarity. In the case of *trans*-**14a**, all atoms except P and Mn are disordered over two positions, and only one conformation {50.1(2)% and 52.8(2)% for the two dmpe ligands, 50.5(2)% for the isonitrile ligand, and 56.0(3)% for the ethyl ligand} is shown. In the case of *trans*-**14b**, one dmpe ligand and the N atom are both disordered over two positions, and only one conformation {51.4(3)% for the dmpe ligand and 55(2)% for N} is shown. Atoms below with an ‘A’ suffix are the atoms related to those with the same identifying number without a suffix, but in the conformation not

shown in the figure. For *trans-14a*,^v bond distances (Å) and angles (deg): Mn–C(1) 2.222(2), Mn–C(1A) 2.226(3), Mn–C(3) 1.803(4), Mn–C(3A) 1.813(3), C(1)–C(2) 1.528(4), C(1A)–C(2A) 1.526(6), C(3)–N(1) 1.207(5), C(3A)–N(1A) 1.214(4), N(1)–C(4) 1.456(5), N(1A)–C(4A) 1.458(5), Mn–C(3)–N(1) 168.2(6), Mn–C(3A)–N(1A) 171.0(6), C(3)–N(1)–C(4) 148.3(5), C(3A)–N(1A)–C(4A) 146.0(5), Mn–C(1)–C(2) 120.4(2), Mn–C(1A)–C(2A) 120.6(3), $\Sigma(\text{P–Mn(1)–P})$ (*cis*) 360.04(4). For *trans-14b*, bond distances (Å) and angles (deg): Mn–C(1) 2.212(2), Mn–C(3) 1.794(2), C(1)–C(2) 1.520(4), C(3)–N(1) 1.223(7), C(3)–N(1A) 1.219(9), N(1)–C(4) 1.391(7), N(1A)–C(4) 1.394(9), C(1)–Mn–C(3) 174.1(1), Mn–C(3)–N(1) 173.1(7), Mn–C(3)–N(1A) 165.4(6), C(3)–N(1)–C(4) 159(1), C(3)–N(1A)–C(4) 159(1), Mn–C(1)–C(2) 122.8(2), $\Sigma(\text{P–Mn(1)–P})$ (*cis*) 360.34(6).

Attempts to purify either of the two isomers of **14b** from the reaction mixture failed, and the additional products formed in the reaction of **14b** with CNXyl are presumed to result from phosphine substitution by excess *o*-xylyl isonitrile and/or multiple isonitrile insertion reactions. Support for these reaction pathways was provided by crystallization of [(dmpe)Mn(CNXyl)₃{C(=NXyl)CEt(=NXyl)}] (**15**) from the reaction mixture, which features an octahedral coordination environment composed of a single dmpe ligand, three isonitrile ligands, and a $\kappa^1\text{-C(=NXyl)CEt(=NXyl)}$ ligand *trans* to one of the isonitriles (Figure 3.9 and Scheme 3.3).^w NMR spectra of complex **15**, which could be isolated in approximately 90% purity, show two ³¹P NMR signals (53.9 and 66.2 ppm) and three xylyl-Me ¹H NMR signals (correlating to four ¹³C NMR signals

^v Due to approximately 50:50 positional disorder in the isonitrile ligand, two possible sets of N–C_{terminal}, C–N–C, and Mn–C–N values exist. The first set of values is tabulated in this caption, while the second set of values is C(3)–N(1A) and C(3A)–N(1) = 1.307(5) and 1.362(5) Å; C(3A)–N(1)–C(4) and C(3)–N(1A)–C(4A) = 137.4(4)° and 131.4(4)°; Mn–C(3)–N(1A) and Mn–C(3A)–N(1): 146.9(5)° and 144.7(6)°. Only the first set of values is consistent with literature values, and DFT calculations also afforded bond lengths and angles in much closer agreement to the first set of values: N–C_{terminal} = 1.22 Å, C–N–C = 147.2°, and Mn–C–N = 169.2°. Therefore, only the first set of values is discussed further.

^w Examples of manganese complexes with iminoacyl ligands (all of which are κ^2 -coordinated) can be found in ref. 502.

in the ^1H - ^{13}C HSQC spectrum) integrating to a total of five isonitrile ligands per dmpe ligand and ethyl substituent. Unlike ethyl complexes **14a,b**, the MnCH_2 environment in the ^1H NMR spectrum of **15** displays no coupling to ^{31}P , due to a separation of 5 bonds between the MnCH_2 protons and phosphorus.

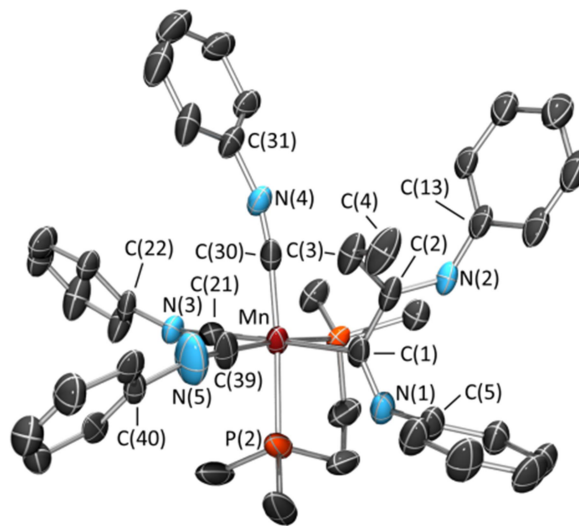


Figure 3.9: X-ray crystal structure of $[(\text{dmpe})\text{Mn}(\text{CNXyl})_3\{\text{C}(=\text{NXyl})\text{CEt}(=\text{NXyl})\}]$ (**15**), with ellipsoids drawn at 50% probability. Methyl groups on the *o*-xylyl ligands and all hydrogen atoms have been omitted for clarity. The phenyl group of one isonitrile ligand is disordered over two positions and only the dominant conformation {51.4(6)%} is shown. C(40A) is the counterpart to C(40) in the conformation not shown. Bond distances (Å) and angles (deg): Mn–C(1) 2.110(5), Mn–C(21) 1.837(5), Mn–C(30) 1.848(6), Mn–C(39) 1.832(6), C(1)–C(2) 1.522(8), C(2)–C(3) 1.540(7), C(3)–C(4) 1.522(7), C(1)–N(1) 1.307(6), C(2)–N(2) 1.291(6), N(1)–C(5) 1.425(7), N(2)–C(13) 1.419(7), C(21)–N(3) 1.198(7), C(30)–N(4) 1.198(6), C(39)–N(5) 1.133(6), N(3)–C(22) 1.408(6), N(4)–C(31) 1.401(6), N(5)–C(40) 1.486(5), N(5)–C(40A) 1.49(1), Mn–C(1)–C(2) 120.2(3), Mn–C(1)–N(1) 121.2(4), C(1)–N(1)–C(5) 125.3(5), C(2)–C(3)–C(4) 113.4(5), C(2)–N(2)–C(13) 123.6(4), C(1)–C(2)–C(3) 118.6(4), C(1)–C(2)–N(2) 117.8(4), Mn–C(21)–N(3) 175.8(5), Mn–C(30)–N(4) 171.9(4), Mn–C(39)–N(5) 177.3(5), C(21)–N(3)–C(22) 160.3(5), C(30)–N(4)–C(31) 166.5(5), C(39)–N(5)–C(40) 155.1(5), C(39)–N(5)–C(40A) 169.7(6).

3.6 – Summary and Conclusions for Chapter 3

Girolami and Wilkinson reported the synthesis and NMR spectra of *trans*-[(dmpe)₂MnH(C₂H₄)] (***trans*-10**) decades ago, but until now the reactivity of this complex has remained largely unexplored. We have now obtained an X-ray crystal structure which confirmed that the *trans* hydride-ethylene structure reported in solution based on NMR spectroscopy is maintained in the solid state. Analysis of the solid state structure, in combination with DFT calculations, suggests significant metallacyclopropane character.

Two potential pathways for reactions of **10** with hydridic reagents were discussed, involving either ethylene substitution or initial isomerization to a 5-coordinate ethyl intermediate [(dmpe)₂MnEt] (**13**). DFT calculations and trapping experiments with isonitriles demonstrated the accessibility of **13** from ***trans*-10**. Isolated ethyl complex [(dmpe)₂MnEt(CN*t*Bu)] (**14a**) is a rare example of a thermally stable β -hydride-containing alkyl complex, showing negligible decomposition over 12 hours at 80 °C.

This work contributes to fundamental understanding of the equilibrium between transition metal ethylene hydride and ethyl complexes. As described in the Section 3.3, examples of 1st row transition metal ethylene hydrides are extremely scarce (the equilibrium typically lies to the side of the ethyl isomer), and the equilibrium between ethylene hydride and alkyl complexes has rarely been investigated. Compound ***trans*-10** provided a unique opportunity to study this process, and key computational findings are (a) two isomers of a *cis* ethylene hydride are energetically accessible from ***trans*-10** (***cis*-10[⊥]** and ***cis*-10^{||}**), differing in the orientation of the alkene relative to the plane formed by manganese, the hydride, and the ethylene centroid, (b) the *trans* ethylene hydride isomer is 39 kJ mol⁻¹ lower in energy than the most energetically favorable *cis* isomer (***cis*-10^{||}**), primarily due to increased steric hindrance between the dmpe ligands in either isomer of ***cis*-10**, (c) the most energetically favorable *cis* ethylene hydride complex (***cis*-10^{||}**) is 10 kJ mol⁻¹ higher in energy than the β -agostic ethyl isomer (**13 ^{β -agostic}**), (d) the barrier to 1,2-insertion, converting ***cis*-10^{||}** to **13 ^{β -agostic}**, is only 5 kJ mol⁻¹, (e) an α -agostic ethyl isomer (**13 ^{α -agostic}**) is energetically accessible, 42 kJ mol⁻¹ higher in energy than **13 ^{β -agostic}**,

(f) the barrier to conversion of $\mathbf{13}^{\beta\text{-agostic}}$ to $\mathbf{13}^{\alpha\text{-agostic}}$ is 58 kJ mol^{-1} , and (g) an energy minimum for a non-agostic ethyl complex with a *cis* vacant coordination site was not located, but a structure optimized with the Mn–C $_{\alpha}$ –C $_{\beta}$ angle restrained to 109.5° ($\mathbf{13}^{109.5}$) was 49 kJ mol^{-1} higher in energy than $\mathbf{13}^{\beta\text{-agostic}}$.

Chapter 4

Synthesis of Silylene Hydride Complexes and Reactivity with Ethylene to Afford Silene Hydride Complexes

Portions of this chapter have been reprinted (adapted) with permission from Price, J. S.; Emslie, D. J. H.; Britten, J. F. Manganese Silylene Hydride Complexes: Synthesis and reactivity with Ethylene to Afford Silene Hydride Complexes, *Angew. Chem. Int. Ed.* **2017**, *56*, 6223-6227. Copyright 2017 Wiley-VCH.

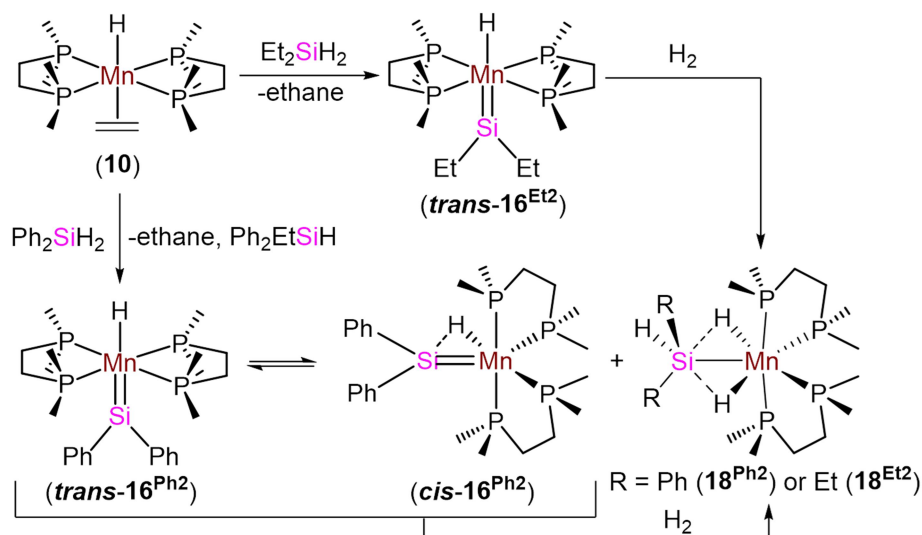
4.1 – Introduction to Chapter 4

Manganese hydride complexes with silicon-based co-ligands could be potential precursors for use in CVD of Mn-containing thin films. Complexes bearing electronically unstabilized silylene or silene ligands are extremely reactive, and no group 7 examples have yet been reported. Overviews of transition metal silylene and silene complexes are provided in sections 1.6 and 1.7. Herein, we show that $[(\text{dmpe})_2\text{MnH}(\text{C}_2\text{H}_4)]$ (**10**), which we discussed as a potential precursor for new manganese chemistry in Chapter 3, can be used to access silylene hydride complexes. These are the first examples of isolable group 7 complexes bearing an unstabilized terminal silylene ligand. Furthermore, we also show the unprecedented transformation of a silylene hydride complex to a silene hydride complex. One of the two silene hydride complexes prepared in this work is the first isolated example of a 1st row transition metal complex bearing a sterically and electronically unstabilized silene ligand, and the other is the first such complex to be crystallographically characterized.

4.2 – Synthesis and Characterization of Manganese Silylene Hydride Complexes

Girolami and Wilkinson's *trans*- $[(\text{dmpe})_2\text{MnH}(\text{C}_2\text{H}_4)]$ (*trans*-**10**) complex¹⁷² reacted with H_2SiEt_2 (4.5 equiv.) at room temperature to form $[(\text{dmpe})_2\text{MnH}(=\text{SiEt}_2)]$ (**16**^{Et2}) with release of ethane (scheme 4.1). Compound **16**^{Et2} gave rise to one ³¹P

resonance, a hydride ^1H NMR signal at -10.46 ppm, and a ^{29}Si resonance at 365.3 ppm, characteristic of a C_{2v} symmetric *trans* silylene hydride complex (note: 1-2% of an unidentified product was always observed in ^1H NMR spectra of $\mathbf{16}^{\text{Et}2}$, and may be the *cis* isomer). An X-ray crystal structure of $\mathbf{16}^{\text{Et}2}$ (Figure 4.1) confirmed this assignment, revealing an octahedral geometry at manganese, trigonal planar geometry at silicon ($\Sigma(\text{C}-\text{Si}-\text{X}) = 360.0(1)^\circ$; $\text{X} = \text{C}$ or Mn), and a $\text{Mn}-\text{H}$ distance of $1.60(3)$ - $1.62(3)$ Å. The $\text{Mn}-\text{Si}$ distance in $\mathbf{16}^{\text{Et}2}$ is $2.1880(12)$ - $2.1948(12)$ Å, which compares well with the $\text{Fe}-\text{Si}$ distance of $2.154(1)$ Å in $[\text{CpFe}(\text{SiMe}_3)(\text{CO})(=\text{SiMe}_2)]$,⁵⁰³ taking into consideration the larger ionic radius of $\text{Mn}(\text{I})$ vs $\text{Fe}(\text{II})$, and is much shorter than the $\text{Mn}-\text{Si}$ distances of $2.2789(9)$ - $2.3571(7)$ Å in the *N*-heterocyclic silylene complexes $[(\text{CO})_4\text{Mn}(=\text{SiR}\{\text{PhC}(\text{N}^t\text{Bu})_2\})_2]^+$ ($\text{R} = \text{Cl}, \text{NPh}_2$),³⁷² and $2.402(2)$ - $2.434(3)$ Å in the bridging silylene complexes $[\{\text{CpMnH}(\text{CO})_2\}_2(\mu\text{-SiH}_2)]$ ³⁷⁷ and $[\{\text{Mn}(\text{CO})_4\}_2\{\mu\text{-SiPh}_2\}_2]$.³⁷⁵



Scheme 4.1: Reactions of $[(\text{dmpe})_2\text{MnH}(\text{C}_2\text{H}_4)]$ (**10**) with H_2SiR_2 to form (when $\text{R} = \text{Et}$) *trans*- $[(\text{dmpe})_2\text{MnH}(=\text{SiEt}_2)]$ (*trans*-**16**^{Et2}), or (when $\text{R} = \text{Ph}$) a mixture of *cis*- and *trans*- $[(\text{dmpe})_2\text{MnH}(=\text{SiPh}_2)]$ (*cis*-**16**^{Ph2} and *trans*-**16**^{Ph2}) along with $[(\text{dmpe})_2\text{MnH}_2(\text{SiHPh}_2)]$ (**18**^{Ph2}). Subsequent reactions of the silylene hydride complexes (*trans*-**16**^{Et2} or *cis*- and *trans*-**16**^{Ph2}) with H_2 to form $[(\text{dmpe})_2\text{MnH}_2(\text{SiHR}_2)]$ (**18**^{Et2}: $\text{R} = \text{Et}$, **18**^{Ph2}: $\text{R} = \text{Ph}$) are also included. Only one isomer of **18**^{R2} is shown.

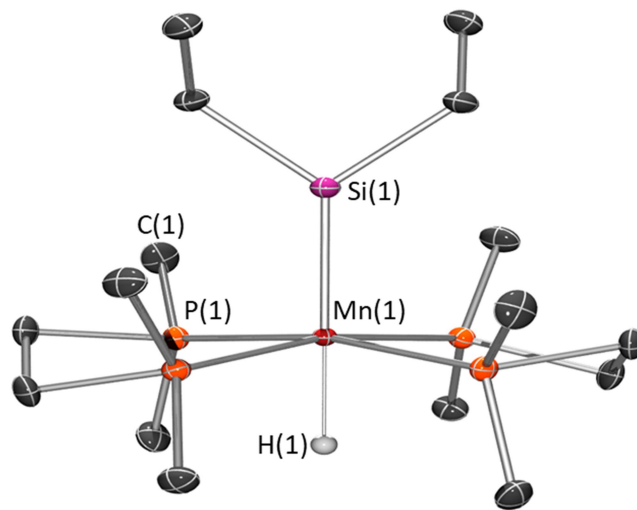


Figure 4.1: X-ray crystal structure of *trans*-[(dmpe)₂MnH(=SiEt₂)] (*trans*-**16**^{Et2}) with ellipsoids drawn at 50% probability. Most hydrogen atoms have been omitted for clarity and the hydrogen atom on Mn was located from the difference map and refined isotropically. The unit cell contained four independent and essentially isostructural molecules, and only one is shown. Atom labels with suffixes A-C are complementary to those without the suffix in the molecule shown. Distances (Å) and angles (deg): Mn(1)–Si(1) 2.195(1), Mn(1A)–Si(1A) 2.188(1), Mn(1B)–Si(1B) 2.192(1), Mn(1C)–Si(1C) 2.191(1), Mn(1)–H(1) 1.61(3), Mn(1A)–H(1A) 1.61(3), Mn(1B)–H(1B) 1.61(3), Mn(1C)–H(1C) 1.60(3), Si(1)–C(1) 1.933(2), Si(1A)–C(1A) 1.929(2), Si(1B)–C(1B) 1.929(2), Si(1C)–C(1C) 1.933(3), H(1)–Mn(1)–Si(1) 180.0, H(1A)–Mn(1A)–Si(1A) 180.0, H(1B)–Mn(1B)–Si(1B) 180.0, H(1C)–Mn(1C)–Si(1C) 180.0, Mn(1)–Si(1)–C(1) 130.45(7), Mn(1A)–Si(1A)–C(1A) 130.6(8), Mn(1B)–Si(1B)–C(1B) 130.50(7), Mn(1C)–Si(1C)–C(1C) 130.59(8), C(1)–Si(1)–C(1′) 99.1(2), C(1A)–Si(1A)–C(1A′) 98.8(2), C(1B)–Si(1B)–C(1B′) 99.0(2), C(1C)–Si(1C)–C(1C′) 98.8(2).

The reaction to form **16**^{Et2} and ethane likely occurs via an undetected 5-coordinate manganese ethyl complex, [(dmpe)MnEt] (**13**), formed by isomerization of **10** to place the hydride and alkene *cis* to one another, followed by 1,2-insertion (see sections 3.4–3.5). This ethyl complex can undergo σ -bond metathesis with H₂SiEt₂ {or Si–H bond oxidative addition (OA) followed by C–H bond reductive elimination (RE)} to form a

low-coordinate hydrosilyl intermediate, [(dmpe)₂Mn(SiHEt₂)] (**17^{Et2}**), which isomerizes to **16^{Et2}** by α -hydride elimination.

Compound **10** also reacted with H₂SiPh₂ at 60 °C to afford [(dmpe)₂MnH(=SiPh₂)] (**16^{Ph2}**) as an approximate 50:50 mixture with [(dmpe)₂MnH₂(SiHPh₂)] (**18^{Ph2}**), releasing ethane and HSiEtPh₂ (scheme 4.1). Compound **18^{Ph2}** may form by initial σ -bond metathesis (or OA/RE) between [(dmpe)₂MnEt] (**13**) and H₂SiPh₂ to afford “(dmpe)₂MnH” (**12**) and HSiEtPh₂, followed by oxidative addition of a second equivalent of H₂SiPh₂.^x Compounds **16^{Ph2}** and **18^{Ph2}** could not be separated, but the mixture could be converted entirely to **18^{Ph2}** by reaction with H₂. Similarly, compound **16^{Et2}** reacted cleanly with H₂ to generate [(dmpe)₂MnH₂(SiHEt₂)] (**18^{Et2}**) (Scheme 4.1). A detailed discussion of silyl dihydride complexes **18^{R2}**, along with solution and solid state characterization, can be found in Chapter 6. Compound **16^{Ph2}** was characterized in solution, and shown to exist as an 88:12 mixture of interconverting silylene hydride isomers: a major C₁-symmetric *cis*-isomer with a hydride ¹H NMR signal at –16.22 ppm, a ²⁹Si NMR shift of 210.2 ppm, and four broad ³¹P environments at –20 °C; and a minor C_{2v} *trans*-isomer with one ³¹P environment, a hydride ¹H NMR signal at –9.78 ppm, and a ²⁹Si NMR shift of 285.1 ppm.

Maintaining a toluene solution of **16^{Ph2}**/**18^{Ph2}** at –30 °C afforded crystals containing a 50:50 mixture of *cis*-**16^{Ph2}** and *central*-**18^{Ph2}** (confirmed by NMR spectroscopy) with superimposed (dmpe)₂Mn fragments and phenyl rings. Distinct silicon

^x Formation of HSiEtPh₂ in the reaction to form **16^{Ph2}** and **18^{Ph2}** could alternatively occur via the following sequence: 1) dissociation of ethylene from [(dmpe)₂MnH(C₂H₄)] (**10**), and oxidative addition of H₂SiPh₂ to form **18^{Ph2}**, 2) concurrent formation of **16^{Ph2}** (*cis*- and *trans*-isomers) via the mechanism proposed in the text, 3) reaction of **16^{Ph2}** with ethylene (formed in step 1) to generate silene complex **19^{Ph2}**, and 4) an equilibrium between **19^{Ph2}** and [(dmpe)₂Mn(CH(Me)(SiPh₂H)] (**24^{Ph2}**) or [(dmpe)₂Mn(SiPh₂Et)], either of which could undergo σ -bond metathesis with additional H₂SiPh₂ to form HSiEtPh₂ and [(dmpe)₂Mn(SiHPh₂)] (**17^{Ph2}**), which would isomerize to **16^{Ph2}** by α -hydride elimination. Indeed, **19^{Ph2}** does react rapidly and cleanly with H₂SiPh₂ at 60 °C to form **16^{Ph2}** and HSiEtPh₂.

atom positions are observed for *cis-16*^{Ph2} and *central-18*^{Ph2}, but the resulting structures are only suitable to establish connectivity. In the structure of *cis-16*^{Ph2} (Figure 4.2 left), the four phosphorus atoms and silicon form an approximate trigonal bipyramid, with the *Si*-phenyl groups perpendicular to the equatorial plane. Silicon is trigonal planar, and electron density consistent with the hydride ligands in *cis-16*^{Ph2} and co-crystallized *central-18*^{Ph2} was located on either side of the Mn–Si bond (resulting from crystallographic disorder in the case of *cis-16*^{Ph2}), above and below the C(1)/Si/C(1') plane. DFT calculations (gas phase, all-electron, PBE, TZ2P, ZORA, D3-BJ) support a close interaction between the hydride ligand and the silicon atom in *cis-16*^{Ph2}, yielding distances of 2.168 and 1.665 Å for the Mn–Si and Mn–H bonds, a Si–H distance of 1.726 Å, and angles of 51.5 and 49.0° for the H–Mn–Si and H–Si–Mn linkages (Figure 4.2 right). These values compare well with those of other silylene hydride featuring strong Si–H interactions, including the X-ray structures of [(C₅Me₄Et)(OC)₂WH{=SiHC(SiMe₃)₃}] and [{1,2-C₂H₄(P^tBu₂)₂}NiH(=SiMe₂)]⁺,^{325,333} and the neutron structure of [Cp*(dmpe)MoH(=SiEt₂)]³²⁶ (Si–H [Å] = 1.71(6), 1.64(7), 1.68(1). H–M–Si [°]: 46(2), 49(2), and 45.5(4). H–Si–M [°]: 50(2), 51(2), and 51.5(4)).

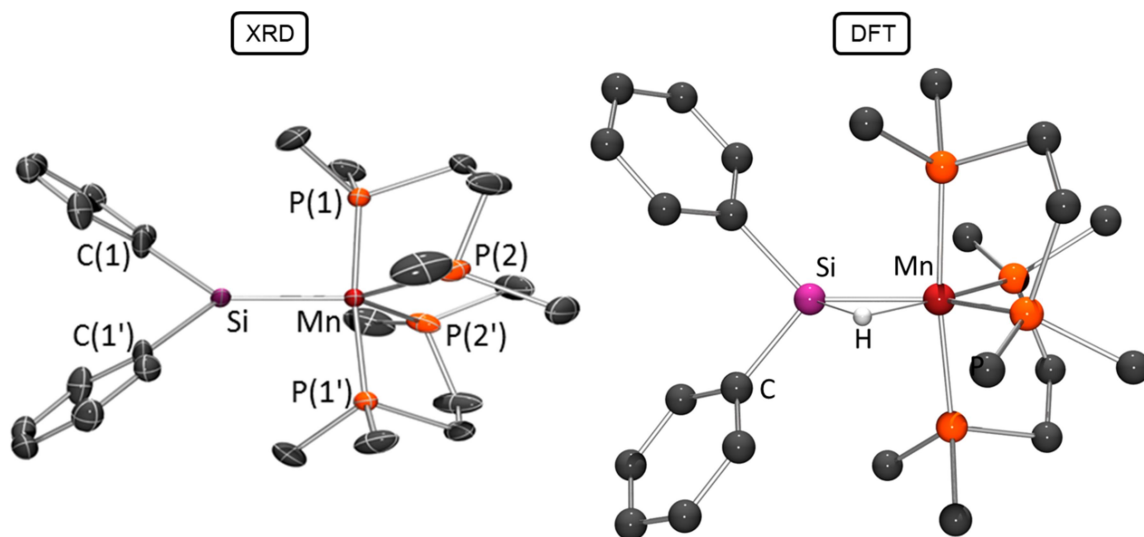


Figure 4.2: Left: X-ray crystal structure of *cis*-[(dmpe)₂MnH(=SiPh₂)] (*cis*-**16**^{Ph₂}). *cis*-**16**^{Ph₂} co-crystallized with the *central* isomer of [(dmpe)₂MnH₂(SiHPh₂)] (**18**^{Ph₂}), with superimposed (dmpe)₂Mn and phenyl groups, and only the structure of *cis*-**16**^{Ph₂} is shown. Hydrogen atoms have been omitted for clarity (and the bridging metal hydride environment was not located from the difference map). The unit cell contains two independent and essentially isostructural molecules, and only one is shown. Atom labels with the suffix A are complementary to those without a suffix in the structure shown. Distances (Å) and angles (deg): Mn(1)–Si(1) 2.133(2), Mn(1A)–Si(1A) 2.148(2), Si(1)–C(1) 1.916(2), Si(1A)–C(1C) 1.926(3), Mn(1)–Si(1)–C(1) 130.72(7), Mn(1A)–Si(1A)–C(1A) 131.31(8), C(1)–Mn(1)–C(1′) 98.6(1), C(1A)–Mn(1A)–C(1A′) 97.4(2). Right: geometry optimized (DFT calcd.) structure of *cis*-[(dmpe)₂MnH(=SiPh₂)] (*cis*-**16**^{Ph₂}). Most hydrogen atoms have been omitted for clarity.

Compound **16**^{Ph₂} is the first silylene hydride complex observed to exist as distinct isomers with and without an M–H–Si interaction, providing a unique opportunity to probe the nature of the Mn–Si and Si–H interactions. Surprisingly, DFT calculations show slightly shorter Mn–Si distances in *cis*-**16**^{R₂} versus *trans*-**16**^{R₂} (Mn–Si [Å]: 2.168–2.175 (*cis*), 2.184–2.187 (*trans*)). However, the Mn–Si Mayer bond orders for *cis*-**16**^{R₂} (1.25

and 1.19) are notably less than those for *trans*-**16**^{R2} (1.54 and 1.52), and the same trend is observed in Nalewajski-Mrozek and Gopinathan-Jug bond orders.

4.3 – DFT Fragment Interaction Analysis of Silylene Hydride Complexes

Fragment interaction analysis of *cis*- and *trans*-**16**^{Et2} using the combined Extended Transition State and Natural Orbitals for Chemical Valence (ETS-NOCV) method revealed similarities in the bonding between the (dmpe)₂MnH and SiEt₂ fragments in both isomers of **16**^{Et2} (Figures 4.3 and 4.4). In particular, bonding in both complexes involves σ -donation from the silylene highest occupied molecular orbital (HOMO) to the (dmpe)₂MnH lowest unoccupied molecular orbital (LUMO), accompanied by π_{\parallel} -backdonation into a silylene orbital that is σ -antibonding with respect to the Si–C bonds. However, π_{\perp} -backdonation primarily involves the silylene LUMO and a filled Mn–H σ -bonding orbital (HOMO–3) in *cis*-**16**^{Et2}, versus a filled manganese d-orbital in *trans*-**16**^{Et2}. The Hirshfeld charge on the SiEt₂ fragment is more negative in *trans*-**16**^{Et2} than *cis*-**16**^{Et2} (–0.29 vs –0.18), indicative of less effective σ -donation and/or more effective π -backdonation in the former. Nevertheless, the silicon atoms in both isomers of **16**^{Et2} and **16**^{Ph2} are electrophilic, based on positive Hirshfeld charges on the silicon atoms (0.20 to 0.22), negative Hirshfeld charges on manganese (–0.25 to –0.27), and positive electrostatic potentials at silicon.

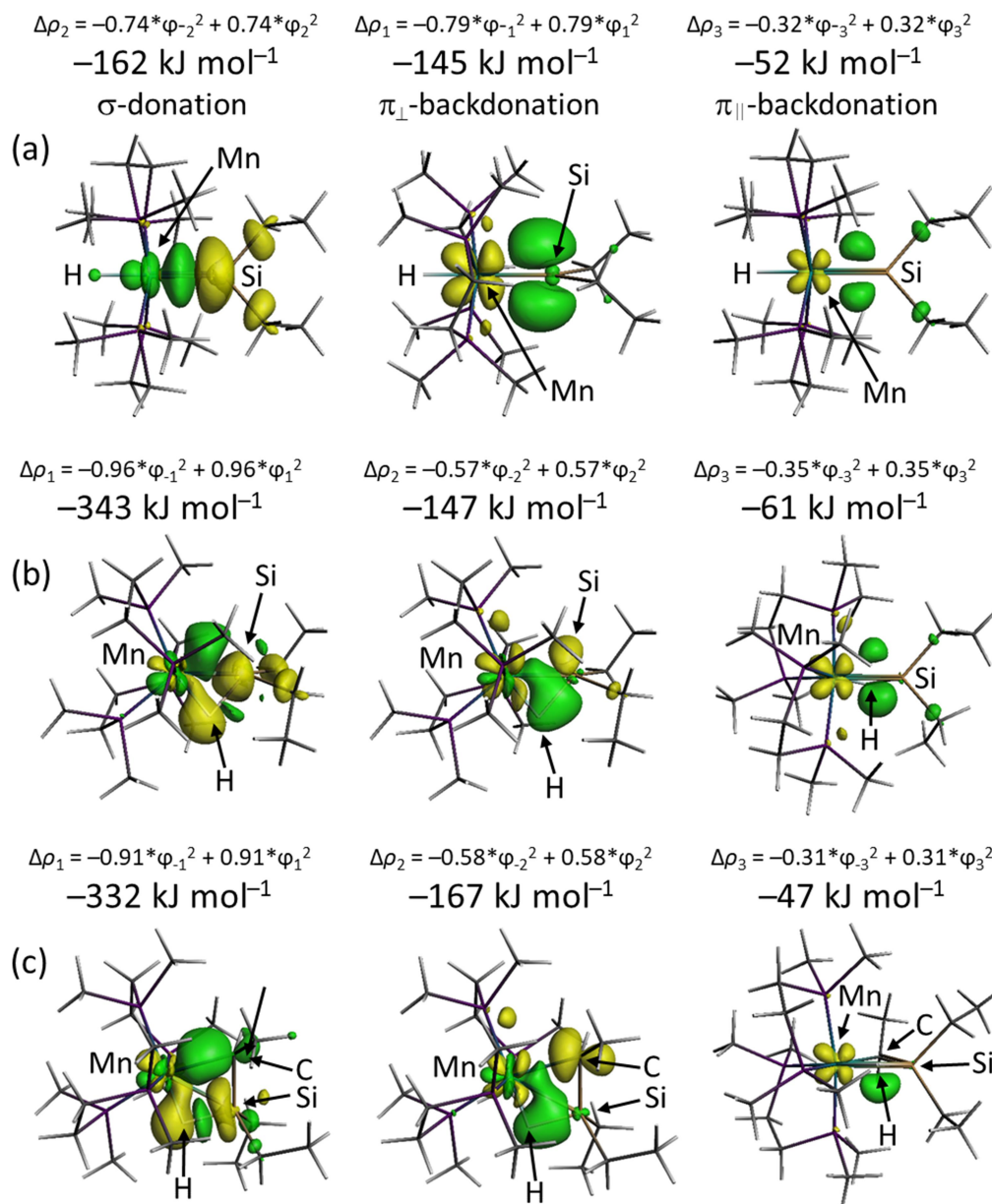


Figure 4.3: Deformation density contributions $\Delta\rho_1$, $\Delta\rho_2$, and $\Delta\rho_3$ to bonding between the SiEt_2 and $(\text{dmpe})_2\text{MnH}$ fragments in a) *trans*- $[(\text{dmpe})_2\text{MnH}(\text{=SiEt}_2)]$ (***trans*-16^{Et2}**), b) *cis*- $[(\text{dmpe})_2\text{MnH}(\text{=SiEt}_2)]$ (***cis*-16^{Et2}**), and c) $[(\text{dmpe})_2\text{MnH}(\text{Et}_2\text{Si}=\text{CHMe})]$ (**19^{Et2}**). Increased (green) and decreased (yellow) electron density is presented relative to the fragments; isosurfaces are set to 0.003.

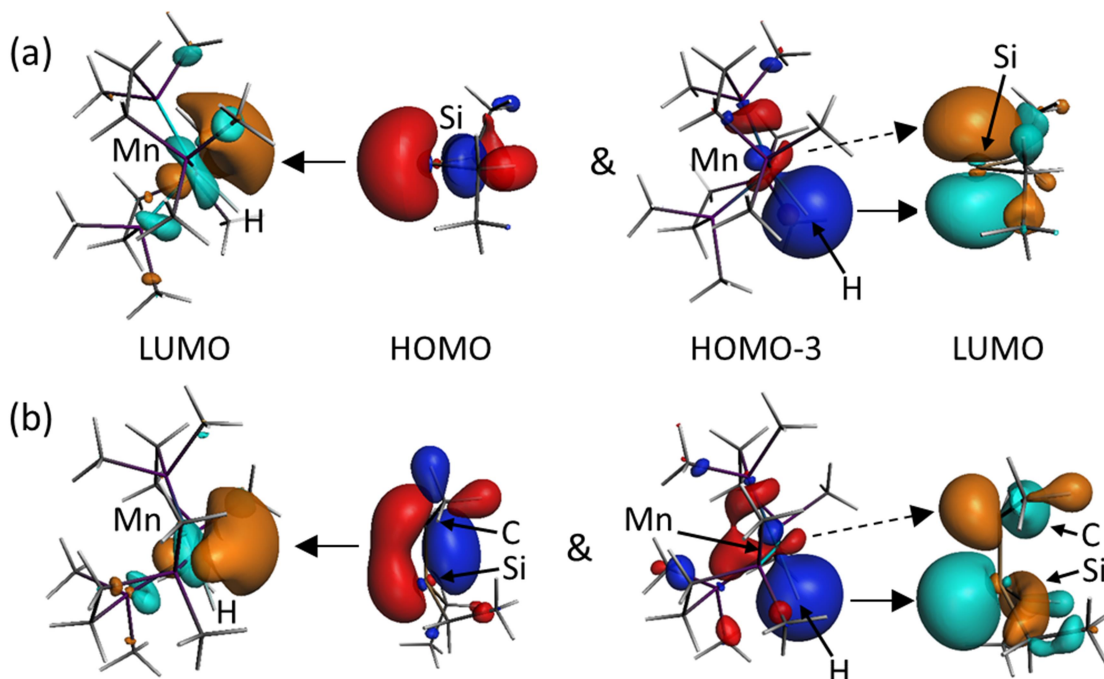
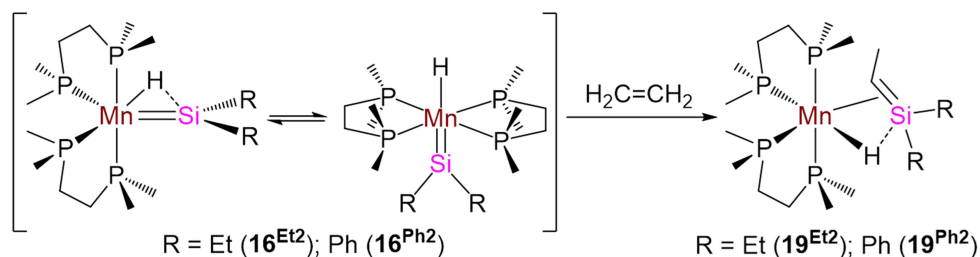


Figure 4.4: Key fragment orbitals contributing to $\Delta\rho_1$ and $\Delta\rho_2$ in a) *cis*-[(dmpe)₂MnH(=SiEt₂)] (*cis*-16^{Et2}) and b) [(dmpe)₂MnH(Et₂Si=CHMe)] (19^{Et2}); isosurfaces are set to 0.04.

4.4 – Synthesis and Characterization of Silene Hydride Complexes

Both 16^{Et2} and 16^{Ph2} reacted with ethylene (1.7 atm, 25 °C) to form silene hydride products, *cis*-[(dmpe)₂MnH(R₂Si=CHMe)] (19^{Et2}: R = Et, 19^{Ph2}: R = Ph) (Scheme 4.2), conceptually achieving addition of the carbene isomer of ethylene (CHMe) to the silylene (SiEt₂ or SiPh₂); compound 19^{Et2} was isolated in pure form, whereas 19^{Ph2} was isolated as an approximately 50:50 mixture with 18^{Ph2}, which was present in the starting material. Compounds 19^{R2} gave rise to hydride ¹H NMR signals at –15.30 and –14.56 ppm, ²⁹Si resonances at –2.95 and 1.47 ppm, low frequency ¹³C NMR signals at –19.37 and –22.93 ppm, and a characteristic silene ¹J_{C,H} coupling constant of 137 and 136 Hz, for R = Et, Ph respectively.



Scheme 4.2: Reaction of silylene hydride complexes $[(\text{dmpe})_2\text{MnH}(=\text{SiR}_2)]$ $\{\text{R} = \text{Et (16}^{\text{Et2}})$ or $\text{Ph (16}^{\text{Ph2}})\}$ with ethylene to form $[(\text{dmpe})_2\text{MnH}(\text{R}_2\text{Si}=\text{CHMe})]$ $\{\text{R} = \text{Et (19}^{\text{Et2}})$ or $\text{Ph (19}^{\text{Ph2}})\}$.

An X-ray crystal structure of $\mathbf{19}^{\text{Ph2}}$ (Figure 4.5) revealed a distorted octahedral geometry in which the hydride interacts with the silicon atom of the silene. The silene Si–C(1) distance in $\mathbf{19}^{\text{Ph2}}$ is 1.781(5) Å, which is at the short end of the range previously reported for silene complexes (1.773(4)–1.838(11) Å),^{y,413–417,419,431} and the Mn–C(1) distance is over 0.10 Å shorter than the M–Si distance (2.270(4) vs 2.409(2) Å), as observed for all other silene complexes. The sum of the X–C(1)–X (X = Si, H or C) and C–Si–C angles (346(2) and 343.5(2)°) are also consistent with considerable silene character. However, the Mn–H and H–Si distances of 1.56(5) and 1.55(4) Å (calcd. 1.653 and 1.648 Å), as well as a large $^1J_{\text{Si,H}}$ coupling with a magnitude of 90 Hz in $\mathbf{19}^{\text{Ph2}}$, clearly indicate a significant interaction between the hydride ligand and silicon.

^y Pt and Ni silene complexes featuring coordination to a stabilized silene; see ref. 411 and 418.

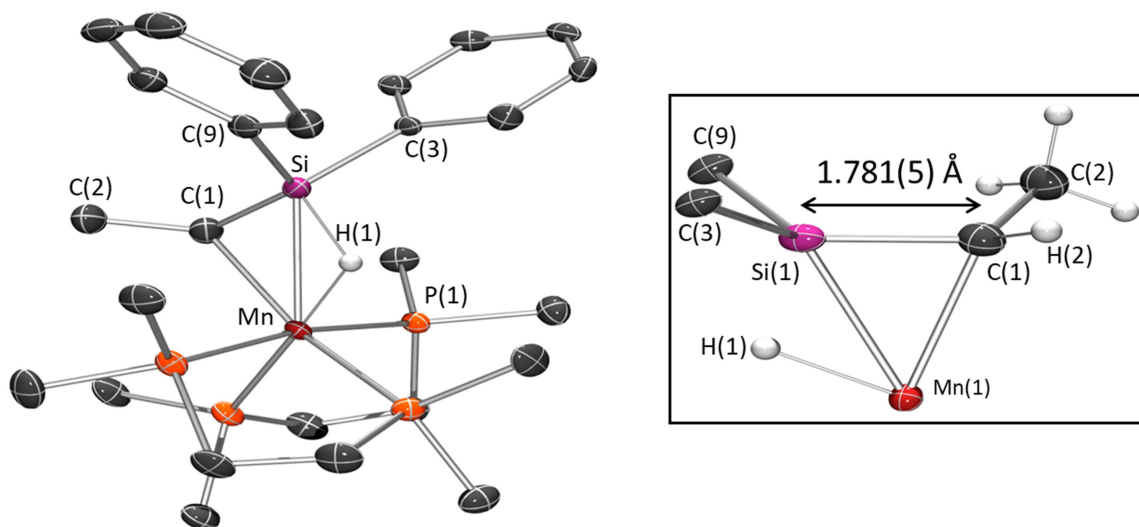


Figure 4.5: X-ray crystal structure of $[(\text{dmpe})_2\text{MnH}(\text{Ph}_2\text{Si}=\text{CHMe})]$ ($\mathbf{19}^{\text{Ph}2}$) with ellipsoids drawn at 50 % probability. Most hydrogen atoms have been eliminated for clarity, and hydrogen atoms on Mn(1) and C(1) (H(1) and H(2)) were located from the difference map and refined isotropically. Inset shows the metal, silene, and hydride core, with most H atoms, the dmpe ligands, and the most of the phenyl substituents on Si (aside from the *ipso* carbons) removed for clarity. Distances (Å) and angles (deg): Mn(1)–Si(1) 2.409(2), Mn(1)–C(1) 2.270(4), Mn(1)–H(1) 1.56(5), Si(1)–C(1) 1.781(4), Si(1)–C(3) 1.898(4), Si(1)–C(9) 1.906(5), Si(1)–H(1) 1.55(4), C(1)–C(2) 1.532(6), C(2)–H(2) 1.11(4), Mn(1)–C(1)–Si(1) 71.8(1), Mn(1)–Si(1)–C(1) 63.5(1), Si(1)–Mn(1)–C(1) 44.6(1), C(1)–Si(1)–H(1) 103(2), Mn(1)–H(1)–Si(1) 103(2), H(1)–Mn(1)–Si(1) 39(2), C(1)–Si(1)–C(3) 120.7(2), C(1)–Si(1)–C(9) 119.5(2), C(3)–Si(1)–C(9) 103.3(2).

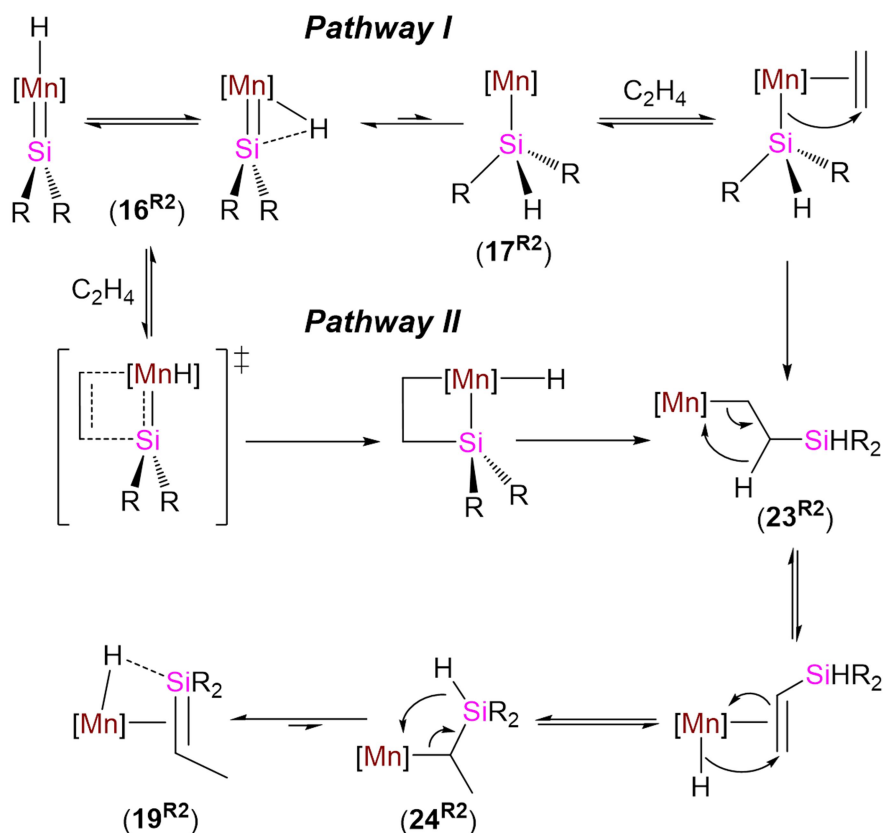
4.5 – Fragment Interaction Analysis of Silene Hydride Complex $[(\text{dmpe})_2\text{MnH}(\text{Et}_2\text{Si}=\text{CHMe})]$

Fragment interaction and ETS-NOCV calculations on $[(\text{dmpe})_2\text{MnH}(\text{Et}_2\text{Si}=\text{CHMe})]$ ($\mathbf{19}^{\text{Et}2}$) (Figures 4.3 and 4.4) revealed three major interactions between the silene and $(\text{dmpe})_2\text{MnH}$ fragments. The first two contributions involve σ -donation from the silene π -bond (HOMO) to the LUMO of the $(\text{dmpe})_2\text{MnH}$

fragment, combined with π_{\parallel} -backdonation from a filled Mn–H σ -bonding orbital (HOMO–3) into the silene π^* orbital (LUMO), whereas the third contribution appears to involve π_{\perp} -backdonation to silicon. Parallels in the bonding descriptions for *cis*-**16**^{Et2} and **19**^{Et2} arise from the very similar geometries of the (dmpe)₂MnH fragments in these complexes, and the analogous symmetries and orientations of the HOMO and LUMO of the silylene and silene fragments relative to the Mn–H bond.

4.6 – Potential Mechanisms for Silene Hydride Synthesis

Several mechanisms could be proposed for the formation **19**^{R2}, but the reactions of **17**^{R2} with *d*₄-ethylene to form *cis*-[(dmpe)₂MnH(R₂Si=CDCD₃)] (*d*₄-**19**^{E2}; R = Et, *d*₄-**19**^{Ph2}; R = Ph) rule out a mechanism involving initial insertion of ethylene into a Mn–H bond. Alternative possibilities are shown in Scheme 4.3. In pathway I, a low-coordinate silyl complex, [(dmpe)₂Mn(SiHR₂)] (R = Et (**17**^{E2}) or Ph (**17**^{Ph2})), is accessed from the *cis*-silylene hydride complex. From this point, two cycles of 1,2-insertion and β -hydride elimination would afford the silene hydride product. In pathway II, the Si=C double bond of the silene initially engages in 2+2 cycloaddition with ethylene to form a metallasilacyclobutane, which then undergoes Si–H bond-forming reductive elimination. These pathways involve primary alkyl {[(dmpe)₂Mn(CH₂CH₂SiHR₂)]}; R = Et (**23**^{E2}) or Ph (**23**^{Ph2})} and secondary alkyl {[(dmpe)₂Mn{CH(Me)(SiHR₂)}]}; R = Et (**24**^{E2}) or Ph (**24**^{Ph2})} intermediates, which we have implicated as catalytically competent species in ethylene hydrosilylation (see Chapter 8).



Scheme 4.3: Two potential pathways for the formation of $[(dmpe)_2MnH(R_2Si=CHMe)]$ (19^{Et2} : R = Et, 19^{Ph2} : R = Ph) via reaction of $[(dmpe)_2MnH(=SiR_2)]$ (16^{Et2} : R = Et, 16^{Ph2} : R = Ph) with ethylene. Key: [Mn] = $(dmpe)_2Mn$, [MnH] = $(dmpe)_2MnH$.

Mechanism II lacks precedent in silicon chemistry, although silylene 2+2 cycloaddition chemistry has been observed for isocyanates,⁵⁰⁴ proposed as a possibility for nitriles,³⁴³ isothiocyanates,⁵⁰⁵ and ketones,⁵⁰⁶ and observed for alkynes in combination with Schrock-type titanium silylene complexes.³⁶⁵ By contrast, mechanism I is supported by: 1) the likely intermediacy of $[(dmpe)_2Mn(SiHR_2)]$ (17^{Et2} : R = Et, 17^{Ph2} : R = Ph) in the reaction of **10** to form 16^{Et2} (*vide supra*); 2) DFT calculations, which show that 17^{R2} , which are the low-coordinate hydrosilyl isomers of 16^{R2} , exist as minima located 25 and 42 kJ mol^{-1} higher in energy than *cis*- 16^{Et2} and *cis*- 16^{Ph2} respectively; and 3) the reactions of 16^{Ph2} and 16^{Et2} with D_2 which exclusively form $[(dmpe)_2MnD_2(SiHR_2)]$

($d_2\text{-18}^{\text{Ph}2}$: R = Ph, $d_2\text{-18}^{\text{Et}2}$: R=Et), indicative of reactivity stemming from intermediate $17^{\text{R}2}$ rather than directly from a silylene hydride.

4.7 – Summary and Conclusions for Chapter 4

Silylene hydride complexes $[(\text{dmpe})_2\text{MnH}(=\text{SiR}_2)]$ ($16^{\text{Et}2}$: R = Et, $16^{\text{Ph}2}$: R = Ph) were prepared from the reaction of $[(\text{dmpe})_2\text{MnH}(\text{C}_2\text{H}_4)]$ (**10**) with secondary hydrosilanes, and are the first group seven examples to be observed bearing an unstabilized silylene ligand. Complex $16^{\text{Et}2}$ crystallized as the *trans* isomer, while the diphenyl analogue $16^{\text{Ph}2}$ crystallized as the *cis* isomer. Uniquely, $16^{\text{Ph}2}$ existed in solution as interconverting *cis* and *trans* isomers with and without an interligand Si–H interaction.

Silene hydride complexes $[(\text{dmpe})_2\text{MnH}(\text{R}_2\text{Si}=\text{CHMe})]$ ($19^{\text{Et}2}$: R = Et, $19^{\text{Ph}2}$: R = Ph) were prepared by exposing silylene hydride complexes $16^{\text{R}2}$ to ethylene. Complex $19^{\text{Ph}2}$ and complex $19^{\text{Et}2}$ are the first crystallographically characterized or isolated, respectively, examples of a 1st row transition metal complex with a sterically and electronically unstabilized silene ligand. Furthermore, the silylene-hydride to silene-hydride transformation is, to our knowledge, also unique.

Fragment interaction calculations were conducted on both isomers of silylene hydride $16^{\text{Et}2}$, and the silene hydride complex $19^{\text{Et}2}$. In each case, the interaction between the metal and Si-based ligand (silylene or silene) was observed to have three contributions; σ -donation, π_{\parallel} -backdonation, and π_{\perp} -backdonation. Of note are the similarities between the Mn–Si interaction in *cis*-silylene and silene complexes, and that two orthogonal π -backdonation interactions were calculated.

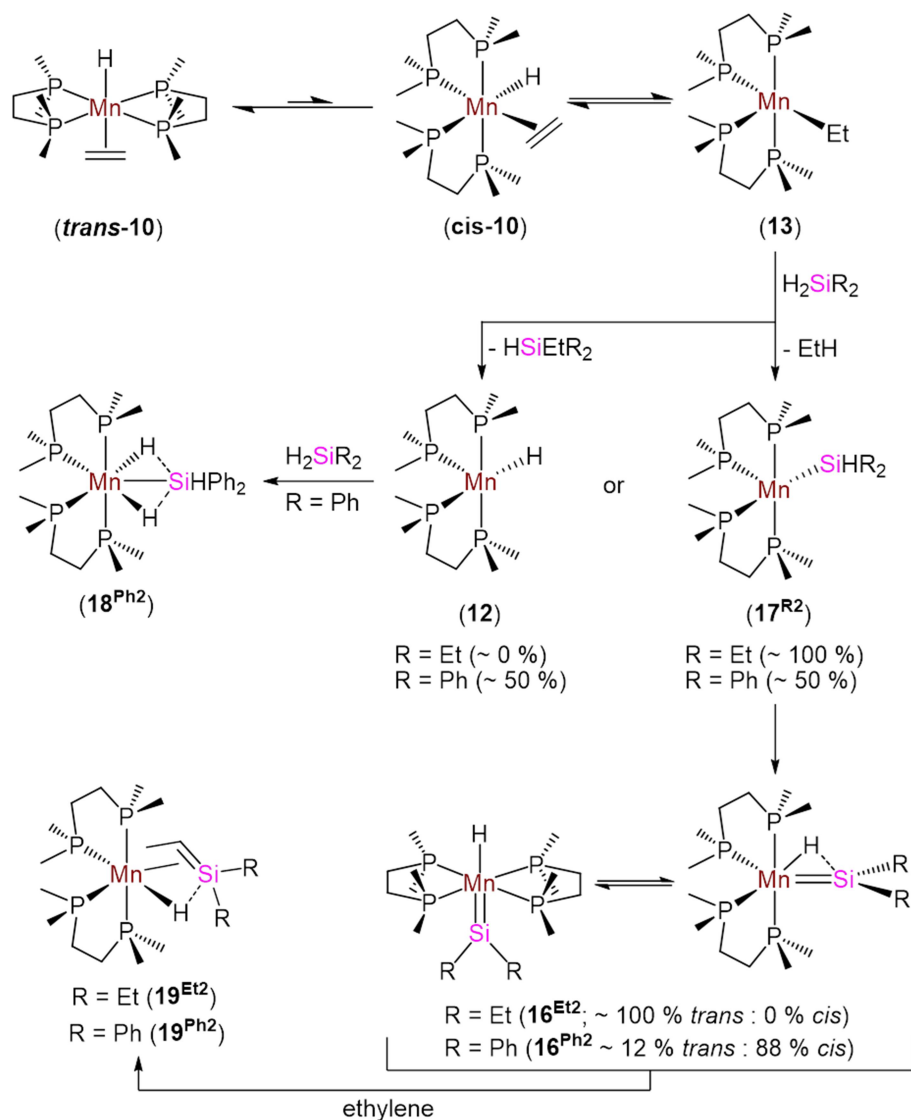
Chapter 5

Synthesis of Manganese Disilyl Hydride Complexes and Reactivity with Ethylene to Afford Silene Hydride Complexes

Portions of this chapter have been reprinted (adapted) with permission from Price, J. S.; Emslie, D. J. H.; Vargas-Baca, I. [(dmpe)₂MnH(C₂H₄)] as a Source of Low-Coordinate Ethyl Manganese(I) Species: Reactions with Primary Silanes, H₂, and Isonitriles, *Organometallics* **2018**, *37*, 3010-3023 (Copyright 2018 American Chemical Society), and Price, J. S.; Emslie, D. J. H. Interconversion and reactivity of manganese silyl, silylene, and silene complexes, *Chem. Sci.* **2019**, Advance Articles, DOI: 10.1039/C9SC04513A (Published by The Royal Society of Chemistry).

5.1 – Introduction to Chapter 5

In Chapter 4, we discussed reactions of the ethylene hydride complex, [(dmpe)₂MnH(C₂H₄)] (**10**),^{120,172} with secondary silanes (H₂SiR₂); Scheme 5.1. The reaction of **10** with H₂SiEt₂ afforded the *trans* silylene hydride complex *trans*-[(dmpe)₂MnH(=SiEt₂)] (*trans*-**16**^{Et2}) via ethane elimination. By contrast, the reaction of **10** with H₂SiPh₂ afforded ethane and [(dmpe)₂MnH(=SiPh₂)] (**16**^{Ph2}), as a mixture of a *trans* isomer (minor) and a *cis* isomer (major; featuring a Mn–H–Si bridging interaction), as well as [(dmpe)₂MnH₂(SiHPh₂)] (**18**^{Ph2}) and HSiEtPh₂.⁵⁰⁷ Compounds **16**^{Et2} is the only isolated example of a group 7 complex bearing an unstabilized terminal silylene ligand, and the phenyl derivative (**16**^{Ph2}) is the first silylene hydride complex observed to exist as distinct isomers with and without a M–H–Si interaction. Silylene hydride complexes **16**^{R2} were found to react with ethylene to form silene hydride complexes [(dmpe)₂MnH(R₂Si=CHMe)] (**19**^{Et2}: R = Et, **19**^{Ph2}: R = Ph); an unprecedented transformation.



Scheme 5.1: Reactions of $[(\text{dmpe})_2\text{MnH}(\text{C}_2\text{H}_4)]$ (**10**) with R_2SiH_2 ($\text{R} = \text{Et}, \text{Ph}$) to afford silylene hydride compounds **16^{R2}** and silyl dihydride complex **18^{Ph2}**, and subsequent reactivity with ethylene to afford silene hydride complexes **19^{R2}**. *cis-10*, **13**, **17^{R2}**, and **12** are hypothesized intermediates, for which DFT calculations have located energy minima. Only one isomer is shown for all complexes, except **10** and **16^{R2}**.

The reactions to form **16^{R2}** proceed (Scheme 5.1) via isomerization of *trans-10* to yield *cis* isomer *cis-10*, followed by 1,2-insertion to generate a coordinatively unsaturated ethyl complex (**13**), reaction with H_2SiR_2 to afford a low-coordinate manganese silyl

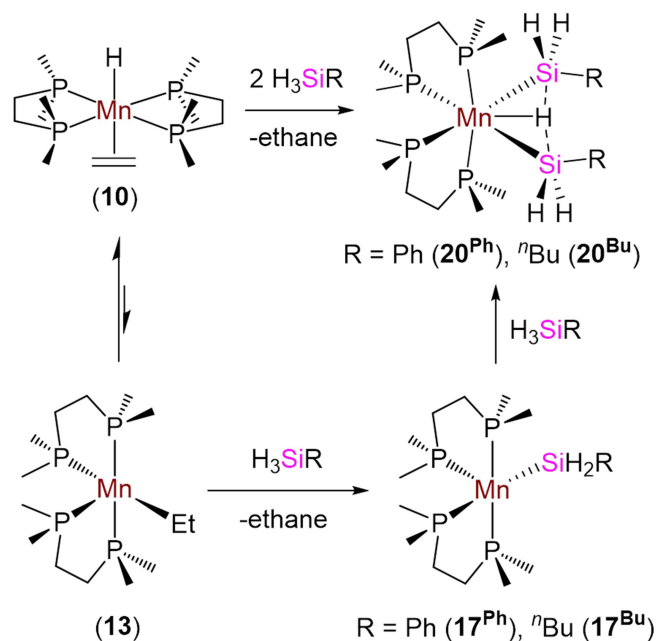
complex (**17**^{R2}; formed via σ -bond metathesis or Si–H bond oxidative addition followed by C–H bond-forming reductive elimination), and finally α -hydride elimination. In the reaction of **10** with H₂SiPh₂, the formation of complex **18**^{Ph2} also likely proceeds via ethyl intermediate **13**. However, in this case the reaction of **13** with H₂SiPh₂ also generates HSiEtPh₂ and a low-coordinate manganese hydride complex (**12**), which oxidatively adds a second equivalent of H₂SiPh₂ (Scheme 5.1). The reaction pathway in Scheme 5.1 relies upon conversion of alkene hydride complex **10** to a coordinatively unsaturated alkyl isomer, and this isomerization is discussed in Chapter 3.

Herein, we report that complex **10** reacts with primary hydrosilanes to generate disilyl hydride complexes, which can act as ‘masked’ sources of either a 5-coordinate silyl complex or a silylene hydride complex with an H substituent on the silicon centre. Upon exposure to ethylene, these manganese disilyl hydride complexes react in a similar manner to silylene hydride complexes to form silene hydride complexes with a H substituent on Si. These are, to our knowledge, the first example of transition metal silene complexes with an H substituent on silicon, and themselves react with an additional equivalent of ethylene to form new silene hydride complexes with two alkyl substituents on silicon, the product of apparent insertion of ethylene into the Si–H bond (a reaction which, to our knowledge, is unprecedented). Manganese silyl complexes, transition metal silylene complexes, and transition metal silene complexes are reviewed in sections 1.5, 1.6, and 1.7, respectively.

5.2 – Synthesis and Characterization of Manganese Disilyl Hydride Complexes

In contrast to reactions of [(dmpe)₂MnH(C₂H₄)] (**10**) with the secondary silanes H₂SiEt₂ and H₂SiPh₂ (*vide supra*), exposure of **10** to an excess of the primary silanes H₃SiPh or H₃SiⁿBu at 60 °C formed the disilyl hydride complexes [(dmpe)₂MnH(SiH₂R)₂] (**20**^{Ph}: R = Ph, **20**^{Bu}: R = ⁿBu) with elimination of ethane

(Scheme 5.2).^z Both complexes gave rise to two ³¹P NMR resonances (60.2 and 67.4 ppm for **20^{Ph}**, 58.6 and 72.6 ppm for **20^{Bu}**), a single ²⁹Si NMR resonance (−4.2 and 1.6 ppm respectively), two diastereotopic Si–H ¹H NMR resonances (5.28 and 5.31 ppm for **20^{Ph}**, 4.36 and 4.53 ppm for **20^{Bu}**), and a single metal hydride ¹H NMR signal (−14.55 and −13.27 ppm respectively).



Scheme 5.2: Reactions of $[(\text{dmpe})_2\text{MnH}(\text{C}_2\text{H}_4)]$ (**10**) with primary hydrosilanes to afford disilyl hydride complexes $[(\text{dmpe})_2\text{MnH}(\text{SiH}_2\text{R})_2]$ (**20^{Ph}**: R = Ph, **20^{Bu}**: R = ⁿBu). Only one isomer of all complexes is shown.

These reactions, like those involving secondary hydrosilanes (*vide supra*), presumably proceed via initial isomerization of **10** to the 5-coordinate ethyl species $[(\text{dmpe})_2\text{MnEt}]$ (**13**), which reacts with a single equivalent of hydrosilane to generate a 5-coordinate silyl complex $[(\text{dmpe})_2\text{Mn}(\text{SiH}_2\text{R})]$ (**17^{Ph}**: R = Ph, **17^{Bu}**: R = ⁿBu); Scheme 5.2. However, unlike in the reactions involving H_2SiR_2 , a second equivalent of primary

^z The reaction of **10** with 10 equivalents of H_3SiPh proceeded more quickly than the analogous reaction to 5 equivalents, implying that isomerization of $[(\text{dmpe})_2\text{MnH}(\text{C}_2\text{H}_4)]$ (**10**) to an ethyl isomer is not the rate-determining step.

hydrosilane oxidatively adds to the metal centre to generate the observed disilyl hydride products. Presumably, such reactivity is not observed for secondary hydrosilanes due to their increased steric bulk.

Crystals of 7-coordinate $[(\text{dmpe})_2\text{MnH}(\text{SiH}_2\text{Ph})_2]$ (**20^{Ph}**) were obtained by cooling a saturated solution in hexanes to $-30\text{ }^\circ\text{C}$, and an X-ray structure (Figure 5.1) revealed an octahedral arrangement of the four phosphorus and two silicon atoms about manganese, with a disphenoidal arrangement of the phosphorus donors, and the hydride ligand (located from the difference map) situated equidistant between the two silicon atoms. Complex **20^{Ph}** is the first structurally characterized disilyl hydride complex of manganese with non-chelating silyl ligands, although Tobita et al. previously reported a series of disilyl hydride and silyl hydrosilane complexes in which both silicon-based donors are tethered by a xanthene backbone (Figure 5.2).²⁹⁵ The Mn–Si distance of $2.3851(2)\text{ \AA}$ in **20^{Ph}** is within the range previously observed for manganese silyl hydride complexes $\{2.254(1)\text{--}2.4702(9)\text{ \AA}\}$,²¹¹ and is shorter than those in Tobita's most closely related disilyl hydride complex **T3** in Figure 5.2: $d(\text{Mn--Si}) = 2.4026(7)\text{--}2.4069(7)\text{ \AA}$.²⁹⁵

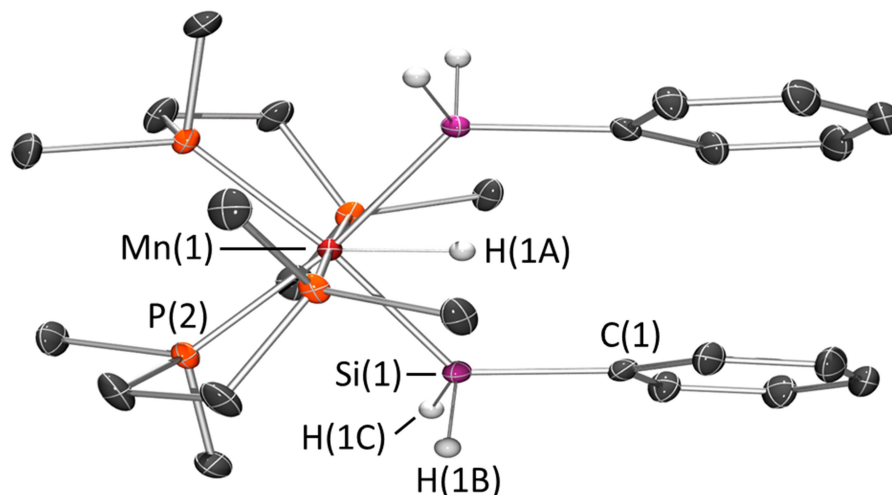


Figure 5.1: X-ray crystal structure of $[(dmpe)_2MnH(SiH_2Ph)_2]$ (20^{Ph}) with ellipsoids drawn at 50% probability. Most hydrogen atoms have been omitted for clarity. Hydrogen atoms on Mn and Si were located from the difference map and refined isotropically. Dmpe ligands are disordered over two positions and only the dominant conformation {94.7(8)%} is shown. Bond distances (Å) and angles (deg): Mn–H(1A) 1.49(2), Mn–Si 2.3851(2), Si–H(1A) 1.9163(8), Si–H(1B) 1.44(2), Si–H(1C) 1.44(1), Si–Si 3.8319(4), Si–C 1.9091(7), H(1A)–Mn–Si 53.418(7), Si–Mn–Si 106.83(1).

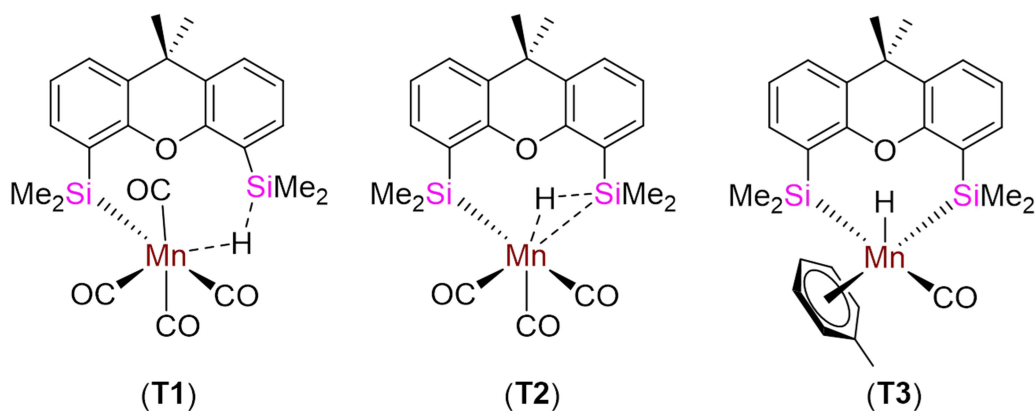


Figure 5.2: Disilyl hydride and silyl hydrosilane complexes reported by Tobita et al.²⁹⁵

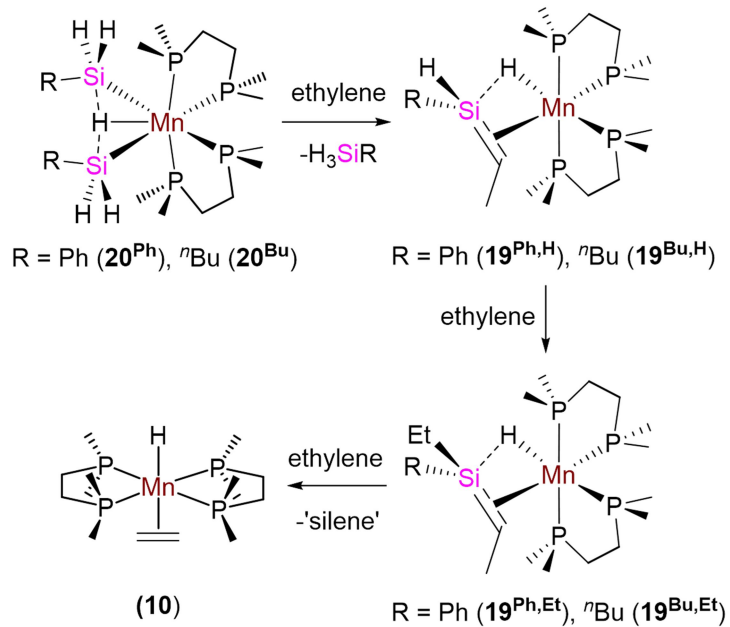
The central position of the hydride ligand between the two silyl ligands in 20^{Ph} and 20^{Bu} appears to be maintained on the NMR time scale in solution, given that the 1H

NMR spectra indicate C_2 symmetry between 25 and -87 °C. In the solid state (for $\mathbf{20}^{\text{Ph}}$), the Si(1)–H(1A) distance is 1.9163(8) Å (calcd: 1.92 Å), which is significantly longer than a typical Si–H single bond (1.48 Å),⁵⁰⁸ but much shorter than the sum of the Van der Waals radii (3.1 Å).⁵⁰⁹ The related calculated distance in a model of $\mathbf{20}^{\text{Bu}}$ where ^nBu groups were replaced by methyl groups ($\mathbf{20}^{\text{Me}}$), 1.88 Å, also falls into this range. These geometries are suggestive of a nonclassical silyl hydride ligand resulting from incomplete oxidative addition to the metal centre, leaving some degree of Si–H bonding intact.²²⁷⁻²²⁹ Computationally, this bonding picture in both $\mathbf{20}^{\text{Ph}}$ and $\mathbf{20}^{\text{Me}}$ is supported by fractional Mayer bond orders for the Mn–Si ($\mathbf{20}^{\text{Ph}}$: 0.83, $\mathbf{20}^{\text{Me}}$: 0.82-0.83), Mn–H ($\mathbf{20}^{\text{Ph}}$: 0.53, $\mathbf{20}^{\text{Me}}$: 0.53), and Si–H_{MnH} ($\mathbf{20}^{\text{Ph}}$: 0.25-0.26, $\mathbf{20}^{\text{Me}}$: 0.25) linkages. Coupling constants between ^{29}Si and the metal hydride were measured as -31 Hz ($\mathbf{20}^{\text{Ph}}$) and -30 Hz ($\mathbf{20}^{\text{Bu}}$),^{aa} and DFT calculations afforded similar ^{29}Si – ^1H coupling constants of -24 Hz ($\mathbf{20}^{\text{Ph}}$) and -27 Hz ($\mathbf{20}^{\text{Me}}$), indicative of a nonclassical silyl hydride bonding environment.^{233,241}

5.3 – Reactions of Manganese Disilyl Hydride Complexes with Ethylene

The disilyl hydride complexes [(dmpe)₂MnH(SiH₂R)₂] ($\mathbf{20}^{\text{Ph}}$: R = Ph, $\mathbf{20}^{\text{Bu}}$: R = ^nBu) reacted with ethylene at room temperature to afford the silene hydride complexes [(dmpe)₂MnH(RHSi=CHMe)] ($\mathbf{19}^{\text{Ph,H}}$: R = Ph, $\mathbf{19}^{\text{Bu,H}}$: R = ^nBu). This reaction mirrors the reactions of silylene hydride complexes $\mathbf{16}^{\text{R}2}$ with ethylene (*vide supra*: Scheme 1).⁵⁰⁷ Moreover, complexes $\mathbf{19}^{\text{R,H}}$ reacted with a second equivalent of ethylene to form silene hydride complexes with two hydrocarbyl groups on Si, [(dmpe)₂MnH(REtSi=CHMe)] ($\mathbf{19}^{\text{Ph,Et}}$: R = Ph, $\mathbf{19}^{\text{Bu,Et}}$: R = ^nBu); the products of apparent ethylene insertion into the Si–H bond (Scheme 5.3, Figure 5.3). This silene SiH to SiR conversion reaction is unprecedented. Complexes $\mathbf{19}^{\text{R,Et}}$ also reacted further with ethylene to generate [(dmpe)₂MnH(C₂H₄)] ($\mathbf{10}$), potentially by substitution of the silene ligand which undergoes subsequent decomposition to unidentified products.

^{aa} These coupling constants were measured using ^{29}Si -edited ^1H – ^1H COSY, as described in Chapter 6. These data were published in ref. 510.



Scheme 5.3: Reactions of disilyl hydride complexes $[(\text{dmpe})_2\text{MnH}(\text{SiH}_2\text{R})_2]$ (20^{Ph} : R = Ph, 20^{Bu} : R = ^nBu) with one, two, or three equivalents of ethylene to afford SiH-containing silene hydride complexes $[(\text{dmpe})_2\text{MnH}(\text{RHSi}=\text{CHMe})]$ ($19^{\text{Ph,H}}$: R = Ph, $19^{\text{Bu,H}}$: R = ^nBu), silene hydride complexes with two hydrocarbyl groups on Si $[(\text{dmpe})_2\text{MnH}(\text{REtSi}=\text{CHMe})]$ ($19^{\text{Ph,Et}}$: R = Ph, $19^{\text{Bu,Et}}$: R = ^nBu), and ethylene hydride complex $[(\text{dmpe})_2\text{MnH}(\text{C}_2\text{H}_4)]$ (**10**), respectively. Only one isomer is shown for each silene hydride complex.

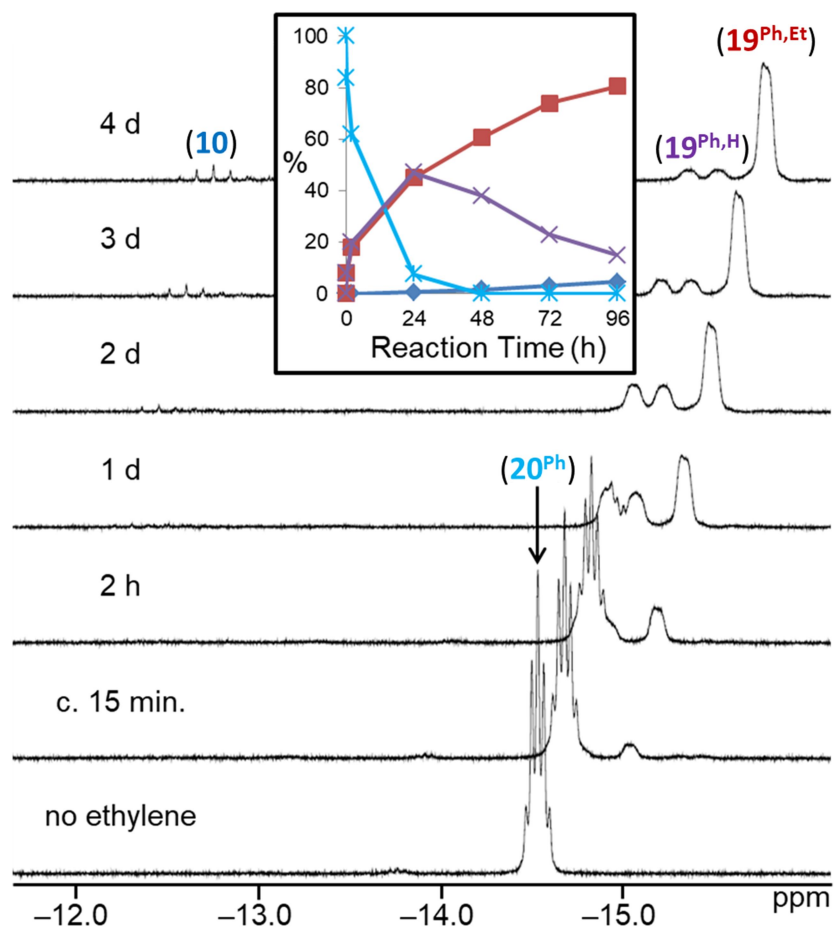


Figure 5.3: ^1H NMR spectra (298 K, C_6D_6 , 600 MHz) for the reaction of $[(dmpe)_2MnH(SiH_2Ph)_2]$ (20^{Ph}) with ethylene over time (initial, $n_{\text{C}_2\text{H}_4} \approx n_{\text{silane}}$).^{bb} The x-axis corresponds to the bottom spectrum, and for clarity, each spectrum above that is shifted by 0.15 ppm to lower frequency. The inset shows the relative concentration of hydride-containing species versus time; reactant $[(dmpe)_2MnH(SiH_2Ph)_2]$ (20^{Ph} ; light blue *), silene hydride $[(dmpe)_2MnH(PhHSi=CHMe)]$ ($19^{Ph,H}$; purple x), silene hydride $[(dmpe)_2MnH(PhEtSi=CHMe)]$ ($19^{Ph,Et}$; red ■), and $[(dmpe)_2MnH(C_2H_4)]$ (10 ; dark blue ◆).

^{bb} Over the 4 days that this reaction was monitored by ^1H NMR spectroscopy, the ethylene concentration in solution decreased by 40 %. Relative concentrations in Fig. 5.3 were calculated by integrating ^1H NMR data; integration relative to the residual solvent signal from C_6D_6 indicated that the total moles of manganese-containing species in the inset in Figure 5.3 remained constant.

A range of byproducts was observed in the syntheses of silene hydride complexes, including primary, secondary, and tertiary hydrosilanes $\{\text{H}_{(3-n)}\text{SiEt}_n\text{R}$ ($n = 0, 1, 2$; $\text{R} = \text{Ph}, {}^n\text{Bu}\}$;^{cc} the latter two are formed by stepwise manganese-catalysed hydrosilylation reactions between the primary hydrosilane byproduct and excess ethylene (see Chapter 8). For $\text{R} = {}^n\text{Bu}$, silene SiH to SiEt conversion did not proceed until all of the primary hydrosilane byproduct had been consumed, so conversion of $\mathbf{20}^{\text{Bu}}$ to $\mathbf{19}^{\text{Bu,H}}$, and then to $\mathbf{19}^{\text{Bu,Et}}$, proceeded in a stepwise fashion. By contrast, for $\text{R} = \text{Ph}$, silene SiH to SiEt conversion commenced as soon as $\mathbf{19}^{\text{Ph,H}}$ was available (Figure 5.3).

Compounds $\mathbf{19}^{\text{Bu,H}}$ and $\mathbf{19}^{\text{Ph,Et}}$ were isolated as a red oil and a brown solid, respectively, in $> 95\%$ purity. By contrast, $\mathbf{19}^{\text{Ph,H}}$ and $\mathbf{19}^{\text{Bu,Et}}$ were characterized *in situ* by NMR spectroscopy (Table 5.1). Compounds $\mathbf{19}^{\text{Ph,H}}$ and $\mathbf{19}^{\text{Bu,Et}}$ were not isolated due to the formation of mixtures of products (e.g. $\mathbf{19}^{\text{Ph,H}}$ accompanied by $\mathbf{19}^{\text{Ph,Et}}$ and $\mathbf{10}$), combined with instability in solution over a period of days at room temperature.

^{cc} In the reaction of $\mathbf{20}^{\text{Ph}}$ with ethylene, no tertiary hydrosilane was observed. However, small amounts of vinyl hydrosilane were.

Table 5.1: Selected ^1H , ^{13}C , ^{29}Si and ^{31}P NMR chemical shifts (ppm) and coupling constants (Hz) for silene hydride complexes $[(\text{dmpe})_2\text{MnH}(\text{RR}'\text{Si}=\text{CHMe})]$ ($\mathbf{19}^{\text{Ph}2}$: R = R' = Ph; $\mathbf{19}^{\text{Et}2}$: R = R' = Et; $\mathbf{19}^{\text{Ph,H}}$: R = Ph, R' = H; $\mathbf{19}^{\text{Bu,H}}$: R = ^nBu , R' = H; $\mathbf{19}^{\text{Ph,Et}}$: R = Ph, R' = Et; $\mathbf{19}^{\text{Bu,Et}}$: R = ^nBu , R' = Et); in C_6D_6 ($\mathbf{19}^{\text{R}2}$ and $\mathbf{19}^{\text{Ph,Et}}$) or d_8 -toluene ($\mathbf{19}^{\text{R,H}}$ and $\mathbf{19}^{\text{Bu,Et}}$). Unless otherwise noted, values are from NMR spectra at 298 K. For $\mathbf{19}^{\text{R,H}}$, NMR environments are reported for both observed isomers.

	$\mathbf{19}^{\text{Ph,H}}$	$\mathbf{19}^{\text{Bu,H}}$	$\mathbf{19}^{\text{Ph,Et}}$	$\mathbf{19}^{\text{Bu,Et}}$	$\mathbf{19}^{\text{Ph}2}$	$\mathbf{19}^{\text{Et}2}$
Mn <u>H</u>	-14.5, -14.7	-14.9, ^a -15.0 ^b	-14.9	-15.3	-14.6	-15.3
Si <u>H</u>	4.5 ^c	3.7 ^c	–	–	–	–
Si= <u>CH</u> CH ₃	0.1, 0.2	-0.1, ^a -0.2 ^b	0.2	-0.1	0.4	0.0
Si= <u>CH</u> CH ₃	1.9 ^c	1.8, ^a 1.7 ^b	1.9	1.7	2.1	1.8
Si= <u>C</u>	-21.0, -21.2	-19.3, ^a -20.8 ^b	-21.7	-19.3	-22.9	-19.4
^{29}Si	-7.1, ^d -17.4 ^d	-8.9, ^a -17.0 ^b	0.7	-6.5	-1.5	-3.0
^{31}P	63.3- 85.5	65.8-79.1	65.7-79.2	65.5-79.3	62.7-78.3	65.5-79.3
$^1J_{\text{C,H}}^{\text{e}}$	139 ^f	138, ^a 139 ^b	137	138	136	137

a. Due to the minor isomer of $\mathbf{19}^{\text{Bu,H}}$.

b. Due to the major isomer of $\mathbf{19}^{\text{Bu,H}}$.

c. Both isomers have identical chemical shifts.

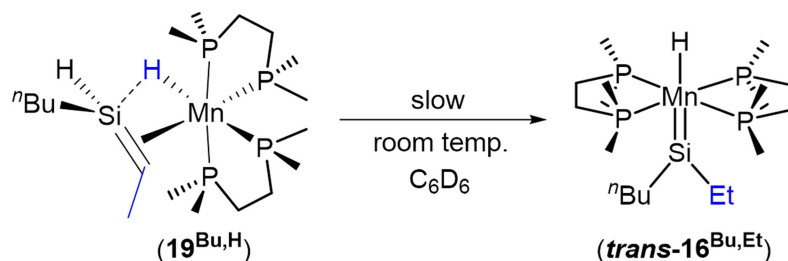
d. Measured at 213 K {because this environment was not located by $^{29}\text{Si}\{^1\text{H}\}$ or 2D $^1\text{H}-^{29}\text{Si}$ (HSQC or HMBC) NMR spectroscopy at 298 K}.

e. Coupling between the Si=C and Si=CHCH₃ environments.

f. $^1J_{\text{C,H}}$ could only be resolved for one isomer

In solution (in the absence of ethylene or free hydrosilanes), SiH-containing silene hydride complex $\mathbf{19}^{\text{Bu,H}}$ underwent isomerization to the silylene hydride complex *trans*- $[(\text{dmpe})_2\text{MnH}(=\text{SiEt}^n\text{Bu})]$ (*trans*- $\mathbf{16}^{\text{Bu,Et}}$; Scheme 5.4), with 20% conversion after 2 days

at room temperature in C_6D_6 .^{dd} NMR spectra of *trans*-**16**^{Bu,Et} feature an MnH 1H NMR peak at -10.48 ppm (a pentet with $^2J_{H,P}$ of 51 Hz), two sharp singlets in the $^{31}P\{^1H\}$ NMR spectrum at 80.35 and 80.50 ppm, and a high-frequency peak in the $^{29}Si\{^1H\}$ NMR spectrum at 364 ppm. These data are consistent with a high-symmetry base-free silylene complex, and are nearly identical to the NMR data for *trans*- $[(dmpe)_2MnH(=SiEt_2)]$ (*trans*-**16**^{Et2}).^{ee} Isomerization was accompanied by formation of small amounts ($\sim 10\%$ combined relative to **16**^{Bu,Et}) of an unidentified manganese hydride complex (with a pentet 1H NMR peak at -9.06 ppm; $^2J_{H,P} = 47$ Hz) and the silene hydride complex $[(dmpe)_2MnH(^nBuEtSi=CHMe)]$ (**19**^{Bu,Et}).



Scheme 5.4: Solution decomposition of $[(dmpe)_2MnH(^nBuHSi=CHMe)]$ (**19**^{Bu,H}) to form silylene complex *trans*- $[(dmpe)_2MnH(=SiEt^nBu)]$ (*trans*-**16**^{Bu,Et}) as the major product.

Isomerization of a silene hydride complex to a silylene hydride complex is, to our knowledge, unprecedented. However, this isomerization is related to Tilley and Bergman's report of an equilibrium between the silylene alkyl complex $[Cp^*(Me_3P)Ir(Me)(=SiMe_2)]^+$ and the silene hydride isomer,

^{dd} DFT calculations indicated that isomerization of SiH-containing silene hydride complexes **19**^{R,H} to silylene hydride complexes *trans*- $[(dmpe)_2MnH(=SiEtR)]$ (*trans*-**16**^{Et,R}) is thermodynamically favourable for R = Ph and ⁿBu; minima for the latter were located 20-34 kJ mol⁻¹ lower in energy than the lowest energy silene hydride isomer. In addition, *cis* silylene hydride isomers were determined to be 1 (**16**^{PhEt}) and 9 (**16**^{Bu,Et}) kJ mol⁻¹ higher in energy than the respective *trans* isomers.

^{ee} NMR data for *trans*- $[(dmpe)_2MnH(=SiEt_2)]$ (*trans*-**16**^{Et2}) includes an MnH 1H NMR peak at -10.46 ppm (pentet with $^2J_{H,P}$ of 51 Hz), a single sharp singlet in the $^{31}P\{^1H\}$ NMR spectrum at 80.95, and a ^{29}Si NMR chemical shift of 365 ppm.

$[\text{Cp}^*(\text{Me}_3\text{P})\text{IrH}(\text{Me}_2\text{Si}=\text{CH}_2)]^+$, which relies upon reversible α -Me and β -H elimination from a trimethylsilyl intermediate (see Scheme 1.14).⁴¹⁴

For silene hydride complexes $\mathbf{19}^{\text{R,H}}$ (those with a hydride substituent on Si), two sets of NMR signals were observed due to a pair of isomers present in solution with a 1:1 ($\mathbf{19}^{\text{Ph,H}}$; Figure 5.3) or 1.9:1 ($\mathbf{19}^{\text{Bu,H}}$) ratio, whereas only a single set of NMR signals (indicative of a single isomer) were observed for $\mathbf{19}^{\text{R,Et}}$ (silene hydride complexes with two hydrocarbyl substituents on Si). NMR spectra of the silene hydride complexes feature (for each isomer) four ^{31}P NMR signals, a single ^{29}Si NMR environment (at -17.4 to 0.7 ppm), a low frequency ^{13}C NMR signal for the $\text{Si}=\underline{\text{C}}$ environment (at -19.3 to -21.7 ppm), and a silene $^1J_{\text{C,H}}$ coupling constant (137-139 Hz) intermediate between those typical for sp^2 and sp^3 hybridized carbon atoms; Table 5.1. Additionally, the MnH signal was located at -14.5 to -15.3 ppm in the ^1H NMR spectra of $\mathbf{19}^{\text{R,H}}$ and $\mathbf{19}^{\text{R,Et}}$, and the SiH , $\text{Si}=\underline{\text{C}}\text{H}(\text{CH}_3)$ and $\text{Si}=\text{CH}(\underline{\text{C}}\text{H}_3)$ signals were observed at 3.7 to 4.5 ppm, -0.2 to 0.2 ppm, and 1.7 to 1.9 ppm, respectively. These data are very similar to those for $[(\text{dmpe})_2\text{MnH}(\text{R}_2\text{Si}=\text{CHMe})]$ ($\mathbf{19}^{\text{Ph}2}$: R = Ph, $\mathbf{19}^{\text{Et}2}$: R = Et; pertinent NMR data are included in Table 5.1), which have been spectroscopically, and (for $\mathbf{19}^{\text{Ph}2}$) crystallographically, characterized (Chapter 4). To the best of our knowledge, $\mathbf{19}^{\text{R,H}}$ are the first spectroscopically observed^{ff} examples of transition metal silene complexes with a hydrogen substituent on silicon.

Despite numerous attempts, we were unable to obtain X-ray quality crystals of $\mathbf{19}^{\text{R,H}}$ or $\mathbf{19}^{\text{R,Et}}$. Therefore, we turned to DFT calculations in order to gain further insight into the structures of these complexes {ADF, gas-phase, all-electron, PBE, D3-BJ, TZ2P, ZORA}. For all four complexes, energy minima were located for four *cis* silene hydride isomers^{gg} with E or Z silene stereochemistry, and differing in the orientation of the silene

^{ff} Iron or cobalt silene complexes with hydrogen substituents on Si have been detected in the gas phase by mass spectrometry and postulated as an intermediate in the gas-phase activation of H_3SiEt by Co cations; see ref. 429.

^{gg} Not including enantiomers where the stereochemistry at manganese is switched from Λ to Δ .

methyl substituent ($\text{RR}'\text{Si}=\text{CHMe}$) relative to the two dmpe ligands, as shown in Figure 5.4 (see Figure 5.5 for the lowest energy isomer of $\mathbf{19}^{\text{Bu,H}}$). In all cases, isomers i and ii are within a few kJ mol^{-1} of one another, and are 13-22 kJ mol^{-1} lower in energy than isomers iii and iv, consistent with observation of just 2 isomers in the solution NMR spectra of $\mathbf{19}^{\text{R,H}}$.^{hh} By contrast, the apparent formation of a single isomer of compounds $\mathbf{19}^{\text{R,Et}}$ suggests that these reactions proceed under kinetic control.

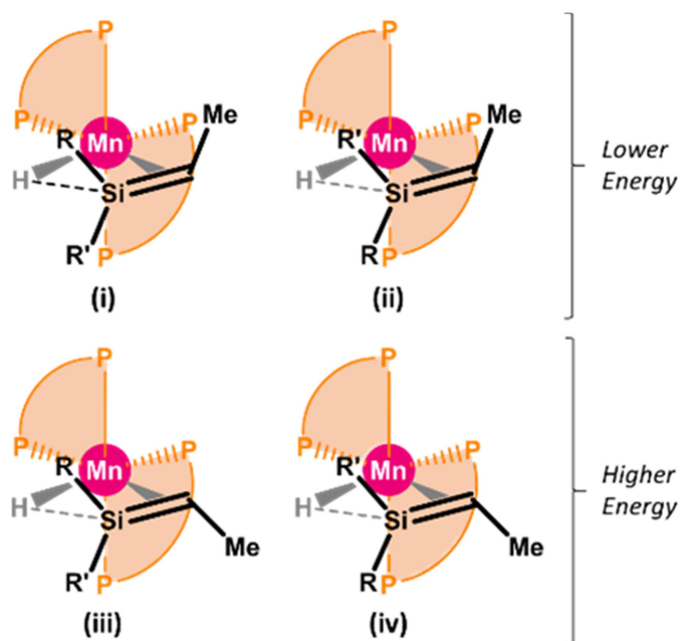


Figure 5.4: Calculated isomers (i-iv) of silene hydride complexes $[(\text{dmpe})_2\text{MnH}(\text{RR}'\text{Si}=\text{CHMe})]$ ($\mathbf{19}^{\text{Ph,H}}$: $\text{R} = \text{Ph}$, $\text{R}' = \text{H}$; $\mathbf{19}^{\text{Bu,H}}$: $\text{R} = \text{}^n\text{Bu}$, $\text{R}' = \text{H}$; $\mathbf{19}^{\text{Ph,Et}}$: $\text{R} = \text{Ph}$, $\text{R}' = \text{Et}$; $\mathbf{19}^{\text{Bu,Et}}$: $\text{R} = \text{}^n\text{Bu}$, $\text{R}' = \text{Et}$) featuring Si-H interligand interactions.

^{hh} The dominant isomer for $\mathbf{19}^{\text{Bu,H}}$ was assigned as isomer I given that the $\text{SiH } ^1\text{H}$ NMR signal for this isomer exhibits a large (18 Hz) $^3J_{\text{H},\text{P}}$ coupling to one of the phosphorus donor atoms, and in the calculated structures of isomers (i) and (ii) (for a model of $\mathbf{19}^{\text{Bu,H}}$ where the ^nBu group was replaced with an Et group), only isomer (i) exhibited a $^1\text{H}-^{31}\text{P}$ coupling of comparable magnitude (23 Hz). As well, isomer I of $\mathbf{19}^{\text{Bu,H}}$ is slightly (4 kJ mol^{-1}) lower in energy than isomer (ii).

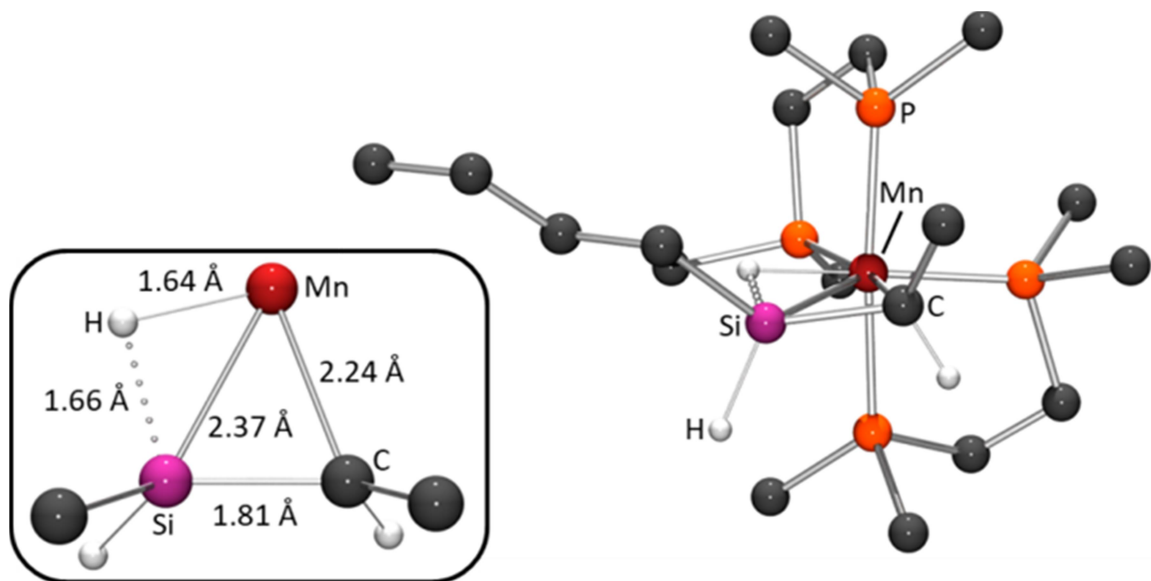


Figure 5.5: Calculated structure (ball and stick diagram) for the lowest energy isomer of silene hydride complex $[(dmpe)_2Mn(nBuHSi=CHMe)]$ ($\mathbf{19}^{Bu,H}$). All hydrogen atoms have been omitted for clarity except those on Mn or the Si=C unit. The inset shows a top-down view of the Mn silene hydride core, with selected bond distances.

In the calculated structures of silene hydride isomers i and ii, the Si=C bond distances of 1.80-1.81 Å fall within the range for previously reported transition metal silene complexes (1.78(2)-1.838(11) Å),²¹¹ and correspond to Mayer bond orders ranging from 0.96 to 1.10 (cf. 0.70-0.91 for Si-C single bonds in the same complexes). Also, as in $\mathbf{19}^{R2}$ (Chapter 4), significant interligand interactions exist between silicon and the hydride. Computationally, this is illustrated by short Si-H_{Mn} distances (1.64-1.66 Å), with substantial Mayer bond orders (0.45-0.49),ⁱⁱ and is also reflected by a large negative $^{29}Si-^1H_{Mn}$ coupling constant of -80 Hz (measured using ^{29}Si -edited 2D $^1H-^1H$ COSY NMR spectroscopy; see Chapter 6) for the major isomer of $\mathbf{19}^{Bu,H}$ (cf. -30 to -31 Hz for $\mathbf{20}^R$ and > 0 in classical silyl hydride complexes).^{241,260,510} Short Mn-Si distances (2.35-2.42 Å) with Mayer bond orders of 0.49-0.53, and Mn-H distances of 1.64-1.66 Å with Mayer bond orders of 0.52-0.56, combined with the short Si=C distance (*vide supra*),

ⁱⁱ By comparison, terminal Si-H distances and Mayer bond orders in $\mathbf{19}^{R,H}$ are 1.50-1.51 Å and 0.82-0.86, respectively.

support the identification $19^{\text{R,H}}$ and $19^{\text{R,Et}}$ as *cis* silene hydride complexes, as opposed to 5-coordinate alkyl complexes with a strong β -Si-H-Mn interaction.

5.3 – DFT Calculations on Low-Coordinate Silyl and Silylene Hydride Intermediates Derived from 20^{R}

The reactions of the disilyl hydride complexes $[(\text{dmpe})_2\text{MnH}(\text{SiH}_2\text{R})_2]$ (20^{Ph} : R = Ph, 20^{Bu} : R = *n*Bu) with C_2H_4 (*vide supra*) likely proceed via either (a) 5-coordinate mono-silyl intermediates, $[(\text{dmpe})_2\text{Mn}(\text{SiH}_2\text{R})]$ (17^{Ph} : R = Ph, 17^{Bu} : R = *n*Bu), or (b) silylene-hydride intermediates, $[(\text{dmpe})_2\text{MnH}(=\text{SiHR})]$ ($16^{\text{Ph,H}}$: R = Ph, $16^{\text{Bu,H}}$: R = *n*Bu), formed by sequential hydrosilane reductive elimination and α -hydride elimination from disilyl hydride complexes 20^{R} (Scheme 5.6; *vide infra*). Therefore, DFT calculations (ADF, gas-phase, all-electron, PBE, D3-BJ, TZ2P, ZORA) were carried out to assess the thermodynamic accessibility of such intermediates (Table 5.2, Figure 5.6).

Table 5.2: Thermodynamic parameters calculated by DFT for the formation of intermediates in Figure 5.6 from disilyl hydride complexes $[(\text{dmpe})_2\text{MnH}(\text{SiH}_2\text{R})_2]$ $\{20^{\text{Ph}}$ (R = Ph) / 20^{Bu} (R = *n*Bu) $\}$; ΔE (calculated before ZPE correction), ΔH , $\Delta\text{G}^{298.15\text{K}}$, $\Delta\text{G}^{335\text{K}}$ (kJ mol^{-1} at 298.15 K or, for $\Delta\text{G}^{335\text{K}}$, 335 K), and ΔS ($\text{J mol}^{-1}\text{K}^{-1}$ at 298.15 K).^a

	<i>trans</i> - 17^{R}	<i>cis</i> - 17^{R} <i>rotamer 1</i>	<i>cis</i> - 17^{R} <i>rotamer 2</i>	<i>cis</i> - $16^{\text{R,H}}$	<i>trans</i> - $16^{\text{R,H}}$
ΔE	146/156	131/145	165/n.o.	110/115	115/122
ΔH	135/150	123/138	152/n.o.	117/124	100/111
ΔS	242/265	197/232	225/n.o.	234/216	199/234
$\Delta\text{G}^{298.15\text{K}}$	63/71	64/69	85/n.o.	47/60	41/41
$\Delta\text{G}^{335\text{K}}$	54/62	57/60	76/n.o.	39/52	34/33

a. n.o. = not observed (*i.e.* energy minimum not located).

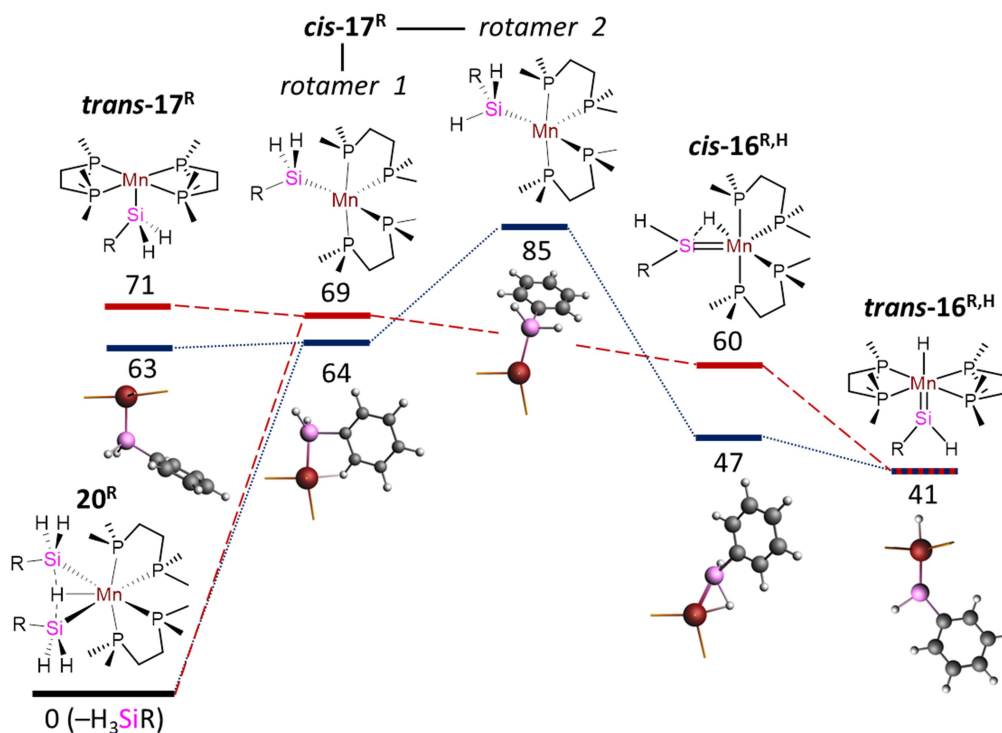


Figure 5.6: DFT calculated Gibbs free energies at 298.15 K ($\Delta G^{298.15\text{K}}$; kJ mol^{-1}) to access reactive intermediates (and the H_3SiR byproduct) from disilyl hydride complexes $[(\text{dmpe})_2\text{MnH}(\text{SiH}_2\text{R})_2]$ (20^{Ph} : R = Ph, blue dotted lines; 20^{Bu} : R = $n\text{Bu}$, red dashed lines). Calculated intermediates (left to right) are: (i) an isomer of $[(\text{dmpe})_2\text{Mn}(\text{SiH}_2\text{R})]$ with an equatorial dmpe arrangement ($\text{trans-17}^{\text{Ph}}$: R = Ph, $\text{trans-17}^{\text{Bu}}$: R = $n\text{Bu}$), (ii) an isomer of $[(\text{dmpe})_2\text{Mn}(\text{SiH}_2\text{R})]$ with a disphenoidal dmpe arrangement and a hydrocarbyl substituent on silicon oriented towards the vacant coordination site {rotamer 1 of cis-17^{R} : R = Ph ($\text{cis-17}^{\text{Ph}}$), $n\text{Bu}$ ($\text{cis-17}^{\text{Bu}}$)}, (iii) an isomer of $[(\text{dmpe})_2\text{Mn}(\text{SiH}_2\text{R})]$ with a disphenoidal dmpe arrangement and an SiH substituent oriented towards the vacant coordination site {rotamer 2 of cis-17^{R} : R = Ph ($\text{cis-17}^{\text{Ph}}$); a minimum was not located for R = $n\text{Bu}$ }, (iv) an isomer of $[(\text{dmpe})_2\text{MnH}(\text{=SiHR})]$ with interacting *cis*-disposed silylene and hydride ligands ($\text{cis-16}^{\text{Ph,H}}$: R = Ph, $\text{cis-16}^{\text{Bu,H}}$: R = $n\text{Bu}$), and (v) *trans*- $[(\text{dmpe})_2\text{MnH}(\text{=SiHR})]$ ($\text{trans-16}^{\text{Ph,H}}$: R = Ph, $\text{trans-16}^{\text{Bu,H}}$: R = $n\text{Bu}$). Geometry optimized cores of the phenyl analogues of reactive intermediates are depicted below each energy level, showing Mn in red, Si in pink, C in dark grey, and H in light grey, accompanied by stick bonds to the phosphorus donor atoms.

In the case of low-coordinate silyl species, energy minima were located for structures in which the silyl group is either *cis* (*cis-17^R*) or *trans* (*trans-17^R*) to the vacant coordination site generated by hydrosilane reductive elimination. At 298 K, ΔG for the formation of these monosilyl compounds and free hydrosilane from **20^R** is very similar (63-71 kJ mol⁻¹).

In the global minima for the *cis* isomers (rotamer 1 of *cis-17^R*), the hydrocarbyl substituent on silicon engages in a γ -agostic interaction with manganese (via an *ortho-CH* bond in *cis-17^{Ph}* or a CH₂CH₂CH₂CH₃ bond in *cis-17^{Bu}*), with Mn–H _{γ} distances of 1.91-1.93 Å. The Mn–H _{γ} –C _{γ} angles in this rotamer of *cis-17^R* are 115.9° and 131.4°, respectively, and the presence of a γ -agostic interaction is further supported by Mayer bond orders of 0.22-0.24 between Mn and H _{γ} , and 0.13-0.15 between Mn and C _{γ} .

For the phenyl analogue **17^{Ph}**, a higher-energy *cis* isomer was located, corresponding to a rotamer where one of the two hydrogen substituents on silicon is now oriented in the direction of the vacant coordination site (rotamer 2 of *cis-17^{Ph}*; Figure 5.6, Table 5.2). Relative to rotamer 1, this structure features an acute Mn–Si–H_{Si} angle of 101° (cf. 119°), an Mn–H_{Si} Mayer bond order of 0.06 (cf. < 0.05), a marginally elongated Si–H_{Si} distance of 1.53 Å (cf. 1.51 Å), and a marginally lower Si–H_{Si} Mayer bond order of 0.80 (cf. 0.85), together suggestive of a weak α -Si–H–Mn interaction. Rotamer 2 of **17^R** is presumably involved in silylene hydride formation via α -hydride elimination, and indeed, all attempts to locate an analogous energy minimum for the ⁿBu analogue structure led instead to a silylene hydride structure (*cis-16^{Bu,H}*; *vide infra*).

As with the 5-coordinate silyl species (*vide supra*), multiple energy minima (Table 5.2, Figure 5.6) were located for silylene hydride structures [(dmpe)₂MnH(=SiHR)] (**16^{Ph,H}**: R = Ph, **16^{Bu,H}**: R = ⁿBu). The two lowest energy structures are (a) a *cis* silylene hydride isomer with a significant interaction between silicon and the neighbouring hydride ligand (the Si···H_{Mn} distances are 1.68 Å, with Mayer bond orders of 0.52; cf. 0.84-0.85 for the terminal Si–H bonds), and (b) a *trans* silylene hydride isomer. These isomers are isostructural to the X-ray crystal structures of

cis-[(dmpe)₂MnH(=SiPh₂)] (**16**^{Ph₂}) and *trans*-[(dmpe)₂MnH(=SiEt₂)] (**16**^{Et₂}), respectively (Chapter 4). Calculated ΔG values to access **16**^{R,H} from **20**^R range from 41 kJ mol⁻¹ (*trans* isomers) to 47-60 kJ mol⁻¹ (*cis* isomers) at 298.15 K, decreasing to 33-34 kJ mol⁻¹ (*trans* isomers) and 39-52 kJ mol⁻¹ (*cis* isomers) at 335 K, highlighting their thermodynamic accessibility.

In silylene hydride complexes **16**^{R,H}, Mn–Si double bond character is apparent from relatively short Mn–Si distances (2.16-2.20 Å), Mn–Si Mayer bond orders ranging from 1.17 (*cis*-**16**^{R,H}) to 1.54-1.57 (*trans*-**16**^{R,H}), and a planar or near-planar environment about Si ($\sum(\text{R-Si-R}) > 356^\circ$). These parameters are comparable to those for the two isomers of [(dmpe)₂MnH(=SiR₂)] (**16**^{R₂}; R = Et or Ph) discussed in Chapter 4.

5.4 – High Temperature NMR Spectra of **20**^R: *in situ* Generation of *trans*-Silylene Hydride (*trans*-**16**^{R,H}) Species

At 335 K, ¹H NMR spectra of the disilyl hydride complexes [(dmpe)₂MnH(SiH₂R)₂] (**20**^{Ph}: R = Ph, **20**^{Bu}: R = ⁿBu) revealed the formation of a small amount of a new manganese complex and free hydrosilane (H₃SiR; R = Ph or ⁿBu). This process is reversible, and clean spectra of **20**^R were observed upon cooling back to room temperature. The new manganese complex exhibits a high frequency (9.83 or 9.53 ppm) and a low frequency (–9.01 or –9.60 ppm) ¹H NMR signal. The former is in the range observed for the terminal =SiRH (R = hydrocarbyl substituent) environment in diamagnetic silylene complexes of Mo, W, Fe, Ru, Os, and Ir, (6.34-12.1 ppm; see Section 1.6.6), while the latter is consistent with a metal hydride environment. The low frequency hydride signal is a pentet (²J_{1H,31P} = 54 or 51 Hz) consistent with a hydride ligand apical to a plane of four equivalent phosphine donors. Taken together, these data indicate that the new complex observed at elevated temperature is *trans*-[(dmpe)₂MnH(=SiHR)] (*trans*-**16**^{Ph,H}: R = Ph, *trans*-**16**^{Bu,H}: R = ⁿBu); the most thermodynamically accessible silyl or silylene species in Figure 5.6.

Characterization of *trans-16*^{R,H} by ²⁹Si NMR spectroscopy was not possible since the new species were formed at very low concentrations (~4% and ~2% relative to **20**^{Ph} or **20**^{Bu}, respectively). However, EXSY NMR spectroscopy at 335 K indicates exchange between the two diastereotopic SiH protons in **20**^{Ph} or **20**^{Bu}, the free hydrosilane SiH peak, the high frequency *trans-16*^{R,H} silylene SiH environment, and the MnH signals from both **20**^R and *trans-16*^{R,H} (shown in Figure 5.7 for R = ⁿBu).^{jj} This is consistent with an equilibrium in which **20**^R eliminates free H₃SiR to form *trans-16*^{R,H} (*vide infra*).

^{jj} In the case of **20**^{Ph}, an additional low frequency ¹H NMR signal (a broad singlet with < 2% intensity relative to the MnH peak of **20**^{Ph}) was observed at -12.1 ppm (335 K), which could potentially be from the MnH environment of *cis*-[(dmpe)₂MnH(=SiHPh)] (*cis-16*^{Ph,H}). However, EXSY NMR spectroscopy did not show chemical exchange between this peak and those from **20**^{Ph} or *trans-16*^{Ph,H} (potentially due to broadness and low intensity of the signal). A further low frequency ¹H NMR signal (also a broad singlet, but present in the room temperature and high temperature NMR spectra in similar intensities; ~1.5% relative to the MnH region of **20**^{Ph}) was observed at -13.8 ppm, which could potentially be from another isomer of **20**^{Ph}; this environment was observed by EXSY NMR spectroscopy to be in chemical exchange with the SiH and MnH environments of both **20**^{Ph} and *trans-16*^{Ph,H}.

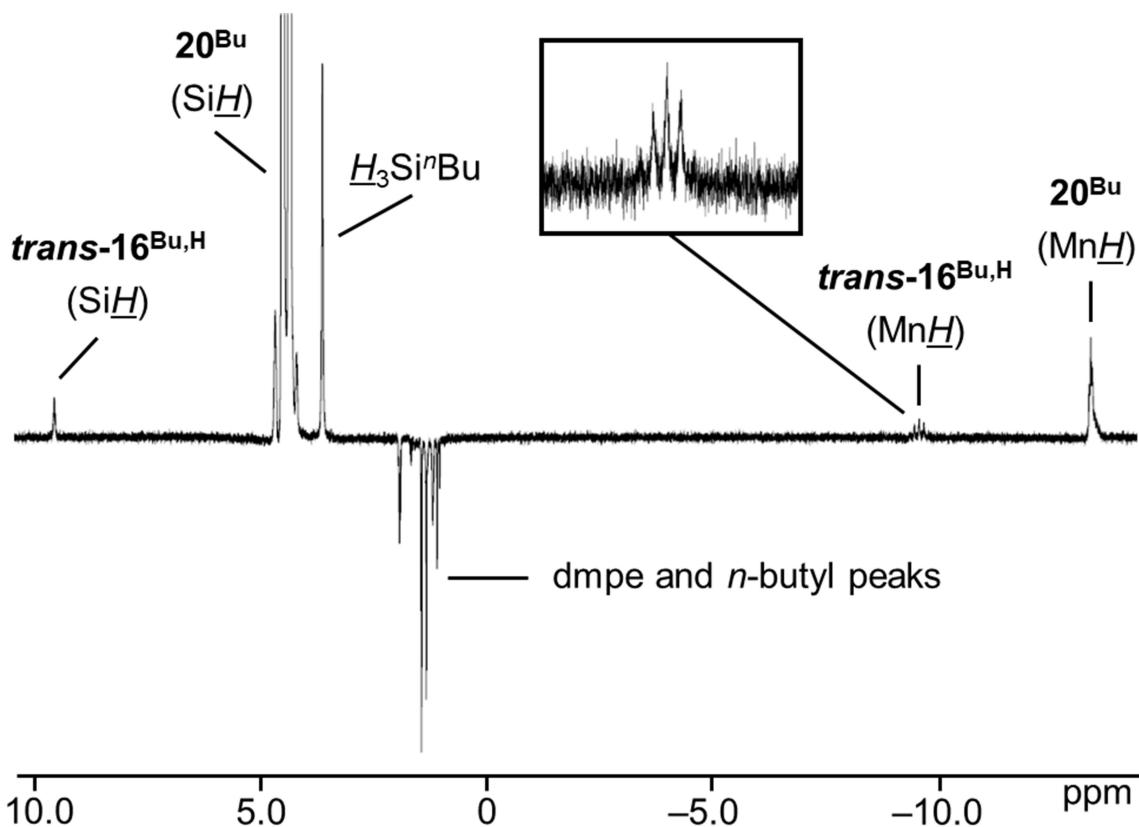
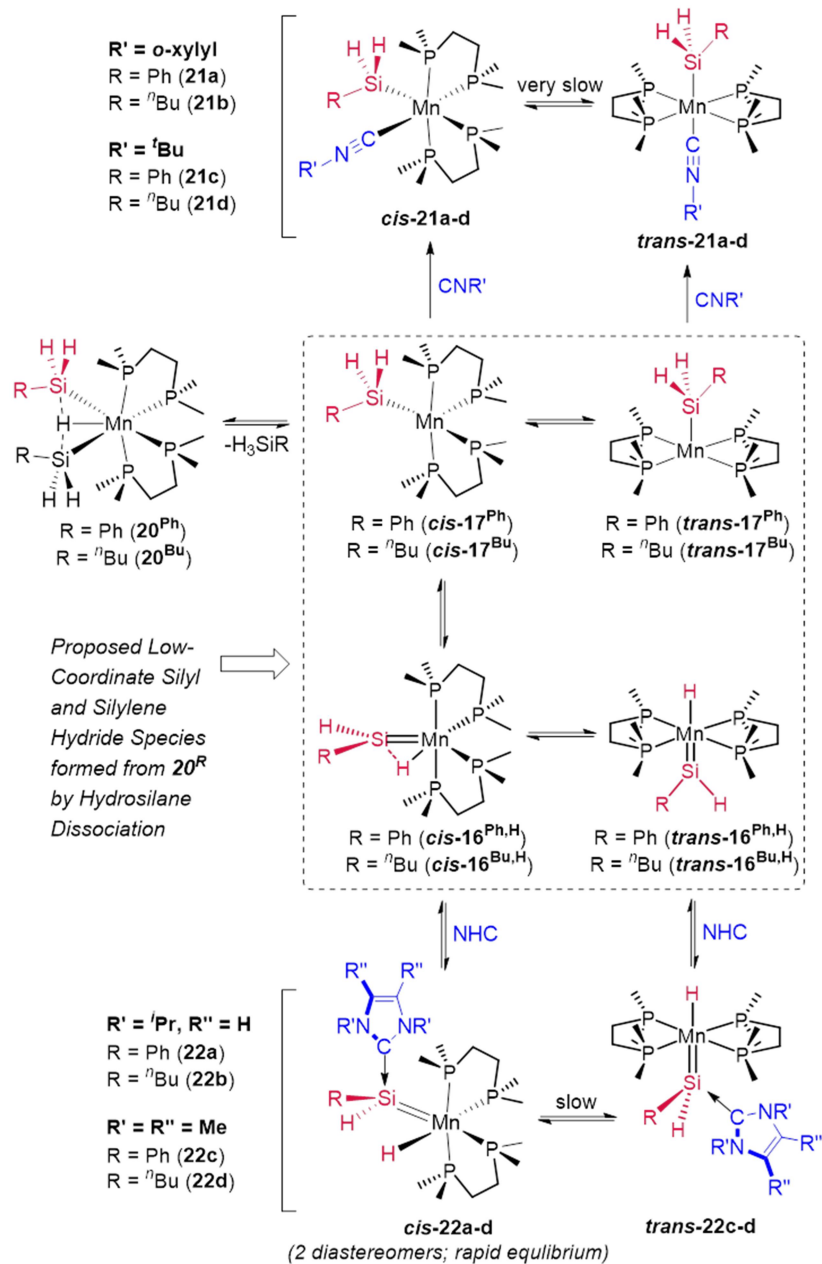


Figure 5.7: 1D NOESY/EXSY NMR spectrum of a solution of $[(\text{dmpe})_2\text{MnH}(\text{SiH}_2^n\text{Bu})_2]$ (20^{Bu}) at 335 K with excitation at the SiH signal of 20^{Bu} , showing chemical exchange between the SiH and MnH environments of $[(\text{dmpe})_2\text{MnH}(\text{SiH}_2^n\text{Bu})_2]$ (20^{Bu}) and *trans*- $[(\text{dmpe})_2\text{MnH}(=\text{SiH}^n\text{Bu})]$ (*trans*- $16^{\text{Bu,H}}$), and the SiH environment of free $\text{H}_3\text{Si}^n\text{Bu}$. Positive (EXSY) peaks are indicative of chemical exchange and negative (NOESY) peaks are indicative of through-space coupling (500 MHz, C_6D_6).

5.5 – Trapping Experiments with Isonitriles and *N*-Heterocyclic Carbenes

To provide experimental corroboration for the accessibility of 5-coordinate silyl $[(\text{dmpe})_2\text{Mn}(\text{SiH}_2\text{R})]$ (17^{Ph} : R = Ph, 17^{Bu} : R = ^nBu) and silylene hydride $[(\text{dmpe})_2\text{MnH}(=\text{SiHR})]$ ($16^{\text{Ph,H}}$: R = Ph, $16^{\text{Bu,H}}$: R = ^nBu) species from 20^{R} , reactions with neutral donor ligands were carried out, with a view towards coordination to manganese in 17^{R} or silicon in $16^{\text{R,H}}$ (Scheme 5.5).



Scheme 5.5: Trapping of putative silyl (**17^R**) and silylene hydride (**16^{R,H}**) intermediates: synthesis of silyl isonitrile complexes [(dmpe)₂Mn(SiH₂R)(CNR')] (**21a**: R = Ph, R' = *o*-xylyl; **21b**: R = ⁿBu, R' = *o*-xylyl; **21c**: R = Ph, R' = ^tBu; **21d**: R = ⁿBu, R' = ^tBu) and NHC-stabilized silylene hydride complexes [(dmpe)₂MnH{=SiHR(NHC)}] (**22a**: NHC = ⁱPrNHC, R = Ph; **22b**: NHC = ⁱPrNHC, R = ⁿBu; **22c**: NHC = ^{Me}NHC, R = Ph; **22d**: NHC = ^{Me}NHC, R = ⁿBu).

Addition of *o*-xylylN≡C or ^tBuN≡C to solutions of **20^R** resulted in hydrosilane elimination, and isolation of yellow or orange silyl isonitrile complexes [(dmpe)₂Mn(SiH₂R)(CNR')] {R' = *o*-xylyl, R = Ph (**21a**) or ⁿBu (**21b**); R' = ^tBu, R = Ph (**21c**) or ⁿBu (**21d**)}, effectively trapping silyl complexes **17^R** (Scheme 5.5). In solution, all four reactions initially led to mixtures of two complexes identified by NMR spectroscopy as *cis* (85-97%) and *trans* (3-15%) isomers of **21a-d**. Slow isomerization was observed between the *cis* and *trans* isomers of **21a-d** in solution, and unexpectedly, these isomerization reactions proceeded in the direction of the *trans* isomers at elevated temperature (resulting in an increase in the proportion of *trans* isomer to 44-74% after heating solutions containing exclusively the *cis* isomer at 65-80° for 4-21 days), and in the opposite direction upon leaving the same solutions at room temperature for 3 weeks (e.g. leaving *cis/trans* mixtures of **21a,b** containing 44-48% *trans* isomer at room temperature resulted in solutions containing 99% *cis* isomer after 3 weeks).

X-ray quality crystals were obtained for the four silyl isonitrile complexes **21a-d**, in each case as the *cis* isomer (Figure 5.8). All four structures are octahedral with Mn–Si distances of 2.3552(5)-2.3618(5) Å and Mn–C distances of 1.805(4)-1.847(3) Å. The isonitrile ligands show elongated C_{Mn}–N distances of 1.176(4)-1.225(9) Å and non-linear C–N–C angles of 159.2(8)-167.5(1)°, indicative of appreciable π-backbonding.

In contrast to reactions with isonitriles, reactions of disilyl hydride complexes **20^R** with 1,3-diisopropylimidazolin-2-ylidene (ⁱPrNHC) or 1,3,4,5-tetramethyl-4-imidazolin-2-ylidene (^{Me}NHC) afforded the base-stabilized silylene hydride complexes [(dmpe)₂MnH{=SiHR(NHC)}] {NHC = ⁱPrNHC, R = Ph (**22a**) or ⁿBu (**22b**); NHC = ^{Me}NHC, R = Ph (**22c**) or ⁿBu (**22d**)}, trapping the proposed silylene hydride species **16^{R,H}** (Scheme 5.5). Compounds **22b-d** were isolated as analytically pure red powders, whereas **22a** evaded purification.

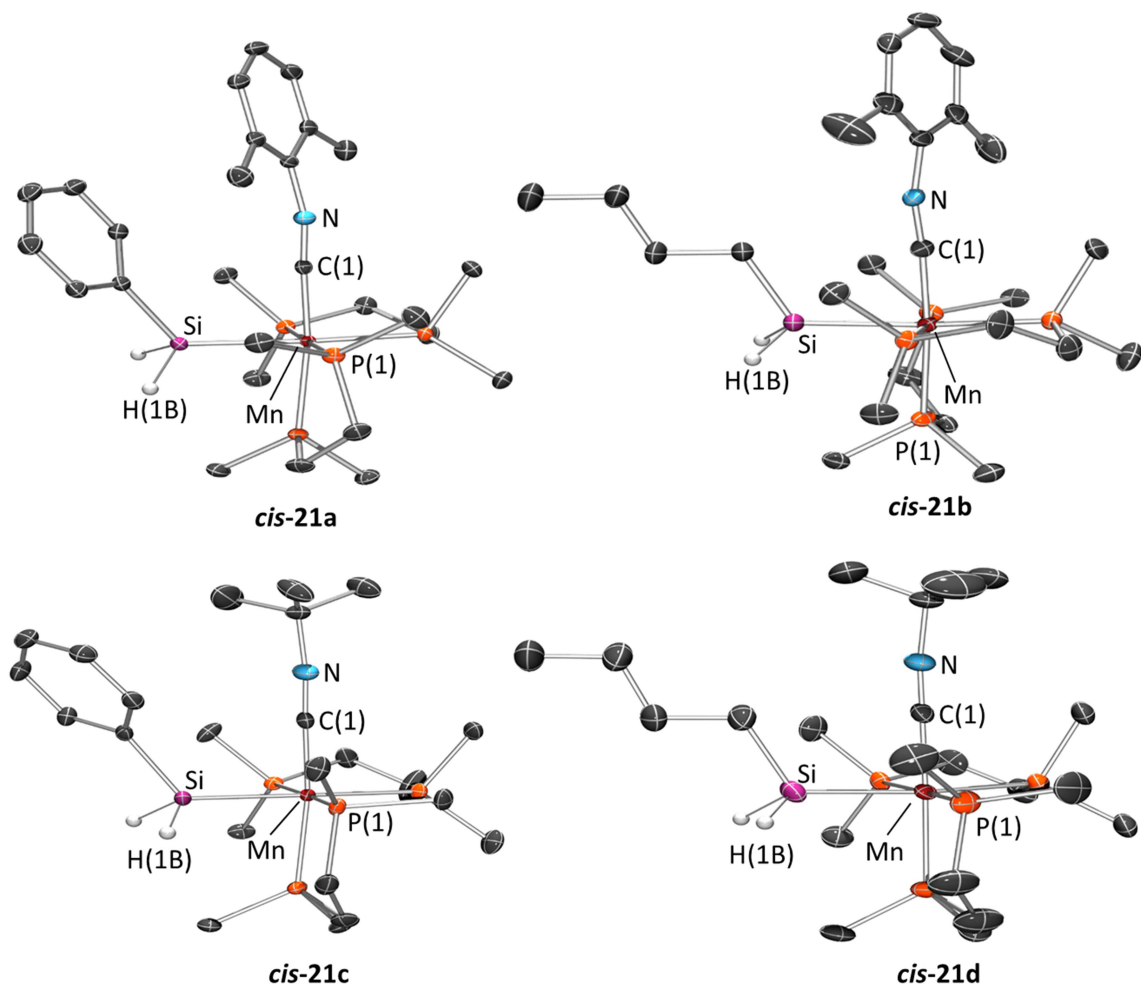


Figure 5.8: X-ray crystal structures of (top left) *cis*-[(dmpe)₂Mn(SiH₂Ph)(CN^xxylyl)] (*cis*-**21a**), (top right) *cis*-[(dmpe)₂Mn(SiH₂^tBu)(CN^xxylyl)] (*cis*-**21b**), (bottom left) *cis*-[(dmpe)₂Mn(SiH₂Ph)(CN^tBu)] (*cis*-**21c**), and (bottom right) *cis*-[(dmpe)₂Mn(SiH₂^tBu)(CN^tBu)] (*cis*-**21d**), with ellipsoids drawn at 50% probability. Hydrogen atoms on Si were located from the difference map and refined isotropically, and all other hydrogen atoms have been omitted for clarity. In the case of *cis*-**21a**, the dmpe ligands are disordered over two positions, and only the dominant (95%) are shown. In the case of *cis*-**21b**, the dmpe ligands and N atom are disordered (one dmpe and the N atom over two positions and the other dmpe over three), and only the dominant conformation (66% for the dmpe ligands, and 72% for N) is shown. In the case of *cis*-**21c**, the unit cell contains two independent and essentially isostructural molecules (one of

which has been shown) both of which have one dmpe ligand disordered over two positions and the other over three, and only the dominant conformation (96% and 81%) is shown. In the case of *cis-21d*, the unit cell contains two independent and essentially isostructural molecules both of which have one dmpe ligand disordered over two positions and the other over three, and one has both butyl groups disordered and only the structure without butyl disorder is shown with the dominant (62%) dmpe configuration. Atom labels with suffixes correspond to those without suffixes in conformations or molecules not shown. For *cis-21a*, bond distances (Å) and angles (deg): Mn–Si 2.3618(5), Mn–C(1) 1.820(1), C(1)–N(1) 1.200(1), N(1)–C(2) 1.386(1), Si–H(1A) 1.45(1), Si–H(1B) 1.47(2), Si–C(10) 1.920(1), Mn–C(1)–N(1) 176.3(1), C(1)–N(1)–C(2) 167.5(1), Mn–Si–C(10) 123.66(4), Mn–Si–H(1A) 115.9(7), Mn–Si–H(1B) 115.5(7). For *cis-21b*, bond distances (Å) and angles (deg): Mn–Si 2.360(1), Mn–C(1) 1.805(4), C(1)–N(1) 1.225(9), C(1)–N(1A) 1.22(2), N(1)–C(2) 1.394(9), N(1A)–C(2) 1.39(2), Si–C(10) 1.910(4), Si–H(1A) 1.40(6), Si–H(1B) 1.48(5), Mn–C(1)–N(1) 173.1(5), Mn–C(1)–N(1A) 166(1), C(1)–N(1)–C(2) 159.2(8), C(1)–N(1A)–C(2) 161(2), Mn–Si–C(10) 118.7(2), Mn–Si–H(1A) 118(2), Mn–Si–H(1B) 115(2). For *cis-21c*, bond distances (Å) and angles (deg): Mn(1)–Si(1) 2.3562(7), Mn(1C)–Si(1C) 2.3568(7), Mn(1)–C(1) 1.841(2), Mn(1C)–C(1C) 1.847(3), C(1)–N(1) 1.181(4), C(1C)–N(1C) 1.176(4), N(1)–C(2) 1.442(4), N(1C)–C(2C) 1.441(4), Si(1)–C(6) 1.920(3), Si(1C)–C(6C) 1.925(3), Si(1)–H(1A) 1.46(3), Si(1)–H(1B) 1.45(4), Si(1C)–H(1CA) 1.39(4), Si(1C)–H(1CB) 1.44(3), Mn(1)–C(1)–N(1) 177.7(2), Mn(1C)–C(1C)–N(1C) 177.4(2), C(1)–N(1)–C(2) 167.4(3), C(1C)–N(1C)–C(2C) 172.6(3), Mn(1)–Si(1)–C(6) 124.08(8), Mn(1C)–Si(1C)–C(6C) 123.54(8), Mn(1)–Si(1)–H(1A) 117(1), Mn(1)–Si(1)–H(1B) 116(2), Mn(1C)–Si(1C)–H(1CA) 114(2), Mn(1C)–Si(1C)–H(1CB) 117(1). For *cis-21d*, bond distances (Å) and angles (deg): Mn(1)–Si(1) 2.3551(5), Mn(1C)–Si(1C) 2.3559(7), Mn(1)–C(1) 1.838(2), Mn(1C)–C(1C) 1.828(2), Si(1)–C(6) 1.914(2), Si(1C)–C(6C) 1.930(3), Si(1C)–C(6D) 1.88(1), Si(1)–H(1A) 1.48(2), Si(1)–H(1B) 1.42(3), Si(1C)–H(1CA) 1.44(2), Si(1C)–H(1CB) 1.46(2).

A variety of NHC-stabilized silylene complexes have been reported for V, Cr, W, Fe, Co, Rh, and Ni (see Section 1.6.7), and relative to base-free silylene complexes, they

feature longer metal–silicon bond distances, pyramidalization at silicon, and lower frequency ^{29}Si NMR chemical shifts (typically 25-100 ppm,^{kk} compared with > 200 ppm for base-stabilized silylene complexes).³⁰⁴

Room temperature NMR spectra of $^{i\text{Pr}}\text{NHC}$ adducts **22a,b** revealed two sets of broad NMR signals in the process of coalescence/decoalescence, due to a pair of rapidly interconverting isomers. Cooling the solutions afforded two sets of well resolved NMR signals corresponding to compounds with a disphenoidal arrangement of the phosphorus donor atoms, each with a single $\text{Si}\underline{H}$ signal (5.1 to 6.4 ppm), a single $\text{Mn}\underline{H}$ resonance (–12.3 to –12.6 ppm), a single ^{29}Si NMR environment (22.2 to 29.6 ppm), and four unique ^{31}P NMR environments (65.6-81.9 ppm). These data are indicative of NHC-coordinated *cis* silylene hydride complexes existing as a pair of interconverting diastereomers (due to chirality at Si and Mn).

In contrast, NMR spectra of the $^{\text{Me}}\text{NHC}$ silylene hydride complexes (**22c,d**) revealed the same two rapidly interconverting *cis* diastereomers plus a third isomer which afforded a sharp set of ^1H and ^{31}P NMR signals at room temperature. This third isomer corresponds to an NHC-coordinated *trans* silylene hydride complex, as evidenced by a single $\text{Mn}\underline{H}$ (–14.9 or –15.0 ppm) signal with a pentet coupling pattern ($^2J_{\text{H,P}} = 48\text{-}49$ Hz) and two sharp signals in the $^{31}\text{P}\{^1\text{H}\}$ NMR spectra (78.7-80.6 ppm) due to diastereotopic phosphorus atoms. The ^1H NMR $\text{Si}\underline{H}$ and ^{29}Si NMR chemical shifts in these *trans* isomers (4.9-5.8 ppm and 22.4 ppm, respectively)^{ll} are similar to those in the *cis* isomers.

At 335 K, the two *cis* diastereomers of **22a-d** gave rise to a single set of averaged signals, with the $\text{Mn}\underline{H}$ peak at –12.5 to –12.7 ppm (pentets for *cis*-**22a,c,d** with $^2J_{\text{H,P}} = 32\text{-}34$ Hz, while the NMR spectrum of **22b** remained a broad singlet in the process of

^{kk} A handful of NHC-stabilized silylene complexes have also been reported with ^{29}Si chemical shifts lower than 25 ppm (see ref. 354-357), and this has been rationalized by adoption of a zwitterionic bonding motif which results in limited π -backdonation to the Si centre from the metal (see ref. 357).

^{ll} We could not determine the ^{29}Si NMR chemical shift of *trans*-**22c** due to the low proportion of *trans* isomer in solution (*cis* : *trans* ratio of 14 : 1).

coalescence), accompanied by (in solutions of **22c,d** only) a set of sharp signals for the *trans* isomer. For **22c,d**, EXSY NMR spectroscopy at 335 K showed cross peaks between the MnH and SiH ^1H NMR signals due to both the *cis* and *trans* isomers (i.e. chemical exchange between all *four* environments). This equilibrium between *cis*- and *trans*-**22c,d** mirrors that discussed in Chapter 4 between the *cis* and *trans* isomers of base-free $[(\text{dmpe})_2\text{MnH}(=\text{SiPh}_2)]$ (**16^{Ph2}**).

Possible mechanisms for ambient temperature exchange between the *cis* diastereomers of **22a-d** are (a) phosphine donor dissociation, isomerization of the 5-coordinate product, and phosphine re-coordination, or (b) NHC dissociation to generate *cis*- $[(\text{dmpe})_2\text{MnH}(=\text{SiHR})]$ (*cis*-**16^{Ph,H}**: R = Ph, *cis*-**16^{Bu,H}**: R = ⁿBu), followed by re-coordination to the opposite face of the silylene ligand.^{mmm} The latter mechanism would imply that **22a-d**, like disilyl hydride complexes **20^R**, could react as sources of either base-free silylene hydride complexes **16^{R,H}**, or 5-coordinate silyl complexes **17^R**. The accessibility of this pathway is implied by the reactions of **22d** with ^tBuNC, and **22b** with ethylene, which afforded $[(\text{dmpe})_2\text{Mn}(\text{SiH}_2^{\text{nBu}})(\text{CN}^{\text{tBu}})]$ (**21d**) and $[(\text{dmpe})_2\text{MnH}(\text{nBuHSi}=\text{CHMe})]$ (**19^{Bu,H}**),ⁿⁿ respectively; these are the same complexes formed in reactions of these reagents with **20^{Bu}**. Furthermore, the accessibility of **17^R** provides a mechanism for the observed exchange between the SiH and MnH environments in the EXSY NMR spectra of **22c,d** at 335 K (*vide supra*).

^{mmm} The lability of NHCs in **22a-d** was also illustrated by initial generation of mixtures of reagents and products upon addition of free NHCs to **20^R**; complete conversion to **22a-d** required removal of the free hydrosilane byproducts. For **22b-d**, this was achieved by periodically removing all solvent and hydrosilane byproducts *in vacuo*. By contrast, for **22a** this was achieved by the reaction of the H_3SiPh byproduct with excess ^{iPr}NHC to form 1-phenyl-2,5-diisopropyl-3,4-dehydro-2,5-diazasilinane; this reaction has previously been reported at 100 °C (see ref. 511), and in our hands 98% conversion was observed after 24 h at 55 °C (consistent with the reaction conditions involved in the synthesis of **22a**).

ⁿⁿ Unlike the reaction of **20^{Bu}** with ethylene, the reaction of **22b** with ethylene does not generate $\text{H}_3\text{Si}^{\text{nBu}}$ as a byproduct, and under these conditions, complex **19^{Bu,H}** reacted readily with a further equivalent of ethylene, so that both **19^{Bu,H}** and **19^{Bu,Et}** were formed concurrently.

X-ray quality crystals were obtained for complexes **22a-d** by recrystallization from concentrated hexanes solutions (**22a,b**), toluene layered with pentane (**22c**), or a dilute hexanes solution (**22d**) at $-30\text{ }^{\circ}\text{C}$. The solid state structures of **22a-c** (Figure 5.9; top row and bottom left) feature a *cis* arrangement of the hydride and base-stabilized silylene ligands, corresponding to one of the two *cis* diastereomers observed in solution.^{oo} By contrast, **22d** crystallized as the *trans* isomer (Figure 5.9; bottom right). In all four structures {complementary DFT calculations modelled **22b,d** with an *n*Bu group in place of the Et group; [(dmpe)₂MnH{=SiHEt(NHC)}] where NHC = *i*PrNHC (**22b***) or ^{Me}NHC (**22d***)}, NHC coordination to silicon resulted in elongated Mn–Si distances (2.255(1)-2.299(1) Å; calcd. 2.26-2.30 Å for both isomers of **22a,b*,c,d***), and correspondingly weaker Mayer bond orders of 1.03-1.08, relative to base-free silylene complexes **16^{R,H}** (2.16-2.20 Å and 1.17-1.57, respectively). Unlike base-free analogues (*vide supra*), *cis*-**22a-d** display only negligible interligand Si–H interactions (with Mayer bond orders ≤ 0.13). Additionally, substantial pyramidalization at silicon was observed for both isomers of **22a-d**, where the sum of the angles around silicon (for non-NHC substituents) ranged from 322(3) to 342(2) $^{\circ}$ (calcd. 336.1-341.5 $^{\circ}$; cf. $> 356^{\circ}$ in **16^{R,H}**). Nevertheless, the Mn–Si distances are significantly shorter than those in related silyl complexes **21a-d** (the Mn–Si distances in **21a-d** range from 2.3552(5)-2.3618(5) Å {calcd. 2.35-2.36 Å (*cis*) and 2.41-2.42 Å (*trans*)}, with Mayer bond orders of 0.89-0.93}),^{pp} indicative of residual Mn–Si multiple bond character in **22a-d**.

^{oo} In the structures of *cis*-**22a,b**, the dmpe ligands are disordered, and modelling this disorder allowed the structures of both diastereomers observed in solution to be elucidated.

^{pp} **21b,d** were computationally modelled with Et groups in place of *n*Bu groups; [(dmpe)₂Mn(SiH₂Et)(CNR)] (**21b***: R = *o*-xylyl, **21d***: R = *t*Bu).

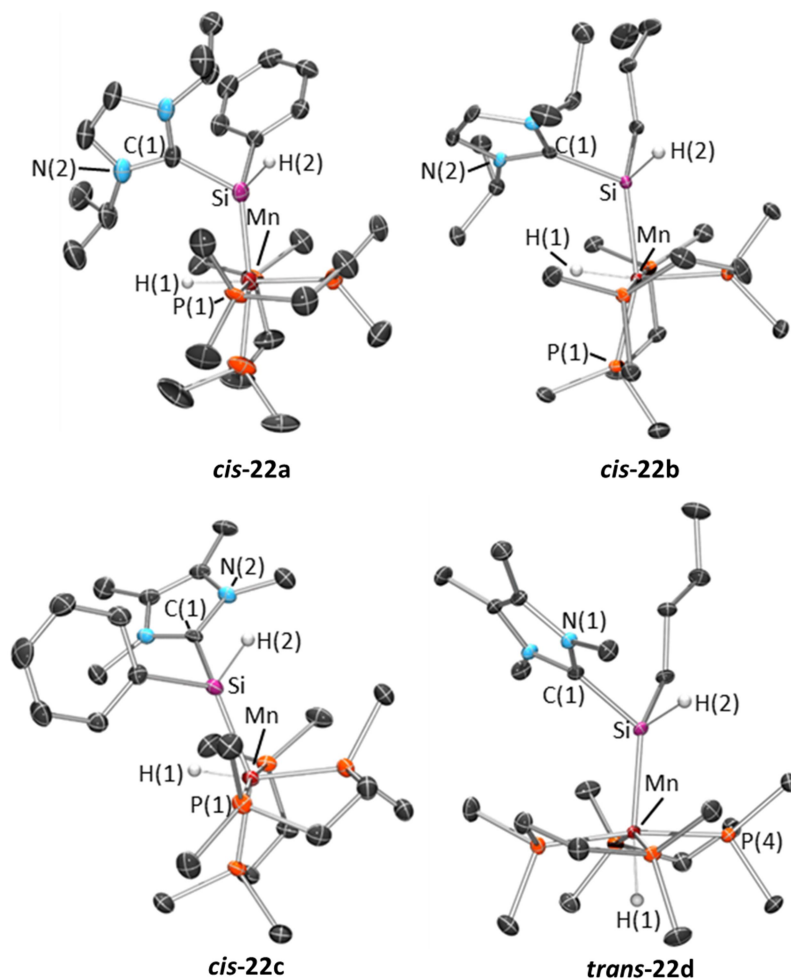
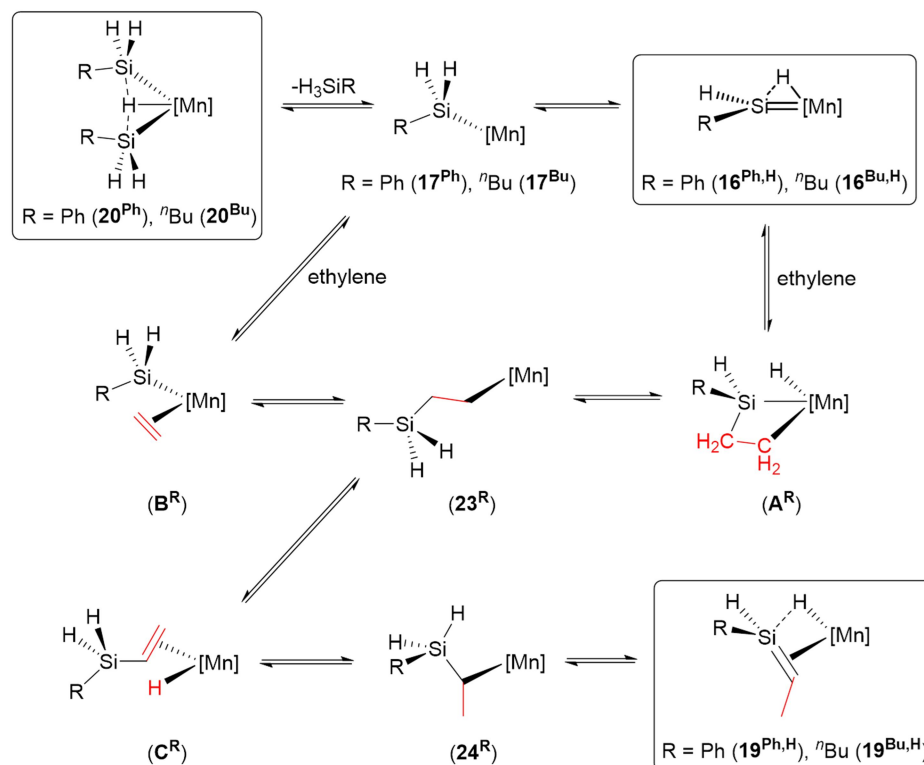


Figure 5.9: X-ray crystal structures of (top left) *cis*-[(dmpe)₂MnH{=SiHPh(ⁱPrNHC)}] (*cis*-22a), (top right) *cis*-[(dmpe)₂MnH{=SiHⁿBu(ⁱPrNHC)}] (*cis*-22b), (bottom left) *cis*-[(dmpe)₂MnH{=SiHPh(^{Me}NHC)}] (*cis*-22c), and (bottom right) *trans*-[(dmpe)₂MnH{=SiHⁿBu(^{Me}NHC)}] (*trans*-22d) with ellipsoids drawn at 50% probability. Hydrogen atoms on Mn and Si were located from the difference map and refined isotropically, and all others have been omitted for clarity. In the case of *cis*-22a, the dmpe ligands are disordered over 3 positions, the dominant (51%) of which is shown. In the case of *cis*-22b, the dmpe ligands are disordered over 2 positions, the dominant (95%) of which is shown. For *cis*-22a, bond distances (Å) and angles (deg): Mn–Si 2.292(2), Mn–H(1) 1.58(6), Si–C(1) 2.004(6), Si–C(10) 1.954(5), Si–H(2) 1.49(5), H(1)–Mn–Si 86(2), Mn–Si–C(10) 133.0(2), Mn–Si–H(2) 118(2), Mn–Si–C(1) 122.9(2). For *cis*-22b, bond

distances (Å) and angles (deg): Mn–Si 2.299(1), Mn–H(1) 1.45(2), Si–C(1) 1.994(3), Si–C(10) 1.927(3), Si–H(2) 1.43(3), H(1)–Mn–Si 78(1), Mn–Si–C(10) 125.15(9), Mn–Si–H(2) 120(1), Mn–Si–C(1) 118.47(8). For *cis*-**22c**, bond distances (Å) and angles (deg): Mn–Si 2.255(1), Mn–H(1) 1.29(3), Si–C(1) 1.956(4), Si–C(8) 1.939(4), Si–H(2) 1.51(3), H(1)–Mn–Si 62(1), Mn–Si–C(8) 121.6(1), Mn–Si–H(2) 124(1), Mn–Si–C(1) 121.3(1). For *trans*-**22d**, bond distances (Å) and angles (deg): Mn–Si 2.2956(6), Mn–H(1) 1.52(3), Si–C(1) 1.985(1), Si–C(8) 1.948(2), Si–H(2) 1.46(1), H(1)–Mn–Si 173.0(9), Mn–Si–C(8) 125.96(5), Mn–Si–H(2) 119.4(7), Mn–Si–C(1) 125.70(4), Σ P–Mn–P (cis only) 356.93(4).

5.6 – Pathways for Reactions of **20^R** with Ethylene

In Chapter 4, we showed that the silylene hydride complexes, [(dmpe)₂MnH(=SiR₂)] (**16^{Ph2}**: R = Ph, **16^{Et2}**: R = Et), react with ethylene to form the silene hydride complexes [(dmpe)₂MnH(R₂Si=CHMe)] (**19^{Ph2}**: R = Ph, **19^{Et2}**: R = Et), potentially via a 5-coordinate silyl isomer. Given that disilyl hydride complexes **20^R** exist in equilibrium with analogous low-coordinate silyl and silylene hydride complexes (*vide supra*), it is likely that the reactions of **20^R** with ethylene proceed via a parallel mechanism, as illustrated in Scheme 5.6. The initial steps in this scheme involve either (a) ethylene coordination to a silylene hydride intermediate (**16^{R,H}**) followed by 2+2 cycloaddition (to form **A^R**) and subsequent Si–H bond-forming reductive elimination, or (b) coordination of ethylene to a low coordinate silyl intermediate (**17^R**), forming **B^R**, followed by 1,2-insertion. Both of these pathways generate primary alkyl complex **23^R**, which can provide access to **19^{R,H}** by sequential β -hydride elimination (to form **C^R**), 1,2-insertion to generate secondary alkyl complex **24^R**, and a second β -hydride elimination involving the hydrogen substituent on silicon. Consistent with this mechanism, the reactions of [(dmpe)₂MnH(SiH₂ⁿBu)₂] (**20^{Bu}**) or [(dmpe)₂Mn{=SiHⁿBu(ⁱPrNHC)}] (**22b**) with *d*₄-ethylene yielded [(dmpe)₂MnH(ⁿBuHSi=CDCD₃)] as the only observed isotopomer of **19^{Bu,H}**.

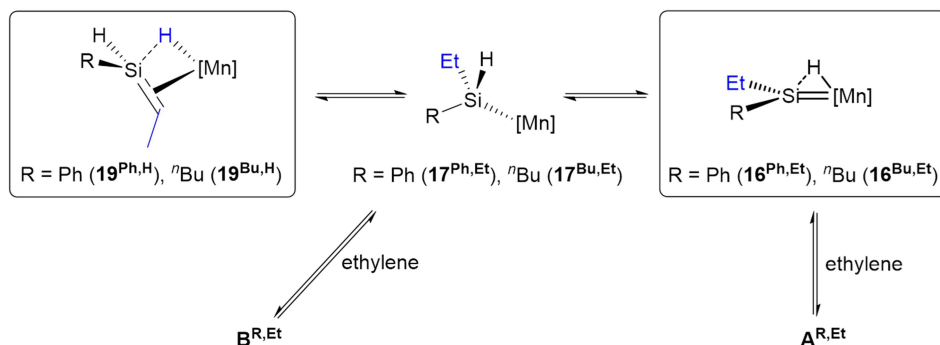


Scheme 5.6: Proposed pathways for reactions of disilyl hydride complexes $[(\text{dmpe})_2\text{MnH}(\text{SiH}_2\text{R})_2]$ (20^{Ph} : $R = \text{Ph}$, 20^{Bu} : $R = n\text{Bu}$) with ethylene to form silene hydride complexes $[(\text{dmpe})_2\text{MnH}(\text{RHSi}=\text{CHMe})]$ ($19^{\text{Ph,H}}$; $R = \text{Ph}$, $19^{\text{Bu,H}}$: $R = n\text{Bu}$). $[\text{Mn}] = \text{Mn}(\text{dmpe})_2$. Only one isomer of $16^{\text{R,H}}$ is shown. Boxes indicate complexes which have been isolated or spectroscopically observed.

After conversion of 20^R to $19^{\text{R,H}}$, reaction with a second equivalent of ethylene resulted in conversion of a silene SiH group in $19^{\text{R,H}}$ to an SiEt group, yielding $19^{\text{R,Et}}$ (*vide supra*). This reactivity likely involves the experimentally observed isomerization of $19^{\text{R,H}}$ to silylenes $16^{\text{R,Et}}$ (*vide supra*), presumably via a low-coordinate silyl intermediate ($17^{\text{R,Et}}$ in Scheme 5.7) formed from $19^{\text{R,H}}$ by C–H bond-forming 1,2-insertion. Conversion to $19^{\text{R,Et}}$ can then take place via previously discussed pathways (Scheme 5.6) involving reactions of the silylene or low-coordinate silyl species with ethylene to afford

intermediates $\mathbf{A}^{\text{R,Et}}$ and $\mathbf{B}^{\text{R,Et}}$, respectively ($\mathbf{A}^{\text{R,Et}}$ and $\mathbf{B}^{\text{R,Et}}$ are analogues of \mathbf{A}^{R} and \mathbf{B}^{R} in Scheme 5.6, but with an ethyl group in place of one hydrogen atom on silicon).^{9q}

Deuterium labelling studies were employed to provide experimental support for these mechanistic proposals. Specifically, $[(\text{dmpe})_2\text{MnH}(^n\text{BuHSi}=\text{CDCD}_3)]$ ($d_4\text{-}\mathbf{19}^{\text{Bu,H}}$) isomerized to exclusively form *trans*- $[(\text{dmpe})_2\text{MnH}(=\text{Si}^n\text{Bu}(\text{CHDCD}_3))] (trans\text{-}d_4\text{-}\mathbf{16}^{\text{Bu,Et}})$, and the reaction of $[(\text{dmpe})_2\text{MnH}(^n\text{BuHSi}=\text{CHMe})]$ ($\mathbf{19}^{\text{Bu,H}}$) with d_4 -ethylene yielded $[(\text{dmpe})_2\text{MnH}(^n\text{BuEtSi}=\text{CDCD}_3)]$ ($d_4\text{-}\mathbf{19}^{\text{Bu,Et}}$). Additionally, $[(\text{dmpe})_2\text{MnH}(=\text{SiEt}_2)]$ ($\mathbf{16}^{\text{Et}_2}$) exclusively forms $[(\text{dmpe})_2\text{MnH}(\text{Et}_2\text{Si}=\text{CDCD}_3)]$ ($d_4\text{-}\mathbf{19}^{\text{Et}_2}$) upon exposure to d_4 -ethylene (see Chapter 4).



Scheme 5.7: Initial steps in the pathway proposed for reactions of silene hydride complexes $[(\text{dmpe})_2\text{MnH}(\text{RHSi}=\text{CHMe})]$ ($\mathbf{19}^{\text{Ph,H}}$; R = Ph, $\mathbf{19}^{\text{Bu,H}}$: R = ^nBu) with ethylene to afford $[(\text{dmpe})_2\text{MnH}(\text{REtSi}=\text{CHMe})]$ ($\mathbf{19}^{\text{Ph,Et}}$; R = Ph, $\mathbf{19}^{\text{Bu,Et}}$: R = ^nBu). $[\text{Mn}] = \text{Mn}(\text{dmpe})_2$. Intermediates $\mathbf{A}^{\text{R,Et}}$ and $\mathbf{B}^{\text{R,Et}}$ are analogous to intermediates \mathbf{A}^{R} and \mathbf{B}^{R} in Scheme 5.6, but with an ethyl group in place of one hydrogen atom on silicon. Only one isomer of $\mathbf{16}^{\text{R,Et}}$ is shown. Boxes indicate complexes which have been isolated or spectroscopically observed.

^{9q} Alternative pathways requiring initial dissociation of a phosphine donor in $\mathbf{19}^{\text{R,H}}$ followed by ethylene coordination (with subsequent oxidative coupling or 1,2-insertion reactivity) cannot be ruled out.

5.7 – Summary and Conclusions for Chapter 5

$[(\text{dmpe})_2\text{MnH}(\text{C}_2\text{H}_4)]$ (**10**) reacted with two equivalents of primary hydrosilanes to generate disilyl hydride complexes $[(\text{dmpe})_2\text{MnH}(\text{SiH}_2\text{R})_2]$ (**20^{Ph}**: R = Ph, **20^{Bu}**: R = ⁿBu), presumably via a 5-coordinate ethyl intermediate $[(\text{dmpe})_2\text{MnEt}]$ (**13**). Crystallographic and NMR characterization of **20^R** suggests the presence of nonclassical Si–H interligand interactions. These are the first reported manganese disilyl hydride complexes where the Si donors are not chelating.

The disilyl hydride manganese complexes **20^R** reversibly dissociate H_3SiR to access low-coordinate silyl ($[(\text{dmpe})_2\text{Mn}(\text{SiH}_2\text{R})]$; **17^R**) and silylene hydride ($[(\text{dmpe})_2\text{MnH}(\text{=SiHR})]$; **16^{R,H}**) complexes. The *trans* isomers of the silylene hydride complexes were observed in small amounts (< 5% relative to the disilyl hydride) by NMR spectroscopy at 335 K, and are the first spectroscopically observed examples of group 7 $\text{L}_x\text{M}=\text{SiHR}$ compounds. DFT calculations support the thermodynamic accessibility of *cis*- and *trans*- isomers of these low coordinate silyl and silylene species, and both sets of intermediates were trapped by coordination of isocyanides (to manganese) or *N*-heterocyclic carbenes (to silicon).

The reactivity of **20^R** with ethylene was investigated, affording silene hydride complexes $[(\text{dmpe})_2\text{MnH}(\text{RHSi}=\text{CHMe})]$ (**19^{R,H}**). This reaction represents a unique method to access silene complexes (analogous to reactions of ethylene with $[(\text{dmpe})_2\text{MnH}(\text{=SiR}_2)]$ compounds discussed in Chapter 4), and the resulting silene complexes are the first spectroscopically observed transition metal examples with an *SiH* substituent. As such, they displayed unusual reactivity: for example, **19^{Bu,H}** slowly converted to a more stable silylene hydride isomer, $[(\text{dmpe})_2\text{MnH}(\text{=SiEt}^n\text{Bu})]$ (**16^{Bu,Et}**); the first example of isomerization of a silene hydride complex to a silylene hydride complex. Furthermore, **19^{R,H}** reacted with a second equivalent of ethylene to convert the *SiH* substituent to an *SiEt* substituent, which is an unprecedented transformation for a silene ligand.

Chapter 6

Manganese Silyl Dihydride Complexes: A Spectroscopic, Crystallographic and Computational Study of Nonclassical Silicate and Hydrosilane Hydride Isomers

Portions of this chapter have been reprinted (adapted) with permission from Price, J. S.; Emslie, D. J. H.; Berno, B. Manganese Silyl Dihydride Complexes: A Spectroscopic, Crystallographic, and Computational Study of Nonclassical Silicate and Hydrosilane Hydride Isomers, *Organometallics* **2019**, *38*, 2347-2362. Copyright 2019 American Chemical Society.

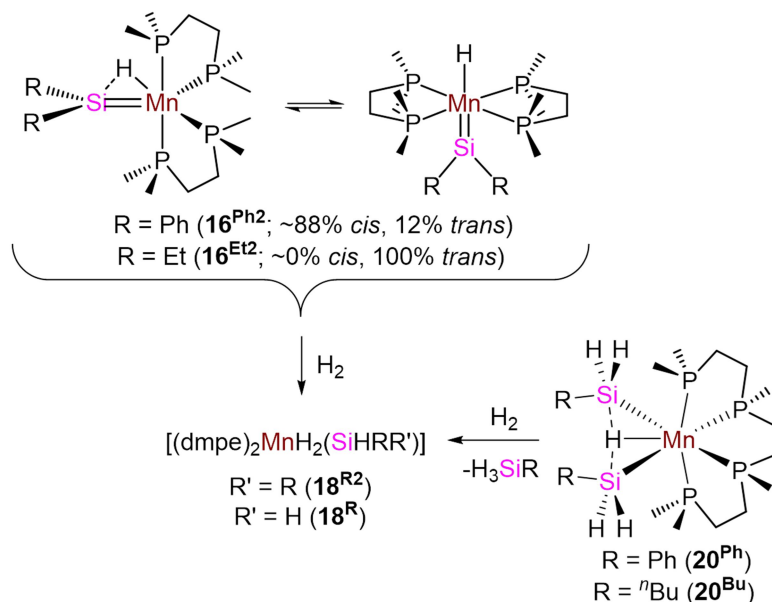
6.1 – Introduction to Chapter 6

Section 1.5.5 provided a brief introduction to ‘nonclassical’ hydrosilane complexes and silicate (H_2SiR_3^-) complexes, both of which involve substantial but incomplete Si–H bond oxidative addition. These complexes are notable for containing significant interactions between MnSi and MnH environments, which can be evaluated crystallographically (by the Si–H distance; albeit with low accuracy when measured by XRD) and spectroscopically (e.g. using the ^{29}Si – ^1H coupling constant, although proper interpretation of the NMR data requires knowledge of both the magnitude and sign of $J_{\text{Si,H}}$).

Chapter 4 briefly noted that silyl dihydride complex $[(\text{dmpe})_2\text{MnH}_2(\text{SiHPh}_2)]$ (**18^{Ph2}**) was formed as a byproduct in the synthesis of the silylene hydride complex $[(\text{dmpe})_2\text{MnH}(\text{=SiPh}_2)]$ (**16^{Ph2}**), and that silyl dihydride complexes **18^{Ph2}** and $[(\text{dmpe})_2\text{MnH}_2(\text{SiHEt}_2)]$ (**18^{Et2}**) could be prepared pure by exposure of silylene hydride complexes to H_2 . Herein we discuss the synthesis and characterization of the silyl dihydride complexes **18^{R2}** and $[(\text{dmpe})_2\text{MnH}_2(\text{SiH}_2\text{R})]$ {R = Ph (**18^{Ph}**), R = ⁿBu (**18^{Bu}**)}, with an examination of the nature of Si–H interactions in different geometric isomers via NMR spectroscopy (including determination of the sign and magnitude of $J_{\text{Si,H}}$) combined with X-ray diffraction and DFT calculations.

6.2 – Synthesis of Silyl Dihydride Complexes

Both silylene hydride complexes $[(\text{dmpe})_2\text{MnH}(=\text{SiR}_2)]$ ($\mathbf{16}^{\text{Ph}2}$: R = Ph, $\mathbf{16}^{\text{Et}2}$: R = Et; see Chapter 4 for synthesis and characterization) and disilyl hydride complexes $[(\text{dmpe})_2\text{MnH}(\text{SiH}_2\text{R})_2]$ ($\mathbf{20}^{\text{Ph}}$: R = Ph, $\mathbf{20}^{\text{Bu}}$: R = n Bu; see Chapter 5 for synthesis and characterization) reacted with H_2 to afford a family of silyl dihydride complexes $[(\text{dmpe})_2\text{MnH}_2(\text{SiHRR}')]^{\dagger}$ ($\mathbf{18}^{\text{Ph}2}$: R = R' = Ph; $\mathbf{18}^{\text{Et}2}$: R = R' = Et; $\mathbf{18}^{\text{Ph}}$: R = Ph, R' = H; $\mathbf{18}^{\text{Bu}}$: R = n Bu, R' = H) differing in the number and nature of the hydrocarbyl substituents on silicon (Scheme 6.1). Both of these reactions presumably proceed via a low-coordinate silyl intermediate $[(\text{dmpe})_2\text{Mn}(\text{SiH}_{3-x}\text{R}_x)]$ ($\mathbf{17}$), generated either by 1,1-insertion from silylene hydride complexes $\mathbf{16}^{\text{R}2}$, or hydrosilane reductive elimination from disilyl hydride complexes $\mathbf{20}^{\text{R}}$ (see Chapter 5 for a discussion of the accessibility of $\mathbf{17}$ from $\mathbf{20}^{\text{R}}$). Thermal decomposition of $\mathbf{20}^{\text{R}}$ (12 h at 90 °C) also yielded $\mathbf{18}^{\text{R}}$ as the dominant manganese complexes in solution, accompanied by H_2SiR_2 (R = Ph or n Bu) and other unidentified products, although the mechanism for this reaction is unknown.



Scheme 6.1: Syntheses of $[(\text{dmpe})_2\text{MnH}_2(\text{SiHR}_2)]$ {R = Ph ($\mathbf{18}^{\text{Ph}2}$), R = Et ($\mathbf{18}^{\text{Et}2}$)} and $[(\text{dmpe})_2\text{MnH}_2(\text{SiH}_2\text{R})]$ {R = Ph ($\mathbf{18}^{\text{Ph}}$), R = n Bu ($\mathbf{18}^{\text{Bu}}$)}.

6.3 – 1D NMR Characterization of Silyl Dihydride Complexes

Room temperature solution NMR spectra (^1H , ^{13}C , and ^{31}P)^{rr} of **18** display very broad signals indicative of multiple isomers in rapid equilibrium. However, upon cooling, NMR spectra corresponding to both a low symmetry (apparent C_2 symmetry) and a high symmetry (apparent C_{2v} symmetry) isomer were observed (shown for **18^R** in Figure 6.1).

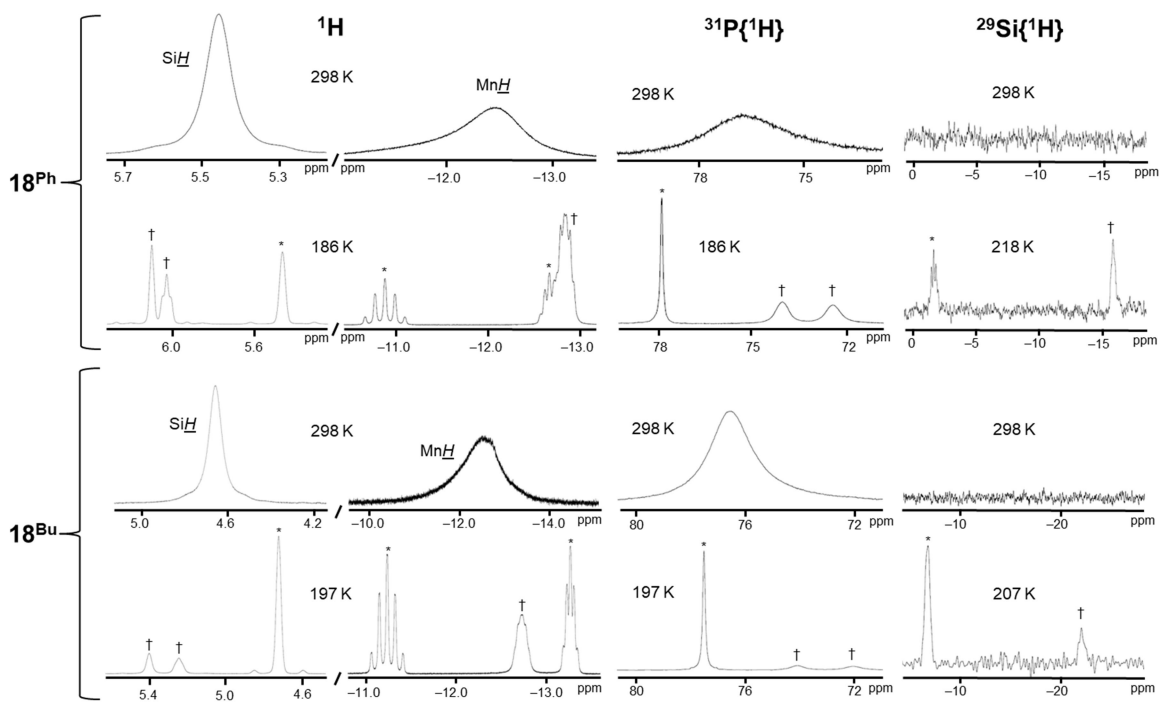
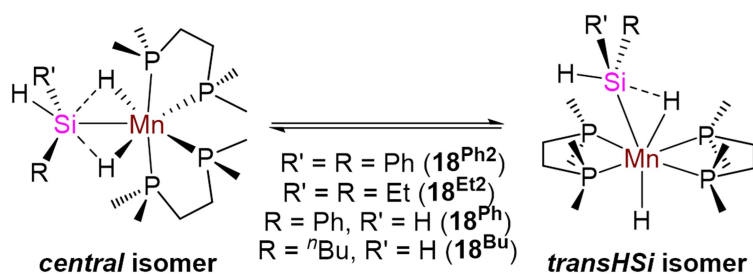


Figure 6.1: Selected regions of the room temperature and low temperature NMR spectra for (top) $[(\text{dmpe})_2\text{MnH}_2(\text{SiH}_2\text{Ph})]$ (**18^{Ph}**) and (bottom) $[(\text{dmpe})_2\text{MnH}_2(\text{SiH}_2^{\text{nBu}})]$ (**18^{Bu}**) showing, from left to right, the silicon hydride and metal hydride regions of the ^1H NMR spectra, the $^{31}\text{P}\{^1\text{H}\}$ NMR spectra, and $^{29}\text{Si}\{^1\text{H}\}$ NMR spectra. Signals in the low temperature spectra are assigned to low symmetry (\dagger ; *central*) and high symmetry ($*$; *transHSi*) isomers.

^{rr} Many ^{13}C NMR signals and all ^{29}Si NMR signals were not located due to broadness at room temperature.

NMR signals for the low symmetry isomer of **18** feature one low frequency MnH ^1H NMR resonance at -12.5 to -12.8 ppm, integrating to two protons, one ($\mathbf{18}^{\text{R}2}$) or two ($\mathbf{18}^{\text{R}}$) terminal SiH resonance(s) (6.0 - 6.6 ppm for $\mathbf{18}^{\text{Ph}2}$ and $\mathbf{18}^{\text{Ph}}$; 5.0 - 5.4 ppm for $\mathbf{18}^{\text{Et}2}$ and $\mathbf{18}^{\text{Bu}}$), two ^{31}P NMR resonances (71.0 - 75.2 ppm), and a single ^{29}Si resonance (10.0 ppm for $\mathbf{18}^{\text{Ph}2}$, 14.2 ppm for $\mathbf{18}^{\text{Et}2}$, -15.7 ppm for $\mathbf{18}^{\text{Ph}}$, and -22.0 ppm for $\mathbf{18}^{\text{Bu}}$). The two relatively broad ^{31}P NMR signals, and the complex ^{31}P coupling pattern of the MnH signals, are indicative of a disphenoidal arrangement of the phosphorus donors. These data are consistent with a *central* isomer (Scheme 6.2) featuring a meridional H–Si–H bonding motif involving the silyl and metal hydride ligands (as opposed to a *lateral* isomer with an H–H–Si bonding motif; *vide infra*).



Scheme 6.2: Isomers of $[(\text{dmpe})_2\text{MnH}_2(\text{SiHR}_2)]$ $\{\text{R} = \text{Ph}$ ($\mathbf{18}^{\text{Ph}2}$), $\text{R} = \text{Et}$ ($\mathbf{18}^{\text{Et}2}$) $\}$ and $[(\text{dmpe})_2\text{MnH}_2(\text{SiH}_2\text{R})]$ $\{\text{R} = \text{Ph}$ ($\mathbf{18}^{\text{Ph}}$), $\text{R} = \text{}^n\text{Bu}$ ($\mathbf{18}^{\text{Bu}}$) $\}$ observed in solution.

In contrast, low temperature NMR spectra for the high symmetry isomer of **18** consist of *two* low frequency MnH ^1H NMR resonances located between -10.9 and -14.4 ppm (1H each), a single terminal SiH ^1H NMR resonance $\{4.7$ - 6.2 ppm; integrating to 1H ($\mathbf{18}^{\text{R}2}$) or 2H ($\mathbf{18}^{\text{R}}$) $\}$, and single ^{31}P NMR (77.5 - 78.5 ppm) and ^{29}Si NMR (23.8 ppm for $\mathbf{18}^{\text{Et}2}$; -1.6 ppm for $\mathbf{18}^{\text{Ph}}$; -6.9 ppm for $\mathbf{18}^{\text{Bu}}$; not located for $\mathbf{18}^{\text{Ph}2}$ due to the low concentration of this isomer) resonances. The single sharp ^{31}P NMR signal and pentet coupling pattern of the higher frequency MnH signal in this isomer of **18** ($^2J_{\text{H,P}} = 52$ - 56 Hz) are indicative of two equivalent dmpe ligands lying in a plane with a hydride

ligand in an apical site.^{ss} By contrast, the ${}^2J_{\text{P,H}}$ coupling constants for the lower frequency MnH signal in the same isomer of $\mathbf{18}^{\text{Et}2}$ and $\mathbf{18}^{\text{R}}$ are significantly smaller (22-23 Hz; the analogous signal in $\mathbf{18}^{\text{Ph}2}$ is a multiplet from which ${}^2J_{\text{P,H}}$ could not be determined), consistent with literature examples of ${}^2J_{\text{P,H}}$ for the proton involved in $\eta^2\text{-(H-SiR}_3\text{)}$ coordination in nonclassical hydrosilane complexes.^{tt} These data are consistent with a *transHSi* isomer (Scheme 6.2) featuring *trans*-disposed hydride and nonclassical hydrosilane ligands (as opposed to a *transH*₂ isomer with *trans* disposed silyl and dihydrogen ligands; *vide infra*), with rapid rotation of the hydrosilane ligand about the Mn–(hydrosilane centroid) axis.

The *central:transHSi* ratios observed by NMR spectroscopy are 87:13 for $\mathbf{18}^{\text{Ph}2}$ (271 K), 75:25 for $\mathbf{18}^{\text{Et}2}$ (229 K), 62:38 for $\mathbf{18}^{\text{Ph}}$ (186 K), and 27:73 for $\mathbf{18}^{\text{Bu}}$ (205 K). To our knowledge, this is only the second report of an equilibrium between two silyl dihydride isomers which differ in whether the silyl group interacts with one or both hydride co-ligands; in 2006 Sakaba reported a pair of isostructural tungsten silyl dihydride complexes, $[(\text{CO})_2\text{Cp}^*\text{WH}_2(\text{SiHRPh})]$ (R = H, Ph), existing in solution as an equilibrium between two isomers; one complex crystallized as an isomer with two close Si–H interactions (1.91(3) and 2.00(4) Å), while the other crystallized as an isomer with a single close Si–H interaction (2.02(4) Å).⁵¹³

Interconversion between the *central* and *transHSi* isomers of $\mathbf{18}$ could hypothetically involve initial HSiR₃ or H₂ dissociation. However, the terminal SiH environment(s) and the metal hydride environments do not undergo facile exchange at room temperature; upon selective deuteration of the metal hydride environment in $\mathbf{18}^{\text{Et}2}$, $\mathbf{18}^{\text{Ph}}$, and $\mathbf{18}^{\text{Bu}}$, no deuterium incorporation into the terminal SiH environment was

^{ss} These coupling constants are very similar to the ${}^2J_{\text{H,P}}$ coupling of 56.5 Hz in Wilkinson and Girolami's $[(\text{dmpe})_2\text{MnH}(\text{C}_2\text{H}_4)]$ ($\mathbf{10}$), which also contains a hydride ligand apical to a plane formed by two κ^2 -dmpe ligands; see ref.120.

^{tt} For selected examples, see refs. 244, 249, 272, 273, and 512.

observed after 12 hours in solution.^{uu} This indicates that isomerization (which is rapid at room temperature for all four members of the family), does not involve hydrosilane dissociation to form 5-coordinate "(dmpe)₂MnH" (**12**) as an intermediate. Likewise, addition of D₂ to **18^{Ph}** did not result in any observable deuteration of the complex after 72 h in solution at room temperature, suggesting that H₂ dissociation to form a 5-coordinate "(dmpe)₂Mn(SiR₃)" intermediate (**17**) does not play a significant role in isomerization. However, after heating a solution of [(dmpe)₂MnD₂(SiH₂ⁿBu)] (**d₂-18^{Bu}**) for three days at 70-80 °C, the MnH and terminal SiH signals both achieved 50% deuterium incorporation, suggesting that hydrosilane elimination may be possible at elevated temperatures. Furthermore, hydrosilane exchange reactions were found to occur in the presence of excess free silane, including very slow reactions at room temperature. For example, [(dmpe)₂MnH₂(SiHPh₂)] (**18^{Ph2}**) reacted with ~6 equiv. of PhSiH₃ to generate [(dmpe)₂MnH₂(SiH₂Ph)] (**18^{Ph}**); after three days at room temperature this reaction had proceeded to a 2 : 1 mixture of **18^{Ph2}** : **18^{Ph}**, whereas heating overnight at 90 °C afforded complete conversion to **18^{Ph}**, with no remaining **18^{Ph2}** observed by ¹H NMR spectroscopy.

6.4 – X-ray Crystal Structures of Silyl Dihydride Complexes

X-ray quality crystals of **18^{Ph2}** and **18^{Ph}** (Figure 6.2; Table 6.1) were obtained from toluene (**18^{Ph2}**) or hexanes (**18^{Ph}**) at -30 °C, and in both cases the *central* isomer (the low symmetry isomer observed in solution) was obtained. The geometry at manganese can be described as capped octahedral, with the four phosphorus donors and two *cis*-hydride ligands at the points of a distorted octahedron, and the silyl ligand positioned close to the H–H edge; nearly equidistant from the two hydride ligands, but with a 30.4-37.6° angle between the H(1A)–Si–H(1B) and H(1A)–Mn–H(1B) planes. The Si–H(1A) and Si–H(1B) distances of 1.75(4)-1.79(2) Å in **18^{Ph2}** and 1.77(4)-1.82(3) Å in **18^{Ph}** are suggestive of significant H–Si interactions, consistent with an η³-

^{uu} Selective deuteration of the metal hydride environment in **18^{Ph2}** was not carried out because the starting complex, **16^{Ph2}**, could not be purified.

coordinated silicate (H_2SiR_3^-) ligand. Crystallographically well-characterized monometallic examples of *central* $\eta^3\text{-H}_2\text{SiR}_3$ ligand systems have been reported for Fe,²⁴⁷ Co,²⁷¹ Mo,²⁷⁴ Rh,²⁷³ and Ru,^{244,248,251,270,272,275} and exhibit Si–H distances ranging from 1.69(3)–2.15 Å, encompassing the distances in $\mathbf{18}^{\text{Ph}2}$ and $\mathbf{18}^{\text{Ph}}$. As in these literature examples, the substituents on silicon in $\mathbf{18}^{\text{Ph}2}$ and $\mathbf{18}^{\text{Ph}}$ form a distorted square pyramid with both $\mu\text{-H}$ atoms in the square plane.

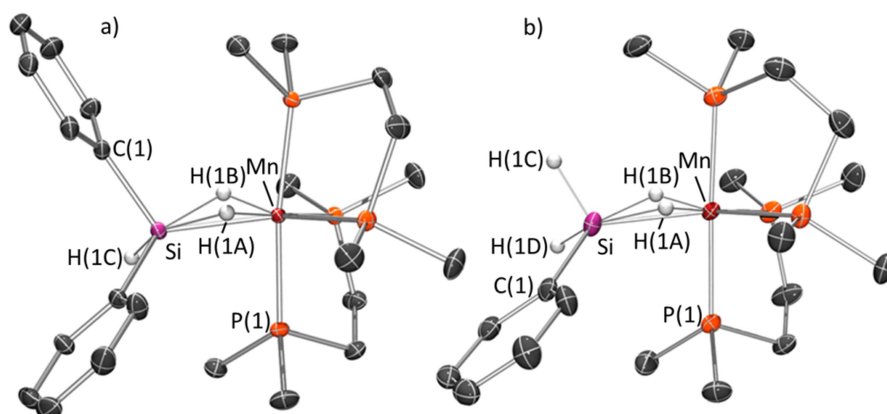


Figure 6.2: X-ray crystal structures of (a) the *central* isomer of $[(\text{dmpe})_2\text{MnH}_2(\text{SiHPh}_2)]$ (*central-18*^{Ph2}), and (b) the *central* isomer of $[(\text{dmpe})_2\text{MnH}_2(\text{SiH}_2\text{Ph})]$ (*central-18*^{Ph}). Ellipsoids are drawn at 50% probability. Hydrogen atoms on Mn and Si were located from the difference map and refined isotropically. All other hydrogen atoms have been omitted for clarity. Bond distances (Å) and angles (deg) for *central-18*^{Ph2}: Mn(1)–Si(1) 2.3176(3), Mn(1)–H(1A) 1.46(3), Mn(1)–H(1B) 1.62(3), Si(1)–H(1A) 1.79(2), Si(1)–H(1B) 1.75(4), Si(1)–H(1C) 1.37(4), Mn(1)–Si(1)–C(1) 117.65(3), Mn(1)–Si(1)–C(7) 119.69(3), H(1A)–Mn(1)–Si(1) 50(1), H(1B)–Mn(1)–Si(1) 49(1), H(1A)–Mn(1)–H(1B) 92(2). Bond distances (Å) and angles (deg) for *central-18*^{Ph}: Mn(1)–Si(1) 2.3148(8), Mn(1)–H(1A) 1.49(3), Mn(1)–H(1B) 1.54(3), Si(1)–H(1A) 1.82(3), Si(1)–H(1B) 1.77(4), Si(1)–H(1C) 1.44(3), Si(1)–H(1D) 1.48(3), Mn(1)–Si(1)–C(1) 120.48(9), H(1A)–Mn(1)–Si(1) 52(1), H(1B)–Mn(1)–Si(1) 50(1), H(1A)–Mn(1)–H(1B) 97(2).

By contrast, crystallization of $\mathbf{18}^{\text{Bu}}$ from hexanes at $-30\text{ }^\circ\text{C}$ afforded a structure (a in Figure 6.3) consistent with the *transHSi* isomer (the high symmetry isomer observed in

solution). The geometry at manganese can be described as octahedral, with a hydride ligand coordinated *trans* to a hydrosilane ligand. Unfortunately, four-fold disorder of the silicon moiety prevented location of the three hydrogen atoms bound to Si (two terminal on Si and one bridging between Si and Mn) from the difference map. However, DFT calculations on a model of *transHSi-18*^{Bu} where the ⁿBu group has been replaced by an Et group (*transHSi-18*^{Et}) afforded a structure with very similar placement of the terminal manganese hydride ligand and the heavy atoms around Mn and Si (b in Figure 6.3): the calculated Mn–Si distance is 2.36 Å (cf. 2.388(3) Å in the X-ray structure), and the Mn–Si–C(1) and Si–Mn–H(1) angles are 121.8° and 162.3° (cf. 121.8(3)° and 163.0(6)°, respectively, in the X-ray structure).^{vv} The calculated structure of *transHSi-18*^{Et} also features two terminal Si–H bonds (Si–H = 1.52 Å) accompanied by one hydrogen atom (H_{MnSi}) bridging between Mn and Si, with bond lengths and angles (Si–H_{MnSi} = 1.79 Å; Mn–H_{MnSi} = 1.56 Å; Mn–H_{MnSi}–Si = 49.2°) suggestive of a nonclassical hydrosilane ligand; the result of incomplete hydrosilane oxidative addition. Other crystallographically characterized monometallic complexes featuring a nonclassical η²-(Si–H)-coordinated hydrosilane ligand accompanied by at least one non-interacting metal hydride ligand have been reported for Fe,⁵¹⁴ Nb,²³⁷ Mo,²⁷⁴ W,⁵¹⁵ and Ru.^{243,244,249,252,253,512,516}

^{vv} Discussed values are those from the dominant disordered conformer.

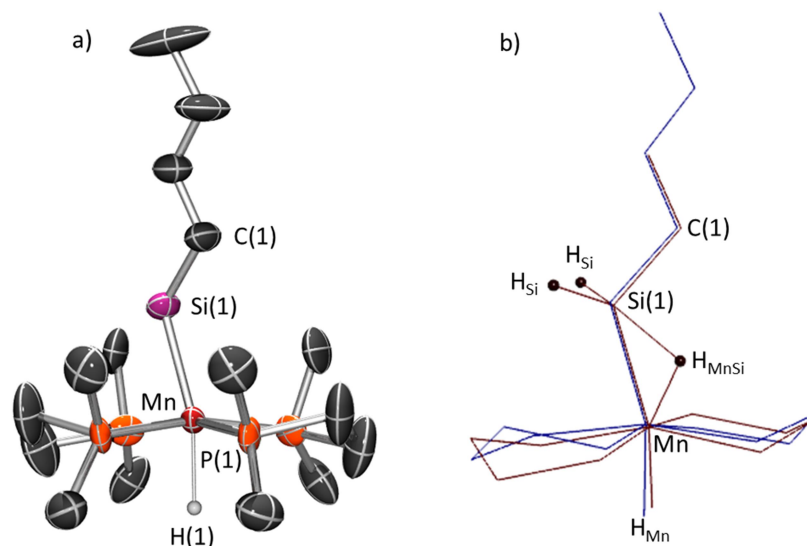


Figure 6.3: a) X-ray crystal structure of the *transHSi* isomer of $[(\text{dmpe})_2\text{MnH}_2(\text{SiH}_2^n\text{Bu})]$ (*transHSi-18^{Bu}*) with ellipsoids drawn at 50% probability. The terminal metal hydride atom was located from the difference map and refined isotropically. All other hydrogen atoms have been omitted for clarity. The Si atom is disordered over 4 positions (2 sets of 2 related by symmetry), the butyl group is disordered over 2 positions (related by symmetry), and the dmpe ligands are disordered over 8 positions (4 sets of 2 related by symmetry). Only one conformation is shown for clarity, with occupancies of 36.8(3)% and 16.0(1)% for silicon and the dmpe ligands, respectively. Bond distances (Å) and angles (deg), where Si(1A) is the Si position that is not shown in the depicted conformation: Mn(1)–Si(1) 2.388(3), Mn(1)–Si(1A) 2.386(3), Mn(1)–H(1) 1.75(5), Mn(1)–Si(1)–C(1) 121.8(3), Mn(1)–Si(1A)–C(1) 127.8, H(1)–Mn(1)–Si(1) 163.0(7), H(1)–Mn(1)–Si(1A) 158(1). b) Overlay of the X-ray crystal structure (blue) of *transHSi-[(dmpe)₂MnH₂(SiH₂ⁿBu)]* (*transHSi-18^{Bu}*) and DFT calculated structure (red) of *transHSi-[(dmpe)₂MnH₂(SiH₂Et)]* (*transHSi-18^{Et}*), with selected H atoms in the calculated structure depicted as spheres. Methyl groups on the dmpe ligands, and most hydrogen atoms, have been omitted for clarity.

6.5 – DFT Calculations on Silyl Dihydride Complexes

To investigate the nature of Si–H ‘interligand’ interactions in the *central* and *transHSi* isomers of **18**, and the thermodynamic stability of alternative isomers (*transH₂*, *lateralH₂*, and *lateralHSi*; Figure 6.4), we turned to DFT calculations {ADF, gas-phase, all-electron, PBE, D3-BJ, TZ2P, ZORA; **18^{Bu}** was modelled as [(dmpe)₂MnH₂(SiH₂Et)] (**18^{Et}**), with an ethyl group in place of the ⁿBu group}. These calculations yielded energy minima (see Figure 6.5) corresponding to four sets of isomers; the two experimentally observed isomers shown in Scheme 6.2 (*central* and *transHSi*, with good agreement in the relevant bond lengths and angles; Table 6.1) and two higher energy isomers: *transH₂* and *lateralH₂* (Figure 6.4, Table 6.2, and for **18^{Et2}**, Figure 6.6). However, in no case was an energy minimum located for a *lateralHSi* isomer (Figure 6.4).

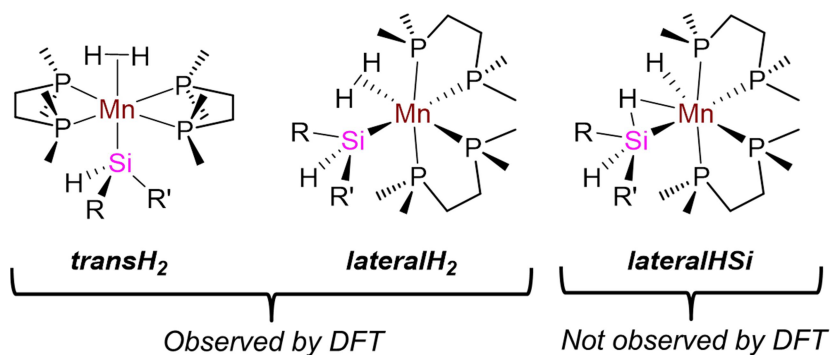


Figure 6.4: Structures of experimentally unobserved *transH₂*, *lateralH₂*, and *lateralHSi* isomers of [(dmpe)₂MnH₂(SiHRR’)] (**18^{Ph2}**: R = R’ = Ph; **18^{Et2}**: R = R’ = Et; **18^{Ph}**: R = Ph, R’ = H; **18^{Et}**: R = Et, R’ = H). Of these, energy minima were only located for the *transH₂* and *lateralH₂* isomers by DFT calculations. For structures of the experimentally observed *central* and *transHSi* isomers (for which energy minima were also located via DFT), see Scheme 6.2.

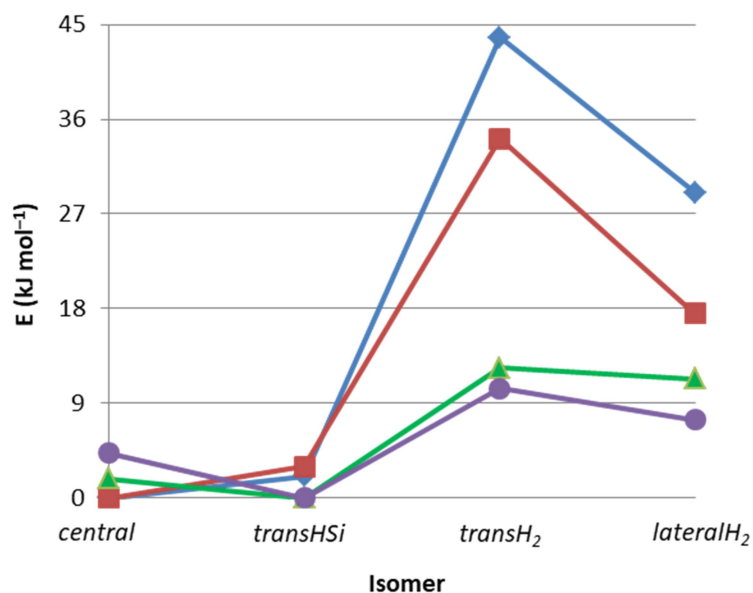


Figure 6.5: Relative total bonding energies (kJ mol^{-1}) of the *central*, *transHSi*, *transH₂*, and *lateralH₂* isomers of $[(\text{dmpe})_2\text{MnH}_2(\text{SiHPh}_2)]$ (**18^{Ph2}**; blue ♦), $[(\text{dmpe})_2\text{MnH}_2(\text{SiHEt}_2)]$ (**18^{Et2}**; red ■), $[(\text{dmpe})_2\text{MnH}_2(\text{SiH}_2\text{Ph})]$ (**18^{Ph}**; green ▲), and $[(\text{dmpe})_2\text{MnH}_2(\text{SiH}_2\text{Et})]$ (**18^{Et}**; purple ●).

As in the X-ray structures of **18^{Ph2}** and **18^{Ph}**, the *central* isomers have an octahedral arrangement of the phosphorous and H_{Mn} atoms, with silicon located approximately between the two bridging H_{MnSi} atoms (the angle between the $\text{H}_{\text{MnSi}1}/\text{Mn}/\text{H}_{\text{MnSi}2}$ and $\text{H}_{\text{MnSi}1}/\text{Si}/\text{H}_{\text{MnSi}2}$ planes ranges from 17 to 36°). The *transHSi* isomers feature an approximately octahedral arrangement of the phosphorous donors, H_{Mn} , and an η^2 -nonclassical hydrosilane ligand, with H_{Mn} approximately *trans* to the centroid of the $\text{Si}-\text{H}_{\text{MnSi}}$ bond, and the four phosphorous donors distorted away from the nonclassical hydrosilane unit. Similarly, the *transH₂* isomer is octahedral with *trans*-disposed dihydrogen and silyl ligands. By contrast, the *lateralH₂* isomer features *cis*-disposed H_2 and silyl ligands, with Mn, Si, and both H atoms of the dihydrogen ligand located nearly in a plane. The geometry at manganese is approximately octahedral, although the dihydrogen ligand is displaced in the direction of the neighboring silyl

ligand (centroid_{H2}–Mn–Si = 79-82°). In all four calculated isomers of **18**^{Ph2}, **18**^{Ph}, **18**^{Et2}, and **18**^{Et}, the Mn–Si–C angles lie between 114 and 126°, while the Mn–Si–H_{Si} angles range from 111 to 118°.

Table 6.1: Selected angles (deg) and distances (Å) (and Mayer bond orders) for experimentally observed *central* and *transHSi* isomers from calculated {or X-ray} structures of **18**. Atom labels correspond to those for **18**^{Et2} in Figure 6.6.

[(dmpe) ₂ MnH ₂ (SiHRR')]	18 ^{Ph2}	18 ^{Et2}	18 ^{Ph}	18 ^{Bu} / 18 ^{Et}	
SiHRR'	SiHPh ₂	SiHEt ₂	SiH ₂ Ph	SiH ₂ Et {XRD: SiH ₂ ⁿ Bu}	
<i>central isomer</i>	Mn–Si	2.31 (0.63) {2.3176(3)}	2.35 (0.69)	2.31 (0.69) {2.3148(8)}	2.32 (0.69)
	Mn–H _{MnSi}	1.57, 1.59 (0.62, 0.67) {1.46(3), 1.62(3)}	1.56, 1.57 (0.70, 0.71)	1.57, 1.58 (0.66, 0.70) {1.49(3), 1.54(3)}	1.57 (0.68, 0.70)
	Si–H _{MnSi}	1.82, 1.85 (0.28, 0.33) {1.75(4), 1.79(2)}	1.85, 1.88 (0.25, 0.26)	1.84, 1.87 (0.28, 0.29) {1.77(4), 1.82(3)}	1.83, 1.88 (0.27, 0.28)
	Si–H _{Si}	1.52 (0.81) {1.37(4)}	1.51 (0.81)	1.50, 1.51 (0.83, 0.88) {1.44(3), 1.48(3)}	1.51, 1.52 (0.84)
	H _{MnSi} –Mn–Si	51.9, 52.9 {49(1), 50(1)}	52.0, 53.1	52.3, 53.4 {50(1), 52(1)}	51.8, 53.5
	H _{MnSi} –Mn–H _{MnSi}	98.3 {92(2)}	103.8	101.1 {97(2)}	103.0
	Mn–Si–C	116.5, 118.4 {117.65(3), 119.69(3)}	117.5, 120.3	119.6 {120.48(9)}	119.9
	Mn–Si–H _{Si}	116.3 {114(2)}	111.7	114.9, 117.7 {115(1), 120(1)}	113.8, 116.9
	H _{MnSi} /Mn/H _{MnSi} plane to H _{MnSi} /Si/H _{MnSi} plane	36.4 {37.6}	16.6	30.7 {30.4}	22.2
	<i>transHSi isomer</i>	Mn–Si	2.36 (0.77)	2.39 (0.71)	2.35 (0.81)
Mn–H _{MnSi}		1.57 (0.57)	1.57 (0.64)	1.57 (0.62)	1.56 (0.63)
Mn–H _{Mn}		1.56 (0.82)	1.57 (0.83)	1.57 (0.80)	1.57 (0.83) {1.75(5)}
Si–H _{MnSi}		1.80 (0.34)	1.75 (0.33)	1.82 (0.31)	1.79 (0.30)
Si–H _{Si}		1.52 (0.74)	1.52 (0.80)	1.51, 1.52 (0.79, 0.86)	1.52 (0.81, 0.82)
H _{MnSi} –Mn–Si		49.6	47.1	50.8	49.2
H _{Mn} –Mn–Si		162.3	162.4	161.7	162.3 {158(1), 163.0(7)}
H _{Mn} –Mn– SiH _{MnSi} (centroid)		178.1	178.7	177.2	178.4
Mn–Si–C		118.3, 119.0	116.2, 118.1	120.0	121.8 {121.8(3), 127.8}
Mn–Si–H _{Si}		115.6	112.6	115.9, 116.1	114.2, 115.3

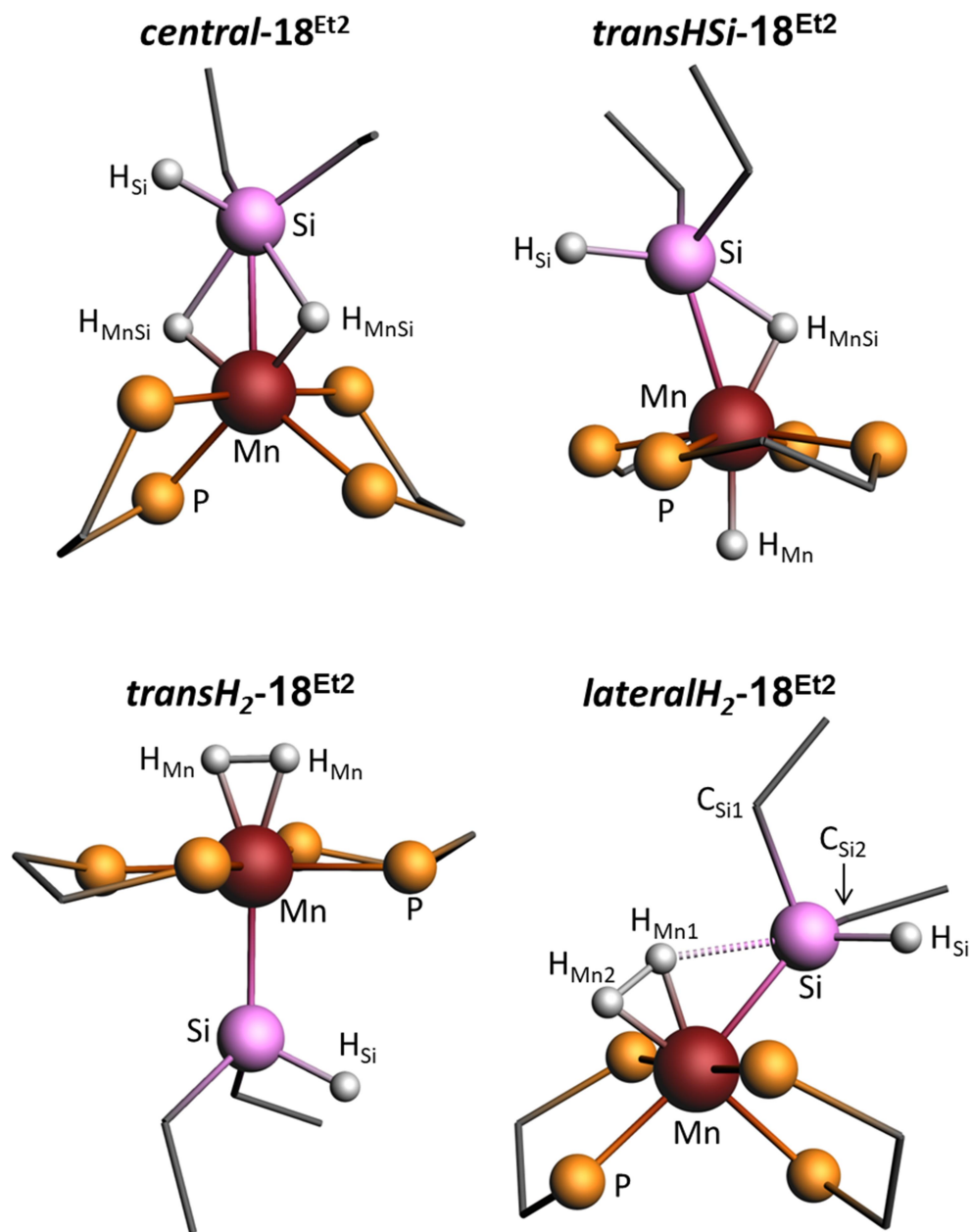


Figure 6.6: Geometry optimized structures of the isomers of $[(dmpe)_2MnH_2(SiHEt_2)]$ (18^{Et_2}) determined by DFT calculations. Spheres represent Mn (red), Si (pink), P (orange), and H (white), whereas carbon atoms are represented by grey vertices. P-methyl groups and most H atoms have been omitted for clarity.

Table 6.2: Selected angles (deg) and distances (Å) (and Mayer bond orders) for experimentally unobserved *transH₂* and *lateralH₂* isomers from calculated structures of **18**. Atom labels correspond to those for **18^{Et2}** in Figure 6.6.

[(dmpe) ₂ MnH ₂ (SiHRR')]	18^{Ph2}	18^{Et2}	18^{Ph}	18^{Bu}/18^{Et}	
SiHRR'	SiHPh ₂	SiHEt ₂	SiH ₂ Ph	SiH ₂ Et {XRD: SiH ₂ ^t Bu}	
<i>transH₂</i> isomer	Mn–Si	2.41 (0.95)	2.41 (0.89)	2.37 (0.96)	2.36 (0.93)
	Mn–H _{Mn}	1.58, 1.59 (0.55)	1.58 (0.61)	1.59 (0.56)	1.59 (0.59, 0.60)
	Si–H _{Mn1}	3.93, 3.96 (<0.05)	3.94, 3.95 (<0.05)	3.91, 3.92 (<0.05)	3.90 (<0.05)
	Si–H _{Si}	1.51 (0.78)	1.52 (0.77)	1.51, 1.52 (0.81)	1.52, 1.53 (0.79, 0.80)
	H _{Mn} –H _{Mn}	0.96 (0.43)	0.99 (0.38)	0.96 (0.44)	0.98 (0.41)
	H _{Mn} –Mn–H _{Mn}	35.3	36.7	35.3	36.1
	H ₂ (centroid)–Mn–Si	177.0	177.3	175.1	174.2
	Mn–Si–C	122.9, 124.2	120.9, 121.6	123.6	124.8
	Mn–Si–H _{Si}	111.4	113.9	115.0, 115.8	114.8, 115.7
	<i>lateralH₂</i> isomer	Mn–Si	2.39 (0.91)	2.40 (0.90)	2.35 (0.91)
Mn–H _{Mn1}		1.57 (0.48)	1.56 (0.53)	1.57 (0.51)	1.57 (0.53)
Mn–H _{Mn2}		1.59 (0.62)	1.59 (0.63)	1.59 (0.62)	1.59 (0.62)
Si–H _{Mn1}		2.17 (0.12)	2.12 (0.13)	2.16 (0.14)	2.13 (0.14)
Si–H _{Mn2}		3.05 (<0.05)	3.03 (<0.05)	3.07 (<0.05)	3.04 (<0.05)
Si–H _{Si}		1.52 (0.76)	1.53 (0.76)	1.52 (0.79, 0.82)	1.52, 1.53 (0.80, 0.81)
H _{Mn1} –H _{Mn2}		0.99 (0.40)	1.00 (0.39)	1.01 (0.41)	1.00 (0.41)
H _{Mn1} –Mn–Si		62.6	60.6	63.5	62.1
H _{Mn1} –Mn–H _{Mn2}		36.6	36.8	37.2	37.0
H ₂ (centroid)–Mn–Si		80.4	79.0	82.2	80.7
Mn–Si–C ₁		117.1	113.8	120.8	119.4
Mn–Si–C ₂		125.9	123.6	–	–
Mn–Si–H _{Si}		113.9	113.2	115.8, 116.7	116.2
H _{Mn1} –Mn–Si–C ₁		19.5	5.5	–12.0	0.5
H _{Mn1} –Mn–Si–C ₂		–103.4	–118.6	–	–
H _{Mn1} –Mn–Si–H _{Si}	135.0	121.1	111.3, –131.3	121.6, –121.0	

For all complexes (**18^{Ph2}**, **18^{Ph}**, **18^{Et2}**, and **18^{Et}**), the *central* and *transHSi* isomers are within 4 kJ mol^{–1} of each other (Figure 6.5), consistent with their observation by solution NMR spectroscopy (*vide supra*). In contrast, the two higher energy isomers (*transH₂* and *lateralH₂*) are 8–44 kJ mol^{–1} higher in energy than the most stable experimentally observed isomer, with a larger energy difference in the case of more

sterically hindered $\mathbf{18}^{\text{R}2}$ complexes (Figure 6.5). These isomers likely exist in equilibrium with the experimentally observed isomers, but in concentrations too low for NMR spectroscopic observation. In fact, a *transH₂* or *lateralH₂* isomer is presumably formed initially in the synthesis of $\mathbf{18}$ via the reactions of H₂ with silylene hydride complexes $\mathbf{16}^{\text{R}2}$ or disilyl hydride complexes $\mathbf{20}^{\text{R}}$ (*vide supra*).

Both experimentally observed isomers (*central* and *transHSi*) feature nonclassical bonding situations. This is apparent from Mayer bond orders of 0.25-0.34 between silicon and the bridging hydride ligands (Si–H_{MnSi}), as well as Mn–Si Mayer bond orders ranging from 0.63 to 0.81 (cf. 0.89 to 0.96 for the *transH₂* and *lateralH₂* isomers, which feature silyl ligands without strong interactions to neighboring hydride ligands; *vide infra*). The *transHSi* isomers can simply be described as nonclassical hydrosilane complexes; structures intermediate between classical η^2 -hydrosilane and classical silyl hydride extremes, as a consequence of substantial but incomplete Si–H bond oxidative addition. By contrast, the similar Si–H_{MnSi} and Mn–H_{MnSi} Mayer bond orders involving both H_{MnSi} atoms in the *central* isomers are indicative of a nonclassical η^3 -H₂SiHRR' (silicate) anion.^{ww}

In contrast to the nonclassical *central* and *transHSi* isomers, the *transH₂* and *lateralH₂* isomers can be described as silyl η^2 -H₂ complexes. These isomers feature significant H–H interactions, reflected by H–H distances of 0.96-1.01 Å (relative to 0.75 Å for free H₂), Mayer H–H bond orders of 0.38-0.44, and acute H–Mn–H angles of 35.3-37.2° (Table 6.2). Nevertheless, the *lateralH₂* isomers feature small but non-negligible Si–H_{Mn1} Mayer bond orders (0.12-0.14), a Mn–H_{Mn1} Mayer bond order which is 0.09-0.14 lower than that of Mn–H_{Mn2}, as well as acute (79-82°) angles between the centroid of the H₂ ligand, Mn and Si (Table 6.2). These features suggest a minor degree of bonding between Si and H_{Mn1}, and the lower extent of Si–H_{Mn1} bonding in the *lateralH₂* versus the *central* or *transHSi* isomers is also reflected in Si–Mn–H_{Mn1} angles

^{ww} The calculated Si–H_{MnSi} distances are different from one another by 0.03-0.05 Å, consistent with a limited degree of second order Jahn-Teller distortion, as described in reference 232.

of 60.6-63.5° in the former, which are much more obtuse than the corresponding Si–Mn–H angles in the latter (*central*; 51.8-53.5°, *transHSi*; 47.1-50.8°).

The lack of substantial interligand Si–H interactions in the *lateralH₂* isomers lies in contrast to the literature on transition metal complexes with a meridional Si–H–H arrangement of SiR₃ and H moieties, which suggests that complexes featuring a hydrosilane and a hydride ligand (i.e. the proposed *lateralHSi* isomer in Figure 6.4) should typically be favored relative to a silyl dihydrogen complex (i.e. the *lateralH₂* isomer).^{237,249,253} Such a preference has been rationalized^{xx} based primarily on H–H and Si–H bond strengths.⁵¹⁹ In this work, the expected trend is reflected in the experimental observation of the *transHSi* isomer of **5** but not the *transH₂* isomer.

Our inability to locate an energy minimum for a *lateralHSi* isomer (*vide supra*) was surprising, and prompted us to investigate sterically less encumbered PH₃ analogues of **18**; ([$(\text{PH}_3)_4\text{MnH}_2(\text{SiHRR}')$): **18**^{Ph₂;PH₃}; R = R' = Ph, **18**^{Et₂;PH₃}; R = R' = Et, **18**^{Ph;PH₃}; R = H, R' = Ph, and **18**^{Et;PH₃}; R = H, R' = Et). These calculations afforded energy minima corresponding to the four previously calculated isomers (*central*, *transHSi*, *transH₂*, and *lateralHSi*), as well as a *lateralHSi* isomer (relative energies are plotted in Figure 6.7). In all cases these *lateralHSi* isomers were lower in energy than the *lateralH₂* isomers, and feature a significant Si–H_{Mn1} interaction (Si–H_{Mn1} dist. 1.88-1.93 Å, Mayer bond order 0.25-0.32, Si–Mn–H_{Mn1} angle 51.3-54.0°) and minimal H_{Mn1}–H_{Mn2} interactions (H–H dist. 1.57-1.63 Å, Mayer bond order 0.05-0.08, H_{Mn1}–Mn–H_{Mn2} angle 60.7-63.4°), consistent with *cis*-disposed hydride and nonclassical hydrosilane ligands. Computational

^{xx} See refs. 234, 250, 267, and 517. Examples of dihydrogen silyl complexes have also been observed, and some computational results have suggested that these complexes should have similar energies to hydrosilane hydride complexes; see refs. 245 and 518.

observation of the *lateralHSi* isomers for the PH_3 analogues, but not the dmpe complexes, suggests that the *lateralHSi* isomers are sterically disfavored in the dmpe complexes.^{yy}

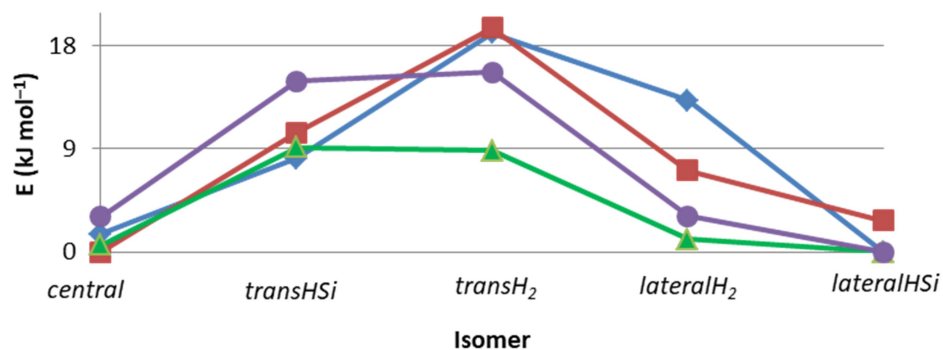


Figure 6.7: Relative total bonding energies (kJ mol^{-1}) of the *central*, *transHSi*, *transH₂*, *lateralH₂*, and *lateralHSi* isomers of silyl dihydride complexes where the two dmpe ligands have been replaced with four PH_3 ligands; $[(\text{PH}_3)_4\text{MnH}_2(\text{SiHPh}_2)]$ (**18^{Ph₂;PH₃}**; blue ♦), $[(\text{PH}_3)_4\text{MnH}_2(\text{SiHEt}_2)]$ (**18^{Et₂;PH₃}**; red ■), $[(\text{PH}_3)_4\text{MnH}_2(\text{SiH}_2\text{Ph})]$ (**18^{Ph;PH₃}**; green ▲), and $[(\text{PH}_3)_4\text{MnH}_2(\text{SiH}_2\text{Et})]$ (**18^{Bu;PH₃}**; purple ●).

6.6 – Determination of Sign and Magnitude of $J_{\text{Si,H}}$

As noted previously (section 1.5.5), the ^{29}Si - ^1H coupling constant ($J_{\text{Si,H}}$) can provide a sensitive experimental measure of where a structure lies along the continuum from a classical hydrosilane complex to a classical silyl hydride complex. However, this requires knowledge of both the magnitude and sign of $J_{\text{Si,H}}$.

Scherer has used standard 2D ^1H - ^1H COSY NMR spectroscopy to unambiguously determine the sign of $J_{\text{Si,H}}$ in transition metal silyl hydride/hydrosilane complexes; specifically, those where silicon bears at least one terminal hydrogen substituent.^{241,256} This method takes advantage of passive coupling; coupling which is not

^{yy} The experimentally and computationally unobserved *lateralHSi* isomer of dmpe-coordinated **18** would require $\text{H}_{\text{MnI}}-\text{Mn}-\text{Si}-\text{X}$ dihedral angles of approximately 60° ($\times 2$) and 180° ($\times 1$), where X represents any one of the 3 substituents on silicon, bringing the hydrocarbyl substituent(s) on silicon into closer proximity to the dmpe ligands than in a *lateralH₂* isomer.

directly responsible for the formation of a particular cross-peak.⁵²⁰ For example, in an AMX spin system (A and M are proton environments, and X is a spin $\frac{1}{2}$ nucleus) where active A–M coupling gives rise to a ^1H – ^1H COSY cross-peak, passive A–X and M–X coupling results in additional splitting of the cross-peak into a doublet where a diagonal line can be drawn between the two peaks which compose the doublet; the slope of which can be used to determine the relative sign of the two passive coupling constants (J_{XA} and J_{XM}).⁵²⁰

In Scherer's experiment, this involves measurement of the vector between ^{29}Si satellites of a ^1H – ^1H COSY cross-peak between a terminal SiH signal (H_{Si}) and a metal-coordinated hydride signal (H_{M}).^{241,256} If the slope of this vector is positive, then the two passive $J_{\text{Si,H}}$ couplings ($J_{\text{Si,H}}$ to H_{M} , *the sign of which is unknown*, and $^1J_{\text{Si,H}}$ to H_{Si} , *which is known to be negative*²⁶⁴) have the same sign, so $J_{\text{Si,H}}$ to H_{M} is negative. By contrast, if the slope is negative, the two passive $J_{\text{Si,H}}$ couplings have opposite signs, and $J_{\text{Si,H}}$ to H_{M} is positive; $^1J_{\text{Si,H}}$ coupling to the terminal SiH proton (H_{Si}) therefore serves as an internal reference.^{241,256} The magnitudes of the two passive $J_{\text{Si,H}}$ couplings can also be measured directly from the 2D ^1H – ^1H COSY NMR spectrum, since the horizontal and vertical distances between the ^{29}Si satellites provide the magnitudes of $J_{\text{Si,H}}$ to H_{M} and H_{Si} .

However, for silyl dihydride complexes **18**, we had difficulty obtaining standard ^1H – ^1H dqf COSY NMR spectra with well-defined ^{29}Si satellites (Figure 6.8); in some cases the signal could not be detected from the noise, while in others the signals were too broad for accurate measurement, or could not be resolved from the parent cross-peak. In an effort to more clearly resolve the ^{29}Si satellites of the COSY NMR cross-peaks, two modifications of a standard 2D COSY experiment were investigated. One modification involved applying broadband ^{31}P decoupling during FID acquisition of a dqf COSY ^1H – ^1H NMR experiment (a 2D ^1H – $^1\text{H}\{^{31}\text{P}\}$ dqf COSY NMR experiment), as a means to increase the signal/noise and improve resolution of the cross-peaks by concentrating the signal (which is spread into a multiplet by coupling to four ^{31}P atoms) over a smaller area. The second modification was ^{29}Si editing to filter out all of the signal which is not

interacting with ^{29}Si . This 2D ^{29}Si _edited ^1H - ^1H COSY NMR experiment eliminates the parent cross-peak (which contains 95% of the intensity), allowing ^{29}Si satellites which overlap with the parent cross-peak to be resolved. Furthermore, it increases the signal-to-noise for the ^{29}Si satellites by removing unnecessary signal, allowing for a much higher receiver gain.

Figure 6.8 shows a comparison of the cross-peaks required to measure the sign of $J_{\text{Si,H}}$ for various protons in ^1H - ^1H dqf COSY, ^1H - $^1\text{H}\{^{31}\text{P}\}$ dqf COSY, and ^{29}Si _edited ^1H - ^1H COSY NMR spectra for the two experimentally observed isomers of $[(\text{dmpe})_2\text{MnH}_2(\text{SiHEt}_2)]$ ($\mathbf{18}^{\text{Et}2}$) at 229 K. These experiments used the same NMR sample, the same number of scans, and identical td1eff values (leading to nearly identical experiment times), and it can be seen that the ^1H - $^1\text{H}\{^{31}\text{P}\}$ dqf COSY experiment provided only a marginal improvement in resolution relative to a standard ^1H - ^1H dqf COSY spectrum; likely because decoupling was only possible in the direct dimension, so the signal remained spread out in the indirect dimension (the y-axis). By contrast, the ^{29}Si _edited ^1H - ^1H COSY experiment provided substantially more intense ^{29}Si satellites and allowed for more accurate identification of ^{29}Si satellite peak positions, as well as observation of satellites buried under the parent cross-peak in the standard ^1H - ^1H dqf COSY spectrum. Therefore, all further discussion focuses on the results of ^{29}Si _edited ^1H - ^1H COSY experiments.

The top row of Figure 6.8 shows the cross-peak, in *central-18* $^{\text{Et}2}$, between the terminal SiH proton (H_{Si}) and the hydride ligands bridging between Si and Mn ($2 \times \text{H}_{\text{MnSi}}$; equivalent on the NMR timescale). The middle row of Figure 6.8 shows the cross-peak, in *transHSi-18* $^{\text{Et}2}$, between the terminal SiH proton (H_{Si}) and the single hydride bridging between Si and Mn (H_{MnSi}). The positive slope of the line between the ^{29}Si satellites on both of these cross-peaks is indicative of negative $J_{\text{Si,H}}$ values for the H_{MnSi} protons in *central-18* $^{\text{Et}2}$ and *transHSi-18* $^{\text{Et}2}$ (-47 and -54 Hz, respectively). By contrast, the bottom row of Figure 6.8 shows the cross-peak between H_{MnSi} and the terminal hydride ligand, H_{Mn} , in *transHSi-18* $^{\text{Et}2}$. In this case, because $J_{\text{Si,H}}$ has been determined to

be negative for H_{MnSi} in *transHSi-18*^{Et2} (*vide supra*), the negative slope of the line between the ²⁹Si satellites indicates that $J_{Si,H}$ for H_{Mn} in *transHSi-18*^{Et2} is positive (5 Hz), as expected for a 2-bond ²⁹Si–¹H coupling.

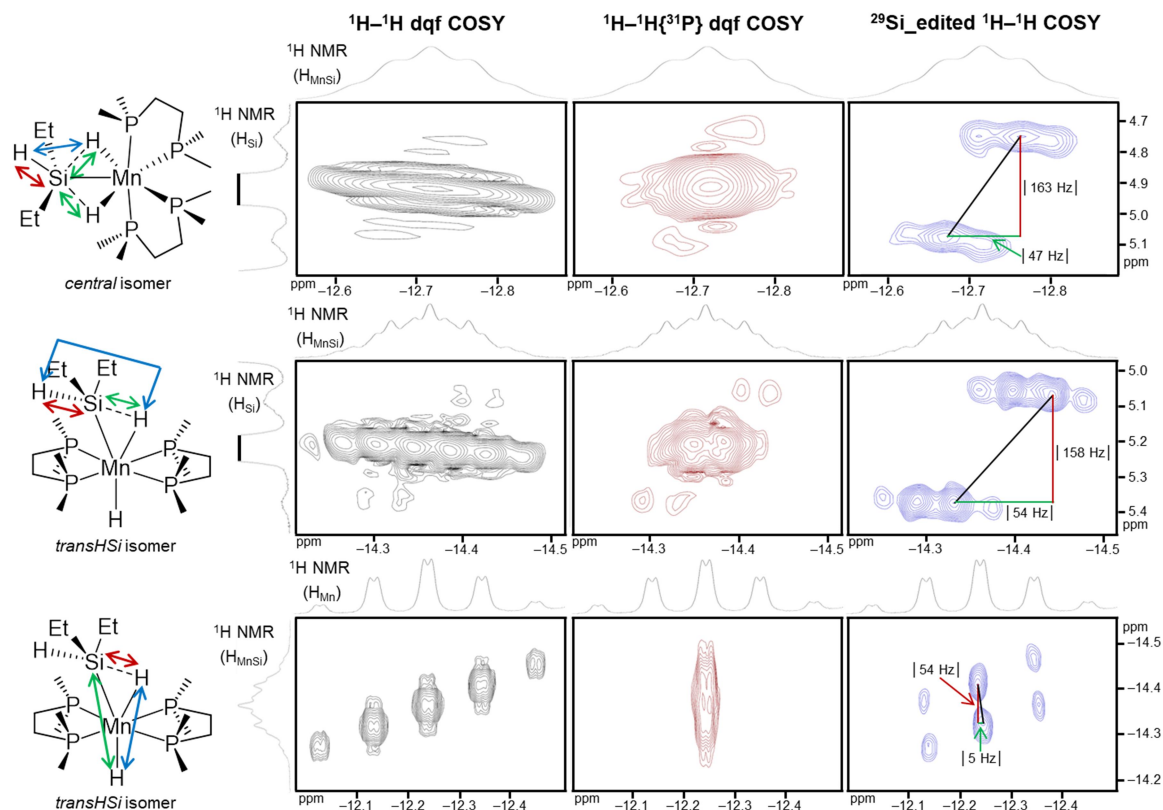


Figure 6.8: Comparisons of ¹H–¹H COSY spectra (500 MHz, *d*₈-toluene) of [(dmpe)₂MnH₂(SiHEt₂)] (**18**^{Et2}) at 229 K showing cross-peaks (with ²⁹Si satellites) used to measure the sign and magnitude of $J_{Si,H}$ via coupling between (top row) *central* isomer H_{Si} and H_{MnSi} environments, (middle row) *transHSi* isomer H_{Si} and H_{MnSi} environments, and (bottom row) *transHSi* isomer H_{MnSi} and H_{Mn} environments. From left to right within a row, the same spectral regions are shown with equivalent acquisition parameters (e.g. ns, tdl) in the standard ¹H–¹H dqf COSY spectrum (black), the ¹H–¹H{³¹P} dqf COSY spectrum (red), and the ²⁹Si-edited ¹H–¹H COSY spectrum (blue). Peak labels match those in Figure 6.6. In the structures to the left of each row, the blue arrow indicates the two ¹H environments whose active coupling gives rise to the cross-peak shown, the red

arrow indicates the passive ^1H - ^{29}Si coupling used as an internal reference in the measurement, and the green arrow indicates the passive ^1H - ^{29}Si coupling being measured. The lines on the cross-peaks in the ^{29}Si _edited ^1H - ^1H COSY spectra represent the vector between the ^{29}Si satellites (black line; used to determine relative sign), the magnitude of the coupling used as the internal reference (red line), and the magnitude of $J_{\text{Si,H}}$ for which the sign is being determined (green line).

Analogous trends were observed for the *central* and *transHSi* isomers of $\mathbf{18}^{\text{Ph}2}$ and $\mathbf{18}^{\text{R}}$ (Table 6.3). However, we were unable to observe coupling constants from particularly weak cross-peaks, precluding determination of the sign of $J_{\text{Si,H}}$ for H_{MnSi} in the *central* isomers of $\mathbf{18}^{\text{Ph}2}$ and $\mathbf{18}^{\text{Bu}}$ or for H_{Mn} in the *transHSi* isomer of $\mathbf{18}^{\text{Ph}2}$ (present as a minor isomer; 13%). DFT-calculated coupling constants are also provided in Table 6.3, and are in good agreement with those determined experimentally.

Table 6.3: ^{29}Si -H coupling constants ($J_{\text{Si,H}}$) measured by ^{29}Si _edited ^1H - ^1H COSY NMR spectroscopy (and calculated by DFT) for silyl dihydride complexes $\mathbf{18}$ (Hz).

Complex	$\mathbf{18}^{\text{Ph}2}$	$\mathbf{18}^{\text{Et}2}$	$\mathbf{18}^{\text{Ph}}$	$\mathbf{18}^{\text{Bu}}/\mathbf{18}^{\text{Et}}$
Silyl group	SiHPh ₂	SiHEt ₂	SiH ₂ Ph	SiH ₂ ⁿ Bu ^a
$J_{\text{Si,H}}$ for H_{MnSi} in the <i>central</i> isomer	n.o. ^b (-45, -49)	-47 (-35, -45)	<0° (-41, -44)	n.o. ^b (-38, -43)
$J_{\text{Si,H}}$ for H_{MnSi} in the <i>transHSi</i> isomer	-41 (-38)	-54 (-47)	-38 (-26)	-43 (-33)
$J_{\text{Si,H}}$ for H_{Mn} in the <i>transHSi</i> isomer	n.o. ^b (13)	5 (12)	9 (13)	9 (14)

a. In the calculated complex, $\mathbf{18}^{\text{Et}}$, the silyl group is SiH₂Et.

b. n.o. = not observed.

c. This cross-peak was too broad to accurately measure.

For the *central* isomer of $\mathbf{18}^{\text{Et}2}$, the $J_{\text{Si,H}}$ coupling constant for H_{MnSi} is -47 Hz, and the average calculated values for $\mathbf{18}$ range from -40 to -47 Hz. Literature values of $J_{\text{Si,H}}$ for H_{MnSi} in η^3 -coordinated silicate (H_2SiR_3^-) complexes typically range in magnitude from 11 to 54 Hz.^{244,247,248,272,273,275} To the best of our knowledge, the sign of $J_{\text{Si,H}}$ has not been experimentally determined for these literature complexes, but calculations have, in at least one case, been performed and indicate a negative sign.²⁴⁷ Assuming that all of these $J_{\text{Si,H}}$ values are negative, the $J_{\text{Si,H}}$ coupling constants for H_{MnSi} in $\mathbf{18}$ lie towards the more negative end of the reported range, indicative of nonclassical silicate complexes with relatively strong Si- H_{MnSi} interactions.

For the *transHSi* isomer of **18**, the $J_{\text{Si,H}}$ coupling constants for H_{MnSi} range from -38 to -54 Hz (calcd. -26 to -47 Hz), falling within the region typically associated with nonclassical hydrosilane complexes (0 to -70 Hz; *vide infra*), indicative of partial oxidative addition of the Si– H_{MnSi} bond. Using both experimental and calculated values, two clear trends can be observed in $J_{\text{Si,H}}$ for H_{MnSi} in the *transHSi* isomers; more negative $J_{\text{Si,H}}$ coupling constants were seen for aliphatic versus aromatic analogues, and for disubstituted versus monosubstituted analogues. This trend appears to reflect the trend in calculated bond metrics (*vide supra*), for which stronger Si–H interactions were observed in aliphatic and disubstituted analogues (relative to aromatic and monosubstituted analogues respectively). The former can be rationalized based on a larger degree of π backdonation to hydrosilanes with aryl substituents, whereas the latter is presumably steric in origin, with disubstituted hydrosilanes decreasing the extent of Si–H bond oxidative addition.

6.7 – Summary and Conclusions for Chapter 6

Silyl dihydride complexes of manganese, $[(\text{dmpe})_2\text{MnH}_2(\text{SiHRR}')] (\mathbf{18})$, were synthesized via the reactions of H_2 with silylene hydride ($\mathbf{16}^{\text{R}2}$) and disilyl hydride ($\mathbf{20}^{\text{R}}$) complexes. These reactions suggest that both $\mathbf{16}^{\text{R}2}$ and $\mathbf{20}^{\text{R}}$ exist in equilibrium with a shared low-coordinate silyl species, $[(\text{dmpe})_2\text{Mn}(\text{SiH}_{3-x}\text{R}_x)] (\mathbf{17})$, accessed via 1,1-insertion from $\mathbf{16}^{\text{R}2}$, and hydrosilane reductive elimination from $\mathbf{20}^{\text{R}}$.

Complexes **18** provide an uncommon opportunity to study silyl dihydride complexes differing in the number (1 vs 2) and nature (aromatic vs alkyl) of the hydrocarbyl substituents on silicon. In solution, these complexes exist as an equilibrium mixture of a *central* isomer featuring a meridional H–Si–H arrangement of the silyl and hydride ligands, and a *transHSi* isomer with *trans*-disposed hydrosilane and hydride ligands. These isomers contain a single silicon centre involved in either one or two Si–H–Mn bridging interactions, and combined XRD, DFT, and NMR spectroscopic studies indicate that the *central* and *transHSi* isomers can be considered to contain a nonclassical

silicate ($\eta^3\text{-H}_2\text{SiR}_3$) anion, and a nonclassical hydrosilane ligand, respectively. Additionally, DFT calculations indicate the thermodynamic accessibility of *lateralH₂* and *transH₂* isomers with *cis*- and *trans*-disposed silyl and dihydrogen ligands, respectively (these isomers may be present in solution at concentrations below that detectable by NMR spectroscopy). Furthermore, a *lateralHSi* isomer featuring *cis*-disposed hydride and nonclassical hydrosilane ligands was observed in DFT calculations on sterically-minimized PH₃ analogues of **18**.

Measurement of the sign and magnitude of $J_{\text{Si,H}}$ in the *central* and *lateralHSi* isomers of **18** was made possible using a modification of Scherer's method, employing 2D ^1H - ^1H COSY NMR spectroscopy with ^{29}Si editing to remove all of the signal which is not interacting with ^{29}Si . This ^{29}Si _edited ^1H - ^1H COSY experiment allowed accurate location of ^{29}Si satellites which were unobserved in 'standard' ^1H - ^1H dqf COSY experiments. Additionally, it allowed determination of small $J_{\text{Si,H}}$ couplings (e.g. 5 Hz) where the pertinent signals are broadened by ^{31}P coupling; previous methods to determine the magnitude of similar couplings relied upon experiments requiring non-standard NMR probes which can simultaneously be tuned to ^{29}Si and ^{31}P (e.g. $^{29}\text{Si}\{^{31}\text{P}\}$ INEPT^{zz} and ^{29}Si - ^1H - $\{^{31}\text{P}\}$ HMQC^{aaa} experiments). By contrast, the ^{29}Si _edited ^1H - ^1H COSY experiment used in this report can be run on a standard double resonance NMR probe with a single broadband channel.

The utility of the ^{29}Si _edited ^1H - ^1H COSY NMR experiment was also highlighted by measurement of the sign and magnitude of $J_{\text{Si,H}}$ for H_{MnSi} in the nonclassical disilyl hydride complexes $[(\text{dmpe})_2\text{MnH}(\text{SiH}_2\text{R})_2]$ (**20^{Ph}**: R = Ph, **20^{Bu}**: R = ⁿBu). These experiments afforded coupling constants of -31 Hz (**20^{Ph}**) and -30 Hz (**20^{Bu}**), which are

^{zz} For examples of these experiments used to determine $J_{\text{Si,H}}$, see refs. 249 and 512.

^{aaa} For an example of such an experiment used to measure $J_{\text{Si,H}}$ in a nonclassical hydrosilane complex, see ref. 251.

in good agreement with the calculated values of -24 and -27 Hz, respectively (see Chapter 5).^{bbb}

^{bbb} Using 2D $^{29}\text{Si}-^1\text{H}$ HMBC NMR spectroscopy, we measured a magnitude for $J_{\text{Si,H}}$ of 36 Hz in **20^{Ph}**, and were unable to measure $J_{\text{Si,H}}$ for **20^{Bu}**.

Chapter 7

Reactions of Manganese Disilyl Hydride Complexes with Reagents Containing Unsaturated Polar Bonds

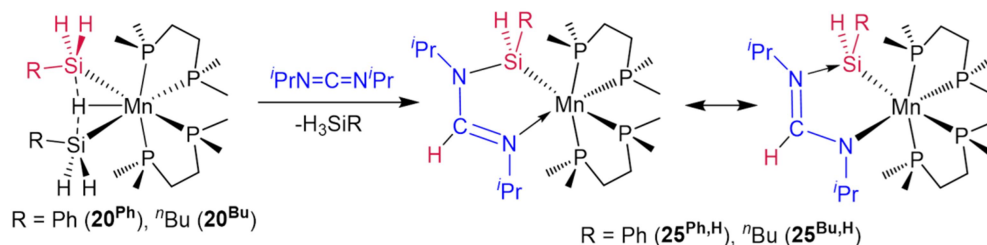
7.1 – Introduction to Chapter 7

Chapter 5 described the synthesis of manganese disilyl hydride complexes $[(\text{dmpe})_2\text{MnH}(\text{SiH}_2\text{R})_2]$ ($\mathbf{20}^{\text{Ph}}$: R = Ph, $\mathbf{20}^{\text{Bu}}$: R = *n*Bu), and reactions of $\mathbf{20}^{\text{R}}$ with ethylene to form silene hydride complexes $[(\text{dmpe})_2\text{MnH}(\text{RHSi}=\text{CHMe})]$ ($\mathbf{19}^{\text{Ph,H}}$: R = Ph, $\mathbf{19}^{\text{Bu,H}}$: R = *n*Bu). We proposed that these reactions could proceed via initial formation of a 5-coordinate silyl ($\mathbf{17}^{\text{R}}$) or a silylene hydride ($\mathbf{16}^{\text{R2}}$) intermediate, accessed from $\mathbf{20}^{\text{R}}$ by hydrosilane elimination, followed by (for $\mathbf{16}^{\text{R2}}$) α -hydride elimination. In addition, Chapter 6 described reactions of $\mathbf{20}^{\text{R}}$ with H_2 to form silyl dihydride complexes $[(\text{dmpe})_2\text{MnH}_2(\text{SiH}_2\text{R})]$ ($\mathbf{18}^{\text{R}}$), presumably proceeding via some silyl intermediate, $\mathbf{17}^{\text{R}}$. Herein, we report the reactions of $\mathbf{20}^{\text{Ph}}$ with reagents containing unsaturated polar bonds, specifically diisopropylcarbodiimide and carbon dioxide, for comparison with the aforementioned reactivity involving apolar C=C bonds.

7.2 – Synthesis and Characterization of $[(\text{dmpe})_2\text{Mn}\{\kappa^2\text{-SiHR}(\text{N}^i\text{PrCHN}^i\text{Pr})\}]$

Disilyl hydride complexes $[(\text{dmpe})_2\text{MnH}(\text{SiH}_2\text{R})_2]$ ($\mathbf{20}^{\text{Ph}}$: R = Ph, $\mathbf{20}^{\text{Bu}}$: R = *n*Bu) reacted with diisopropylcarbodiimide $\{\text{C}(\text{N}^i\text{Pr})_2\}$ to form the manganese(I) amidinylsilyl complexes $[(\text{dmpe})_2\text{Mn}\{\kappa^2\text{-SiHR}(\text{N}^i\text{PrCHN}^i\text{Pr})\}]$ ($\mathbf{25}^{\text{Ph,H}}$: R = Ph, $\mathbf{25}^{\text{Bu,H}}$: R = *n*Bu); Scheme 7.1. These metallacycles feature a 5-membered M–Si–N–C–N ring, where one of the two hydrogen substituents originating from a silyl ligand in $\mathbf{20}^{\text{R}}$ is located on the central carbon atom of the $^i\text{PrNCN}^i\text{Pr}$ unit. Complexes $\mathbf{25}^{\text{R,H}}$ are chiral at the metal centre and silicon, and in solution, two diastereomers were observed (in thermodynamic ratios

of 2.8:1 and 2.3:1, respectively),^{ccc} each with an NC(*H*)N signal at 7.58-7.70 ppm and an Si*H* signal at 5.50-6.26 ppm in the ¹H NMR spectra, as well as a ²⁹Si NMR peak between 81.1 and 87.1 ppm.



Scheme 7.1: Reactions of disilyl hydride complexes [(dmpe)₂MnH(SiH₂R)₂] (**20^{Ph}**: R = Ph, **20^{Bu}**: R = ⁿBu) with diisopropylcarbodiimide to afford the amidinylsilyl complexes [(dmpe)₂Mn{κ²-SiHR(N^{*i*}PrCHN^{*i*}Pr)}] (**25^{Ph,H}**: R = Ph, **25^{Bu,H}**: R = ⁿBu). Only one diastereomer of **25^{R,H}** is shown, as two canonical structures.

The ²⁹Si NMR chemical shifts in **25^{R,H}** (*vide supra*) are comparable to those of base-stabilized silylene complexes, and a similarly high frequency resonance (65.4 ppm) has been used to suggest that the bonding environment in [Cp*(OC)₂Mo(κ²{Si,*N*}-Si{*p*-tol}₂{N(H)C₅H₄N})] (which contains a comparable M–Si–N–C–N metallacycle) involves a contribution from a base-stabilized silylene resonance structure.⁵²¹ However, ²⁹Si resonances at only slightly lower frequencies have also been reported for aminosilyl complexes such as [Cp*(OC)₂Fe{SiMe₂(NR₂)}] (R = Me, ^{*i*}Pr, Ph; ²⁹Si δ = 53-47 ppm).⁵²²

X-ray quality crystals of amidinylsilyl complex **25^{Ph,H}** were obtained from a concentrated hexanes solution layered with hexamethyldisiloxane at –30 °C. The resulting structure contains disorder due to two overlapping diastereomers of **25^{Ph,H}**, and Figure 7.1 shows just one of these two components. At first glance, the X-ray crystal

^{ccc} No EXSY NMR cross-peaks were observed to show chemical interchange between the two diastereomers of **25^{R,H}** (up to 60 °C). However, such an equilibrium was inferred by heating solutions starting with different ratios of the two isomers (obtained for preferential recrystallization), yielding solutions with consistent (i.e. thermodynamic) ratios.

structure and DFT calculations ($\mathbf{25}^{\text{Bu,H}}$ was modelled with the ^nBu group replaced by an Et group) indicate that the monoanionic $\{\kappa^2\text{-SiHR}(\text{N}^i\text{PrCHN}^i\text{Pr})\}$ ligand can be described as a bidentate amidinylsilyl ligand, with Mn–Si distances of 2.347(1)-2.358(1) Å (calcd. 2.32 for $\mathbf{25}^{\text{R,H}}$, with Mayer bond orders of 0.93-0.95), and Mn–N distances of 2.137(3)-2.141(3) Å (calcd. 2.12-2.13 for $\mathbf{25}^{\text{R,H}}$, with Mayer bond orders of 0.58-0.59). The Mn–Si distances lie at the shorter end of the range observed for Mn(I) silyl complexes with dmpe co-ligands (e.g. 2.35-2.44 Å in $\mathbf{21a-d}$; Chapter 5), but are longer than those in related NHC-stabilized silylene hydride complexes (2.26-2.30 Å in $\mathbf{22a-d}$; Chapter 5). However, the two C–N distances in the metallacycle are more similar than would be expected for localized single and double bonds. The C–N bonds closer to silicon and manganese are 1.350(4)-1.350(5) Å (calcd. 1.34-1.35 Å for $\mathbf{25}^{\text{R,H}}$, with Mayer bond orders of 1.23-1.25) and 1.296(6)-1.299(5) Å (calcd. 1.31 Å for $\mathbf{25}^{\text{R,H}}$, with Mayer bond orders of 1.50), respectively; cf. 1.46 Å for a typical C–N single bond and 1.21 Å for a typical C–N double bond.⁵²³ Furthermore, the Si–N distances of 1.805(3)-1.813(3) Å (calcd. 1.82 Å for $\mathbf{25}^{\text{R,H}}$, with Mayer bond orders of 0.69-0.74) are longer than those in free aminosilanes (1.70-1.76 Å).⁵²⁴ Together, these bond metrics suggest that $\mathbf{25}^{\text{R,H}}$ may be better described using a combination of the two resonance structures in Scheme 7.1; one with anionic aminosilyl and neutral imine donors on manganese (left), and the other with a neutral base-stabilized silylene and an anionic amido donor on manganese (right). Similar resonance structures have been employed to describe the bonding situation in a pair of M–Si–N–C–N metallacycles (M = Mo, Ru) where the N donor on the metal is part of a pyridine ring, as well as in related M–Si–O–C–E (E = O, N) metallacycles.^{505,521,525}

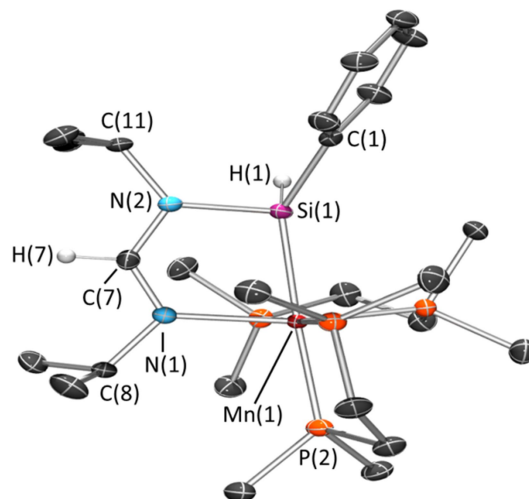
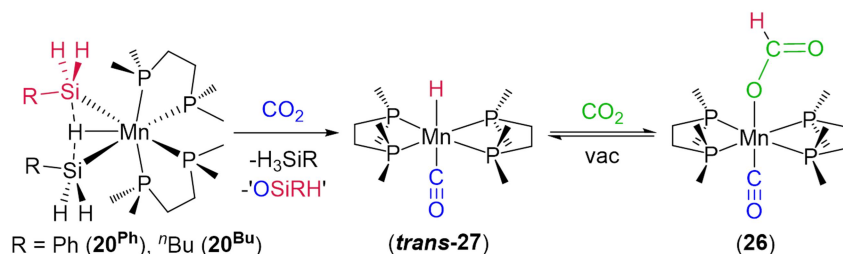


Figure 7.1: X-ray crystal structure of $[(dmpe)_2Mn\{\kappa^2\text{-SiHPh}(N^iPrCHN^iPr)\}]$ (**25^{Ph,H}**) with ellipsoids at 50% probability. Most hydrogen atoms have been omitted for clarity. H(1) and H(7) were located from the difference map and refined isotropically. Two independent and essentially isostructural molecules were observed in the unit cell, only one of which is shown. Atom labels with an A suffix correspond to those without a suffix in the structure not shown. Bond distances (Å) and angles (deg): Mn(1)–Si(1) 2.347(1), Mn(1A)–Si(1A) 2.358(1), Mn(1)–N(1) 2.137(3), Mn(1A)–N(1A) 2.141(3), Si(1)–H(1) 1.44(5), Si(1A)–H(1A) 1.50(6), Si(1)–C(1) 1.934(4), Si(1A)–C(1A) 1.938(3), Si(1)–N(2) 1.815(3), Si(1A)–N(2A) 1.805(4), N(2)–C(7) 1.348(4), N(2A)–C(7A) 1.349(5), N(2)–C(11) 1.478(6), N(2A)–C(11A) 1.482(6), N(1)–C(7) 1.301(6), N(1A)–C(7A) 1.298(6), N(1)–C(8) 1.490(4), N(1A)–C(8A) 1.485(6), C(7)–H(7) 0.98(4), C(7A)–H(7A) 0.96(6), N(1)–Mn(1)–Si(1) 80.14(9), N(1A)–Mn(1A)–Si(1A) 79.45(9), Mn(1)–Si(1)–C(1) 136.4(1), Mn(1A)–Si(1A)–C(1A) 132.8(1), Mn(1)–Si(1)–H(1) 118(2), Mn(1A)–Si(1A)–H(1A) 120(2), Mn(1)–Si(1)–N(2) 100.5(1), Mn(1A)–Si(1A)–N(2A) 100.6(1), Si(1)–N(2)–C(7) 114.6(3), Si(1A)–N(2A)–C(7A) 115.1(3), Si(1)–N(2)–C(11) 126.2(2), Si(1A)–N(2A)–C(11A) 125.7(2), N(2)–C(7)–N(1) 123.9(3), N(2A)–C(7A)–N(1A) 123.3(3), C(7)–N(1)–Mn(1) 120.4(3), C(7A)–N(1A)–Mn(1A) 121.1(3), C(7)–N(1)–C(8) 114.0(3), C(7A)–N(1A)–C(8A) 113.8(3), C(11)–N(2)–C(7) 117.9(3), C(11A)–N(2A)–C(7A) 119.2(3), C(8)–N(1)–Mn(1) 125.5(2), C(8A)–N(1A)–Mn(1A) 125.1(3).

7.3 – Synthesis and Characterization of *trans*-[(dmpe)₂Mn(CO)(κ¹-O₂CH)] (**26**)

Whereas the reactions of **20^R** with diisopropylcarbodiimide yielded structures in which the NCN unit remained intact, reactions with carbon dioxide afforded *trans*-[(dmpe)₂Mn(CO)(κ¹-O₂CH)] (**26**; Scheme 7.2), in which one equivalent of CO₂ has been converted to CO. Synthesis of this carbonyl formate complex was accompanied by silane (H₃SiR) elimination and the formation of benzene-soluble byproducts thought to be polysiloxanes {(SiHRO)_n, R = Ph or ⁿBu};⁵²⁶ these byproducts gave rise to ¹H NMR signals at 4.8-5.5 ppm in the SiH region, cumulatively integrating to a single SiH residue per equivalent of **26**, and correlated to ²⁹Si NMR signals ranging from -21 to -36 ppm (for R = Ph, further reactivity between the byproducts ensued). Such reactivity mirrors reported reactions of free silylenes with CO₂, which also yield polysiloxanes.³⁰⁰



Scheme 7.2: Reaction of disilyl hydride complexes [(dmpe)₂MnH(SiH₂R)₂] (**20^{Ph}**: R = Ph, **20^{Bu}**: R = ⁿBu) with carbon dioxide to afford the formate complex *trans*-[(dmpe)₂Mn(CO)(κ¹-O₂CH)] (**26**).

Compound **26** was obtained in pure form by sublimation to afford a 60 : 40 mixture of **26** and known *trans*-[(dmpe)₂MnH(CO)] (*trans*-27),¹⁷³ the product of CO₂ elimination from the formate ligand, followed by re-exposure to CO₂ to re-form **26**. In fact, **26** was only stable at room temperature under an atmosphere of CO₂, eliminating CO₂ slowly under argon (either as a solid or in solution) or under vacuum (approx. 2% conversion after 20 min.). DFT calculations afforded a ΔG of less than 0.1 kJ mol⁻¹ for this process at 298.15 K, reflecting the observed thermodynamic reversibility; to the best

of our knowledge, this is the first example of reversible CO₂ insertion/deinsertion into a manganese–hydride bond.^{ddd}

NMR spectra of **26** feature a single ³¹P NMR environment at 68.3 ppm, and only five ¹H NMR signals {four from the dmpe ligands between 1.23 and 1.90 ppm, and one (a pentet with $J_{31\text{P}-1\text{H}}$ of 2 Hz) for the formyl proton at 8.68 ppm}. Complex **26** also formed cleanly upon exposure of [(dmpe)₂MnH(=SiEt₂)] (**16**^{Et2}) to CO₂, whereas reaction of [(dmpe)₂MnH(C₂H₄)] (**10**) with CO₂ only afforded **26** in low yield, accompanied by free dmpe and unidentified byproducts.

X-ray quality crystals of **26** were obtained from a concentrated toluene solution layered with hexamethyldisiloxane at –30 °C, and confirmed the expected octahedral geometry with *trans*-disposed carbonyl and κ¹-formate ligands (Figure 7.2). The equatorial dmpe ligands form a statistically perfect plane ($\sum\text{P-Mn-P} = 359.98(4)\text{-}360.01(4)^\circ$), the C–Mn–O angles are 172.23(5)-173.31(5)°, and the various bonding parameters related to the terminal formate unit {Mn–O distances of 2.086(1)-2.096(1) Å, O–C distances of 1.266(2)-1.275(2) Å, O=C distances of 1.229(2)-1.237(2) Å, and Mn–O–C angles of 178.5(1)-179.3(1)°} are all within the range previously observed for terminal manganese formate complexes.²¹¹

^{ddd} For examples of irreversible CO₂ insertion into a terminal Mn–H bond, see refs. 170 and 527.

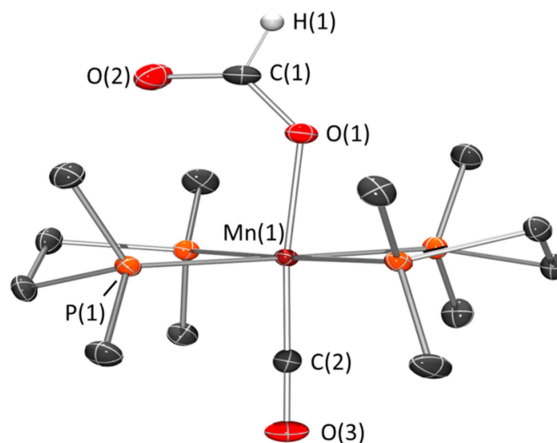


Figure 7.2: X-ray crystal structure of *trans*-[(dmpe)₂Mn(CO)(κ¹-O₂CH)] (**26**), with ellipsoids drawn at 50% probability. H(1) was located from the difference map and refined isotropically. Most hydrogen atoms have been omitted for clarity. Two independent and essentially isostructural molecules are observed in the unit cell, one of which is shown. Atom labels with the A suffix correspond to atoms labels without a suffix in the structure not shown. Bond distances (Å) and angles (deg): Mn(1)–O(1) 2.096(1), Mn(1A)–O(1A) 2.086(1), Mn(1)–C(2) 1.751(1), Mn(1A)–C(2A) 1.742(1), O(1)–C(1) 1.275(2), O(1A)–C(1A) 1.266(2), C(1)–O(2) 1.229(2), C(1A)–O(2A) 1.237(2), C(1)–H(1) 0.97(2), C(1A)–H(1A) 0.98(2), C(2)–O(3) 1.191(2), C(2A)–O(3A) 1.175(2), C(2)–Mn(1)–O(1) 173.31(5), C(2A)–Mn(1A)–O(1A) 172.23(5), Mn(1)–C(2)–O(3) 178.5(1), Mn(1A)–C(2A)–O(3A) 179.3(1), Mn(1)–O(1)–C(1) 133.78(9), Mn(1A)–O(1A)–C(1A) 133.53(9), O(1)–C(1)–O(2) 128.8(1), O(1A)–C(1A)–O(2A) 128.9(1), O(1)–C(1)–H(1) 116(1), O(1A)–C(1A)–H(1A) 114(1), O(2)–C(1)–H(1) 115(1), O(2A)–C(1A)–H(1A) 117(1).

7.4 – Potential Pathways for Reactions of Disilyl Hydride Complexes with {C(N^{*i*}Pr)₂} or CO₂

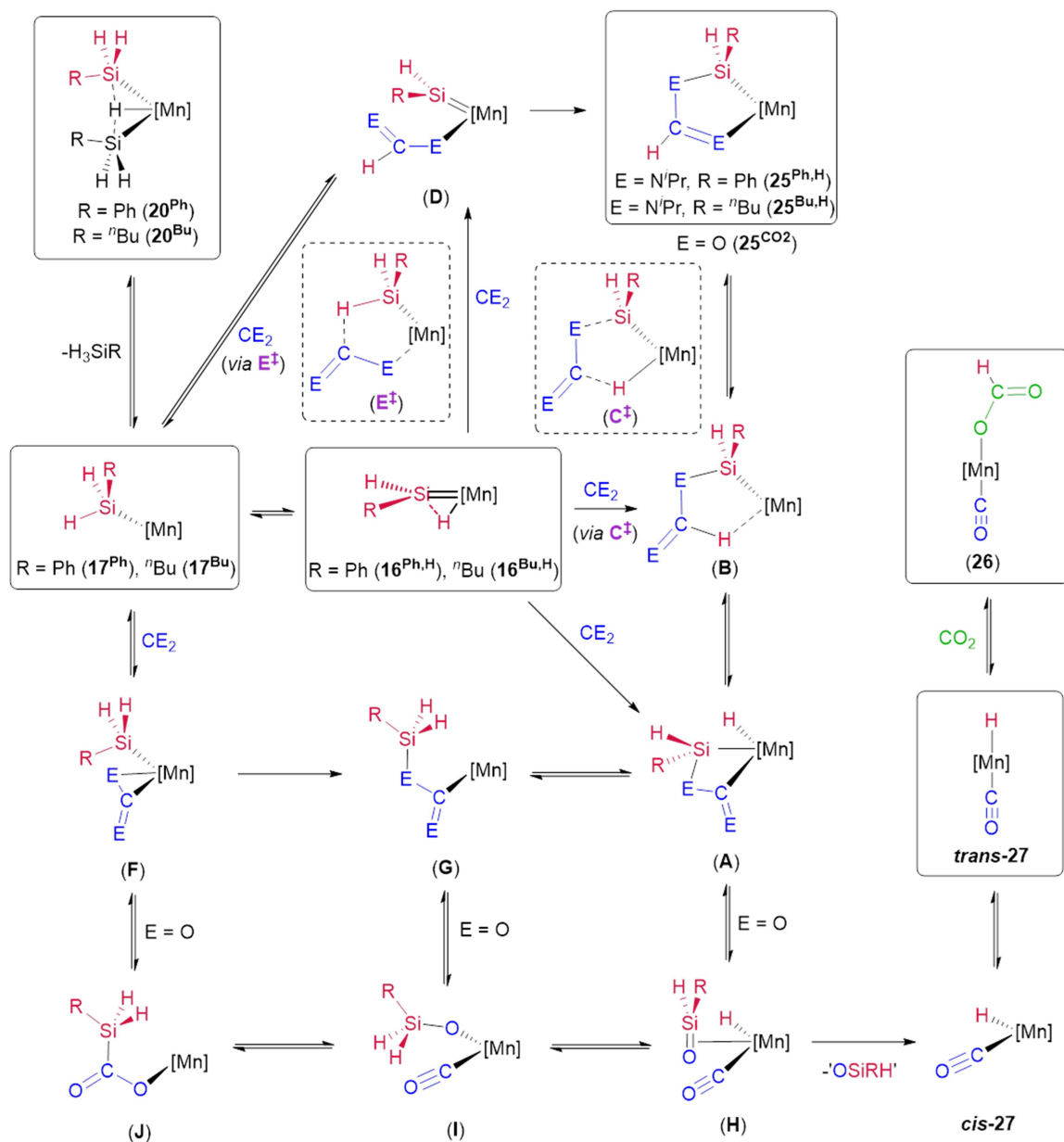
Reactions of the disilyl hydride complexes **20^R** with C(N^{*i*}Pr)₂ or CO₂ afforded [(dmpe)₂Mn{κ²-SiHR(N^{*i*}PrCHN^{*i*}Pr)}] (**25^{Ph,H}**; R = Ph, **25^{Bu,H}**; R = ^{*n*}Bu) and [(dmpe)₂Mn(CO)(κ¹-O₂CH)] (**26**), respectively (*vide supra*). These reactions (Scheme

7.3) could proceed via a 5-coordinate silyl species (17^R) or a silylene hydride complex ($16^{R,H}$), both of which have been shown to be accessible from 20^R through combined computational studies, high temperature ^1H NMR spectroscopy, and trapping reactions with isonitriles and NHCs (Chapter 5).

The silylene hydride intermediates ($16^{R,H}$) present several plausible reaction pathways to the observed reaction products (Scheme 7.3). One possibility involves initial 2+2 cycloaddition of the Mn=Si double bond and a C=E (E = N^{*i*}Pr, O) bond to afford a metallacyclobutane intermediate **A**. This cycloaddition reaction could proceed either in a concerted or two-step process (via initial base coordination to the silicon centre), and similar mechanistic steps have been proposed for reactions of ruthenium silylene hydride complexes with RC≡N,³⁴³ RNCO,⁵⁰⁴ and MesNCS.^{505,528} Subsequent C–H bond-forming reductive elimination from **A** would then generate intermediate **B**, and isomerization would afford compound **25**; the observed product {R = Ph ($25^{\text{Ph,H}}$) or ^{*n*}Bu ($25^{\text{Bu,H}}$)} in reactions with {C(N^{*i*}Pr)₂}.

It is also conceivable that intermediate **B** could be formed directly from $16^{R,H}$ and CE₂ via an outer sphere mechanism involving formal 2+3 cycloaddition of the Si=M–H unit across one of the C=E bonds. Such a process (either concerted or two-step), via a transition state with a M–Si–E–C–H ring system (analogous to C^\ddagger), has been suggested for reactions of ruthenium silylene complexes with MesNCO^{505,528} and CO₂,⁵²⁹ and a similar transition state was also suggested for the reaction of a tungsten silylene hydride complex with acetone.³²⁷

An alternative route to compound **25** could involve CE₂ insertion into the Mn–H bond of a silylene hydride complex ($16^{R,H}$) to afford silylene formate or formamidinate {HC(NR)₂} intermediate **D**, with subsequent cyclization (involving nucleophilic attack of the formate or formamidinate anion on the silylene).



Scheme 7.3: Potential pathways for the reactions of $[(\text{dmpe})_2\text{MnH}(\text{SiH}_2\text{R})_2]$ (20^{Ph} : $\text{R} = \text{Ph}$, 20^{Bu} : $\text{R} = \text{}^n\text{Bu}$) with $\text{E}=\text{C}=\text{E}$ ($\text{E} = \text{N}^i\text{Pr}$, O). $[\text{Mn}] = \text{Mn}(\text{dmpe})_2$. For some compounds, more than one isomer is likely to be accessible (e.g. *cis* vs *trans*, the presence/absence of an interaction between silicon and an adjacent hydride ligand, or coordination/lack of coordination of lone pairs on E to the metal centre), but for clarity, only one isomer is shown. Solid boxes indicate known complexes and intermediates.

The reactions of **20^R** with CO₂ and C(N^{*i*}Pr)₂ could also proceed via 5-coordinate silyl intermediates **17^R** instead of silylene hydride intermediates **16^{R,H}** (Scheme 7.3). In one such mechanism, intermediate **D** could be accessed directly from silyl intermediates **17^R** via initial 2+3 cycloaddition of the Mn–Si–H moiety on silyl complexes **17^R** across one of the E=C bonds {forming a delocalized M–Si–H–C–E ring system (**E[‡]**)}. This is analogous to mechanisms proposed by Whited et al. in the reaction of a ruthenium silylene hydride with CO₂,⁵²⁹ and computationally investigated (though discarded as higher in energy) by We and Lin et al. for the reactions of a tungsten silylene hydride complex with acetonitrile and acetone.⁵³⁰

Alternatively, reactions of **17^R** could involve initial CO₂/C(N^{*i*}Pr)₂ coordination to afford manganese(III) intermediate **F**, followed by Si–E bond-forming reductive elimination to generate acyl intermediate **G**, which could then undergo oxidative addition of an Si–H bond across the metal centre to form previously mentioned metallacyclobutyl intermediate **A**. While 1,2-insertion reactions involving C(NR)₂ and silyl ligands typically form silylamidinate {R₃SiC(NR)₂} ligands,⁵³¹ N–Si bond-formation has been observed in the reaction of [(C₅H₄N)(OC)CpFe(SiR₃)] with diisopropylcarbodiimide to generate a –C(=N^{*i*}Pr)N(^{*i*}Pr)(SiR₃) ligand.⁵³² Additionally, Tobita et al. proposed an equivalent mechanism for the reactions of ruthenium silylene hydride complexes with aldehydes (involving Si–O bond-forming 1,2-insertion of an η²-aldehyde ligand into a metal–silyl bond).⁵³³ These two mechanistic proposals are reflected in our proposed transformation from intermediate **F** to **G**, while the latter report includes subsequent oxidative addition of the Si–H bond to form a metallacyclic structure analogous to intermediate **A**.⁵³³

The above reaction pathways provide access to structure **25**; the final product in reactions with carbodiimides. However, in the case of CO₂, further reactivity ensues to generate **26**, where CO ligand formation is accompanied by polysiloxane {(RHSiO)_n} elimination; this reactivity bears some resemblance to the C–S bond cleavage observed upon reaction of [Cp*(CO)RuH{=SiHC(SiMe₃)₃}] with MesNCS.^{505,528}

One potential route to compound **26** involves cleavage of the O–C bond in **A** to afford intermediate **H**, containing a hydride and a neutral sila-aldehyde ligand (O=SiHR; sila-aldehyde complexes of Mn are unknown, but Tobita recently reported a stable W complex with a η^2 -coordinated sila-aldehyde ligand,³³⁸ and silanone complexes have been proposed as reactive intermediates in the generation of polysiloxanes⁵³⁴), followed by sila-aldehyde elimination {yielding a polysiloxane, (RHSiO)_n} to afford compound **27** (*cis* or *trans*), which we have shown reversibly inserts CO₂ to afford **26**.

Two additional pathways could be envisaged to generate intermediate **H**, in both cases proceeding via intermediate **I**, which contains a siloxide (OSiH₂R) and a carbonyl ligand.

Firstly, the C(O)OSiR₃ ligand in compound **G** could undergo α -siloxide elimination to form **I**. To our knowledge, this type of reaction has not previously been proposed. However, it resembles the CNMes extrusion reaction observed for a C(NMes){SSiH₂C(SiMe₃)₃} ligand on ruthenium.^{505,528} Furthermore, the reverse process (1,1-insertion involving a siloxy group and a carbonyl ligand) has been observed in the reaction of [(Me₃P)Re(OSi^tBu)₃] with CO.⁵³⁵ Then compound **H** can be accessed from **I** by β -hydride elimination; β -hydride elimination from a siloxide ligand also has not been reported, but the reverse reaction (siloxide generating 1,2-insertion of a silanone into a metal hydride bond) has been proposed as a step in the catalytic disproportionation of siloxanes.⁵³⁶

Alternatively, intermediate **I** could be accessed from **F** by Si–C bond-forming 1,2-insertion to generate silyl carboxylate (R₃SiCO₂) complex **J**, followed by CO extrusion. Reactions of silyl ligands with CO₂ have been reported to form silyl carboxylate (R₃SiCO₂) complexes,^{537,538} and CO extrusion from some of these complexes has been observed to yield siloxide groups⁵³⁸ (DFT calculations have suggested that this step involves an outer-sphere migration of the SiR₃ moiety from C to O).⁵³⁹

7.5 – Summary and Conclusions for Chapter 7

Manganese disilyl hydride complexes **20^R** reacted with E=Si=E (E= ⁱPrN or O) to generate manganese(I) amidinylsilyl (**25^R**) or formate (**26**) complexes. The former features a rare TM–Si–N–C–N 5-membered ring, and the latter was found to undergo reversible CO₂ dissociation to generate a manganese(I) hydride complex (**27**). This reactivity presumably proceeds via one of two potential intermediates discussed in Chapter 5 for the reactions of **20^R** with ethylene; either a 5-coordinate silyl species (**17^R**) or a silylene hydride complex (**16^{R2}**). This work demonstrates the potential for manganese disilyl hydride complexes **20^R** to be precursors to a wide variety of novel manganese-containing species.

Chapter 8

Catalytic Hydrosilylation of Ethylene

Portions of this chapter have been reprinted (adapted) from Price, J. S.; Emslie, D. J. H. Interconversion and reactivity of manganese silyl, silylene, and silene complexes, *Chem. Sci.* **2019**, Advance Articles, DOI: 10.1039/C9SC04513A. Published by The Royal Society of Chemistry.

8.1 – Introduction of Chapter 8

Chapters 4 and 5 showed that silyl, silylene, and silene complexes can be prepared from reactions of $[(\text{dmpe})_2\text{MnH}(\text{C}_2\text{H}_4)]$ (**10**) with hydrosilanes, in some cases followed by ethylene. Therefore, we decided to investigate the potential for **10** to catalyze ethylene hydrosilylation in combination with primary and secondary hydrosilanes. Alkene hydrosilylation is an industrially important transition metal-catalyzed process for alkylsilane production,^{381,382,384,385} and the most common olefin hydrosilylation catalyst used in industry is Karstedt's catalyst, $[\text{Pt}_2\{\text{O}(\text{SiMe}_2\{\text{CH}=\text{CH}_2\})_2\}_3]$.³⁸⁴ However, the development of catalytic systems based on first row transition metals such as manganese is of interest due to high abundance, low cost, reduced toxicity, and improved environmental compatibility.⁵⁴⁰ In this regard, manganese mediated hydrosilylation of polar unsaturated bonds has been well studied,⁵⁴¹ but only a handful of manganese catalysts have been reported for alkene hydrosilylation.⁵⁴²

The typical mechanism for alkene hydrosilylation (Chalk-Harrod mechanism; see Scheme 1.34 in Chapter 1) involves oxidative addition of a hydrosilane to generate a silyl hydride complex, followed by alkene coordination, C–H bond-forming 1,2-insertion, and finally Si–C bond-forming reductive elimination. However, in some cases alkene coordination is followed by C–Si bond-forming 1,2-insertion and then C–H bond-forming reductive elimination (modified Chalk-Harrod mechanism; see Scheme 1.34 in Chapter 1). Furthermore, catalytic cycles which proceed via a monosilyl complex rather

than a silyl hydride complex have been reported, including hydrosilylation reactions utilizing a cationic palladium(II) or cobalt(III) alkyl pre-catalyst.^{383,384}

8.2 – Catalytic Hydrosilylation of Ethylene

At 60 °C, addition of 7 mol% of [(dmpe)₂MnH(C₂H₄)] (**10**) to primary or secondary hydrosilanes (H₃SiPh, H₃Si^{*n*}Bu, H₂SiPh₂ or H₂SiEt₂) in C₆D₆ under ethylene (1.7 atm initial pressure) led to catalytic incorporation of one or two equivalents of ethylene into the Si–H bonds of the free hydrosilanes, leading to a mixture of new hydrosilanes (Table 8.1). The major products in reactions of secondary hydrosilanes were tertiary hydrosilanes (HSiEtPh₂ or HSiEt₃), while reactions involving primary hydrosilanes first formed secondary hydrosilanes (H₂SiEt^{*n*}Bu or H₂SiEtPh), followed by reaction with an additional equivalent of ethylene to generate the tertiary hydrosilane (HSiEt₂Ph or HSiEt₂^{*n*}Bu) as the major product. Hydrosilylation reactions with H₃Si^{*n*}Bu, H₂SiPh₂, and H₂SiEt₂ produced fewer byproducts than those with H₃SiPh (as noted in Table 8.1). Additionally, hydrosilylation with H₂SiEt₂ progressed much more rapidly than that with H₂SiPh₂. By contrast, no reactivity was observed when **10** was exposed to ethylene and the tertiary hydrosilanes HSiEt₃ or HSiEtPh₂; various other hydrosilylation catalysts exhibit higher activities than **10**, especially precious metal catalysts,^{384,543} but the ability of **10** to selectively form tertiary but not quaternary hydrosilanes from ethylene is uncommon.^{eee}

^{eee} For examples of ethylene hydrosilylation selective for producing secondary hydrosilanes, see refs. 340 and 544. For examples of ethylene hydrosilylation selective for producing quaternary silanes, see refs. 251 and 545.

Table 8.1: Ratio of hydrosilane products (assigning the tertiary hydrosilane product a value of 100) observed by ^1H NMR spectroscopy after hydrosilylation of ethylene catalysed by $[(\text{dmpe})_2\text{MnH}(\text{C}_2\text{H}_4)]$ (**10**) pre-catalyst (7 mol%) with 1.7 atm ethylene (initially $n_{\text{silane}} \approx n_{\text{ethylene}}$; for reactions with H_3SiR , the headspace was re-filled with ethylene after 1 week) at 60 °C in C_6D_6 after 50 days (H_3SiPh), 25 days ($\text{H}_3\text{Si}^n\text{Bu}$) or 6 days (H_2SiR_2).

Substrate	R/R'	Substrate	H_2SiEtR	$\text{HSiEtRR}'$	$\text{HSiViRR}'$	Unidentified ^a
H_3SiPh	Ph/Et	0	0	100	< 5	20 ^b
$\text{H}_3\text{Si}^n\text{Bu}$	ⁿ Bu/Et	0	< 5	100	20	10 ^c
H_2SiPh_2	Ph/Ph	50	n.a.	100	< 5	20
H_2SiEt_2	Et/Et	6	n.a.	100	11	< 5

- a. Relative amounts of unidentified SiH -containing silanes were determined assuming that they contain a single SiH proton.
 b. At least seven unassigned SiH environments were observed.
 c. Two unassigned SiH environments were observed

Organic byproducts were observed during conversion of secondary to tertiary silanes, but not conversion of primary to secondary silanes. The major byproduct was a hydrosilane with a vinyl group (Vi) in place of an ethyl substituent (HSiEtViR , $\text{R} = \text{Et}$ or ⁿBu or HSiPhViR , $\text{R} = \text{Et}$ or Ph), accompanied by one or more unidentified SiH -containing silanes (Table 8.1). Vinyl silanes are commonly observed byproducts in olefin (e.g. $\text{H}_2\text{C}=\text{CHR}$) hydrosilylation, formed by β -hydride elimination from an $\text{M}(\text{CH}_2\text{CHRSiR}_3)$ intermediate in the catalytic cycle,⁵⁴⁶ and were an impetus for the initial proposal of a modified Chalk-Harrod catalytic cycle involving C–Si rather than C–H bond-forming 1,2-insertion from an alkene-coordinated silyl hydride intermediate.³⁸²

During catalysis using primary and secondary hydrosilanes, a variety of manganese-containing complexes were observed by NMR spectroscopy, including disilyl hydride complexes (for reactions involving primarily hydrosilanes only), silylene hydride

complexes (for reactions involving secondary silanes only),^{fff} silyl dihydride complexes, silene hydride complexes, and ethylene hydride complex **10**. Furthermore, all of these classes of complex are catalytically active. For example, [(dmpe)₂MnH(Et₂Si=CHMe)] (**19^{Et2}**) and [(dmpe)₂MnH(=SiEt₂)] (**16^{Et2}**) are catalysts for ethylene hydrosilylation using secondary hydrosilanes, and [(dmpe)₂MnH(SiH₂ⁿBu)₂] (**20^{Bu}**) and [(dmpe)₂MnH₂(SiH₂ⁿBu)] (**18^{Bu}**) are active for ethylene hydrosilylation by H₃SiⁿBu. Reactions involving **19^{Et2}**, **16^{Et2}**, and **20^{Bu}** rapidly generated distributions of Mn-containing species and hydrosilane products which are very similar to those formed when [(dmpe)₂MnH(C₂H₄)] (**10**) was used as the pre-catalyst. By contrast, when **18^{Bu}** was employed, hydrosilylation proceeded at a slower rate, and even after 24 hours the dominant manganese-containing species was **18^{Bu}**.

8.3 – Monitoring Ethylene Hydrosilylation by H₃SiⁿBu Over Time

In order to monitor ethylene hydrosilylation reactions under conditions where ethylene concentration does not vary significantly during the course of the reaction, multiple aliquots from a stock solution of **10** and H₃SiⁿBu in C₆D₆ were placed under a large excess of ethylene in a sealed 50 mL flask (initial pressure 1.7 atm, n_{C₂H₄} ≈ 40 × n_{silane}) and heated at 60 °C for various time periods prior to analysis by NMR spectroscopy (Figure 8.1). Key observations were; (a) nearly complete conversion of the primary hydrosilane to secondary hydrosilane H₂SiEtⁿBu was observed *before* any formation of the tertiary silane (HSiEt₂ⁿBu) product or vinyl silane (HSiEtViⁿBu) byproduct, (b) during hydrosilylation by the primary hydrosilane H₃SiⁿBu, the dominant metal-containing species was the SiH-containing silene hydride [(dmpe)₂MnH(ⁿBuHSi=CHMe)] (**19^{Bu,H}**), with small amounts of the disilyl hydride [(dmpe)₂MnH(SiH₂ⁿBu)₂] (**20^{Bu}**), (c) after 13 hours, almost all H₃SiⁿBu had been consumed, (d) from 13 to 18 hours, conversion of H₂SiEtⁿBu to HSiEt₂ⁿBu proceeded rapidly with concurrent formation of the vinylsilane byproduct HSiEtViⁿBu (see below

^{fff} Silylene complexes were only observed during catalysis when most of the ethylene had been consumed.

for experiments to determine the manganese species present *between* 13 and 18 hours), (e) after 18 hours, **10** was the dominant manganese species in solution {accompanied by small amounts of the silene hydride [(dmpe)₂MnH(ⁿBuEtSi=CⁿEtMe)] (**19^{Bu,Et}**) and the silyl dihydride [(dmpe)₂MnH₂(SiHEtⁿBu)] (**18^{Bu,Et}**)}, and conversion of H₂SiEtⁿBu to HSiEt₂ⁿBu now proceeded more slowly, and (f) after 12 days, > 99.5% of the H₂SiEtⁿBu intermediate had been consumed yielding 81% HSiEt₂ⁿBu, 16% HSiEtViⁿBu, and 3% of an unidentified SiH-containing byproduct (assuming that this species contains one SiH proton), which is non-volatile at room temperature (5 mTorr); at this point, the only Mn-containing species in the reaction mixture was [(dmpe)₂MnH(C₂H₄)] (**10**). Relative amounts of the different hydrosilane and MnH-containing species in solution during ethylene hydrosilylation by H₃SiⁿBu are plotted as a function of time in Figure 8.1.

Between 13 and 18 hours in Figure 8.1, conversion of H₂SiEtⁿBu to HSiEt₂ⁿBu proceeded rapidly (to more than 50% conversion), and then slowed down dramatically, as the resting state of the catalyst switched to [(dmpe)₂MnH(C₂H₄)] (**10**). However, during secondary to tertiary hydrosilane conversion, [(dmpe)₂MnH(ⁿBuHSi=CHMe)] (**19^{Bu,H}**) cannot be regenerated, indicating that a different manganese species may have spiked in concentration *between* the 13 and 18 hour data points (this species is presumably responsible for the rapid H₂SiEtⁿBu to HSiEt₂ⁿBu conversion observed during this time period). Consequently, the reaction in Figure 8.1 was repeated and stopped after most but not all of the primary hydrosilane had been consumed {the resulting mixture of hydrosilanes and Mn-containing species in C₆D₆ was similar to that observed at 13 h in Figure 8.1; i.e. mostly secondary hydrosilane H₂SiEtⁿBu and [(dmpe)₂MnH(ⁿBuHSi=CHMe)] (**19^{Bu,H}**), with a small amount of the primary hydrosilane, H₃SiⁿBu}. This mixture was then sealed under a near-stoichiometric (relative to the hydrosilane) amount of ethylene in an NMR tube, and monitored by NMR spectroscopy at 56 °C in 5 minute intervals (Figure 8.2).

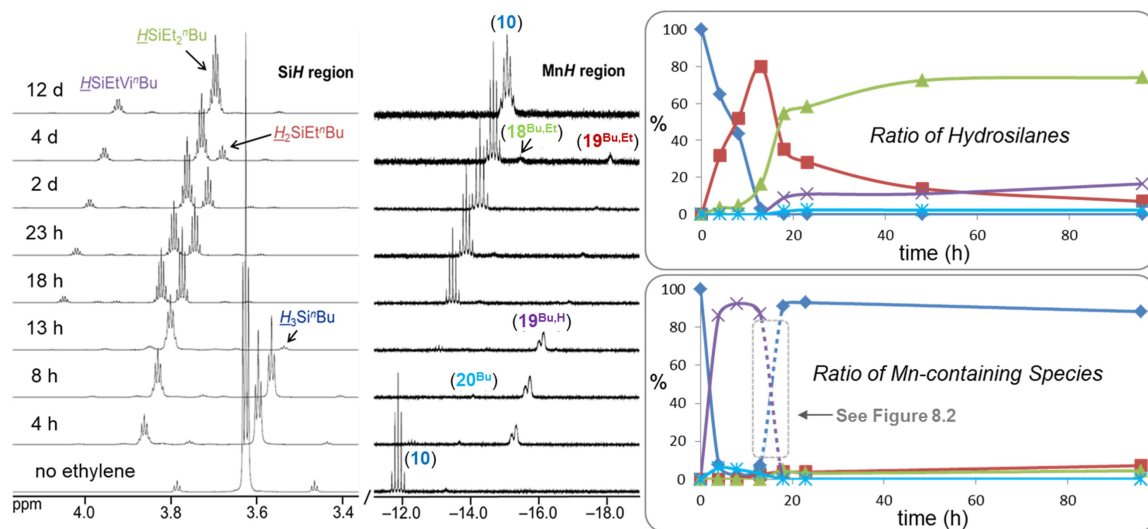


Figure 8.1: SiH (left) and MnH (middle) regions of the ¹H NMR spectra (298 K, 500 or 600 MHz) for the hydrosilylation of ethylene by H₃SiⁿBu using [(dmpe)₂MnH(C₂H₄)] (10) pre-catalyst (7 mol% relative to the hydrosilane) under ~1.7 atm of ethylene (initial, n_{C₂H₄} ≈ 40 × n_{silane}) in C₆D₆ and after various time intervals at 60° C. The x-axis corresponds to the bottom ¹H NMR spectrum, and for clarity, each spectrum above that is shifted by 0.3 (SiH region) or 0.4 (MnH region) ppm to lower frequency. Right: graphs showing the ratio of (top) hydrosilanes (dark blue ♦ = H₃SiⁿBu; red ■ = H₂SiEtⁿBu; green ▲ = HSiEt₂ⁿBu; purple × = HSiViEtⁿBu; light blue * = unidentified SiH-containing silane) and (bottom) MnH-containing species {dark blue ♦ = [(dmpe)₂MnH(C₂H₄)] (10); light blue * = [(dmpe)₂MnH(SiH₂ⁿBu)₂] (20^{Bu}); green ▲ = [(dmpe)₂MnH₂(SiHEtⁿBu)] (18^{Bu,Et}); purple × = [(dmpe)₂MnH(ⁿBuHSi=CHMe)] (19^{Bu,H}); red ■ = [(dmpe)₂MnH(ⁿBuEtSi=CHMe)] (19^{Bu,Et})} in these reactions, as measured by ¹H NMR spectroscopy.

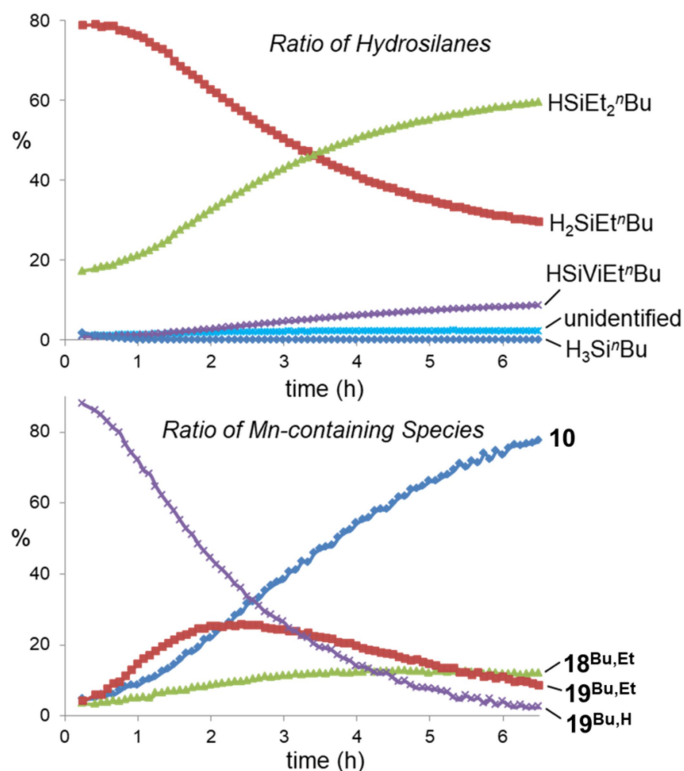


Figure 8.2: Graphs showing the ratio of (top) hydrosilanes (dark blue \blacklozenge = $\text{H}_3\text{Si}^n\text{Bu}$; red \blacksquare = $\text{H}_2\text{SiEt}^n\text{Bu}$; green \blacktriangle = $\text{HSiEt}_2^n\text{Bu}$; purple \times = $\text{HSiViEt}^n\text{Bu}$; light blue $*$ = unidentified SiH -containing silane) and (bottom) MnH -containing species {dark blue \blacklozenge = $[(\text{dmpe})_2\text{MnH}(\text{C}_2\text{H}_4)]$ (**10**); red \blacksquare = $[(\text{dmpe})_2\text{MnH}(^n\text{BuEtSi}=\text{CHMe})]$ (**19**^{Bu,Et}); green \blacktriangle = $[(\text{dmpe})_2\text{MnH}_2(\text{SiHEt}^n\text{Bu})]$ (**18**^{Bu,Et}); purple \times = $[(\text{dmpe})_2\text{MnH}(^n\text{BuEtSi}=\text{CHMe})]$ (**19**^{Bu,Et})} measured over time by ^1H NMR spectroscopy (in C_6D_6 at 56°C) for the hydrosilylation of ethylene (initial, $n_{\text{C}_2\text{H}_4} \approx n_{\text{silane}}$) by a mixture of hydrosilanes corresponding to the 13 h mark in Figure 8.1.

In Figure 8.2, consumption of remaining primary hydrosilane was complete after 10 minutes, followed by rapid secondary to tertiary hydrosilane conversion and a spike in the concentration of a new silene hydride complex, $[(\text{dmpe})_2\text{MnH}(^n\text{BuEtSi}=\text{CHMe})]$ (**19**^{Bu,Et}), while the concentrations of **19**^{Bu,H} (the resting state of the catalyst during primary to secondary hydrosilane conversion) and $[(\text{dmpe})_2\text{MnH}(\text{C}_2\text{H}_4)]$ (**10**) (the Mn-containing species dominant after the 18 h mark) diminished and increased, respectively.

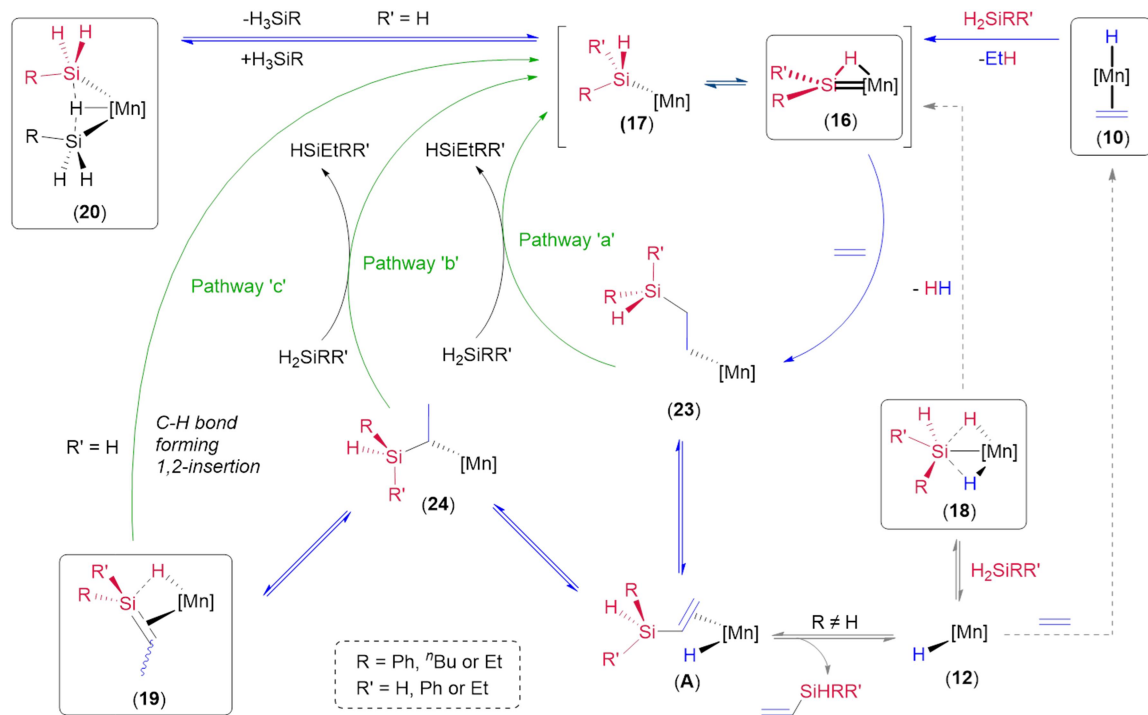
Furthermore, a small amount (~12%) of the silyl dihydride complex $[(\text{dmpe})_2\text{MnH}_2(\text{SiHEt}^n\text{Bu})]$ ($\mathbf{18}^{\text{Bu,Et}}$) grew in over this time period, and vinylsilane ($\text{HSiViEt}^n\text{Bu}$) production was observed to accompany the formation of $\mathbf{10}$ and $\mathbf{18}^{\text{Bu,Et}}$. The slowdown in the rate of catalysis between 13 and 18 hours in Figure 8.1 can therefore be attributed to a change in the resting state of the catalyst, from more active silene hydride complexes $\mathbf{19}^{\text{Bu,H}}$ and $\mathbf{19}^{\text{Bu,Et}}$, to $\mathbf{10}$ and $\mathbf{18}^{\text{Bu,Et}}$, both of which are formed via vinylsilane elimination (*vide infra*), and re-enter the catalytic cycle slowly ($\mathbf{18}^{\text{Bu,Et}}$ is particularly slow to enter the cycle; *vide supra*).

8.4 – Proposed Catalytic Cycles of Ethylene Hydrosilylation

A catalytic cycle (Scheme 8.1) can be envisaged based on the reaction pathways already proposed for (a) reaction of ethylene with disilyl hydride complexes $\mathbf{20}^{\text{R}}$ (formed in reactions of $\mathbf{10}$ with primary hydrosilanes; Chapter 5) to afford silene hydride complexes $\mathbf{19}^{\text{R,H}}$, and (b) reaction of ethylene with silylene hydride complexes $\mathbf{16}^{\text{R2}}$ (formed in reactions of $\mathbf{10}$ with secondary hydrosilanes; Chapter 4) to afford silene hydride complexes $\mathbf{19}^{\text{R2}}$. These reactions are identified with blue reaction arrows in Scheme 8.1. In the presence of free hydrosilane substrate, the catalytic cycle can be completed (green reaction arrows) by reaction of hydrosilanes with primary alkyl intermediate $\mathbf{23}$ (pathway 'a' in Scheme 8) or secondary alkyl intermediate $\mathbf{24}$ (pathway 'b' in Scheme 8.1); via oxidative addition followed by reductive elimination, or σ -bond metathesis. Energy minima for alkyl intermediates $\mathbf{23}$ and $\mathbf{24}$ were found to lie 46–67 kJ mol^{-1} higher in energy than the respective silene hydride resting states, indicating their thermodynamic accessibility from complexes observed by NMR spectroscopy.

Alternatively, for conversion of primary to secondary hydrosilanes, the catalytic cycle in Scheme 8.1 can be completed by C–H bond-forming 1,2-insertion from intermediate $\mathbf{19}^{\text{R,H}}$ (pathway 'c', green reaction arrow) to generate silyl and silylene hydride species $\mathbf{17}^{\text{R,Et}}$ and $\mathbf{16}^{\text{R,Et}}$. Isomerization of $\mathbf{19}^{\text{Bu,H}}$ to $\mathbf{16}^{\text{Bu,Et}}$ has been observed in the absence of ethylene and hydrosilanes (Chapter 5), and this pathway is also thought to

be involved in the reactions of $[(\text{dmpe})_2\text{MnH}(\text{RHSi}=\text{CHMe})]$ ($\mathbf{19}^{\text{R,H}}$) with ethylene to afford $[(\text{dmpe})_2\text{MnH}(\text{REtSi}=\text{CHMe})]$ ($\mathbf{19}^{\text{R,Et}}$) in which an SiH group is converted to an SiEt group (Chapter 5). If pathway 'c' is involved in the catalysis, the resulting $[\text{Mn}]\text{SiHREt}$ ($\mathbf{17}^{\text{R,Et}}$) complex must react with free H_3SiR to form $[\text{Mn}]\text{SiH}_2\text{R}$ ($\mathbf{17}^{\text{R}}$) and eliminate H_2SiREt (likely via an unobserved disilyl hydride intermediate analogous to $\mathbf{20}^{\text{R}}$), given that the observed reactivity converts primary hydrosilanes to *free* secondary hydrosilanes prior to the formation of significant amounts of tertiary hydrosilane products. The accessibility of this reaction pathway is highlighted by the reaction of $[(\text{dmpe})_2\text{MnH}(=\text{SiR}_2)]$ $\{\text{R} = \text{Ph}$ ($\mathbf{16}^{\text{Ph}_2}$) or Et ($\mathbf{16}^{\text{Et}_2}$) $\}$ with excess $\text{H}_3\text{Si}^n\text{Bu}$ at 20 °C to afford $[(\text{dmpe})_2\text{MnH}(\text{SiH}_2^n\text{Bu})_2]$ ($\mathbf{20}^{\text{R}}$) and free H_2SiPh_2 or H_2SiEt_2 , respectively. This reaction was complete in several hours (for $\mathbf{16}^{\text{Et}_2}$) or minutes (for $\mathbf{16}^{\text{Ph}_2}$).



Scheme 8.1: Proposed catalytic cycle for ethylene hydrosilylation by primary and secondary hydrosilanes. $[\text{Mn}] = \text{Mn}(\text{dmpe})_2$. Only one isomer is shown for complexes **16** and **18**. Boxes represent complexes observed by NMR spectroscopy during catalysis.

Unidentified SiH-containing byproducts {formed in larger amounts in reactions with H₂SiPh₂ and H₃SiPh (after conversion to H₂SiEtPh); Table 8.1} may arise from reactions of **23** (or less likely **24**) with hydrosilanes resulting in C–Si rather than C–H bond-formation to eliminate a disilylated organic product and generate manganese hydride intermediate [(dmpe)₂MnH] (**12**), which can re-enter the proposed catalytic cycle (*vide infra*) as shown in Scheme 8.1. This reactivity bears resemblance to that of [(dmpe)₂MnEt] (**13**, which is an isomer of **10**; see Chapter 3) with H₂SiPh₂ to afford a 1:1 mixture of (a) [(dmpe)₂MnH(=SiPh₂)] (**16**^{Ph₂}) and ethane, the products of C–H bond-forming oxidative addition / reductive elimination (or σ-bond metathesis) followed by α-hydride elimination, and (b) [(dmpe)₂MnH₂(SiHPh₂)] (**18**^{Ph₂}) and Ph₂SiEtH, the products of C–Si bond-forming oxidative addition / reductive elimination (or σ-bond metathesis) to form [(dmpe)₂MnH] (**12**), followed by oxidative addition of a second equivalent of H₂SiPh₂ (see Chapter 4).

Pathways 'a', 'b' and 'c' described above (green reaction arrows in Scheme 8.1) generate the observed disilyl hydride (**20**^R), silylene hydride (**16**) and silene hydride (**19**) complexes. However, they do not explain the formation of vinyl silane byproducts. These byproducts can be accessed by vinylsilane dissociation from intermediate **A**,^{ggg} forming low-coordinate hydride species **12**, which can react with either of the available organic substrates: ethylene to form **10**, or hydrosilanes to form silyl dihydride complexes (**18**); Scheme 8.1. While **10** reacts with primary or secondary hydrosilanes (but not tertiary hydrosilanes) to generate ethane and low-coordinate silyl species **17**, complex **18** can slowly rejoin the catalytic cycle by H₂ elimination to afford **17**. Support for this H₂ elimination process was obtained experimentally at elevated temperatures. For example, heating a solution of [(dmpe)₂MnH₂(SiH₂Ph)] (**18**^{Ph}) under D₂ at 70-80 °C overnight resulted in > 90% deuterium incorporation into the MnH environments, exclusively. Furthermore, reactions of **18**^{Bu} with ^tBuNC, and [(dmpe)₂MnD₂(SiH₂Ph)] (**d₂-18**^{Ph}) with

^{ggg} In hydrosilylation reactions with *d*₄-ethylene, the vinyl byproducts contain fully deuterated vinyl groups, in keeping with the proposed pathway for their formation.

o-xylylNC, afforded $[(\text{dmpe})_2\text{Mn}(\text{SiH}_2^{\text{R}}\text{Bu})(\text{CN}^t\text{Bu})]$ (**21d**) and $[(\text{dmpe})_2\text{Mn}(\text{SiH}_2\text{Ph})(\text{CNXyl})]$ (**21a**), respectively, after 1 h at 75 °C.

In an effort to determine whether pathway 'a' (via primary alkyl intermediate **23**), 'b' (via secondary alkyl intermediate **24**), or 'c' (via a silene hydride complex with an SiH substituent; **19^{R,H}**) in Scheme 8.1 is operative, catalysis was carried out using *d*₄-ethylene; pathway 'a' would generate CD₂CD₂H groups, whereas pathways 'b' and 'c' would generate CHDCD₃ groups.^{hhh} Hydrosilylation of C₂D₄ by the secondary hydrosilane H₂SiEt₂ yielded *d*₄-HSiEt₃, primarily as HSiEt₂(CD₂CD₂H) (97%), with a minor amount of HSiEt₂(CDHCD₃) (3%), as determined by ¹H, ²H, and ¹³C{¹H} NMR analysis (Appendix 2), indicating that pathway 'a' in Scheme 8.1 is dominant. By contrast, C₂D₄ hydrosilylation by H₃Si^RBu under identical conditions yielded a solution containing 20% HSi^RBu(CD₂CD₂H)₂, and 80% HSi^RBu(CD₂CD₂H)(CDHCD₃); Appendix 2. Given that H₂SiEt₂ has been shown to react almost exclusively via pathway 'a' (affording a CD₂CD₂H substituent on silicon), and H₂Si^RBuEt can be expected to react analogously, this product distribution indicates that H₃Si^RBu is converted to H₂Si^RBuEt primarily via pathway 'b' and/or 'c' (~77%), with a lesser contribution from pathway 'a' (~23%).

DFT calculations indicate that alkyl intermediates **23** and **24** are very similar in energy (within 5 kJ mol⁻¹). Therefore, the preferential reactivity of secondary silanes towards less hindered **23** (pathway 'a') may be sterically driven. By contrast, for conversion of primary to secondary hydrosilanes, where pathway 'b' and/or 'c' is dominant, it is not obvious why pathway 'b' would be preferred over pathway 'a'. Pathway 'c' is therefore a viable alternative, especially given that 'c' has been demonstrated (*vide supra*) in room temperature stoichiometric reactions involving silenes with a hydrogen substituent on silicon (**19^{R,H}**). Furthermore, it is notable that silenes (**19^{R,H}**) are the

^{hhh} Hydrosilylation reactions involving C₂D₄ (with either H₃Si^RBu or H₂SiEt₂) proceeded to completion (i.e. complete consumption of the secondary hydrosilane reagent/intermediate) after 4 days at 60 °C, while analogous reactions using a higher pressure of C₂H₄ still contained 6-7% of the secondary hydrosilane (H₂SiEt^RBu intermediate or H₂SiEt₂ reagent), suggestive of an inverse kinetic isotope effect.

dominant metal-containing species during the first phase of catalysis (conversion of primary to secondary hydrosilanes).

8.5 – Summary and Conclusions for Chapter 8

All of the silyl, silylene and silene complexes prepared in Chapters 4 and 5 were accessed via reactions of $[(dmpe)_2MnH(C_2H_4)]$ (**10**) with hydrosilanes and/or ethylene. Therefore, ethylene hydrosilylation was investigated using **10** as a pre-catalyst, resulting in stepwise conversion of primary to secondary to tertiary hydrosilanes. Manganese complexes observed during catalysis include (a) disilyl hydride complexes (**20^R**), (b) silylene hydride complexes (**16**), (c) silene hydride complexes (**19**), (d) silyl dihydride complexes (**18**), and (e) the ethylene hydride pre-catalyst (**10**). All of these species are catalytically active (although the silyl dihydride complexes **18** are significantly less active than the others), and a catalytic cycle is proposed on the basis of these observations, the aforementioned stoichiometric reactions, and hydrosilylation of d_4 -ethylene. This catalytic cycle is unusual due to the involvement of silylene hydride and silene hydride complexes, potentially as on-cycle species. While the catalytic system discussed in this chapter displays very low activity relative to many previously reported catalysts, especially those containing precious metals, it is unusual in that it selectively forms tertiary but not quaternary hydrosilanes from ethylene, and utilizes a relatively inexpensive and environmentally benign metal centre.

Chapter 9

Synthesis of Manganese Hydride Complexes with Various Co-ligands (not including Si-based co-ligands)

Portions of this chapter have been reprinted (adapted) with permission from Price, J. S.; Emslie, D. J. H.; Vargas-Baca, I.; Britten, J. F. [(dmpe)₂MnH(C₂H₄)] as a Source of a Low-Coordinate Ethyl Manganese(I) Species: Reactions with Primary Silanes, H₂, and Isonitriles, *Organometallics* **2018**, *37*, 3010-3023. Copyright 2018 American Chemical Society.

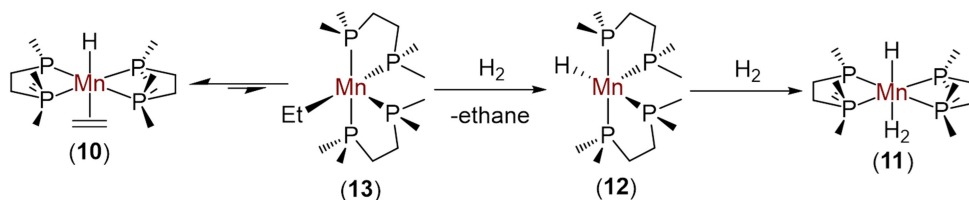
9.1 – Introduction to Chapter 9

As discussed in Chapter 3, Girolomi and Wilkinson's ethylene hydride complex *trans*-[(dmpe)₂MnH(C₂H₄)] (**trans-10**)^{120,172} could react with neutral reagents via either substitution of the ethylene ligand, or via initial isomerization to a 5-coordinate Mn(I) ethyl species [(dmpe)₂MnEt] (**13**).⁵⁴⁷ Reactions of **10** with hydrosilane reagents (Chapters 4-5) yielded a variety of new manganese hydride complexes with different silicon-based ligands. Herein, we present the syntheses of additional manganese hydride complexes “(dmpe)₂MnHL” (L = neutral ligand) from **10** by exposure to neutral reagents from groups 13 (B, Al), 14 (Sn), and 15 (P), as well as H₂.

9.2 – Reaction of *trans*-[(dmpe)₂MnH(C₂H₄)] with H₂

Complex **10**, *trans*-[(dmpe)₂MnH(C₂H₄)], has previously been reported to be unreactive with H₂ at room temperature.¹²⁰ However, we found that **10** does in fact react *extremely* slowly with H₂ at room temperature, and more rapidly at elevated temperatures (Scheme 9.1); [(dmpe)₂MnH(H₂)] (**1**) and ethane were formed over 5 days at 60 °C in benzene, in >95% purity (77% crude isolated yield), via initial isomerization of **10** to the 5-coordinate ethyl intermediate [(dmpe)₂MnEt] (**13**). When this synthesis was carried out in C₆D₆, significant deuterium incorporation was observed in the CH₂ and CH₃

environments of the dmpe ligands (consistent with Jones' report that complex **11** undergoes H/D exchange between C₆D₆ and the dmpe ligands at elevated temperature).¹⁷³



Scheme 9.1: Synthesis of [(dmpe)₂MnH(H₂)] (**11**). **12** and **13** are unobserved intermediates.

Complex **11** was previously prepared via the reaction of [$\{(\text{dmpe})_2\text{Mn}(\mu\text{-AlH}_4)\}_2$] with water¹²⁰ and it was determined spectroscopically that the dmpe ligands are arranged equatorially with the hydride ligand *trans* to dihydrogen.¹⁷³ In this work, X-ray quality crystals of **11** (Figure 9.1 left) were obtained by recrystallization from a concentrated solution in hexanes at $-30\text{ }^\circ\text{C}$, confirming that the dmpe ligands lie in a plane, with the manganese atom displaced 0.15-0.16 Å from the plane. Unfortunately, we were unable to locate the hydride and dihydrogen ligands in the difference map. However, DFT calculations (ADF, gas-phase, all-electron, PBE, D3-BJ, TZ2P, ZORA) suggest that the equatorial belt of phosphorus donors is displaced towards the hydride ligand and away from the (bulkier) neutral axial donor (Figure 9.1 right),ⁱⁱⁱ analogous to the situation in **10** (Chapter 3, Figure 3.1).

The computationally determined H–H distance (1.017 Å, Mayer bond order of 0.40) of the H₂ ligand in **11** is consistent with the presence of a dihydrogen ligand (as opposed to two *cis* disposed hydride ligands, which generally feature longer than 1.6 Å of separation),⁵⁴⁸ as proposed by Jones on the basis of variable temperature NMR studies.¹⁷³ This H–H distance lies between the two estimates reported by Jones on the basis of T₁ NMR measurements (assuming free dihydrogen rotation or not; 0.90(2) and 1.13(2) Å respectively),¹⁷³ and is greater than those reported for other manganese dihydrogen

ⁱⁱⁱ Such a structure was obtained upon geometry optimization starting from coordinates with the dmpe ligands displaced towards either the H₂ or H ligands.

complexes (0.81-0.91 Å, determined from T_1 or J_{HD} NMR studies),¹⁹⁹⁻²⁰¹ all of which are cationic.

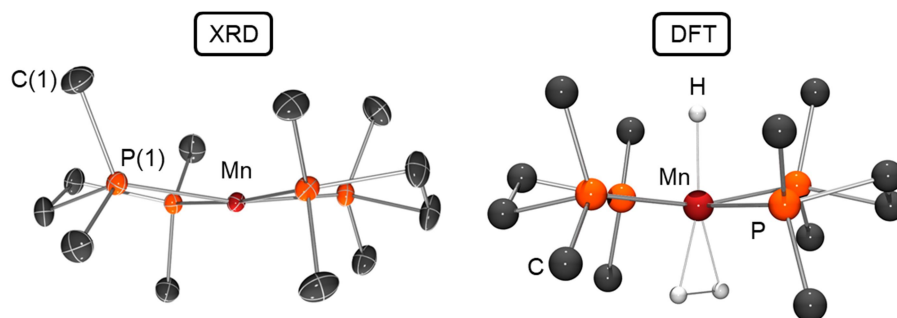


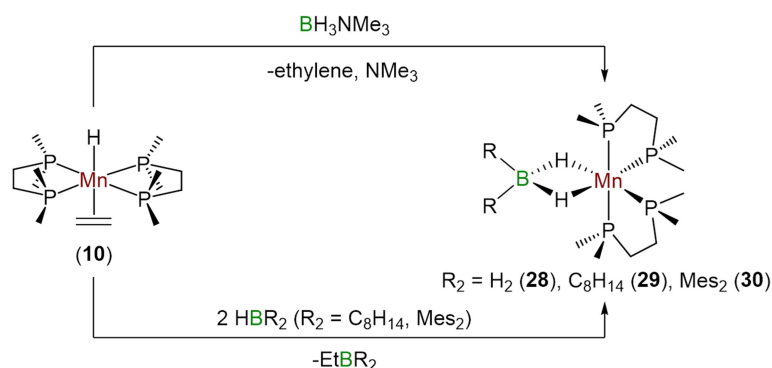
Figure 9.1: Left: X-ray crystal structure of $[(\text{dmpe})_2\text{MnH}(\text{H}_2)]$ (**11**) with ellipsoids drawn at 50% probability. Hydrogen atoms have been omitted for clarity. H and H_2 ligands were not located from the difference map, and Mn is disordered over two positions, with only one conformation {51.5(1)%} shown; Mn(1A) is the Mn atom not shown in this conformation. Bond distances (Å) and angles (deg): Mn(1)–P(1) 2.1850(7), Mn(1A)–P(1) 2.2201(8), Mn(1)–P(2) 2.2000(6), Mn(1A)–P(2) 2.2032(7), Mn(1)–P(3) 2.2132(7), Mn(1A)–P(3) 2.1953(8), Mn(1)–P(4) 2.2143(6), Mn(1A)–P(4) 2.1907(7), $\Sigma(\text{P}–\text{Mn}(1)–\text{P})$ (*cis*) 358.96(4), $\Sigma(\text{P}–\text{Mn}(1\text{A})–\text{P})$ (*cis*) 359.13(6). Right: geometry optimized (DFT calcd.) structure of $[(\text{dmpe})_2\text{MnH}(\text{H}_2)]$ (**11**).

9.3 – Reactions of *trans*- $[(\text{dmpe})_2\text{MnH}(\text{C}_2\text{H}_4)]$ with Hydroboranes; Synthesis and Characterization of Borohydride Complexes of Manganese(I)

Exposure of *trans*- $[(\text{dmpe})_2\text{MnH}(\text{C}_2\text{H}_4)]$ (**10**) to the hydroborane reagents ‘ HBR_2 ’ ($\text{BH}_3\cdot\text{NMe}_3$,^{jjj} 9-BBN, or HBMe_2) at 60 °C (from 9-BBN or HBMe_2) or 90 °C (from $\text{BH}_3\cdot\text{NMe}_3$) yielded the Mn(I) borohydride complexes $[(\text{dmpe})_2\text{Mn}(\mu\text{-H})_2\text{BR}_2]$ (**28**: R = H, **29**: $\text{R}_2 = \text{C}_8\text{H}_{14}$, **30**: R = Mes). Analytically pure samples were only obtained for **30** (34 % yield), while **28** was obtained in > 95 % purity (by NMR spectroscopy; 22 % yield) and pure samples of **29** were not obtained (solutions of > 95 % purity by NMR

^{jjj} The NMe_3 adduct of BH_3 was used as a source of trihydroborane because free BH_3 (or, more specifically, the B_2H_6 dimer) is a pyrophoric and highly toxic gas.

spectroscopy were obtained by removing red crystals from a collection of yellow and red crystals obtained during recrystallization from hexanes at $-30\text{ }^{\circ}\text{C}$). The reaction with $\text{BH}_3\cdot\text{NMe}_3$ proceeded with ethylene elimination, whereas the reactions with 9-BBN and HBMe_2 afforded EtBR_2 byproducts (Scheme 9.2). Attempts to extend this reactivity to aluminum were unsuccessful; **10** reacted with DIBAL to produce an unidentified product, which proceeded to decompose at room temperature to numerous hydride containing products.



Scheme 9.2: Synthesis of borohydride Mn(I) complexes $[(\text{dmpe})_2\text{Mn}(\mu\text{-H})_2\text{BR}_2]$ (**28**: $\text{R} = \text{H}$, **29**: $\text{R}_2 = \text{C}_8\text{H}_{14}$, **30**: $\text{R} = \text{Mes}$).

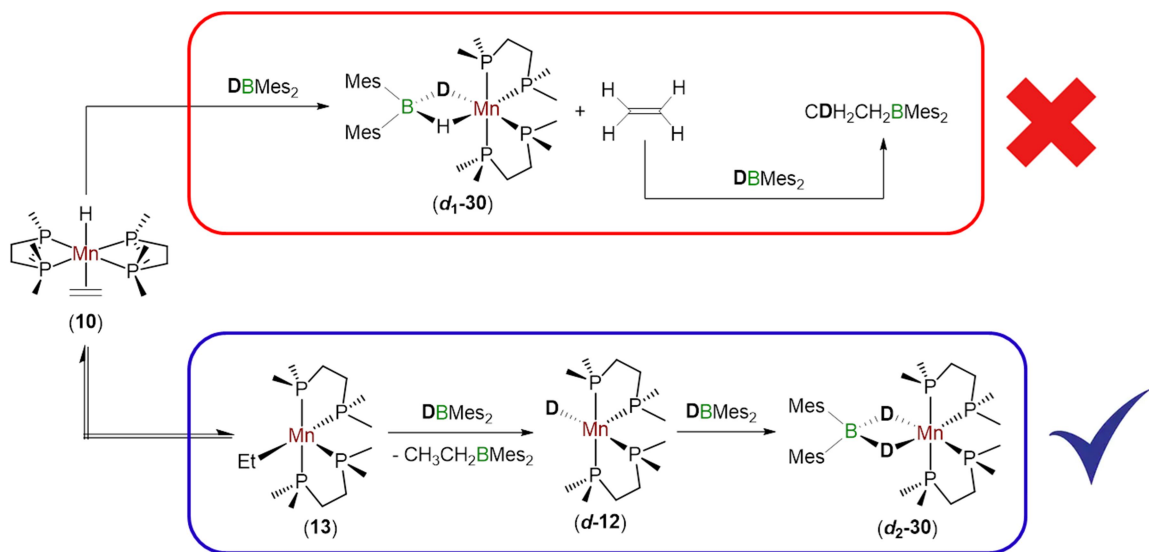
In the synthesis of $[(\text{dmpe})_2\text{Mn}(\mu\text{-H})_2\text{BH}_2]$ (**28**), the observed ethylene byproduct suggests a simple substitution mechanism. By contrast, the EtBR_2 byproducts observed in reactions of 9-BBN or HBMe_2 with **10** indicate two possible mechanisms; i) ethylene substitution, followed by hydroboration of the released ethylene by a second equivalent of free HBR_2 ,^{kkk} or ii) initial isomerization of the ethylene hydride complex **10** to a 5-coordinate ethyl intermediate $[(\text{dmpe})_2\text{MnEt}]$ (**13**), which would react with one equivalent of HBR_2 (via either oxidative addition followed by C–B bond forming reductive elimination, or σ -bond metathesis) to generate an ethylborane (EtBR_2) and the 5-coordinate hydride complex $[(\text{dmpe})_2\text{MnH}]$ (**12**), to which a second equivalent of

^{kkk} Ethylene was found to insert into the B–H bond of free 9-BBN or HBMe_2 at room temperature, with 90% (9-BBN reaction) or 100% (HBMe_2 reaction) conversion to EtBR_2 after 1 h at $60\text{ }^{\circ}\text{C}$ in C_6D_6 under an initial atmosphere of 1.7 atm ethylene.

hydroborane could coordinate. The former mechanism parallels that observed for reactions of **10** with $\text{BH}_3\cdot\text{NMe}_3$ and phosphines (*vide infra*), whereas the latter is analogous to the reactions of **10** with H_2 (*vide supra*) or hydrosilanes (Chapters 4-5).^{507,547}

To determine which of these two mechanisms is active, we turned to deuterium labelling. In the reaction of two equivalents of DBMes_2 with **10**, the former mechanism (ethylene substitution) would be expected to generate partially deuterated EtBMes_2 (with a single D incorporated into the β ethyl position) and $[(\text{dmpe})_2\text{Mn}(\mu\text{-D})(\mu\text{-H})\text{BMes}_2]$ (***d*₁-30**), while the second mechanism {via $[(\text{dmpe})_2\text{MnEt}]$ (**13**)} would be expected to generate fully protonated EtBMes_2 and $[(\text{dmpe})_2\text{Mn}(\mu\text{-D})_2\text{BMes}_2]$ (***d*₂-30**); Scheme 9.3. Monitoring this reaction by ^1H and ^2H NMR spectroscopy (Figure 9.2) revealed the latter set of products (the EtBMes_2 ethyl environments in the ^1H NMR spectrum are a quartet and triplet, and the only signal in the ^2H NMR is shifted to slightly lower frequency relative to the $\text{Mn}\underline{\text{H}}_2\text{BR}_2$ proton environmentⁱⁱⁱ). The reactions of **10** with 9-BBN and HBMes_2 therefore proceed via a different mechanism than the reaction with $\text{BH}_3\cdot\text{NMe}_3$. The reason for this difference is unclear but could suggest that the $\text{BH}_3\cdot\text{NMe}_3$ adduct remains intact during the first step of the reaction with **10**; this is also consistent with the more forcing conditions required to promote the reaction with $\text{BH}_3\cdot\text{NMe}_3$, relative to 9-BBN or HBMes_2 .

ⁱⁱⁱ The slight difference in δ for the $\text{Mn}\underline{\text{D}}$ environment in the ^2H NMR spectrum of ***d*₂-30** and the $\text{Mn}\underline{\text{H}}$ environment in the ^1H NMR spectrum of **30** is due to isotope shift.



Scheme 9.3: Reaction of *trans*-[(*dmp*)₂MnH(C₂H₄)] (**10**) with DBMes₂. Only one potential isomer of **13** and *d*-**12** is shown.

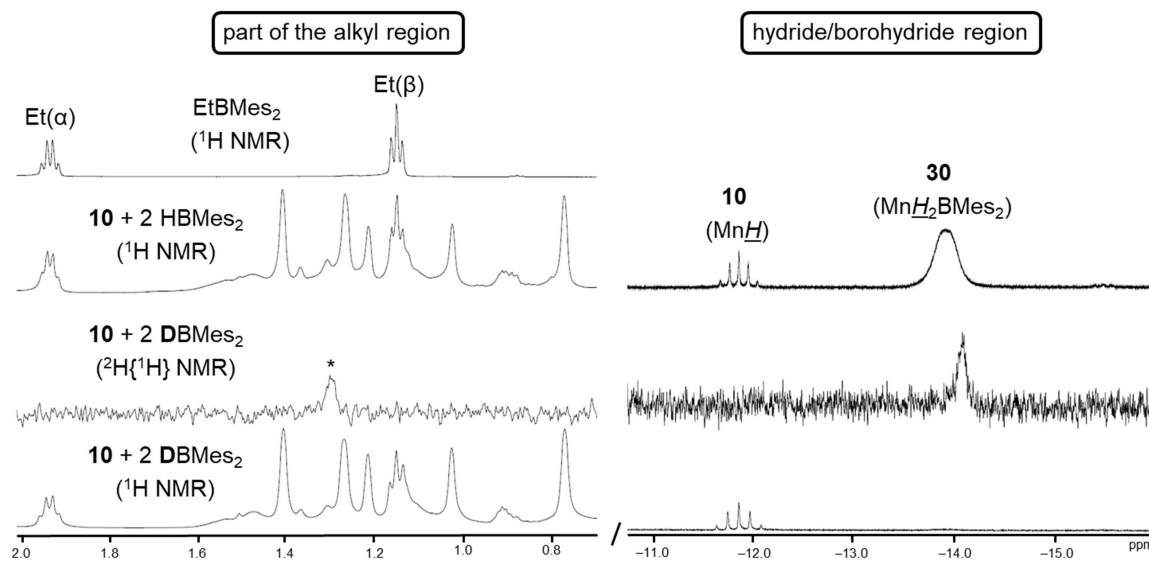


Figure 9.2: Regions of the ¹H NMR spectra (*n* = 1; 500 or 600 MHz, *n*= 2; 77 MHz) in C₆D₆ at 298 K containing the *Et*BMes₂ (left) and metal hydride/borohydride (right) environments for, from bottom to top, ¹H NMR for the reaction of 2 DBMes₂ with **10** after heating overnight at 60 °C, ²H NMR for the reaction of 2 DBMes₂ with **10** after heating overnight at 60 °C, ¹H NMR for the reaction of 2 HBMes₂ with **10** after heating overnight at 60 °C, and ¹H NMR for EtBMes₂. * is from an impurity in the C₆D₆ used.

In the syntheses of $[(\text{dmpe})_2\text{Mn}(\mu\text{-H})_2\text{BR}_2]$ (**29**: $\text{R}_2 = \text{C}_8\text{H}_{14}$, **30**: $\text{R} = \text{Mes}$), an intermediate was observed by NMR spectroscopy (Figure 9.3), with a high-field ^1H NMR signal (**29**: -13.1 ppm **30**: -13.0 ppm). For the intermediate formed from the 9-BBN reaction, four ^{31}P environments (57.8-85.8 ppm) and a sharp peak at -15.5 ppm in the ^{11}B NMR spectrum were observed, and the high-field ^1H NMR peak was a broad singlet. In contrast, the intermediate formed from the HBMe_2 reaction features a single sharp signal in the $^{31}\text{P}\{^1\text{H}\}$ NMR spectrum at -4.0 ppm, a broad ^{11}B NMR environment at 68.1 ppm, and the high-field ^1H NMR peak was an apparent triplet ($J = 73.5$ Hz). These data suggest that these intermediates are not isostructural, and both contain hydride or borohydride ligands with (for the 9-BBN intermediate) a low-symmetry disphenoidal or (for the HBMe_2 intermediate) a high-symmetry equatorial dmpe coordination environment. Furthermore, the $^{31}\text{P}\{^1\text{H}\}$ NMR spectrum of the intermediate generated from the 9-BBN reaction contained a small signal at -5.4 ppm, and the $^{31}\text{P}\{^1\text{H}\}$ NMR spectrum of the intermediate generated from the HBMe_2 reaction contained a broad signal at 73.5 ppm; these suggest that each mixture contained a small amount of a complex isostructural to the major intermediate complex in the other reaction mixture.

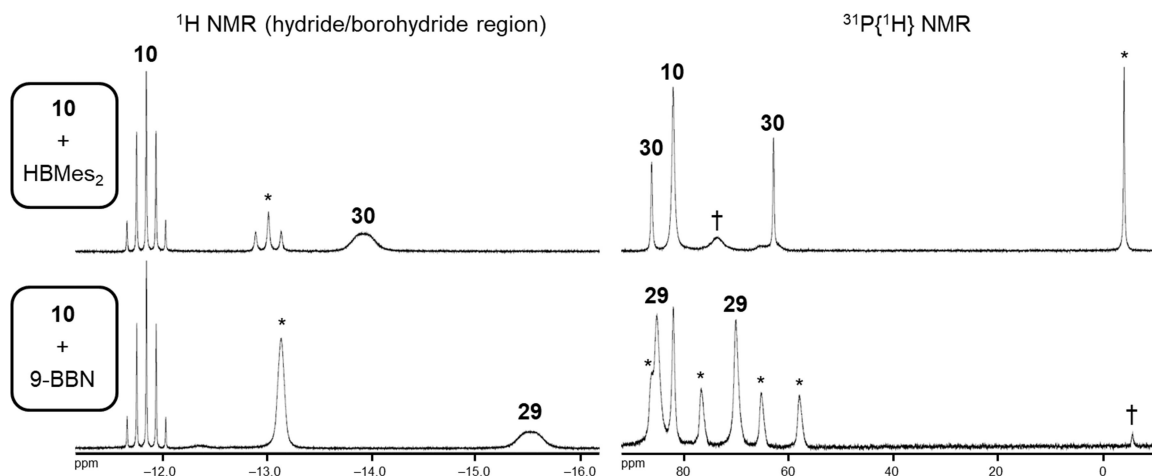


Figure 9.3: Left: (boro)hydride region of the ^1H NMR spectra, and right: $^{31}\text{P}\{^1\text{H}\}$ NMR spectra, for reactions of *trans*- $[(\text{dmpe})_2\text{MnH}(\text{C}_2\text{H}_4)]$ (**10**) with (bottom) 9-BBN or (top) HBMe_2 before completion. $*$ = peaks attributed to the dominant intermediate isomer, and \dagger = peaks attributed to the minor intermediate isomer. C_6D_6 , 600 MHz, 298 K.

Attempts to isolate these intermediates were unsuccessful; when a limiting amount (1 equivalent) of 9-BBN was allowed to react with *trans*-[(dmpe)₂MnH(C₂H₄)] (**10**) at room temperature until complete consumption of the hydroborane (1 week), a mixture of starting material **10**, borohydride product **29**, and this intermediate were observed with a ratio of 1.3 : 0.5 : 2.0 (assuming that the (boro)hydride environment in the unidentified intermediate contains a single proton). Upon heating this mixture (with no free hydroborane present), the intermediate cleanly decomposed to a single unidentified hydride-containing complex (with a ¹H NMR pentet at -11.9 ppm, *J*_{H,P} 55.4 Hz), not the borohydride complex [(dmpe)₂Mn(μ-H)₂BC₈H₁₄] (**29**), suggesting that the intermediate contains a single equivalent of hydroborane. Furthermore, the reaction of **10** with DBMes₂ yielded an intermediate with the (boro)hydride environment fully replaced by deuterium, implying a structure where the hydrogen residual from the MnH environment in **10** no longer occupies a hydridic position. Therefore, possible identities of these intermediates would be σ-hydroborane complexes with *cis*- or *trans*- disposed ethyl ligands, [(dmpe)₂MnEt(HBR₂)] (Figure 9.4), which could be formed by coordination of free hydroborane to [(dmpe)₂MnEt] (**13**) in Scheme 9.3, with the reaction proceeding to form transient [(dmpe)₂MnH] (**12**) upon C–B bond forming reductive elimination of EtBR₂. However, it is unclear why the ³¹P NMR chemical shifts for the high-symmetry products are so dissimilar to what is normally observed in dmpe complexes of Mn (usually > 50 ppm), or why the (boro)hydride ¹H NMR environment is an apparent triplet. No intermediate was observed in the reaction of **10** with BH₃·NMe₃, and perhaps its inaccessibility explains why that reaction proceeds via an alternative mechanism; *vide supra*.

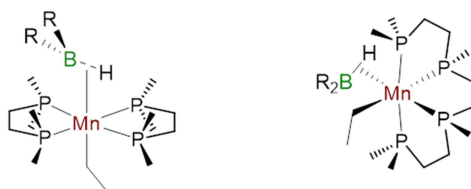


Figure 9.4: Potential structures of intermediates in the reaction of *trans*-[(dmpe)₂MnH(C₂H₄)] (**10**) with 9-BBN or HBMes₂.

Borohydride complexes $[(\text{dmpe})_2\text{Mn}(\mu\text{-H})_2\text{BR}_2]$ (**28-30**) yielded NMR spectra (Figure 9.5) featuring two ^{31}P NMR signals consistent with a disphenoidal dmpe coordination geometry at Mn (62.6-88.6 ppm), and a single MnH_2BR_2 ^1H environment (integrating to two protons) indicating chemical equivalence of the two bridging borohydride protons (**28**: -16.5 ppm, **29**: -15.6 ppm, **30**: -14.0 ppm). The single ^{11}B NMR environments (**28**: 25.3 ppm, **29**: 43.2 ppm, **30**: 27.5 ppm) are located within the range associated with tetrahedral borate environments.^{549,550} However, the moderate downfield shift in the ^{11}B NMR environment for **28** relative to the bulk of tetrahydroborate complexes^{551,552} is suggestive of some contribution from a boryl dihydride resonance structure. For $[(\text{dmpe})_2\text{Mn}(\mu\text{-H})_2\text{BH}_2]$ (**28**), a single environment (integrating to two protons) was located for the two terminal MnH_2BH_2 hydrides at 5.1 ppm. EXSY NMR spectroscopy did not provide evidence for chemical interchange between the bridging and terminal borohydride environments in **28** up to 339 K; this lies in contrast to the majority of tetrahydroborate complexes of transition metals, for which the bridging and terminal environments rapidly interchange.⁵⁵³ In the case of $[(\text{dmpe})_2\text{Mn}(\mu\text{-H})_2\text{BMes}_2]$ (**30**), the NMR spectra are consistent with hindered rotation at the B-C bond, leading to magnetic inequivalence of the two sides of each mesityl ring.

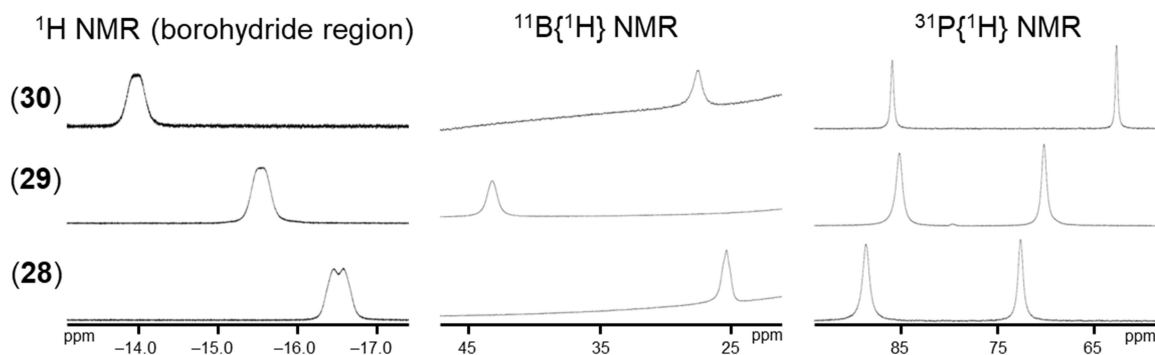


Figure 9.5: NMR spectra for borohydride complexes $[(\text{dmpe})_2\text{Mn}(\mu\text{-H})_2\text{BR}_2]$ (**28**: R = H, **29**: R₂ = C₈H₁₄, **30**: R = Mes) in *d*₈-toluene (**28**, **30**) or C₆D₆ (**29**) at 298 K. From left to right, the MnH_2BR_2 region of the ^1H NMR spectra (600 MHz), the $^{11}\text{B}\{^1\text{H}\}$ NMR spectra (192 MHz), and the $^{31}\text{P}\{^1\text{H}\}$ NMR spectra (243 MHz).

In the ^1H NMR spectra of $[(\text{dmpe})_2\text{Mn}(\mu\text{-H})_2\text{BR}_2]$ (**28**: $\text{R} = \text{H}$, **29**: $\text{R}_2 = \text{C}_8\text{H}_{14}$, **30**: $\text{R} = \text{Mes}$), the $\text{Mn}\underline{\text{H}}_2\text{BR}_2$ and (for **28** only) $\text{MnH}_2\text{B}\underline{\text{H}}_2$ signals are broad, and in the case of **28**, they also feature unusual coupling patterns. However, upon decoupling the ^{11}B nuclei these signals collapsed into sharp singlets. Furthermore, variable temperature (174–339 K) ^1H NMR spectroscopy of $[(\text{dmpe})_2\text{Mn}(\mu\text{-H})_2\text{BH}_2]$ (**28**) shows that both the $\text{Mn}\underline{\text{H}}_2\text{BH}_2$ and $\text{MnH}_2\text{B}\underline{\text{H}}_2$ signals transform from sharp singlets at low temperature to multiplets approaching the expected 1:1:1:1 quartet at high temperature due to coupling to ^{11}B (Figure 9.6); the ^{10}B satellites were not resolved, but could contribute the broadness of the signals. Together, this suggests that these borohydride signals are in the process of quadrupolar collapse due to the proximity of these environments to quadrupolar ^{11}B .

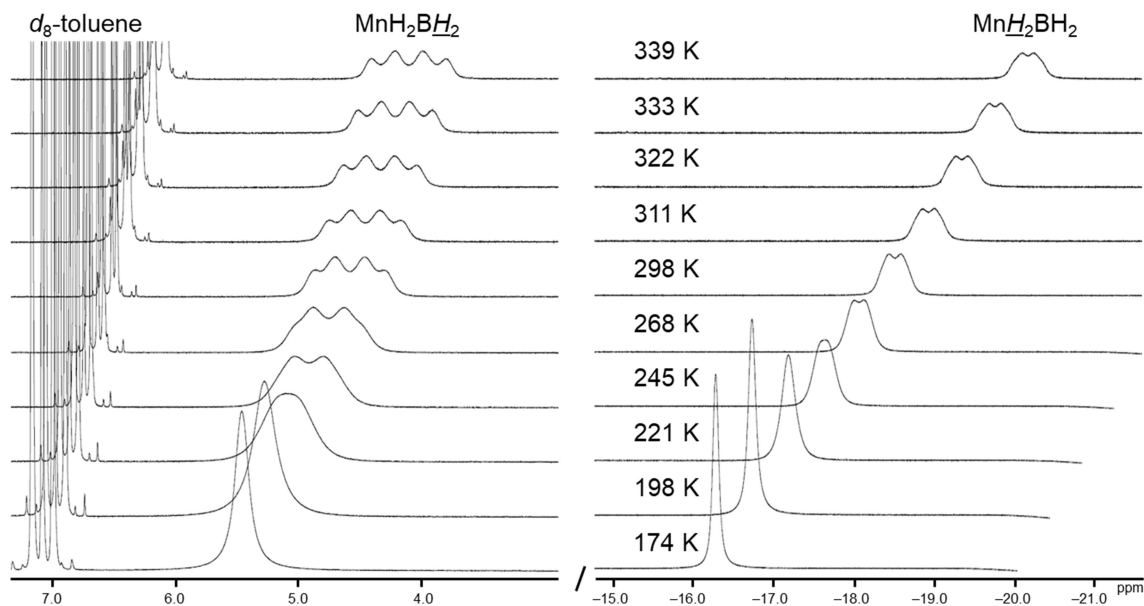


Figure 9.6: Variable temperature (174–339 K) ^1H NMR spectra of $[(\text{dmpe})_2\text{Mn}(\mu\text{-H})_2\text{BH}_2]$ (**28**) zoomed into the (left) terminal $\text{MnH}_2\text{B}\underline{\text{H}}_2$ and (right) bridging $\text{Mn}\underline{\text{H}}_2\text{BH}_2$ regions in d_8 -toluene at 500 MHz. Chemical shift scale refers to the spectrum at c. 178 K, and each additional spectrum above that is shifted to lower frequency by 0.1 ppm ($\text{MnH}_2\text{B}\underline{\text{H}}_2$ region) or 0.4 ppm ($\text{Mn}\underline{\text{H}}_2\text{BH}_2$ region) for clarity.

X-ray crystal structures were obtained for borohydride complexes **28-30** (Figure 9.7), and in each case feature an octahedral environment around Mn composed of the two dmpe ligands (with a disphenoidal geometry) and a borohydride ligand (with two bridging hydrides, located from the difference map, occupying the remaining coordination sites on Mn, and the angles between the H(1)–Mn–H(2) and H(1)–B–H(2) planes ranging from 0.2-8.3°).

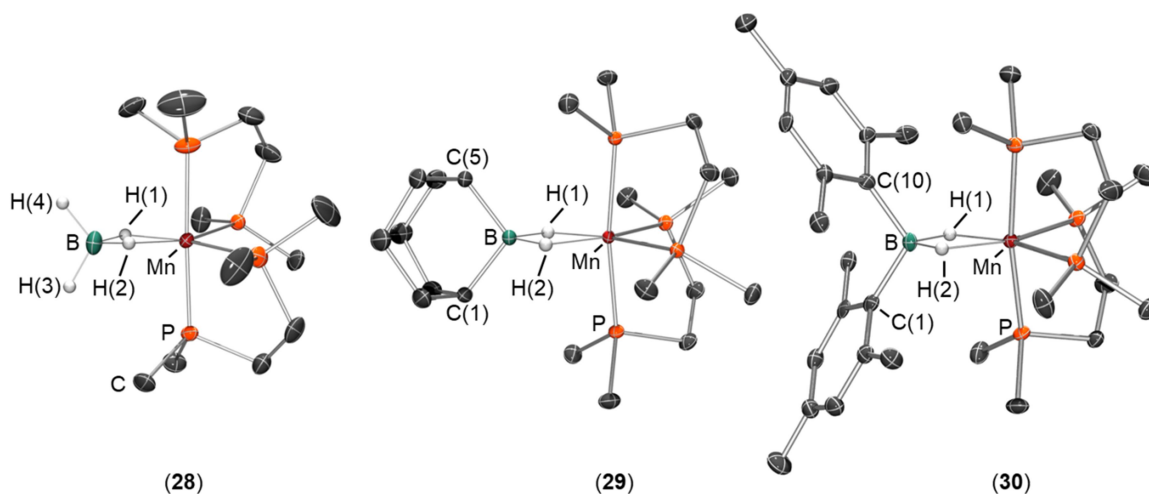


Figure 9.7: X-ray crystal structures of $[(dmpe)_2Mn(\mu-H)_2BR_2]$ (**28**: R = H, **29**: $R_2 = C_8H_{14}$, **30**: R = Mes) with ellipsoids drawn at 50% probability. Most hydrogen atoms have been omitted for clarity. Hydrogen atoms on Mn and B were located from the difference map and refined isotropically. For **28**, distances (Å) and angles (deg): Mn–B 2.170(4), Mn–H(1) 1.76(4), Mn–H(2) 1.78(4), B–H(1) 1.34(4), B–H(2) 1.31(4), B–H(3) 1.19(5), B–H(4) 1.18(4), H(1)–Mn–H(2) 75(2), H(1)–B–H(2) 109(2), $\angle\{H(1)–Mn–H(2) \text{ plane to } H(1)–B–H(2) \text{ plane}\}$ 8.3. For **29**, distances (Å) and angles (deg): Mn–B 2.206(2), Mn–H(1) 1.71(2), Mn–H(2) 1.66(3), B–H(1) 1.31(2), B–H(2) 1.25(2), B–C(1) 1.624(2), B–C(5) 1.626(3), H(1)–Mn–H(2) 70(1), H(1)–B–H(2) 99(1), $\angle\{H(1)–Mn–H(2) \text{ plane to } H(1)–B–H(2) \text{ plane}\}$ 3.5. For **30**, distances (Å) and angles (deg): Mn–B 2.245(3), Mn–H(1) 1.69(4), Mn–H(2) 1.72(4), B–H(1) 1.24(3), B–H(2) 1.19(4), B–C(1) 1.647(5), B–C(10) 1.647(6), H(1)–Mn–H(2) 65(2), H(1)–B–H(2) 97(2), $\angle\{H(1)–Mn–H(2) \text{ plane to } H(1)–B–H(2) \text{ plane}\}$ 0.2.

Description of the “R₂BH₂” moiety as a borohydride ligand (a single anionic ligand involving two 3-centre-2-electron bonds to Mn), as opposed to a boryl dihydride (three anionic ligands) or hydroborane hydride (an anionic hydride and neutral hydroborane) bonding motif, is supported by acute H(1)–Mn–H(2) angles⁵⁵⁰ of 65(2)-75(2)° and high symmetry {B–H(1) and B–H(2) distances are statistically equivalent}, respectively. Furthermore, the relatively⁵⁵³ long Mn–B distances of 2.170(4)-2.245(3) Å are characteristic of complexes with significant B–H_M interactions (borohydride or σ -hydroborane complexes).⁵⁵⁰

Complexes **29-30** are the first structurally characterized borohydride complexes of manganese with hydrocarbyl substituents on the borate ligand, and therefore allow a direct comparison of the effects that terminal hydride (**28**), alkyl (**29**), and aromatic (**30**) substituents on boron have on the “Mn(μ -H)₂B” core. Proceeding along this series from **28** to **30** (with increasing steric bulk at the boron centre), the Mn–B distances increase from 2.170(4) to 2.245(3) Å and the H–Mn–H angles decrease from 75(2) to 65(2)°. Furthermore, the Mn–P distances *trans* to the hydrogen atoms in the borohydride ligands (**28**: 2.193(1)-2.197(1) Å, **29**: 2.2112(6)-2.2176(5) Å, **30**: 2.215(1)-2.216(1) Å) are significantly shorter than to those perpendicular to the MnH₂ plane (**28**: 2.219(1)-2.229(1) Å, **29**: 2.2433(5)-2.2463(5) Å, **30**: 2.267(1)-2.268(1) Å).

In a borohydride complex with terminal hydrides on boron (e.g. **28**), the terminal B–H distances would be expected to be shorter than the bridging B–H distances. The X-ray data for [(dmpe)₂Mn(μ -H)₂BH₂] (**28**) does appear to support this trend {d(B–H_{terminal}) = 1.18(4)-1.19(5) Å, d(B–H_{bridging}) = 1.31(4)-1.34(4) Å}, but large standard deviations in the bond distances prevent conclusions from being drawn. However, DFT calculations yielded a geometry optimized structure of **28** with B–H_{terminal} distances (1.21-1.22 Å, Mayer bond order of 0.81) significantly shorter than the B–H_{bridging} distances (1.32 Å, Mayer bond order of 0.55). Furthermore, significant Mayer bond orders were observed between Mn and both the boron atom (0.43) and bridging hydrides (0.48), though the

calculated structure does slightly underestimate the Mn–B distance (2.13 Å relative to 2.170(4) Å observed in the solid state).

Unlike the previously reported aluminum analogue $[(\text{dmpe})_2\text{Mn}(\mu\text{-H})_2\text{AlH}(\mu\text{-H})_2\text{AlH}(\mu\text{-H})_2\text{Mn}(\text{dmpe})_2]$,^{120,172} **28** is monomeric {though with an isostructural ‘ $(\text{dmpe})_2\text{Mn}(\mu\text{-H})_2\text{E}$ ’ (E = Al, B) unit}. This difference is due to the inability of B to obtain a coordination number of 5, which would be required to access the dimeric structure. The observed monomeric structure is beneficial in terms being a potential precursor for applications in vapour-phase deposition; **28** sublimates at 80 °C (5 mTorr).

Borohydride complexes have been reported for many transition metals. While a number of borohydride complexes of divalent Mn(II) are known, the first (and, to our knowledge, only) monometallic, low-valent Mn(I) complexes with non-chelating borohydride ligands are $[(\text{Ar}^{\text{Dipp}^2}\text{NC})_2(\text{OC})_2\text{Mn}(\mu\text{-H})_2\text{BHR}]$ (R = H, OSO_2CF_3 ; Figure 9.8), reported by Figueroa in 2017.⁵⁵² The Mn–B distances (2.170(4) to 2.245(3) Å) observed in complexes **28-30** are comparable to those in Figueroa’s borohydride complex $[(\text{Ar}^{\text{Dipp}^2}\text{NC})_2(\text{OC})_2\text{Mn}(\mu\text{-H})_2\text{BH}(\text{OSO}_2\text{CF}_3)]$ (2.08(3)-2.142(7) Å),^{mmm} as well as the dimetallic bridging BH_4 complex reported by Riera in 1993 (2.048(4) Å)⁵⁵⁴ and a series of chelating borohydride complexes reported by Ghosh (2.137(4)-2.1817(19) Å);⁵⁵⁵ Figure 9.8.

^{mmm} The Mn–B distance was not reported for $[(\text{Ar}^{\text{Dipp}^2}\text{NC})_2(\text{OC})_2\text{Mn}(\mu\text{-H})_2\text{BH}_2]$, and the atomic coordinates are not available through the CSD.

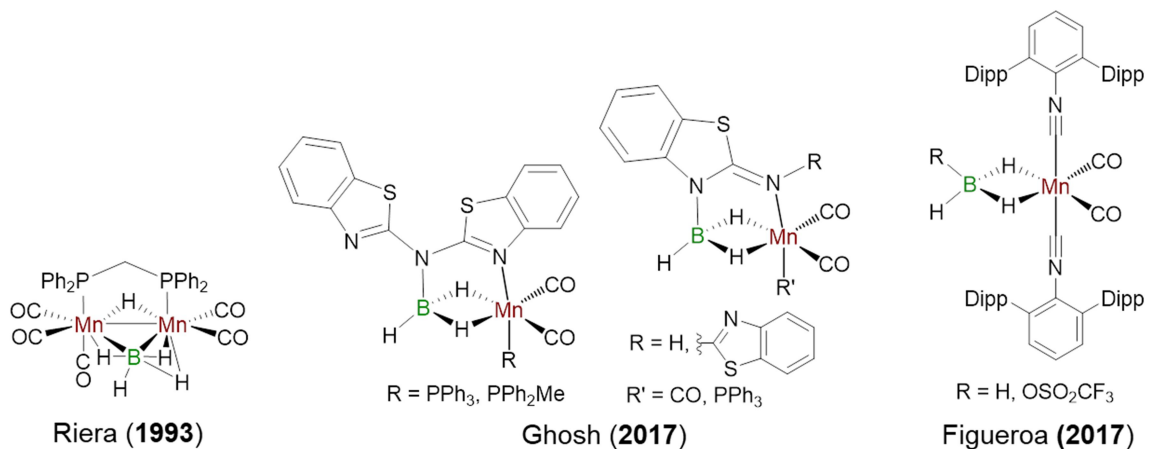
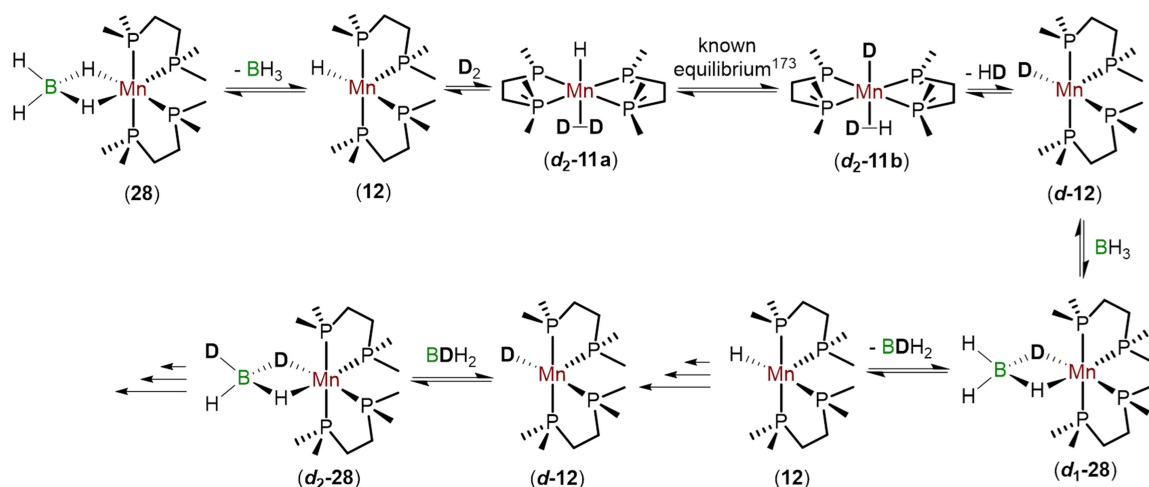


Figure 9.8: Structurally characterized borohydride complexes of Mn(I).

Exposure of $[(\text{dmpe})_2\text{Mn}(\mu\text{-H})_2\text{BH}_2]$ (**28**) to D_2 (initial pressure of 1.7 atm) for 12 h at 90°C led to 40 % deuterium incorporation into both the MnH_2BH_2 and MnH_2BH_2 environments, with HD and H_2 byproducts. This reaction (Scheme 9.4) may proceed by initial BH_3 dissociation to generate $[(\text{dmpe})_2\text{MnH}]$ (**12**), followed by reaction with D_2 to form $[(\text{dmpe})_2\text{MnH}(\text{D}_2)]$ (***d*₂-11a**). Spectroscopic studies by Jones et al. have shown chemical exchange between the MnH and $\text{Mn}(\text{H}_2)$ positions in **11**.¹⁷³ This would allow $[(\text{dmpe})_2\text{MnH}(\text{D}_2)]$ (***d*₂-11a**) to isomerize to $[(\text{dmpe})_2\text{MnD}(\text{DH})]$ (***d*₂-11b**), from which HD elimination would yield a deuterated analogue of **12** $\{[(\text{dmpe})_2\text{MnD}]$ (***d*-12**) $\}$, to which the free BH_3 could re-associate to form $[(\text{dmpe})_2\text{Mn}(\mu\text{-H})(\mu\text{-D})\text{BH}_2]$ (***d*₁-28**). Subsequent cycles of these reactions $\{$ which involve initial elimination and subsequent association of partially deuterated free borane (in each case, via fully protonated **12**), and in some cases HD in place of D_2 $\}$ would allow step-wise deuterium incorporation.

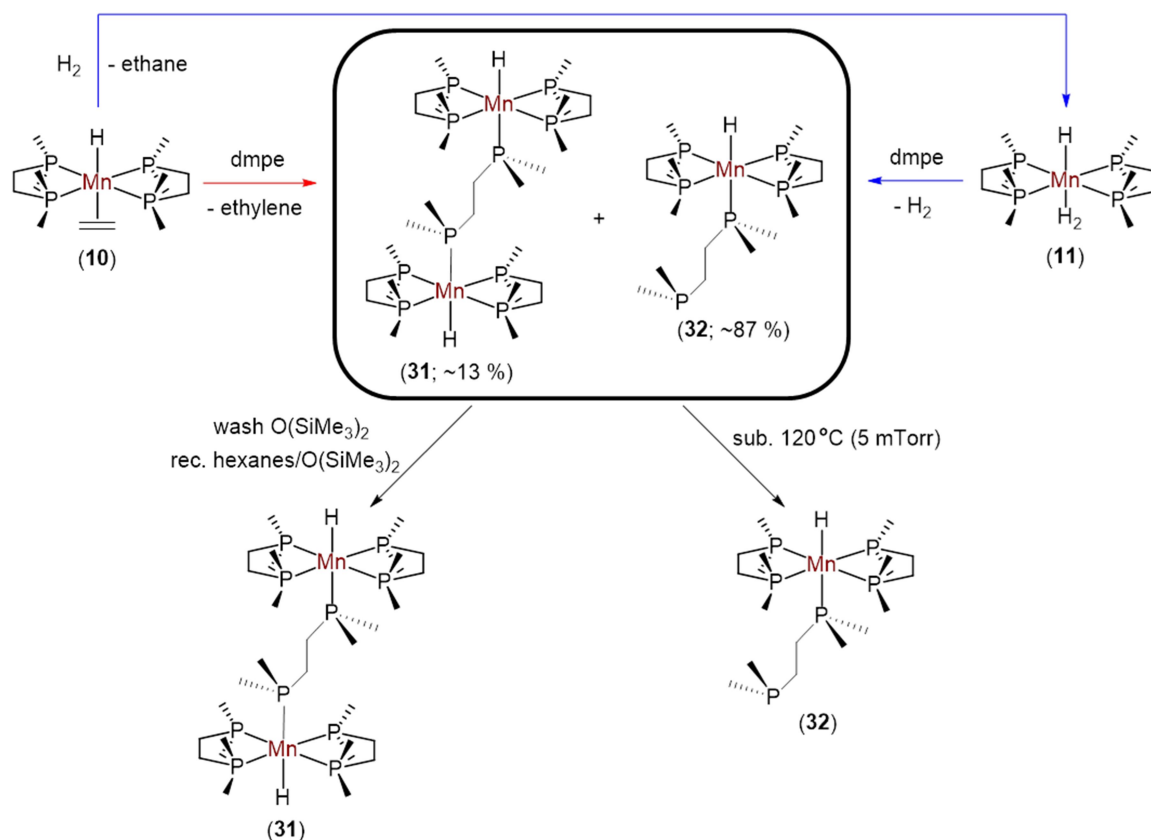


Scheme 9.4: Potential mechanism for deuterium incorporation into $[(\text{dmpe})_2\text{Mn}(\mu\text{-H})_2\text{BH}_2]$ (**28**) by D_2 . Only one isomer of **12_{d_n}** is shown.

9.4 – Synthesis and Characterization of κ^1 -dmpe Hydride Complexes of Manganese

^1H NMR spectra of solutions containing crude borohydride complexes **28-30** all contained a peak at -15.7 ppm, presumably from an identical hydride-containing complex. Closer inspection of these spectra revealed that there are actually two sets of NMR peaks with nearly overlapping MnH signals (0.03 ppm apart), which have been identified by NMR spectroscopy as $[\{(\text{dmpe})_2\text{MnH}\}_2(\mu\text{-dmpe})]$ (**31**) and $[(\text{dmpe})_2\text{MnH}(\kappa^1\text{-dmpe})]$ (**32**); *vide infra*. For both complexes, the MnH peak is a pentet ($^2J_{\text{H,P}} = 49$ Hz) of doublets ($^2J_{\text{H,P}} = 13$ Hz) from coupling to two ^{31}P environments; one with four equivalent P donors and the other with one (upon ^{31}P decoupling, both signals became singlets). The larger coupling constant is comparable to that in Mn(I) hydride complexes where the hydride is located apical to an equatorial plane consisting of two dmpe ligands (e.g. 56.5 Hz in **10**).¹²⁰ These data are consistent with pentaphosphino manganese(I) hydride complexes with *trans* hydride and either μ -dmpe or terminal κ^1 -dmpe ligands (the additional dmpe ligand is presumably generated by decomposition of one or more of the products or intermediates).

The same mixture of pentaphosphino hydride complexes was independently prepared by the reaction of *trans*-[(dmpe)₂MnH(C₂H₄)] (**10**) with excess free dmpe either under inert atmosphere (overnight at 105 °C) or an atmosphere of H₂ (3 days at 60 °C), with either ethylene or ethane observed as the reaction byproduct, respectively (Scheme 9.5). While the former synthesis proceeded via ethylene elimination, the latter proceeded by initial reaction of **10** with H₂ to generate [(dmpe)₂MnH(H₂)] (**11**; *vide infra*, Scheme 9.1) and ethane, followed by substitution of H₂ by the free phosphine (Jones et al. have shown that the H₂ ligand in **11** is prone to substitution reactions by even very weak ligands such as N₂).¹⁷³ Potentially due to the milder conditions required, the reaction under H₂ proceeded more cleanly.



Scheme 9.5: Synthesis {under inert atmosphere (red reaction arrow) or an atmosphere of H₂ (blue reaction arrows)} and purification of [{(dmpe)₂MnH}₂(μ-dmpe)] (**31**) and [(dmpe)₂MnH(κ¹-dmpe)] (**32**) from *trans*-[(dmpe)₂MnH(C₂H₄)] (**10**). Only one isomer of **31** and **32** is shown.

Washing the crude mixture with $O(\text{SiMe}_3)_2$, followed by recrystallization of the residual solid from a concentrated hexanes solution layered with $O(\text{SiMe}_3)_2$ at $-30\text{ }^\circ\text{C}$, allowed for the isolation of dimetallic $[\{(\text{dmpe})_2\text{MnH}\}_2(\mu\text{-dmpe})]$ (**31**) as orange crystals (Scheme 9.5). The NMR spectra of **31** (Figure 9.9 bottom) indicate 2.5 equivalents of dmpe (5 P moieties) per MnH environment with two broad singlets at 78.9 and 26.5 ppm in the $^{31}\text{P}\{^1\text{H}\}$ NMR spectrum; one for the κ^2 -coordinated ligands, and one for the bridging ligand. For the bridging ligand, the alkyl region of the ^1H NMR spectrum contains a single PCH_3 signal (a doublet with $^2J_{\text{H,P}} = 3.6\text{ Hz}$, integrating to $6 \times$ the MnH area) and a single PCH_2 signal (a multiplet, integrating to $2 \times$ the MnH area). The apparent C_{2v} symmetry of **31** indicates that the complex contains *trans* disposed hydride and bridging dmpe ligands (*trans,trans*- $[\{(\text{dmpe})_2\text{MnH}\}_2(\mu\text{-dmpe})]$; *trans,trans*-**31**).

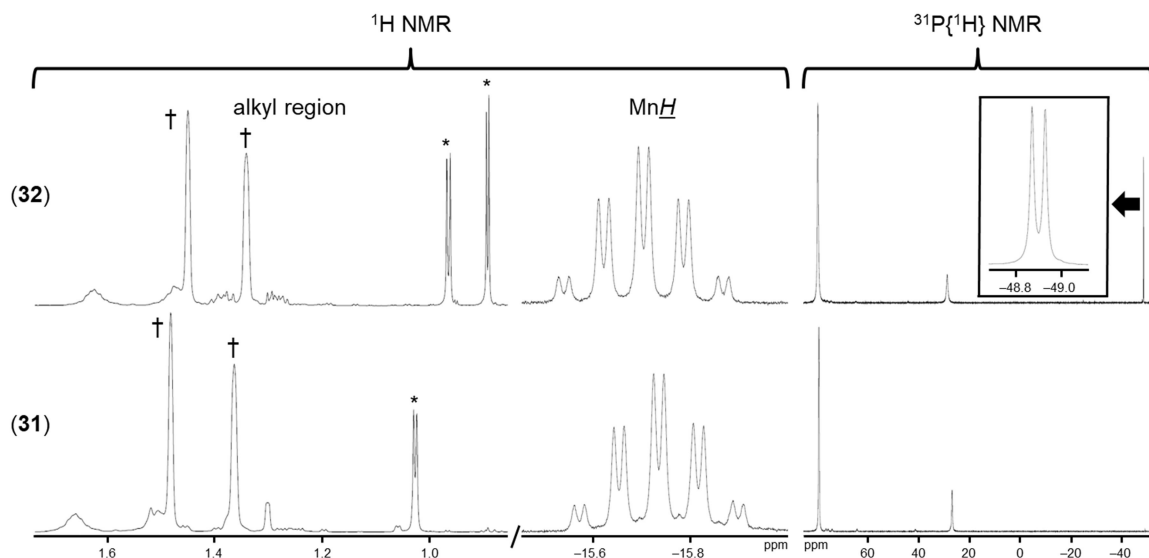


Figure 9.9: Alkyl (left) and hydride (middle) regions of the ^1H NMR spectrum, and the full $^{31}\text{P}\{^1\text{H}\}$ NMR spectrum (right) of (top) $[(\text{dmpe})_2\text{MnH}(\kappa^1\text{-dmpe})]$ (**32**) and (bottom) $[\{(\text{dmpe})_2\text{MnH}\}_2(\mu\text{-dmpe})]$ (**31**) in C_6D_6 at 298 K (600 MHz). * and † represent PCH_3 environments from the κ^1 - and chelating dmpe ligands, respectively.

Upon allowing complex **31** to sit in C_6D_6 at room temperature, a new set of NMR signals slowly appeared (immediately after recrystallization, they were present in the

baseline; approx. 5% relative to the major isomer), with a single MnH ^1H NMR environment at -11.7 ppm featuring a very complex coupling pattern, and five resolved ^{31}P NMR environments (40.91-76.12 ppm). Due to the low symmetry of this product, these NMR signals have been tentatively assigned to an alternative isomer of **31** with a disphenoidal arrangement of the chelating dmpe ligands; *cis,cis*-[$\{(\text{dmpe})_2\text{MnH}\}_2(\mu\text{-dmpe})$] (*cis,cis*-**31**).

By contrast, when the crude mixture of **31** and **32** was sublimed at 120 °C *in vacuo*, monometallic [$(\text{dmpe})_2\text{MnH}(\kappa^1\text{-dmpe})$] (**32**) was isolated as a yellow powder. The NMR spectra of **32** (Figure 9.9 top) indicate 3 equivalents of dmpe (6 P moieties) per MnH environment. Two broad singlets (at 79.3 and 28.4 ppm), along with a sharp doublet ($J_{\text{P,P}} = 14$ Hz, -48.9 ppm), were observed in the $^{31}\text{P}\{^1\text{H}\}$ NMR spectrum. One of the high-frequency signals is from the κ^2 -coordinated ligands, and the other from the donor atom on the κ^1 -coordinated phosphine. The low-frequency $^{31}\text{P}\{^1\text{H}\}$ NMR signal is consistent (both in frequency and line sharpness) with a PR_3 environment which is not coordinated to a metal centre (cf. the $^{31}\text{P}\{^1\text{H}\}$ signal from free dmpe is a sharp singlet at -48.1 ppm), and has therefore been attributed to the pendent phosphine on the κ^1 -coordinated ligand. For the terminal dmpe ligand, the alkyl region of the ^1H NMR spectrum contained two PCH_3 signals (both doublets with $^2J_{\text{H,P}} = 3.8$ and 2.9 Hz, each integrating to $6 \times$ the MnH area) and two PCH_2 signals (both multiplets, each integrating to $2 \times$ the MnH area). These data, combined with apparent C_{2v} symmetry, indicate that **32** features *trans* disposed hydride and κ^1 -coordinated dmpe ligands; *trans,trans*-[$(\text{dmpe})_2\text{MnH}(\kappa^1\text{-dmpe})$]; (*trans,trans*-**32**).

Spectroscopically pure samples of *trans,trans*-**32** were not obtained, as the sublimed sample contained some minor impurities (including a low-symmetry species with a MnH environment at -11.7 ppm, which may be an alternative isomer of **32** with the chelating dmpe ligands forming a disphenoidal geometry). It is currently unclear whether sublimation of the crude reaction mixture only extracts complex **32** already present in the mixture, or whether decomposition of **31** occurs at the sublimation

temperature to generate additional **32**. The volatility of compound **32** suggests that it could potentially be utilized as a precursor for vapour-phase deposition of Mn-containing thin films.

Upon recrystallization of reaction mixtures containing [$\{(\text{dmpe})_2\text{MnH}\}_2(\mu\text{-dmpe})$] (**31**) from hexanes or $\text{O}(\text{SiMe}_3)_2$ at $-30\text{ }^\circ\text{C}$, X-ray quality crystals were obtained for both the high- and low- symmetry isomers of **31**. These structures (Figure 9.10) feature two octahedral Mn centres separated by a bridging dmpe ligand, with the remaining five coordination sites occupied by two chelating dmpe ligands and a hydride.

The X-ray crystal structure of **31** obtained from hexanes is consistent with the dominant isomer observed in solution by NMR spectroscopy (*trans,trans-31*; *vide supra*); Figure 9.10 left. Each octahedral Mn core is related to the other by an inversion centre. The Mn–P distances are 2.2055(4)-2.2138(4) Å for the two chelating dmpe ligands, which are significantly shorter than the Mn–P distance of 2.2331(4) Å to the bridging dmpe ligand, reflecting the higher *trans* influence of hydride vs. phosphine ligands.

In contrast to the structure of *trans,trans-31*, the X-ray crystal structure of **31** obtained from $\text{O}(\text{SiMe}_3)_2$ (Figure 9.10 right) features a disphenoidal coordination geometry of the two chelating dmpe ligands, and the bridging phosphine ligand is *cis* disposed to the hydride ligand (*cis,cis-31*). This structure could be the source of the NMR signals tentatively identified as a ‘minor isomer’ in solutions of **31** (*vide supra*). Unfortunately, poor crystal quality precluded any quantitative analysis of the bonding metrics in *cis,cis-31*.

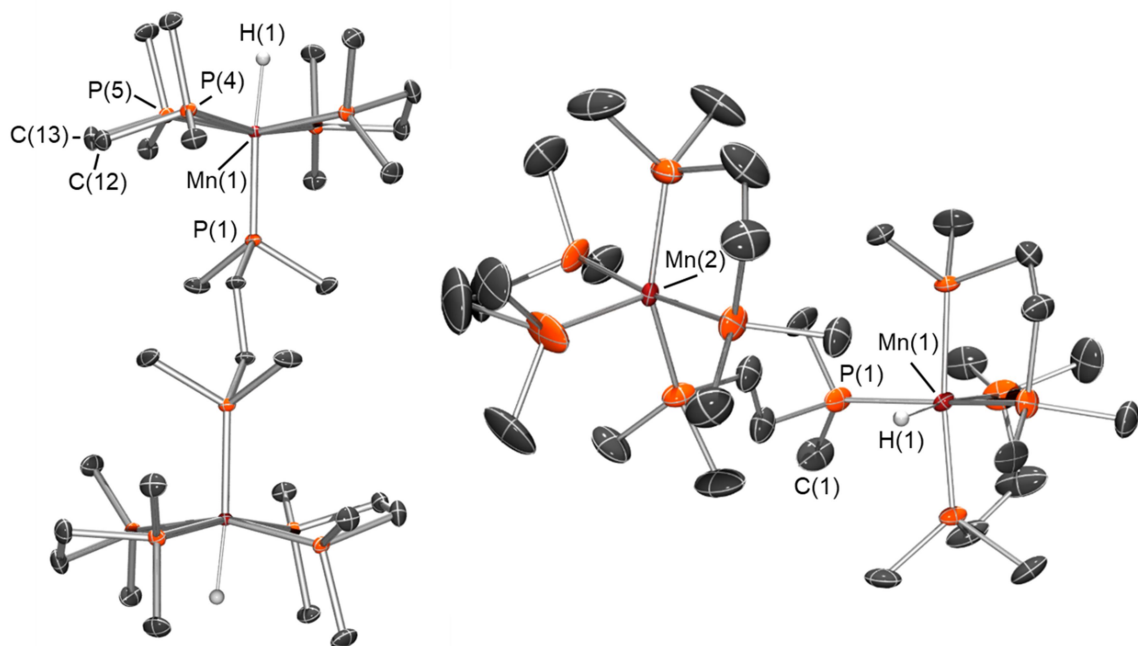
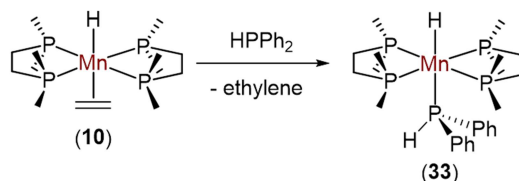


Figure 9.10: X-ray crystal structures of (left) *trans,trans*-[$\{(\text{dmpe})_2\text{MnH}\}_2(\mu\text{-dmpe})$] (*trans,trans*-**31**) and (right) *cis,cis*-[$\{(\text{dmpe})_2\text{MnH}\}_2(\mu\text{-dmpe})$] (*cis,cis*-**31**) with ellipsoids drawn at 50% probability. Most hydrogen atoms have been omitted for clarity. Hydrogen atoms on Mn(1) were located from the difference map and refined isotropically {the hydride on Mn(2) in the *cis,cis* isomer was not located from the difference map and is not included in the figure or CIF}. For *trans,trans*-**31**, distances (Å) and angles (deg): Mn(1)–P(1) 2.2331(4), Mn(1)–P(2) 2.2138(4), Mn(1)–P(3) 2.2065(4), Mn(1)–P(4) 2.2114(4), Mn(1)–P(5) 2.2055(4), Mn(1)–H(1) 1.53(1), P(1)–Mn(1)–H(1) 174.8(6), $\Sigma(\text{P}–\text{Mn}–\text{P})$ (*cis*, equatorial) 355.02(2). For *cis,cis*-**31**, all dmpe ligands were disordered over two positions, and only the major conformation (84.3(2)%) is shown. Due to poor quality data, bond metrics are not discussed.

9.5 – Reaction of *trans*-[$(\text{dmpe})_2\text{MnH}(\text{C}_2\text{H}_4)$] with HPPPh₂

Heating **10** with an excess of HPPPh₂ at 90 °C yielded the monometallic pentaphosphino hydride complex [$(\text{dmpe})_2\text{MnH}(\text{PPh}_2)$] (**33**), accompanied by

elimination of free ethylene (Scheme 9.6). This parallels the reaction of **10** with dmpe (*vide supra*), and presumably proceeded via straightforward ethylene substitution.



Scheme 9.6: Synthesis of [(dmpe)₂MnH(PHPh₂)] (**33**).

The NMR spectra of **33** are very similar to those observed for the dominant species in solutions of complexes **31** and **32**, and feature a single MnH ¹H NMR environment at -14.08 ppm {a pentet (²J_{H,P} = 51 Hz) of doublets (²J_{H,P} = 12) due to coupling to two ³¹P environments} and two ³¹P NMR signals (Figure 9.11 bottom). While the terminal PH environment was not immediately apparent in the ¹H NMR spectrum, this was due to serendipitous overlap of both peaks of the doublet with larger aromatic ¹H NMR signals. However, this signal was conclusively located at 7.28 ppm by ¹H{³¹P} (Figure 9.11 top) and ³¹P-¹H HMBC NMR spectroscopy. Furthermore, cooling a solution of **33** in *d*₈-toluene led to temperature-dependent migration of ¹H NMR signals, allowing the doublet to be resolved at 207 K (Figure 9.12). Very large ³¹P-¹H coupling constants were measured from ¹H, ³¹P, and/or ³¹P-¹H HMBC NMR spectroscopy at both 298 K (288 Hz; Figure 9.11) and 207 K (282 Hz; Figure 9.12). The apparent C_{2v} symmetry of **33** in solution suggests a geometry about Mn involving *trans*-disposed hydride and HPPH₂ ligands.

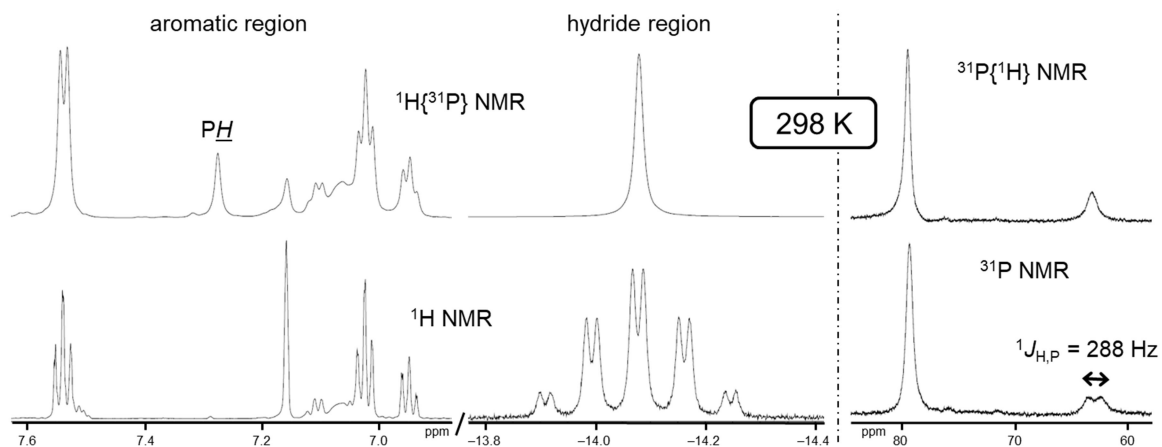


Figure 9.11: NMR spectra (C_6D_6) of $[(dmpe)_2MnH(PHPh_2)]$ (**33**) at 298 K; aromatic (left) and hydride (middle) regions of the 1H (bottom) and $^1H\{^{31}P\}$ (top) NMR spectra (600 MHz), and $^{31}P\{^1H\}$ (top right) and ^{31}P (bottom right) NMR spectra (243 MHz).

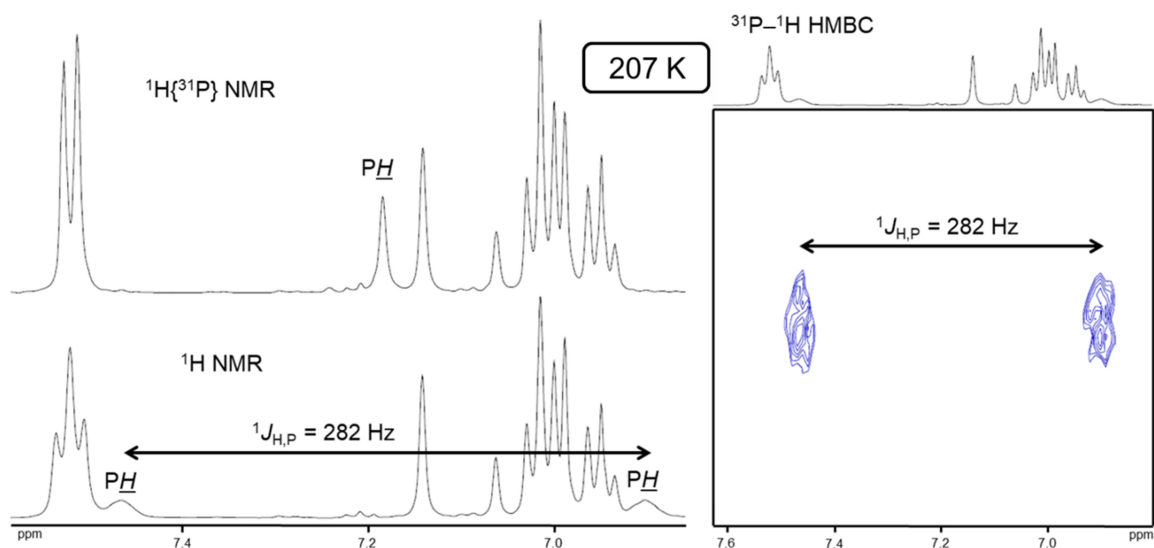


Figure 9.12: NMR spectra (d_8 -toluene, 500 MHz) of $[(dmpe)_2MnH(PHPh_2)]$ (**33**) at 207 K; aromatic region of the 1H (bottom left) and $^1H\{^{31}P\}$ (top left) NMR spectra, and (right) the region of the ^{31}P - 1H HMBC spectrum showing the cross-peak between the terminal PH signal and the major ^{31}P environment.

Solutions of **33** contained a second set of 1H NMR signals in very small concentrations (negligible upon initially dissolving, growing to $\sim 10\%$ after 4 days at

room temperature), including a MnH environment (at -11.4 ppm) with a complex coupling pattern. This impurity could potentially be an alternative isomer of **33** with a disphenoidal dmpe arrangement, and *cis* disposed HPPh_2 and hydride ligands (similar to that observed for *cis,cis-31*; *vide supra*). Unfortunately, low concentrations and the broadness of the NMR signals prevented identification. Furthermore, complex **33** is unstable in solution and slowly decomposed to yield numerous unidentified products, as well as free HPPh_2 , hindering attempts to obtain an analytically pure sample.

X-ray quality crystals of $[(\text{dmpe})_2\text{MnH}(\text{PPh}_2)]$ (**33**) were obtained from a hexanes solution at -30 °C (Figure 9.13), and revealed an octahedral environment about the manganese centre composed of the two chelating dmpe ligands equatorially coordinated, and the hydride *trans* to the HPPh_2 ligand $\{\angle\text{H-Mn-P}_{\text{HPPh}_2} = 165(3)^\circ\}$ with $\text{Mn-P-C}_{\text{ipso}}$ angles of $122.9(1)$ - $126.2(1)^\circ$, and a $\text{Mn-P-H}(1\text{P})$ angle of $116(2)^\circ$.ⁿⁿⁿ

The Mn-P distances involving the chelating dmpe ligands in **33** $\{2.2091(7)$ to $2.2255(7)$ Å $\}$ are similar to those involving the chelating dmpe ligands in *trans,trans-31*. By contrast, the $\text{Mn-P}_{\text{HPPh}_2}$ distances of $2.2048(8)$ - $2.206(2)$ Å in **33** are significantly shorter than the $\text{Mn-P}_{\kappa 1}$ distance of $2.331(4)$ Å in *trans,trans-7*, which is consistent with the expected greater degree of π -backdonation from the electron rich Mn(I) centre to a HPPh_2 ligand relative than to a trialkylphosphine ligand.

ⁿⁿⁿ The two phenyl substituents in **33** are tilted towards the axis formed by the Mn-H bond.

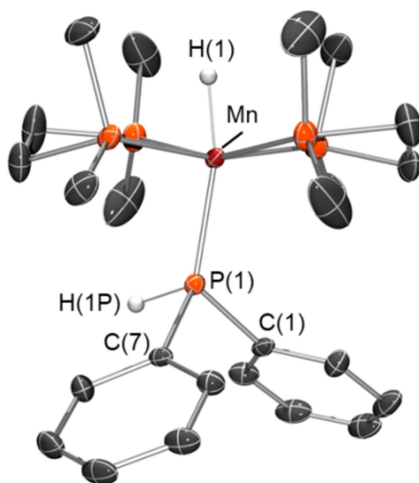


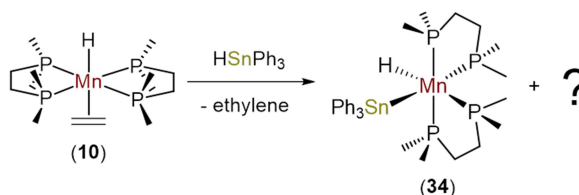
Figure 9.13: X-ray crystal structure of $[(\text{dmpe})_2\text{MnH}(\text{PHPh}_2)]$ (**33**) with ellipsoids drawn at 50% probability. Most hydrogen atoms have been omitted for clarity. Hydrogen atoms on Mn(1) and P(1) were located from the difference map and refined isotropically. The HPPh_2 ligand was disordered over two positions, and only the major conformer {86.8(2)%} is shown.^{ooo} Distances (Å) and angles (deg), where atoms with the ‘A’ suffix refer to those in the minor disordered HPPh_2 ligand analogous to those without that suffix: Mn(1)–P(1) 2.2048(8), Mn(1)–P(1A) 2.206(2), Mn(1)–P(2) 2.2195(7), Mn(1)–P(3) 2.2202(8), Mn(1)–P(4) 2.2255(7), Mn(1)–P(5) 2.2091(7), Mn(1)–H(1) 1.38(7), P(1)–H(1P) 1.35(5), P(1)–Mn(1)–H(1) 165(3), P(1A)–Mn(1)–H(1) 165(3), Mn(1)–P(1)–H(1P) 116(2), Mn(1)–P(1)–C(1) 126.2(1), Mn(1)–P(1A)–C(1A) 124.8(5), Mn(1)–P(1)–C(7) 122.9(1), Mn(1)–P(1A)–C(7A) 124.0(6), $\Sigma(\text{P}–\text{Mn}–\text{P})$ (*cis*, equatorial) 355.11(6).

Complexes **31** and **33** are, to our knowledge, the first pentaphosphino hydride complexes of manganese to be crystallographically characterized. Furthermore, the only previously reported spectroscopically characterized example, $[(\text{F}_3\text{P})_5\text{MnH}]$,^{164,165,556} differs significantly from an electronic standpoint (PF_3 is a poor σ -donor and strong π -acceptor, comparable to carbon monoxide).

^{ooo} The HPPh_2 location in the minor conformation wasn’t located from the difference map.

9.6 – Reactions of *trans*-[(dmpe)₂MnH(C₂H₄)] (**10**) with Hydrotin Reagents

Exposure of *trans*-[(dmpe)₂MnH(C₂H₄)] (**10**) to HSnPh₃ generated a dark pine-green solution containing a manganese(II)-stannyl complex identified as [(dmpe)₂MnH(SnPh₃)] (**34**; *vide infra*), along with ethylene and, presumably, additional unidentified products (Scheme 9.7). The ¹H NMR spectrum of **34** featured five broad signals over a wide range of chemical shifts, characteristic of one or more paramagnetic complexes, suggesting oxidation of the metal centre. Unfortunately, attempts to purify complex **34** were unsuccessful because it is unstable under vacuum, decomposing to a number of species including SnPh₄. As well, reactions of **10** with HSnⁿBu₃ resulted in paramagnetic species (determined by ¹H NMR spectroscopy), though no ethylene was formed, and attempts to identify the product(s) were unsuccessful. The reaction of **10** with stannyl hydride reagents clearly differs from the other reactions of **10** discussed in this work (including reactions with lighter group 14 hydrosilane reagents; Chapters 4-5) by involving 1-electron redox chemistry.



Scheme 9.7: Reaction of *trans*-[(dmpe)₂MnH(C₂H₄)] (**10**) with HSnPh₃.

Large turquoise crystals of [(dmpe)₂MnH(SnPh₃)] (**34**) were obtained from toluene at –30 °C (Figure 9.14), and the structure was found to be octahedral about the manganese centre with a disphenoidal arrangement of the two chelating dmpe ligands, and *cis* disposed stannyl (–SnPh₃) and hydride ligands. While the metal hydride ligand lies exactly *trans* to a phosphine ($\angle\text{H–Mn–P}(4) = 176(2)^\circ$), the stannyl ligand is angled towards the hydride ($\angle\text{H–Mn–Sn} = 71(2)^\circ$) presumably due to steric repulsion from the methyl groups of one or more dmpe ligands.

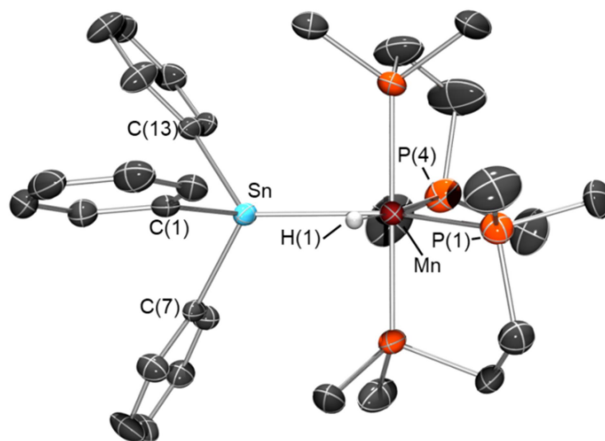


Figure 9.14: X-ray crystal structure of $[(\text{dmpe})_2\text{MnH}(\text{SnPh}_3)]$ (**34**) with ellipsoids drawn at 50% probability. Most hydrogen atoms have been omitted for clarity. The hydrogen atom on Mn(1) was located from the difference map and refined isotropically. Distances (Å) and angles (deg): Mn(1)–Sn(1) 2.5944(7), Sn(1)–H(1) 2.52(5), Mn(1)–H(1) 1.47(5), Mn(1)–P(1) 2.259(1), Mn(1)–P(2) 2.235(1), Mn(1)–P(3) 2.240(1), Mn(1)–P(4) 2.247(1), P(1)–Mn(1)–Sn(1) 146.34(3), H(1)–Mn(1)–Sn(1) 71(2), H(1)–Mn(1)–P(4) 176(2), Mn(1)–Sn(1)–C(1) 117.11(9), Mn(1)–Sn(1)–C(7) 119.80(7), Mn(1)–Sn(1)–C(13) 122.21(9), P(2)–Mn(1)–P(3) 176.85(4).

The Mn–Sn distance in **34** of 2.5944(7) Å is within the range previously reported for manganese complexes with non-bridging Sn(IV) ligands; 2.446–2.693 Å,²¹¹ and significantly shorter than the two structurally characterized manganese stannyl hydride (or η^2 -hydrostannane) complexes, $[(\text{OC})_2\text{Cp}^{\text{Me}}\text{MnH}(\text{SnPh}_3)]$ {d(Mn–Sn) = 2.636(1) Å}⁵⁵⁷ and $[(\text{OC})_4\text{Mn}(\mu\text{-H})(\mu\text{-dppm})\text{Mn}(\text{CO})_3(\text{SnPh}_3)]$ {d(Mn–Sn) = 2.6415(7) Å}.⁵⁵⁸ In contrast to $[(\text{OC})_2\text{Cp}^{\text{Me}}\text{MnH}(\text{SnPh}_3)]$, which was described as featuring an η^2 hydrostannane ligand in the process of oxidative addition across a manganese centre {d(Sn–H) = 2.16(4) Å, $\angle\text{Sn–Mn–H} = 55(2)^\circ$ },⁵⁵⁷ the bonding metrics in **34** {d(Sn–H) = 2.52(5) Å, $\angle\text{Sn–Mn–H} = 71(2)^\circ$ } suggests that no significant interligand stannyl-hydride interaction is present. $[(\text{dmpe})_2\text{MnH}(\text{SnPh}_3)]$ (**34**) is, to our knowledge, the first reported example of a manganese(II) complex which contains both hydride and stannyl ligands.

However, the mechanism for the formation of **34** is unclear, it could not be isolated in pure form, and the mechanism of decomposition to form SnPh_4 remains obscure.

9.7 – Summary and Conclusions for Chapter 9

trans- $[(\text{dmpe})_2\text{MnH}(\text{C}_2\text{H}_4)]$ (**10**) has been shown to be a versatile precursor from which to access a variety of new manganese hydride complexes; the previously reported dihydrogen complex $[(\text{dmpe})_2\text{MnH}(\text{H}_2)]$ (**11**), the borohydride complexes $[(\text{dmpe})_2\text{Mn}(\mu\text{-H})_2\text{BR}_2]$ (**28**: R = H, **29**: $\text{R}_2 = \text{C}_8\text{H}_{14}$, **30**: R = Mes), pentaphosphino hydride complexes $[\{(\text{dmpe})_2\text{MnH}(\text{PR}_3)\}_n]$ (**31**: $\text{PR}_3 = 0.5 \text{ dmpe}$, $n = 2$; **32**: $\text{PR}_3 = \kappa^1\text{-dmpe}$, $n = 1$; **33**: $\text{PR}_3 = \text{HPPH}_2$, $n = 1$), and the stannyl hydride complex $[(\text{dmpe})_2\text{MnH}(\text{SnPh}_3)]$ (**34**). In some cases, these reactions proceeded by ethylene substitution, and in others via initial isomerization of **10** to $[(\text{dmpe})_2\text{MnEt}]$ (**13**) followed by ethane or ethylborane elimination (the mechanism to form **34**, however, remains unclear).

X-ray crystal structures were obtained for the borohydride complexes **28-30**, and provided an opportunity to examine the effect that different terminal substituents on boron (H, alkyl, aromatic) have on structural parameters. Complexes **29-30** are the first examples of manganese borohydride complexes with hydrocarbyl substituents on boron, and complex **28** was shown to undergo H/D exchange under an atmosphere of D_2 .

$[\{(\text{dmpe})_2\text{MnH}\}_2(\mu\text{-dmpe})]$ (**31**), $[(\text{dmpe})_2\text{MnH}(\kappa^1\text{-dmpe})]$ (**32**), and $[(\text{dmpe})_2\text{MnH}(\text{PPh}_2)]$ (**33**) were prepared, and **31** and **33** are the first pentaphosphino hydride complexes of manganese to be structurally characterized. Compound **31** features a dmpe ligand bridging between two well-separated Mn centres, and X-ray crystal structures were obtained for two isomers with an equatorial or disphenoidal arrangement of the chelating dmpe ligands on each metal centre.

Unlike the reactions of **10** with hydroboranes and phosphines, **10** reacted with HSnPh_3 to afford the divalent manganese complex $[(\text{dmpe})_2\text{MnH}(\text{SnPh}_3)]$ (**34**) via 1-electron oxidation. Compound **34** is the first manganese(II) stannyl hydride complex to

have been structurally characterized, and its structure features *cis*-disposed hydride and stannyl ligands without a significant Sn···H interligand interaction (in contrast to previously reported $[(OC)_2^{Me}CpMnH(SnPh_3)]$, for which such an interaction was observed).

Chapter 10

Future Directions

10.1 – Future Directions Pertaining to Vapour-phase Deposition of Mn-containing Thin Films

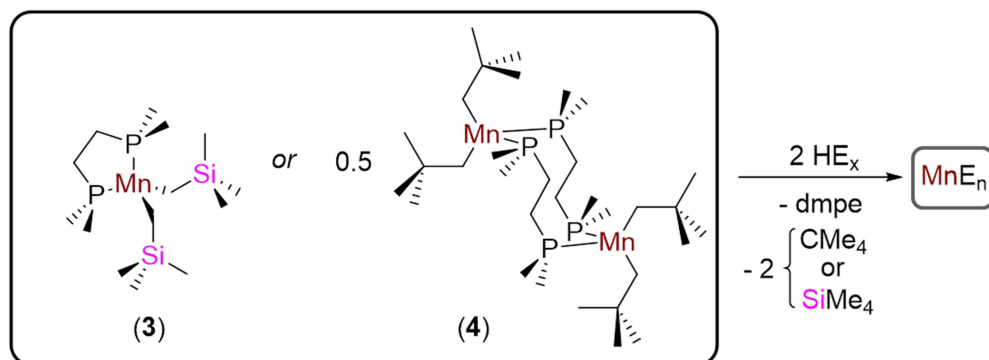
Chapter 2 includes solution-state reactions involving dialkylmanganese(II) complexes (**1** and **2**) or their Lewis base adducts (**3-8**) with H_2 or $ZnEt_2$, which resulted in electroless deposition of elemental manganese or a Mn:Zn alloy, respectively. Furthermore, the 1:1 dmpe adducts of $Mn(CH_2EMe_3)_2$ ($E = C, Si$; complexes **3** and **4**) exhibited desirable properties for an ALD or CVD precursor. Because of this, future work in this area will include attempts to deposit Mn and Mn:Zn alloy films by ALD using complexes **3** or **4** in combination with H_2 or $ZnEt_2$ as a co-reactant.

Initial efforts in this direction will be to determine if the electroless deposition observed in Chapter 2 could be mirrored in an ALD-type experiment (which involves reactivity at a vapour-surface interface).^{PPP} If a thin film could successfully be deposited using these precursor/co-reactant combinations, it will be necessary to determine i) if the film growth is self-limiting, ii) the rate of film growth, iii) the chemical composition of the film, iv) which substrates the film could be deposited on (e.g. silica, H-terminated silicon, various metals), and v) the deposition temperature range for which ALD could be observed. Furthermore, additional co-reactants could be investigated for deposition of elemental thin films using the same dialkylmanganese(II) precursors (**3** or **4**). These could include other hydride sources such as hydrosilanes or hydroboranes, as well as other ethyl sources such as $AlEt_3$ or BEt_3 . This work will involve initial solution-state test

^{PPP} It cannot be assumed that reactivity at a surface-vapour interface will mimic that observed in solution. One reason for this is that upon absorption to a surface, the environment around the metal centre will be significantly different than in the free molecule (for example, by complete or partial phosphine dissociation from **3** or **4**).

reactions similar to those described in section 2.5 for H_2 and ZnEt_2 , and promising results will be followed up in a manner described above (i.e. attempts to deposit a film by ALD).

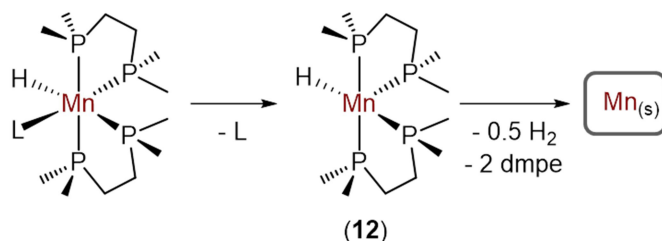
Other work in this area could involve determination if dialkylmanganese(II) complexes could be generic Mn-containing precursors for ALD of a variety of Mn-containing thin films. For example, reactions with H_2O , H_2S , NH_3 , or HF could potentially yield various Mn-containing films (MnS_n , MnO_n , MnN_n , or MnF_n , respectively); Scheme 10.1. Deposition of Mn-containing films by ALD, with the exception of manganese oxide films, remains a relatively unexplored area of research (see section 1.2.8).



Scheme 10.1: Potential deposition of Mn-containing films using proton-source co-reactants. For example, $\text{E} = \text{O}, \text{S}, \text{N}, \text{or F}$, and $x = 1$ or 0.5 .

Lastly, deposition of Mn-containing films by CVD using Mn(I) hydride complexes could be explored. Deposition of elemental manganese could be envisaged by the reactivity outlined in Scheme 10.2; initial dissociation of the neutral non-dmpe co-ligand (which, when free of the metal centre, would be neutral, volatile, and thermally stable) to generate the reactive intermediate $[(\text{dmpe})_2\text{MnH}]$ (**12**), which could decompose to form $\text{Mn}_{(s)}$ and volatile byproducts by dmpe dissociation and bimolecular H–H bond-forming reductive elimination. Some hydride complexes in this work have displayed promising physical properties (thermal stability and volatility) for acting as vapour-phase precursors, including $[(\text{dmpe})_2\text{MnH}(\text{C}_2\text{H}_4)]$ (**10**), $[(\text{dmpe})_2\text{MnH}(\kappa^1\text{-dmpe})]$ (**32**) and

$[(dmpe)_2Mn(\mu-H)_2BH_2]$ (**28**). The thermal stability and volatility of many other manganese hydride complexes reported in this work have yet to be determined. For hydride complexes which are determined to have these necessary (for CVD) physical properties, CVD experiments will be conducted and the resulting films will be analyzed as discussed above for ALD, with the exception of determination of self-limiting growth, which is not relevant for CVD.



Scheme 10.2: Potential CVD reactivity to obtain thin films of elemental manganese from manganese(I) hydride precursors. L represents a neutral, volatile ligand (e.g. HBR₂, PR₃). Only one isomer of all complexes are shown.

10.2 – Future Directions Pertaining to Dialkylmanganese(II) Chemistry

In 2010, the Cámpora group reported that the reaction of $[(bipy)Mn(CH_2SiMe_3)_2]$ with a quarter equivalent of O₂ yielded the mixed valence species $[\{Mn_2(CH_2SiMe_3)_3(\mu-O)(bipy)\}_2]$.¹⁰⁰ It would be interesting to observe the differences in structure between this species and those produced by an analogous reaction of the dmpe and/or dmpm adducts of Mn(CH₂EMe₃)₂ (E = C, Me) discussed in Chapter 2. Exposure of some of the dialkylmanganese(II) complexes discussed in this work to trace oxygen led to a change in colour from yellow/orange/red to green (an excess of oxygen resulted in an exothermic conversion to a black powder), suggesting formation of a molecular higher valent alkyl species. In addition, similar chemistry could be explored with limiting and stoichiometric equivalents of other reagents such as S₈ or P₄.

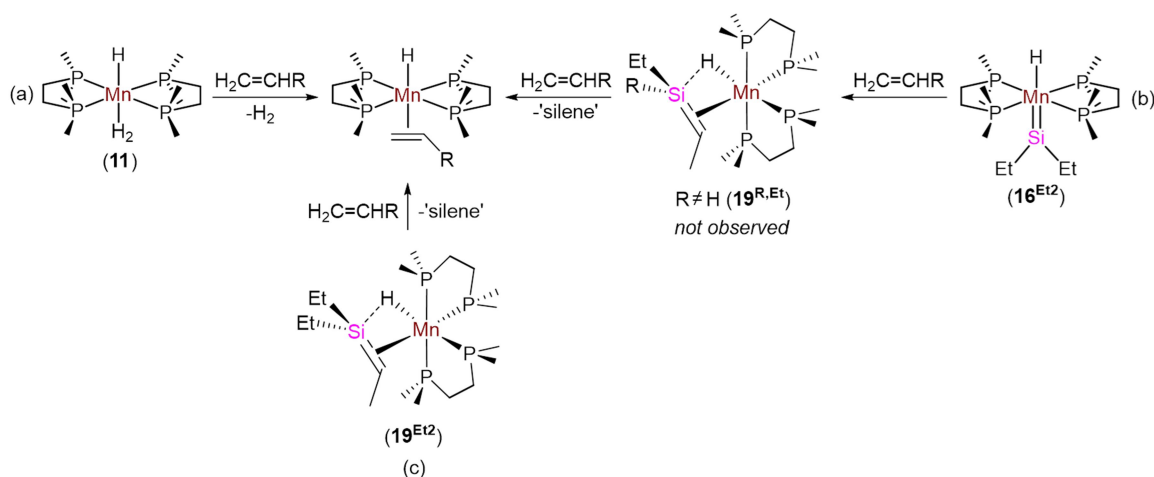
10.3 – Future Directions Pertaining to the Structure of [(dmpe)₂MnH(C₂H₄)] (**10**)

Chapter 3 highlighted that [(dmpe)₂MnH(C₂H₄)] (**10**) is unusual for a 1st row transition metal complex in that it is observed in solution and the solid state as an alkene hydride complex, as opposed to an ethyl species (the product of 1,2-insertion). DFT calculations indicated that this is due to the unique steric environment provided by the two chelating dmpe ligands. A combination of these DFT calculations and trapping experiments showed that complex **10** is in equilibrium with the 5-coordinate ethyl complex [(dmpe)₂MnEt] (**13**), from which reactions with main group hydrides could proceed. Further work in this area could examine how altering the steric and electronic nature of both the phosphine and alkene ligands in complex **10** would affect the alkene hydride to ethyl equilibrium.

Initial work could be carried out computationally by comparing the difference in energy between these species (as well as the *cis* alkene hydride isomer) when different phosphine or alkene groups were used. It would be relatively simple to repeat the calculations described in Chapter 3 using input coordinates with, for example, CF₃ or phenyl groups in place of methyl group on the phosphine, a propyl linker in place of the ethylene linker on the phosphine, or a sterically bulky substituent could replace one of the hydrogen atoms on the alkene.

Experimentally, analogues of **10** with different alkene ligands can be prepared by H₂ substitution from [(dmpe)₂MnH(H₂)] (**11**), in a manner similar to Jones' synthesis of **10** and a 1-pentene analogue of **10** (a in Scheme 10.3).¹⁷³ Alternatively, such complexes could be prepared by exposing the silylene hydride complex [(dmpe)₂MnH(=SiEt₂)] (**16**^{Et2}) to different terminal alkenes; preliminary results show that **16**^{Et2} reacts with 3-trimethylsilylpropene and 1-octene to form the alkene hydride complexes *trans*-

[(dmpe)₂MnH(alkene)] (alkene = H₂C=CHCH₂SiMe₃ or H₂C=CH(CH₂)₅CH₃).^{qqq} In the reactions of terminal alkenes with **16**^{Et2}, no intermediate was observed spectroscopically to suggest the formation of a transient silene complex, however it is possible that this mechanism passes through an unobserved silene hydride intermediate in an analogous manner to the reactions of silene hydride complexes with multiple equivalents of ethylene (described in Chapter 5); b in Scheme 10.3. Presumably, similar reactivity would be observed from [(dmpe)₂MnH(Et₂Si=CHMe)] (**19**^{Et2}), though there is no apparent benefit to using this higher-value complex as a reagent relative to using **16**^{Et2} (c in Scheme 10.3).

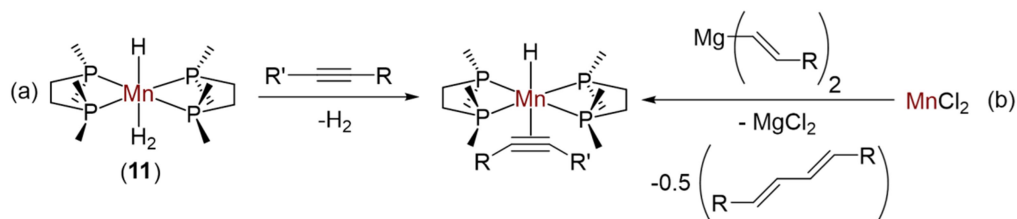


Scheme 10.3: Potential routes (a-c) to the synthesis of derivatives of [(dmpe)₂MnH(C₂H₄)] (**10**) with different alkene ligands. Only one isomer of each complex is shown, R ≠ H.

Lastly, attempts could be made to prepare the alkyne analogue of complex **10**, to compare the structure and reactivity of this species to that of the alkene hydride complex reported in this work. A potential synthetic route could involve substitution of H₂ from [(dmpe)₂MnH(H₂)] (**11**) by a free alkyne (a in Scheme 10.4). Alternatively, a pathway

^{qqq} These complexes featured a ¹H NMR environment at -13.05 ppm (3-trimethylsilylpropene complex) or -12.87 ppm (1-octene complex) corresponding to the MnH environment. An X-ray crystal structure was obtained for the 3-trimethylsilylpropene analogue.

can be envisaged analogous to the initial synthesis of $[(dmpe)_2MnH(C_2H_4)]$ (**10**) with a divinyl magnesium reagent in place of $MgEt_2$ (b in Scheme 10.4).



Scheme 10.4: Potential routes (a-b) to the synthesis of $[(dmpe)_2MnH(\text{alkyne})]$ complexes. For route b, $R' = H$.

10.4 – Future Directions Pertaining to DFT Calculations

In Chapters 4, 5, and 7, various mechanisms were proposed for the synthesis of a number of different manganese complexes, and in Chapter 8 a potential catalytic cycle for ethylene hydrosilylation was proposed. In some cases, DFT calculations were employed to demonstrate the thermodynamic accessibility of some of the proposed intermediates (as well as, in some cases, trapping studies and high temperature NMR spectroscopy). Furthermore, we gained some insight into the mechanism for ethylene hydrosilylation by deuterium labelling experiments. In all cases, however, multiple potential reaction pathways were proposed. DFT calculations can be employed to analyze each of the proposed reaction pathways (involving locating energy minima for all potential intermediates, potential energy profiles for each transformation, and transition states) to determine which of the proposed reaction pathways is of lowest energy for each case. Such knowledge could potentially allow for rational design of new reaction chemistry.

10.5 – Future Directions Pertaining to Manganese Silylene Hydride Complexes

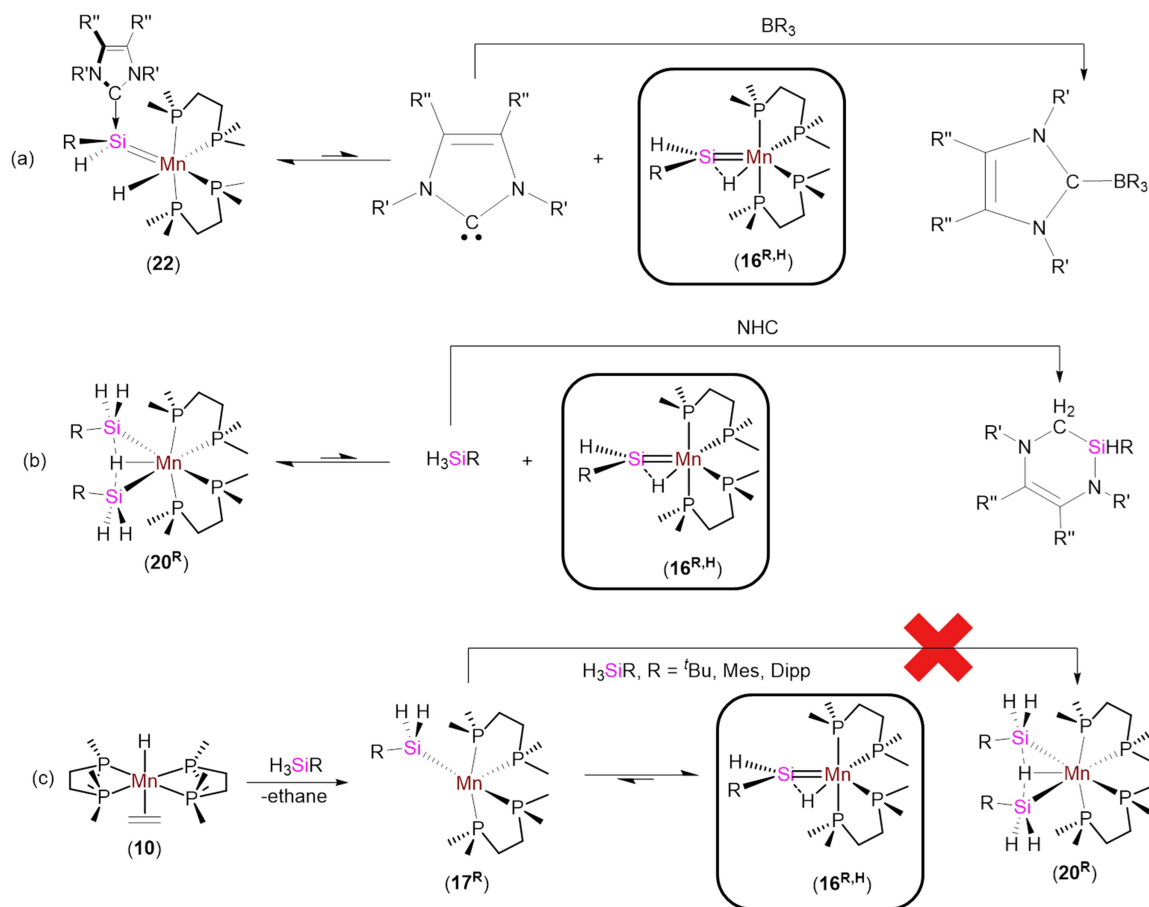
The synthesis of silylene hydride complex $[(dmpe)_2MnH(=SiEt_2)]$ (**16**^{Et2}) required very mild reaction conditions (i.e. the reaction mixture could not be heated above

ambient temperature), and therefore took a full month before 100% conversion was observed. When heated above 30 °C, **16**^{Et2} decomposed to form a new complex tentatively identified as $[(\text{dmpe})\{\kappa^3\text{-P}(\text{Me})_2\text{CH}_2\text{CH}_2\text{P}(\text{Me})\text{CH}_2\text{SiEt}_2\}\text{MnH}_2]$, which features two hydride ligands and a tridentate bis(phosphine)-silyl ligand, by ¹H NMR spectroscopy. Tilley et al. reported that an analogous structure was formed from the decomposition of $[\text{Cp}^*(\text{dmpe})\text{MoH}(\text{=SiR}_2)]$ (R = Me, Ph).³²⁶ Future work in this area could involve isolating and fully characterizing this species.

Chapter 5 discussed the use of DFT calculations, trapping experiments, and high temperature NMR spectroscopy to show the accessibility of base-free silylene hydride complexes with a hydrogen substituent on Si ($[(\text{dmpe})_2\text{MnH}(\text{=SiHR})]$; **16**^{R,H}) from disilyl hydride complexes $[(\text{dmpe})_2\text{MnH}(\text{SiH}_2\text{R})_2]$ (**20**^R). Further work in this field could involve isolation of these complexes; to date no manganese complexes with an electronically unstabilized terminal silylene ligand featuring a terminal SiH substituent have been isolated. Three potential routes to obtaining such complexes are shown in Scheme 10.5. First, reactivity could be envisaged where NHC-stabilized silylene hydride complexes featuring a terminal SiH substituent $\{[(\text{dmpe})_2\text{MnH}\{\text{=SiHR}(\text{NHC})\}]\}$ (**22a-d**) react with a reagent capable of abstracting the NHC; a in Scheme 10.5. Given that complexes **22** are presumably in an equilibrium with free NHC and the base-free silylene complex (see Chapter 5), reagents could be chosen which will preferentially react with free NHCs and added stoichiometrically to remove the free NHC from this equilibrium.^{†††} The Fillipou group has used B(*p*-tol)₃ to obtain a base-free silylyne complex from an NHC-stabilized silylyne complex, with elimination of an NHC-borane adduct.³⁴⁹ Preliminary results in this area involved the reaction of excess BPh₃ with $[(\text{dmpe})_2\text{MnH}\{\text{=SiH}^n\text{Bu}(\text{}^{i\text{Pr}}\text{NHC})\}]\}$ (**22b**), which resulted in clean conversion to a single hydride-containing species and a byproduct tentatively identified by NMR spectroscopy as an adduct of BPh₃ and ⁱPrNHC. Presumably, this reaction involved initial NHC abstraction to form the base-free silylene hydride complex $[(\text{dmpe})_2\text{MnH}(\text{=SiH}^n\text{Bu})]$

^{†††} Care should be taken not to add an excess of the abstraction reagent because it could potentially react with the highly reactive target base-free silylene hydride complex.

(**16^{Bu,H}**), which proceeded to react with a second equivalent of BPh₃ to form an as-yet unidentified species (2 equiv. of BPh₃ were consumed in the reaction).



Scheme 10.5: Potential routes to isolation of manganese complexes bearing electronically unstabilized terminal silylene ligands with a terminal SiH substituent; $[(dmpe)_2MnH(=SiHR)]$ (**16^{R,H}**). Only one isomer is shown for all complexes.

A related pathway would be removal of free hydrosilane from a solution containing a disilyl hydride complex $[(dmpe)_2MnH(SiH_2R)_2]$ (**20^R**), which is in equilibrium with a base-free silylene hydride complex and a free hydrosilane (Chapter 5); b in Scheme 10.5. A possible reagent for this is ⁱPrNHC, which irreversibly reacts with free hydrosilanes (care must be taken not to add an excess of NHC, or it will form the NHC-stabilized silylene complex **22a**).⁵¹¹ Alternatively, attempts can be made to form

such a complex directly from $[(\text{dmpe})_2\text{MnH}(\text{C}_2\text{H}_4)]$ (**10**), using very bulky primary hydrosilanes H_3SiR (e.g. $\text{R} = \text{}^t\text{Bu}$, Mes, Dipp); *c* in Scheme 10.5. Perhaps the steric bulk will inhibit addition of a second equivalent of hydrosilane to the putative silyl intermediate $[(\text{dmpe})_2\text{Mn}(\text{SiH}_2\text{R})]$ (**17^R**); the presumed intermediate in the reactions of **10** with H_3SiR ($\text{R} = \text{}^n\text{Bu}$, Ph) in Chapter 5. This would allow the silyl intermediate to isomerize to a base-free silylene hydride complex $[(\text{dmpe})_2\text{MnH}(=\text{SiHR})]$ in a manner similar to that observed in the reaction of **10** with secondary hydrosilanes (Chapter 4).^{sss}

Chapters 4, 6, and 7 include discussion of the reactions of silylene hydride complexes **16^{R2}** with H_2 , ethylene, CO_2 , and diisopropylcarbodiimide (reactions of disilyl hydride complexes **20^R**, which are in equilibrium with silylene hydride complexes, with H_2 and ethylene were also discussed in Chapters 5-6). Investigation of the reactivity of manganese silylene hydride complexes can be further expanded to additional reagents such as ketones and imines.

Reactions of silylene hydride complexes **16^{R2}** with H_2 or (potentially) ethylene are proposed to proceed via a 5-coordinate silyl intermediate accessed by 1,1-insertion. The accessibility of this complex can be confirmed by trapping experiments with isonitriles, similar to how an isostructural complex was trapped from solutions of disilyl hydride complexes **20^R** (Chapter 5).

10.6 – Future Directions Pertaining to Manganese Silene Hydride Complexes

In the synthesis of $[(\text{dmpe})_2\text{MnH}(\text{Ph}_2\text{Si}=\text{CHMe})]$ (**19^{Ph2}**), an unidentified hydride-containing intermediate was observed by NMR spectroscopy. Identification of this

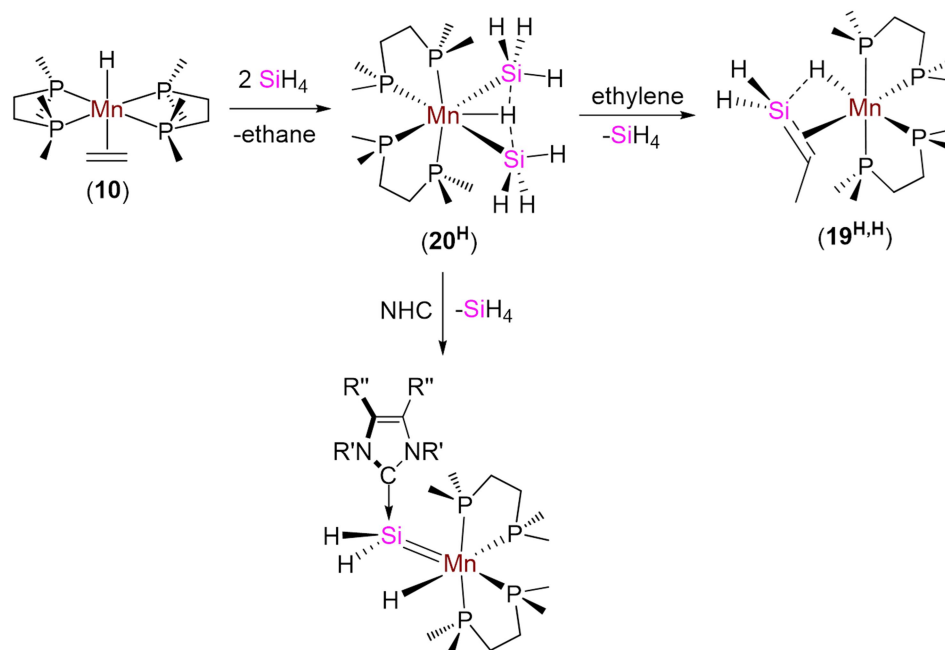
^{sss} It is also possible that the increased steric bulk in the primary hydrosilane reagent will inhibit reaction with **10** from occurring at all.

species (potentially via low temperature NMR spectroscopy) could provide corroboration for the proposed synthetic mechanism (Chapter 4).^{†††}

Chapter 5 also contained a discussion of the first spectroscopically observed transition metal silene hydride complexes featuring a hydrogen substituent on Si; [(dmpe)₂MnH(RHSi=CHMe)] (**19**^{R,H}; R = ⁿBu, Ph). However, we were unsuccessful at obtaining X-ray quality crystals, so the literature currently contains no solid state structural characterization of these types of complexes. Future work in this area could involve preparing derivatives of **19**^{R,H} where the non-H substituent on Si is a group which would allow for easier crystallization. Use of different primary hydrosilanes in the initial synthesis of disilyl hydride complexes **20**^R (the precursors to **19**^{R,H}) should allow a family of such complexes to be prepared. Examples of R groups which may promote crystallization of **19**^{R,H} are Me, ⁱPr, or *p*-ⁱPrPh (though it should be noted that H₃SiMe and H₃SiⁱPr are gases at room temperature, and the latter is not commercially available).

To date, no spectroscopically or crystallographically observed silene complexes of transition metals have been reported which contain *two* hydrogen substituents on Si. Attempts to obtain such a complex could involve reactivity analogous to that presented in Chapter 5 but with SiH₄ in place of a primary hydrosilane. This could initially yield a disilyl hydride complex [(dmpe)₂MnH(SiH₃)₂] (**20**^H) which could then react with ethylene to form the target silene hydride complex [(dmpe)₂MnH(H₂Si=CHMe)] (**19**^{H₂}); Scheme 10.6. In addition, isolation or observation of a manganese silylene complex with two terminal SiH substituents (**16**^{H₂}) would be of interest in its own right. Such a complex would presumably be in equilibrium with the proposed disilyl hydride intermediate (and could potentially be observed at high temperature by NMR spectroscopy or trapped by NHC coordination; Scheme 10.6).

^{†††} It is possible that this intermediate is simply another isomer of *cis*-**19**^{Ph₂} (see Chapter 5 for discussion of different possible isomers), which is kinetically more accessible but isomerizes to a lower-energy (observed) product over time.



Scheme 10.6: Potential routes for accessing a silene hydride complex or an NHC-stabilized silylene hydride complex with two terminal SiH substituents. Only one isomer is shown for all complexes.

Absent from this work is an investigation of the reactivity of manganese silene hydride complexes **19**.^{uuu} This investigation could reflect what we have done for silylene hydride complexes, including what has been proposed for future directions in that field (see Chapter 7 or section 10.5). For example, reactions with various small molecules (e.g. ketones, alkynes, CO₂, C(N^tPr)₂, imines) could be carried out for silene hydrides with and without- an SiH substituent.

10.7 – Future Directions Pertaining to Silyl Dihydride Complexes

Chapter 6 discussed the structures of silyl dihydride complexes [(dmpe)₂MnH₂(SiHRR’)] (**18**), which feature nonclassical silyl hydrosilane or silicate

^{uuu} With the exception of the stoichiometric reaction with ethylene or hydrosilanes, and the catalytic hydrosilylation of ethylene.

ligands. The strength of the Si–H interactions is commonly inferred from the Si–H distances. However, X-ray crystallography is notoriously inaccurate in locating hydrogen atoms. Therefore, in this work we turned to DFT calculations to analyze these distances. Future work in this field could involve obtaining neutron structures, for which accurate Si–H distances could be obtained (along with other key bonding metrics such as the Mn–H distances and Si–Mn–H angle).

The silyl dihydride complexes discussed in chapter 6 exist in solution as an equilibrium between multiple isomers, two of which (*central* and *transHSi*) were observed by NMR spectroscopy. The ratios of observed *central* : *transHSi* isomers ranged from 87 : 13 to 27 : 72. Further work in this field could involve investigating how the steric and electronic properties of the substituents on Si affect this equilibrium. Analogues of **18** could be prepared with various silicon substituents including hydrogen, halogens, or bulky aromatic groups (such as Dipp).

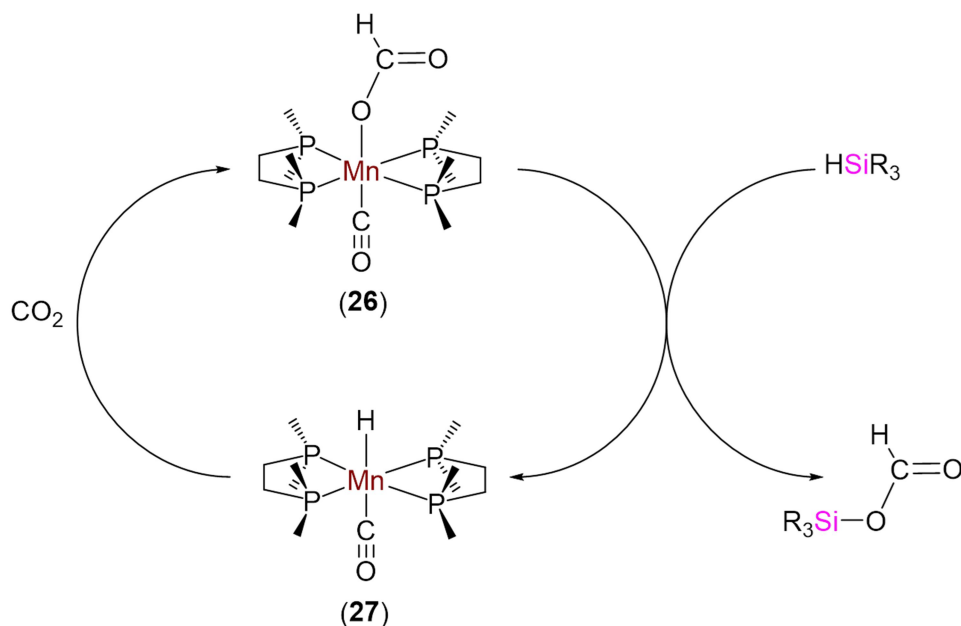
Lastly, Chapter 6 introduced ^{29}Si -edited ^1H – ^1H COSY NMR spectroscopy, which could be used for measuring the sign and magnitude of the ^{29}Si – ^1H coupling constants (by a modification of the Scherer method). This method was able to locate ^{29}Si satellites with greater accuracy than standard ^1H – ^1H COSY spectroscopy (used by Scherer), and in some cases was able to locate signals which could not be located at all in the ^1H – ^1H COSY experiment. However, these experiments were very time-consuming, so further work in this area could involve optimizing the ^{29}Si -edited ^1H – ^1H COSY experiment (such as by applying a double quantum filter (dqf) sequence).

10.8 – Future Directions Pertaining to Reactions of Disilyl Hydride Complexes with CO_2 and $\text{C}(\text{N}^i\text{Pr})_2$

Chapter 7 contained a discussion of the reactions of disilyl hydride complexes $[(\text{dmpe})_2\text{MnH}(\text{SiH}_2\text{R})]$ (**20^R**) with diisopropylcarbodiimide $\{\text{C}(\text{N}^i\text{Pr})_2\}$ to form the manganese(I) amidinylsilyl complexes $[(\text{dmpe})_2\text{Mn}\{\kappa^2\text{-SiHR}(\text{N}^i\text{PrCHN}^i\text{Pr})\}]$ (**25^{R,H}**). Given the similarities between reactions of either **20^R** or silylene hydride complexes **16^{R2}**

with either H₂, ethylene, or CO₂, which form isostructural products (Chapters 4-7), this chemistry can be expanded to determine if similar manganese(I) amidinylsilyl complexes could be formed from reactions of C(N^tPr)₂ and silylene hydride complexes. Furthermore, the reactivity of complexes **25^{R,H}** towards a variety of small molecules can be investigated.

Reactions of CO₂ with disilyl hydride complexes **20^R** or silylene hydride complex **16^{Et2}** were shown to yield *trans*-[(dmpe)₂Mn(CO)(κ¹-O₂CH)] (**26**) with polysiloxane byproducts. In Chapter 7, the polysiloxane byproducts were only characterized by NMR spectroscopy, and further characterization would be useful. Examples of characterization techniques which could be employed are Gel Permeation Chromatography (for measuring molecular weight average and distribution) and IR spectroscopy (to obtain chemical information to supplement that provided by NMR spectroscopy).⁵⁵⁹ In addition, the polysiloxane byproduct formed from the reaction of [(dmpe)₂MnH(SiH₂Ph)₂] (**20^{Ph}**) and CO₂ {(SiHPhO)_n} was observed to react with the free hydrosilane byproduct H₃SiPh. This reaction bears further examination, as does characterization of this as-yet unidentified product. Lastly, formate complex **26** could be investigated for activity towards the catalytic hydrosilylation of CO₂ to form formoxysilanes. Though highly speculative, a potential catalytic cycle (Scheme 10.7) could involve i) O–Si bond-forming σ-bond metathesis (or oxidative addition followed by O–Si bond-forming reductive elimination) of **26** and free hydrosilane to generate the target formoxysilane (silyl formate) and [(dmpe)₂MnH(CO)] (**27**), and ii) 1,2-insertion of a C=O bond in CO₂ into the Mn–H bond in **27** to reform complex **26**. The second of these two steps has been observed in this work (Chapter 7).



Scheme 10.7: Potential catalytic cycle for hydrosilylation of CO_2 using *trans*- $[(\text{dmpe})_2\text{Mn}(\text{CO})(\kappa^1\text{-O}_2\text{CH})]$ (**26**). For clarity, a tertiary hydrosilane is shown as feedstock, though this chemistry could also potentially apply to other hydrosilanes.

10.9 – Future Directions Pertaining to Catalytic Hydrosilylation

Chapter 8 includes discussion that $[(\text{dmpe})_2\text{MnH}(\text{C}_2\text{H}_4)]$ (**10**), and the various silicon-containing complexes prepared from reactions of **10** with hydrosilanes (in some cases followed by ethylene or H_2), are all catalytically active towards the hydrosilylation of ethylene. A potential catalytic cycle was proposed which involves a number of unobserved intermediates. Further work in this area (aside from DFT calculations; section 10.4) can involve attempting to trap the proposed primary or secondary alkyl intermediates (**23** or **24**), perhaps by the reaction of silene hydride complexes (which are proposed to be in equilibrium with these intermediates) with nucleophiles which could coordinate to the metal centre. Additionally, the substrate scope could be expanded to other unsaturated reagents such as imines, ketones, and aldehydes.

10.10 – Future Directions Pertaining to Manganese Hydride Complexes with non-Si Co-ligands

Chapter 9 highlights reactions of complex $[(dmpe)_2MnH(C_2H_4)]$ (**10**) with a variety of main group species to form new manganese hydride complexes “ $(dmpe)_2MnHL$ ” (L = neutral ligand). However, many of the synthetic procedures are very low yielding and require optimization. In addition, many of these complexes require further spectroscopic or crystallographic characterization. This work was not carried out due to time constraints, but will be required prior to publication.

A variety of complexes reported in Chapter 9 have only been tentatively identified, and further characterization is required to confidently identify and understand them. These include intermediates in the reactions of **10** with 9-BBN or $HBMes_2$ (tentatively identified as *cis* and *trans* isomers of $[(dmpe)_2MnEt(HBR_2)]$), as well as ‘impurities’ in solutions of $[{(dmpe)_2MnH}_2(\mu-dmpe)]$ (**31**), $[(dmpe)_2MnH(\kappa^1-dmpe)]$ (**32**), and $[(dmpe)_2MnH(HPPH_2)]$ (**33**) (which have been tentatively identified as isomers of these complexes with a disphenoidal arrangement of the chelating dmpe ligands). As well, attempts should be made to identify the as-yet unidentified product of the reaction of complex **10** with $H\text{Sn}^n\text{Bu}_3$ (including obtaining an X-ray crystal structure).

The reaction of complex **10** with $H\text{SnPh}_3$ to form $[(dmpe)_2MnH(\text{SnPh}_3)]$ (**34**) is an unusual reaction (compared to reactions of **10** with other reagents in this thesis) in that it involves conversion to a divalent species. The mechanism for formation of **34**, as well as the mechanism for its decomposition (under vacuum, **34** decomposes to form various species including SnPh_4) is currently unclear and work could be done to understand this. Furthermore, the source of the deep green colour of solutions containing **34** could be indicative of unusual electronic transitions and could be explored further.^{vvv}

^{vvv} It is unclear at this point if the source of this colour is complex **34** or another species in solution.

Chapter 11

Experimental Methods

11.1 – General Details

11.1.1: Laboratory Equipment and Apparatus

An argon-filled MBraun UNIlab glove box equipped with a $-30\text{ }^{\circ}\text{C}$ freezer was employed for the manipulation and storage of all oxygen- and moisture- sensitive compounds. Air-sensitive preparative reactions were performed on a double-manifold high-vacuum line equipped with a two stage Welch 1402 belt-drive vacuum pump (ultimate pressure 1×10^{-4} Torr) using standard techniques.⁵⁶⁰ The vacuum was measured periodically using a Kurt J. Lesker 275i convection enhanced Pirani gauge. Commonly utilized specialty glassware included thick walled flasks equipped with Teflon stopcocks, a swivel frit assembly, Wilmad-LabGlass LPV EPR tubes, Starna 1-Q-10/GS UV-Vis-NIR cells with spectrosil far-UV quartz windows (transparent from 170 nm to 2700 nm), quartz to pyrex graded seals and Teflon stopcocks, and J-Young or Wilmad-LabGlass LPV NMR tubes. A VWR Clinical 200 Large Capacity Centrifuge (with 28° fixed-angle rotors that hold 12×15 mL or 6×50 mL tubes, and in combination with VWR high-performance polypropylene conical centrifuge tubes) located within a glove box was used where indicated. Where indicated, a Branson 2510 ultrasonic bath was used to sonicate reaction mixtures. Residual oxygen and moisture was removed from the argon stream by passage through an Oxisorb-W scrubber from Matheson Gas Products.

11.1.2: Solvents

Benzene, diethylether, pentane, octane, and hexamethyldisiloxane were purchased from Aldrich, hexanes, toluene, DME and THF were purchased from Caledon, and deuterated solvents were purchased from ACP Chemicals. Benzene, diethylether, DME THF, pentane, octane, hexamethyldisiloxane, hexanes and toluene were initially dried and distilled at atmospheric pressure from sodium/benzophenone (first eight solvents) or

sodium (toluene). All solvents were stored over an appropriate drying agent (hexamethyldisiloxane, benzene, diethylether, toluene, d_8 -toluene, $C_6D_6 = Na/Ph_2CO$; hexanes, pentane = $Na/Ph_2CO/tetraglyme$) and introduced to reactions or solvent storage flasks via vacuum transfer with condensation at $-78\text{ }^\circ\text{C}$.

11.1.3: Starting Materials

Dmpe, dmpm, H_3SiPh , H_3Si^nBu , H_2SiEt_2 , H_2SiPh_2 , D_2 , 1,4-dioxane, *tert*-butyl isocyanide, *o*-xylyl isocyanide, d_4 -ethylene, 1,3-diisopropylimidazolium chloride, potassium *tert* butoxide, trimethylsilylmethylmagnesium chloride solution (1.0 M in diethyl ether), ethylmagnesium chloride solution (2.0 M in diethyl ether), 2-mesitylmagnesium bromide solution (1.0 M in THF), CO_2 , diisopropylcarbodiimide, $BH_3 \cdot NMe_3$, 9-BBN, $BF_3 \cdot Et_2O$, $HPPPh_2$, $LiAlH_4$, $LiAlD_4$, DIBAL, $HSnPh_3$, and HSn^nBu_3 were purchased from Sigma-Aldrich. Manganese dichloride, neopentyl chloride, and diethyl zinc (min. 95 % in Sure-Pak cylinder) were purchased from Strem Chemicals. Argon, ethylene, and hydrogen gas were purchased from PraxAir. 1,3,4,5-tetramethyl-4-imidazolin-2-ylidene (^{Me}NHC) was obtained from Green Centre Canada. Bis(trimethylsilylmethyl)magnesium (0.25 equivalents of 1,4-dioxane was present in the product),⁵⁶¹ dineopentylmagnesium (0.8 equivalents of 1,4-dioxane was present in the product),⁹⁶ $MgEt_2$,⁵⁶¹ $FBMes_2$,⁵⁶² 1,3-diisopropylimidazolin-2-ylidene (^{iPr}NHC),⁵⁶³ $HBMes_2$,⁵⁶⁴ and $[(dmpe)_2MnH(C_2H_4)]$ (**1**)^{120,172} were prepared according to the literature. $DBMes_2$ was prepared in a manner analogous to $HBMes_2$, with $LiAlD_4$ in place of $LiAlH_4$.

11.1.4: Instrumentation and Analysis

Combustion elemental analyses were performed a) in house on a Thermo EA1112 CHNS/O analyzer {samples for elemental analysis (typically 1-4 mg) were packed and sealed in pre-weighed 3×6 mm smooth wall tin capsules inside the glovebox. After removal from the glovebox, these capsules were packed into 5×8 mm pressed aluminum capsules containing approximately 10 mg of V_2O_5 }, b) by the London Metropolitan University in London, UK, or c) by Midwest Microlabs in Indianapolis, USA.

NMR spectroscopy was performed on Bruker AV200, DRX-500, AV-500, AV-600, and AV-700 spectrometers. Spectra were obtained at 298 K unless otherwise indicated. All ^1H NMR spectra were referenced relative to SiMe_4 through a resonance of the protio impurity of the solvent used: C_6D_6 (δ 7.16 ppm) and d_8 -toluene (δ 2.08 ppm, 6.97 ppm, 7.01 ppm, and 7.09 ppm). The ^2H NMR spectra were referenced relative to the solvent used $\{\text{C}_6\text{D}_6$ (δ 7.16 ppm) $\}$ or the $\text{C}_6\text{H}_5\text{D}$ impurity in C_6H_6 (δ 7.15 ppm). Also, all ^{13}C NMR spectra were referenced relative to SiMe_4 through a resonance of the ^{13}C in the solvents: C_6D_6 (δ 128.06 ppm) and d_8 -toluene (δ 20.43, 125.13, 127.96, 128.87, and 137.48 ppm). The ^{29}Si NMR spectra were referenced using an external standard of hexamethyldisiloxane in CDCl_3 (6.53 ppm), the ^{31}P NMR spectra were referenced using an external standard of 85% H_3PO_4 in D_2O (0.0 ppm), and the ^{11}B NMR spectra were referenced using neat $\text{BF}_3\cdot\text{Et}_2\text{O}$ (0.0 ppm). Relative intensities of overlapping peaks were calculated, where appropriate, using the SOLA feature of Bruker Topspin 3.2. Relative concentrations of species were determined by integration of ^1H NMR spectra, unless otherwise indicated.

^1H - ^1H COSY NMR spectra (and variations thereof) used to measure $J_{\text{Si,H}}$ from the Scherer method (see Chapter 6) were performed on Bruker AV-500 instruments at the highest temperatures where all peaks are completely resolved. Spectral widths were chosen to ensure all peaks were encompassed. ^1H - $^1\text{H}\{^{31}\text{P}\}$ dqf COSY NMR spectroscopy required input of a ^{31}P chemical shift to be used in calculating the frequency used for ^{31}P decoupling; 75 ppm was used for all samples (of $\mathbf{18^R}$, $\mathbf{18^{R2}}$, and $\mathbf{20^R}$) because it was close to the ^{31}P chemical shifts observed for these complexes. ^{29}Si -edited ^1H - ^1H COSY NMR spectroscopy required input of a transmitter frequency for the pulses on ^{29}Si (calculated from the ^{29}Si chemical shifts; δ_{Si}) and an estimated $J_{\text{Si,H}}$ used to calculate the delay required to preferentially select, by polarization transfer, those protons interacting with ^{29}Si (excluding all others). The former was chosen separately for each complex based on an average of the chemical shifts of the *central* and *transHSi* isomers. Determination of the latter involved starting with a ‘best guess’ determined from 1D ^1H NMR spectra (usually the coupling constant between ^{29}Si and a terminal *SiH* proton),

followed by repeatedly collecting a 1D slice of a ^1H - ^{29}Si HSQC experiment varying in estimated $J_{\text{Si,H}}$, with the value leading to the greatest intensity of the cross-peak of interest being chosen for use in the 2D experiment. Pertinent parameters (optimized for each sample based on values which gave the best results for ^{29}Si -edited ^1H - ^1H COSY NMR experiments) used for all three COSY-type experiments (number of scans, experiment time, td1eff , td2eff , temperature, and for ^{29}Si -edited ^1H - ^1H COSY only, δ_{Si} and estimated $J_{\text{Si,H}}$) are available in the ESI to reference 510, as are symbolic pulse sequences used for ^1H - $^1\text{H}\{^{31}\text{P}\}$ dqf COSY and ^{29}Si -edited ^1H - ^1H COSY NMR experiments. For all COSY experiments, pulsed field gradients were used for coherence selection and artifact suppression.

Evans NMR measurements were conducted on the Bruker DRX-500 spectrometer in a manner described in the supporting information for ref. 565, and values are the average of two independent experiments. For **2**, $\chi_{[\text{M}(\text{corr})]}$ values above and below room temperature were collected using two different sets of samples; the values from 298 to 335 K were adjusted to give the same room temperature value by correcting the mass used from 8.3 to 8.6 mg, which is within the error of the mass balance.

Single-crystal X-ray crystallographic analyses were performed on crystals coated in Paratone oil and mounted on either a SMART APEX II diffractometer with a 3 kW sealed-tube Mo generator and SMART6000 CCD detector or on a STOE IPDS II diffractometer with an image plate detector in the McMaster Analytical X-Ray (MAX) Diffraction Facility. A semi-empirical absorption correction was applied using redundant data. Raw data was processed using XPREP (as part of the APEX v2.2.0 software), and solved by either SHELXS-97 (direct)⁵⁶⁶ or SHELXT (intrinsic)⁵⁶⁷ methods. The structure was completed by difference Fourier synthesis and refined with full-matrix least-squares procedures based on F^2 . In all cases, non-hydrogen atoms were refined anisotropically and hydrogen atoms were generated in ideal positions and then updated with each cycle of refinement {with the exception of hydrogen atoms on Mn, Si, and sometimes C or P (see figure captions in each chapter for a complete list of these H atoms) which were

located from the difference map and refined isotropically}. Refinement was performed using Olex2.⁵⁶⁸

Powder X-ray diffraction experiments were performed on a Bruker D8 Advance powder diffractometer with Cu K α radiation ($\lambda = 0.154$ nm) operated at 40 kV and 40 mA. Powders were packed in 0.5 mm o.d. special glass (SG; wall thickness 0.01 mm) capillary tubes for X-ray diffraction (purchased from Charles Supper Co.) and sealed by inverting to submerge the open end in a pool of Apiezon H-grease within the glovebox. Calculated powder patterns were generated from the low-temperature single crystal data (for complexes **2-8**) and a file downloaded from the Cambridge Crystallographic Database (for complex **1**)⁹⁹ using Mercury. Experimental powder diffractograms were generated and viewed using Gadds, Powdercell, Crystal Sleuth, Diffrac.eva, Topaz, and PANalytical HighScore.

UV/Vis spectra were obtained on a Cary 50 UV/Visible Spectrometer using 10 mM to 10 μ M solutions in hexanes. Melting points were measured on a DigiMelt SRS MPA 160 melting point apparatus; between 1 and 2 mg of each sample was flame-sealed in a thin glass tube under an atmosphere of argon. X-Ray photoelectron spectra were collected on either a Thermo Scientific Thetaprobe or a K-Alpha (Thermo Scientific, E. Grinstead, UK) both of which are located at the University of Toronto. A monochromated Al K-Alpha was used with a spot size of 400 μ m. An initial survey spectrum was collected at low energy resolution for composition, as well as the high energy resolution spectrum of the Zn 2p, Zn Aug, and Mn 2p regions.

IR spectra were performed on transmission mode on a Nicolet 6700 FT-IR spectrometer or a Bruker Tensor 27 IR spectrometer as a suspension in Nujol, or as a solution in hexanes or octane, in both cases using CaF₂ plates (for solution measurements, a liquid cell purchased from International Crystal Laboratories was used).

SQUID measurements were collected on a Quantum Design MPMS between 5 K and 300 K at applied fields ranging from 100 Oe (for most) to 10 000 Oe (for complexes

3 and **6**). Roughly 50 mg of sample was placed in a sealed sample rod assembly for transport of air-sensitive samples into the magnetometer (with the exception of **3**, where between 2.9 and 3.4 mg of sample was placed in a flame-sealed glass capillary).

Thermal stability data was obtained by sealing approx. 10 mg of powder under argon in a flask with a Teflon valve. This flask was heated to the desired temperature for 24 hours and then cooled to room temperature for visual inspection as well as PXRD and/or ^1H NMR spectroscopy. When ‘very little’ is used to describe the extent of decomposition, this indicates that the compound darkened in colour, but that decomposition was not observed by PXRD or ^1H NMR spectroscopy.

11.1.5: DFT Calculations

All calculated structures were fully optimized with the ADF DFT package (SCM, versions 2014.05 to 2018.104).⁵⁶⁹ Calculations were conducted in the gas phase within the generalized gradient approximation using the 1996 Perdew-Burke-Ernzerhof exchange and correlation functional (PBE),⁵⁷⁰ using the scalar zeroth-order approximation (ZORA)⁵⁷¹ for relativistic effects, and Grimme’s DFT-D3-BJ dispersion correction.⁵⁷² Preliminary geometry optimizations were conducted with frozen cores corresponding to the configuration of the preceding noble gas (core = medium) using double- ζ basis sets with one polarization function (DZP), a Voronoi grid with an integration value of 5, and default convergence criteria for energy and gradients. These structures were further refined using all-electron triple- ζ basis sets with two polarization functions (TZ2P) and fine integration grids (Voronoi 7 or Becke⁵⁷³ verygood-quality).

Bond orders were calculated within the Mayer,⁵⁷⁴ Gopinathan-Jug,⁵⁷⁵ and Nalewajski-Mrozek^{576,577} formalisms. Visualization of the computational results was performed using the ADF-GUI (SCM) or Biovia Discovery Studio Visualizer. Electron density at the bond critical points were obtained using the BADER keyword.⁵⁷⁸ NBO analysis⁵⁷⁹ was carried out using nbo 6.0 within ADF 2014.5.

Bonding between the '(dmpe)₂MnR' (R = H, Et) moiety and neutral ethylene in **10**, isonitrile ligands in the two isomers of **14a-b**, silylene ligands in **16^{Et2}**, and silene ligands in **19^{Et2}** was analyzed in detail by fragment calculations (Ziegler-Rauk Energy Decomposition Analysis⁵⁸⁰ and the ETS-NOCV method^{577,581}). In such calculations, fragments had structures as calculated in each optimized whole molecule. Relaxation (optimization) of the individual fragments yielded the preparation energy, i.e. the energetic cost of geometric distortion of the interacting fragments. BSSE values were not calculated, as their contribution is negligible for large interacting molecules.

Analytical frequency calculations⁵⁸² were conducted on all geometry optimized structures (including geometry optimized fragments) to ensure that the geometry optimization led to an energy minimum and to obtain thermodynamic parameters. In a handful of cases, slightly negative frequencies (frequency range from -1 to -25 cm⁻¹) were observed but were shown to be spurious imaginary frequencies using the SCANFREQ command.⁵⁸³ In one case (**transH₂-18^{Ph2}**), the observed negative frequency (-9 cm⁻¹) was determined to be a dirty mode caused by low barrier rotation of the Mn-Si bond.

Transition states were optimized by minimizing energy gradients while ensuring that the Hessian had a negative eigenvalue for the normal coordinate that contains atomic motions consistent with the transformation (using the TransitionState subkey in the Geometry key block).

NMR coupling constants were calculated (using geometry optimized coordinates derived as discussed above) with the CPL program of the ADF package⁵⁸⁴ from wave functions obtained by hybrid PBE0⁵⁸⁵ (ZORA)⁵⁷¹ calculations using the TZ2P basis sets with additional steep basis functions (TZ2P-J). This method was benchmarked against published data calculated for nonclassical hydrosilane complexes. The literature results²⁴¹ were reproduced with acceptable accuracy for [(C₅H₄Me)MnH(SiHPh₂)(CO)₂] (our method: -52 Hz, literature calcd.: -68 Hz, literature expt.: -63 Hz²⁴¹), [Cp₂TiH(SiHPh₂)(PMe₃)] (our method: -22 Hz, literature calcd.: -28 Hz, literature expt.:

(281 Hz²³⁸), and [Cp₂TiH(SiHClPh)(PMe₃)] (our method: 19 Hz, literature calcd.: 23 Hz, literature expt.: 15 Hz²⁵⁶).

All reported computational values in this work were for diamagnetic structures (obtained using restricted calculations).^{xxx} Models of **16**^{Bu,H} and **17**^{Bu} were calculated with the ⁿBu substituent replaced with an Et group and the two dmpe ligands were replaced with four PH₃ groups {*cis*-**17**^{Et;PH₃}: *cis*-[(H₃P)₄Mn(SiH₂Et)], *trans*-**17**^{Et;PH₃}: *trans*-[(H₃P)₄Mn(SiH₂Et)], *cis*-**16**^{Et,H;PH₃}: *cis*-[(H₃P)₄MnH(=SiHEt)], *trans*-**16**^{Et,H;PH₃}: *trans*-[(H₃P)₄MnH(=SiHEt)]}. The resulting minima were compared to those from two additional sets of calculations conducted to model potential paramagnetic structures using the UNRESTRICTED command⁵⁸⁶ in conjunction with forcing two or four unpaired electrons (using the CHARGE command) and explicit occupation numbers (using the OCCUPATIONS command). Similar models were also obtained for various isomers of **13** and **18**^{Et;PH₃}. In all cases resulting minima were >28 kJ mol⁻¹ higher in energy than the corresponding diamagnetic structure.^{www} Paramagnetic minima of *cis*-**17**^{Et;PH₃}, *trans*-**17**^{Et;PH₃}, and *cis*-**16**^{Et,H;PH₃} resulted in isostructural silyl complexes.

11.1.6: Additional Notes

All prepared complexes are air sensitive, and their products upon reaction with air are malodorous. Therefore, all syntheses were conducted under an atmosphere of argon.

11.2 – Synthetic Procedures and Characterization Pertaining to the Work of Chapter 2

Various data is available in the ESI to reference 565, including room temperature ¹H NMR spectra of complexes **2-8**, variable temperature ¹H NMR spectra of complexes **2-5** and **7-8**, variable temperature ¹H NMR spectra used to obtain Evans measurements for **2,5**, and **7**, PXRD diffractograms of complexes **1-8**, SQUID data tables and plots for complexes **2-8** (including fits to an exchange expression for **2** and **5-8**), UV/Vis spectra

^{www} A single exception to this is an isomer of **13** with an equatorial arrangement of dmpe donors (**13**^{trans}); see Chapter 3.

of complexes **2-3** and **5-8**, ^1H NMR spectra and PXRD diffractograms for the results of reactions of **1-8** with H_2 or ZnEt_2 , and XPS of solids deposited from the reactions of ZnEt_2 with **2** or **7**. The identification numbers in reference 565 match those in this thesis. CSD 1450874-1450881 contain the supplementary crystallographic data for **2-7** and **9**.

Bis(trimethylsilylmethyl)manganese(II) (**1**)⁹⁹ and $[\{\text{Mn}(\text{CH}_2\text{SiMe}_3)(\mu\text{-CH}_2\text{SiMe}_3)(\text{PEt}_3)\}_2]$ (**9**)¹¹² were prepared according to literature procedures.

$[\{\text{Mn}(\text{CH}_2\text{CMe}_3)(\mu\text{-CH}_2\text{CMe}_3)_2\}_2\{\text{Mn}(\mu\text{-CH}_2\text{CMe}_3)_2\text{Mn}\}]$ (**2**). MnCl_2 (2 g, 15.9 mmol) was suspended in 20 mL of diethyl ether. $\text{Mg}(\text{CH}_2\text{CMe}_3)_2(1,4\text{-dioxane})_{0.8}$ (4.9 g, 20.7 mmol) was dissolved separately in 40 mL of diethyl ether and added dropwise to the MnCl_2 suspension over 20 minutes. The reaction was stirred at room temperature for four days with regular sonication. The resulting yellow/light brown suspension was centrifuged to remove MgCl_2 , and the solvent was removed from the resulting solution *in vacuo*. Crude **2** was extracted into toluene forming a dark brown solution, and the solvent was again removed *in vacuo*. The remaining solid was recrystallized from hexanes (~ 10 mL) at $-30\text{ }^\circ\text{C}$ to afford large brown crystals. The mother liquors were then concentrated and maintained for several days at $-30\text{ }^\circ\text{C}$ to afford a 2nd batch of crystals; the total yield was 60 % (1.88 g). Note that on one occasion, a white solid was obtained rather than the expected dark brown solid. This solid was likely the Et_2O or 1,4 dioxane adduct of dineopentylmanganese(II), and was converted to pure **2** by extended exposure to dynamic vacuum. Compound **2** was found to sublime at $90\text{ }^\circ\text{C}$ (5 mTorr) and to melt between 99 and $102\text{ }^\circ\text{C}$. X-ray quality crystals were obtained from hexanes at $-30\text{ }^\circ\text{C}$. ^1H NMR (C_6D_6 , 500 MHz, 298 K): δ 32.6. ^1H NMR (d_8 -toluene, 500 MHz, 298 K): δ 28.2. ^1H NMR (d_8 -toluene, 500 MHz, 233 K): δ 14.9, 28.9, 65.9. **Vis**: $\lambda_{\text{max}} = 464\text{ nm}$. **Anal.** Found (Calcd): C, 60.18 (60.90); H, 10.75 (11.24).

$[\text{Mn}(\text{CH}_2\text{SiMe}_3)_2(\text{dmpe})]$ (**3**) and $[\{\text{Mn}(\text{CH}_2\text{CMe}_3)_2(\mu\text{-dmpe})\}_2]$ (**4**). The 1:1 dialkylmanganese(II):dmpe adducts were prepared according to literature procedures.¹¹¹ Complex **3** was purified by sublimation ($60\text{ }^\circ\text{C}$ at 5 mTorr) to a bright yellow powder,

and complex **4** was purified by recrystallization from hexanes to afford a white powder (**4** also sublimed cleanly between 80 °C and 100 °C at 5 mTorr). X-ray quality crystals of **3** and **4** were obtained from hexanes at –30 °C. Complex **3**: $^1\text{H NMR}$ (C_6D_6 , 500 MHz, 298 K): δ 20.6, 44.0, 58.1. $^1\text{H NMR}$ (d_8 -toluene, 500 MHz, 298 K): δ 20.6, 43.4, 56.4. $^1\text{H NMR}$ (d_8 -toluene, 500 MHz, 233 K): δ 26.2, 76 (v. broad). **Anal.** Found (Calcd): C, 44.16 (44.31); H, 10.36 (10.09). Complex **4**: $^1\text{H NMR}$ (C_6D_6 , 500 MHz, 298 K): δ 25.2, 46.3, 59.1. $^1\text{H NMR}$ (d_8 -toluene, 500 MHz, 298 K): δ 25.1, 45.6, 56.5. $^1\text{H NMR}$ (d_8 -toluene, 500 MHz, 233 K): δ 30.6, 67 (v. broad). **Anal.** Found (Calcd): C, 56.02 (55.32); H, 11.11 (11.03).

$[\{\text{Mn}(\text{CH}_2\text{SiMe}_3)(\mu\text{-CH}_2\text{SiMe}_3)_2(\mu\text{-dmpe})\}]$ (**5**). $[\{\text{Mn}(\mu\text{-CH}_2\text{SiMe}_3)_2\}_\infty]$ (**1**) (67.1 mg, 0.294 mmol of Mn) and $[\text{Mn}(\text{CH}_2\text{SiMe}_3)_2(\text{dmpe})]$ (**3**) (110.9 mg, 0.292 mmol) were dissolved in toluene at –78 °C. The resulting light orange solution was stirred for 1 hour at –78 °C and 3 hours at room temperature before solvent was removed *in vacuo*. The resulting powder was dissolved in 1 mL of hexanes, centrifuged to remove a white solid impurity, and maintained at –30 °C for several days to produce orange/red crystals (which were of X-ray quality), which when crushed yielded an orange powder (87.2 mg; 49 % yield). An additional set of X-ray quality crystals were obtained by recrystallization from a concentration solution of **5** in toluene at –30 °C. The product was found to melt cleanly between 145 and 146 °C when heated quickly. $^1\text{H NMR}$ (C_6D_6 , 500 MHz, 298 K): δ 5.2, 12.7, 19 (v. broad). $^1\text{H NMR}$ (d_8 -toluene, 500 MHz, 298 K): δ 5.2, 12.7, 19 (v. broad). $^1\text{H NMR}$ (d_8 -toluene, 5000 MHz, 233 K): δ 2.5, 7.6, 12.1, 19 (v. broad). **Vis:** $\lambda_{\text{max}} = 477$ nm. **Anal.** Found (Calcd): C, 43.01 (43.40); H, 9.58 (9.93).

$[\{\text{Mn}(\text{CH}_2\text{CMe}_3)(\mu\text{-CH}_2\text{CMe}_3)_2(\mu\text{-dmpe})\}]$ (**6**). Tetrametallic **2** (110 mg, 0.14 mmol) and dimetallic **4** (200 mg, 0.29 mmol) were dissolved in 5 mL of toluene. The solution was stirred overnight at room temperature, and then maintained at –30 °C for several days to obtain black crystals. The mother liquor was concentrated and maintained at –30 °C for several days to obtain a second batch of crystals, leading to a total yield of 92 % (279 mg). The product sublimed at 110 °C at 5 mTorr and melted with

some decomposition between 149 and 151.5 °C. $^1\text{H NMR}$ (C_6D_6 , 500 MHz, 298K): δ 12.8, 26 (v. broad). $^1\text{H NMR}$ (d_8 -toluene, 500 MHz, 298 K): δ 12.2, 25 (v. broad). $^1\text{H NMR}$ (d_8 -toluene, 500 MHz, 233 K): δ 4.0, 11.3, 31 (v. broad). **Vis:** $\lambda_{\text{max}} = 486$ nm. **Anal.** Found (Calcd): C, 57.06 (57.34); H, 11.23 (11.11).

[{Mn(CH₂SiMe₃)(μ -CH₂SiMe₃)₂(dmpm)] (7). A suspension of [$\{\text{Mn}(\mu\text{-CH}_2\text{SiMe}_3)_2\}_\infty$] (**1**) (119 mg, 0.52 mmol per Mn) in toluene (20 mL) was cooled to -78 °C. A solution of dmpm (180 mg, 1.3 mmol) in toluene (2 mL) was then added dropwise, and after stirring for 30 minutes at -78 °C and 1.5 hours at room temperature, the suspension turned to a clear orange solution. The solvent was then removed *in vacuo* and the solid was extracted with hexanes. After centrifuging to remove residual solid, the clear red hexanes solution was maintained at -30 °C for several days. The resulting red crystals were of X-ray quality. Crushing the crystals afforded a light pink powder (99 mg; 52 % yield). Complex **7** sublimed cleanly at 100 °C (5 mTorr) and melted without significant decomposition when heated rapidly to 176 °C (note: partial melting commenced at 160 °C). $^1\text{H NMR}$ (C_6D_6 , 500 MHz, 298 K): δ 3.1, 7.9, 15.5, 24 (v. broad). $^1\text{H NMR}$ (d_8 -toluene, 500 MHz, 298 K): δ 3.1, 7.7, 15.4, 25 (v. broad). $^1\text{H NMR}$ (d_8 -toluene, 500 MHz, 233 K): δ 2.5, 8.4, 15.4, 25 (v. broad). **Vis:** $\lambda_{\text{max}} = 476$ nm. **Anal.** Found (Calcd): C, 42.24 (42.40); H, 9.86 (9.83).

[{Mn(CH₂CMe₃)(μ -CH₂CMe₃)₂(dmpm)] (8). dmpm (220 mg, 1.61 mmol) was added to a solution of tetrametallic **2** (310 mg, 0.39 mmol) in a 4:1 mixture of hexanes and toluene (10 mL total). The reaction mixture was stirred for 24 hours after which time the solvent was removed *in vacuo* to give a brown powder (70 % yield). Both recrystallization over days at -30 °C from saturated hexanes, and slow evaporation of hexanes yielded thin red needles from which poor quality X-ray crystal structures could be obtained. The product sublimed between 100 and 120 °C at 5 mTorr and melted without decomposition between 161 and 165 °C. $^1\text{H NMR}$ (C_6D_6 , 500 MHz, 298 K): δ 8.1, 13.8, 21 (v. broad). $^1\text{H NMR}$ (d_8 -toluene, 500 MHz, 298 K): δ 8.1, 13.8, 21 (v.

broad). ^1H NMR (d_8 -toluene, 500 MHz, 233 K): δ 4.9, 11.4, 12.9, 19 (v. broad). **Vis:** $\lambda_{\text{max}} = 481$ nm. **Anal.** Found (Calcd): C, 56.16 (56.60); H, 11.34 (11.02).

Reactions with $\text{H}_{2(\text{g})}$. Approx. 10 mg of each complex was dissolved in approx. 0.6 mL of C_6D_6 (with the exception of [$\{\text{Mn}(\mu\text{-CH}_2\text{SiMe}_3)_2\}_\infty$], which was suspended in approx. 0.6 mL of d_8 -toluene). The resulting solution (or suspension) was placed in a thick-walled NMR tube with a J-Young Teflon valve and was freeze-pump-thawed ($\times 3$). The NMR tube was then placed under an atmosphere of hydrogen gas, cooled to -95 °C using a liquid nitrogen-acetone bath, sealed at this low temperature, and warmed to room temperature to provide approx. 1.7 atm of hydrogen gas. Reactions were then observed by ^1H NMR spectroscopy as a function of time and temperature. Upon reaction completion, gases were removed by exposing to dynamic argon, and solutions were decanted. Shiny metallic mirrors on the walls of the NMR tubes were sonicated into around 2 mL of toluene (rarely, the mirrors were physically scratched into suspension). The resulting silver-black powder was then washed twice with 5 mL of toluene and once with 5 mL of hexanes, dried *in vacuo*, and examined by PXRD.

Reactions with diethyl zinc. These reactions were conducted in a manner analogous to those with H_2 , with the following modifications: Approx. 10-15 mg of each manganese complex was used, and rather than addition of H_2 , 1-3 equivalents of neat diethyl zinc was added to the solution (or suspension) in the NMR tube within the glovebox, and the Teflon valve was immediately closed to ensure that volatile reaction byproducts did not escape. The resulting silver mirrors were sonicated to yield silver-black powders (in most cases pyrophoric) which were examined by PXRD, as well as XPS in some cases.

11.3 – Synthetic Procedures and Characterization Pertaining to the Work of Chapter 3

Various data is available in the ESI to reference 547, including tables of calculated (for isomers of **10**, isomers of **13**, and isomers of **14a,b**) and

crystallographically (for **10**) determined bond lengths and angles, tables of bond orders, Hirshfeld charges, zero-point energies, and total bonding energies for calculated structures (isomers of **10**, isomers of **13**, and isomers of **14a,b**), fragment interaction analyses for **10** and **14a,b**, potential energy profiles for isomerizations of **10** and **13**, and selected NMR spectra for **14a,b** and **15**. The identification numbers in this chapter of the thesis (X→Y) relate to those in reference 547 (X→Y) in the following manner; *trans*-**10**→**1**, *cis*-**10**→**A**, **11**→**5**, **12**→**D**, **13**→**B**, **14**→**6**, and **15**→**7**. CSD 1846647 and 1846650-1846652 contain the supplementary crystallographic data for **10**, **14a,b**, and **15**.

[(dmpe)₂MnH(C₂H₄)] (**10**) was prepared according to the literature.¹²⁰

[(dmpe)₂MnEt(CN^{*t*}Bu)] (**14a**). An excess of *tert*-butyl isonitrile (250 mg, 3.01 mmol) was added to a solution of [(dmpe)₂MnH(C₂H₄)] (**10**) (129.8 mg, 0.34 mmol) in 10 mL of benzene. The reaction mixture was stirred in a sealed flask at 80 °C for 5 h, after which the solvent was removed *in vacuo* leading to an orange oily solid. Recrystallization from hexamethyldisiloxane at –30 °C afforded 53.2 mg of yellow solid. Concentrating the mother liquor and allowing the solution to sit again at –30 °C afforded another 20.0 mg of the yellow solid, providing a combined yield of 46% (73.2 mg, 0.16 mmol). Upon dissolution in solution, the bulk of the sample was observed to be the *trans* isomer, but a small amount of *cis* isomer was observed in the baseline. To obtain NMR characterization of the *cis* isomer, the reaction was carried out on a smaller scale (13.5 mg **10** and 24 mg CN^{*t*}Bu) in approx. 0.6 mL of C₆D₆ at 50 °C for 1.5 h, which provided a 3 : 6 : 1 ratio of **10** : *cis*-**14a** : *trans*-**14a**, and was analyzed *in situ* (with excess free isonitrile present). This ratio could be improved to 6 : 12 : 1 by removing the solvent *in vacuo* and re-dissolving. X-ray quality crystals of *trans*-**14a** were obtained from a saturated solution in pentane at –30 °C. *cis*-**14a** (selected): ¹H NMR (C₆D₆, 600 MHz, 298 K): δ 1.83 (t, 3H, ³J_{H,H} 8 Hz, CH₂CH₃), 1.54 (d, 3H, ²J_{H,P} 7 Hz, PCH₃), 1.47 (d, 3H, ²J_{H,P} 6 Hz, PCH₃), 1.29 (m, 6H, PCH₃), 1.28 (s, 9H, CNC(CH₃)₃), 1.14 (d, 3H, ²J_{H,P} 5 Hz, PCH₃), 1.04 (d, 3H, ²J_{H,P} 3 Hz, PCH₃), 0.22 (m, 1H, CH₂CH₃), –0.12 (m, 1H, CH₂CH₃). ¹³C{¹H} NMR (C₆D₆, 151 MHz, 298 K): δ 35.24 (m, PCH₂), 32.29 (s, CNC(CH₃)₃),

24.25 (s, PCH₃), 23.53 (d, ³J_{C,P} 10 Hz, CH₂CH₃), 23.32 (d, ¹J_{C,P} 17 Hz, PCH₃), 22.22 (d, ¹J_{C,P} 16 Hz, PCH₃), 19.51 (s, PCH₃), 17.25 (d, ¹J_{C,P} 15 Hz, PCH₃), 14.25 (d, ¹J_{C,P} 13 Hz, PCH₃), -2.47 (m, CH₂CH₃). ³¹P{¹H} NMR (C₆D₆, 243 MHz, 298 K): δ 81 (br. s, 1P), 74.43 (br. s, 1P), 61.58 (br. s, 2P). ¹H NMR (*d*₈-toluene 500 MHz, 207 K): δ 1.98 (t, 3H, ³J_{H,H} 7 Hz, CH₂CH₃), 1.60 (d, 3H, ²J_{H,P} 6 Hz, PCH₃), 1.51 (d, 3H, ²J_{H,P} 6 Hz, PCH₃), 1.30 (m, 3H, PCH₃), 1.27 (s, 9H, CNC(CH₃)₃), 1.26 (m, 3H, PCH₃), 1.08 (d, 3H, ²J_{H,P} 4 Hz, PCH₃), 1.01 (d, 3H, ²J_{H,P} 3 Hz, PCH₃), 0.92 (d, 3H, ²J_{H,P} 5 Hz, PCH₃), 0.88 (d, 3H, ²J_{H,P} 3 Hz, PCH₃), 0.26 (m, 1H, CH₂CH₃),^{xxx} -0.11 (m, 1H, CH₂CH₃).^{yyy} ¹³C{¹H} NMR (*d*₈-toluene, 126 MHz, 207 K): δ 53.98 (s, CNC(CH₃)₃), 34.88 (m, PCH₂), 33.00 (m, PCH₂), 32.01 (s, CNC(CH₃)₃), 30.88 (m, PCH₂), 29.57 (m, PCH₂), 23.82 (d, ³J_{C,P} 11 Hz, CH₂CH₃), 23.51 (br. s, PCH₃), 22.94 (d, ¹J_{C,P} 17 Hz, PCH₃), 22.05 (d, ¹J_{C,P} 12 Hz, PCH₃), 21.50 (d, ¹J_{C,P} 15 Hz, PCH₃), 18.97 (s, PCH₃), 16.28 (d, ¹J_{C,P} 14 Hz, PCH₃), 13.94 (d, ¹J_{C,P} 12 Hz, PCH₃), 12.45 (m, PCH₃), -2.66 (m, CH₂CH₃). ³¹P{¹H} (*d*₈-toluene, 202 MHz, 207 K): δ 82.02 (s, 1P), 75.24 (s, 1P), 62.09 (s, 1P), 61.63 (s, 1P). *trans*-14a: ¹H NMR (C₆D₆, 600 MHz, 298 K): δ 1.51 (m, 4H, PCH₂), 1.43 (m, 4H, PCH₂), 1.41 (t, 3H, ³J_{H,H} 8 Hz, CH₂CH₃), 1.40 (s, 12H, PCH₃), 1.29 (s, 12H, PCH₃), 1.12 (s, 9H, CNC(CH₃)₃), -0.47 (p of q, 2H, ³J_{H,P} 8 Hz, ³J_{H,H} 8 Hz, CH₂CH₃). ¹³C{¹H} NMR (C₆D₆, 151 MHz, 298 K): δ 205.95 (s, CNC(CH₃)₃), 53.79 (s, CNC(CH₃)₃), 32.62 (s, CNC(CH₃)₃), 32.12 (app. p, PCH₂), 24.63 (s, CH₂CH₃), 21.03 (s, PCH₃), 16.49 (s, PCH₃), 1.40 (p, ²J_{C,P} 17 Hz, CH₂CH₃). ³¹P{¹H} (C₆D₆, 202 MHz, 298 K): δ 74.66 (s). IR: ν(CN) (nujol, cm⁻¹) = 1915 (*cis*-14a), 1828 (*trans*-14a). ν(CN) (octane, cm⁻¹) = 1923 (*cis*-14a), 1829 (*trans*-14a). Anal. Found (Calcd): C, 49.25 (48.82); H, 9.60 (9.92); N, 2.79 (3.00).

[(dmpe)₂MnEt(CNXyl)] (14b). 143.1 mg (0.37 mmol) of [(dmpe)₂MnH(C₂H₄)] (10) and 292.7 mg (2.23 mmol) of *o*-xylyl isonitrile were dissolved in 10 mL of benzene. The reaction mixture was heated at 50-55 °C for 2 days, after which time the solvent was

^{xxx} ³¹P decoupling collapsed the multiplet to a doublet (²J_{H,H} = 11 Hz) of quartets (³J_{H,H} = 7 Hz), measured at 500 MHz.

^{yyy} ³¹P decoupling collapsed the multiplet to a doublet (²J_{H,H} = 11 Hz) of quartets (³J_{H,H} = 7 Hz), measured at 500 MHz.

removed *in vacuo* to afford a dark brown oil. Attempts to recrystallize **14b** from a variety of solvents failed to yield a pure product. However, X-ray quality crystals were obtained by recrystallization from toluene layered with hexanes at $-30\text{ }^{\circ}\text{C}$ which resulted in a green-brown oily residue with a small number of small bright orange crystals which could be picked out manually. To obtain NMR characterization of the *trans* isomer, the mother liquor from the aforementioned crystallization was maintained at $-40\text{ }^{\circ}\text{C}$, yielding a green solid which contained *trans-14b* and **15** in a 1 : 6 ratio. To obtain NMR characterization of the *cis* isomer, the reaction was carried out on a smaller scale (17.7 mg **10** and 23.2 mg CNXyl) in C_6D_6 at $50\text{ }^{\circ}\text{C}$ for 2.5 h, which provided a 7 : 1.25 : 1 : 2.5 ratio of **10** : *cis-14b* : *trans-14b* : **15**, and was analyzed *in situ* (with excess free isonitrile present). *cis-14b* (selected): $^1\text{H NMR}$ (C_6D_6 , 600 MHz, 298 K): δ 6.95 (d, 2H, $^3J_{\text{H,H}}$ 7 Hz, *m*), 6.76 (m, 1H, *p*), 2.52 (s, 6H, xylyl- CH_3), 1.92 (t, 3H, $^3J_{\text{H,H}}$ 8 Hz, CH_2CH_3), 1.62 (m, 3H, PCH_3), 1.50 (d, 3H, $^2J_{\text{H,P}}$ 6 Hz, PCH_3), 1.30 (m, 3H, PCH_3), 0.27 (m, 1H, CH_2CH_3), 0.03 (m, 1H, CH_2CH_3). $^{13}\text{C}\{^1\text{H}\}$ NMR (C_6D_6 , 151 MHz, 298 K): δ 23.8 (CH_2CH_3), 21.11 (s, xylyl- CH_3), -1.3 (CH_2CH_3). *trans-14b*: $^1\text{H NMR}$ (C_6D_6 , 600 MHz, 298 K): δ 6.93 (d, 2H, $^3J_{\text{H,H}}$ 7 Hz, *m*), 6.71 (t, 1H, $^3J_{\text{H,H}}$ 8 Hz, *p*), 2.33 (s, 6H, xylyl- CH_3), 1.54 (m, 8H, PCH_2), 1.37 (t, 3H, $^3J_{\text{H,H}}$ 8 Hz, CH_2CH_3), 1.35 (s, 12H, PCH_3), 1.20 (m, 12H, PCH_3), -0.43 (p of q, 2H, $^3J_{\text{H,P}}$ 8 Hz, $^3J_{\text{H,H}}$ 8 Hz, CH_2CH_3). $^{13}\text{C}\{^1\text{H}\}$ NMR (C_6D_6 , 151 MHz, 298 K): δ 136.28 (*i*), 131.42 (s, *o*), 128.25 (m, *m*), 120.39 (s, *p*), 32.16 (m, PCH_2), 24.24 (m, CH_2CH_3), 21.20 (s, PCH_3), 20.81 (s, xylyl- CH_3), 16.27 (s, PCH_3), 3.37 (CH_2CH_3). $^{31}\text{P}\{^1\text{H}\}$ (C_6D_6 , 202 MHz, 298 K): δ 75.85 (s).

[(dmpe)Mn(CNXyl) $_3$ {C(=NXyl)CEt(=NXyl)}] (**15**). The mixture of *trans-14b* and **15** (see synthesis of **14b**) was then heated under vacuum at $140\text{ }^{\circ}\text{C}$ for 2 hours. The resulting brown solid resisted further purification (approximately 90% pure by NMR spectroscopy). However, **15** was characterized by NMR spectroscopy and X-ray quality crystals were obtained by recrystallization of the crude mixture of *trans-14b* and **15** (see synthesis of **14b**) from a dilute solution in hexanes at $-30\text{ }^{\circ}\text{C}$. $^1\text{H NMR}$ (C_6D_6 , 600 MHz, 298 K): δ 7.04 (d, 2H, $^3J_{\text{H,H}}$ 8 Hz, *m*), 6.73–6.82 {*m*, *m* (8H) and *p* (5H)}, 2.85 (q, 2H, $^3J_{\text{H,H}}$ 8 Hz, CH_2CH_3), 2.47 (s, 12H, xylyl- CH_3), 2.44 (s, 12H, xylyl- CH_3), 1.99 (br. s, 6H,

xylyl- \underline{CH}_3), 1.64 (d, 6H, $^2J_{H,P}$ 8 Hz, \underline{PCH}_3), 1.34 (m, 4H, \underline{PCH}_2), 1.20 (d, 6H, $^2J_{H,P}$ 7 Hz, \underline{PCH}_3), 0.69 (t, 3H, $^3J_{H,H}$ 8 Hz, $\underline{CH}_2\underline{CH}_3$). $^{13}\text{C}\{\text{H}\}$ NMR (C_6D_6 , 151 MHz, 298 K): δ 179.44 (s, $\underline{CCH}_2\underline{CH}_3$), 156.33, 150.51, 134.13, 133.80, 133.34, 133.11, 132.31, 131.01 (8 \times s, *o* and *i*), 128.06 (m, *m*), 127.93 (m, *m*), 125.47 (s, *p*), 123.57 (s, *p*), 121.62 (s, *p*), 120.20 (s, *p*), 31.38 (m, \underline{PCH}_2), 30.76 (m, \underline{PCH}_2), 26.68 (s, $\underline{CH}_2\underline{CH}_3$), 20.71 (s, xylyl- \underline{CH}_3), 20.39 (s, xylyl- \underline{CH}_3), 20.05 (s, xylyl- \underline{CH}_3), 19.14 (s, xylyl- \underline{CH}_3), 17.34 (d, $^1J_{C,P}$ 20 Hz, \underline{PCH}_3), 16.82 (d, $^1J_{C,P}$ 20 Hz, \underline{PCH}_3), 9.02 (s, $\underline{CH}_2\underline{CH}_3$). $^{31}\text{P}\{\text{H}\}$ (C_6D_6 , 243 MHz, 298 K): δ 66.15 (s, 1P), 53.90 (s, 1P).

11.4 – Synthetic Procedures and Characterization Pertaining to the Work of Chapter 4

Various data is available in the ESI to reference 507, including tables of calculated and crystallographically determined bond lengths and angles, bond orders, Hirshfeld charges, total bonding energies, Slater-type molecular orbitals involved in Mn–ligand interactions (not including interactions with dmpe), electrostatic potential diagrams, and fragment interaction analyses for calculated structures, and selected NMR spectra. The identification numbers in this chapter ($\underline{X}\rightarrow\underline{Y}$) of the thesis relate to those in reference 507 ($\underline{X}\rightarrow\underline{Y}$) in the following manner; $\underline{10}\rightarrow\underline{1}$, $\underline{16}^{\text{Et}2}\rightarrow\underline{2a}$, $\underline{16}^{\text{Ph}2}\rightarrow\underline{2b}$, $\underline{17}^{\text{Et}2}\rightarrow\underline{A}$, $\underline{18}^{\text{Et}2}\rightarrow\underline{3a}$, $\underline{18}^{\text{Ph}2}\rightarrow\underline{3b}$, $\underline{19}^{\text{Et}2}\rightarrow\underline{4a}$, and $\underline{19}^{\text{Ph}2}\rightarrow\underline{4b}$. CSD 1529213-1529215 contain the supplementary crystallographic data for $\underline{16}^{\text{Et}2}$, $\underline{16}^{\text{Ph}2}$, and $\underline{19}^{\text{Ph}2}$.

$[(\text{dmpe})_2\text{MnH}(=\text{SiEt}_2)]$ ($\underline{16}^{\text{Et}2}$). An excess of H_2SiEt_2 (734 mg, 8.32 mmol) was added to $[(\text{dmpe})_2\text{MnH}(\text{C}_2\text{H}_4)]$ ($\underline{10}$) (463.1 mg, 1.78 mmol) in 30 mL of benzene. The reaction mixture was stirred in a sealed flask at room temperature for a month, turning from clear bright yellow to a clear vibrant red/brown solution and the solvent was removed *in vacuo*. The resulting brown powder was dissolved in 2.5 mL of hexanes and a yellow residue was removed by centrifuging. Following this, the supernatant liquid was concentrated to 2 mL, and stored at $-30\text{ }^\circ\text{C}$ for two weeks resulting in brown crystals. Yield = 277 mg (52%). X-ray quality crystals were obtained by recrystallizing from a

dilute solution in hexanes at $-30\text{ }^{\circ}\text{C}$. ^1H NMR (C_6D_6 , 600 MHz, 298 K): δ 1.88 (m, 4H, $\text{P}(\underline{\text{C}}\underline{\text{H}}_2)$), 1.74 (m, 4H, $\text{P}(\underline{\text{C}}\underline{\text{H}}_2)$), 1.34 (br. s, 12H, $\text{P}(\underline{\text{C}}\underline{\text{H}}_3)$), 1.34 (q, 4H, $^3J_{\text{H,H}}$ 7.8 Hz, $\text{Si}\underline{\text{C}}\underline{\text{H}}_2\text{CH}_3$), 1.22 (br. s, 12H, $\text{P}(\underline{\text{C}}\underline{\text{H}}_3)$), 1.09 (t, 6H, $^3J_{\text{H,H}}$ 7.9 Hz, $\text{Si}\underline{\text{C}}\underline{\text{H}}_2\text{CH}_3$), -10.46 (p, 1H, $^2J_{\text{H,P}}$ 51.4 Hz, $\text{Mn}\underline{\text{H}}$). $^{13}\text{C}\{^1\text{H}\}$ (C_6D_6 , 151 MHz, 298 K): δ 34.63 (p, $J_{\text{C,P}}$ 12.2 Hz, $\text{P}(\underline{\text{C}}\underline{\text{H}}_2)$), 29.50 (br. s, $\text{P}(\underline{\text{C}}\underline{\text{H}}_3)$), 29.35 (s, $\text{Si}\underline{\text{C}}\underline{\text{H}}_2\text{CH}_3$), 8.19 (s, $\text{Si}\underline{\text{C}}\underline{\text{H}}_2\text{CH}_3$). $^{29}\text{Si}\{^1\text{H}\}$ (C_6D_6 , 119 MHz, 298 K): δ 365.30 (m). $^{31}\text{P}\{^1\text{H}\}$ (C_6D_6 , 243 MHz, 298 K): δ 80.95 (s). **Anal.** Found (calcd.): C, 44.31 (43.44); H, 9.90 (9.80).

$[(\text{dmpe})_2\text{MnH}(\text{=SiPh})_2]$ (16^{Ph_2}). Three equivalents of H_2SiPh_2 (296.6 mg, 1.61 mmol) were added to $[(\text{dmpe})_2\text{MnH}(\text{C}_2\text{H}_4)]$ (**10**) (201.3 mg, 0.52 mmol) in 25 mL of benzene. The solution was stirred at $60\text{ }^{\circ}\text{C}$ for five days, turning from a clear bright yellow solution to a deep dark purple solution, and then the solvent was removed *in vacuo*. The resulting dark oil was washed with 5 mL hexanes and crystallized from 2 mL of toluene at $-30\text{ }^{\circ}\text{C}$ to get dark purple cubic single crystals of X-ray quality (88.4 mg). A further 32.1 mg could be obtained by cooling the hexanes mother liquors at $-30\text{ }^{\circ}\text{C}$. In the solid state structure, the *cis* isomer (*cis*- 16^{Ph_2}) was obtained as a mixture with $[(\text{dmpe})_2\text{MnH}_2(\text{SiHPh}_2)]$ (18^{Ph_2}), usually in ratios of roughly 1 : 1, due to the tendency to co-crystallize. In the case of the X-ray quality crystals, a ratio of 1 : 1 was confirmed both through XRD and ^1H NMR data. Total yield of 23% of 16^{Ph_2} (45% if including 18^{Ph_2}). In solution, 16^{Ph_2} exists as an equilibrium of a *cis*- and *trans*- isomer (in C_6D_6 at 298 K there is a 88 : 12 *cis*- 16^{Ph_2} : *trans*- 16^{Ph_2} ratio). *cis*- 16^{Ph_2} : ^1H NMR (C_6D_6 , 500 MHz, 298 K): δ 7.81 (d of m, 4H, $^3J_{\text{H,H}}$ 6.3 Hz, *o*), 7.22 (t, 4H, $^3J_{\text{H,H}}$ 7.0 Hz, *m*), 7.17 (t, 2H, $^3J_{\text{H,H}}$ 7.0 Hz, *p*), 0-2.2 (series of broad signals from dmpe), -16.22 (s, 1H, $\text{Mn}\underline{\text{H}}$). $^{13}\text{C}\{^1\text{H}\}$ NMR (C_6D_6 , 151 MHz, 298 K): δ 156.81 (s, *ipso*), 134.83 (s, *o*), 127.14 (s, *m*), 126.00 (s, *p*), could not locate dmpe signals. $^{29}\text{Si}\{^1\text{H}\}$ NMR (C_6D_6 , 119 MHz, 298 K): δ 210.2. $^{31}\text{P}\{^1\text{H}\}$ NMR (C_6D_6 , 202 MHz, 298 K): δ 78.29 (br. s), 69.11 (br. s). *trans*- 16^{Ph_2} : ^1H NMR (C_6D_6 , 500 MHz, 298 K): δ 7.50 (d of m, 4H, $^3J_{\text{H,H}}$ 6.6 Hz, *o*), 7.18 (t, 4H, $^3J_{\text{H,H}}$ 7.6 Hz, *m*), 7.07 (t, 2H, $^3J_{\text{H,H}}$ 7.4 Hz, *p*), 1.97 (br. s, 4H, $\text{P}(\underline{\text{C}}\underline{\text{H}}_2)$), 1.69 (br. s, 4H, $\text{P}(\underline{\text{C}}\underline{\text{H}}_2)$), 1.37 (s, 12H, $\text{P}(\underline{\text{C}}\underline{\text{H}}_3)$), 1.17 (s, 12H, $\text{P}(\underline{\text{C}}\underline{\text{H}}_3)$), -9.78 (p, 1H, $^2J_{\text{H,P}}$ 55.0 Hz, $\text{Mn}\underline{\text{H}}$). $^{13}\text{C}\{^1\text{H}\}$ NMR (C_6D_6 , 126 MHz, 298 K): δ 160.42 (s, *ipso*), 131.95 (s, *o*), 127.14

(s, *p*), 126.00 (s, *m*), 34.13 (m, P(CH₂)), 29.77 (m, P(CH₃)), 28.64 (s, P(CH₃)), 21.73 (m, P(CH₂)). ²⁹Si{¹H} NMR (C₆D₆, 119 MHz, 298 K): δ 285.1. ³¹P{¹H} NMR (C₆D₆, 202 MHz, 298 K): δ 80.29 (br. s). **Anal.** Found (calcd. based on 1:1 ratio of **16**^{Ph2} : **18**^{Ph2} as observed by NMR for the sample submitted): C, 53.77 (53.43); H, 7.83 (8.22).

[(dmpe)₂MnH₂(SiHEt₂)] (**18**^{Et2}). Method a) Approx. 15 mg of [(dmpe)₂MnH(=SiEt₂)] (**16**^{Et2}) was dissolved in approx. 0.6 mL of C₆D₆ and the solution was freeze/pump/thawed three times in an NMR tube with a J-young valve to remove dissolved argon. The NMR tube was then placed under 1 atm of H₂ at -95 °C, sealed, and warmed to room temperature. 100% conversion to [(dmpe)₂MnH₂(SiHEt₂)] (**18**^{Et2}) was observed by ¹H NMR after allowing the reaction mixture to sit at room temperature overnight (leading to a very pale clear yellow solution). Method b) An excess of H₂SiEt₂ (228 mg, 2.58 mmol) was added to [(dmpe)₂MnH(C₂H₄)] (**10**) (89 mg, 0.23 mmol) in 10 mL of benzene. The reaction mixture was freeze/pump/thawed in a 50 mL storage flask three times, and then was placed under 1 atm of H₂ at -95 °C, sealed, and warmed to room temperature. After stirring at 30-40 °C for one week, the clear bright yellow solution turned to a pale clear yellow solution. At this point, the solvent was removed *in vacuo* and resulting pale yellow solid was recrystallized from a concentrated solution of hexanes at -30 °C giving a pale yellow powder. Yield = 20 mg (19%). X-ray quality crystals (very pale yellow cubes) were obtained from pentane at -30 °C, though a crystal structure could not be obtained due to severe disorder and/or twinning. In solution, **18**^{Et2} exists as an equilibrium mixture of a *central* and *transHSi* isomer (in C₆D₆ at 298 K there is a 78 : 22 ratio of isomers *central-18*^{Et2} : *transHSi-18*^{Et2}). *central-18*^{Et2}: ¹H NMR (C₆D₆, 600 MHz, 298 K): δ 4.97 (br. s, 1H, SiH), 0.4–1.7 (series of broad signals from dmpe and SiEt₂), -12.67 (br. s, 2H, MnHSi), ³¹P{¹H} NMR (C₆D₆, 243 MHz, 298 K): broad pair of signals ranging from 65-80 ppm. ¹H NMR (*d*₈-toluene, 500 MHz, 224 K): δ 4.97 (br. s with ²⁹Si sat., 1H, ¹J_{H,Si} 166 Hz, SiH), 0.4–1.9 (series of broad signals from dmpe and SiEt₂), -12.71 (p, 2H, ²J_{H,P} 23.3 Hz, MnHSi). ²⁹Si{¹H} (*d*₈-toluene, 99 MHz, 224 K): δ 14.20. ³¹P{¹H} (*d*₈-toluene, 202 MHz, 224 K): δ 75.19 (br. s, 2P), 71.69 (br. s, 2P). *transHSi-18*^{Et2}: ¹H NMR (C₆D₆, 600 MHz, 298 K): δ 5.20 (br. s, 1H, SiH), -12.26

Ph.D. Thesis — Jeffrey S. Price; McMaster University – Chemistry

(br. s, 1H, Mn \underline{H} Si), 0.4–1.7 (series of broad signals from dmpe and SiEt₂), –12.28 (br. s, 1H, Mn \underline{H} Si), –14.23 (br. s, 1H, Mn \underline{H} Si). ³¹P{¹H} NMR (C₆D₆, 243 MHz, 298 K): δ 77.74. ¹H NMR (*d*₈-toluene, 500 MHz, 224 K): δ 5.26 (br. s with ²⁹Si sat., 1H, ¹J_{H,Si} 150 Hz, Si \underline{H}), 0.4–1.9 (series of broad signals from dmpe and SiEt₂), –12.22 (p of d, 1H, ²J_{H,P} 52.5 Hz, Mn \underline{H} Si), –14.38 (m, 1H, Mn \underline{H} Si). ²⁹Si{¹H} (*d*₈-toluene, 99 MHz, 224 K): δ 23.78. ³¹P{¹H} (*d*₈-toluene, 202 MHz, 224 K): δ 78.37 (br. s). **Anal.** Found (calcd.): C, 43.46 (43.24); H, 10.10 (10.20). **IR:** ν(SiH, MnH) (Nujol, cm⁻¹): 1877 (with shoulder to lower wavenumber), 2015. ν(SiH, MnH) (hexanes, cm⁻¹): 1734, 1864, 2031 (with two shoulders to lower wavenumber).

[(dmpe)₂MnD₂(SiHEt₂)] (*d*₂-**18**^{Et2}): *d*₂-**18**^{Et2} was prepared in a manner identical to that described above for **18**^{Et2} (method a) utilizing D₂ in place of H₂. 100% conversion was observed after one day at room temperature, including deuterium incorporation exclusively to the Mn-*H*-Si bridging position, and no incorporation of deuterium into the Si-*H* bond over time at room temperature. ¹H NMR spectrum of *d*₂-**18**^{Et2} (C₆D₆) is identical to that for **18**^{Et2} with no signals at –12.28, –12.67, or –14.23 ppm.

[(dmpe)₂MnH₂(SiHPh₂)] (**18**^{Ph2}): Method a) Approx. 15 mg of a mixture of [(dmpe)₂MnH(=SiPh)₂] (**16**^{Ph2}) and [(dmpe)₂MnH₂(SiHPh₂)] (**18**^{Ph2}) was dissolved in approx. 0.6 mL of C₆D₆, and the solution was freeze/pump/thawed three times in an NMR tube with a J-young valve to remove dissolved argon. The NMR tube was then placed under 1 atm of H₂ at –95 °C and sealed at this temperature. 100% conversion to [(dmpe)₂MnH₂(SiHPh₂)] (**18**^{Ph2}) was observed by ¹H NMR spectroscopy after allowing the reaction mixture to warm to room temperature, leading to a pale yellow clear solution. Method b) [(dmpe)₂MnH(C₂H₄)] (**10**) (133.7 mg, 0.35 mmol) was dissolved in 10 mL of benzene. To this bright yellow solution was added 192 mg (1.04 mmol) of H₂SiPh₂ and the resulting mixture was placed in a 50 mL storage flask and freeze/pump/thawed three times before being placed under 1 atm of H₂ at –95 °C. The flask was then sealed, and the mixture was heated at 60 °C for 5 days leading to a pale yellow clear solution. The solvent was removed *in vacuo* and the resulting yellow oil was washed with 2 mL of

hexanes. The remaining yellow solid was dissolved in toluene and layered with hexanes or hexamethyldisiloxane (two different fractions) yielding a combined 136.2 mg (72% yield) of bright yellow crystals. $\mathbf{18}^{\text{Ph}2}$ exists as an equilibrium mixture of *central* and *transHSi* isomers (298 K, C_6D_6 or d_8 -toluene) in a 87 : 13 ratio. X-ray quality crystals of the dominant isomer (*central-18*^{Ph2}) were prepared by recrystallization from toluene at -30 °C. ***central-18*^{Ph2}**: ^1H NMR (C_6D_6 , 500 MHz, 298 K): δ 8.17 (d, 2H, $^3J_{\text{H,H}}$ 5.6 Hz, *o*), 7.87 (d, 2H, $^3J_{\text{H,H}}$ 6.1 Hz, *o*), 7.41 (t, 2H, $^3J_{\text{H,H}}$ 6.6 Hz, *m*), 7.28 (t, 1H, $^3J_{\text{H,H}}$ 6.6 Hz, *p*), 7.24 (t, 2H, $^3J_{\text{H,H}}$ 6.8 Hz, *m*), 7.15 (t, 1H, $^3J_{\text{H,H}}$ 6.6 Hz, *p*), 6.62 (app. t with ^{29}Si satellites, 1H, $^3J_{\text{H,P}}$ 9.4 Hz, $^1J_{\text{H,Si}}$ 177.8 Hz, SiH), 1.47 (br. s, 6H, $\text{P}(\underline{\text{C}}\text{H}_3)$), 1.34 (m, 4H, $\text{P}(\underline{\text{C}}\text{H}_2)$), 1.08 (m, 2H, $\text{P}(\underline{\text{C}}\text{H}_2)$), 1.01 (br. d, $^2J_{\text{H,P}}$ 5.3 Hz, $\text{P}(\underline{\text{C}}\text{H}_3)$), 0.91 (br. s, 2H, $\text{P}(\underline{\text{C}}\text{H}_2)$), 0.89 (br. s, 12H, $\text{P}(\underline{\text{C}}\text{H}_3)$), -12.40 (m, 2H, MnHSi). $^{13}\text{C}\{^1\text{H}\}$ NMR (C_6D_6 , 151 MHz, 298 K): δ 152.07 (*ipso*), 151.63 (*ipso*), 136.48 (*o*), 136.05 (*o*), 127.38 (*m*), 127.22 (*m*), 126.73 (*p*), 35.08 ($\text{P}(\underline{\text{C}}\text{H}_2)$), 32.42 ($\text{P}(\underline{\text{C}}\text{H}_2)$), 30.74 ($\text{P}(\underline{\text{C}}\text{H}_3)$), 23.82 ($\text{P}(\underline{\text{C}}\text{H}_3)$), 23.47 ($\text{P}(\underline{\text{C}}\text{H}_3)$), 21.42 ($\text{P}(\underline{\text{C}}\text{H}_3)$). $^{29}\text{Si}\{^1\text{H}\}$ NMR (d_8 -toluene, 119 MHz, 298 K): δ 10.01. $^{31}\text{P}\{^1\text{H}\}$ NMR (C_6D_6 , 202 MHz, 298 K): 72.02 (v. broad m). ***transHSi-18*^{Ph2}**: ^1H NMR (C_6D_6 , 500 MHz, 298 K): aromatic and dmpe signals not resolved, δ 6.34 (br. s, 1H, SiH), -11.43 (p, 1H, $^2J_{\text{H,P}}$ 55.4 Hz, MnHSi), -12.75 (br. s, 1H, MnHSi). $^{31}\text{P}\{^1\text{H}\}$ NMR (C_6H_6 , 202 MHz, 298 K): δ 78.30 (v. broad m). **Anal.** Found (calcd.): C, 53.30 (53.33); H, 8.55 (8.39). **IR:** $\nu(\text{SiH}, \text{MnH})$ (Nujol, cm^{-1}): 1767, 1807, 1974.

$[(\text{dmpe})_2\text{MnD}_2(\text{SiHPh}_2)]$ (d_2 - $\mathbf{18}^{\text{Ph}2}$): d_2 - $\mathbf{18}^{\text{Ph}2}$ was prepared in a manner identical to that described above for $\mathbf{18}^{\text{Ph}2}$ (method a) utilizing D_2 in place of H_2 . 100% conversion was achieved almost immediately upon warming to room temperature, including deuterium incorporation exclusively at the MnH environment, and no incorporation of deuterium into the terminal Si-H bond. ^1H NMR spectra of d_2 - $\mathbf{18}^{\text{Ph}2}$ are identical to those for $\mathbf{18}^{\text{Ph}2}$ with no signals at -11.43 , -12.40 , or -12.75 ppm. Also observed in solution is $\mathbf{18}^{\text{Ph}2}$ (as a residue from the starting solution of $\mathbf{16}^{\text{Ph}2}$ and $\mathbf{18}^{\text{Ph}2}$) at a ratio of 3 : 1 d_2 - $\mathbf{18}^{\text{Ph}2}$: $\mathbf{18}^{\text{Ph}2}$ which is identical to the portion of $\mathbf{16}^{\text{Ph}2}$: $\mathbf{18}^{\text{Ph}2}$ in the starting material used.

$[(\text{dmpe})_2\text{MnH}(\text{Et}_2\text{Si}=\text{CHMe})]$ ($\mathbf{19}^{\text{Et}2}$): $[(\text{dmpe})_2\text{MnH}(\text{Et}_2\text{Si}=\text{CHMe})]$ ($\mathbf{16}^{\text{Et}2}$) (55.1 mg, 0.12 mmol) was dissolved in 5 mL of benzene. The solution was freeze/pump/thawed

three times in a 50 mL storage flask, then placed under 1 atm of ethylene at $-95\text{ }^{\circ}\text{C}$. The flask was sealed and warmed to room temperature, and after stirring for 3.5 h, the solution had turned from a clear red/brown solution to a clear light orange. Following this, solvent was removed *in vacuo* and the resulting orange oil was recrystallized from hexamethyldisiloxane at $-30\text{ }^{\circ}\text{C}$ to afford an orange solid (20.5mg, 35% yield). X-ray quality crystals were not obtained. ^1H NMR indicates that samples of $\mathbf{19}^{\text{Et}2}$ contain 0.1 equivalents of hexamethyldisiloxane which could not be removed by exposure of the solid to vacuum. ^1H NMR (C_6D_6 , 600 MHz, 298 K): δ 1.79 (d, 3H, $^3J_{\text{H,H}}$ 7.2 Hz, Si=CHCH $\underline{\text{H}}_3$), 1.56 (m, 1C, P(CH $\underline{\text{H}}_2$)), 1.49 (d, 3H, $^2J_{\text{H,P}}$ 6.7 Hz, P(CH $\underline{\text{H}}_3$)), 1.45(m, 2C, P(CH $\underline{\text{H}}_2$)), 1.42 (d, 3H, $^3J_{\text{H,H}}$ 5.4 Hz, P(CH $\underline{\text{H}}_3$)), 1.34 (t, 3H, $^3J_{\text{H,H}}$ 7.9 Hz, SiCH $\underline{2}$ CH $\underline{\text{H}}_3$), 1.31 (t, 3H, $^3J_{\text{H,H}}$ 7.8 Hz, SiCH $\underline{2}$ CH $\underline{\text{H}}_3$), 1.28 (d, 3H, $^3J_{\text{H,H}}$ 5.5 Hz, P(CH $\underline{\text{H}}_3$)), 1.26 (d, 3H, $^3J_{\text{H,H}}$ 5.3 Hz, P(CH $\underline{\text{H}}_3$)), 1.17 (d, 3H, $^3J_{\text{H,H}}$ 5.1 Hz, P(CH $\underline{\text{H}}_3$)), 1.14 (m, 4C, P(CH $\underline{\text{H}}_2$)), 0.96 (m, 9H, P(CH $\underline{\text{H}}_3$), 2H, SiCH $\underline{2}$ CH $\underline{\text{H}}_3$), 0.95 (m, 1C, P(CH $\underline{\text{H}}_2$)), 0.80 (d of q, 1H, $^1J_{\text{H,H}}$ 14.1 Hz, $^3J_{\text{H,H}}$ 7.5 Hz, SiCH $\underline{2}$ CH $\underline{\text{H}}_3$) 0.58 (d of q, 1H, $^1J_{\text{H,H}}$ 14.1 Hz, $^3J_{\text{H,H}}$ 7.5 Hz, SiCH $\underline{2}$ CH $\underline{\text{H}}_3$), -0.02 (m, 1H, Si=CHCH $\underline{\text{H}}_3$), -15.34 (br. s, 1H, MnH $\underline{\text{H}}\text{Si}$). $^{13}\text{C}\{^1\text{H}\}$ NMR (C_6D_6 , 151 MHz, 298 K): δ 37.43 (t, 1C, $J_{\text{C,P}}$ 25.5 Hz, P(CH $\underline{\text{H}}_2$)) 35.34 (d of d, 1C, $J_{\text{C,P}}$ 19.9, 17.5 Hz, P(CH $\underline{\text{H}}_2$)), 33.47 (t, 1C, $J_{\text{C,P}}$ 16.8 Hz, P(CH $\underline{\text{H}}_2$)), 33.28 (d, 1C $J_{\text{C,P}}$ 18.3 Hz, P(CH $\underline{\text{H}}_3$)), 32.94 (m, 1C, P(CH $\underline{\text{H}}_2$)), 28.04 (s, 1C, P(CH $\underline{\text{H}}_3$)), 26.50 (d, 1C, $J_{\text{C,P}}$ 10.4 Hz, P(CH $\underline{\text{H}}_3$)), 25.16 (s, 1C, P(CH $\underline{\text{H}}_3$)), 22.99 (m, 2C, P(CH $\underline{\text{H}}_3$) and Si=CHCH $\underline{\text{H}}_3$), 22.73 (m, 1C, P(CH $\underline{\text{H}}_3$)), 20.72 (s, 1C, P(CH $\underline{\text{H}}_3$)), 15.52 (s, 1C, P(CH $\underline{\text{H}}_3$)), 10.22 (s, 1C, SiCH $\underline{2}$ CH $\underline{\text{H}}_3$), 10.05 (s, 1C, SiCH $\underline{2}$ CH $\underline{\text{H}}_3$), 7.56 (m, 1C, SiCH $\underline{2}$ CH $\underline{\text{H}}_3$), 5.15 (s, 1C, SiCH $\underline{2}$ CH $\underline{\text{H}}_3$), -19.37 (s, 1C, Si=CHCH $\underline{\text{H}}_3$). $^{29}\text{Si}\{^1\text{H}\}$ NMR (C_6D_6 , 119 MHz, 298 K): δ -2.95 . $^{31}\text{P}\{^1\text{H}\}$ NMR (C_6D_6 , 243 MHz, 298 K): δ 79.32 (br. s, 1P), 70.74 (br. s, 1P), 67.68 (br. s, 1P), 65.54 (br. s, 1P). **Anal.** Found (calcd. with 0.1 equiv. O(SiMe $_3$) $_2$): C, 46.01 (45.90); H, 9.97 (10.11).

$[(\text{dmpe})_2\text{MnH}(\text{Et}_2\text{Si}=\text{C}\text{D}\text{C}\text{D}_3)]$ ($d_4\text{-19}^{\text{Et}2}$): $d_4\text{-19}^{\text{Et}2}$ was prepared by dissolving approx. 15 mg of $[(\text{dmpe})_2\text{MnH}(=\text{SiEt}_2)]$ ($\mathbf{16}^{\text{Et}2}$) in approx. 0.6 mL of C_6D_6 . The solution was placed in an NMR tube fitted with a J-young valve and freeze/pump/thawed three times to remove dissolved argon. 1 atm of d_4 -ethylene was then admitted into the NMR tube at $-95\text{ }^{\circ}\text{C}$, which was sealed, warmed to room temperature, and left for two hours.

100% conversion was observed by ^1H NMR spectroscopy, which shows peaks identical to those of $\mathbf{19}^{\text{Et}2}$, but with no signals at 1.79 or -0.02 ppm.

$[(\text{dmpe})_2\text{MnH}(\text{Ph}_2\text{Si}=\text{CHMe})]$ ($\mathbf{19}^{\text{Ph}2}$): A mixture of $[(\text{dmpe})_2\text{MnH}(\text{=SiPh})_2]$ ($\mathbf{16}^{\text{Ph}2}$) and $[(\text{dmpe})_2\text{MnH}_2(\text{SiHPh}_2)]$ ($\mathbf{18}^{\text{Ph}2}$) (total of 126.4 mg, containing 0.12 mmol of $\mathbf{16}^{\text{Ph}2}$) was dissolved in 20 mL of benzene. The dark purple solution was freeze/pump/thawed 3 times in a 50 mL storage flask, and then placed under 1 atm of ethylene at -95 °C. The flask was sealed, and upon thawing, the reaction mixture turned a bright clear orange indicative of complete conversion to an unidentified intermediate. Following five hours of stirring at room temperature, most of the intermediate had converted to the target complex ($\mathbf{19}^{\text{Ph}2}$), and the residual intermediate was removed by removal of the solvent *in vacuo* and recrystallizing the resulting orange oil from hexanes. The orange powder which precipitated after leaving the solution at -30 °C for a week contained $[(\text{dmpe})_2\text{MnH}(\text{Ph}_2\text{Si}=\text{CHMe})]$ ($\mathbf{19}^{\text{Ph}2}$) mixed with $[(\text{dmpe})_2\text{MnH}_2(\text{SiHPh}_2)]$ ($\mathbf{18}^{\text{Ph}2}$), which was present in the starting solution and did not react with ethylene. Yield = 81.2 mg (61% of $\mathbf{19}^{\text{Ph}2}$). X-ray quality orange crystals were obtained from recrystallization in dilute hexanes at -30 °C. **^1H NMR (C_6D_6 , 600 MHz, 298 K):** δ 8.05 (d, 2H, $^3J_{\text{H,H}}$ 8.0 Hz, *o*), 8.01 (d, 2H, $^3J_{\text{H,H}}$ 7.2 Hz, *o*), 7.16 (t, 2H, $^3J(^1\text{H}-^1\text{H})$ 7.6 Hz, *m*), 7.10 (t, 2H, $^3J(^1\text{H}-^1\text{H})$ 7.4 Hz, *m*), 7.05 (t of t, 1H, $^3J(^1\text{H}-^1\text{H})$ 7.2 Hz, $^4J_{\text{H,H}}$ 1.2 Hz, *p*), 7.00 (t of t, 1H, $^3J_{\text{H,H}}$ 7.5 Hz, $^4J_{\text{H,H}}$ 1.0 Hz, *p*), 2.14 (d, 3H, $^3J_{\text{H,H}}$ 7.4 Hz, Si=CHCH $\underline{\text{H}}_3$), 1.72 (d, 3H, $^3J_{\text{H,H}}$ 5.4 Hz, P(CH $\underline{\text{H}}_3$)), 1.51 (d, 3H, $^3J_{\text{H,H}}$ 6.4 Hz, P(CH $\underline{\text{H}}_3$)), 1.47 (m, 2H, P(CH $\underline{\text{H}}_2$)), 1.36 (m, 2H, P(CH $\underline{\text{H}}_2$)), 1.35 (m, 2H, P(CH $\underline{\text{H}}_2$)), 1.30 (m, 2H, P(CH $\underline{\text{H}}_2$)), 1.14 (d, 3H, $^3J_{\text{H,H}}$ 5.5 Hz, P(CH $\underline{\text{H}}_3$)), 1.01 (d, 6H, $^3J_{\text{H,H}}$ 5.5 Hz, P(CH $\underline{\text{H}}_3$)), 0.94 (d, 3H, $^3J_{\text{H,H}}$ 5.0 Hz, P(CH $\underline{\text{H}}_3$)), 0.59 (d, 3H, $^3J_{\text{H,H}}$ 5.2 Hz, P(CH $\underline{\text{H}}_3$)), 0.54 (d, 3H, $^3J_{\text{H,H}}$ 5.6 Hz, P(CH $\underline{\text{H}}_3$)), 0.39 (m, 1H, Si=CHCH $\underline{\text{H}}_3$), -14.56 (m, 1H, MnH $\underline{\text{S}}\text{i}$). **$^{13}\text{C}\{^1\text{H}\}$ NMR (C_6D_6 , 151 MHz, 298 K):** 144.60 (s, *ipso*), 144.33 (s, *ipso*), 135.64 (s, *o*), 135.56 (s, *o*), 127.8 (*p*), 127.58 (s, *m*), 35.75 (m, P(CH $\underline{\text{H}}_2$)), 34.48 (app. t, $J_{\text{C,P}}$ 17.1 Hz, P(CH $\underline{\text{H}}_2$)), 33.68 (d, $J_{\text{C,P}}$ 18.9 Hz, P(CH $\underline{\text{H}}_3$)), 33.09 (m, P(CH $\underline{\text{H}}_2$)), 26.03 (d, $J_{\text{C,P}}$ 8.9 Hz, P(CH $\underline{\text{H}}_3$)), 25.66 (s, P(CH $\underline{\text{H}}_3$)), 24.21 (s, P(CH $\underline{\text{H}}_3$)), 23.36 (m, Si=CHCH $\underline{\text{H}}_3$), 22.64 (d, $J_{\text{C,P}}$ 14.4 Hz, P(CH $\underline{\text{H}}_3$)), 21.87 (d, $J_{\text{C,P}}$ 10.0 Hz, P(CH $\underline{\text{H}}_3$)), 21.12 (d, $J_{\text{C,P}}$ 21.1 Hz, P(CH $\underline{\text{H}}_3$)), 15.43 (s, P(CH $\underline{\text{H}}_3$)), -22.93 (s, Si=CHCH $\underline{\text{H}}_3$). **^{29}Si (C_6D_6 , 119 MHz,**

298 K): -1.47 (d, $^1J_{\text{Si,H}}$ $^{31}\text{P}\{^1\text{H}\}$ (C_6D_6 , 243 MHz, **298 K):** 78.31 (s), 69.14 (s), 66.52 (s), 62.72 (s). **Anal.** Found (calcd. based on 50:50 mixture observed for the submitted sample by ^1H NMR): C, 54.42 (54.24); H, 8.46 (8.38).

$[(\text{dmpe})_2\text{MnH}(\text{Ph}_2\text{Si}=\text{CDCD}_3)]$ ($d_4\text{-19}^{\text{Ph}_2}$): $d_4\text{-19}^{\text{Ph}_2}$ was prepared by dissolving approx. 15 mg of a mixture of $[(\text{dmpe})_2\text{MnH}(=\text{SiPh}_2)]$ (16^{Ph_2}) and $[(\text{dmpe})_2\text{MnH}_2(\text{SiHPh}_2)]$ (18^{Ph_2}) (3:1 ratio) in approx. 0.6 mL of C_6D_6 . The solution was placed in an NMR tube fitted with a J-young valve and freeze/pump/thawed three times to remove dissolved argon. 1 atm of d_4 -ethylene was admitted into the NMR tube at -95 °C, the tube was sealed, and the reaction mixture was warmed to room temperature. 100% consumption of 16^{Ph_2} was observed by ^1H NMR after 5 minutes at room temperature, producing $d_4\text{-19}^{\text{Ph}_2}$ and an unidentified intermediate which slowly converted into $d_4\text{-19}^{\text{Ph}_2}$; 95% complete after 2 days. ^1H NMR spectroscopy of $d_4\text{-19}^{\text{Ph}_2}$ shows identical peaks to 19^{Ph_2} , but with no signals at 2.14 or 0.39 ppm. Also observed in solution is 18^{Ph_2} residual from the starting solution.

11.5 – Synthetic Procedures and Characterization Pertaining to the Work of Chapter 5

Various data for complex 20^{R} is available in the ESI to reference 547, including tables of calculated and crystallographically determined bond lengths and angles, bond orders, Hirshfeld charges, and total bonding energies for calculated structures, along with selected NMR spectra. Various data is also available of other complexes in this chapter in the ESI to reference 587, including tables of calculated and crystallographically determined bond lengths, bond orders, total bonding energies, Hirshfeld charges, and thermodynamic parameters for calculated structures, and selected NMR spectra. The identification numbers in this chapter of the thesis ($\underline{\text{X}} \rightarrow \text{Y}$) relate to those in reference 547 ($\text{X} \rightarrow \underline{\text{Y}}$) in the following manner; *trans*-10 \rightarrow 1, *cis*-10 \rightarrow A, 12 \rightarrow D, 13 \rightarrow B, 16 \rightarrow 2, 17 \rightarrow C, 18 \rightarrow 3, and 20 \rightarrow 4. The identification numbers in this chapter of the thesis ($\underline{\text{X}} \rightarrow \text{Y}$) relate to those in reference 587 ($\text{X} \rightarrow \underline{\text{Y}}$) in the following manner; 10 \rightarrow 1, 12 \rightarrow A, 16 \rightarrow 3, 17 \rightarrow 2,

18→5, 19→6, 20→4, 21→7, 22→8, 23→D, 24→F A→B, B→C, and C→E. CSD 1846648 and 1946403-1946410 contain the supplementary crystallographic data for **20^{Ph}**, **21a-d**, and **22a-d**.

[(dmpe)₂MnH(SiH₂Ph)₂] (20^{Ph}): An excess of phenylsilane (770 mg, 7.12 mmol) was added to a solution of [(dmpe)₂MnH(C₂H₄)] (**10**) (543.7 mg, 1.41 mmol) in 30 mL of toluene. The reaction mixture was stirred in a 100 mL sealed flask at 60 °C for 4 h, after which time the solvent was removed *in vacuo* leading to a dark orange oil. Note that ethane is formed as a by-product in this reaction, so after 30 minutes, the reaction mixture was temporarily allowed to cool to room temperature and the excess gas was vented into the Schlenk line before continuing heating at 60 °C. Washing twice with 10 mL of hexanes produced a yellow solid, which was dissolved in 9 mL of toluene and residual solid was removed by centrifugation. Layering the resulting solution with 20 mL of hexanes and storing at –30 °C for days afforded large orange crystals of **20^{Ph}** with a yield of 63% (509.2 mg, 0.89 mmol). Note that on some occasions, instead of large orange crystals a yellow powder was obtained. X-ray quality crystals were obtained from a saturated solution of **20^{Ph}** in hexanes at –30 °C. **¹H NMR (C₆D₆, 600 MHz, 298 K):** δ 8.12 (d, 4H, ³J_{H,H} 7 Hz, *o*), 7.31 (t, 4H, ³J_{H,H} 7 Hz, *m*), 7.24 (t, 2H, ³J_{H,H} 7 Hz, *p*), 5.31 (s with ²⁹Si sat., 2H, ¹J_{H,Si} 158 Hz, SiH), 5.28 (s with ²⁹Si sat., 2H, ¹J_{H,Si} 167 Hz, SiH), 1.50 (d, 6H, ²J_{H,P} 5 Hz, PCH₃), 1.39 (m, 2H, PCH₂), 1.16 (m, 2H, PCH₂), 1.03 (d, 6H, ²J_{H,P} 7 Hz, PCH₃), 1.02 (m, 2H, PCH₂), 0.98 (d, 6H, ²J_{H,P} 6 Hz, PCH₃), 0.91 (m, 2H, PCH₂), 0.91 (d, 6H, ²J_{H,P} 3 Hz, PCH₃), –14.55 (p, 1H, ²J_{H,P} 20 Hz, J_{H,Si} –31 Hz, ^{zzz} MnH). **¹³C{¹H} NMR (C₆D₆, 151 MHz, 298 K):** δ 147.34 (s, *i*), 137.03 (s, *o*), 127.37 (s, *m*), 127.23 (s, *p*), 32.76 (m, PCH₂), 32.15 (m, PCH₂), 23.66 (d, ¹J_{C,P} 6 Hz, PCH₃), 23.62 (d, ¹J_{C,P} 6 Hz, PCH₃), 22.65 (d, ¹J_{C,P} 15 Hz, PCH₃), 22.55 (d, ¹J_{C,P} 16 Hz, PCH₃), 21.81 (d, ¹J_{C,P} 17 Hz, PCH₃), 17.25 (d, ¹J_{C,P} 25 Hz, PCH₃). **²⁹Si{¹H} NMR (C₆D₆, 119 MHz, 298 K):** δ –4.20 (m). **²⁹Si NMR (d₈-toluene, 119 MHz, 298 K):** δ –4.18 (t of m, ¹J_{Si,H}

^{zzz} Measured using ²⁹Si_{edited} ¹H–¹H COSY NMR spectroscopy as described in Chapter 6.

168 Hz). $^{31}\text{P}\{^1\text{H}\}$ NMR (C_6D_6 , 243 MHz, 298 K): δ 67.42 (s, 2P), 60.24 (s, 2P). **Anal.** Found (Calcd): C, 50.47 (50.52); H, 8.49 (8.30).

$[(\text{dmpe})_2\text{MnH}(\text{SiH}_2^{\text{Bu}})_2]$ (20^{Bu}): An excess of *n*-butyl silane (293 mg, 3.32 mmol) was added to a solution of $[(\text{dmpe})_2\text{MnH}(\text{C}_2\text{H}_4)]$ (**10**) (503.2 mg, 1.31 mmol) in 25 mL of benzene. The reaction mixture was stirred in a 50 mL sealed flask at 60 °C for 2 days, after which time the solvent was removed *in vacuo* leading to a yellow solid. Note that ethane is formed as a by-product in this reaction so after a few hours the reaction mixture was temporarily allowed to cool to room temperature and the excess gas was vented into the Schlenk line before continuing at 60 °C. Recrystallization in hexanes at –30 °C yielded 357.6 mg of 20^{Bu} , and removing the solvent *in vacuo* from the mother liquor and recrystallization of the residue in toluene at –30 °C yielded an additional 178.5 mg, for a total yield of 77% (536.1 mg, 1.01 mmol) of yellow powder. ^1H NMR (C_6D_6 , 600 MHz, 298 K): δ 4.53 (m with ^{29}Si sat., 2H, $^1J_{\text{H,Si}}$ 178 Hz, SiH), 4.36 (m with ^{29}Si sat., 2H, $^1J_{\text{H,Si}}$ 159 Hz, SiH), 1.95 (m, 4H, $\text{SiH}_2\text{CH}_2\text{CH}_2\text{CH}_3$), 1.67 (t of q, 4H, $^3J_{\text{H,H}}$ 7 Hz, $\text{SiH}_2\text{CH}_2\text{CH}_2\text{CH}_3$), 1.47 (m, 2H, PCH_2), 1.40 (d, 6H, $^2J_{\text{H,P}}$ 6 Hz, PCH_3), 1.31 (d, 6H, $^2J_{\text{H,P}}$ 6 Hz, PCH_3), 1.22 (m, 4H, $\text{SiH}_2\text{CH}_2\text{CH}_2\text{CH}_3$), 1.21 (m, 4H, PCH_2), 1.08 (t, 6H, $^3J_{\text{H,H}}$ 7 Hz, $\text{SiH}_2\text{CH}_2\text{CH}_2\text{CH}_3$), 1.03 (d, 6H, $^2J_{\text{H,P}}$ 6 Hz, PCH_3), 0.97 (d, 6H, $^2J_{\text{H,P}}$ 4 Hz, PCH_3), 0.84 (m, 2H, PCH_2), –13.27 (t, 1H, $^2J_{\text{H,P}}$ 17 Hz, $J_{\text{H,Si}}$ –30 Hz, $^{\text{aaaa}}\text{MnH}$). $^{13}\text{C}\{^1\text{H}\}$ NMR (C_6D_6 , 151 MHz, 298 K): δ 34.72 (s, $\text{SiH}_2\text{CH}_2\text{CH}_2\text{CH}_3$), 33.94 (m, PCH_2), 30.12 (m, PCH_2), 27.12 (s, $\text{SiH}_2\text{CH}_2\text{CH}_2\text{CH}_3$), 24.00 (d, $^1J_{\text{C,P}}$ 6 Hz, PCH_3), 23.96 (d, $^1J_{\text{C,P}}$ 6 Hz, PCH_3), 21.60 (s, $\text{SiH}_2\text{CH}_2\text{CH}_2\text{CH}_3$), 20.55 (d, $^1J_{\text{C,P}}$ 13 Hz, PCH_3), 19.31 (d, $^1J_{\text{C,P}}$ 23 Hz, PCH_3), 17.97 (d, $^1J_{\text{C,P}}$ 15 Hz, PCH_3), 17.86 (d, $^1J_{\text{C,P}}$ 16 Hz, PCH_3), 14.53 (s, $\text{SiH}_2\text{CH}_2\text{CH}_2\text{CH}_3$). $^{29}\text{Si}\{^1\text{H}\}$ NMR (C_6D_6 , 119 MHz, 298 K): δ 1.62 (p, $^2J_{\text{Si,P}}$ 23 Hz). ^{29}Si NMR (C_6D_6 , 119 MHz, 298 K): δ 1.63 (t of m, $^1J_{\text{Si,H}}$ 165 Hz). $^{31}\text{P}\{^1\text{H}\}$ (C_6D_6 , 243 MHz, 298 K): δ 72.62 (s, 2P), 58.56 (s, 2P). **Anal.** Found (Calcd): C, 45.17 (45.27); H, 10.39 (10.45).

^{aaaa} Measured using ^{29}Si _edited ^1H – ^1H COSY NMR spectroscopy as described in Chapter 6.

trans-[(dmpe)₂MnH(=SiEtⁿBu)] (**16**^{Bu,Et}). Approx. 15 mg of [(dmpe)₂MnH(SiH₂ⁿBu)₂] (**20**^{Bu}) was dissolved in approx. 0.6 mL of C₆D₆ and placed in a J-young NMR tube, and this solution was freeze-pump-thawed (×3). The resulting solution was placed under an atmosphere of ethylene gas, cooled to –95 °C, sealed at this low temperature, and allowed to stand for 1-3 days at room temperature (until complete consumption of **20**^{Bu}). The solvent and free hydrosilane byproducts were then removed *in vacuo* (note that solvent and hydrosilanes must be removed before the H₃SiⁿBu is completely consumed by ethylene hydrosilylation; i.e. as soon as possible after **20**^{Bu} is consumed), and the resulting reddish/brown oil was dissolved in approx. 0.6 mL of C₆D₆. This solution of **19**^{Bu,H} was allowed to stand at room temperature, with >65% conversion to **16**^{Bu,Et} after 1 week. The resulting clear, bronze solution contained impurities of **19**^{Bu,Et} and an unidentified MnH-containing species, as well as significant deuteration from solvent activation in the MnH and various alkyl environments. Characterization was performed by NMR spectroscopy *in situ* {spectra were collected after 18 (¹H and ³¹P{¹H}), 14 (1D TOCSY and various 2D experiments), 17 (1D ²⁹Si–HSQC), 11 (¹³C{¹H}), 16 (²⁹Si–¹H HMBC), or 10 (²⁹Si{¹H}) days}, and NMR spectra in C₆H₆ were conducted by removing the C₆D₆ *in vacuo* after 18 days of isomerization, and dissolving the resulting oil in C₆H₆. Selected NMR data are as follows; ¹H NMR (C₆D₆, 600 MHz, **298 K**): δ 1.90 (m, 4H, PCH₂), 1.75 (m, 4H, PCH₂), 1.46 (m, various ⁿBu environments), 1.39 (m, 2H, SiCH₂CH₂CH₂CH₃), 1.36 (s, 12H, PCH₃), 1.35 (q, 2H, ³J_{H,H} 8.5 Hz, SiCH₂CH₃), 1.23 (s, 12H, PCH₃), 1.11 (t, 3H, ³J_{H,H} 7.9 Hz, SiCH₂CH₃) 1.00 (t, 3H, ³J_{H,H} 6.5 Hz, SiCH₂CH₂CH₂CH₃), –10.48 (p, 1H, ²J_{H,P} 51.2 Hz, MnH). ²H NMR (C₆H₆, 77 MHz, **298 K**):^{bbbb} 1.39 (br. s, alkyl), 1.28 (br. s, alkyl), 1.12 (br. s, alkyl), 0.98 (br. s, alkyl), –10.54 (app. t, ²J_{D,P} 7.8 Hz, MnD). ¹³C{¹H} NMR (C₆D₆, 151 MHz, **298 K**): δ 38.04 (s, ⁿBu environment), 34.65 (p, ²J_{C,P} 12.3 Hz, PCH₂), 30.07 (s, SiCH₂CH₃), 29.53 (d, ²J_{C,P} 8.9 Hz, PCH₃), 29.41 (s, PCH₃), 27.42 (s, ⁿBu environment), 26.95 (s, ⁿBu environment), 14.25 (s, SiCH₂CH₂CH₂CH₃), 8.33 (s, SiCH₂CH₃). ²⁹Si{¹H} NMR (C₆D₆,

^{bbbb} All ²H NMR environments are due to room-temperature activation of the C₆D₆ solvent.

119 MHz, 298 K): δ 364.49 (m). $^{31}\text{P}\{^1\text{H}\}$ NMR (C_6D_6 , 243 MHz, 298 K): 80.50 (s, 2P), 80.35 (s, 2P).

trans-[(dmpe)₂MnH{=SiⁿBu(CDHCD₃)}] (*d*₄-**16**^{Bu,Et}). *d*₄-**16**^{Bu,Et} was prepared in a manner analogous to **16**^{Bu,Et}, with *d*₄-ethylene in place of ethylene and a 4 day reaction time for the exposure of **20**^{Bu} to C₂D₄ (with the headspace being evacuated and refilled with *d*₄-ethylene at the 2 day mark). Characterization was performed by NMR spectroscopy *in situ*, and NMR spectra in C₆H₆ were conducted by removing the C₆D₆ *in vacuo* and dissolving the resulting oil in C₆H₆. NMR data are consistent with those from **16**^{Bu,Et}, with the following exceptions; no ¹H NMR peak for the β ethyl environment (1.11 ppm in **16**^{Bu,Et}), an isotopic shift in the ¹H NMR peak for the α ethyl environment (singlet) to 1.29 ppm (cf. 1.35 ppm in **16**^{Bu,Et}), and isotopic shifts of the α and β ethyl ¹³C NMR peaks to 29.4 and 7.5 ppm, respectively (¹H NMR collected at 600 MHz, ¹³C{¹H} NMR collected at 151 MHz, both at 298 K). ²H NMR (C₆H₆, 77 MHz, 298 K): δ 1.28 (s, 1D, SiCDHCD₃), 1.00 (s, 3D, SiCDHCD₃).

trans-[(dmpe)₂MnH(=SiHPh)] (**16**^{Ph,H}). Approx. 15 mg of [(dmpe)₂MnH(SiH₂Ph)₂] (**20**^{Ph}) was dissolved in approx. 0.6 mL of C₆D₆ and placed in a J-young NMR tube. NMR spectra were collected at 311, 322, and 333 K, with increasing concentrations of *trans*-[(dmpe)₂MnH(=SiHPh)] (**16**^{Ph,H}) observed at higher temperatures (at 333 K, approx. 4% of the solution was *trans*-**16**^{Ph,H}). Selected NMR data for *trans*-**16**^{Ph,H} is as follows: ¹H NMR (C₆D₆, 500 MHz, 333 K): δ 9.83 (s, 1H, =SiH), -9.01 (app. t, 1H, ²J_{H,P} 54 Hz, MnH).

trans-[(dmpe)₂MnH(=SiHⁿBu)] (**16**^{Bu,H}). Approx. 15 mg of [(dmpe)₂MnH(SiH₂ⁿBu)₂] (**20**^{Bu}) was dissolved in approx. 0.6 mL of C₆D₆ and placed in a J-young NMR tube. NMR spectra were collected at 311, 322, and 333 K, with increasing concentrations of *trans*-[(dmpe)₂MnH(=SiHⁿBu)] (**16**^{Bu,H}) observed at higher temperatures (at 333 K, approx. 2% of the solution was *trans*-**16**^{Bu,H}). Selected NMR data for *trans*-**16**^{Bu,H} is as follows: ¹H NMR (C₆D₆, 500 MHz, 333 K): δ 9.53 (s, 1H, =SiH), -9.60 (app. t, 1H, ²J_{H,P} 51 Hz, MnH).

[(dmpe)₂MnH(PhHSi=CHMe)] (19^{Ph,H}). Approx. 15 mg of [(dmpe)₂MnH(SiH₂Ph)₂] (**20^{Ph}**) was dissolved in approx. 0.6 mL of C₆D₆ and placed in a J-young NMR tube, and the solution was freeze-pump-thawed (×3). The resulting solution was placed under an atmosphere of ethylene gas, cooled to –95 °C, and sealed at this low temperature. After standing at room temperature for 24 h, the solvent and free hydrosilane byproducts were removed *in vacuo* and the resulting solid was dissolved in *d*₈-toluene. Characterization was performed by NMR spectroscopy *in situ*. The following NMR data encompasses signals from both observed isomers (which are in a 1 : 1 ratio); **¹H NMR (*d*₈-toluene, 600 MHz, 298 K):** δ 7.94 (d, 2H, ³J_{H,H} 7.0 Hz, *o*), 7.88 (d, 2H, ³J_{H,H} 6.9 Hz, *o*), 7.22 (t, 2H, ³J_{H,H} 7.4 Hz, *m*), 7.16 (t, 1H, ³J_{H,H} 6.2 Hz, *p*), 4.45 (br. s, 1H, SiH), 4.45 (br. s, 1H, SiH), 1.93 (d, 3H, ³J_{H,H} 5.8 Hz, Si=C(H)CH₃), 1.92 (d, 3H, ³J_{H,H} 4.5 Hz, Si=C(H)CH₃), 1.89 (d, 3H, ²J_{H,P} 7.4 Hz, PCH₃), 1.51 (d, 3H, ²J_{H,P} 5.1 Hz, PCH₃), 1.46 (d, 3H, ²J_{H,P} 6.6 Hz, PCH₃), 1.44 (d, 3H, ²J_{H,P} 6.4 Hz, PCH₃), 1.42 (m, 3H, PCH₃), 0.57 (d, 3H, ²J_{H,P} 5.0 Hz, PCH₃), 0.45 (d, 3H, ²J_{H,P} 5.7 Hz, PCH₃), 0.17 (m, 1H, Si=C(H)CH₃), 0.07 (m, 1H, Si=C(H)CH₃), –14.54 (br. s, 1H, MnH), –14.70 (br. s, 1H, MnH). **¹³C{¹H} NMR (*d*₈-toluene, 151 MHz, 298 K):** δ –20.95 (s, ¹J_{C,H} 140 Hz, Si=C(H)CH₃), –21.17 (s, Si=C(H)CH₃). **³¹P{¹H} NMR (C₆D₆, 243 MHz, 298 K):** δ 84.96, 83.81, 81.82, 74.95, 72.01, 70.48, 66.81, 63.30. **¹H NMR (*d*₈-toluene, 500 MHz, 213 K):** δ 8.08 (d, 2H, ³J_{H,H} 6.9 Hz, *o*), 8.02 (d, 2H, ³J_{H,H} 7.2 Hz, *o*), 4.61 (s with ²⁹Si sat., 1H, ¹J_{H,Si} 194.8 Hz, SiH), 4.61 (s with ²⁹Si sat., 1H, ¹J_{H,Si} 194.8 Hz, SiH), 2.09 (m, 3H, Si=C(H)CH₃), 2.06 (m, 3H, Si=C(H)CH₃), 0.28 (m, 1H, Si=C(H)CH₃), 0.11 (m, 1H, Si=C(H)CH₃), –14.47 (m, 1H, MnH), –14.64 (m, 1H, MnH). **¹³C{¹H} NMR (*d*₈-toluene, 126 MHz, 213 K):** δ –21.63 (s, Si=C(H)CH₃), –21.85 (s, Si=C(H)CH₃). **²⁹Si NMR (*d*₈-toluene, 99 MHz, 213 K):** δ –7.11, –17.42.

[(dmpe)₂MnH(ⁿBuHSi=CHMe)] (19^{Bu,H}). Approx. 15 mg of [(dmpe)₂MnH(SiH₂ⁿBu)₂] (**20^{Bu}**) was dissolved in approx. 0.6 mL of C₆D₆ and placed in a J-young NMR tube, and this solution was freeze-pump-thawed (×3). The resulting solution was placed under an atmosphere of ethylene gas, cooled to –95 °C, sealed at this low temperature, and allowed to stand for 3 days at room temperature. The solvent and

free hydrosilane byproducts were then removed *in vacuo* and the resulting oil was dissolved in approx. 0.6 mL of C₆D₆. The reaction mixture was allowed to stand for 1 hour and the solvent was removed again in *vacuo*, yielding a red oil. The red oil was then dissolved in *d*₈-toluene and analyzed by NMR spectroscopy *in situ*, with two isomers present in solution (in a 1 : 1.9 ratio at room temperature). **Dominant isomer:** ¹H NMR (*d*₈-toluene, 600 MHz, 298 K): δ 3.74 (d with ²⁹Si sat., 1H, ³J_{H,P} 17.8 Hz, ¹J_{H,Si} 192.2 Hz, SiH), 1.74 (m, 2H, SiCH₂CH₂CH₂CH₃), 1.68 (d, 3H, ³J_{H,H} 7.5 Hz, Si=C(H)CH₃), 1.54 (m, 2H, SiCH₂CH₂CH₂CH₃), 1.54-0.87 (various m, 8H, PCH₂), 1.43 (d, 3H, ²J_{H,P} 6.6 Hz, PCH₃), 1.32 (d, 3H, ²J_{H,P} 5.0 Hz, PCH₃), 1.23 (d, 3H, ²J_{H,P} 4.7 Hz, PCH₃), 1.22 (d, 3H, ²J_{H,P} 5.5 Hz, PCH₃), 1.11 (d, 3H, ²J_{H,P} 5.0 Hz, PCH₃), 1.01 (t, 3H, ³J_{H,H} 7.3 Hz, SiCH₂CH₂CH₂CH₃), 0.99-0.95 (m, 6H, PCH₃), 0.97 (m, 1H, SiCH₂CH₂CH₂CH₃), 0.84 (d, 3H, ²J_{H,P} 5.6 Hz, PCH₃), 0.78 (m, 1H, SiCH₂CH₂CH₂CH₃), -0.16 (m, 1H, Si=C(H)CH₃), -14.99 (br. s, 1H, MnH). ¹³C{¹H} NMR (*d*₈-toluene, 151 MHz, 298 K): δ 35.37 (app. t, J_{C,P} 24.7 Hz, PCH₂), 34.65 (m, PCH₂), 33.96 (d of d, ¹J_{C,P} 25.4 Hz, ²J_{C,P} 20.0 Hz, PCH₂), 32.96 (m, PCH₂), 32.16 (d, ¹J_{C,P} 19.0 Hz, PCH₃), 30.27 (s, SiCH₂CH₂CH₂CH₃), 28.07 (m, PCH₃), 26.77 (s, SiCH₂CH₂CH₂CH₃), 25.84 (d, ¹J_{C,P} 10.9 Hz, PCH₃), 24.30 (br. s, PCH₃), 22.10 (t, ³J_{C,P} 8.4 Hz, Si=C(H)CH₃), 21.82 (d, ¹J_{C,P} 13.9 Hz, PCH₃), 20.92 (m, PCH₃), 19.97 (m, PCH₃), 14.40 (s, SiCH₂CH₂CH₂CH₃), 12.86 (s, SiCH₂CH₂CH₂CH₃), 10.85 (m, PCH₃), -20.75 (s, ¹J_{C,H} 139 Hz, Si=C(H)CH₃). ²⁹Si NMR (*d*₈-toluene, 119 MHz, 298 K): δ -16.98. ³¹P{¹H} NMR (*d*₈-toluene, 243 MHz, 298 K): δ 79.13 (s, 1P), 74.04 (s, 1P), 70.04 (s, 1P), 68.86 (s, 1P). **Minor isomer:** ¹H NMR (*d*₈-toluene, 600 MHz, 298 K): δ 3.66 (m with ²⁹Si sat., 1H, ¹J_{H,Si} 188.5 Hz, SiH), 1.83 (d, 3H, ³J_{H,H} 7.0 Hz, Si=C(H)CH₃), 1.74 (m, 2H, SiCH₂CH₂CH₂CH₃), 1.54 (m, 2H, SiCH₂CH₂CH₂CH₃), 1.54-0.87 (various m, 8H, PCH₂), 1.43 (d, 3H, ²J_{H,P} 6.6 Hz, PCH₃), 1.32 (d, 6H, ²J_{H,P} 5.0 Hz, PCH₃), 1.20 (d, 3H, ²J_{H,P} 5.7 Hz, PCH₃), 1.18 (d, 3H, ²J_{H,P} 5.7 Hz, PCH₃), 0.98 (t, 3H, ³J_{H,H} 7.3 Hz, SiCH₂CH₂CH₂CH₃), 0.99-0.95 (m, 6H, PCH₃), 0.89 (d, 3H, ²J_{H,P} 5.2 Hz, PCH₃), 0.88 (m, 1H, SiCH₂CH₂CH₂CH₃), 0.60 (m, 1H, SiCH₂CH₂CH₂CH₃), -0.09 (m, 1H, Si=C(H)CH₃), -14.86 (br. s, 1H, MnH). ¹³C{¹H} NMR (*d*₈-toluene, 151 MHz, 298 K): δ 35.37 (app. t, J_{C,P} 24.7 Hz, PCH₂), 34.65 (m,

PCH₂), 33.96 (d of d, ¹J_{C,P} 25.4 Hz, ²J_{C,P} 20.0 Hz, PCH₂), 32.96 (m, PCH₂), 30.34 (s, SiCH₂CH₂CH₂CH₃), 26.70 (s, SiCH₂CH₂CH₂CH₃), 25.95 (m, PCH₃), 24.07 (br. s, PCH₃), 23.87 (m, PCH₃), 23.72 (t, ³J_{C,P} 7.5 Hz, Si=C(H)CH₃), 23.31 (m, PCH₃), 21.17 (m, PCH₃), 16.07 (s, SiCH₂CH₂CH₂CH₃), 15.56 (m, PCH₃), 14.37 (s, SiCH₂CH₂CH₂CH₃), -19.32 (s, ¹J_{C,H} 138 Hz, Si=C(H)CH₃). ²⁹Si NMR (*d*₈-toluene, 119 MHz, 298 K): δ -8.87. ³¹P{¹H} NMR (*d*₈-toluene, 243 MHz, 298 K): δ 79.13 (s, 1P), 72.39 (s, 1P), 70.04 (s, 1P), 65.75 (s, 1P).

[(dmpe)₂MnH(ⁿBuHSi=CDCD₃)] (*d*₄-**19**^{Bu,H}). *d*₄-**19**^{Bu,H} was prepared in a manner analogous to the first steps in the preparation of *d*₄-**19**^{Bu,H}, with NMR spectra taken immediately after re-dissolving in C₆D₆. ¹H NMR data is consistent with that for **19**^{Bu,H}, though without peaks for the Si=C(H)CH₃ and Si=C(H)CH₃ environments (which are deuterated). ²H NMR (C₆D₆, 77 MHz, 298 K): δ 1.85 (s, Si=C(D)CD₃ minor isomer), 1.69 (s, Si=C(D)CD₃ major isomer), -0.10 (br. s, Si=C(D)CD₃ both isomers).

[(dmpe)₂MnH(PhEtSi=CHMe)] (**19**^{Ph,Et}). 177.7 mg (0.311 mmol) of [(dmpe)₂MnH(SiH₂Ph)₂] (**20**^{Ph}) was dissolved in 10 mL of benzene, and the solution was placed in a 50 mL storage flask and freeze-pump-thawed (×3). The resulting solution was placed under an atmosphere of ethylene gas, cooled to -95 °C, and sealed at this low temperature. After stirring at room temperature for two days, the solvent was removed *in vacuo* and the resulting reddish-orange oil was recrystallized from a concentrated solution of hexamethyldisiloxane at -30 °C, yielding 20.6 mg (0.040 mmol, 13%) of a brown solid. Small impurities could not be removed, and the resulting complex decomposed slowly at room temperature (overnight at room temperature, a variety of hydride resonances appeared in the ¹H NMR spectrum). ¹H NMR (C₆D₆, 600 MHz, 298 K): δ 7.89 (d, 2H, ³J_{H,H} 7.0 Hz, *o*), 7.22 (t, 2H, ³J_{H,H} 7.2 Hz, *m*), 7.16 (t, 1H, ³J_{H,H} 7.2 Hz, *p*), 1.88 (d, 3H, ³J_{H,H} 7.3 Hz, Si=C(H)CH₃), 1.58 (d, 3H, ³J_{H,P} 5.5 Hz, PCH₃), 1.56–1.09 (m, 6H, PCH₂), 1.51 (d, 3H, ³J_{H,P} 6.7 Hz, PCH₃), 1.29 (d, 3H, ³J_{H,P} 5.1 Hz, PCH₃), 1.24 (d, 3H, ³J_{H,P} 4.6 Hz, PCH₃), 1.18 (t, 3H, ³J_{H,H} 7.7 Hz, SiCH₂CH₃), 1.04 (m, 1H, PCH₂), 1.02 (m, 1H, SiCH₂CH₃), 0.97 (d, 3H, ³J_{H,P} 4.6 Hz, PCH₃), 0.93 (d, 3H, ³J_{H,P}

4.9 Hz, PCH_3), 0.91 (m, 1H, PCH_2), 0.89 (d, 3H, $^3J_{H,P}$ 5.5 Hz, PCH_3), 0.85 (m, 1H, $SiCH_2CH_3$), 0.54 (d, 3H, $^3J_{H,P}$ 5.3 Hz, PCH_3), 0.18 (m, 1H, $Si=C(H)CH_3$), -14.89 (m, 1H, MnH). $^{13}C\{^1H\}$ NMR (C_6D_6 , 151 MHz, 298 K): δ 142.81 (s, *i*), 136.22 (s, *o*), 127.68 (s, *p*), 127.30 (s, *m*), 37.47 (t, $J_{C,P}$ 25.0 Hz, PCH_2), 35.69 (d of d, $^1J_{C,P}$ 25.0 Hz, $^3J_{C,P}$ 20.1 Hz, PCH_2), 33.59 (m, PCH_2), 33.59 (m, PCH_3), 32.98 (t of d, $J_{C,P}$ 19.2 Hz, $J_{C,P}$ 7.5 Hz, PCH_2), 28.30 (s, PCH_3), 26.14 (d, $^1J_{C,P}$ 10.3 Hz, PCH_3), 24.84 (s, PCH_3), 22.69 (s, $Si=C(H)CH_3$), 22.68 (d, $^1J_{C,P}$ 13.7 Hz, PCH_3), 21.12 (m, PCH_3), 20.64 (d, $^1J_{C,P}$ 14.9 Hz, PCH_3), 14.86 (s, PCH_3), 9.95 (s, $SiCH_2CH_3$), 9.56 (s, $SiCH_2CH_3$), -21.74 (s, $^1J_{C,H}$ 137 Hz, $Si=C(H)CH_3$). ^{29}Si NMR (C_6D_6 , 119 MHz, 298 K): δ 0.72. $^{31}P\{^1H\}$ NMR (C_6D_6 , 243 MHz, 298 K): δ 79.17 (s, 1P), 68.61 (s, 1P), 65.65 (s, 2P). Low temperature (selected): 1H NMR (d_8 -toluene, 500 MHz, 213 K): δ 7.99 (d, 1H, $^3J_{H,H}$ 6.4 Hz, *o*), 7.88 (d, 1H, $^3J_{H,H}$ 6.6 Hz, *o*), 7.27 (t, 1H, $^3J_{H,H}$ 6.8 Hz, *m*), 7.20 (t, 1H, $^3J_{H,H}$ 6.8 Hz, *m*), 7.17 (m, 1H, *p*), 1.91 (d, 3H, $^3J_{H,H}$ 6.7 Hz, $Si=C(H)CH_3$), 1.58 (d, 3H, $^2J_{H,P}$ 4.2 Hz, PCH_3), 1.51 (d, 3H, $^2J_{H,P}$ 5.8 Hz, PCH_3), 1.26 (m, 2H, $SiCH_2CH_3$), 1.19 (d, 3H, $^2J_{H,P}$ 2.7 Hz, PCH_3), 0.55 (d, 3H, $^2J_{H,P}$ 3.5 Hz, PCH_3), 0.18 (m, 1H, $Si=C(H)CH_3$), -14.91 (m, 1H, MnH). ^{29}Si NMR (d_8 -toluene, 99 MHz, 213 K): δ 0.51. $^{31}P\{^1H\}$ NMR (C_6D_6 , 202 MHz, 203 K): δ 79.51 (app. q, $^2J_{P,P}$ 29.9 Hz, 1P), 69.00 (s, 1P), 65.80 (m, 2P).

$[(dmpe)_2MnH(^nBuEtSi=CHMe)]$ ($19^{Bu,Et}$). Approx. 15 mg of $[(dmpe)_2MnH(^nBuHSi=CHMe)]$ ($19^{Bu,H}$; >95% pure) was dissolved in approx. 0.6 mL of C_6D_6 . The reaction mixture was freeze-pump-thawed ($\times 3$) in a J-young NMR tube, and then was placed under 1 atm of ethylene at -95 °C, sealed at this temperature, and warmed to room temperature. After standing at room temperature for 14 days, the resulting mixture contained primarily $[(dmpe)_2MnH(^nBuEtSi=CHMe)]$ ($19^{Bu,Et}$) and $[(dmpe)_2MnH(C_2H_4)]$ (**10**), along with a series of small impurities including $[(dmpe)_2MnH(^nBuHSi=CHMe)]$ ($19^{Bu,H}$), and was analyzed by NMR spectroscopy *in situ*. Selected NMR data are as follows; 1H NMR (d_8 -toluene, 600 MHz, 298 K): δ 1.69 (d, 3H, $^3J_{H,H}$ 6.0 Hz, $Si=C(H)CH_3$), 1.47 (d, 3H, $^3J_{H,H}$ 6.7 Hz, PCH_3), 1.41 (m, 3H, PCH_3), 1.28 (m, 3H, $SiCH_2CH_3$), 1.27 (m, 6H, PCH_3), 1.15 (m, 3H, PCH_3), 0.96 (m, 3H, PCH_3), 0.95 (m, 3H, PCH_3), 0.94 (m, 3H, PCH_3), -0.11 (m, 1H, $Si=C(H)CH_3$), -15.33

(m, 1H, MnH). $^{13}\text{C}\{\text{H}\}$ NMR (C_6D_6 , 151 MHz, 298 K): δ -19.28 (s, $^1J_{\text{C,H}}$ 137 Hz, Si=C(H)CH₃). ^{29}Si NMR (C_6D_6 , 119 MHz, 298 K): δ -6.45. $^{31}\text{P}\{\text{H}\}$ NMR (C_6D_6 , 243 MHz, 298 K): δ 65.45 (s, 1P), 67.57 (s, 1P), 70.66 (s, 1P), 79.26 (s, 1P).

$[(\text{dmpe})_2\text{MnH}(\text{BuEtSi}=\text{C}\text{D}\text{C}\text{D}_3)]$ ($d_4\text{-19}^{\text{Bu,Et}}$). Approx. 15 mg of $[(\text{dmpe})_2\text{MnH}(\text{SiH}_2^{\text{Bu}})_2]$ ($\mathbf{20}^{\text{Bu}}$) was dissolved in approx. 0.6 mL of C_6D_6 . The reaction mixture was freeze-pump-thawed ($\times 3$) in a J-young NMR tube, and then was placed under 1 atm of ethylene at -95 °C, sealed at this temperature, and warmed to room temperature. After standing at room temperature for 30 hours, the solvent and free hydrosilane byproducts were removed *in vacuo*. The resulting dark red/brown oil ($\mathbf{19}^{\text{Bu,H}}$) was dissolved in approx. 0.6 mL of C_6D_6 , and the resulting solution was freeze-pump-thawed ($\times 3$) in a J-young NMR tube, placed under 1 atm of d_4 -ethylene at -95 °C, sealed at this temperature, and warmed to room temperature where it was monitored over time by NMR spectroscopy. ^1H NMR data was consistent with that for $\mathbf{19}^{\text{Bu,Et}}$, though without peaks for the Si=C(H)CH₃ and Si=C(H)CH₃ environments (which are deuterated).

cis- $[(\text{dmpe})_2\text{Mn}(\text{SiH}_2\text{Ph})(\text{CNxylyl})]$ (*cis*- $\mathbf{21a}$). A slight excess of *o*-xylyl isocyanide (28.6 mg, 0.218 mmol) was added to a solution of 118.3 mg (0.207 mmol) $[(\text{dmpe})_2\text{MnH}(\text{SiH}_2\text{Ph})_2]$ ($\mathbf{20}^{\text{Ph}}$) in 10 mL of benzene. The reaction mixture was stirred overnight at room temperature in a sealed flask, after which the solvent was removed *in vacuo*. The resulting yellow solid was washed with hexanes and recrystallized from a concentrated solution of toluene at -30 °C, yielding 79.1 mg of bright orange crystals. A further 8.7 mg of orange crystals could be obtained by concentrating the mother liquor, layering with hexanes, and allowing to stand at -30 °C, for a total yield of *cis*- $\mathbf{21a}$ of 87.8 mg (0.148 mmol, 71%). X-ray quality crystals were obtained by complete evaporation of toluene from a concentrated solution of *cis*- $\mathbf{21a}$ at room temperature under argon. For elemental analysis, residual toluene was removed by heating at 50 °C for 2 h at 5 mTorr, resulting in a bright yellow powder. ^1H NMR (C_6D_6 , 600 MHz, 298 K): δ 8.05 (d of d, 2H, $^3J_{\text{H,H}}$ 7.2 Hz, $^4J_{\text{H,H}}$ 1.8 Hz, *o*), 7.07 (m, 2H, *m*), 7.06 (m, 1H, *p*), 6.87 (d, 2H, $^3J_{\text{H,H}}$ 7.4 Hz, xylyl-*m*), 6.76 (t, 1H, $^3J_{\text{H,H}}$ 7.4 Hz, xylyl-*p*), 5.05 (d of d with ^{29}Si

Ph.D. Thesis — Jeffrey S. Price; McMaster University – Chemistry

sat., 1H, $^3J_{\text{H,P}}$ 19.2 Hz, $^3J_{\text{H,P}}$ 7.7 Hz, $^1J_{\text{H,Si}}$ 138.7 Hz, SiH), 4.73 (m with ^{29}Si sat., 1H, $^1J_{\text{H,Si}}$ 137.5 Hz, SiH), 2.05 (s, 6H, xylyl-CH₃), 1.74 (d, 3H, $^2J_{\text{H,P}}$ 7.0 Hz, PCH₃), 1.68 (m, 1H, PCH₂), 1.64 (d, 3H, $^2J_{\text{H,P}}$ 6.5 Hz, PCH₃), 1.61–1.44 (m, 3H, PCH₂), 1.32 (d, 3H, $^2J_{\text{H,P}}$ 6.0 Hz, PCH₃), 1.23 (d, 3H, $^2J_{\text{H,P}}$ 6.0 Hz, PCH₃), 1.20 (d, 3H, $^2J_{\text{H,P}}$ 6.2 Hz, PCH₃), 1.18 (m, 2H, PCH₂), 1.18 (d, 3H, $^2J_{\text{H,P}}$ 5.7 Hz, PCH₃), 1.07 (m, 1H, PCH₂), 1.01 (d, 3H, $^2J_{\text{H,P}}$ 4.7 Hz, PCH₃), 0.75 (d, 3H, $^2J_{\text{H,P}}$ 4.4 Hz, PCH₃), 0.75 (m, 1H, PCH₂). $^{13}\text{C}\{^1\text{H}\}$ NMR (C₆D₆, 151 MHz, 298 K): δ 149.06 (s, *i*), 137.34 (s, *o*), 134.02 (s, xylyl-*i*), 132.76 (s, xylyl-*o*), 128.04 (s, xylyl-*m*), 127.01 (s, *p*), 125.95 (s, *m*), 122.26 (s, xylyl-*p*), 33.79 (t of d, $J_{\text{C,P}}$ 20.2 Hz, $J_{\text{C,P}}$ 5 Hz, PCH₂), 32.48 (t, $J_{\text{C,P}}$ 19.9 Hz, PCH₂), 32.10 (m, PCH₂), 23.70 (m, PCH₃), 22.96 (m, PCH₃), 22.55 (d, $^1J_{\text{C,P}}$ 8.8 Hz, PCH₃), 21.53 (d of d, $J_{\text{C,P}}$ 20.8 Hz, $J_{\text{C,P}}$ 5.6 Hz, PCH₃), 20.66 (m, PCH₃), 20.35 (s, xylyl-CH₃), 20.22 (m, PCH₃), 19.82 (d, $^1J_{\text{C,P}}$ 26.4 Hz, PCH₃), 16.83 (d of d, $J_{\text{C,P}}$ 21.2 Hz, $J_{\text{C,P}}$ 4.6 Hz, PCH₃). ^{29}Si NMR (C₆D₆, 119 MHz, 298 K): δ 6.97. $^{31}\text{P}\{^1\text{H}\}$ NMR (C₆D₆, 243 MHz, 298 K): δ 74.77 (s, 2P), 64.51 (s, 1P), 55.54 (s, 1P). **Anal.** Found (calcd.): C, 54.89 (54.63); H, 8.61 (8.15); N, 2.32 (2.36).

trans-[(dmpe)₂Mn(SiH₂Ph)(CNxylyl)] (*trans*-21a). Method a) Approx. 15 mg of *cis*-[(dmpe)₂Mn(SiH₂Ph)(CNxylyl)] (*cis*-21a) was dissolved in approx. 0.6 mL of C₆D₆, and this solution was placed in an NMR tube with a J-Young Teflon valve and heated at 80-90°C for 5 days. The resulting solution contained a mixture of *cis*-7a (51%) and *trans*-21a (49%), and was analyzed by NMR spectroscopy *in situ*. Method b) Approx. 15 mg of [(dmpe)₂MnD₂(SiH₂Ph)] (*d*₂-18^{Ph}) was dissolved in approx. 0.6 mL of C₆D₆. To the reaction mixture was added an excess (5 mg) of *o*-xylyl isocyanide. The reaction mixture was placed in an NMR tube with a J-Young Teflon valve and heated at 75 °C for one hour, and NMR characterization was performed *in situ*. The resulting solution contained a mixture of *cis*-21a (91%) and *trans*-21a (9%). Data for the *trans* isomer is presented below. ^1H NMR (C₆D₆, 600 MHz, 298 K): δ 7.82 (d of d, 2H, $^3J_{\text{H,H}}$ 7.8 Hz, $^4J_{\text{H,H}}$ 1.3 Hz, *o*), 7.22 (t, 2H, $^3J_{\text{H,H}}$ 7.1 Hz, *m*), 7.16 (m, 1H, *p*), 6.85 (d, 2H, $^3J_{\text{H,H}}$ 7.1 Hz, xylyl-*m*), 6.71 (t, 1H, $^3J_{\text{H,H}}$ 7.5 Hz, xylyl-*p*), 4.42 (p with ^{29}Si sat., 2H, $^3J_{\text{H,P}}$ 8.4 Hz, $^1J_{\text{H,Si}}$ 140.5 Hz, SiH), 2.27 (s, 6H, xylyl-CH₃), 1.72 (m, 4H, PCH₂), 1.50 (m, 4H, PCH₂), 1.34

(s, 12H, PCH_3), 1.27 (s, 12H, PCH_3). $^{13}\text{C}\{^1\text{H}\}$ NMR (C_6D_6 , 151 MHz, 298 K): δ 152.72 (s, *i*), 136.11 (s, *o*), 133.93 (s, xylyl-*i*), 132.11 (s, xylyl-*o*), 128.53 (s, xylyl-*m*), 127.47 (s, *m*), 126.03 (s, *p*), 122.17 (s, xylyl-*p*), 32.61 (m, PCH_2), 22.00 (br. s, PCH_3), 20.51 (s, xylyl- CH_3), 20.21 (br. s, PCH_3). ^{29}Si NMR (C_6D_6 , 119 MHz, 298 K): δ -5.19. $^{31}\text{P}\{^1\text{H}\}$ NMR (C_6D_6 , 243 MHz, 298 K): δ 72.47.

***cis*-[(dmpe)₂Mn(SiH₂ⁿBu)(CNxylyl)] (*cis*-21b).** An excess of *o*-xylyl isocyanide (78.6 mg, 0.599 mmol) was added to a solution of 145.2 mg (0.274 mmol) [(dmpe)₂MnH(SiH₂ⁿBu)₂] (**20^{Bu}**) in 10 mL of benzene. The reaction mixture was stirred overnight at room temperature in a sealed flask, after which the solvent was removed *in vacuo*. The resulting orange solid was extracted with 2.5 mL of hexanes, and the resulting solution was stored at -30 °C, yielding 33.3 mg of ***cis*-21b** as an orange powder. Additional yield was obtained by dissolving the residual solid in toluene, layering with hexamethyldisiloxane, and letting stand at -30 °C to give an additional 22.7 mg (for a total yield of 56.0 mg, 0.098 mmol, 36%). X-ray quality crystals (bright orange diamonds) were obtained from a concentrated solution of toluene layered with hexamethyldisiloxane at -30 °C. ^1H NMR (C_6D_6 , 600 MHz, 298 K): δ 6.91 (d, 2H, $^3J_{\text{H,H}}$ 7.4 Hz, xylyl-*m*), 6.76 (t, 1H, $^3J_{\text{H,H}}$ 7.5 Hz, xylyl-*p*), 4.15 (m with ^{29}Si sat., 1H, $^1J_{\text{H,Si}}$ 134.5 Hz, SiH), 3.99 (m with ^{29}Si sat., 1H, $^1J_{\text{H,Si}}$ 133.8 Hz, SiH), 2.46 (s, 6H, xylyl- CH_3), 2.02 (t of t, 2H, $^3J_{\text{H,H}}$ 7.7 Hz, $\text{SiCH}_2\text{CH}_2\text{CH}_2\text{CH}_3$), 1.71 (m, 1H, PCH_2), 1.71 (d, 3H, $^2J_{\text{H,P}}$ 6.6 Hz, PCH_3), 1.68 (d, 3H, $^2J_{\text{H,P}}$ 6.4 Hz, PCH_3), 1.63 (t of q, 2H, $^3J_{\text{H,H}}$ 7.4 Hz, $\text{SiCH}_2\text{CH}_2\text{CH}_2\text{CH}$), 1.54 (m, 3H, PCH_2), 1.27 (d, 3H, $^2J_{\text{H,P}}$ 6.4 Hz, PCH_3), 1.23 (d, 3H, $^2J_{\text{H,P}}$ 5.9 Hz, PCH_3), 1.22 (m, 2H, $\text{SiCH}_2\text{CH}_2\text{CH}_2\text{CH}_3$), 1.22 (m, 1H, PCH_2), 1.18 (m, 6H, PCH_3), 1.15 (m, 1H, PCH_2), 1.04 (m, 1H, PCH_2), 1.03 (d, 3H, $^2J_{\text{H,P}}$ 4.9 Hz, PCH_3), 1.02 (t, 3H, $^3J_{\text{H,H}}$ 7.3 Hz, $\text{SiCH}_2\text{CH}_2\text{CH}_2\text{CH}_3$), 0.77 (d, 3H, $^2J_{\text{H,P}}$ 4.7 Hz, PCH_3), 0.73 (m, 1H, PCH_2). $^{13}\text{C}\{^1\text{H}\}$ NMR (C_6D_6 , 151 MHz, 298 K): δ 134.66 (s, xylyl-*i*), 132.18 (s, xylyl-*o*), 128.41 (xylyl-*m*), 122.10 (s, xylyl-*p*), 35.55 (s, $\text{SiCH}_2\text{CH}_2\text{CH}_2\text{CH}_3$), 33.87 (t of d, $J_{\text{C,P}}$ 19.8 Hz, $J_{\text{C,P}}$ 6.9 Hz, PCH_2), 32.88 (t of d, $J_{\text{C,P}}$ 23.5 Hz, $J_{\text{C,P}}$ 8.6 Hz, PCH_2), 32.53 (t, $^1J_{\text{C,P}}$ 18.9 Hz, PCH_2), 31.45 (t, $^1J_{\text{C,P}}$ 20.2 Hz, PCH_2), 27.08 (s, $\text{SiCH}_2\text{CH}_2\text{CH}_2\text{CH}_3$), 23.93 (d of d, $^1J_{\text{C,P}}$ 13.0 Hz, $^3J_{\text{C,P}}$ 2.3 Hz, PCH_3), 23.39 (d of d, $^1J_{\text{C,P}}$ 8.4 Hz, $^3J_{\text{C,P}}$ 3.7 Hz, PCH_3),

22.67 (d, $^1J_{C,P}$ 9.1 Hz, $P\text{CH}_3$), 22.50 (d of d, $^1J_{C,P}$ 20.2 Hz, $^3J_{C,P}$ 6.5 Hz, $P\text{CH}_3$), 21.13 (s, xylyl- CH_3), 20.46 (m, $P\text{CH}_3$), 18.80 (d, $^1J_{C,P}$ 21.3 Hz, $P\text{CH}_3$), 18.46 (d, $^1J_{C,P}$ 22.4 Hz, $P\text{CH}_3$), 18.30 (m, $\text{SiCH}_2\text{CH}_2\text{CH}_2\text{CH}_3$), 16.87 (d of d, $^1J_{C,P}$ 20.4 Hz, $^3J_{C,P}$ 5.6 Hz, $P\text{CH}_3$), 14.58 (s, $\text{SiCH}_2\text{CH}_2\text{CH}_2\text{CH}_3$). ^{29}Si NMR (C_6D_6 , 119 MHz, 298 K): δ 7.28 (m). $^{31}\text{P}\{^1\text{H}\}$ NMR (C_6D_6 , 243 MHz, 298 K): δ 75.15 (s, 2P), 64.29 (s, 1P), 54.93 (s, 1P). Anal. Found (calcd.): C, 52.08 (52.35); H, 8.85 (9.14); N, 2.29 (2.44).

trans-[(dmpe) $_2\text{Mn}(\text{SiH}_2^{\text{n}}\text{Bu})(\text{CNxylyl})]$ (*trans*-**21b**). Approx. 15 mg of *cis*-[(dmpe) $_2\text{Mn}(\text{SiH}_2^{\text{n}}\text{Bu})(\text{CNxylyl})]$ (*cis*-**21b**) was dissolved in approx. 0.6 mL of C_6D_6 , and this solution was placed in an NMR tube with a J-Young Teflon valve and heated at 80–90 °C for 5 days. The resulting solution contained a mixture of *cis*-**21b** (56%) and *trans*-**21b** (44%), and was analyzed by NMR spectroscopy *in situ*. Data for the *trans* isomer is presented below. ^1H NMR (C_6D_6 , 600 MHz, 298 K): δ 6.87 (d, 2H, $^3J_{\text{H,H}}$ 7.3 Hz, xylyl-*m*), 6.72 (t, 1H, $^3J_{\text{H,H}}$ 7.4 Hz, xylyl-*p*), 3.58 (m with ^{29}Si sat., 2H, $^1J_{\text{H,Si}}$ 135.5 Hz, SiH), 2.31 (s, 6H, xylyl- CH_3), 1.92 (app. p, 2H, $^3J_{\text{H,H}}$ 7.5 Hz, $\text{SiCH}_2\text{CH}_2\text{CH}_2\text{CH}_3$), 1.67 (m, 4H, $P\text{CH}_2$), 1.65 (app. sextet, 2H, $^3J_{\text{H,H}}$ 8.7 Hz, $\text{SiCH}_2\text{CH}_2\text{CH}_2\text{CH}_3$), 1.50 (m, 4H, $P\text{CH}_2$), 1.42 (s, 12H, $P\text{CH}_3$), 1.31 (s, 12H, $P\text{CH}_3$), 1.07 (t, 3H, $^3J_{\text{H,H}}$ 7.3 Hz, $\text{SiCH}_2\text{CH}_2\text{CH}_2\text{CH}_3$), 0.69 (m, 2H, $\text{SiCH}_2\text{CH}_2\text{CH}_2\text{CH}_3$). $^{13}\text{C}\{^1\text{H}\}$ NMR (C_6D_6 , 151 MHz, 298 K): δ 134.29 (s, xylyl-*i*), 132.12 (s, xylyl-*o*), 128.48 (s, xylyl-*m*), 121.95 (s, xylyl-*p*), 37.05 (s, $\text{SiCH}_2\text{CH}_2\text{CH}_2\text{CH}_3$), 32.80 (m, $P\text{CH}_2$), 27.35 (s, $\text{SiCH}_2\text{CH}_2\text{CH}_2\text{CH}_3$), 22.39 (s, $P\text{CH}_3$), 21.18 (s, $\text{SiCH}_2\text{CH}_2\text{CH}_2\text{CH}_3$), 20.61 (s, xylyl- CH_3), 20.42 (s, $P\text{CH}_3$), 14.63 (s, $\text{SiCH}_2\text{CH}_2\text{CH}_2\text{CH}_3$). ^{29}Si NMR (C_6D_6 , 119 MHz, 298 K): δ 0.24. $^{31}\text{P}\{^1\text{H}\}$ NMR (C_6D_6 , 243 MHz, 298 K): δ 73.03.

cis-[(dmpe) $_2\text{Mn}(\text{SiH}_2\text{Ph})(\text{CN}^t\text{Bu})]$ (*cis*-**21c**). An excess of *tert*-butyl isocyanide (57.0 mg, 0.686 mmol) was added to a solution of 60.9 mg (0.107 mmol) [(dmpe) $_2\text{MnH}(\text{SiH}_2\text{Ph})_2$] (**20^{Ph}**) in 10 mL of benzene. The reaction mixture was stirred for an hour in a sealed flask at room temperature, after which the solvent was removed *in vacuo*. The resulting yellow solid was extracted with hexanes, and the resulting solution was stored at –30 °C, yielding 12.1 mg of *cis*-**21c** as a light yellow powder. Additional

yield was obtained by dissolving the residual solid in a minimal amount of toluene, layering with hexamethyldisiloxane, and storing at $-30\text{ }^{\circ}\text{C}$ to give an additional 15.8 mg (total yield of 27.9 mg, 0.051 mmol, 48 %). X-ray quality crystals (pale yellow) were obtained from a concentrated solution of toluene layered with hexamethyldisiloxane at $-30\text{ }^{\circ}\text{C}$. **^1H NMR (C_6D_6 , 600 MHz, 298 K):** δ 8.14 (d of m, 2H, $^3J_{\text{H,H}}$ 7.6 Hz, *o*), 7.32 (t, 2H, $^3J_{\text{H,H}}$ 7.5 Hz, *m*), 7.21 (t, 1H, $^3J_{\text{H,H}}$ 7.3 Hz, *p*), 4.98 (d of d of d with ^{29}Si sat., 1H, $^3J_{\text{H,P}}$ 16.2 Hz, $^3J_{\text{H,P}}$ 7.0 Hz, $^3J_{\text{H,P}}$ 3.4 Hz, $^1J_{\text{H,Si}}$ 136.9 Hz, SiH), 4.78 (q with ^{29}Si sat., 1H, $^3J_{\text{H,P}}$ 7.8 Hz, $^1J_{\text{H,Si}}$ 138.2 Hz, SiH), 1.75 (m, 1H, PCH₂), 1.66 (d, 3H, $^2J_{\text{H,P}}$ 6.9 Hz, PCH₃), 1.63 (m, 1H, PCH₂), 1.53 (d, 3H, $^2J_{\text{H,P}}$ 7.0 Hz, PCH₃), 1.39 (m, 1H, PCH₂), 1.38 (m, 1H, PCH₂), 1.36 (d, 3H, $^2J_{\text{H,P}}$ 6.1 Hz, PCH₃), 1.30 (d, 3H, $^2J_{\text{H,P}}$ 6.1 Hz, PCH₃), 1.29 (m, 1H, PCH₂), 1.24 (d, 3H, $^2J_{\text{H,P}}$ 5.9 Hz, PCH₃), 1.17 (d, 3H, $^2J_{\text{H,P}}$ 5.9 Hz, PCH₃), 1.09 (m, 2H, PCH₂), 1.06 (d, 3H, $^2J_{\text{H,P}}$ 4.7 Hz, PCH₃), 1.02 (s, 9H, CNC(CH₃)₃), 0.96 (m, 1H, PCH₂), 0.82 (d, 3H, $^2J_{\text{H,P}}$ 5.1 Hz, PCH₃). **$^{13}\text{C}\{^1\text{H}\}$ NMR (C_6D_6 , 151 MHz, 298 K):** δ 152.01 (s, *i*), 137.30 (s, *o*), 126.95 (s, *m*), 125.64 (s, *p*), 54.62 (s, CNC(CH₃)₃), 34.10 (t of d, $J_{\text{C,P}}$ 21.5 Hz, $J_{\text{C,P}}$ 5.5 Hz, PCH₂), 33.28 (t of d, $J_{\text{C,P}}$ 22.8 Hz, $J_{\text{C,P}}$ 7.9 Hz, PCH₂), 32.97 (t, $J_{\text{C,P}}$ 20.3 Hz, PCH₂), 31.76 (s, CNC(CH₃)₃), 30.89 (t, $J_{\text{C,P}}$ 19.7 Hz, PCH₂), 24.39 (m, PCH₃), 23.78 (m, PCH₃), 23.19 (d, $^1J_{\text{C,P}}$ 7.4 Hz, PCH₃), 22.08 (d of d, $^1J_{\text{C,P}}$ 17.8 Hz, $^3J_{\text{C,P}}$ 5.7 Hz, PCH₃), 20.61 (d, $^1J_{\text{C,P}}$ 13.9 Hz, PCH₃), 19.98 (d, $^1J_{\text{C,P}}$ 23.8 Hz, PCH₃), 19.68 (d, $^1J_{\text{C,P}}$ 21.8 Hz, PCH₃), 18.37 (d of d, $^1J_{\text{C,P}}$ 19.5 Hz, $^3J_{\text{C,P}}$ 4.5 Hz, PCH₃). **$^{29}\text{Si}\{^1\text{H}\}$ NMR (C_6D_6 , 119 MHz, 298 K):** δ 8.46 (m). **$^{31}\text{P}\{^1\text{H}\}$ NMR (C_6D_6 , 243 MHz, 298 K):** δ 77.10 (s, 1P), 74.49 (s, 1P), 67.16 (s, 1P), 57.93 (s, 1P). **Anal.** Found (calcd.): C, 49.76 (50.64); H, 9.52 (8.87); N, 2.64 (2.57).

***trans*-[(dmpe)₂Mn(SiH₂Ph)(CN^{*t*}Bu)] (*trans*-21c).** Approx. 15 mg of *cis*-[(dmpe)₂Mn(SiH₂Ph)(CN^{*t*}Bu)] (*cis*-21c) was dissolved in approx. 0.6 mL of *d*₈-toluene and this solution was placed in an NMR tube with a J-Young Teflon valve and heated at 65-80 °C for 10 days. The resulting solution contained a mixture of *cis*-21c (24%) and *trans*-21c (76%), and was analyzed by NMR spectroscopy *in situ*. Data for the *trans* isomer is presented below. **^1H NMR (*d*₈-toluene, 600 MHz, 298 K):** δ 7.73 (d of m, 2H, $^3J_{\text{H,H}}$ 6.7 Hz, *o*), 7.15 (t, 2H, $^3J_{\text{H,H}}$ 7.1 Hz, *m*), 7.09 (t, 1H, $^3J_{\text{H,H}}$ 6.5 Hz, *p*), 4.30 (p with

^{29}Si sat., 2H, $^3J_{\text{H,P}}$ 8.1 Hz, $^1J_{\text{H,Si}}$ 137.49 Hz, SiH), 1.67 (m, 4H, PCH₂), 1.38 (s, 12H, PCH₃), 1.32, (m, 4H, PCH₂), 1.23 (s, 12H, PCH₃), 1.04 (s, 9H, CNC(CH₃)₃). $^{13}\text{C}\{^1\text{H}\}$ NMR (*d*₈-toluene, 151 MHz, 298 K): δ 153.51 (*i*), 136.12 (*s*, *o*), 127.15 (*s*, *m*), 125.99 (*s*, *p*), 54.43 (*s*, CNC(CH₃)₃), 32.30 (*m*, PCH₂), 31.53 (*s*, CNC(CH₃)₃), 22.01 (*s*, PCH₃), 19.92 (*s*, PCH₃). $^{29}\text{Si}\{^1\text{H}\}$ NMR (*d*₈-toluene, 119 MHz, 298 K): δ -3.19 (*s*). $^{31}\text{P}\{^1\text{H}\}$ NMR (*d*₈-toluene, 243 MHz, 298 K): δ 73.23 (*s*).

cis-[(dmpe)₂Mn(SiH₂ⁿBu)(CN^tBu)] (*cis*-21d). An excess of *tert*-butyl isocyanide (90 mg, 1.083 mmol) was added to a solution of 57.5 mg (0.108 mmol) of [(dmpe)₂MnH(SiH₂ⁿBu)₂] (**20**^{Bu}) in 10 mL of benzene. The reaction mixture was stirred in a sealed flask overnight at room temperature, after which the solvent was removed *in vacuo*. The resulting yellow solid was recrystallized from a concentrated solution of hexamethyldisiloxane at -30 °C, giving a yield of 19.8 mg of *cis*-21d (0.038 mmol, 35%). X-ray quality crystals were obtained from hexamethyldisiloxane at -30 °C. ^1H NMR (C₆D₆, 600 MHz, 298 K): δ 4.12 (m with ^{29}Si sat., 1H, $^1J_{\text{H,Si}}$ 131.7 Hz, SiH), 3.92 (m with ^{29}Si sat., 1H, $^1J_{\text{H,Si}}$ 130.6 Hz, SiH), 2.12 (m, 2H, SiCH₂CH₂CH₂CH₃), 1.77 (*s*, 2H, $^3J_{\text{H,H}}$ 7.4 Hz, SiCH₂CH₂CH₂CH₃), 1.75 (m, 1H, PCH₂), 1.65 (m, 1H, PCH₂), 1.61 (*d*, 3H, $^2J_{\text{H,P}}$ 6.8 Hz, PCH₃), 1.56 (m, 1H, PCH₂), 1.56, (*d*, 3H, $^2J_{\text{H,P}}$ 7.3 Hz, PCH₃), 1.53 (m, 1H, PCH₂), 1.36 (m, 1H, PCH₂), 1.29 (*d*, 3H, $^2J_{\text{H,P}}$ 6.0 Hz, PCH₃), 1.27 (*d*, 3H, $^2J_{\text{H,P}}$ 6.0 Hz, PCH₃), 1.23 (*s*, 9H, CNC(CH₃)₃), 1.23 (*d*, 3H, $^2J_{\text{H,P}}$ 4.9 Hz, PCH₃), 1.18 (*d*, 3H, $^2J_{\text{H,P}}$ 6.1 Hz, PCH₃), 1.17 (m, 2H, SiCH₂CH₂CH₂CH₃), 1.16 (*t*, 3H, $^3J_{\text{H,H}}$ 7.2 Hz, SiCH₂CH₂CH₂CH₃), 1.11 (*d*, 3H, $^2J_{\text{H,P}}$ 4.5 Hz, PCH₃), 1.01 (m, 1H, PCH₂), 0.99 (m, 1H, PCH₂), 0.85 (m, 1H, PCH₂), 0.84 (*d*, 3H, $^2J_{\text{H,P}}$ 4.7 Hz, PCH₃). $^{13}\text{C}\{^1\text{H}\}$ NMR (C₆D₆, 151 MHz, 298 K): δ 54.44 (*s*, CNC(CH₃)), 35.98 (*s*, SiCH₂CH₂CH₂CH₃), 34.44 (*t* of *d*, $J_{\text{C,P}}$ 20.8 Hz, $J_{\text{C,P}}$ 6.2 Hz, PCH₂), 33.87 (*t* of *d*, $J_{\text{C,P}}$ 24 Hz, $J_{\text{C,P}}$ 8.1 Hz, PCH₂), 32.28 (*d* of *d*, $J_{\text{C,P}}$ 19.9 Hz, $J_{\text{C,P}}$ 18.1 Hz, PCH₂), 31.99 (*s*, CNC(CH₃)₃), 30.13 (*t*, $J_{\text{C,P}}$ 19.4 Hz, PCH₂), 27.51 (*s*, SiCH₂CH₂CH₂CH₃), 24.16 (*m*, PCH₃), 23.21 (*d*, $^1J_{\text{C,P}}$ 8.7 Hz, PCH₃), 22.06 (*d* of *d*, $^1J_{\text{C,P}}$ 17.9 Hz, $^3J_{\text{C,P}}$ 5.4 Hz, PCH₃), 20.20 (*d* of *d*, $^1J_{\text{C,P}}$ 12.4 Hz, $^3J_{\text{C,P}}$ 3.1 Hz, PCH₃), 19.12 (*d*, $^3J_{\text{C,P}}$ 5.0 Hz, SiCH₂CH₂CH₂CH₃), 18.16 (*d*, $^1J_{\text{C,P}}$ 24.9 Hz, PCH₃), 17.73 (*d*, $^1J_{\text{C,P}}$ 23.7 Hz, PCH₃), 17.27 (*d* of *d*, $^1J_{\text{C,P}}$ 19.3 Hz, $^3J_{\text{C,P}}$ 5.6 Hz, PCH₃), 14.76 (*s*,

SiCH₂CH₂CH₂CH₃). ²⁹Si{¹H} NMR (C₆D₆, 119 MHz, 298 K): δ 10.12 (m). ³¹P{¹H} NMR (C₆D₆, 243 MHz, 298 K): δ 78.49 (s, 1P), 75.66 (s, 1P), 65.20 (s, 1P), 57.37 (s, 1P). **Anal.** Found (calcd.): C, 47.94 (47.99); H, 9.89 (9.97); N, 2.62 (2.67).

trans-[(dmpe)₂Mn(SiH₂ⁿBu)(CN^tBu)] (*trans*-**21d**). Method a) Approx. 15 mg of *cis*-[(dmpe)₂Mn(SiH₂ⁿBu)(CN^tBu)] (*cis*-**21d**) was dissolved in approx. 0.6 mL of C₆D₆ and this solution was placed in an NMR tube with a J-Young Teflon valve and heated at 80 °C for 20 days. The resulting solution contained mixture of *cis*-**21d** (47%) and *trans*-**21d** (53%), and was analyzed by NMR spectroscopy *in situ*. Method b) approx. 10 mg of [(dmpe)₂MnH₂(SiH₂ⁿBu)] (**18^{Bu}**) was dissolved in approx. 0.6 mL of C₆D₆. To the reaction mixture was added a large excess of ^tBuN≡C. The reaction mixture was placed in an NMR tube with a J-Young Teflon valve and heated at 75 °C for one hour, and NMR characterization was performed *in situ* {the resulting solution contained mixture of *cis*-**21d** (82%) and *trans*-**21d** (18%)}. Data for the *trans* isomer is presented below. ¹H NMR (C₆D₆, 600 MHz, 298 K): δ 3.60 (m with ²⁹Si sat., 2H, ¹J_{H,Si} 131.4 Hz, SiH), 1.96 (p, 2H, ³J_{H,H} 7.6 Hz, SiCH₂CH₂CH₂CH₃), 1.66 (m, 2H, SiCH₂CH₂CH₂CH₃), 1.65 (m, 4H, PCH₂), 1.50 (s, 12H, PCH₃), 1.38 (m, 4H, PCH₂), 1.28 (s, 12H, PCH₃), 1.08 (t, 3H, ³J_{H,H} 7.5 Hz, SiCH₂CH₂CH₂CH₃), 1.06 (s, 9H, CNC(CH₃)₃), 0.68 (m, 2H, SiCH₂CH₂CH₂CH₃). ¹³C{¹H} NMR (C₆D₆, 151 MHz, 298 K): δ 54.24 (s, CNC(CH₃)₃), 37.31 (s, SiCH₂CH₂CH₂CH₃), 32.29 (s, PCH₂), 31.65 (s, CNC(CH₃)₃), 27.41 (s, SiCH₂CH₂CH₂CH₃), 22.45 (m, PCH₃), 21.36 (s, SiCH₂CH₂CH₂CH₃), 20.13 (m, PCH₃), 14.67 (s, SiCH₂CH₂CH₂CH₃). ²⁹Si NMR (C₆D₆, 119 MHz, 298 K): δ 2.51. ³¹P{¹H} NMR (C₆D₆, 243 MHz, 298 K): δ 74.02 (s).

[(dmpe)₂MnH{=SiHPh(ⁱPrNHC)}] (**22a**). 1,3-diisopropylimidazolin-2-ylidene (ⁱPrNHC) (84.7 mg, 0.556 mmol) was added to a solution of 95.1 mg (0.167 mmol) [(dmpe)₂MnH(SiH₂Ph)₂] (**20^{Ph}**) in 10 mL of benzene. The reaction mixture was placed in a 50 mL storage flask, sealed, and stirred overnight at room temperature, then overnight again at 55 °C. The solvent was then removed *in vacuo* and the resulting brownish/red powder was washed with hexanes. The remaining solid was extracted with pentane, and

the resulting solution was stored $-30\text{ }^{\circ}\text{C}$. As well, the residual solid from the extraction was dissolved in a minimal amount of hexamethyldisiloxane and stored at $-30\text{ }^{\circ}\text{C}$. Combining crystals from both batches provided a total yield of 14.4 mg (0.023 mmol, 14% yield) of **22a** as a red powder, though the product contained some unidentified impurities which were not removed. X-ray quality crystals (red blocks) were obtained from hexanes at $-30\text{ }^{\circ}\text{C}$. *Elevated temperature NMR analysis (signals are an average of the chemical shifts for 2 isomers):* **^1H NMR (d_8 -toluene, 500 MHz, 330 K):** δ 7.51 (d, 2H, $^3J_{\text{H,H}}$ 6.8 Hz, *o*), 7.05 (t, 2H, $^3J_{\text{H,H}}$ 7.6 Hz, *m*),⁵⁸⁷ 7 (v. br. m, 2H, $\text{CH}(\text{CH}_3)_2$), 6.97 (t, 1H, $^3J_{\text{H,H}}$ 6.3 Hz, *p*), 6.31 (s, 2H, $\text{HC}=\text{CH}$), 6.18 (br. s, 1H, SiH), 0.6-1.9 (many br. multiplets, 44H, dmpe and $\text{CH}(\text{CH}_3)_2$), -12.54 (p, 1H, $^2J_{\text{H,P}}$ 33.6 Hz, MnH). **$^{31}\text{P}\{^1\text{H}\}$ (d_8 -toluene, 202 MHz, 330 K):** δ 79.60 (m, 2P), 71.79 (s, 1P), 65.38 (s, 1P). *Room temperature NMR analysis (signals are in the process of decoalescing to two sets for the two observed isomers).* Selected NMR signals are as follows; **^1H NMR (d_8 -toluene, 600 MHz, 298 K):** δ 7.55 (d, 2H, $^3J_{\text{H,H}}$ 7.1 Hz, *o*), 7.08 (t, 2H, $^3J_{\text{H,H}}$ 7.4 Hz, *m*), 7.00 (t, 2H, $^3J_{\text{H,H}}$ 7.3 Hz, *p*), 6.80 (br. m, 1H, $\text{CH}(\text{CH}_3)_2$), 6.24 (s, 2H, $\text{HC}=\text{CH}$), 6.16 (br. s, 1H, SiH), 0.6-1.9 (many br. multiplets, 44H, dmpe and $\text{CH}(\text{CH}_3)_2$), -12.43 (m, 1H, MnH minor isomer), -12.56 (m, 1H, MnH major isomer). **$^{13}\text{C}\{^1\text{H}\}$ NMR (d_8 -toluene, 151 MHz, 298 K):** δ 135.66 (s, *o*), 127.06 (s, *m*), 116.47 (s, $\text{HC}=\text{CH}$). **$^{31}\text{P}\{^1\text{H}\}$ NMR (d_8 -toluene, 243 MHz, 298 K):** δ 79.92 (s, 1P, major isomer), 78.38 (s, 1P, major isomer), 78.38 (m, 2P, minor isomer), 73.75 (s, 1P, minor isomer), 71.14 (s, 1P, major isomer), 65.10 (s, 1P, major isomer), 64.42 (s, 1P, minor isomer). *Low temperature NMR analysis (signals for two isomers could be observed in a 0.3 : 1 ratio).* Selected NMR signals are as follows; **Dominant isomer: ^1H NMR (d_8 -toluene, 500 MHz, 213 K):** 8.77 (m, 1H, $\text{CH}(\text{CH}_3)_2$), 7.68 (m, 2H, *o*), 7.20 (t, 2H, $^3J_{\text{H,H}}$ 6.9 Hz, *m*), 7.10 (t, 1H, $^3J_{\text{H,H}}$ 6.8 Hz, *p*), 6.26 (s, 1H, SiH), 6.09 (s, 1H, $\text{HC}=\text{CH}$), 5.86 (s, 1H, $\text{HC}=\text{CH}$), 5.76 (m, 1H, $\text{CH}(\text{CH}_3)_2$), 1.84 (s, 3H, PCH_3), 1.65 (m, 3H, PCH_3), 1.47 (s, 3H, PCH_3), 1.43 (s, 3H, PCH_3), 1.39 (s, 3H, PCH_3), 1.34 (s, 3H, PCH_3), 1.30 (s, 3H, $\text{CH}(\text{CH}_3)_2$), 1.20 (s, 3H, $\text{CH}(\text{CH}_3)_2$), 1.20 (s, 3H, PCH_3), 1.07 (s, 3H, PCH_3), 0.82 (d, 3H, $^3J_{\text{H,H}}$ 4.5 Hz, $\text{CH}(\text{CH}_3)_2$), 0.27 (d, 3H, $^3J_{\text{H,H}}$ 3.8 Hz, $\text{CH}(\text{CH}_3)_2$), -12.47 (m, 1H, MnH). **$^{13}\text{C}\{^1\text{H}\}$ NMR (d_8 -toluene, 126 MHz,**

213 K): δ 156.34 (s, *i*), 135.39 (s, *o*), 127.02 (s, *m*), 116.58 (s, HC=CH), 116.16 (s, HC=CH), 49.69 (s, CH(CH₃)₂), 47.95 (s, CH(CH₃)₂), 37.08 (m, PCH₂), 35.30 (m, PCH₂), 34.00 (m, PCH₃), 33.90 (m, PCH₂), 29.52 (s, PCH₃), 27.74 (s, PCH₃), 26.10 (m, PCH₃), 25.33 (s, PCH₃), 23.66 (s, CH(CH₃)₂), 23.24 (s, CH(CH₃)₂), 22.54 (s, CH(CH₃)₂), 21.96 (s, CH(CH₃)₂). ²⁹Si NMR (*d*₈-toluene, 99 MHz, 213 K): δ 24.11. ³¹P{¹H} (*d*₈-toluene, 202 MHz, 213 K): δ 81.85 (t, ²J_{P,P} 27.2 Hz, 1P), 79.18 (s, 1P), 72.46 (d of d, ²J_{P,P} 41.9 Hz, ²J_{P,P} 20.9 Hz, 1P), 66.34 (m, 1P). **Minor isomer:** ¹H NMR (*d*₈-toluene, 500 MHz, 213 K): 8.03 (m, 1H, CH(CH₃)₂), 7.68 (m, 2H, *o*), 7.19 (t, 2H, ³J_{H,H} 6.9 Hz, *m*), 7.08 (m, 1H, *p*), 6.37 (d with ²⁹Si sat., 1H, ³J_{H,P} 19.0 Hz, ¹J_{H,Si} 123.4 Hz, SiH), 5.59 (br. s, 1H, CH(CH₃)₂), 2.01 (s, 3H, PCH₃), 1.76 (m, 3H, PCH₃), 1.65 (m, 3H, PCH₃), 1.53 (d, 3H, ³J_{H,H} 3.2 Hz, PCH₃), 1.43 (s, 3H, PCH₃), 1.39 (s, 6H, PCH₃), 1.30 (s, 3H, CH(CH₃)₂), 1.12 (s, 3H, CH(CH₃)₂), 0.82 (s, 3H, CH(CH₃)₂), 0.75 (s, 3H, PCH₃), 0.42 (br. s, 3H, CH(CH₃)₂), -12.32 (m, 1H, MnH). ¹³C{¹H} NMR (*d*₈-toluene, 126 MHz, 213 K): δ 135.39 (s, *o*), 127.02 (s, *m*), 29.08 (s, PCH₃), 27.34 (m, PCH₃), 26.54 (m, PCH₃), 22.54 (s, CH(CH₃)₂), 21.50 (m, PCH₃). ²⁹Si NMR (*d*₈-toluene, 99 MHz, 213 K): δ 22.21. ³¹P{¹H} (*d*₈-toluene, 202 MHz, 213 K): δ 79.96 (t, ²J_{P,P} 30.9 Hz, 1P), 79.18 (s, 1P), 74.69 (d, ²J_{P,P} 40.8 Hz, 1P), 65.63 (s, 1P).

[(dmpe)₂MnH{=SiHⁿBu(ⁱPrNHC)}] (**22b**). 1,3-diisopropylimidazolin-2-ylidene (ⁱPrNHC) (70 mg, 0.460 mmol) was added to a solution of 104.1 mg (0.196 mmol) [(dmpe)₂MnH(SiH₂ⁿBu)₂] (**20**^{Bu}) in 10 mL of benzene. The reaction mixture was placed in a 50 mL storage flask, sealed, and stirred for 1 hour at room temperature. Following this, half of the solvent was removed *in vacuo*, and the reaction mixture was stirred for 30 minutes at room temperature before the remainder of the solvent was removed *in vacuo*. This process was repeated (×2): 10 more mL of benzene was added, the solution stirred for 30 minutes, half the solvent was removed *in vacuo*, the solution was stirred again for 30 minutes, and the remainder of the solvent was removed *in vacuo* leaving a red oil. Recrystallization from hexanes at -30 °C yielded 33.9 mg of **22b** as a red powder, and the mother liquor was concentrated and allowed to stand at -30 °C yielding an additional 14.8 mg, for a combined yield of 48.7 mg (0.082 mmol, 42%). X-ray quality crystals

were obtained from hexanes at $-30\text{ }^{\circ}\text{C}$. *Elevated temperature NMR analysis (signals are the average of isomer chemical shifts):* ^1H NMR (d_8 -toluene, 500 MHz, 333 K): δ 6.34 (s, 2H, $\text{HC}=\text{CH}$), 6.29 (br. s, 2H, $\text{CH}(\text{CH}_3)_2$), 5.18 (br. s, 1H, SiH), 2.0-0.9 (various br. signals, 50H, PCH_2 , PCH_3 , $\text{CH}(\text{CH}_3)_2$, and $\text{SiCH}_2\text{CH}_2\text{CH}_2\text{CH}_3$), 0.90 (t, 3H, $^3J_{\text{H,H}}$ 7.1 Hz, $\text{SiCH}_2\text{CH}_2\text{CH}_2\text{CH}_3$), -12.65 (br. s, 1H, MnH). *Room temperature NMR analysis (signals are in the process of decoalescing to two sets for the two observed isomers).* Selected NMR signals are as follows; **Dominant isomer:** ^1H NMR (C_6D_6 , 600 MHz, 298 K): δ 5.11 (br. s with ^{29}Si sat., 1H, $^1J_{\text{H,Si}}$ 112.6 Hz, SiH), 0.85 (br. s, 3H, PCH_3), -12.43 (m, 1H, MnH). ^{13}C NMR (d_8 -toluene, 151 MHz, 298 K): δ 25.42 (m, PCH_3). $^{29}\text{Si}\{^1\text{H}\}$ NMR (C_6D_6 , 119 MHz, 298 K): δ 28.71. **Minor isomer:** ^1H NMR (C_6D_6 , 600 MHz, 298 K): δ 5.43 (br. s with ^{29}Si sat., 1H, $^1J_{\text{H,Si}}$ 116.0 Hz, SiH), 0.56 (br. s, 3H, PCH_3), -12.62 (m, 1H, MnH). $^{13}\text{C}\{^1\text{H}\}$ NMR (d_8 -toluene, 151 MHz, 298 K): δ 28.50 (m, PCH_3). $^{29}\text{Si}\{^1\text{H}\}$ NMR (C_6D_6 , 119 MHz, 298 K): δ 28.71. **Indeterminate isomer or average signals not decoalesced yet:** ^1H NMR (C_6D_6 , 600 MHz, 298 K): δ 6.34 (br. s, 2H, $\text{CH}(\text{CH}_3)_2$), 6.22 (s, 2H, $\text{HC}=\text{CH}$), 2.20-0.98 (various br. signals, 47H, PCH_2 , PCH_3 , $\text{CH}(\text{CH}_3)_2$, and $\text{SiCH}_2\text{CH}_2\text{CH}_2\text{CH}_3$), 0.95 (t, 3H, $^3J_{\text{H,H}}$ 7.1 Hz, $\text{SiCH}_2\text{CH}_2\text{CH}_2\text{CH}_3$). $^{13}\text{C}\{^1\text{H}\}$ NMR (d_8 -toluene, 151 MHz, 298 K): δ 116.66 (s, $\text{HC}=\text{CH}$), 49.55 (s, $\text{CH}(\text{CH}_3)_2$), 14.43 (s, $\text{SiCH}_2\text{CH}_2\text{CH}_2\text{CH}_3$). $^{31}\text{P}\{^1\text{H}\}$ NMR (C_6D_6 , 243 MHz, 298 K): δ 80.49, 78.95, 78.43, 77.17, 76.72, 75.01, 65.08, 63.97. *Low temperature NMR analysis (signals for two isomers could be observed in a 1.2 : 1 ratio).* **Dominant isomer:** ^1H NMR (d_8 -toluene, 500 MHz, 197 K): δ 6.87 (m, 1H, $\text{CH}(\text{CH}_3)_2$), 5.56 (m, 1H, $\text{CH}(\text{CH}_3)_2$), 5.08 (br. s, 1H, $^3J_{\text{H,H}}$ 4.9 Hz, $^1J_{\text{H,Si}}$ 119.5 Hz, SiH), 1.72 (d, 3H, $^2J_{\text{H,P}}$ 3.4 Hz, PCH_3), 1.68 (d, 3H, $^2J_{\text{H,P}}$ 4.2 Hz, PCH_3), 1.45 (br. s, 3H, PCH_3), 1.42 (br. s, 6H, PCH_3), 1.30 (br. s, 3H, PCH_3), 1.22 (d, 3H, $^3J_{\text{H,H}}$ 5.0 Hz, $\text{CH}(\text{CH}_3)_2$), 1.03 (d, 3H, $^3J_{\text{H,H}}$ 5.3 Hz, $\text{CH}(\text{CH}_3)_2$), 0.96 (t, 3H, $^3J_{\text{H,H}}$ 7.6 Hz, $\text{SiCH}_2\text{CH}_2\text{CH}_2\text{CH}_3$), 0.93 (m, 3H, $\text{CH}(\text{CH}_3)_2$), 0.85 (d, 3H, $^3J_{\text{H,H}}$ 4.3 Hz, $\text{CH}(\text{CH}_3)_2$), 0.78 (br. s, 3H, PCH_3), -12.40 (m, 1H, MnH). $^{13}\text{C}\{^1\text{H}\}$ NMR (d_8 -toluene, 126 MHz, 197 K): δ 49.73 (s, $\text{CH}(\text{CH}_3)_2$), 48.63 (s, $\text{CH}(\text{CH}_3)_2$), 33.98 (m, PCH_3), 32.41 (m, PCH_3), 31.89 (s, PCH_3), 29.97 (m, PCH_3), 28.26 (s, PCH_3), 26.84 (br. s, PCH_3), 26.39 (m, PCH_3), 25.37 (m, PCH_3), 23.06 (s, $\text{CH}(\text{CH}_3)_2$), 22.11 (s, $\text{CH}(\text{CH}_3)_2$), 21.84 (s,

CH(CH₃)₂), 14.74 (s, SiCH₂CH₂CH₂CH₃). ²⁹Si NMR (*d*₈-toluene, 99 MHz, 197 K): δ 29.56. ³¹P{¹H} NMR (*d*₈-toluene, 202 MHz, 197 K): δ 79.74 (m, 1P), 78.20 (m, 2P), 65.62 (s, 1P). **Minor isomer:** ¹H NMR (*d*₈-toluene, 500 MHz, 197 K): δ 7.17 (m, 1H, CH(CH₃)₂), 5.63 (m, 1H, CH(CH₃)₂), 5.40 (br. s, 1H, ³J_{H,H} 3.4 Hz, ¹J_{H,Si} 124.8 Hz, SiH), 1.84 (br. s, 3H, PCH₃), 1.77 (br. s, 3H, PCH₃), 1.51 (br. s, 6H, PCH₃), 1.49 (br. s, 3H, PCH₃), 1.21 (d, 3H, ³J_{H,H} 5.0 Hz, CH(CH₃)₂), 1.08 (d, 3H, ³J_{H,H} 3.9 Hz, CH(CH₃)₂), 0.98 (t, 3H, ³J_{H,H} 7.1 Hz, SiCH₂CH₂CH₂CH₃), 0.93 (m, 3H, CH(CH₃)₂), 0.85 (d, 3H, ³J_{H,H} 4.3 Hz, CH(CH₃)₂), 0.50 (br. s, 3H, PCH₃), -12.59 (m, 1H, MnH). ¹³C{¹H} NMR (*d*₈-toluene, 126 MHz, 197 K): δ 49.73 (s, CH(CH₃)₂), 48.85 (s, CH(CH₃)₂), 28.83 (m, PCH₃), 28.18 (m, PCH₃), 27.01 (m, PCH₃), 26.84 (br. s, PCH₃), 25.95 (m, PCH₃), 25.37 (m, PCH₃), 23.63 (s, CH(CH₃)₂), 22.26 (s, CH(CH₃)₂), 21.73 (s, CH(CH₃)₂), 20.49 (s, CH(CH₃)₂), 14.84 (s, SiCH₂CH₂CH₂CH₃). ²⁹Si NMR (*d*₈-toluene, 99 MHz, 197 K): δ 28.78. ³¹P{¹H} NMR (*d*₈-toluene, 202 MHz, 197 K): δ 81.85 (m, 1P), 78.20 (m, 1P), 75.11 (m, 1P), 64.11 (s, 1P). **Indeterminate isomer or average signals not decoalesced yet:** ¹H NMR (*d*₈-toluene, 500 MHz, 197 K): δ 5.98 (s, 1H, HC=CH), 5.92 (s, 1H, HC=CH), 1.87 (br. s, 3H, PCH₃), 1.58 and 1.45 (m, 2H, SiCH₂CH₂CH₂CH₃), 1.10 (m, 2H, SiCH₂CH₂CH₂CH₃). ¹³C{¹H} NMR (*d*₈-toluene, 126 MHz, 197 K): δ 171.74 (s, NCN), 170.98 (s, NCN), 116.87 (s, HC=CH), 116.82 (s, HC=CH), 116.26 (s, HC=CH), 116.17 (s, HC=CH), 37.42 (s, one of SiCH₂CH₂CH₂CH₃), 28.51 (s, one of SiCH₂CH₂CH₂CH₃), 23.52 (s, CH(CH₃)₂), 23.47 (s, CH(CH₃)₂). **Anal.** Found (calcd.): C, 50.83 (50.49); H, 10.22 (10.00); N, 4.72 (4.71).

[(dmpe)₂MnH{=SiHPh(^{Me}NHC)}] (**22c**) 1,3,4,5-tetramethyl-4-imidazolin-2-ylidene (^{Me}NHC) (37.2 mg, 0.300 mmol) was added to a solution of 101.0 mg (0.177 mmol) of [(dmpe)₂MnH(SiH₂Ph)₂] (**20^{Ph}**) in 10 mL of benzene. The reaction mixture immediately turned orange and was stirred overnight at room temperature. Following this, the solvent was removed *in vacuo* and the resulting solid was dissolved again in 10 mL of benzene and stirred again overnight at room temperature. The solvent was again removed *in vacuo*, following which the resulting solid was washed with hexanes, then recrystallized from a concentrated solution of toluene layered with pentane

at $-30\text{ }^{\circ}\text{C}$, yielding 33.3 mg of **22c** as a reddish-brown powder. The mother liquor was then concentrated and layered again at $-30\text{ }^{\circ}\text{C}$ in pentane, yielding an additional 14.6 mg for a total yield of 47.9 mg (0.082 mmol, 46%). X-ray quality crystals (red blocks) were obtained from a concentrated solution in toluene layered with pentane at $-30\text{ }^{\circ}\text{C}$. *Elevated temperature NMR analysis (one set of signals are the average of chemical shifts for the two cis isomers, and another are from the trans isomer, with a 15 : 1 ratio):* **cis-22c**; ^1H NMR (d_8 -toluene, 500 MHz, 339 K): δ 7.98 (br. s, 2H, *o*), 7.17 (t, 2H, $^3J_{\text{H,H}}$ 7.3 Hz, *m*), 7.07 (t, 1H, $^3J_{\text{H,H}}$ 7.7 Hz, *p*), 6.06 (s with ^{29}Si sat., 1H, $^1J_{\text{H,Si}}$ 122.2 Hz, SiH), 3.45 (br. s, 6H, NCH_3), 1.31 (s, 6H, NCCCH_3), -12.60 (p, 1H, $^2J_{\text{H,P}}$ 31.5 Hz, MnH). All remaining ^1H NMR signals could not be identified and range from 0.9 to 1.9 ppm. $^{31}\text{P}\{^1\text{H}\}$ NMR (d_8 -toluene, 202 MHz, 333 K): δ 76.67 (br. s, 2P), 72.56 (br. s, 1P), 65.76 (br. s, 1P). **trans-22c**; ^1H NMR (d_8 -toluene, 500 MHz, 339 K): δ 7.81 (d, 2H, $^3J_{\text{H,H}}$ 7.0 Hz, *o*), 7.13 (m, 2H, *m*), 7.03 (m, 1H, *p*), 5.84 (br. s, 1H, SiH), 3.23 (br. s, 6H, NCH_3), -14.92 (app. t, 1H, $^2J_{\text{H,P}}$ 46.9 Hz, MnH). All remaining ^1H NMR signals could not be identified and range from 0.9 to 1.9 ppm. $^{31}\text{P}\{^1\text{H}\}$ NMR (d_8 -toluene, 202 MHz, 333 K): δ 79.89 (s, 2P), 79.43 (s, 2P). *Room temperature NMR analysis (signals due to the cis isomers are in the process of decoalescing, and one set of sharp signals is observed due to the trans isomer; a 14 : 1 ratio is observed at room temperature between a sum of the two cis isomers and the trans isomer).* Selected NMR signals are as follows; **cis-22c** (major isomer); ^1H NMR (d_8 -toluene, 500 MHz, 298 K): δ 8.24 (br. s, 2H, *o*), 7.23 (br. s, 2H, *m*), 7.12 (br. s, 1H, *p*), 6.08 (s with ^{29}Si sat., 1H, $^1J_{\text{H,Si}}$ 121.3 Hz, SiH), 3.24 (br. s, 6H, NCH_3), 1.22 (s, 6H, NCCH_3), 0.56 (br. s, 3H, PCH_3), -12.56 (m, 1H, MnH). All remaining ^1H NMR signals could not be identified and range from 0.8 to 1.9 ppm. $^{31}\text{P}\{^1\text{H}\}$ NMR (d_8 -toluene, 243 MHz, 298 K): δ 78.38 (br. s, 1P), 77.01 (br. s, 1P), 70.43 (br. s, 1P), 64.52 (br. s, 1P). **cis-22c** (minor isomer), ^1H NMR (d_8 -toluene, 500 MHz, 298 K): 7.77 (br. s, 2H, *o*), 6.08 (s with ^{29}Si sat., 1H, $^1J_{\text{H,Si}}$ 121.3 Hz, SiH), 3.70 (br. s, 6H, NCH_3), 1.22 (s, 6H, NCCH_3), -12.56 (m, 1H, MnH). All remaining ^1H NMR signals could not be identified and range from 0.8 to 1.9 ppm. $^{31}\text{P}\{^1\text{H}\}$ NMR (d_8 -toluene, 243 MHz, 298 K): δ 78.38 (br. s, 1P), 77.01 (br. s, 1P), 72.58 (br. s, 1P), 64.52 (br. s, 1P). **cis-22c** (indeterminate or

both isomers): $^{13}\text{C}\{^1\text{H}\}$ NMR (*d*₈-toluene, 151 MHz, 298 K): δ 126.83 (s, *m*), 126.01 (s, *p*), 124.28 (NCCH₃), 33.96 (s, NCH₃), 7.87 (s, NCCH₃). $^{29}\text{Si}\{^1\text{H}\}$ NMR (*d*₈-toluene, 119 MHz, 298 K): δ 24.29. $^{31}\text{P}\{^1\text{H}\}$ NMR (*d*₈-toluene, 243 MHz, 298 K): δ 78.38 (br. s, 1P, major and minor isomers), 77.01 (br. s, 1P, major and minor isomers), 72.58 (br. s, 1P, minor isomer), 70.43 (br. s, 1P, major isomer), 64.52 (br. s, 1P, major and minor isomers). ***trans*-22c**; ^1H NMR (*d*₈-toluene, 500 MHz, 298 K): δ 7.85 (t, 2H, $^3J_{\text{H,H}}$ 7.1 Hz, *o*), 7.17 (t, 2H, $^3J_{\text{H,H}}$ 7.5 Hz, *m*), 5.83 (app. t with ^{29}Si sat., 1H, $^3J_{\text{H,P}}$ 6.8 Hz, $^1J_{\text{H,Si}}$ 126.6 Hz, SiH), 3.18 (s, 6H, NCH₃), 1.71 (d, 6H, $^2J_{\text{H,P}}$ 4.4 Hz, PCH₃), 1.56 (d, 6H, $^2J_{\text{H,P}}$ 5.3 Hz, PCH₃), 1.47 (d, 6H, $^2J_{\text{H,P}}$ 5.0 Hz, PCH₃), 1.24 (d, 6H, $^2J_{\text{H,P}}$ 4.7 Hz, PCH₃), -14.88 (p, 1H, $^2J_{\text{H,P}}$ 49.3 Hz, MnH). All remaining ^1H NMR signals could not be identified and range from 0.8 to 1.9 ppm. $^{13}\text{C}\{^1\text{H}\}$ NMR (*d*₈-toluene, 151 MHz, 298 K): δ 138.32 (s, *o*), 126.60 (s, *m*), 38.34 (m, PCH₃), 32.89 (m, PCH₃), 24.43 (m, PCH₃), 23.52 (m, PCH₃). $^{31}\text{P}\{^1\text{H}\}$ NMR (*d*₈-toluene, 243 MHz, 298 K): δ 79.84 (br. s, 2P), 78.71 (m, 2P). *Low temperature NMR analysis (signals for the dominant cis, minor cis, and trans isomers could be observed in a 17 : 3 : 1 ratio)*. Selected NMR signals are as follows; ***cis*-22c** (major isomer); ^1H NMR (*d*₈-toluene, 500 MHz, 197 K): δ 8.60 (s, 2H, *o*), 7.44 (t, 2H, $^3J_{\text{H,H}}$ 6.5 Hz, *m*), 7.27 (t, 1H, $^3J_{\text{H,H}}$ 7.9 Hz, *p*), 6.19 (s with ^{29}Si sat., 1H, $^1J_{\text{H,Si}}$ 117.5 Hz, SiH), 3.25 (br. s, 3H, NCH₃), 2.80 (br. s, 3H, NCH₃), 2.08 (m, 3H, PCH₃), 1.90 (s, 3H, PCH₃), 1.80 (s, 3H, PCH₃), 1.47 (s, 3H, PCH₃), 1.39 (s, 3H, PCH₃), 1.23 (s, 3H, PCH₃), 1.19 (s, 3H, PCH₃), 0.9 (br. s, 6H, NCCH₃), 0.61 (s, 3H, PCH₃), -12.47 (m, 1H, MnH). $^{13}\text{C}\{^1\text{H}\}$ NMR (*d*₈-toluene, 126 MHz, 197 K): δ 171.12 (s, NCN), 153.17 (s, *i*), 138.74 (s, *o*), 126.69 (s, *m*), 126.24 (s, *p*), 34.72 (m, NCH₃), 28.30 (m, PCH₃), 26.75 (m, PCH₃), 26.39 (m, PCH₃), 24.90 (m, PCH₃), 23.35 (m, PCH₃), 7.70 (m, NCCH₃), 7.47 (m, NCCH₃). ^{29}Si NMR (*d*₈-toluene, 99 MHz, 197 K): 24.72. $^{31}\text{P}\{^1\text{H}\}$ NMR (*d*₈-toluene, 202 MHz, 197 K): δ 79.51 (br. s, 1P), 77.29 (br. s, 1P), 70.40 (m, 1P), 66.00 (br. s, 1P). ***cis*-22c** (minor isomer); ^1H NMR (*d*₈-toluene, 500 MHz, 197 K): δ 7.88 (d, 2H, $^3J_{\text{H,H}}$ 6.8 Hz, *o*), 7.29 (t, 2H, $^3J_{\text{H,H}}$ 7.8 Hz, *m*), 7.13 (t, 1H, $^3J_{\text{H,H}}$ 6.9 Hz, *p*), 6.16 (s with ^{29}Si sat., 1H, $^1J_{\text{H,Si}}$ 122.5 Hz, SiH), 4.41 (br. s, 3H, NCH₃), 3.09 (br. s, 3H, NCH₃), 1.93 (m, 3H, PCH₃), 1.83 (m, 3H, PCH₃), 1.53 (s, 3H, PCH₃), 1.52 (s, 3H, PCH₃), 1.47 (s, 3H,

PCH₃), 1.40 (m, 3H, PCH₃), 1.27 (s, 3H, PCH₃), 1.13 (s, 3H, PCH₃), -12.20 (m, 1H, MnH). ¹³C{¹H} NMR (*d*₈-toluene, 126 MHz, 197 K): δ 135.67 (s, *o*), 34.90 (m, NCH₃), 28.30 (m, PCH₃), 28.15 (m, PCH₃), 25.87 (m, PCH₃), 23.17 (m, PCH₃). ²⁹Si NMR (*d*₈-toluene, 99 MHz, 197 K): 23.17. ³¹P{¹H} NMR (*d*₈-toluene, 202 MHz, 197 K): δ 80.04 (br. s, 1P), 78.15 (br. s, 1P), 73.59 (br. s, 1P), 66.15 (br. s, 1P). **trans-22c**; ¹H NMR (*d*₈-toluene, 500 MHz, 197 K): δ 8.00 (d, 2H, ³J_{H,H} 6.8 Hz, *o*), 5.96 (m with ²⁹Si sat., 1H, ¹J_{H,Si} 124.2 Hz, SiH), 3.12 (s, 3H, NCH₃), 2.85 (s, 3H, NCH₃), 1.75 (s, 6H, PCH₃), 1.60 (s, 6H, PCH₃), 1.27 (s, 6H, PCH₃), 0.98 (s, 3H, NCCH₃), 0.86 (s, 3H, NCCH₃), -14.57 (p, 1H, ²J_{H,P} 48.9 Hz, MnH). ¹³C{¹H} NMR (*d*₈-toluene, 126 MHz, 197 K): δ 138.17 (*o*), 123.55 (NCCH₃), 33.59 (m, NCH₃), 32.76 (m, NCH₃), 32.03 (PCH₃). ²⁹Si NMR (*d*₈-toluene, 99 MHz, 197 K): 16.63. ³¹P{¹H} NMR (*d*₈-toluene, 202 MHz, 197 K): δ 81.54 (br. s, 2P), 79.67 (s, 2P). **Anal.** Found (calcd.): C, 51.33 (51.19); H, 8.67 (8.76); N, 4.64 (4.78).

[(dmpe)₂MnH{=SiHⁿBu(^{Me}NHC)}] (**22d**). 1,3,4,5-tetramethyl-4-imidazolin-2-ylidene (^{Me}NHC) (50.6 mg, 0.407 mmol) was added to a solution containing 110.8 mg (0.209 mmol) of [(dmpe)₂MnH(SiH₂ⁿBu)₂] (**20^{Bu}**) in 10 mL of benzene. The reaction mixture immediately turned orange and was stirred overnight at room temperature. Following this, the solvent was removed *in vacuo* and the resulting red oil was dissolved again in 10 mL of benzene and stirred again overnight at room temperature. The solvent was again removed *in vacuo*, following which the resulting red oil was dissolved in hexanes. After a couple of minutes, a brown solid precipitated which contains a mixture of [(dmpe)₂MnH{=SiHⁿBu(^{Me}NHC)}] (**22d**) and ^{Me}NHC, which could be removed by centrifugation. The mother liquor was allowed to stand at -30 °C for a month, yielding 20.9 mg (0.037 mmol, 18%) of pure [(dmpe)₂MnH{=SiHⁿBu(^{Me}NHC)}] (**22d**) as a very dark red solid. *Elevated temperature NMR analysis (one set of signals are the average of chemical shifts for the two cis isomers, and another are from the trans isomer, with a 2 : 1 ratio)*: Selected NMR signals are as follows; **cis-22d**; ¹H NMR (*d*₈-toluene, 500 MHz, 333 K): δ 5.17 (s with ²⁹Si sat., 1H, ¹J_{H,Si} 124.4 Hz, SiH), 3.71 (br. s, 6H, NCH₃), 0.96 (m, 2H, SiCH₂CH₂CH₂CH₃), 0.91 (t, 3H, ³J_{H,H} 7.3 Hz, SiCH₂CH₂CH₂CH₃), -12.62 (p,

1H, $^2J_{\text{H,P}}$ 33.4 Hz, MnH). All remaining ^1H NMR signals could not be identified and range from 0.6 to 1.8 ppm. ^{29}Si NMR (*d*₈-toluene, 99 MHz, 333 K): δ 28.97. $^{31}\text{P}\{^1\text{H}\}$ NMR (*d*₈-toluene, 202 MHz, 333 K): δ 75.90 (br. s). *trans*-22d; ^1H NMR (*d*₈-toluene, 500 MHz, 333 K): δ 4.85 (m with ^{29}Si sat., 1H, $^1J_{\text{H,Si}}$ 122.2 Hz, $^3J_{\text{H,H}}$ 3.9 Hz, SiH), 3.26 (br. s, 6H, NCH₃), 0.89 (t, 3H, $^3J_{\text{H,H}}$ 7.2 Hz, SiCH₂CH₂CH₂CH₃), 0.80 (m, 1H, SiCH₂CH₂CH₂CH₃), 0.70 (m, 1H, SiCH₂CH₂CH₂CH₃), -15.07 (p, 1H, $^2J_{\text{H,P}}$ 48.4 Hz, MnH). All remaining ^1H NMR signals could not be identified and range from 0.6 to 1.8 ppm. ^{29}Si NMR (*d*₈-toluene, 99 MHz, 333 K): δ 22.75. $^{31}\text{P}\{^1\text{H}\}$ NMR (*d*₈-toluene, 202 MHz, 333 K): δ 79.87 (br. s, 2P), 79.21 (br. s, 2P). Room temperature NMR analysis (signals due to the *cis* isomers are in the process of decoalescing, and one set of sharp signals is observed due to the *trans* isomer; a 2 : 1 ratio is observed at room temperature between the sum of the two *cis* isomers and the *trans* isomer). Selected NMR signals are as follows; *cis*-22d; ^1H NMR (*d*₈-toluene, 500 MHz, 298 K): δ 5.18 (br. s, 1H, SiH), 3.70 (s, 6H, NCH₃), 1.29 (s, 6H, NCC₃), 0.95 (t, 3H, $^3J_{\text{H,H}}$ 7.3 Hz, SiCH₂CH₂CH₂CH₃), -12.54 (p, 1H, $^2J_{\text{H,P}}$ 33.3 Hz, MnH). $^{13}\text{C}\{^1\text{H}\}$ NMR (*d*₈-toluene, 126 MHz, 298 K): δ 172.49 (s, N₂CN), 124.34 (s, N₂CC), 36.06 (s, one of SiCH₂CH₂CH₂CH₃), 34.22 (s, NCH₃), 14.55 (s, SiCH₂CH₂CH₂CH₃), 27.74 (s, one of SiCH₂CH₂CH₂CH₃), 26.04 (s, one of SiCH₂CH₂CH₂CH₃), 7.96 (s, NCC₃). $^{29}\text{Si}\{^1\text{H}\}$ NMR (*d*₈-toluene, 99 MHz, 298 K): δ 28.66. $^{31}\text{P}\{^1\text{H}\}$ NMR (*d*₈-toluene, 202 MHz, 298 K): δ 78 (br. m, 1P), 74.80 (br. s, 1P), 67.05 (br. s, 1P), 65.49 (br. s, 1P). *trans*-22d; ^1H NMR (*d*₈-toluene, 500 MHz, 298 K): δ 4.87 (s with ^{29}Si sat., 1H, $^1J_{\text{H,Si}}$ 121.7 Hz, $^3J_{\text{H,H}}$ 6.5 Hz, SiH), 3.23 (s, 3H, NCH₃), 3.20 (s, 3H, NCH₃), 1.58 (d, 6H, $^2J_{\text{H,P}}$ 4.2 Hz, PCH₃), 1.54 (d, 6H, $^2J_{\text{H,P}}$ 4.9 Hz, PCH₃), 1.49 (d, 6H, $^2J_{\text{H,P}}$ 5.1 Hz, PCH₃), 1.46 (m, 2H, SiCH₂CH₂CH₂CH₃), 1.40 (d, 6H, $^2J_{\text{H,P}}$ 4.3 Hz, PCH₃), 1.35 (s, 3H, NCC₃), 1.26 (s, 3H, NCC₃), 0.93 (m, 2H, SiCH₂CH₂CH₂CH₃), 0.93 (t, 3H, $^3J_{\text{H,H}}$ 7.2 Hz, SiCH₂CH₂CH₂CH₃), 0.83 (m, 1H, SiCH₂CH₂CH₂CH₃), 0.72 (m, 1H, SiCH₂CH₂CH₂CH₃), -14.98 (p, 1H, $^2J_{\text{H,P}}$ 48.1 Hz, MnH). $^{13}\text{C}\{^1\text{H}\}$ NMR (*d*₈-toluene, 126 MHz, 298 K): δ 175.86 (s, N₂CN), 124.46 (s, N₂CC), 123.66 (s, N₂CC), 36.52 (s, SiCH₂CH₂CH₂CH₃), 35.17 (m, PCH₂), 33.71 (s, NCH₃), 33.63 (s, NCH₃), 33.54 (m, PCH₃), 32.84 (m, PCH₃), 27.71 (s,

SiCH₂CH₂CH₂CH₃), 26.40 (s, SiCH₂CH₂CH₂CH₃), 24.23 (s, PCH₃), 24.13 (s, PCH₃), 14.55 (s, SiCH₂CH₂CH₂CH₃), 8.10 (s, NCCH₃), 7.65 (s, NCCH₃). ²⁹Si{¹H} NMR (*d*₈-toluene, 99 MHz, 298 K): δ 22.44. ³¹P{¹H} NMR (*d*₈-toluene, 202 MHz, 298 K): δ 80.63 (m, 2P), 79.84 (m, 2P). *Low temperature NMR analysis (signals for the two cis isomers and the trans isomer could be observed in a 1 : 1 : 1 ratio)*. Selected NMR signals are as follows; *cis-22d* (includes both *cis* isomers); ¹H NMR (*d*₈-toluene, 500 MHz, 207 K): δ 5.39 (d with ²⁹Si sat., 1H, ³J_{H,P} 13.3 Hz, ¹J_{H,Si} 127.0 Hz, SiH), 5.14 (br. s with ²⁹Si sat., 1H, ³J_{H,H} 6.5 Hz, ¹J_{H,Si} 122 Hz, SiH), 4.01 (s, 3H, NCH₃), 3.93 (br. s, 3H, NCH₃), 3.39 (br. s, 3H, NCH₃), 3.37 (s, 3H, NCH₃), 1.89 (br. s, 3H, PCH₃), 1.89 (br. s, 3H, PCH₃), 1.81 (br. s, 3H, PCH₃), 1.76 (br. s, 3H, PCH₃), 1.72 (br. s, 3H, PCH₃), 1.63 (br. s, 3H, PCH₃), 1.50 (br. s, 3H, PCH₃), 1.50 (br. s, 3H, PCH₃), 1.43 (br. s, 3H, PCH₃), 1.43 (br. s, 3H, PCH₃), 1.43 (br. s, 3H, PCH₃), 1.13 (m, 2H, SiCH₂CH₂CH₂CH₃), 1.10 (br. s, 3H, NCCCH₃), 1.08 (m, 2H, SiCH₂CH₂CH₂CH₃), 1.05 (t, 3H, ³J_{H,H} 7.2 Hz, SiCH₂CH₂CH₂CH₃), 1.04 (t, 3H, ³J_{H,H} 7.5 Hz, SiCH₂CH₂CH₂CH₃), 0.93 (s, 3H, NCCCH₃), 0.83 (br. s, 3H, PCH₃), -12.22 (m, 1H, MnH), -12.36 (m, 1H, MnH). ¹³C{¹H} NMR (*d*₈-toluene, 126 MHz, 207 K): δ 171.27 (s, NCN), 124.58 (NCC), 123.39 (s, NCC), 34.41 (s, NCH₃), 33.56 (s, NCH₃), 29.31 (s, PCH₃), 28.41 (s, SiCH₂CH₂CH₂CH₃), 28.41 (s, SiCH₂CH₂CH₂CH₃), 28.41 (s, PCH₃), 28.18 (s, PCH₃), 28.07 (s, PCH₃), 27.88 (s, PCH₃), 27.46 (m, PCH₃), 26.78 (m, PCH₃), 25.89 (s, PCH₃), 24.15 (s, PCH₃), 21.02 (s, PCH₃), 14.96 (s, SiCH₂CH₂CH₂CH₃), 14.93 (s, SiCH₂CH₂CH₂CH₃), 7.91 (s, NCCH₃), 7.48 (s, NCCH₃). ²⁹Si NMR (*d*₈-toluene, 99 MHz, 207 K): δ 28.07. ³¹P{¹H} NMR (*d*₈-toluene, 202 MHz, 298 K): δ 79.5 (1P), 78.67 (br. s, 1P), 77.28 (br. s, 1P), 76.40 (br. s, 1P), 74.45 (br. s, 1P), 73.12 (d, ²J_{P,P} 33.2 Hz, 1P), 66.97 (br. s, 1P), 65.04 (br. s, 1P). *trans-22d*; ¹H NMR (*d*₈-toluene, 500 MHz, 207 K): δ 4.99 (br. s with ²⁹Si sat., 1H, ³J_{H,H} 6.5 Hz, ¹J_{H,Si} 116 Hz, SiH), 3.06 (s, 3H, NCH₃), 3.01 (s, 3H, NCH₃), 1.76 (s, 6H, PCH₃), 1.72 (s, 6H, PCH₃), 1.63 (s, 6H, PCH₃), 1.47 (s, 6H, PCH₃), 1.15 (s, 3H, NCCCH₃), 1.03 (t, 3H, ³J_{H,H} 7.0 Hz, SiCH₂CH₂CH₂CH₃), 0.98 (m, 2H, SiCH₂CH₂CH₂CH₃), 0.96 (s, 3H, NCCCH₃), -14.67 (p, 1H, ²J_{H,P} 46.6 Hz, MnH). ¹³C{¹H} NMR (*d*₈-toluene, 126 MHz, 207 K): δ 174.12 (s, NCN), 124.21 (s, NCC), 123.18 (s, NCC), 33.28 (s, PCH₃), 33.15 (s, NCH₃),

32.19 (s, P \underline{C} H₃), 28.41 (s, SiCH₂CH₂ \underline{C} H₂CH₃), 24.08 (s, P \underline{C} H₃), 23.29 (s, P \underline{C} H₃), 15.03 (s, SiCH₂CH₂CH₂ \underline{C} H₃), 7.88 (s, NC \underline{C} H₃), 7.48 (s, NC \underline{C} H₃). ²⁹Si NMR (*d*₈-toluene, 99 MHz, 207 K): δ 22.71. ³¹P{¹H} NMR (*d*₈-toluene, 202 MHz, 207 K): δ 80.35 (m, 2P), 79.40 (m, 2P). Indeterminate: ¹³C{¹H} NMR (*d*₈-toluene, 126 MHz, 207 K): δ 36.97 (s), 36.83 (s), 36.36 (s), 35.07 (s), 32.10 (s), 27.14 (s), 26.52 (s). Anal. Found (calcd.): C, 48.72 (48.75); H, 9.65 (9.78); N, 4.80 (4.94).

Reaction of [(dmpe)₂MnH{=SiHⁿBu(ⁱPrNHC)}] (22b) with ethylene. Approx. 15 mg of [(dmpe)₂MnH{=SiHⁿBu(ⁱPrNHC)}] (22b) was dissolved in approx. 0.6 mL of C₆D₆, and the solution was freeze-pump-thawed (×3). The resulting solution was placed under an atmosphere of ethylene gas, cooled to -95 °C, and sealed at this low temperature. The solution was then monitored over time at room temperature by ¹H NMR spectroscopy *in situ*; after 24 h, complete consumption of 22b was observed and the reaction mixture contained approx. 1% 10, 72% 19^{Bu,H}, 23% 19^{Bu,Et}, and 4% of an unidentified MnH-containing species.

11.6 – Synthetic Procedures and Characterization Pertaining to the Work of Chapter 6

Various data is available in the ESI to reference 507, including selected NMR spectra of 18^{R2}. Various data is available in the ESI to reference 510, including selected NMR spectra (for 18^R), selected IR spectra, symbolic pulse sequences and parameters used for new COSY-type NMR experiments, tables of calculated and crystallographically determined bond lengths and angles, bond orders, Hirshfeld charges, and total bonding energies for calculated structures and PH₃ analogues. The identification numbers in this chapter of the thesis (X→Y) relate to those in reference 507 (X→Y) in the following manner; 10→1, 16^{Ph2}→2b, 16^{Et2}→2a, 18^{Ph2}→3b, 18^{Et2}→3a. The identification numbers in this chapter of the thesis (X→Y) relate to those in reference 510 (X→Y) in the following manner; 10→1, 18^{Ph2}→3a, 18^{Et2}→3b, 18^{Ph}→4a, 18^{Bu}→4b, 20^{Ph}→2a, and

20^{Bu}→2b. CSD 1529216 and 1896287-1896288 contain the supplementary crystallographic data for **18^{Ph2}**, **18^{Ph}**, and **18^{Bu}**.

Syntheses and selected characterization data for **18^{Ph2}** and **18^{Et2}** can be found in section 11.4.

[(dmpe)₂MnH₂(SiH₂Ph)] (18^{Ph}). 209.5 mg (0.367 mmol) of **[(dmpe)₂MnH(SiH₂Ph)₂] (20^{Ph})** was dissolved in 10 mL of benzene. The reaction mixture was freeze/pump/thawed in a 50 mL storage flask three times, and then was placed under 1 atm of H₂ at -95 °C, sealed, and warmed to room temperature. After stirring at room temperature for 2 days, the solvent was removed *in vacuo*. The resulting yellow solid was recrystallized from a concentrated solution of hexanes at -30 °C giving a yellow powder which was dried *in vacuo*; 111.1 mg. Concentrating the mother liquor and leaving it at -30 °C yielded an additional 20.9 mg of **18^{Ph}**, for a total yield of 132.0 mg (0.284 mmol, 77 %). X-ray quality crystals were obtained from hexanes. **¹H NMR (*d*₈-toluene, 600 MHz, 298 K):** δ 8.00 (br. s, 2H, *o*-ph), 7.29 (t, 2H, ³J_{H,H} 7.4 Hz, *m*-ph), 7.18 (t, 1H, ³J_{H,H} 7.1 Hz, *p*-ph), 5.45 (br. s, 2H, SiH), 1.5–0.9 (br. singlets, 32H, PCH₃ and PCH₂), -12.54 (br. s, 1H, MnH). **¹³C{¹H} NMR (*d*₈-toluene, 151 MHz, 298 K):** δ 135.83 (s, *o*-ph), 127.28 (s, *m*-ph), 126.82 (s, *p*-ph), 33.13 (br. s.). **³¹P{¹H} NMR (*d*₈-toluene, 202 MHz, 298 K):** δ 76.69 (br. s). ***central-18^{Ph}*: ¹H NMR (*d*₈-toluene, 500 MHz, 186 K):** δ 8.37 (d, 2H, ³J_{H,H} 7.2 Hz, *o*-ph), 7.49 (t, 2H, ³J_{H,H} 7.2 Hz, *m*-ph), 7.34 (t, 1H, ³J_{H,H} 7.0 Hz, *p*-ph), 6.10 (s with ²⁹Si sat., 1H, ¹J_{Si,H} 171.4 Hz, SiH), 6.02 (t with ²⁹Si sat., 1H, ³J_{H,P} 9.5 Hz, ¹J_{Si,H} 175.6 Hz, SiH), 0.8-1.5 (various m, 8H, PCH₂), 1.39 (d, 6H, ²J_{H,P} 2.9 Hz, PCH₃), 1.30 (s, 6H, PCH₃), 0.96 (s, 6H, PCH₃), 0.74 (s, 6H, PCH₃), -12.83 (m, 2H, MnH). **¹³C{¹H} NMR (*d*₈-toluene, 126 MHz, 207 K):** δ 151.39 (s, *i*-ph), 135.59 (s, *o*-ph), 127.30 (s, *m*-ph), 127.04 (s, *p*-ph), 33.44 (m, PCH₂), 32.35 (m, PCH₂), 30.13 (t, J_{C,P} 15 Hz, PCH₃), 22.56 (s, PCH₃), 22.30 (d, ²J_{C,P} 16 Hz, PCH₃), 21.57 (m, PCH₃). **²⁹Si{¹H} NMR (*d*₈-toluene, 119 MHz, 226 K):** δ -15.73 (s). **³¹P{¹H} NMR (*d*₈-toluene, 202 MHz, 186 K):** δ 73.98 (br. s, 2P), 72.38 (br. s, 2P). ***transHSi-18^{Ph}*: ¹H NMR (*d*₈-toluene, 500 MHz, 186 K):** δ 8.15 (d, 2H, ³J_{H,H} 7.1 Hz, *o*-ph), 7.40 (t, 2H, ³J_{H,H} 7.1 Hz,

m-ph), 7.25 (t, 1H, $^3J_{\text{H,H}}$ 7.1 Hz, *p*-ph), 5.46 (s with ^{29}Si sat., 2H, $^1J_{\text{Si,H}}$ 155.0 Hz, SiH), 0.8-1.5 (various m, 8H, PCH₂), 1.34 (s, 12H, PCH₃), 1.07 (s, 12H, PCH₃), -10.88 (p, 1H, $^2J_{\text{H,P}}$ 53.9 Hz, MnH), -12.66 (p, 1H, $^2J_{\text{H,P}}$ 23.1 Hz, MnH). $^{13}\text{C}\{^1\text{H}\}$ NMR (C₆D₆, 126 MHz, 207 K): δ 149.71 (s, *i*-ph), 135.95 (s, *o*-ph), 127.30 (s, *m*-ph), 126.80 (s, *p*-ph), 32.25 (m, PCH₂), 27.73 (m, PCH₃), 20.8 (PCH₃). $^{29}\text{Si}\{^1\text{H}\}$ NMR (*d*₈-toluene, 119 MHz, 226 K): δ -1.63 (m). $^{31}\text{P}\{^1\text{H}\}$ NMR (*d*₈-toluene, 202 MHz, 186 K): δ 77.85 (s). IR: ν (SiH, MnH) (Nujol, cm⁻¹): 1808, 1973, 2025, 2056. ν (SiH, MnH) (hexanes, cm⁻¹): 1738, 1756, 1811, 1990, 2014. Anal. Found (calcd.): C, 46.72 (46.55); H, 8.85 (8.90).

[(dmpe)₂MnH₂(SiH₂ⁿBu)] (**18^{Bu}**). 108.9 mg (0.205 mmol) of [(dmpe)₂MnH(SiH₂ⁿBu)₂] (**20^{Bu}**) was dissolved in 10 mL of benzene. The reaction mixture was freeze/pump/thawed in a 50 mL storage flask three times, and then was placed under 1 atm of H₂ at -95 °C, sealed, and warmed to room temperature. After stirring at room temperature for 3 days, the solvent was removed *in vacuo*. The resulting yellow solid was recrystallized from a concentrated solution of hexanes at -30 °C and dried *in vacuo* to afford a yellow powder. Yield = 41.6 mg (0.094 mmol, 46 %). X-ray quality crystals were obtained from a dilute solution in hexanes at -30 °C. ^1H NMR (*d*₈-toluene, 600 MHz, 298 K): δ 4.65 (br. s, 2H, SiH), 1.76 (p, 2H, $^3J_{\text{H,H}}$ 7.6 Hz, SiH₂CH₂CH₂CH₂CH₃), 1.58 (s, 2H, $^3J_{\text{H,H}}$ 7.4 Hz, SiH₂CH₂CH₂CH₂CH₃), 1.34 (br. s, 8H, PCH₂), 1.23 (br. s, 24H, PCH₃), 1.04 (t, 3H, $^3J_{\text{H,H}}$ 7.3 Hz, SiH₂CH₂CH₂CH₂CH₃), 0.89 (br. s, 2H, SiH₂CH₂CH₂CH₂CH₃), -12.54 (br. s, 2H, MnH). $^{13}\text{C}\{^1\text{H}\}$ NMR (*d*₈-toluene, 151 MHz, 298 K): δ 33.24 (br. s, PCH₂), 32.86 (s, SiH₂CH₂CH₂CH₂CH₃), 27.07 (s, SiH₂CH₂CH₂CH₂CH₃), 14.60 (s, SiH₂CH₂CH₂CH₂CH₃). ^{31}P NMR (*d*₈-toluene, 243 MHz, 298 K): δ 76.51 (s). *central-18^{Bu}*: ^1H NMR (*d*₈-toluene, 500 MHz, 207 K): δ 5.39 (s with ^{29}Si sat., 1H, $^1J_{\text{Si,H}}$ 160.4 Hz, SiH), 5.24 (s with ^{29}Si sat., 1H, $^1J_{\text{Si,H}}$ 168.4 Hz, SiH), 2.01 (m, 2H, SiH₂CH₂CH₂CH₂CH₃), 1.77 (m, 2H, SiH₂CH₂CH₂CH₂CH₃), 1.41 (s, 6H, PCH₃), 1.40 (m, 2H, PCH₂), 1.36 (m, 1H, SiH₂CH₂CH₂CH₂CH₃), 1.26 (s, 6H, PCH₃), 1.21 (m, 2H, PCH₂), 1.18 (s, 6H, PCH₃), 1.18 (m, 1H, SiH₂CH₂CH₂CH₂CH₃), 1.18 (t, 3H, $^3J_{\text{H,H}}$ 7.4 Hz, SiH₂CH₂CH₂CH₂CH₃), 0.99 (m, 2H, PCH₂), 0.88 (m, 2H, PCH₂), 0.79 (s, 6H, PCH₃), -12.75 (m, 2H, MnH). $^{13}\text{C}\{^1\text{H}\}$

NMR (*d*₈-toluene, 126 MHz, 207 K): δ 33.46 (m, PCH₂), 32.37 (m, PCH₂), 32.37 (s, SiH₂CH₂CH₂CH₂CH₃), 30.48 (m, PCH₃), 27.49 (s, SiH₂CH₂CH₂CH₂CH₃), 27.49 (s, SiH₂CH₂CH₂CH₂CH₃), 22.64 (s, PCH₃), 22.25 (m, PCH₃), 15.04 (s, SiH₂CH₂CH₂CH₂CH₃). **²⁹Si{¹H} NMR (*d*₈-toluene, 119 MHz, 207 K):** δ -22.00. **³¹P{¹H} NMR (*d*₈-toluene, 243 MHz, 205 K):** δ 74.06 (br. s, 2P), 72.05 (br. s, 2P). ***transHSi-18*^{Bu}: ¹H NMR (*d*₈-toluene, 500 MHz, 207 K):** δ 4.72 (s with ²⁹Si sat., 2H, ¹J_{Si,H} 151.7 Hz, SiH), 1.92 (m, 2H, SiH₂CH₂CH₂CH₂CH₃), 1.69 (m, 2H, ³J_{H,H} 7.3 Hz, SiH₂CH₂CH₂CH₂CH₃), 1.56 (br. s, 4H, PCH₂), 1.36 (s, 12H, PCH₃), 1.26 (br. s, 4H, PCH₂), 1.12 (s, 12H, PCH₃), 1.12 (t, 3H, ³J_{H,H} 7.3 Hz, SiH₂CH₂CH₂CH₂CH₃), 0.99 (m, 2H, SiH₂CH₂CH₂CH₂CH₃), -11.25 (p, 1H, ²J_{H,P} 51.5 Hz, MnH), -13.28 (p, 1H, ²J_{H,P} 23.0 Hz, MnHSi). **¹³C{¹H} NMR (*d*₈-toluene, 126 MHz, 207 K):** δ 33.46 (s, SiH₂CH₂CH₂CH₂CH₃), 32.37 (m, PCH₂), 27.62 (s, SiH₂CH₂CH₂CH₂CH₃), 27.49 (s, PCH₃), 22.82 (s, SiH₂CH₂CH₂CH₂CH₃), 20.78 (s, PCH₃), 14.91 (s, SiH₂CH₂CH₂CH₂CH₃). **²⁹Si{¹H} NMR (*d*₈-toluene, 119 MHz, 207 K):** -6.91. **³¹P{¹H} NMR (*d*₈-toluene, 243 MHz, 205 K):** 77.48 (s). **IR:** ν (SiH, MnH) (Nujol, cm⁻¹): 1740, 1965, 1995. ν (SiH, MnH) (hexanes, cm⁻¹): 1737, 1830, 1983, 2013. **Anal.** Found (calcd.): C, 43.39 (43.24); H, 9.94 (10.20).

[(dmpe)₂MnD₂(SiH₂R)] (*d*₂-18**^{Ph}: R = Ph, *d*₂-**18**^{Bu}: R = ⁿBu). Roughly 10 mg of the manganese-containing precursor used to synthesize the fully protonated complexes {for **18**^{Ph} [(dmpe)₂MnH(SiH₂Ph)₂] (**20**^{Ph}) and for **18**^{Bu} [(dmpe)₂MnH(SiH₂ⁿBu)₂] (**20**^{Bu})} was dissolved in roughly 0.6 mL of C₆D₆. The reaction mixture was freeze/pump/thawed in a J-young NMR tube three times, and then was placed under 1 atm of D₂ at -95 °C, sealed, and warmed to room temperature and then allowed to sit at room temperature for the reaction times required to prepare the protio analogues. The deuterated complexes were isolated from free hydrosilane byproducts on the NMR scale by removing the solvent and hydrosilane *in vacuo*, and used without further purification. NMR spectra of *d*₂-**18**^{Ph} and *d*₂-**18**^{Bu} differ from the protonated analogues by the absence of peaks in the ¹H NMR spectra corresponding to the MnH environments.**

11.7 – Synthetic Procedures and Characterization Pertaining to the Work of Chapter 7

Tables of calculated and crystallographically determined bond lengths and angles, tables of bond orders, Hirshfeld charges, and total bonding energies for calculated structures and selected NMR spectra for **25^{Ph,H}**, **25^{Bu,H}**, and **26** can be found in Appendix 1. Crystal structures in this chapter have not yet been submitted to the CSD.

[(dmpe)₂Mn{κ²-SiHPh(NⁱPrCHNⁱPr)}] (25^{Ph,H}). An excess of diisopropylcarbodiimide {C(NⁱPr)₂} (67 mg, 0.531 mmol) was added to a solution containing 60.4 mg (0.106 mmol) of [(dmpe)₂MnH(SiH₂Ph)₂] (**20^{Ph}**) in 8 mL of benzene. The reaction mixture was stirred in a sealed flask at 65 °C for two days, leading to a bright red solution which turned a clear orange upon cooling to room temperature. The solvent was then removed *in vacuo*. The resulting orange solid was recrystallized from a concentrated solution of hexanes layered with hexamethyldisiloxane at –30 °C giving a yield of 55.8 mg (0.095 mmol, 90%). X-ray quality crystals were obtained from a saturated solution of **25^{Ph,H}** in hexanes layered with hexamethyldisiloxane at –30 °C.

Dominant isomer: ¹H NMR (C₆D₆, 600 MHz, 298 K): δ 8.09 (d, 2H, ³J_{H,H} 6.8 Hz, *o*), 7.67 (s with shoulders, 1H, NC(H)N), 7.34 (t, 2H, ³J_{H,H} 7.6 Hz, *m*), 7.24 (t, 1H, ³J_{H,H} 7.3 Hz, *p*), 6.26 (d of d with ²⁹Si sat., 1H, ³J_{H,P} 17.9 Hz, ³J_{H,P} 8.0 Hz, ¹J_{H,Si} 136.5, SiH), 3.45 (septet, 1H, ³J_{H,H} 6.8 Hz, C_γH(CH₃)₂), 2.91 (septet, 1H, ³J_{H,H} 6.6 Hz, C_βH(CH₃)₂), 1.99 (m, 1H, PCH₂), 1.83–1.37 (m, 6H, PCH₂), 1.47 (d, 3H, ³J_{H,P} 6.2 Hz, PCH₃), 1.45 (d, 3H, ³J_{H,P} 5.5 Hz, PCH₃), 1.39 (d, 3H, ³J_{H,P} 4.3 Hz, PCH₃), 1.33 (d, 3H, ³J_{H,P} 3.1 Hz, PCH₃), 1.17 (m, 9H, PCH₃), 1.06 (d, 3H, ³J_{H,H} 6.7 Hz, CH(CH₃)₂), 1.02 (d, 3H, ³J_{H,H} 6.8 Hz, CH(CH₃)₂), 0.99 (d, 3H, ³J_{H,H} 6.7 Hz, CH(CH₃)₂), 0.94 (d, 3H, ³J_{H,H} 6.5 Hz, CH(CH₃)₂), 0.78 (m, 1H, PCH₂), 0.73 (d, 3H, ³J_{H,P} 4.7 Hz, PCH₃).

¹³C{¹H} NMR (C₆D₆, 151 MHz, 298 K): δ 159.93 (s, NC(H)N), 153.11 (s, *ipso*), 137.37 (s, *o*), 127.01 (s, *m*), 126.66 (s, *p*), 59.53 (d, ⁴J_{C,P} 8.7 Hz, C_βH(CH₃)₂), 50.08 (s, C_γ(CH₃)₂), 35.24 (m, PCH₂), 29.90 (d, ¹J_{C,P} 16.6 Hz, PCH₃), 29.11 (d of d, ¹J_{C,P} 26.5 Hz, ³J_{C,P} 15.7 Hz, PCH₂), 26.96 (m, PCH₃), 26.12 (s, CH(CH₃)₂), 24.46 (s, CH(CH₃)₂), 24.37 (s, PCH₃), 24.34 (s,

CH(CH₃)₂), 24.26 (s, CH(CH₃)₂), 23.87 (s, PCH₃), 23.73 (d, ¹J_{C,P} 4.8 Hz, PCH₃), 20.51 (m, PCH₃), 13.40 (d, ¹J_{C,P} 11.8 Hz, PCH₃). ²⁹Si{¹H} NMR (C₆D₆, 119 MHz, 298 K): δ 81.11 (m). ³¹P{¹H} NMR (C₆D₆, 243 MHz, 298 K): δ 74.49 (s, 1P), 72.09 (s, 1P), 66.19 (s, 1P), 55.10 (s, 1P). **Minor isomer:** ¹H NMR (C₆D₆, 600 MHz, 298 K): δ 8.22 (d, 2H, ³J_{H,H} 7.8 Hz, *o*), 7.70 (s, 1H, NC(H)N), 7.37 (t, 2H, ³J_{H,H} 7.4 Hz, *m*), 7.24 (t, 1H, ³J_{H,H} 7.2 Hz, *p*), 6.23 (d of d with ²⁹Si sat., 1H, ³J_{H,P} 27.6 Hz, ³J_{H,P} 9.5 Hz, ¹J_{H,Si} 140.1, SiH), 3.48 (septet, 1H, ³J_{H,H} 6.8 Hz, CH(CH₃)₂), 3.07 (septet, 1H, ³J_{H,H} 6.7 Hz, CH(CH₃)₂), 1.94–0.72 (many multiplets, 8H, PCH₂), 1.72 (d, 3H, ³J_{H,P} 6.0 Hz, PCH₃), 1.53 (d, 3H, ³J_{H,P} 4.9 Hz, PCH₃), 1.32 (3H, PCH₃), 1.28 (d, 3H, ³J_{H,P} 4.2 Hz, PCH₃), 1.24 (d, 3H, ³J_{H,P} 2.9 Hz, PCH₃), 1.24 (d, 3H, ³J_{H,P} 2.8 Hz, PCH₃), 1.08 (d, 3H, ³J_{H,P} 5.3 Hz, PCH₃), 1.04 (d, 3H, ³J_{H,H} 6.9 Hz, CH(CH₃)₂), 1.03 (d, 3H, ³J_{H,H} 6.9 Hz, CH(CH₃)₂), 1.01 (d, 3H, ³J_{H,H} 6.8 Hz, CH(CH₃)₂), 0.88 (d, 3H, ³J_{H,H} 6.5 Hz, CH(CH₃)₂), 0.77 (d, 3H, ³J_{H,P} 4.2 Hz, PCH₃). ¹³C{¹H} NMR (C₆D₆, 151 MHz, 298 K): δ 159.93 (s, NC(H)N), 153.11 (s, *ipso*), 137.68 (s, *o*), 127.37 (s, *m*), 126.66 (s, *p*), 59.39 (d, ⁴J_{C,P} 8.3 Hz, CH(CH₃)₂), 50.02 (s, C(CH₃)₂), 36.32 (m, PCH₂), 34.28 (d of d, ¹J_{C,P} 25.0 Hz, ³J_{C,P} 13.4 Hz, PCH₂), 32.40 (m, PCH₂), 30.45 (d, ¹J_{C,P} 10.7 Hz, PCH₃), 26.54 (m, PCH₃), 26.35 (s, PCH₃), 26.16 (s, CH(CH₃)₂), 24.95 (s, PCH₃), 24.64–24.19 (m, CH(CH₃)₂), 24.12 (s, PCH₃), 22.06 (d, ¹J_{C,P} 10.0 Hz, PCH₃), 21.26 (m, PCH₃), 13.62 (m, PCH₃). ²⁹Si{¹H} NMR (C₆D₆, 119 MHz, 298 K): δ 81.11 (m). ³¹P{¹H} NMR (C₆D₆, 243 MHz, 298 K): δ 72.09 (s, 2P), 69.03 (s, 1P), 56.00 (s, 1P). **Anal.** Found (calcd.): C, 51.09 (51.01); H, 9.28 (9.08); N, 4.74 (4.76).

[(dmpe)₂Mn{κ²-SiHⁿBu(NⁱPrCHNⁱPr)}] (**25^{Bu,H}**). An excess of diisopropylcarbodiimide {C(NⁱPr)₂} (165 mg, 1.307 mmol) was added to a solution containing 135.5 mg (0.255 mmol) of [(dmpe)₂MnH(SiH₂ⁿBu)₂] (**20^{Bu}**) in 10 mL of benzene. The reaction mixture was stirred in a sealed flask overnight at room temperature, after which the solvent was removed *in vacuo*. The resulting orange solid was recrystallized from a concentrated solution of **25^{Bu,H}** in hexanes giving a yield of 35.3 mg (0.062 mmol, 24%). X-ray quality crystals could not be obtained. **Dominant isomer:** ¹H NMR (C₆D₆, 600 MHz, 298 K): δ 7.58 (s, 1H, NC(H)N), 5.50 (d of d with

^{29}Si sat., 1H, $^3J_{\text{H,P}}$ 24.2 Hz, $^3J_{\text{H,P}}$ 9.3 Hz, $^1J_{\text{H,Si}}$ 136.5 Hz, SiH, 3.81 (septet, 1H, $^3J_{\text{H,H}}$ 6.8 Hz, CH(CH₃)₂), 3.09 (septet, 1H, $^3J_{\text{H,H}}$ 6.7 Hz, CH(CH₃)₂), 0.9-2.1 (various m, 8H, PCH₂), 1.95 (m, 2H, SiHCH₂CH₂CH₂CH₃), 1.65 (m, 2H, SiHCH₂CH₂CH₂CH₃), 1.45 (d, 3H, $^2J_{\text{H,P}}$ 5.8 Hz, PCH₃), 1.44 (d, 3H, $^2J_{\text{H,P}}$ 5.7 Hz, PCH₃), 1.38 (d, 3H, $^2J_{\text{H,P}}$ 4.9 Hz, PCH₃), 1.32 (d, 3H, $^2J_{\text{H,P}}$ 3.9 Hz, PCH₃), 1.24 (d, 3H, $^2J_{\text{H,P}}$ 2.5 Hz, PCH₃), 1.21 (d, 3H, $^3J_{\text{H,H}}$ 6.8 Hz, CH(CH₃)₂), 1.18 (d, 3H, $^2J_{\text{H,P}}$ 5.7 Hz, PCH₃), 1.18 (d, 3H, $^3J_{\text{H,H}}$ 6.6 Hz, CH(CH₃)₂), 1.13 (m, 5H, SiHCH₂CH₂CH₂CH₃ and SiHCH₂CH₂CH₂CH₃), 1.11 (d, 3H, $^2J_{\text{H,P}}$ 4.2 Hz, PCH₃), 0.97 (d, 3H, $^3J_{\text{H,H}}$ 6.9 Hz, CH(CH₃)₂), 0.86 (d, 3H, $^2J_{\text{H,P}}$ 4.4 Hz, PCH₃), 0.83 (d, 3H, $^3J_{\text{H,H}}$ 6.6 Hz, CH(CH₃)₂). $^{13}\text{C}\{^1\text{H}\}$ NMR (C₆D₆, 151 MHz, 298 K): δ 159.10 (s, NC(H)N), 58.81 (s, CH(CH₃)₂), 50.28 (s, CH(CH₃)₂), 36.28 (app. q, $^1J_{\text{C,P}}$ 20 Hz, PCH₂), 35.48 (s, SiHCH₂CH₂CH₂CH₃), 34.17 (d of d, $^1J_{\text{C,P}}$ 24.5 Hz, $^2J_{\text{C,P}}$ 13.1 Hz, PCH₂), 31.87 (d of d, $^1J_{\text{C,P}}$ 22.7 Hz, $^2J_{\text{C,P}}$ 17.5 Hz, PCH₂), 28.21 (m, PCH₃), 28.13 (s, SiHCH₂CH₂CH₂CH₃), 26.67 (d, $^2J_{\text{C,P}}$ 7.8 Hz, PCH₃), 25.76 (s, CH(CH₃)₂), 25.39 (d, $^2J_{\text{C,P}}$ 4.5 Hz, PCH₃), 25.19 (s, SiHCH₂CH₂CH₂CH₃), 24.99 (s, PCH₃ and CH(CH₃)₂), 24.68 (s, CH(CH₃)₂), 24.42 (br. s, PCH₃), 24.04 (s, CH(CH₃)₂), 21.45 (d, $^2J_{\text{C,P}}$ 20.8 Hz, PCH₃), 20.77 (d, $^2J_{\text{C,P}}$ 12.1 Hz, PCH₃), 14.46 (s, SiHCH₂CH₂CH₂CH₃), 13.70 (d, $^2J_{\text{C,P}}$ 11.5 Hz, PCH₃). $^{29}\text{Si}\{^1\text{H}\}$ NMR (C₆D₆, 119 MHz, 298 K): δ 87.09 (m). $^{31}\text{P}\{^1\text{H}\}$ NMR (C₆D₆, 243 MHz, 298 K): δ 76.19 (s, 1P), 73.51 (s, 1P), 72.21 (s, 1P), 53.57 (s, 1P). **Minor isomer:** ^1H NMR (C₆D₆, 600 MHz, 298 K): δ 7.58 (s, 1H, NC(H)N), 5.59 (d of d with ^{29}Si sat., 1H, $^3J_{\text{H,P}}$ 16.7 Hz, $^3J_{\text{H,P}}$ 8.4 Hz, $^1J_{\text{H,Si}}$ 129.3 Hz, SiH), 3.85 (septet, 1H, $^3J_{\text{H,H}}$ 6.8 Hz, CH(CH₃)₂), 3.04 (septet, 1H, $^3J_{\text{H,H}}$ 6.6 Hz, CH(CH₃)₂), 0.9-2.1 (various m, 8H, PCH₂), 2.05 (m, 2H, SiHCH₂CH₂CH₂CH₃), 1.65 (m, 2H, SiHCH₂CH₂CH₂CH₃), 1.42 (d, 3H, $^2J_{\text{H,P}}$ 6.3 Hz, PCH₃), 1.39 (d, 3H, $^2J_{\text{H,P}}$ 5.8 Hz, PCH₃), 1.33 (d, 3H, $^2J_{\text{H,P}}$ 3.7 Hz, PCH₃), 1.33 (d, 3H, $^2J_{\text{H,P}}$ 3.3 Hz, PCH₃), 1.31 (d, 3H, $^2J_{\text{H,P}}$ 5.7 Hz, PCH₃), 1.25 (d, 3H, $^2J_{\text{H,P}}$ 2.5 Hz, PCH₃), 1.21 (d, 3H, $^3J_{\text{H,H}}$ 6.8 Hz, CH(CH₃)₂), 1.20 (d, 3H, $^3J_{\text{H,H}}$ 4.6 Hz, CH(CH₃)₂), 1.13 (m, 5H, SiHCH₂CH₂CH₂CH₃ and SiHCH₂CH₂CH₂CH₃), 1.10 (d, 3H, $^2J_{\text{H,P}}$ 3.4 Hz, PCH₃), 0.92 (d, 3H, $^3J_{\text{H,H}}$ 6.8 Hz, CH(CH₃)₂), 0.88 (d, 3H, $^2J_{\text{H,P}}$ 4.0 Hz, PCH₃), 0.87 (d, 3H, $^3J_{\text{H,H}}$ 6.9 Hz, CH(CH₃)₂). $^{13}\text{C}\{^1\text{H}\}$ NMR (C₆D₆, 151 MHz, 298 K): δ 159.10 (s, NC(H)N), 58.75 (s, CH(CH₃)₂), 50.15 (s, CH(CH₃)₂), 35.48 (s,

Ph.D. Thesis — Jeffrey S. Price; McMaster University – Chemistry

SiHCH₂CH₂CH₂CH₃), 28.91 (m, PCH₂), 28.13 (s, SiHCH₂CH₂CH₂CH₃), 27.69 (m, PCH₃), 26.53 (d, ²J_{C,P} 8.9 Hz, PCH₃), 25.50 (d, ²J_{C,P} 4.2 Hz, PCH₃), 25.19 (s, SiHCH₂CH₂CH₂CH₃), 25.07 (s, CH(CH₃)₂), 24.84 (s, PCH₃ and CH(CH₃)₂), 24.68 (s, CH(CH₃)₂), 24.42 (br. s, PCH₃), 24.04 (s, PCH₃ and CH(CH₃)₂), 17.65 (d, ²J_{C,P} 10.4 Hz, PCH₃), 14.46 (s, SiHCH₂CH₂CH₂CH₃), 13.09 (d, ²J_{C,P} 11.5 Hz, PCH₃). ²⁹Si{¹H} NMR (C₆D₆, 119 MHz, 298 K): δ 87.09 (m). ³¹P{¹H} NMR (C₆D₆, 243 MHz, 298 K): δ 73.51 (s, 1P), 73.02 (s, 1P), 69.35 (s, 1P), 52.84 (s, 1P). **Anal.** Found (calcd.): C, 48.31 (48.58); H, 9.88 (10.10); N, 5.05 (4.93).

trans-[(dmpe)₂Mn(CO)(κ¹-O₂CH)] (**26**). Method a.) 128.1 mg (0.224 mmol) of [(dmpe)₂MnH(SiH₂Ph)₂] (**20^{Ph}**) was dissolved in 10 mL of benzene. The reaction mixture was freeze/pump/thawed in a 50 mL storage flask three times, placed under 1 atm of CO₂ at room temperature, and then sealed. After stirring at room temperature overnight, the solvent was removed *in vacuo* and the resulting solid was sublimed at 80 °C at 5 mTorr. The sublimed solid was dissolved in approx. 0.6 mL of C₆D₆, and the reaction mixture was freeze/pump/thawed in an NMR tube with a J-young vale three times, before again being placed under 1 atm of CO₂ and sealed. NMR characterization was done *in situ* under an atmosphere of CO₂ because removal of CO₂ (and also removal of solvent) led to partial decomposition to form [(dmpe)₂MnH(CO)] (**27**). X-ray quality crystal were obtained by washing the crude (pre-sublimation) solid with hexamethyldisiloxane, then recrystallizing the solid residue from a concentrated solution of **26** in toluene layered with hexamethyldisiloxane at -30 °C. Methods b-d.) Approx. 10 mg of [(dmpe)₂MnH(SiH₂ⁿBu)₂] (**20^{Bu}**), [(dmpe)₂MnH(=SiEt₂)] (**16^{Et2}**), or [(dmpe)₂MnH(C₂H₄)] (**10**) was dissolved in approx. 0.6 mL of C₆D₆. The resulting solutions were then placed in a thick-walled NMR tube with a J-Young Teflon valve and was freeze-pump-thawed (×3). The NMR tubes were then placed under an atmosphere of carbon dioxide, sealed, and allowed to sit for 1.5h (b), 1.25h (c), or overnight (d). The resulting mixtures (b-d) were analyzed *in situ* without purification, leading to 100% conversion to complex **27** and a polysiloxane byproduct. ¹H NMR (C₆D₆, 600 MHz, 298 K): δ 8.68 (p, 1H, ⁴J_{H,P} 1.8 Hz, OC(H)O), 1.90 (m, 4H, PCH₂), 1.36 (m, 4H, PCH₂),

1.26 (s, 12H, PCH₃), 1.23 (s, 12H, PCH₃). ¹³C{¹H} NMR (C₆D₆, 151 MHz, 298 K): δ 167.93 (s, OC(H)O), 30.94 (p, J_{C,P} 11.6 Hz, PCH₂), 17.95 (m, PCH₃), 15.54 (s, PCH₃). ³¹P{¹H} NMR (C₆D₆, 243 MHz, 298 K): δ 68.33 (s).

11.8 – Synthetic Procedures and Characterization Pertaining to the Work of Chapter 8

Selected NMR spectra are available in the ESI to reference 587. The identification numbers in this chapter of the thesis (X→Y) relate to those in reference 587 (X→Y) in the following manner; **10**→**1**, **12**→**A**, **16**→**3**, **17**→**2**, **18**→**5**, **19**→**6**, **20**→**4**, **21**→**7**, **23**→**D**, **24**→**F**, and **A**→**E**.

Catalytic hydrosilylation of ethylene (used for obtaining hydrosilylation data except those in Figures 8.1 or 8.2). 12-21 mg of hydrosilane, and sufficient precatalyst (**10** or, for H₃Si^{*n*}Bu hydrosilylation either **10**, **20^{Bu}**, or **18^{Bu}** or, for H₂SiEt₂ hydrosilylation either **10** or **16^{Et2}**) to yield a 15 : 1 (silane : [Mn]) molar ratio, were dissolved in approx. 0.6 mL of C₆D₆, placed in a J-young NMR tube, and the solution was freeze-pump-thawed (×3). The resulting solution was placed under an atmosphere of ethylene gas, cooled to –95 °C, and sealed at this low temperature. NMR analysis was conducted *in situ* after intervals at 60 °C, and if the ethylene concentration in solution became low, the freeze-pump-thaw/addition of ethylene process described above was repeated.

Catalytic hydrosilylation of ethylene (used for obtaining data in Figure 8.1). A single stock solution was prepared containing 177 mg (2.01 mmol) of H₃Si^{*n*}Bu and 45 mg (0.12 mmol) of [(dmpe)₂MnH(C₂H₄)] (**10**) in 10 mL C₆D₆. Aliquots (approx. 0.6 mL) of this stock solution were placed in separate 50 mL storage flasks, and were freeze-pump-thawed (×3). The resulting solutions were placed under an atmosphere of ethylene gas, cooled to –95 °C, and sealed at this low temperature. Each flask was heated at 60 °C for a given time period, then cooled to room temperature and the headspace was replaced with argon. NMR spectra were obtained for the resulting solutions, as well as distilled (5 mTorr, 298 K) products.

Catalytic hydrosilylation of ethylene (used for obtaining data in Figure 8.2).

A single aliquot generated as described above (for hydrosilylation of ethylene to obtain data in Figure 8.1) taken after 11 h was placed in a J-young NMR tube. The resulting solution was freeze-pump-thawed ($\times 3$), placed under an atmosphere of ethylene gas, cooled to $-95\text{ }^{\circ}\text{C}$, and sealed at this low temperature. Reaction progress was monitored *in situ* by NMR spectroscopy at $56\text{ }^{\circ}\text{C}$ without cooling to room temperature.

Catalytic hydrosilylation of d_4 -ethylene. 22-29 mg of hydrosilane (either $\text{H}_3\text{Si}^n\text{Bu}$ or H_2SiEt_2), and sufficient $[(\text{dmpe})_2\text{MnH}(\text{C}_2\text{H}_4)]$ (**10**) to produce a 15 : 1 (silane : [Mn]) ratio (6.4-8.5 mg) were dissolved in approx. 0.6 mL C_6D_6 . These solutions were placed in separate 50 mL storage flasks, and were freeze-pump-thawed ($\times 3$). The resulting solutions were placed under approx. 0.5 atm of d_4 -ethylene, cooled to $-95\text{ }^{\circ}\text{C}$, and sealed at this low temperature. Each flask was heated at $60\text{ }^{\circ}\text{C}$ for 4 days, then cooled to room temperature and the headspace was replaced with argon. NMR spectra were obtained for the resulting solutions, as well as distilled (5 mTorr, 298 K) products.

Reactions of silylene hydride complexes with $\text{H}_3\text{Si}^n\text{Bu}$. Approx. 15 mg of silylene hydride complex $[(\text{dmpe})_2\text{MnH}(=\text{SiEt}_2)]$ (**16^{Et2}**) or a mixture of $[(\text{dmpe})_2\text{MnH}(=\text{SiPh}_2)]$ (**16^{Ph2}**) with $[(\text{dmpe})_2\text{MnH}_2(\text{SiHPh}_2)]$ (**18^{Ph2}**) was dissolved in approx. 0.6 mL of C_6D_6 . An excess of free $\text{H}_3\text{Si}^n\text{Bu}$ (approx. 20 mg) was added, and the resulting solution was analyzed by NMR spectroscopy. Complete conversion of the silylene hydride complex to $[(\text{dmpe})_2\text{MnH}(\text{SiH}_2^n\text{Bu})_2]$ (**20^{Bu}**) was observed immediately (for **16^{Ph2}**), or after a few hours (for **16^{Et2}**), with a change in solution colour to pale-yellow.

HSiViEt_2 . ^1H NMR (C_6D_6 , 600 MHz, 298 K): δ 6.08 (d of d of d, 1H, $^3J_{\text{H,H}}$ 20.2 Hz, $^3J_{\text{H,H}}$ 14.7 Hz, $^3J_{\text{H,H}(\text{SiH})}$ 3.0 Hz, $\text{SiCH}=\text{CH}_2$), 5.98 (d of d, 1H, $^3J_{\text{H,H}}$ 14.6 Hz, $^2J_{\text{H,H}}$ 4.1 Hz, $\text{SiCH}=\text{CH}_2$), 5.79 (d of d, 1H, $^3J_{\text{H,H}}$ 20.1 Hz, $^2J_{\text{H,H}}$ 4.1 Hz, $\text{SiCH}=\text{CH}_2$), 4.12 (app. sextet with ^{29}Si sat., 1H, $^3J_{\text{H,H}}$ 3.2 Hz $^1J_{\text{H,Si}}$ 183.6 Hz, SiH), 0.975 (m, 6H, SiCH_2CH_3), 0.59 (q of d, 4H, $^3J_{\text{H,H}}$ 8.0 Hz, $^3J_{\text{H,H}(\text{SiH})}$ 3.4 Hz, SiCH_2CH_3). $^{13}\text{C}\{^1\text{H}\}$ NMR

(C₆D₆, 151 MHz, 298 K): δ 134.61 (s, SiCH=CH₂), 134.24 (s, SiCH=C_H2), 8.23 (s, SiCH₂CH₃), 3.29 (s, SiCH₂CH₃). ²⁹Si NMR (C₆D₆, 119 MHz, 298 K): -10.03.

H₂SiEtⁿBu. ¹H NMR (C₆D₆, 600 MHz, 298 K): δ 3.88 (app. p with ²⁹Si sat., 1H, ³J_{H,H} 3.6 Hz, ¹J_{H,Si} 183.6 Hz, SiH), 1.31 (m, 2H, SiCH₂CH₂CH₂CH₃), 1.29 (m, 2H, SiCH₂CH₂CH₂CH₃), 0.98 (t, 3H, ³J_{H,H} 7.9 Hz, SiCH₂CH₃), 0.85 (t, 3H, ³J_{H,H} 7.1 Hz, SiCH₂CH₂CH₂CH₃), 0.58 (q of t, 2H, ³J_{H,H} 7.4 Hz, ³J_{H,H(SiH)} 3.6 Hz, SiCH₂CH₂CH₂CH₃), 0.56 (q of t, 2H, ³J_{H,H} 7.9 Hz, ³J_{H,H(SiH)} 3.8 Hz, SiCH₂CH₃). ¹³C{¹H} NMR (C₆D₆, 151 MHz, 298 K): δ 27.96 (s, SiCH₂CH₂CH₂CH₃), 26.27 (s, SiCH₂CH₂CH₂CH₃) 13.95 (s, SiCH₂CH₂CH₂CH₃), 9.34 (s, SiCH₂CH₃), 8.86 (s, SiCH₂CH₂CH₂CH₃), 1.65 (s, SiCH₂CH₃). ²⁹Si NMR (C₆D₆, 119 MHz, 298 K): -25.6.

HSiEt₂ⁿBu. Selected NMR data are as follows; ¹H NMR (C₆D₆, 600 MHz, 298 K): δ 3.93 (septet with ²⁹Si sat., 1H, ³J_{H,H} 3.1 Hz ¹J_{H,Si} 177.1 Hz, SiH), 1.33 (m, 2H, SiCH₂CH₂CH₂CH₃), 1.33 (m, 2H, SiCH₂CH₂CH₂CH₃), 1.00 (t, 6H, ³J_{H,H} 7.9 Hz, SiCH₂CH₃), 0.90 (t, 3H, ³J_{H,H} 6.7 Hz, SiCH₂CH₂CH₂CH₃), 0.58 (m, 2H, SiCH₂CH₂CH₂CH₃), 0.57 (q of d, 4H, ³J_{H,H} 7.9 Hz, ³J_{H,H(SiH)} 3.2 Hz, SiCH₂CH₃). ¹³C{¹H} NMR (C₆D₆, 151 MHz, 298 K): δ 27.26 and 26.74 (two s, SiCH₂CH₂CH₂CH₃ and SiCH₂CH₂CH₂CH₃), 14.02 (s, SiCH₂CH₂CH₂CH₃), 10.69 (s, SiCH₂CH₂CH₂CH₃), 8.50 (s, SiCH₂CH₃), 3.20 (s, SiCH₂CH₃). ²⁹Si NMR (C₆D₆, 119 MHz, 298 K): -2.94 (d, ¹J_{H,Si} 179.0 Hz).

HSiViEtⁿBu. Selected NMR data are as follows; ¹H NMR (C₆D₆, 600 MHz, 298 K): δ 6.11 (d of d of d, 1H, ³J_{H,H} 20.3 Hz, ³J_{H,H} 14.8 Hz, ³J_{H,H(SiH)} 3.3 Hz, SiCH=CH₂), 5.99 (d of d, 1H, ³J_{H,H} 14.8 Hz, ²J_{H,H} 4.1 Hz, SiCH=CH₂), 5.81 (d of d, 1H, ³J_{H,H} 20.2 Hz, ²J_{H,H} 4.0 Hz, SiCH=CH₂), 4.16 (app. sextet with ²⁹Si sat., 1H, ³J_{H,H} 3.3 Hz ¹J_{H,Si} 183.8 Hz, SiH). ¹³C{¹H} NMR (C₆D₆, 151 MHz, 298 K): δ 134.98 (s, SiCH=CH₂), 134.12 (s, SiCH=C_H2), 27.06, 26.59, 11.11 (3 s, three of the ⁿBu environments), 8.32 (s, SiCH₂CH₃), 3.70 (s, SiCH₂CH₃). ²⁹Si NMR (C₆D₆, 119 MHz, 298 K): -12.06.

HSiViPh₂. Selected NMR data are as follows; **¹H NMR (C₆D₆, 600 MHz, 298 K)**: δ 6.36 (d of d of d, 1H, ³J_{H,H} 20.1 Hz, ³J_{H,H} 14.3 Hz, ³J_{H,H(SiH)} 3.0 Hz, SiCH=CH₂), 6.06 (d of d, 1H, ³J_{H,H} 14.3 Hz, ²J_{H,H} 3.6 Hz, SiCH=CH₂), 5.85 (d of d, 1H, ³J_{H,H} 20.1 Hz, ²J_{H,H} 3.6 Hz, SiCH=CH₂), 5.33 (d, 1H, ³J_{H,H} 2.9 Hz, SiH).

HSiViEtPh. Selected NMR data are as follows; **¹H NMR (C₆D₆, 600 MHz, 298 K)**: δ 6.20 (d of d of d, 1H, ³J_{H,H} 20.1 Hz, ³J_{H,H} 14.6 Hz, ³J_{H,H(SiH)} 3.1 Hz, SiCH=CH₂), 6.01 (d of d, 1H, ³J_{H,H} 14.8 Hz, ²J_{H,H} 3.7 Hz, SiCH=CH₂), 5.83 (d of d, 1H, ³J_{H,H} 20.1 Hz, ²J_{H,H} 3.7 Hz, SiCH=CH₂), 4.70 (q, 1H, ³J_{H,H} 3.3 Hz, SiH). **²⁹Si NMR (C₆D₆, 119 MHz, 298 K)**: -15.88.

d₄-HSiEt₃ {isotopomer HSiEt₂(-CD₂CD₂H)}. Selected NMR data are as follows; **¹H NMR (C₆D₆, 600 MHz, 298 K)**: δ 3.89 (p with ²⁹Si sat., 1H, ³J_{H,H} 3.2 Hz, ¹J_{H,Si} 177.5 Hz, SiH), 0.98 (t, 6H, ³J_{H,H} 8.0 Hz, SiCH₂CH₃), 0.93 (br. s, 1H SiCD₂CD₂H), 0.54 (q of d, 4H, ³J_{H,H} 7.9 Hz, ³J_{H,H} 3.2 Hz, SiCH₂CH₃). **²H NMR (C₆D₆, 77 MHz, 298 K)**: δ 0.90 (d, 2D, ²J_{H,D} 2.0 Hz, SiCD₂CD₂H), 0.46 (d, 2D, ³J_{H,D} 0.8 Hz, SiCD₂CD₂H). **¹³C{¹H} NMR (C₆D₆, 176 MHz, 298 K)**: δ 8.43 (s, SiCH₂CH₃), 7.64 (p, ¹J_{C,D} 19 Hz, SiCD₂CD₂H), 2.79 (s, SiCH₂CH₃), 1.83 (p, ¹J_{C,D} 18 Hz, SiCD₂CD₂H).

d₄-HSiEt₃ {isotopomer HSiEt₂(-CDHCD₃)}. Selected NMR data are as follows; **¹³C{¹H} NMR (C₆D₆, 176 MHz, 298 K)**: δ 2.11 (t, ¹J_{C,H} 18 Hz, SiCDHCD₃).

d₃-HSiViEt₂ {HSiEt₂(-CD=CD₂)}. Selected NMR data are as follows; **¹H NMR (C₆D₆, 600 MHz, 298 K)**: δ 4.12 (p with ²⁹Si sat., 1H, ³J_{H,H} 3.2 Hz, ¹J_{H,Si} 184.0 Hz, SiH), 0.59 (q of d, 4H, ³J_{H,H} 8.0 Hz, ³J_{H,H} 3.4 Hz, SiCH₂CH₃). **²H{¹H} NMR (C₆D₆, 77 MHz, 298 K)**: δ 6.06 (s, SiCD=CD₂), 5.95 (s, SiCD=CD₂), 5.76 (s, SiCD=CD₂). **¹³C{¹H} NMR (C₆D₆, 176 MHz, 298 K)**: δ 8.23 (s, SiCH₂CH₃), 3.28 (s, SiCH₂CH₃).

d₈-HSiEt₂ⁿBu {isotopomer HSiⁿBu(-CD₂CD₂H)(-CDHCD₃)}. Selected NMR data are as follows; **¹H NMR (C₆D₆, 600 MHz, 298 K)**: δ 3.93 (q with ²⁹Si sat., 1H, ³J_{H,H} 3.2 Hz, ¹J_{H,Si} 177 Hz, SiH), 1.33 (m, 2H, SiCH₂CH₂CH₂CH₃), 1.33 (m, 2H, SiCH₂CH₂CH₂CH₃), 0.95 (br. s, 1H, SiCD₂CD₂H), 0.90 (t, 3H, ³J_{H,H} 6.7 Hz,

SiCH₂CH₂CH₂CH₃), 0.58 (m, 2H, SiCH₂CH₂CH₂CH₃), 0.52 (br. s, 1H, SiCDHCD₃). ²H NMR (C₆D₆, 77 MHz, 298 K): δ 0.92 (d, 2D, ²J_{D,H} 2 Hz, SiCD₂CD₂H), 0.91 (d, 3D, ³J_{D,H} 0.8 Hz, SiCDHCD₃), 0.49 (s, 2D, SiCD₂CD₂H), 0.49 (d, 1D, ²J_{H,D} 2 Hz, SiCDHCD₃). ¹³C{¹H} NMR (C₆D₆, 176 MHz, 298 K): δ 27.27 and 26.74 (two s, SiCH₂CH₂CH₂CH₃ and SiCH₂CH₂CH₂CH₃), 14.0 (s, SiCH₂CH₂CH₂CH₃), 10.67 (s, SiCH₂CH₂CH₂CH₃), 7.73 (p, ¹J_{C,D} 19 Hz, SiCD₂CD₂H), 7.43 (app. p, ¹J_{C,D} 19 Hz, SiCDHCD₃), 2.47 (t, ¹J_{C,D} 18 Hz, SiCDHCD₃), 2.22 (m, ¹J_{C,D} 19 Hz, SiCD₂CD₂H).

*d*₈-HSiEt^{*n*}Bu {isotopomer HSi^{*n*}Bu(–CD₂CD₂H)₂}. Selected NMR data are as follows; ¹H NMR (C₆D₆, 600 MHz, 298 K): δ 3.92 (t with ²⁹Si sat., 1H, ³J_{H,H} 3.2 Hz, ¹J_{H,Si} 177 Hz, SiH), 1.33 (m, 2H, SiCH₂CH₂CH₂CH₃), 1.33 (m, 2H, SiCH₂CH₂CH₂CH₃), 0.95 (br. s, 2H, SiCD₂CD₂H), 0.90 (t, 3H, ³J_{H,H} 6.7 Hz, SiCH₂CH₂CH₂CH₃), 0.58 (m, 2H, SiCH₂CH₂CH₂CH₃). ²H NMR (C₆D₆, 77 MHz, 298 K): δ 0.92 (d, 4D, ²J_{D,H} 2 Hz, SiCD₂CD₂H), 0.49 (s, 4D, SiCD₂CD₂H). ¹³C{¹H} NMR (C₆D₆, 176 MHz, 298 K): δ 27.27 and 26.74 (two s, SiCH₂CH₂CH₂CH₃ and SiCH₂CH₂CH₂CH₃), 14.0 (s, SiCH₂CH₂CH₂CH₃), 10.67 (s, SiCH₂CH₂CH₂CH₃), 7.73 (p, ¹J_{C,D} 19 Hz, SiCD₂CD₂H), 2.22 (m, ¹J_{C,D} 19 Hz, SiCD₂CD₂H).

*d*₇-HSiViEt^{*n*}Bu {isotopomer HSi^{*n*}Bu(–CDHCD₃)(–CD=CD₂)}. Selected NMR data are as follows; ¹H NMR (C₆D₆, 600 MHz, 298 K): δ 4.16 (q with ²⁹Si sat., 1H, ³J_{H,H} 3.3 Hz, ¹J_{H,Si} 184 Hz, SiH). ²H (C₆D₆, 77 MHz, 298 K): δ 6.09 (s, SiCD=CD₂), 5.96 (s, SiCD=CD₂), 5.78 (s, SiCD=CD₂). ¹³C{¹H} (C₆D₆, 176 MHz, 298 K): δ 3.00 (t, ¹J_{C,D} 18.4 Hz, SiCHCD₃).

[(dmpe)₂MnH₂(SiHEtPh)] (18^{Ph,Et}). 18^{Ph,Et} was observed spectroscopically while monitoring ethylene hydrosilylation by H₃SiPh using **10**. Selected NMR data are as follows (assignments are tentative, multiple isomers present); ¹H NMR (C₆D₆, 600 MHz, 298 K): δ 8.17 (d, ³J_{H,H} 6 Hz, *o*), 8.12 (br. s, *o*), 7.87 (d, ³J_{H,H} 7 Hz, *o*), 7.81 (br. s, *o*), 6.62 (app. t, *J* 9.4 Hz, SiH), 5.69 (br. s, SiH), –11.59 (p, ²J_{H,P} 53.7 Hz, MnH), –12.50 (br. s, MnH), –12.68 (br. s, MnH), –13.44 (br. s, MnH).

$[(\text{dmpe})_2\text{MnH}_2(\text{SiHEt}^n\text{Bu})]$ ($18^{\text{Bu,Et}}$). $18^{\text{Bu,Et}}$ was observed spectroscopically while monitoring ethylene hydrosilylation by $\text{H}_3\text{Si}^n\text{Bu}$ using **10**. Selected NMR data are as follows; ^1H NMR (C_6D_6 , 600 MHz, 298 K): δ 4.98 (br. s, 1H, SiH), -12.66 (br. s, 2H, MnH).

11.9 – Synthetic Procedures and Characterization Pertaining to the Work of Chapter 9

Tables of calculated and crystallographically determined bond lengths and angles, along with bond orders, total bonding energies, and Hirshfeld charges for **11** are available in the ESI to reference 547. The identification numbers in this chapter of the thesis ($\underline{\text{X}} \rightarrow \underline{\text{Y}}$) relate to those in reference 547 ($\text{X} \rightarrow \text{Y}$) in the following manner; *trans*-**10** \rightarrow **1**, *cis*-**10** \rightarrow **A**, **11** \rightarrow **5**, **12** \rightarrow **D**, **13** \rightarrow **B**, **16** \rightarrow **2**, **17** \rightarrow **C**, and **18** \rightarrow **3**. CSD 1846649 contains the supplementary crystallographic data for **11** (other crystal structures in this chapter in this chapter have not been submitted to the CSD yet).

$[(\text{dmpe})_2\text{MnH}(\text{H}_2)]$ (**11**). 98.7 mg (0.26 mmol) of $[(\text{dmpe})_2\text{MnH}(\text{C}_2\text{H}_4)]$ (**10**) was dissolved in 10 mL of benzene, and the resulting solution was placed in a sealed flask and freeze-pump-thawed ($\times 3$). The flask was placed under an atmosphere of hydrogen gas at -95 °C using a liquid nitrogen-acetone bath, sealed at this temperature, and warmed to room temperature to provide approx. 1.7 atm of hydrogen gas for reactivity. After stirring at 60 °C for 5 days, the solvent was removed *in vacuo* and the resulting solid was extracted with pentane. Removal of the pentane *in vacuo* yielded a crude pale yellow powder with $>95\%$ purity by NMR (77% isolated yield; 70.4 mg, 0.20 mmol). Recrystallization from a concentrated solution in pentane at -30 °C yielded 48.7 mg of pure **11** (0.14 mmol, 52%). NMR data matches that previously reported via a different synthetic route (with ^{31}P $\delta = 82$ ppm).^{cccc,120,173} X-ray quality crystals were obtained from a concentrated solution of **11** in hexanes at -30 °C.

^{cccc} The ^{31}P chemical shift matches that reported in ref. 173, but not ref. 120.

[(dmpe)₂Mn(μ-H)₂BH₂] (28). BH₃·NMe₃ (23.8 mg, 0.33 mmol) was added to a solution of 127.0 mg (0.33 mmol) of [(dmpe)₂MnH(C₂H₄)] (**10**) in 30 mL of toluene, and the resulting solution was stirred at 90 °C for two days (with the solution turning from bright yellow to dark purple/black within an hour). The solvent was then removed *in vacuo*, and resulting black solid was dissolved in a minimal amount of hexanes and allowed to sit at -30 °C for a few days yielding a purple powder with some impurities. Purification by sublimation (5 mTorr, 80-85 °C) and recrystallization from a concentrated solution in hexanes yielded a combined 27.0 mg of purple solid (0.07 mmol, 22 %). X-ray quality crystals were obtained from a solution in hexanes at -30 °C. **¹H NMR (d₈-toluene, 600 MHz, 298 K):** δ 5.08 (m, 2H, BH), 1.69 (m, 2H, PCH₂), 1.60 (m, 6H, PCH₃), 1.43 (m, 6H, PCH₃), 1.34 (m, 4H, PCH₂), 1.16 (m, 2H, PCH₂), 0.97 (d, 6H, ²J_{H,P} 5.8 Hz, PCH₃), 0.71 (d, 6H, ²J_{H,P} 5.2 Hz, PCH₃), -16.52 (m, 2H, MnH). **¹¹B{¹H} NMR (d₈-toluene, 192 MHz, 298 K):** δ 25.30 (s). **¹³C{¹H} NMR (d₈-toluene, 151 MHz, 298 K):** δ 33.48 (m, PCH₂), 32.78 (m, PCH₂), 29.12 (m, PCH₃), 23.25 (m, PCH₃), 21.82 (s, PCH₃), 20.21 (PCH₃). **³¹P{¹H} NMR (d₈-toluene, 243 MHz, 298 K):** δ 88.56 (s, 2P), 72.54 (s, 2P).

Reaction of [(dmpe)₂Mn(μ-H)₂BH₂] (28) with D₂. Approx. 10 mg of [(dmpe)₂Mn(μ-H)₂BH₂] (**28**) was dissolved in approx. 0.6 mL of C₆D₆, and the resulting solution was placed in a J-young NMR tube and freeze/pump/thawed ×3. After cooling to -95 °C, D₂ was allowed to flow into the J-young NMR tube and the valve was sealed to this temperature. After heating at 90 °C for 12 h, the resulting solution was analyzed by NMR spectroscopy *in situ*. ¹H NMR data matches that for **28**, with 40% reduction in the relative intensity of both the MnH and BH environments.

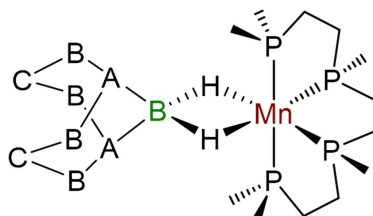


Figure 11.1: $[(\text{dmpe})_2\text{Mn}(\mu\text{-H})_2\text{BC}_8\text{H}_{14}]$ (**29**) with C atom labels used in the NMR list.

$[(\text{dmpe})_2\text{Mn}(\mu\text{-H})_2\text{BC}_8\text{H}_{14}]$ (29**).** 73.7 mg (0.60 mmol) of 9-BBN (purified by two successive recrystallizations from concentrated solutions in DME at $-30\text{ }^\circ\text{C}$) was added to a solution of 116 mg (0.30 mmol)^{dddd} of $[(\text{dmpe})_2\text{MnH}(\text{C}_2\text{H}_4)]$ (**10**) in 20 mL of benzene, and the resulting solution was stirred at $90\text{ }^\circ\text{C}$ overnight (with the solution turning from bright yellow to dark brown). The solvent was then removed *in vacuo*, and resulting black solid was dissolved in a minimal amount hexanes. Allowing this solution to stand at $-30\text{ }^\circ\text{C}$ yielded a mixture of yellow and red crystals; the former were $[(\text{dmpe})_2\text{MnH}]_2(\mu\text{-dmpe})$ (**31**) while the latter was $[(\text{dmpe})_2\text{Mn}(\mu\text{-H})_2\text{BC}_8\text{H}_{14}]$ (**29**). Both sets of crystals were X-ray quality. Picking out red crystals with tweezers allowed isolation of **29** in $> 99\%$ purity. $^1\text{H NMR}$ (C_6D_6 , 600 MHz, 298 K): δ 2.29 (app. nonet, 2H, $^3J_{\text{H,H}}$ 6.0 Hz, $\underline{\text{CH}}_2(\text{C})$), 2.13 (m, 8H, $\underline{\text{CH}}_2(\text{B})$), 1.86 (m, 2H, $\underline{\text{CH}}_2(\text{C})$), 1.67 (m, 2H, $\text{P}\underline{\text{CH}}_2$), 1.55 (m, 6H, $\text{P}\underline{\text{CH}}_3$), 1.40 (s, 6H, $\text{P}\underline{\text{CH}}_3$), 1.36 (br. s, 2H, $\underline{\text{CH}}(\text{A})$), 1.27 (m, 2H, $\text{P}\underline{\text{CH}}_2$), 1.23 (d, 6H, $^2J_{\text{H,P}}$ 5.2 Hz, $\text{P}\underline{\text{CH}}_3$), 1.17 (m, 4H, $\text{P}\underline{\text{CH}}_2$), 0.72 (d, 6H, $^2J_{\text{H,P}}$ 4.7 Hz, $\text{P}\underline{\text{CH}}_3$), -15.55 (br. s, 2H, $\text{Mn}\underline{\text{H}}$). $^{11}\text{B}\{^1\text{H}\}$ NMR (C_6D_6 , 192 MHz, 298 K): δ 43.19 (s). $^{13}\text{C}\{^1\text{H}\}$ NMR (C_6D_6 , 151 MHz, 298 K): δ 36.96 (m, $\underline{\text{CH}}(\text{A})$), 35.94 (m, $\text{P}\underline{\text{CH}}_2$), 35.39 (s, $\underline{\text{CH}}_2(\text{B})$), 34.32 (s, $\underline{\text{CH}}_2(\text{B})$), 31.25 (m, $\text{P}\underline{\text{CH}}_2$ and $\text{P}\underline{\text{CH}}_3$), 25.00 (s, $\underline{\text{CH}}_2(\text{C})$), 24.91 (m, $\text{P}\underline{\text{CH}}_3$), 23.80 (s, $\text{P}\underline{\text{CH}}_3$), 20.79 (s, $\text{P}\underline{\text{CH}}_3$). $^{31}\text{P}\{^1\text{H}\}$ NMR (C_6D_6 , 243 MHz, 298 K): δ 85.08 (s, 2P), 70.11 (s, 2P).

$[(\text{dmpe})_2\text{Mn}(\mu\text{-H})_2\text{BMes}_2]$ (30**).** 172.0 (0.69 mmol) of HBMes_2 was added to a solution of 132.1 mg (0.34 mmol) of $[(\text{dmpe})_2\text{MnH}(\text{C}_2\text{H}_4)]$ (**10**) in 20 mL of toluene, and the resulting solution was stirred at $60\text{ }^\circ\text{C}$ for two days (turning from bright yellow to

^{dddd} Number of moles based on a 9-BBN monomer.

dark purple). The solvent was then removed *in vacuo*, and the resulting purple solid was washed with 10 mL of hexanes, 3 mL of toluene, and dissolved in 12 mL of toluene. The toluene solution was layered with 3 mL of hexanes and stored for days at $-30\text{ }^{\circ}\text{C}$, after which 48.8 mg of a very dark purple solid (both crystals and powder) had crystallized. To obtain a higher yield, the solvent was removed *in vacuo* from the mother liquor, and the resulting solid dissolved in 2 mL of THF which was allowed to sit for days at $-30\text{ }^{\circ}\text{C}$ yielded an additional 22.0 mg of purple crystals (combined yield of 70.8 mg, 0.12 mmol, 34 %). X-ray quality crystals were obtained from a solution in C_6D_6 at $60\text{ }^{\circ}\text{C}$. **^1H NMR (d_8 -toluene, 600 MHz, 298 K):** δ 6.92 (s, 2H, *m*), 6.61 (s, 2H, *m*), 2.84 (s, 6H, *o*- CH_3), 2.26 (s, 6H, *o*- CH_3), 2.23 (s, 6H, *p*- CH_3), 1.51 (m, 2H, PCH_2), 1.38 (m, 6H, PCH_3), 1.26 (d, 6H, $^2J_{\text{H,P}}$ 5.4 Hz, PCH_3), 1.08 (m, 6H, PCH_2), 0.70 (m, 6H, PCH_3), 0.65 (d, 6H, $^2J_{\text{H,P}}$ 4.8 Hz, PCH_3), -13.98 (br. s, 2H, MnH). **$^{11}\text{B}\{^1\text{H}\}$ NMR (d_8 -toluene, 192 MHz, 298 K):** δ 27.46. **$^{13}\text{C}\{^1\text{H}\}$ NMR (d_8 -toluene, 151 MHz, 298 K):** 153.3 (*i*), 140.72 (*s*, *o*), 140.20 (*s*, *o*), 133.59 (*s*, *p*) 129.1 (*m*), 128.7 (*m*), 37.10 (m, PCH_2), 31.93 (m, PCH_2), 27.50 (*s*, *o*- CH_3), 27.40 (*s*, PCH_3), 25.24 (*s*, *o*- CH_3), 24.75 (m, PCH_3), 21.24 (m, PCH_3), 21.12 (*s*, *p*- CH_3), 20.0 (PCH_3). **$^{31}\text{P}\{^1\text{H}\}$ NMR (d_8 -toluene, 243 MHz, 298 K):** δ 85.82 (*s*, 2P), 62.61 (*s*, 2P). **Anal.** Found (calcd.): C, 59.38 (59.42); H, 9.37 (9.31).

$[(\text{dmpe})_2\text{Mn}(\mu\text{-D})_2\text{BMes}_2]$ (d_2 -30). 11.7 mg (0.03 mmol) of $[(\text{dmpe})_2\text{MnH}(\text{C}_2\text{H}_4)]$ (**10**) and 15.3 mg (0.06 mmol) of DBMes_2 were dissolved in approx. 0.6 mL of C_6D_6 . The resulting solution was heated overnight at $60\text{ }^{\circ}\text{C}$, and analyzed by NMR spectroscopy *in situ*. ^1H and ^{11}B NMR data matches that of **30** with the exception of no ^1H NMR signal in the metal hydride environment. **^2H NMR (C_6D_6 , 77 MHz, 298 K):** δ -14.09 (*s*, 2D, MnD).

EtBC₈H₁₄. Approx. 10 mg of $\text{HBC}_8\text{H}_{14}$ was dissolved in approx. 0.6 mL of C_6D_6 , and the resulting solution was placed in a J-young NMR tube and freeze/pump/thawed $\times 3$. After cooling to $-95\text{ }^{\circ}\text{C}$, ethylene was allowed to flow into the J-young NMR tube and the valve was sealed to this temperature. After heating at $60\text{ }^{\circ}\text{C}$ for 1 h, the resulting solution was analyzed by NMR spectroscopy *in situ*. **^1H NMR (C_6D_6 , 600 MHz, 298 K):**

δ 1.84 (m, 6H, C₈H₁₄), 1.76 (br. s, 2H, C₈H₁₄), 1.65 (m, 4H, C₈H₁₄), 1.35 (q, 2H, ³J_{H,H} 7.6 Hz, CH₂CH₃), 1.17 (m, 2H, C₈H₁₄) 1.08 (t, 3H, ³J_{H,H} 7.6 Hz, CH₂CH₃). ¹¹B{¹H} NMR (C₆D₆, 192 MHz, 298 K): δ 87.41 (s). ¹³C{¹H} NMR (C₆D₆, 151 MHz, 298 K): δ 33.39 (s), 31.13 (br. s), 23.63 (s), 20.23 (br. s), 8.41 (s).

EtBMes₂. Approx. 10 mg of HBMes₂ was dissolved in approx. 0.6 mL of C₆D₆, and the resulting solution was placed in a J-young NMR tube and freeze/pump/thawed $\times 3$. After cooling to -95 °C, ethylene was allowed to flow into the J-young NMR tube and the valve was sealed to this temperature. After heating at 60 °C for 1 h, the resulting solution was analyzed by NMR spectroscopy *in situ*. ¹H NMR (C₆D₆, 600 MHz, 298 K): δ 6.74 (s, 4H, *m*), 2.23 (s, 12H, *o*-CH₃), 2.15 (s, 6H, *p*-CH₃), 1.93 (q, 2H, ³J_{H,H} 7.5 Hz, CH₂CH₃), 1.15 (t, 3H, ³J_{H,H} 7.5 Hz, CH₂CH₃). ¹¹B{¹H} NMR (C₆D₆, 192 MHz, 298 K): δ 84.02 (br. s). ¹³C{¹H} NMR (C₆D₆, 151 MHz, 298 K): δ 139.13 (s), 138.34 (s), 128.98 (s), 26.55 (br. s), 22.91 (s), 21.18 (s), 9.38 (s).

Intermediates in the synthesis of 29. Method a) 3.6 mg of 9-BBN (0.030 mmol)^{ffff} and 11.3 mg of [(dmpe)₂MnH(C₂H₄)] (**10**) (0.029 mmol) were dissolved in approx. 0.6 mL of C₆D₆ and the resulting mixture was left for 7 days at room temperature and analyzed *in situ* by NMR spectroscopy indicating a 1.3 : 1.0 : 2.1 ratio of **10** : **29** : intermediates (region of the ¹H NMR spectrum shown in Figure 9.3). Method b) 6.5 mg of 9-BBN (0.05 mmol)^{eeee} and 10.3 mg of [(dmpe)₂MnH(C₂H₄)] (**10**) (0.27 mmol) were dissolved in approx. 0.6 mL of C₆D₆ and the resulting mixture was left for 3 days at room temperature and analyzed *in situ* by ¹H NMR spectroscopy indicating a 0.4 : 1.0 : 0.6 ratio of **10** : **29** : intermediates (region of the ³¹P{¹H} NMR spectrum shown in Figure 9.3). A major (>95%) and minor (<5%) intermediate were both observed in solution. Selected NMR data for the major species are as follows: ¹H NMR (C₆D₆, 600 MHz, 298 K): δ 2.68 (m, 1H), 2.60 (m, 1H), 2.46 (m, 4H), 2.05 (m, 1H), 0.53 (m, 1H), 0.31 (m, 1H), -1.44 (br. s, 1H), -13.14 (br. s, 1H, MnH). ¹¹B NMR (C₆D₆, 192 MHz, 298 K): δ -15.49 (s). ³¹P{¹H} NMR (C₆D₆, 243 MHz, 298 K): δ 85.83 (s, 1P), 76.47 (s, 1P), 64.94

^{eeee} Number of moles based on a 9-BBN monomer.

(s, 1P), 57.83 (s, 1P). Selected NMR data for the minor species are as follows: $^{31}\text{P}\{^1\text{H}\}$ NMR (C_6D_6 , 243 MHz, 298 K): $\delta -5.64$ (s).

Intermediates in the synthesis of 30. 13.0 mg of HBMe_2 (0.052 mmol) and 10.0 mg of $[(\text{dmpe})_2\text{MnH}(\text{C}_2\text{H}_4)]$ (**10**) (0.026 mmol) were dissolved in approx. 0.6 mL of C_6D_6 and the resulting mixture was placed in an NMR tube with J-young valve and heated for 1.5 h at 60 °C. The resulting solution was analyzed *in situ* by NMR spectroscopy indicating a 1.4 : 1.0 : 0.6 ratio of **10** : **30** : intermediates. A major (>95%) and minor (<5%) intermediate were both observed in solution. Selected NMR data for the major species are as follows: ^1H NMR (C_6D_6 , 600 MHz, 298 K): 4.12 (app. t, 2H, J 2.2 Hz), 1.96 (q, 2H, $^3J_{\text{H,H}}$ 7.1 Hz), -13.03 (t, 1H, $J_{\text{H,P}}$ 73.7 Hz, MnH). $^{31}\text{P}\{^1\text{H}\}$ NMR (C_6D_6 , 243 MHz, 298 K): $\delta -4.01$ (s). Selected NMR data for the minor species are as follows: $^{31}\text{P}\{^1\text{H}\}$ NMR (C_6D_6 , 243 MHz, 298 K): $\delta 73.27$ (br. s).

Reaction of $[(\text{dmpe})_2\text{MnH}(\text{C}_2\text{H}_4)]$ (10**) with DIBAL:** 18 mg (0.05 mmol) of $[(\text{dmpe})_2\text{MnH}(\text{C}_2\text{H}_4)]$ (**10**) was dissolved in approx. 0.6 mL C_6D_6 . To this solution was added 24 mg (0.17 mmol) of DIBAL, and the resulting solution was analyzed by NMR spectroscopy *in situ*. Complete consumption of **10** was observed immediately, and the hydride-free product began decomposing to various hydride-containing products within 30 minutes, many of which themselves decomposed to further hydride-containing decomposition products.

$\{[(\text{dmpe})_2\text{MnH}]_2(\mu\text{-dmpe})$ (31**) and $[(\text{dmpe})_2\text{MnH}(\kappa_1\text{-dmpe})]$ (**32**).** Method a) 135.8 mg (0.35 mmol) of $[(\text{dmpe})_2\text{MnH}(\text{C}_2\text{H}_4)]$ (**10**) was dissolved in 10 mL toluene, then added to 149.6 mg (1.00 mmol) of dmpe dissolved in 10 mL of toluene. The resulting solution was sealed in a 50 mL thick-walled storage flask and stirred overnight at 105 °C, after which the solvent was removed *in vacuo*. Recrystallization from a concentrated solution of hexanes at -30 °C yielded 12.3 mg of a waxy yellow solid, and removing the solvent from the mother liquor *in vacuo* and recrystallizing the resulting solution from concentrated hexamethyldisiloxane at -30 °C yielded an additional 39.6 mg of yellow powder. The combined solids were then heated under vacuum at 75 °C

for 5 h to remove unreacted **10**, resulting in 19.8 mg of **31** and **32** in a 1 : 20 ratio.^{fff} A small sample (~10 mg) of [$\{(\text{dmpe})_2\text{MnH}\}_2(\mu\text{-dmpe})$] (**31**) was isolated from **32** by washing a crude mixture of **31** and **32** with hexamethyldisiloxane, followed by recrystallization from a concentrated solution in hexanes layered with hexamethyldisiloxane at $-30\text{ }^\circ\text{C}$, and the product was characterized by NMR spectroscopy. A small sample of [$(\text{dmpe})_2\text{MnH}(\kappa_1\text{-dmpe})$] (**32**) was isolated from **31** by sublimation from a crude mixture of **31** and **32** at $120\text{ }^\circ\text{C}$ (5 mTorr), and the product was characterized by NMR spectroscopy. Method b) 13 mg (0.03 mmol) of [$(\text{dmpe})_2\text{MnH}(\text{C}_2\text{H}_4)$] (**10**) and 11 mg (0.07 mmol) of dmpe were dissolved in approx. 0.6 mL of C_6D_6 and placed in a J-young NMR tube. The resulting solution was freeze/pump/thawed $\times 3$. After cooling to $-95\text{ }^\circ\text{C}$, H_2 was allowed to flow into the J-young NMR tube and the valve was sealed to this temperature. Heating the sealed solution at $60\text{ }^\circ\text{C}$ for 3 days resulted in quantitative conversion of **10** to **31** and **32** in a 1 : 8 ratio, and the products were analyzed *in situ* by NMR spectroscopy. X-ray quality crystals of *trans,trans*-**31** were obtained from a solution of **31** and **29** in hexanes at $-30\text{ }^\circ\text{C}$, and X-ray quality crystal of *cis,cis*-**31** were obtained from a solution of **31** in hexamethyldisiloxane at $-30\text{ }^\circ\text{C}$. Selected NMR data for *trans,trans*-**31** are as follows: $^1\text{H NMR}$ (C_6D_6 , 600 MHz, 298 K): δ 1.66 (m, 8H, $\text{PC}\underline{\text{H}}_2$ -chelating), 1.50 (m, 8H, $\text{PC}\underline{\text{H}}_2$ -chelating), 1.48 (s, 24H, $\text{PC}\underline{\text{H}}_3$ -chelating), 1.36 (s, 24H, $\text{PC}\underline{\text{H}}_3$ -chelating), 1.30 (br. s, 4H, $\text{PC}\underline{\text{H}}_2\text{-}\kappa^1$), 1.02 (d, $^2J_{\text{H,P}}$ 3.5 Hz, 12H, $\text{PC}\underline{\text{H}}_3\text{-}\kappa^1$), -15.74 (p of d, 2H, $^2J_{\text{H,P}}$ 48.8 Hz, $^2J_{\text{H,P}}$ 12.5 Hz, $\text{Mn}\underline{\text{H}}$). $^{31}\text{P}\{^1\text{H}\}$ NMR (C_6D_6 , 243 MHz, 298 K): δ 79.60 (s, 4P, chelating P), 27.16 (s, 1P, $\kappa^1\text{-P}$). Selected NMR data for the complex tentatively identified as *cis,cis*-**31** are as follows: $^1\text{H NMR}$ (C_6D_6 , 600 MHz, 298 K): δ -11.66 (m, $\text{Mn}\underline{\text{H}}$). Selected NMR data for **32** are as follows: $^1\text{H NMR}$ (C_6D_6 , 600 MHz, 298 K): δ 1.62 (m, 4H, $\text{PC}\underline{\text{H}}_2$ -chelating), 1.47 (m, 4H, $\text{PC}\underline{\text{H}}_2$ -chelating), 1.45 (s, 12H, $\text{PC}\underline{\text{H}}_3$ -chelating), 1.38, (m, 2H, $\text{MnP}(\text{Me})_2\text{CH}_2\text{C}\underline{\text{H}}_2\text{PMe}_2$), 1.34 (s, 12H, $\text{PC}\underline{\text{H}}_3$ -chelating), 1.28 (m, 2H, $\text{MnP}(\text{Me})_2\text{C}\underline{\text{H}}_2\text{-CH}_2\text{PMe}_2$), 0.96 (d, 6H, $^2J_{\text{H,P}}$ 3.8 Hz, $\text{MnP}(\text{PC}\underline{\text{H}}_3)_2\text{CH}_2\text{CH}_2\text{PMe}_2$), 0.89 (d, 6H, $^2J_{\text{H,P}}$

^{fff} Different batches of syntheses resulted in varying **31** : **32** ratios, ranging from 5 : 3 to 1 : 20.

2.8 Hz, $\text{MnP}(\text{Me})_2\text{CH}_2\text{CH}_2\text{P}(\text{PCH}_3)_2$), -15.72 (p of d, 1H, $^2J_{\text{H,P}}$ 48.8 Hz, $^2J_{\text{H,P}}$ 12.9 Hz, MnH). $^{13}\text{C}\{^1\text{H}\}$ NMR (C_6D_6 , 151 MHz, 298 K): δ 38.09 (s, $\text{MnP}(\text{Me})_2\text{CH}_2\text{CH}_2\text{PMe}_2$), 34.33 (p, $^1J_{\text{C,P}}$ 11.9 Hz, PCH_2 -chelating), 32.02 (s, PCH_3 -chelating), 26.50 (d of d, $^1J_{\text{C,P}}$ 13.4 Hz, $^2J_{\text{C,P}}$ 7.3 Hz, $\text{MnP}(\text{Me})_2\text{CH}_2\text{CH}_2\text{PMe}_2$), 24.84 (d, $^1J_{\text{C,P}}$ 9.4 Hz, $\text{MnP}(\text{PCH}_3)_2\text{CH}_2\text{CH}_2\text{PMe}_2$), 24.62 (s, PCH_3 -chelating), 13.95 (d, $^1J_{\text{C,P}}$ 16.0 Hz, $\text{MnP}(\text{Me})_2\text{CH}_2\text{CH}_2\text{P}(\text{PCH}_3)_2$). $^{31}\text{P}\{^1\text{H}\}$ NMR (C_6D_6 , 243 MHz, 298 K): δ 79.31 (s, chelating P), 28.40 (s, $\text{MnP}(\text{Me})_2\text{CH}_2\text{CH}_2\text{PMe}_2$), -48.90 (d, $^3J_{\text{P,P}}$ 14.1 Hz, $\text{MnP}(\text{Me})_2\text{CH}_2\text{CH}_2\text{PMe}_2$).

Synthesis of $[(\text{dmpe})_2\text{MnH}(\text{PPh}_2)]$ (33): 199.0 mg (0.52 mmol) of $[(\text{dmpe})_2\text{MnH}(\text{C}_2\text{H}_4)]$ (10) was dissolved in 20 mL of toluene and placed in a 50 mL storage flask. To this solution was added 192.8 mg (1.04 mmol) of HPPH_2 . The reaction mixture was stirred at 90 °C for 2 days to form a dirty brownish solution, and the solvent was then removed *in vacuo*. The brown solid was dissolved in a minimal amount of hexanes and residual solid was removed by centrifugation. After allowing to sit for a week at -30 °C, very dark yellow (X-ray quality) crystals were formed of 33 (57 mg, 0.11 mg, 20%) in >95 % purity. Selected NMR spectra are as follows: ^1H NMR (C_6D_6 , 600 MHz, 298 K): δ 7.54 (app. t, 4H, $^3J_{\text{H,H}}$ 7.9 Hz, $^3J_{\text{H,P}}$ 7.3 Hz, o), 7.28 (d of m, 1H, $^1J_{\text{H,P}}$ 284 Hz, PH), 7.02 (t, 4H, $^3J_{\text{H,H}}$ 7.3 Hz, m), 6.95 (t, 2H, $^3J_{\text{H,H}}$ 7.4 Hz, p), 1.52 (m, 8H, PCH_2), 1.29 (s, 12H, PCH_3), 1.27 (s, 12H, PCH_3), -14.08 (p of d, 1H, $^2J_{\text{H,P}}$ 50.7 Hz, $^2J_{\text{H,P}}$ 11.4 Hz, MnH). $^{13}\text{C}\{^1\text{H}\}$ NMR (C_6D_6 , 151 MHz, 298 K): δ 149.06 (d, $^1J_{\text{C,P}}$ 15.6 Hz, i), 131.71 (d, $^2J_{\text{C,P}}$ 9.3 Hz, o), 127.05 (s, p), 33.36 (p, $J_{\text{C,P}}$ 12.0 Hz, PCH_2), 31.06 (s, PCH_3), 21.46 (s, PCH_3). $^{31}\text{P}\{^1\text{H}\}$ NMR (C_6D_6 , 243 MHz, 298 K): δ 79.34 (s, 4P, dmpe), 63.12 (s, 1P, PPh_2).

Synthesis of $[(\text{dmpe})_2\text{MnH}(\text{SnPh}_3)]$ (34): Method a) 111.4 mg (0.29 mmol) of $[(\text{dmpe})_2\text{MnH}(\text{C}_2\text{H}_4)]$ (10) was dissolved in 10 mL of benzene. To this solution was added 215.0 mg (0.61 mmol) of HSnPh_3 dissolved in 7 mL of benzene. The combined (17 mL) solution began turning green within a few minutes of stirring at room temperature. This solution was stirred overnight at room temperature, followed by

overnight again at 60 °C, forming a clear, pine green solution. The solvent was removed *in vacuo* to yield a light green solid, which slowly turned white upon continued exposure to vacuum (the white solid was identified by NMR spectroscopy as SnPh₄). X-ray quality crystals (large turquoise blocks) were obtained by dissolving the light green solid in a minimal amount of toluene and allowing the resulting solution to sit at –30 °C for a week. A yield was not obtained because the complex was unstable upon exposure to vacuum. Method b) 11.1 mg (0.03 mmol) of [(dmpe)₂MnH(C₂H₄)] (**10**) and 20.2 mg (0.06 mmol) of HSnPh₃ were dissolved in approx. 0.6 mL of C₆D₆. The resulting solution was heating at 65 °C overnight, and analyzed by NMR spectroscopy *in situ*. Selected NMR data tentatively assigned as arising from **34** are as follows: **¹H NMR (C₆D₆, 600 MHz, 298 K):** δ 10.42 (br. s), –8.12 (br. s), –10.80 (br. s), –13.84 (br. s).

Reaction of [(dmpe)₂MnH(C₂H₄)] (10**) with HSnⁿBu₃:** 17.9 mg (0.05 mmol) of [(dmpe)₂MnH(C₂H₄)] (**10**) and 25.7 mg (0.09 mmol) of HSnⁿBu₃ were dissolved in approx. 0.06 mL of C₆D₆, and the resulting solution was heated overnight at 60 °C, and the resulting dark orange solution was analyzed by NMR spectroscopy *in situ*. Selected NMR data tentatively assigned as arising from a paramagnetic Mn-containing species are as follows: **¹H NMR (C₆D₆, 600 MHz, 298 K):** δ 4.01 (br. s), –1.15 (br. s), –3.67 (br. s), –9.01 (br. s), –13.23 (br. s).

Appendix 1

Supplementary Information Related to Chapter 7

Contents	Pages
Figures Showing Calculated Structures	367
Figures Showing Superimposed Calculated and X-ray Structures	368
Tables of Calculated and Crystallographically Determined Bond Lengths, Mayer Bond Orders, and Angles	368-369
Tables of Total Bonding Energies and Thermodynamic Parameters for Calculated Structures	369-370
Tables of Hirshfeld Charges for Calculated Structures	370
Tables of Crystal Data and Crystal Structure Refinement	371-372
Selected NMR Spectra	373-391

Figures Showing Calculated Structures

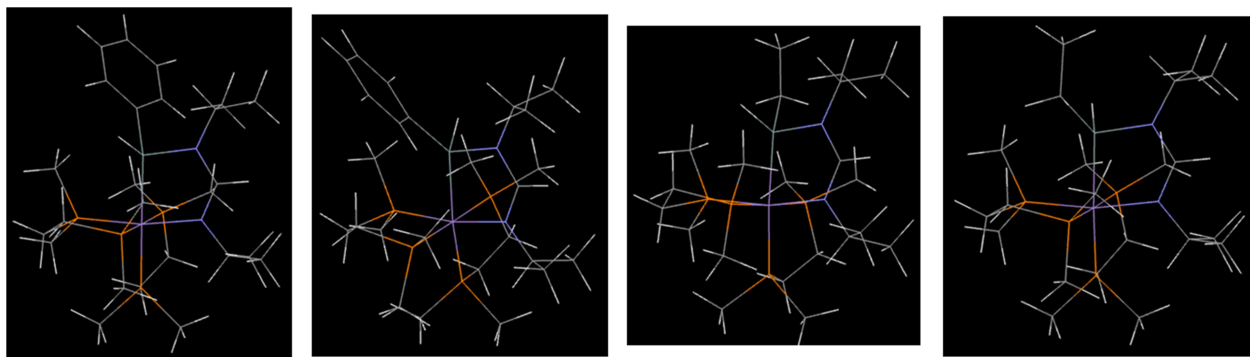


Figure A.1: Calculated structures of, from left to right, two isomers of $[(\text{dmpe})_2\text{Mn}\{\kappa^2\text{-SiHPh}(\text{N}^i\text{PrCHN}^i\text{Pr})\}]$ ($25^{\text{Ph,H}}$) and two isomers of $[(\text{dmpe})_2\text{Mn}\{\kappa^2\text{-SiHEt}(\text{N}^i\text{PrCHN}^i\text{Pr})\}]$ ($25^{\text{Et,H}}$).

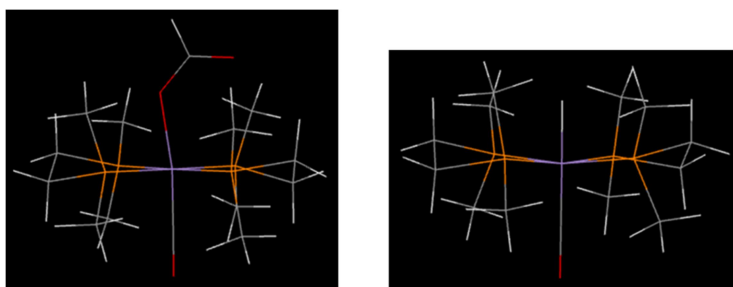


Figure A.2: Calculated structures of, from left to right, *trans*- $[(\text{dmpe})_2\text{Mn}(\text{CO})(\kappa^1\text{-O}_2\text{CH})]$ (**26**) and *trans*- $[(\text{dmpe})_2\text{MnH}(\text{CO})]$ (**27**).

Figures Showing Superimposed Calculated and X-ray Structures

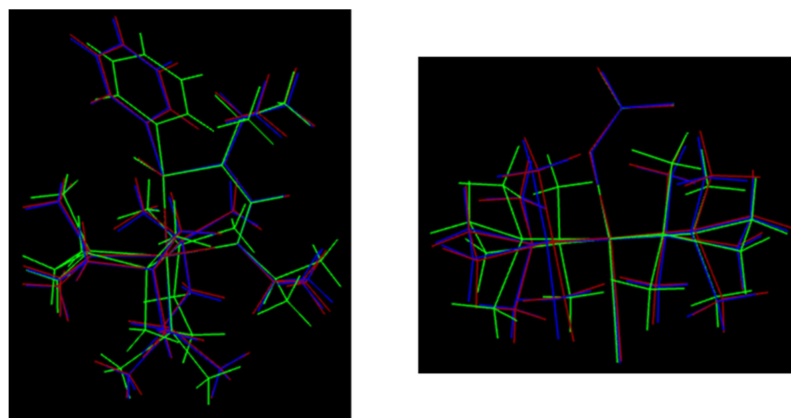


Figure A.3: Superimposed calculated (red) and X-ray (blue and green) structures of, from left to right, $[(dmpe)_2Mn\{\kappa^2-SiHPh(N^iPrCHN^iPr)\}]$ ($25^{Ph,H}$) and $trans-[(dmpe)_2Mn(CO)(\kappa^1-O_2CH)]$ (26). The two X-ray structures in each figure are from two independent and essentially isostructural molecules in the unit cell.

Tables of Calculated and Crystallographically Determined Bond Lengths, Mayer Bond Orders, and Angles

Table A.1: Selected Distances (Å) (and Mayer Bond Orders) for DFT Calculated or XRD Structures of κ^2 -amidinylsilyl Complexes $25^{R,H}$.

Complex (L = dmpe)	Mn-Si	Mn-N	Si-N	Si-H	Si-C	NC-N _{Si}	NC-N _{Mn}	C _{ipr} -N
$[L_2Mn\{\kappa^2-SiHPh(N^iPrCHN^iPr)\}]$ ($25^{Ph,H}$) isomer 1 (DFT)	2.32 (0.95)	2.12 (0.59)	1.82 (0.74)	1.53 (0.74)	1.93 (0.81)	1.35 (1.23)	1.31 (1.50)	1.47, 1.48 (0.89, 0.92)
$[L_2Mn\{\kappa^2-SiHPh(N^iPrCHN^iPr)\}]$ ($25^{Ph,H}$) isomer 2 (DFT)	2.32 (0.93)	2.12 (0.58)	1.82 (0.74)	1.53 (0.75)	1.93 (0.80)	1.34 (1.24)	1.31 (1.50)	1.47, 1.48 (0.90, 0.92)
$[L_2Mn\{\kappa^2-SiHPh(N^iPrCHN^iPr)\}]$ ($25^{Ph,H}$) (XRD) ^a	2.347(1), 2.358(1)	2.137(3), 2.141(3)	1.805(3), 1.813(3)	1.45(4), 1.47(5)	1.934(4), 1.939(3)	1.350(4), 1.350(5)	1.296(6), 1.299(5)	1.480(5)- 1.492(4)
$[L_2Mn\{\kappa^2-SiHEt(N^iPrCHN^iPr)\}]$ ($25^{Et,H}$) isomer 1 (DFT)	2.32 (0.95)	2.13 (0.59)	1.83 (0.70)	1.54 (0.75)	1.94 (0.67)	1.34 (1.25)	1.31 (1.50)	1.47, 1.48 (0.90, 0.93)
$[L_2Mn\{\kappa^2-SiHEt(N^iPrCHN^iPr)\}]$ ($25^{Et,H}$) isomer 2 (DFT)	2.32 (0.93)	2.13 (0.59)	1.83 (0.69)	1.53 (0.75)	1.94 (0.67)	1.34 (1.24)	1.31 (1.50)	1.47, 1.48 (0.90, 0.92)

a. The X-ray structure of $25^{Ph,H}$ includes two independent and essentially isostructural structures in the asymmetric unit and the range of listed values encompasses these two structures.

Table A.2: Selected Angles (°) for DFT Calculated or XRD Structures of κ^2 -amidinylsilyl Complexes **25^{R,H}**.

Complex (L = dmpe)	Mn–Si–R	Si–Mn–N
[L ₂ Mn{ κ^2 -SiHPh(N ⁱ PrCHN ⁱ Pr)}] (25^{Ph,H}) <i>isomer 1</i> (DFT)	H: 118.9, C: 136.5, N: 100.3	80.9
[L ₂ Mn{ κ^2 -SiHPh(N ⁱ PrCHN ⁱ Pr)}] (25^{Ph,H}) <i>isomer 2</i> (DFT)	H: 119.5, C: 134.7, N: 100.7	80.5
[L ₂ Mn{ κ^2 -SiHPh(N ⁱ PrCHN ⁱ Pr)}] (25^{Ph,H}) (XRD) ^a	H: 118(2), 119(2), C: 132.8(1), 136.4(1), N: 100.5(1), 100.6(1)	79.40(9), 80.13(8)
[L ₂ Mn{ κ^2 -SiHEt(N ⁱ PrCHN ⁱ Pr)}] (25^{Et,H}) <i>isomer 1</i> (DFT)	H: 121.1, C: 129.1, N: 100.5	80.8
[L ₂ Mn{ κ^2 -SiHEt(N ⁱ PrCHN ⁱ Pr)}] (25^{Et,H}) <i>isomer 2</i> (DFT)	H: 121.2, C: 128.6, N: 100.6	80.4

a. The X-ray structure of **25^{Ph,H}** includes two independent and essentially isostructural structures in the asymmetric unit and the range of listed values encompasses these two structures.

Table A.3: Selected Angles (°) and Distances (Å) (and Mayer Bond Orders) for DFT Calculated {or XRD} Structures of Formate Complex **26**.^a

Complex	Mn–C	Mn–O	O–C _{Mn}	O _{Mn} –C	O–C _{formate}	C–Mn–O	Mn–O–C	O–C–O
<i>trans</i> - [(dmpe) ₂ Mn(CO)(κ^1 -O ₂ CH)] (26)	1.73 (1.65) {1.742(1), 1.751(1)}	2.10 (0.48) {2.086(1), 2.096(1)}	1.19 (1.86) {1.175(2), 1.191(2)}	1.29 (1.33) {1.266(2), 1.275(2)}	1.24 (1.65) {1.229(2), 1.237(2)}	171.3 {172.23(5), 173.31(5)}	129.6 {133.53(9), 133.78(9)}	128.7 {128.8(1), 128.9(1)}

a. The X-ray structure of **26** includes two independent and essentially isostructural structures in the asymmetric unit and the range of listed values encompasses these two structures.

Tables of Total Bonding Energies and Thermodynamic Parameters for Calculated Structures

Table A.4: Total bonding energy (E), Enthalpy (H), Entropy (S), and Gibbs Free Energy (G) at 298 K for DFT Calculated Structures of κ^2 -amidinylsilyl Complexes **25^{R,H}**.

Complex	E (kJ mol ⁻¹)	H (kJ mol ⁻¹)	S (kJ mol ⁻¹ K ⁻¹)
[(dmpe) ₂ Mn{ κ^2 -SiHPh(N ⁱ PrCHN ⁱ Pr)}] (25^{Ph,H}) <i>isomer 1</i>	-46182.18	[(dmpe) ₂ Mn{ κ^2 -SiHEt(N ⁱ PrCHN ⁱ Pr)}] (25^{Et,H}) <i>isomer 1</i>	-42722.45
[(dmpe) ₂ Mn{ κ^2 -SiHPh(N ⁱ PrCHN ⁱ Pr)}] (25^{Ph,H}) <i>isomer 2</i>	-46181.47	[(dmpe) ₂ Mn{ κ^2 -SiHEt(N ⁱ PrCHN ⁱ Pr)}] (25^{Et,H}) <i>isomer 2</i>	-42720.65

Table A.5: Total bonding energy (E), Enthalpy (H), Entropy (S), and Gibbs Free Energy (G) at 298 K for DFT Calculated Structures of Formate Complex **26**, and Products of CO₂ Abstraction from **26**.

Complex	E (kJ mol ⁻¹)	H (kJ mol ⁻¹)	S (J mol ⁻¹ K ⁻¹)	G (kJ mol ⁻¹)
<i>trans</i> -[(dmpe) ₂ Mn(CO)(κ ¹ -O ₂ CH)] (26)	-29386.52	-28137.27	813.70	-28379.88
<i>trans</i> -[(dmpe) ₂ MnH(CO)] (27)	-27089.63	-25893.17	765.5339	-26121.42
CO ₂	-2231.96	-2192.90	219.8315	-2258.44

Tables of Hirshfeld Charges for Calculated Structures

Table A.6: Hirshfeld Charges for DFT Calculated Structures of κ²-amidinylsilyl Complexes **25**.

Complex	Mn	Si	N _{Si}	N _{Mn}	H _{Si}	$\frac{NC(H)}{C}$	\overline{NCN}	C _{Si}	C _{Pr}
[(dmpe) ₂ Mn{κ ² -SiHPh(N ⁱ PrCHN ⁱ Pr)}] (25^{Ph,H}) <i>isomer 1</i>	-0.225	0.192	-0.117	-0.098	-0.104	0.042	0.066	-0.087	0.014, 0.021
[(dmpe) ₂ Mn{κ ² -SiHPh(N ⁱ PrCHN ⁱ Pr)}] (25^{Ph,H}) <i>isomer 2</i>	-0.225	0.191	-0.116	-0.100	-0.103	0.042	0.064	-0.089	0.015, 0.022
[(dmpe) ₂ Mn{κ ² -SiHEt(N ⁱ PrCHN ⁱ Pr)}] (25^{Et,H}) <i>isomer 1</i>	-0.227	0.195	-0.117	-0.100	-0.108	0.041	0.064	-0.160	0.014, 0.023
[(dmpe) ₂ Mn{κ ² -SiHEt(N ⁱ PrCHN ⁱ Pr)}] (25^{Et,H}) <i>isomer 2</i>	-0.226	0.195	-0.118	-0.100	-0.106	0.041	0.065	-0.160	0.015, 0.023

Table A.7: Hirshfeld Charges for DFT Calculated Structure of Formate Complex **26**.

Complex	Mn	C _{Mn}	O _{Mn}	O _{CO}	$\overline{OC(H)OMn}$	$\overline{OC(H)OMn}$	$\overline{OC(H)OMn}$
<i>trans</i> -[(dmpe) ₂ Mn(CO)(κ ¹ -O ₂ CH)] (26)	-0.141	0.000	-0.200	-0.199	-0.265	0.111	0.018

Tables of Crystal Data and Crystal Structure Refinement**Table A.8:** Crystal and structure refinement data for $[(\text{dmpe})_2\text{Mn}\{\kappa^2\text{-SiHPh}(\text{N}^i\text{PrCHN}^i\text{Pr})\}]$ (**25^{Ph,H}**).

Identification code	MnHSiPh_CDI
Empirical formula	$\text{C}_{25}\text{H}_{53}\text{MnN}_2\text{P}_4\text{Si}$
Formula weight	588.60
Temperature/K	100.0
Crystal system	triclinic
Space group	P-1
$a/\text{\AA}$	9.5886(3)
$b/\text{\AA}$	18.3971(7)
$c/\text{\AA}$	18.7841(7)
$\alpha/^\circ$	75.3350(10)
$\beta/^\circ$	79.6850(10)
$\gamma/^\circ$	83.8060(10)
Volume/ \AA^3	3147.0(2)
Z	4
$\rho_{\text{calc}}/\text{g/cm}^3$	1.242
μ/mm^{-1}	0.677
F(000)	1264.0
Crystal size/ mm^3	$0.25 \times 0.2 \times 0.1$
Radiation	MoK α ($\lambda = 0.71073$)
2Θ range for data collection/ $^\circ$	2.27 to 56.564
Index ranges	$-12 \leq h \leq 12, -24 \leq k \leq 24, -25 \leq l \leq 25$
Reflections collected	80616
Independent reflections	15536 [$R_{\text{int}} = 0.0551, R_{\text{sigma}} = 0.0507$]
Data/restraints/parameters	15536/244/710
Goodness-of-fit on F^2	1.050
Final R indexes [$I \geq 2\sigma(I)$]	$R_1 = 0.0684, wR_2 = 0.1408$
Final R indexes [all data]	$R_1 = 0.0967, wR_2 = 0.1536$
Largest diff. peak/hole / $e \text{\AA}^{-3}$	2.14/-2.24

Table A.9: Crystal and structure refinement data for *trans*-[(dmpe)₂Mn(CO)(κ¹-O₂CH)] (26).

Identification code	Mn_Formate
Empirical formula	C ₁₄ H ₃₃ MnO ₃ P ₄
Formula weight	428.22
Temperature/K	100.0
Crystal system	triclinic
Space group	P-1
a/Å	9.2787(5)
b/Å	15.7180(8)
c/Å	15.7273(8)
α/°	113.535(3)
β/°	93.975(3)
γ/°	94.018(3)
Volume/Å ³	2085.84(19)
Z	4
ρ _{calc} /g/cm ³	1.364
μ/mm ⁻¹	0.947
F(000)	904.0
Crystal size/mm ³	0.4 × 0.4 × 0.3
Radiation	MoKα (λ = 0.71073)
2θ range for data collection/°	3.096 to 61.016
Index ranges	-13 ≤ h ≤ 13, -22 ≤ k ≤ 22, -22 ≤ l ≤ 22
Reflections collected	109835
Independent reflections	12724 [R _{int} = 0.0366, R _{sigma} = 0.0222]
Data/restraints/parameters	12724/0/422
Goodness-of-fit on F ²	1.035
Final R indexes [I ≥ 2σ (I)]	R ₁ = 0.0212, wR ₂ = 0.0503
Final R indexes [all data]	R ₁ = 0.0244, wR ₂ = 0.0519
Largest diff. peak/hole / e Å ⁻³	0.43/-0.25

Selected NMR Spectra for Complexes 25^{R,H} and 26

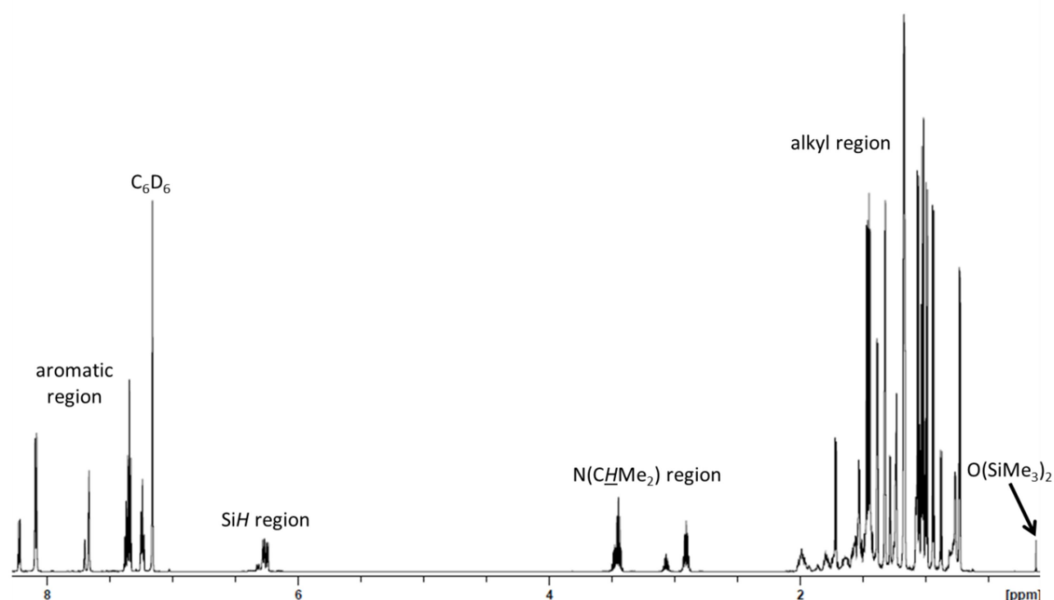


Figure A.4: ¹H NMR spectrum of [(dmpe)₂Mn{κ²-SiHPh(N^{*i*}PrCHN^{*i*}Pr)}] (**25^{Ph,H}**) in C₆D₆ (600 MHz, 298 K).

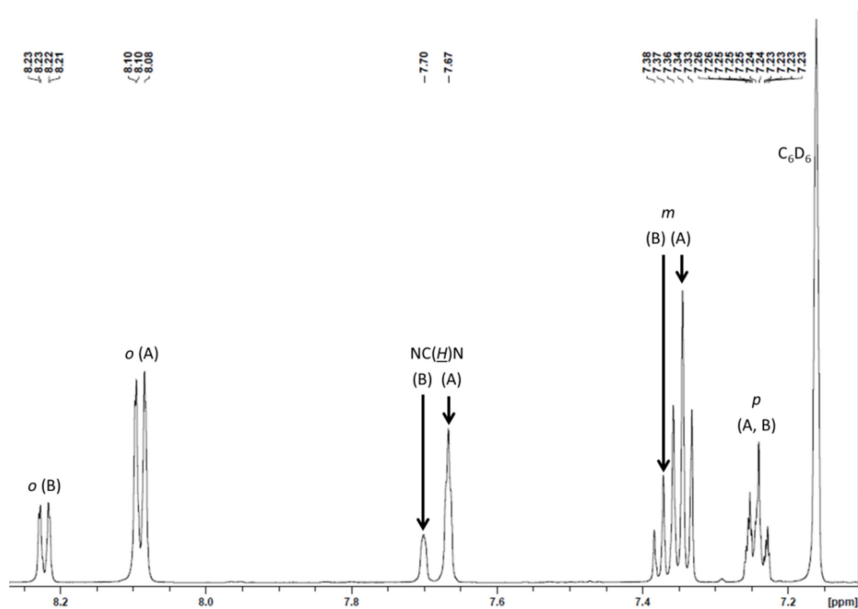


Figure A.5: Expanded aromatic region of the ¹H NMR spectrum of [(dmpe)₂Mn{κ²-SiHPh(N^{*i*}PrCHN^{*i*}Pr)}] (**25^{Ph,H}**) in C₆D₆ (600 MHz, 298 K). A and B represent peaks from the dominant and minor isomers, respectively.

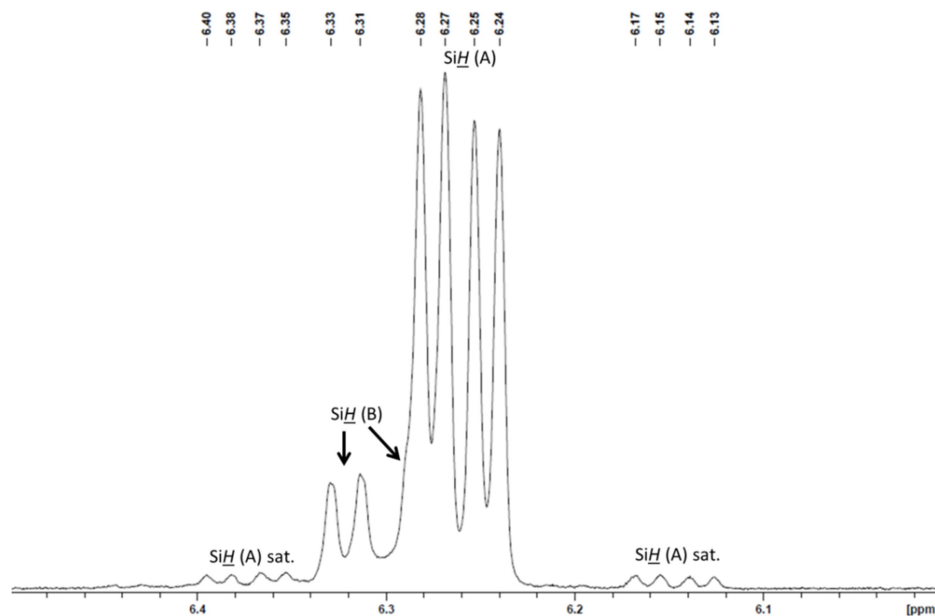


Figure A.6: Expanded SiH region of the ^1H NMR spectrum of $[(\text{dmpe})_2\text{Mn}\{\kappa^2\text{-SiHPh}(\text{N}^i\text{PrCHN}^i\text{Pr})\}]$ ($25^{\text{Ph,H}}$) in C_6D_6 (600 MHz, 298 K). A and B represent peaks from the dominant and minor isomers, respectively.

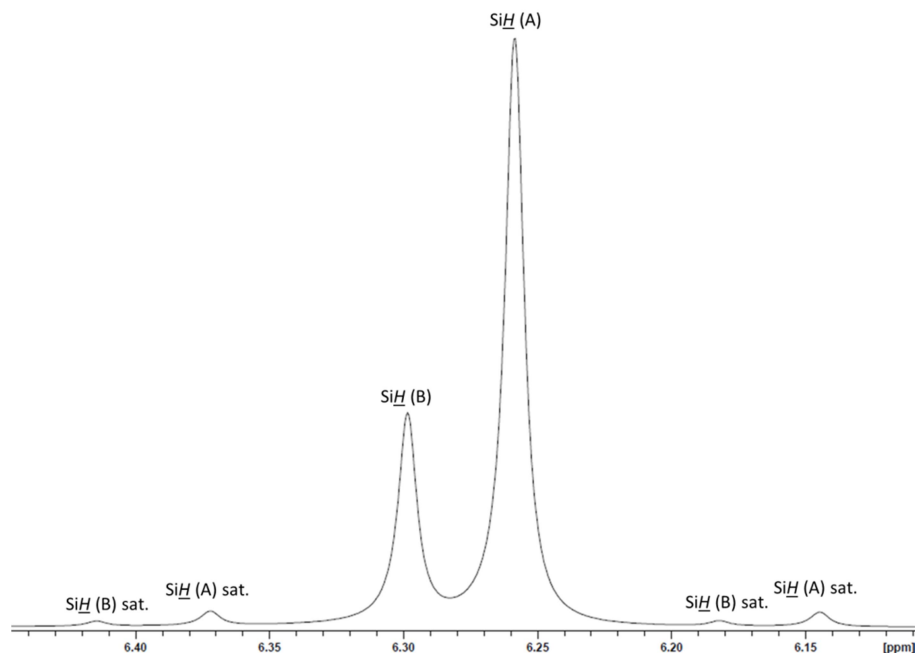


Figure A.7: Expanded SiH region of the $^1\text{H}\{^{31}\text{P}\}$ NMR spectrum of $[(\text{dmpe})_2\text{Mn}\{\kappa^2\text{-SiHPh}(\text{N}^i\text{PrCHN}^i\text{Pr})\}]$ ($25^{\text{Ph,H}}$) in C_6D_6 (600 MHz, 298 K). A and B represent peaks from the dominant and minor isomers, respectively.

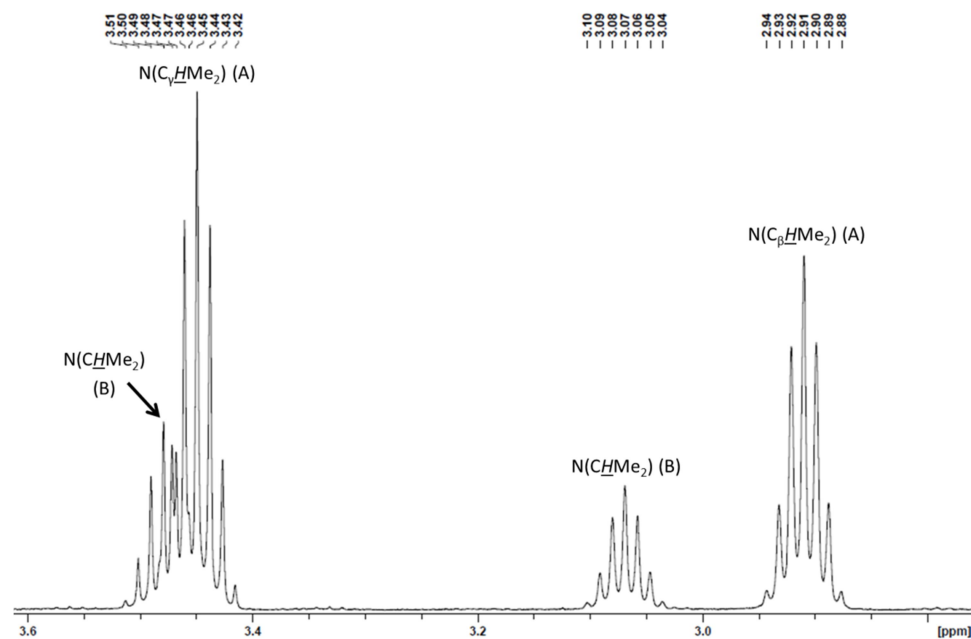


Figure A.8: Expanded $N(\underline{C}HMe_2)$ region of the 1H NMR spectrum of $[(dmpe)_2Mn\{\kappa^2-SiHPh(N^iPrCHN^iPr)\}]$ ($25^{Ph,H}$) in C_6D_6 (600 MHz, 298 K). A and B represent peaks from the dominant and minor isomers, respectively.

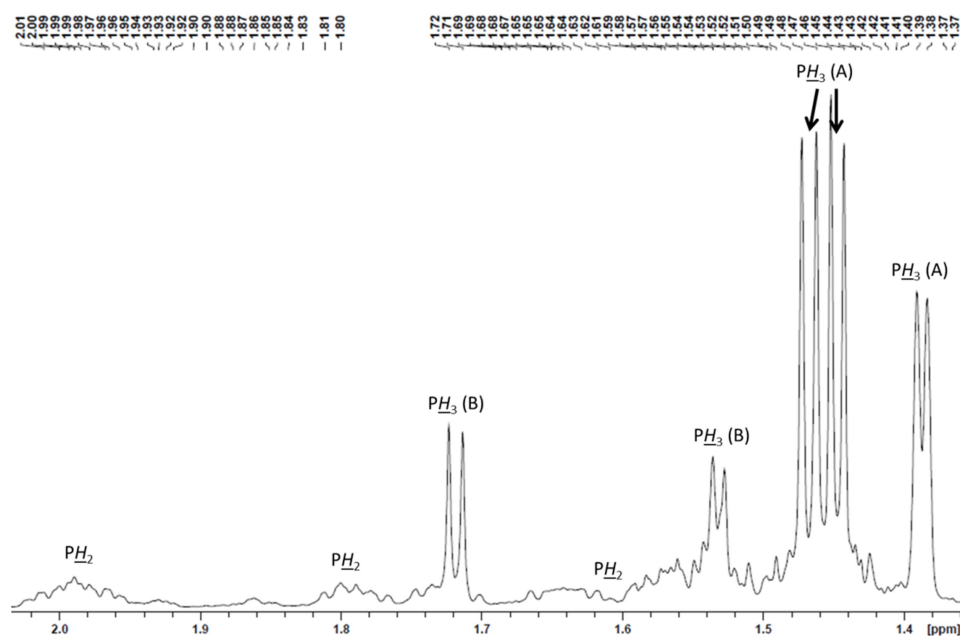


Figure A.9: Expanded high frequency alkyl region of the 1H NMR spectrum of $[(dmpe)_2Mn\{\kappa^2-SiHPh(N^iPrCHN^iPr)\}]$ ($25^{Ph,H}$) in C_6D_6 (600 MHz, 298 K). A and B represent peaks from the dominant and minor isomers, respectively.

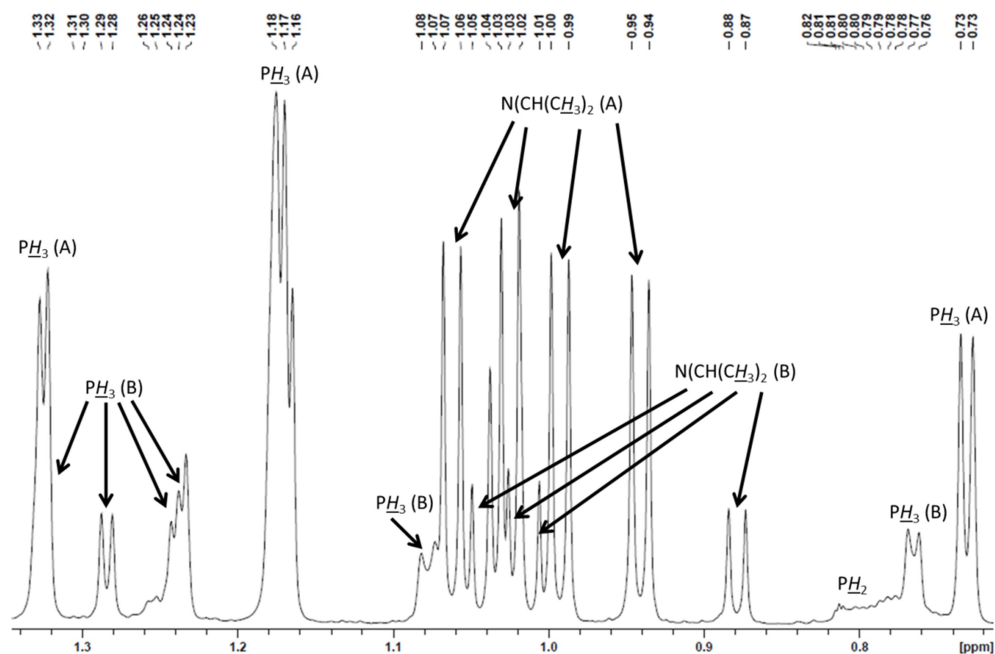


Figure A.10: Expanded low frequency alkyl region of the ^1H NMR spectrum of $[(\text{dmpe})_2\text{Mn}\{\kappa^2\text{-SiHPh}(\text{N}^i\text{PrCHN}^i\text{Pr})\}]$ ($25^{\text{Ph,H}}$) in C_6D_6 (600 MHz, 298 K). A and B represent peaks from the dominant and minor isomers, respectively.

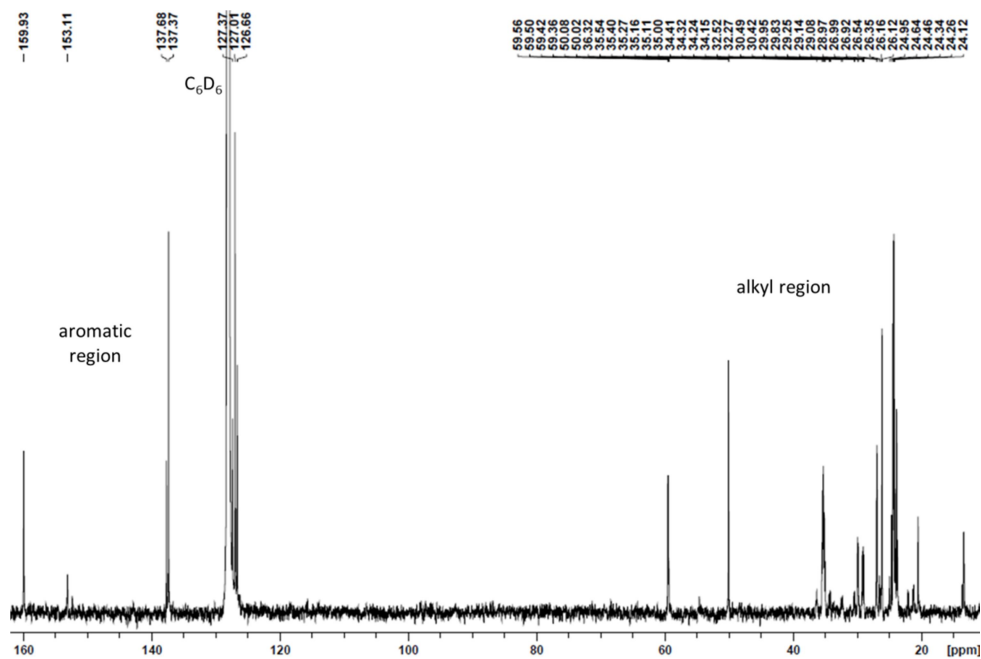


Figure A.11: $^{13}\text{C}\{^1\text{H}\}$ NMR spectrum of $[(\text{dmpe})_2\text{Mn}\{\kappa^2\text{-SiHPh}(\text{N}^i\text{PrCHN}^i\text{Pr})\}]$ ($25^{\text{Ph,H}}$) in C_6D_6 (151 MHz, 298 K).

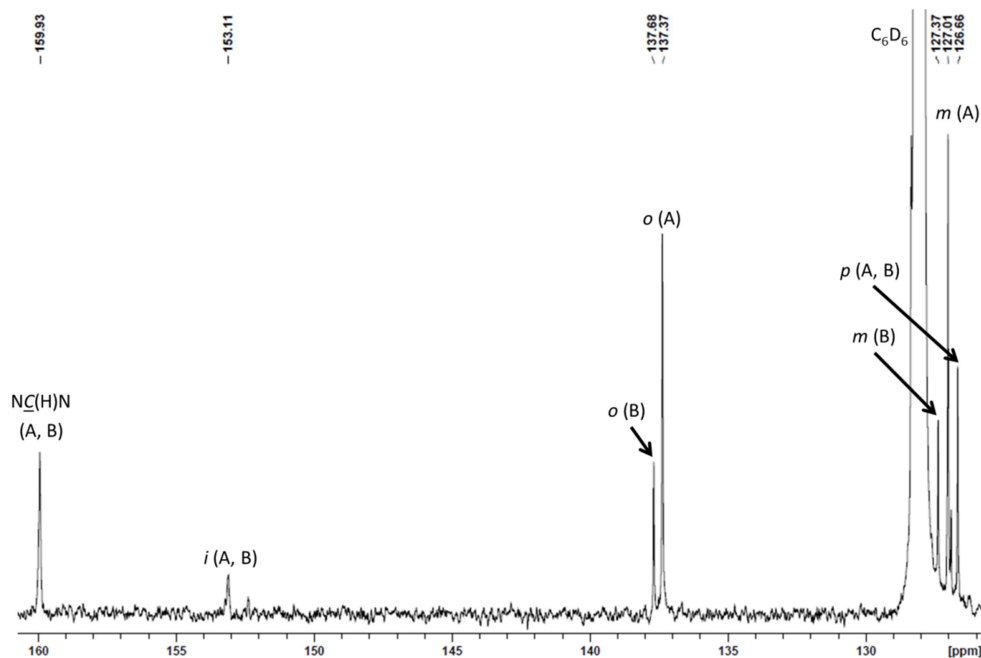


Figure A.12: Expanded aromatic region of the $^{13}\text{C}\{^1\text{H}\}$ NMR spectrum of $[(\text{dmpe})_2\text{Mn}\{\kappa^2\text{-SiHPh}(\text{N}^i\text{PrCHN}^i\text{Pr})\}]$ ($25^{\text{Ph,H}}$) in C_6D_6 (151 MHz, 298 K). A and B represent peaks from the dominant and minor isomers, respectively.

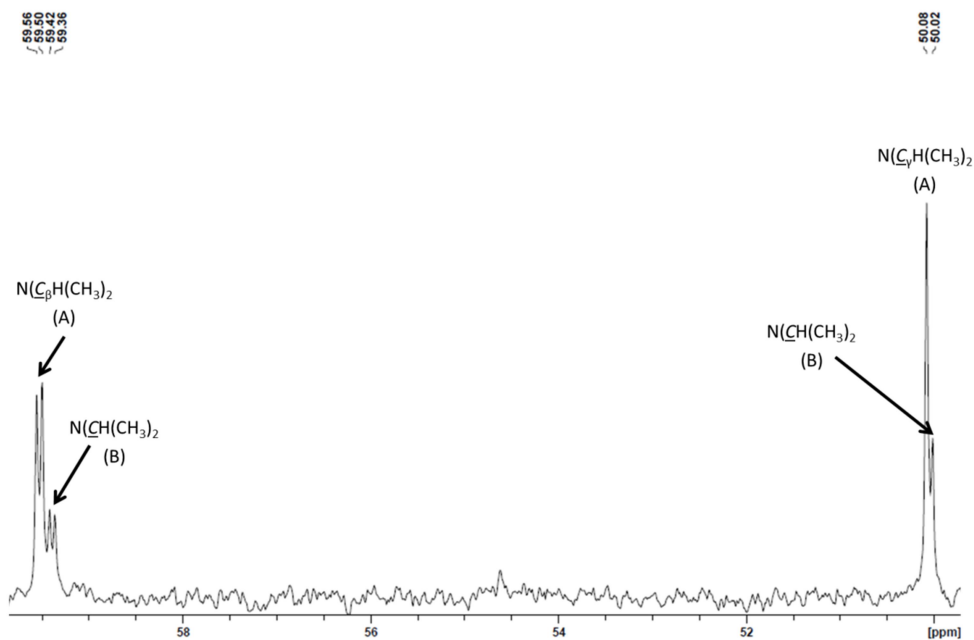


Figure A.13: Expanded $\text{N}(\underline{\text{C}}\text{HMe}_2)$ region of the $^{13}\text{C}\{^1\text{H}\}$ NMR spectrum of $[(\text{dmpe})_2\text{Mn}\{\kappa^2\text{-SiHPh}(\text{N}^i\text{PrCHN}^i\text{Pr})\}]$ ($25^{\text{Ph,H}}$) in C_6D_6 (151 MHz, 298 K). A and B represent peaks from the dominant and minor isomers, respectively.

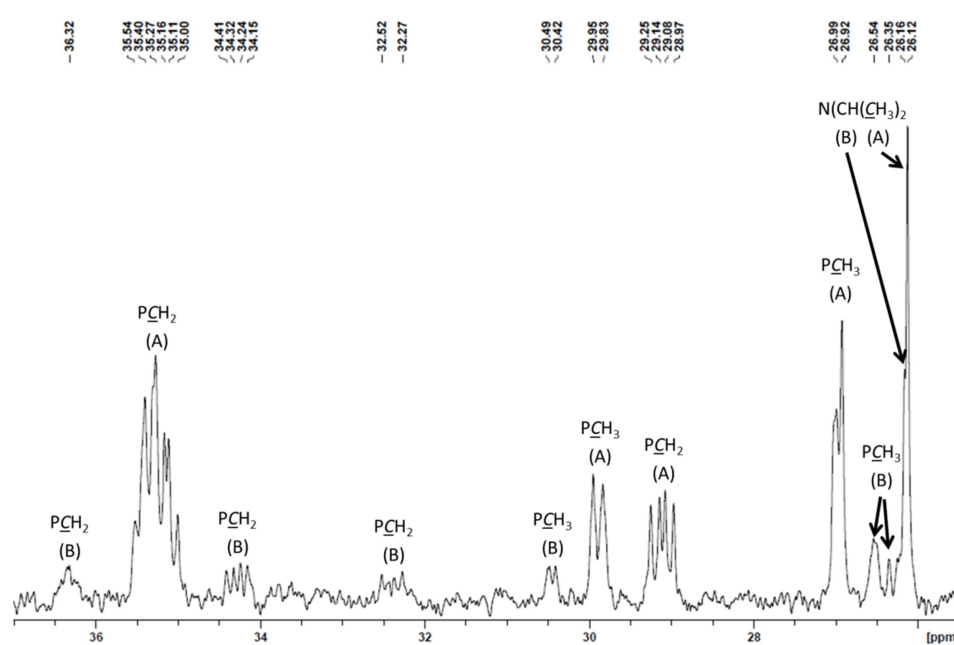


Figure A.14: Expanded high frequency alkyl region of the $^{13}\text{C}\{^1\text{H}\}$ NMR spectrum of $[(\text{dmpe})_2\text{Mn}\{\kappa^2\text{-SiHPh}(\text{N}^i\text{PrCHN}^i\text{Pr})\}]$ ($25^{\text{Ph,H}}$) in C_6D_6 (151 MHz, 298 K). A and B represent peaks from the dominant and minor isomers, respectively.

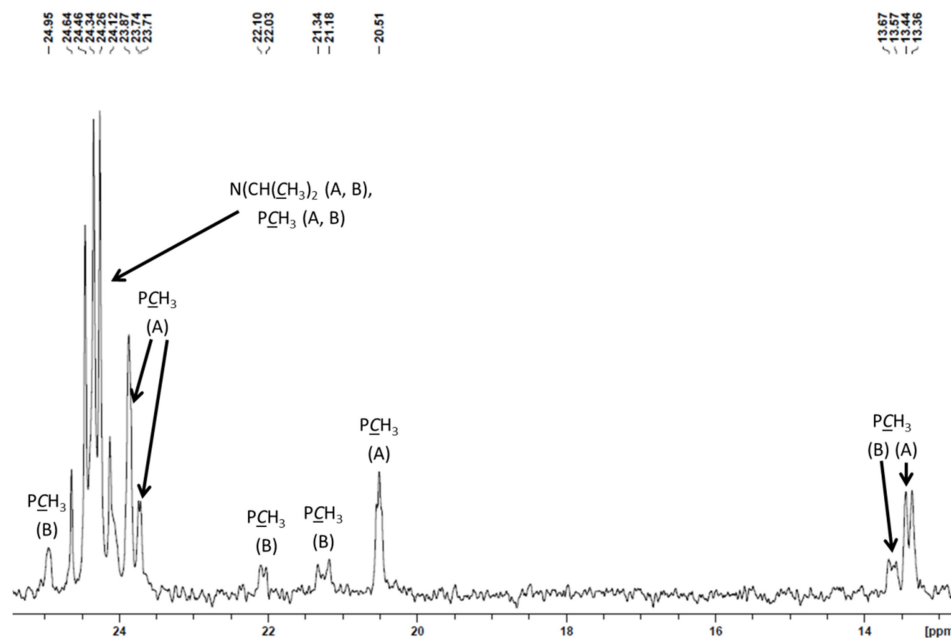


Figure A.15: Expanded low frequency alkyl region of the $^{13}\text{C}\{^1\text{H}\}$ NMR spectrum of $[(\text{dmpe})_2\text{Mn}\{\kappa^2\text{-SiHPh}(\text{N}^i\text{PrCHN}^i\text{Pr})\}]$ ($25^{\text{Ph,H}}$) in C_6D_6 (151 MHz, 298 K). A and B represent peaks from the dominant and minor isomers, respectively.

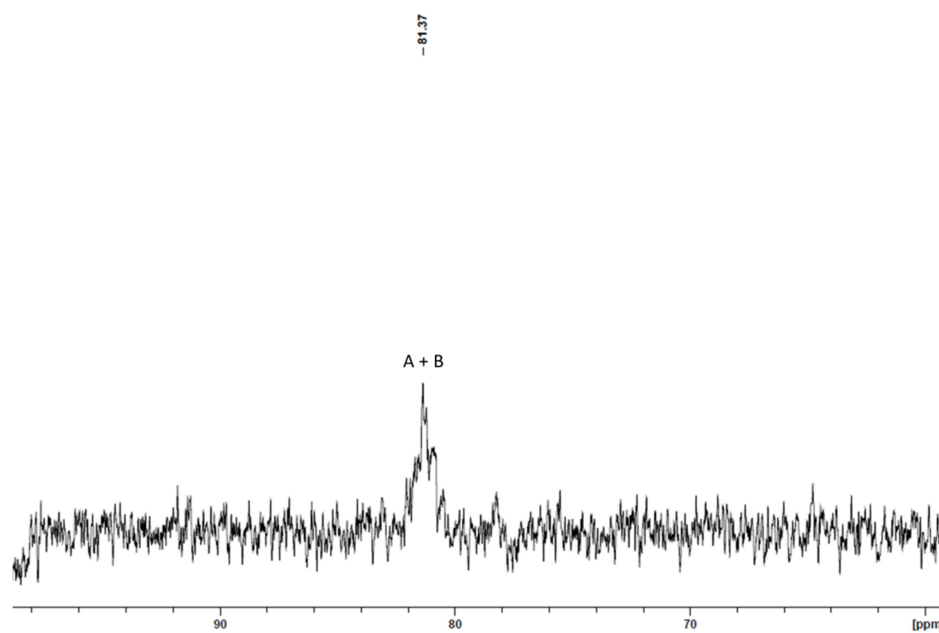


Figure A.16: $^{29}\text{Si}\{^1\text{H}\}$ NMR spectrum of $[(\text{dmpe})_2\text{Mn}\{\kappa^2\text{-SiHPh}(\text{N}^i\text{PrCHN}^i\text{Pr})\}]$ ($25^{\text{Ph,H}}$) in C_6D_6 (119 MHz, 298 K). A and B represent peaks from the dominant and minor isomers, respectively.

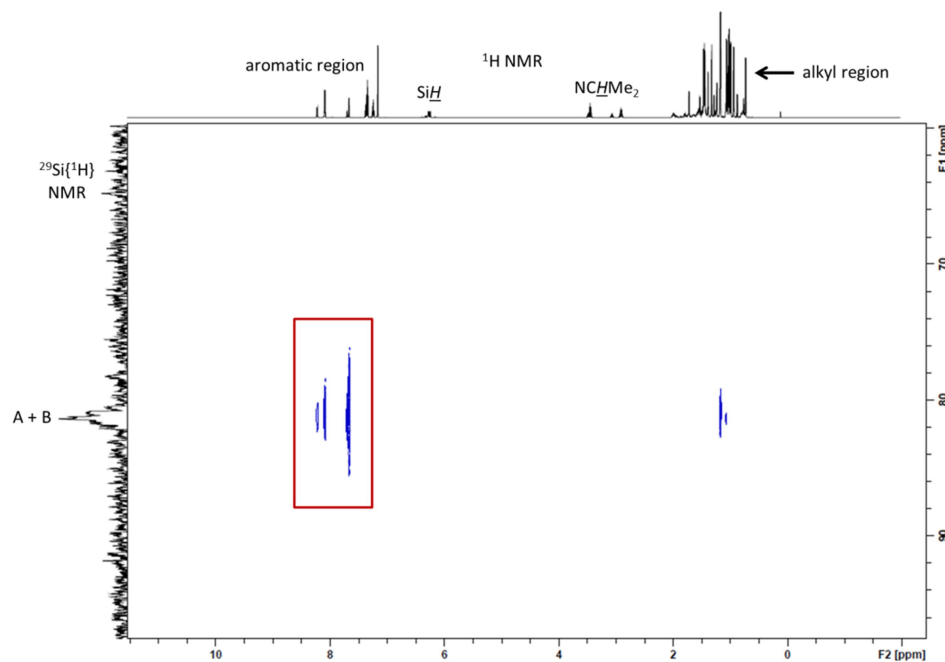


Figure A.17: $^{29}\text{Si}\text{-}^1\text{H}$ HMBC NMR spectrum of $[(\text{dmpe})_2\text{Mn}\{\kappa^2\text{-SiHPh}(\text{N}^i\text{PrCHN}^i\text{Pr})\}]$ ($25^{\text{Ph,H}}$) in C_6D_6 (119 MHz, 298 K). A and B represent peaks from the dominant and minor isomers, respectively.

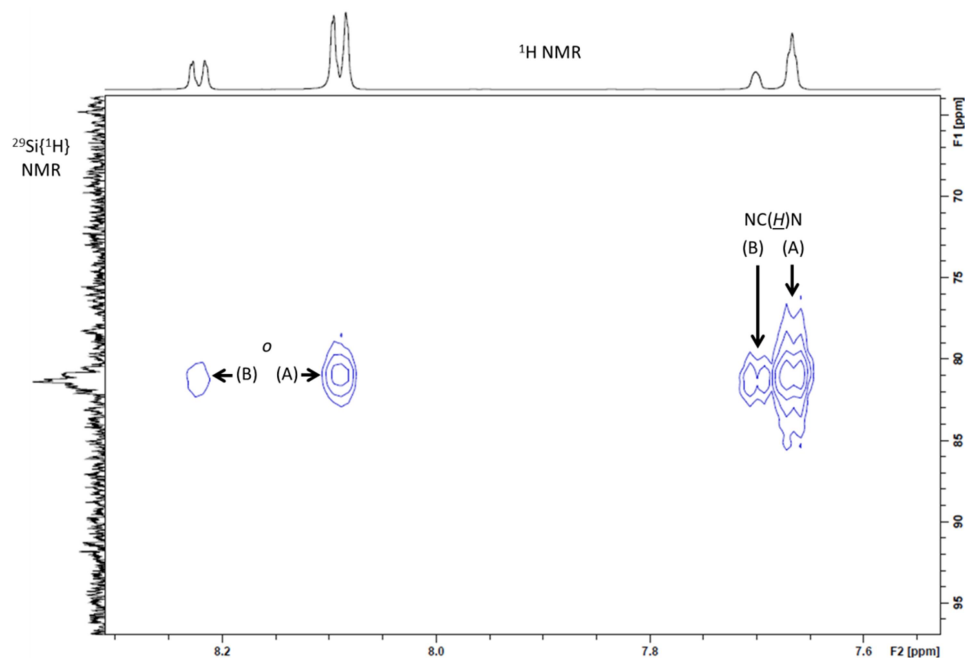


Figure A.18: Expanded aromatic region of the $^{29}\text{Si}\text{-}^1\text{H}$ HMBC NMR spectrum of $[(\text{dmpe})_2\text{Mn}\{\kappa^2\text{-SiHPh}(\text{N}^i\text{PrCHN}^i\text{Pr})\}]$ ($25^{\text{Ph,H}}$) in C_6D_6 (119 MHz, 298 K). A and B represent peaks from the dominant and minor isomers, respectively.

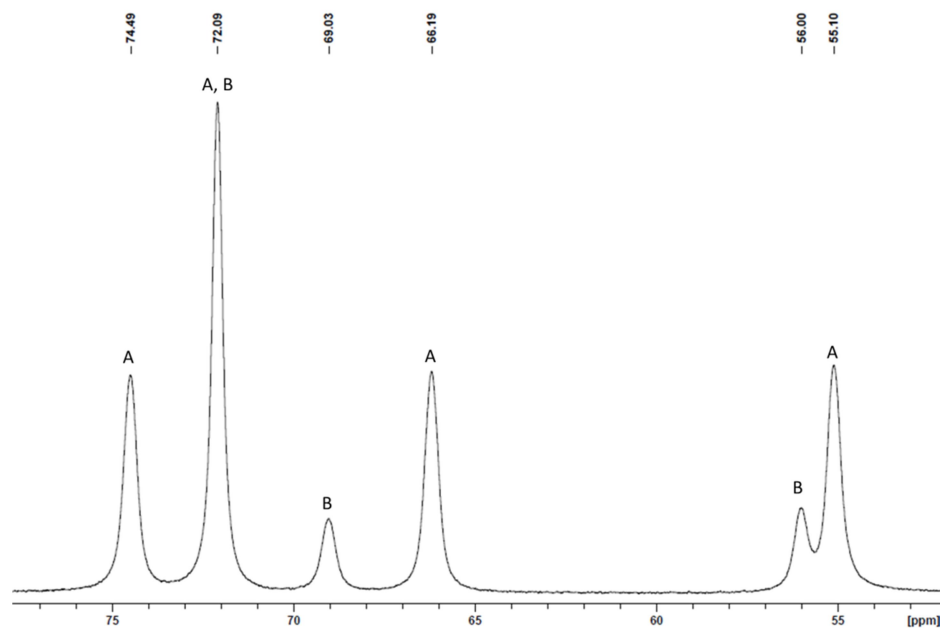


Figure A.19: $^{31}\text{P}\{^1\text{H}\}$ NMR spectrum of $[(\text{dmpe})_2\text{Mn}\{\kappa^2\text{-SiHPh}(\text{N}^i\text{PrCHN}^i\text{Pr})\}]$ ($25^{\text{Ph,H}}$) in C_6D_6 (243 MHz, 298 K). A and B represent peaks from the dominant and minor isomers, respectively.

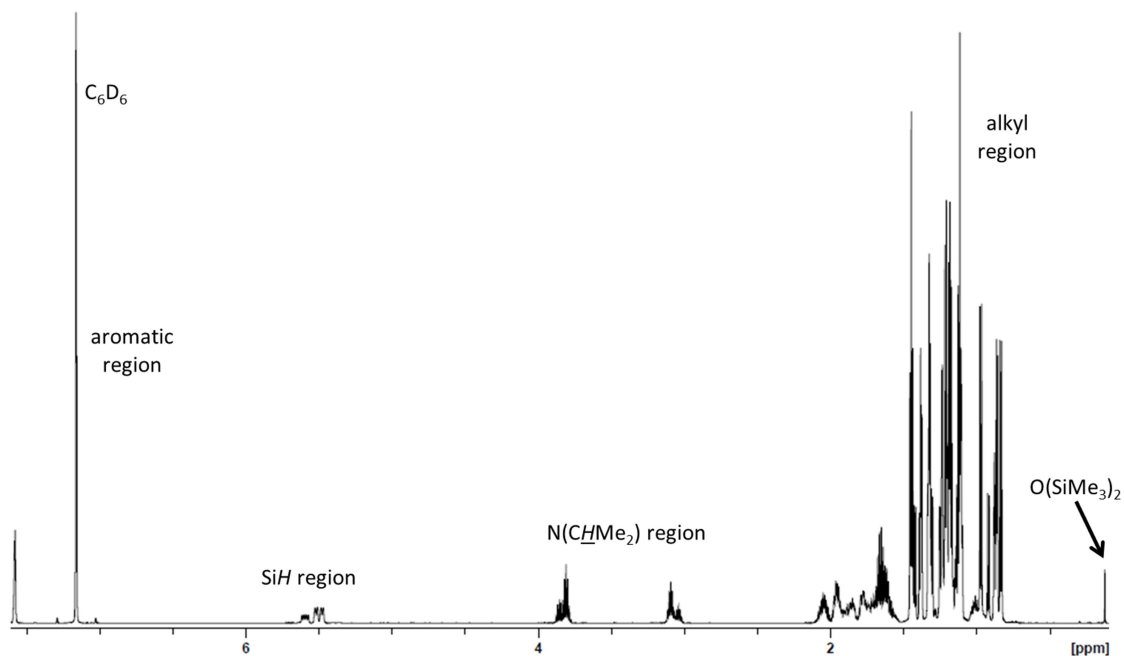


Figure A.20: ^1H NMR spectrum of $[(\text{dmpe})_2\text{Mn}\{\kappa^2\text{-SiH}^n\text{Bu}(\text{N}^i\text{PrCHN}^i\text{Pr})\}]$ ($25^{\text{Bu,H}}$) in C_6D_6 (600 MHz, 298 K).

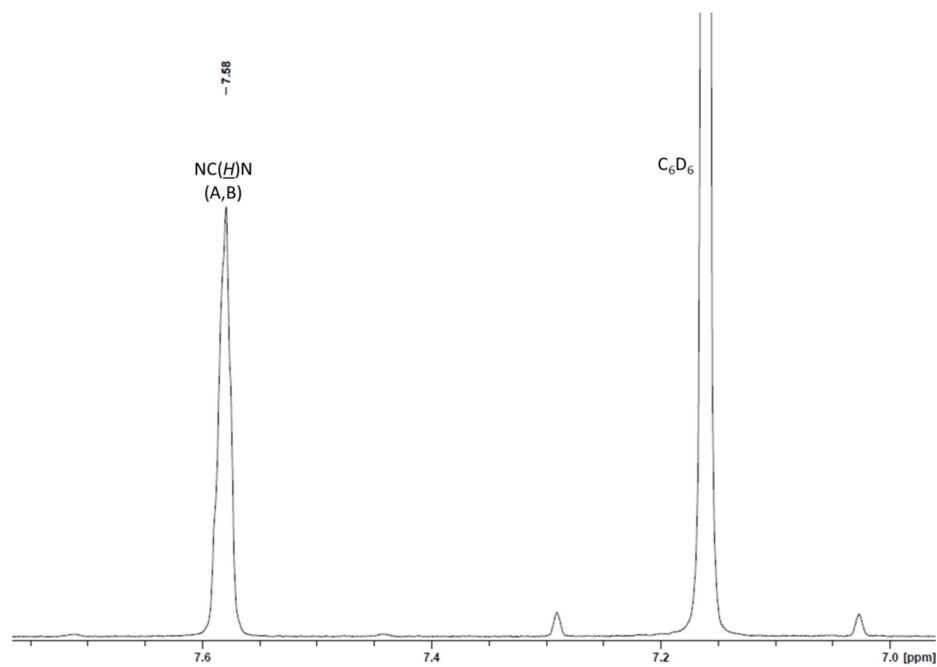


Figure A.21: Expanded $\text{NC}(\text{H})\text{N}$ region of the ^1H NMR spectrum of $[(\text{dmpe})_2\text{Mn}\{\kappa^2\text{-SiH}^n\text{Bu}(\text{N}^i\text{PrCHN}^i\text{Pr})\}]$ ($25^{\text{Bu,H}}$) in C_6D_6 (600 MHz, 298 K). A and B represent peaks from the dominant and minor isomers, respectively.

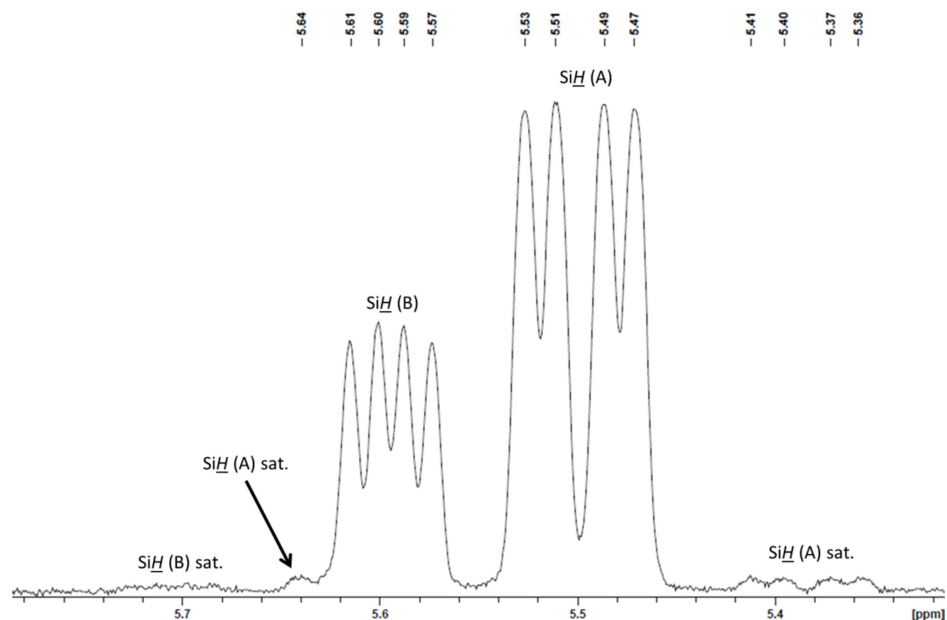


Figure A.22: Expanded SiH region of the ^1H NMR spectrum of $[(\text{dmpe})_2\text{Mn}\{\kappa^2\text{-SiH}^n\text{Bu}(\text{N}^i\text{PrCHN}^i\text{Pr})\}]$ ($25^{\text{Bu,H}}$) in C_6D_6 (600 MHz, 298 K). A and B represent peaks from the dominant and minor isomers, respectively.

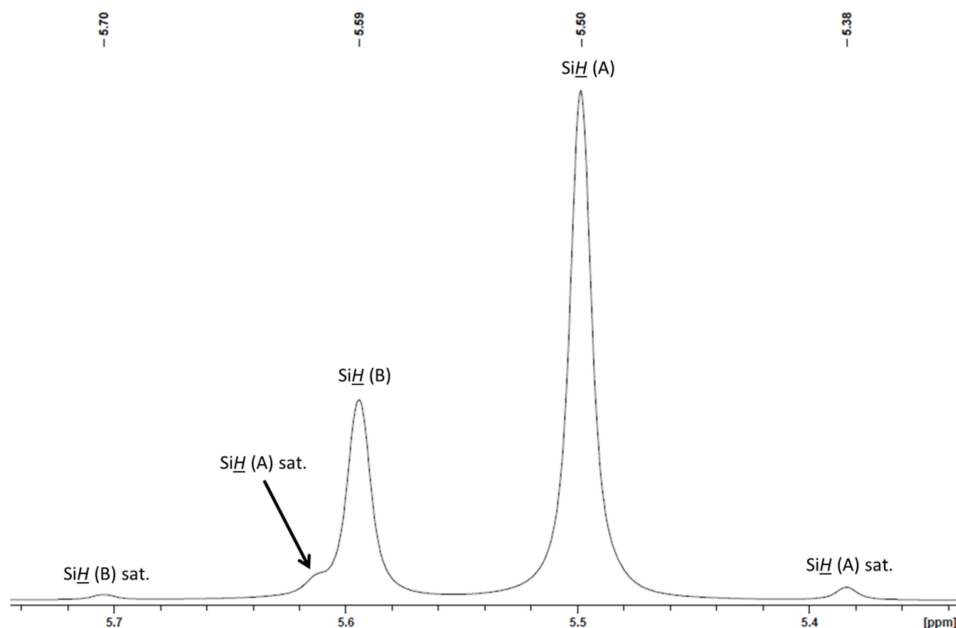


Figure A.23: Expanded SiH region of the $^1\text{H}\{^{31}\text{P}\}$ NMR spectrum of $[(\text{dmpe})_2\text{Mn}\{\kappa^2\text{-SiH}^n\text{Bu}(\text{N}^i\text{PrCHN}^i\text{Pr})\}]$ ($25^{\text{Bu,H}}$) in C_6D_6 (600 MHz, 298 K). A and B represent peaks from the dominant and minor isomers, respectively.

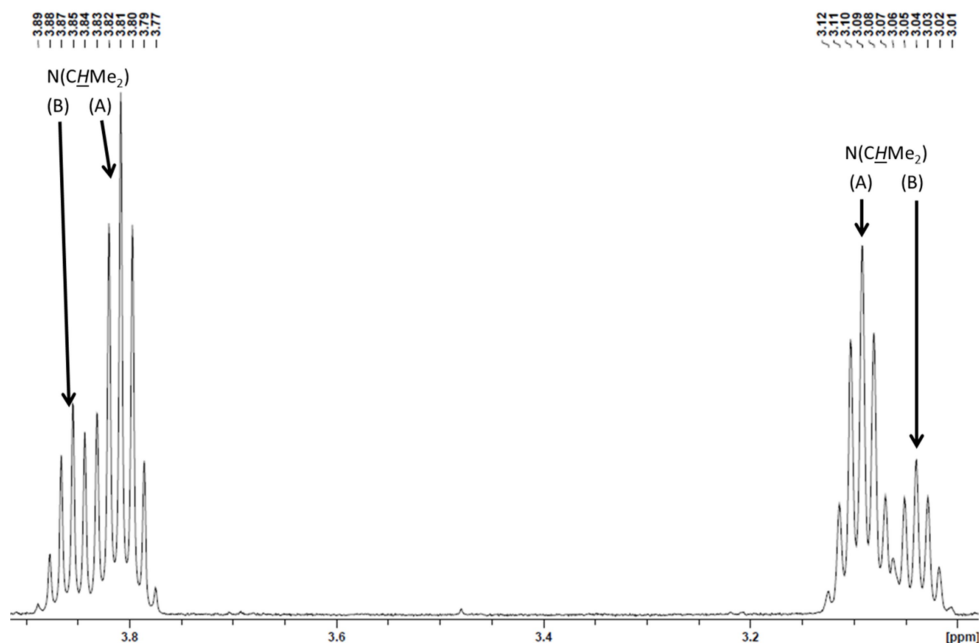


Figure A.24: Expanded $N(CHMe_2)$ region of the 1H NMR spectrum of $[(dmpe)_2Mn\{\kappa^2-SiH^nBu(N^iPrCHN^iPr)\}]$ ($25^{Bu,H}$) in C_6D_6 (600 MHz, 298 K). A and B represent peaks from the dominant and minor isomers, respectively.

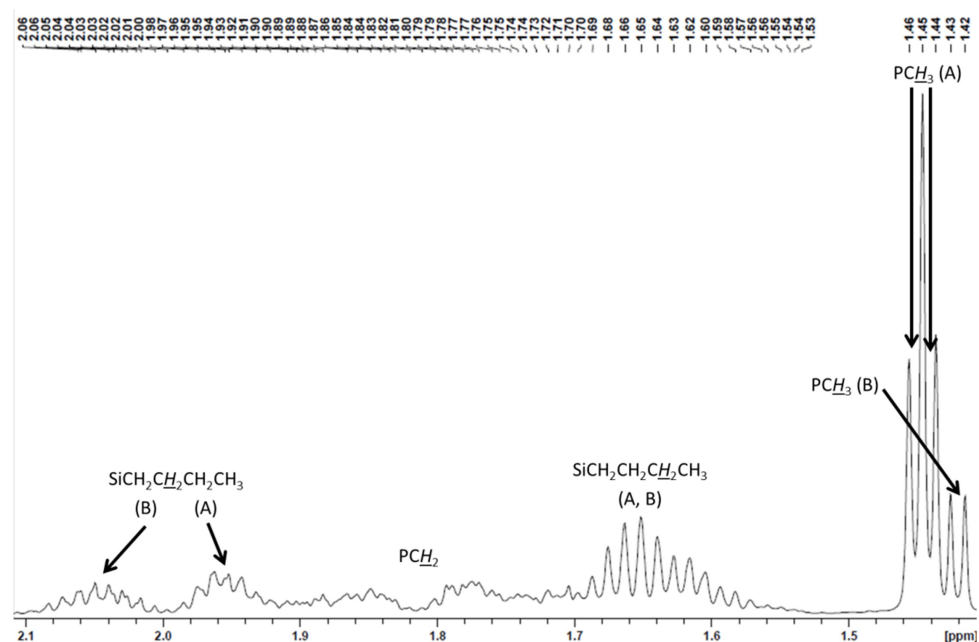


Figure A.25: Expanded high frequency alkyl region of the 1H NMR spectrum of $[(dmpe)_2Mn\{\kappa^2-SiH^nBu(N^iPrCHN^iPr)\}]$ ($25^{Bu,H}$) in C_6D_6 (600 MHz, 298 K). A and B represent peaks from the dominant and minor isomers, respectively.

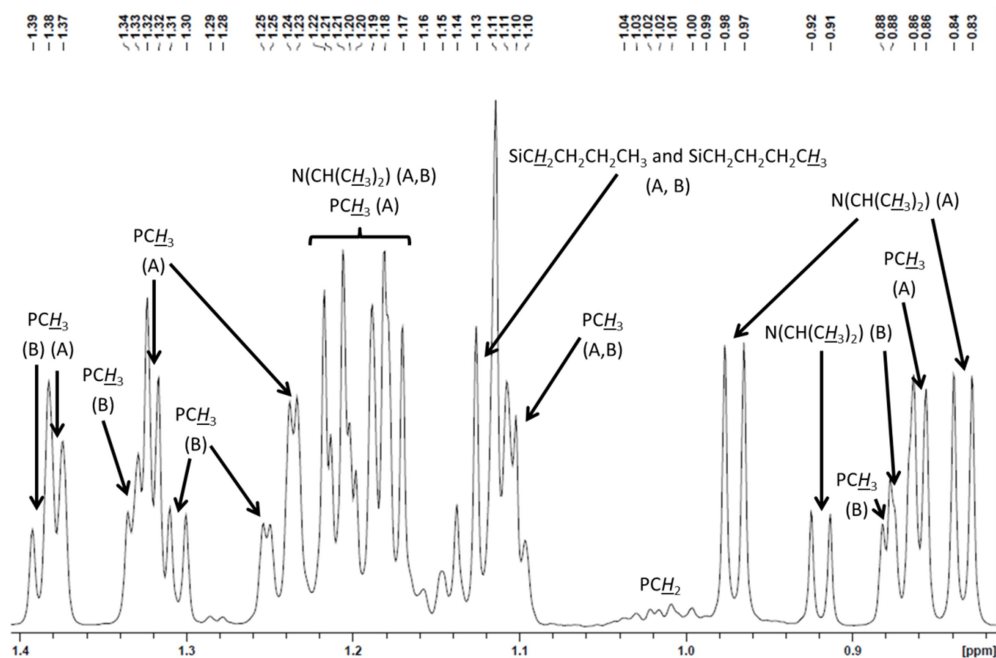


Figure A.26: Expanded low frequency region of the ^1H NMR spectrum of $[(\text{dmpe})_2\text{Mn}\{\kappa^2\text{-SiH}^n\text{Bu}(\text{N}^i\text{PrCHN}^i\text{Pr})\}]$ ($25^{\text{Bu,H}}$) in C_6D_6 (600 MHz, 298 K). A and B represent peaks from the dominant and minor isomers, respectively.

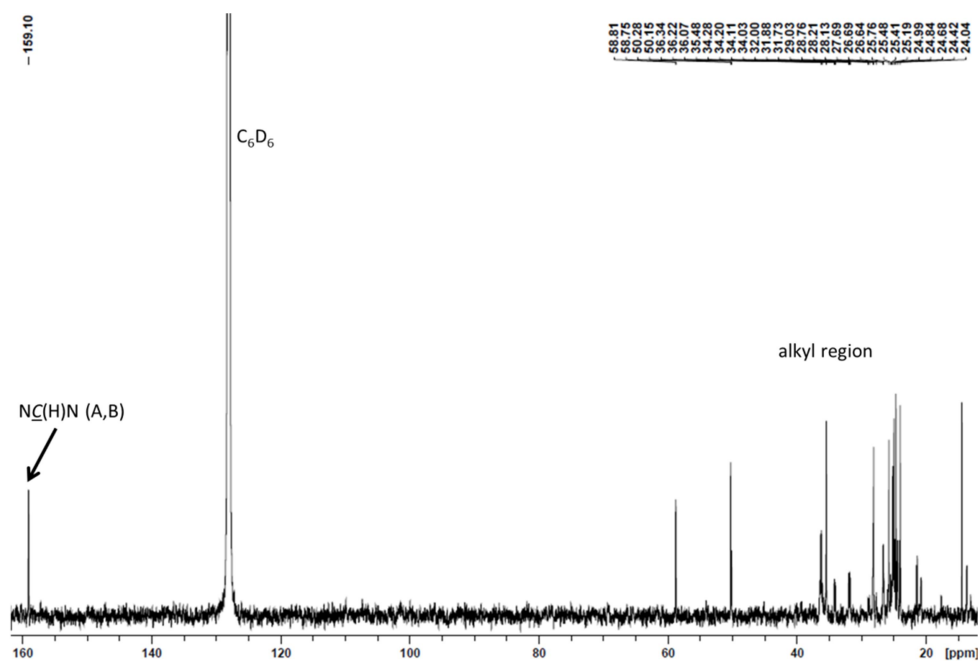


Figure A.27: $^{13}\text{C}\{^1\text{H}\}$ NMR spectrum of $[(\text{dmpe})_2\text{Mn}\{\kappa^2\text{-SiH}^n\text{Bu}(\text{N}^i\text{PrCHN}^i\text{Pr})\}]$ ($25^{\text{Bu,H}}$) in C_6D_6 (151 MHz, 298 K).

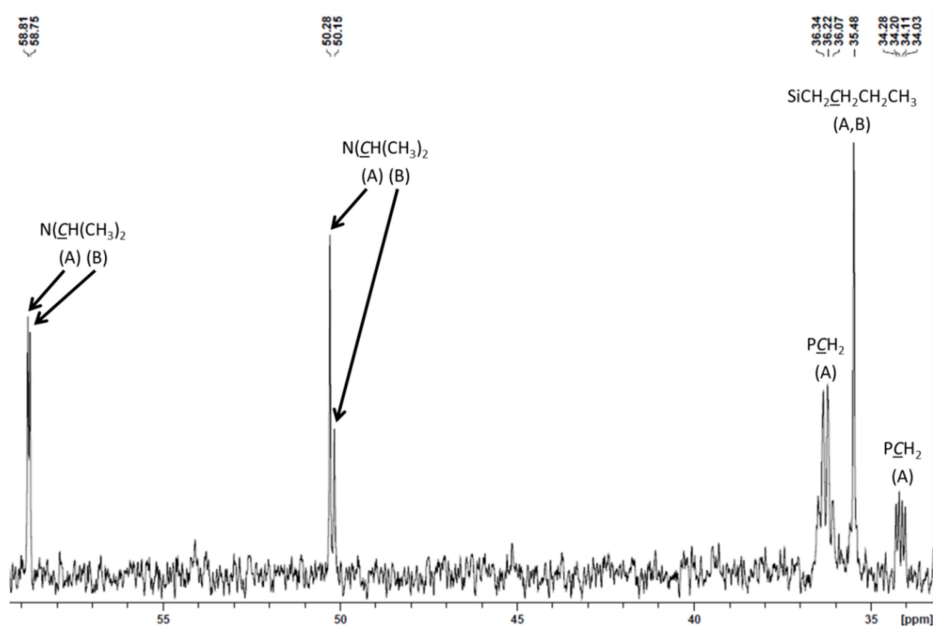


Figure A.28: Expanded high frequency alkyl region of the $^{13}\text{C}\{^1\text{H}\}$ NMR spectrum of $[(\text{dmpe})_2\text{Mn}\{\kappa^2\text{-SiH}^n\text{Bu}(\text{N}^i\text{PrCHN}^i\text{Pr})\}]$ ($25^{\text{Bu,H}}$) in C_6D_6 (151 MHz, 298 K). A and B represent peaks from the dominant and minor isomers, respectively.

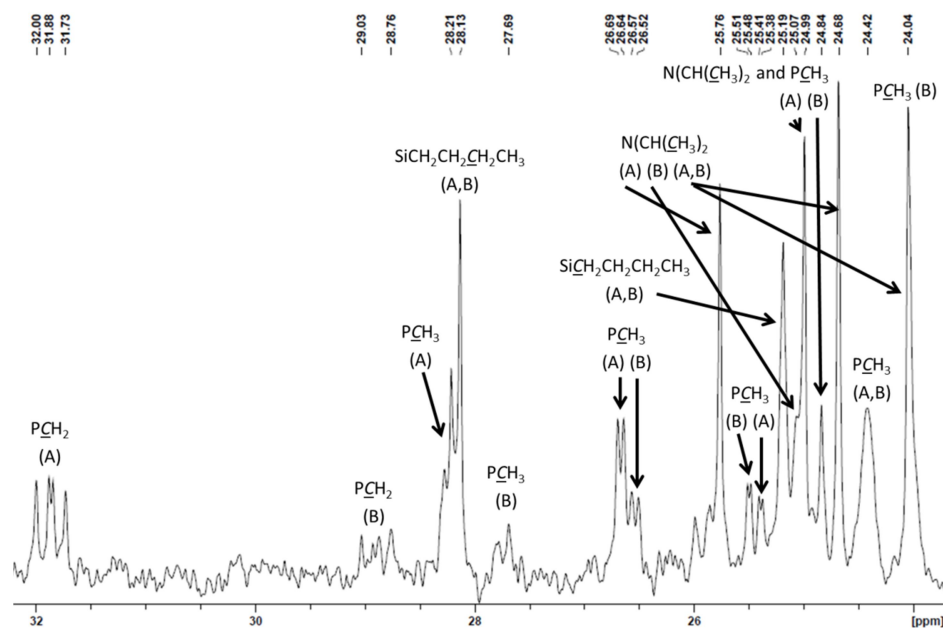


Figure A.29: Expanded middle frequency alkyl region of the $^{13}\text{C}\{^1\text{H}\}$ NMR spectrum of $[(\text{dmpe})_2\text{Mn}\{\kappa^2\text{-SiH}^n\text{Bu}(\text{N}^i\text{PrCHN}^i\text{Pr})\}]$ ($25^{\text{Bu,H}}$) in C_6D_6 (151 MHz, 298 K). A and B represent peaks from the dominant and minor isomers, respectively.

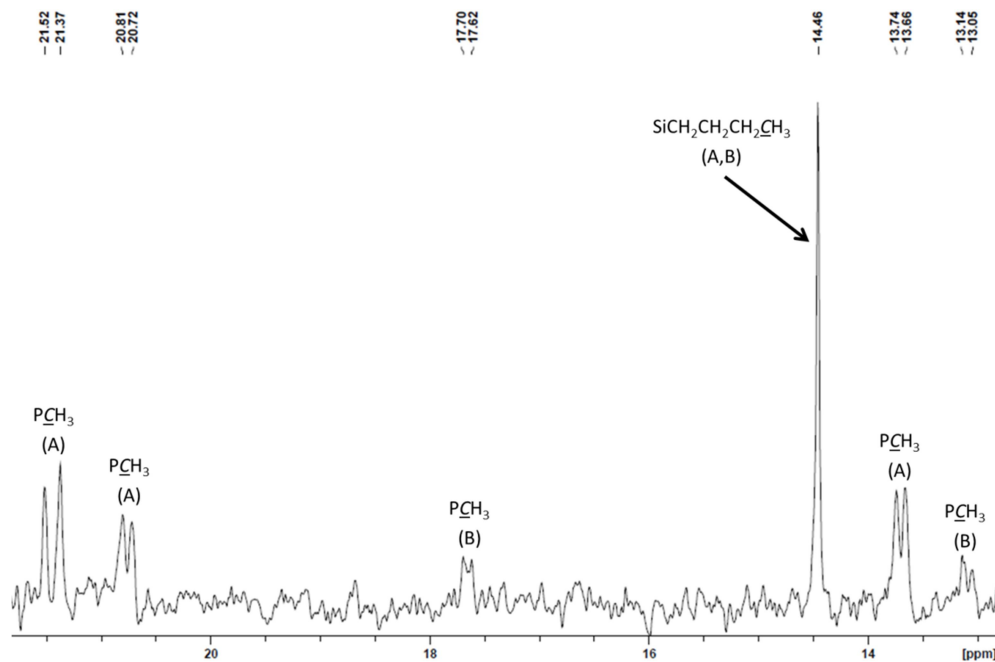


Figure A.30: Expanded low frequency alkyl region of the $^{13}\text{C}\{^1\text{H}\}$ NMR spectrum of $[(\text{dmpe})_2\text{Mn}\{\kappa^2\text{-SiH}^n\text{Bu}(\text{N}^i\text{PrCHN}^i\text{Pr})\}]$ ($25^{\text{Bu,H}}$) in C_6D_6 (151 MHz, 298 K). A and B represent peaks from the dominant and minor isomers, respectively.

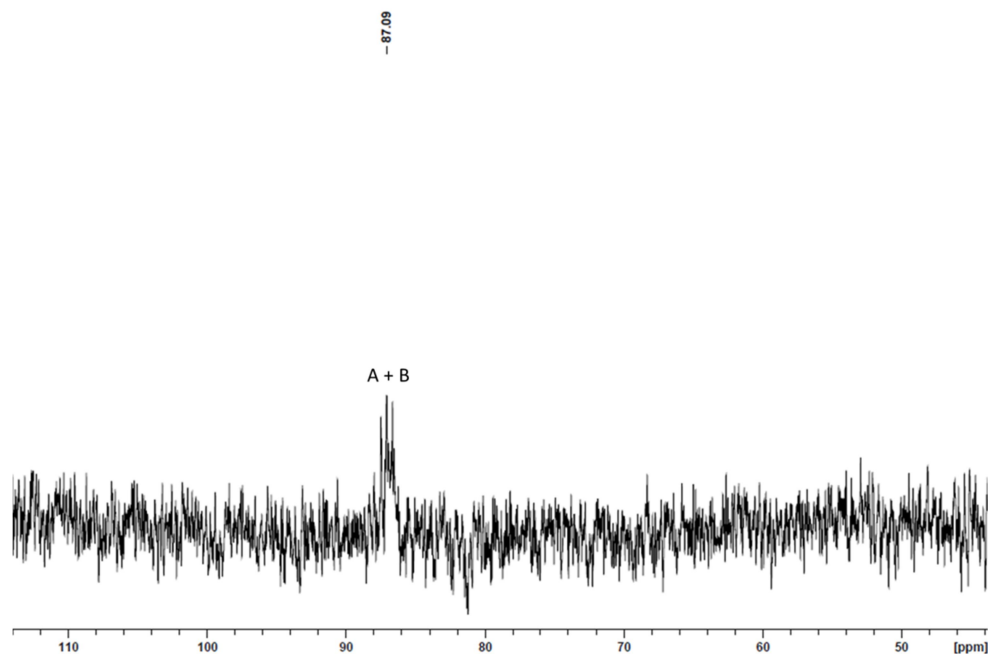


Figure A.31: $^{29}\text{Si}\{^1\text{H}\}$ NMR spectrum of $[(\text{dmpe})_2\text{Mn}\{\kappa^2\text{-SiH}^n\text{Bu}(\text{N}^i\text{PrCHN}^i\text{Pr})\}]$ ($25^{\text{Bu,H}}$) in C_6D_6 (119 MHz, 298 K).

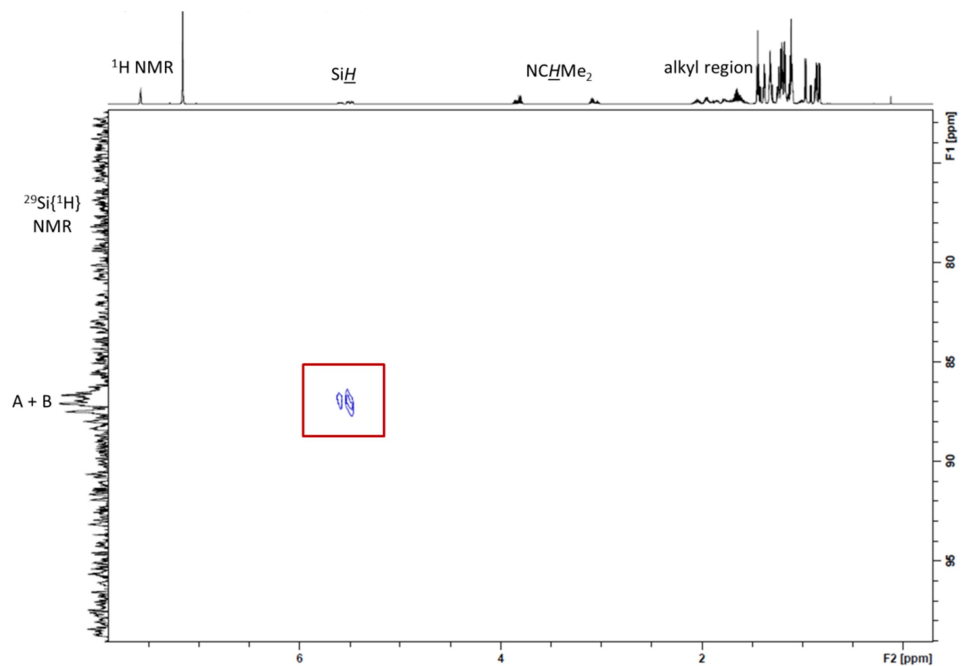


Figure A.32: ^{29}Si - ^1H HSQC NMR spectrum of $[(\text{dmpe})_2\text{Mn}\{\kappa^2\text{-SiH}^n\text{Bu}(\text{N}^i\text{PrCHN}^i\text{Pr})\}]$ ($25^{\text{Bu,H}}$) in C_6D_6 (119 MHz, 298 K).

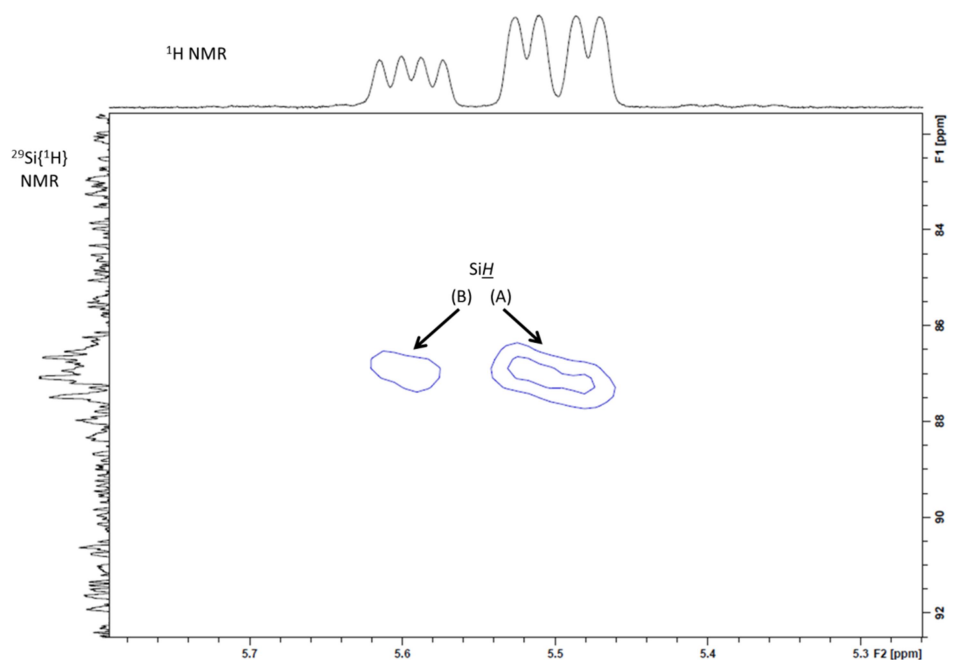


Figure A.33: Expanded SiH region of the ^{29}Si - ^1H HSQC NMR spectrum of $[(\text{dmpe})_2\text{Mn}\{\kappa^2\text{-SiH}^n\text{Bu}(\text{N}^i\text{PrCHN}^i\text{Pr})\}]$ ($25^{\text{Bu,H}}$) in C_6D_6 (119 MHz, 298 K). A and B represent peaks from the dominant and minor isomers, respectively.

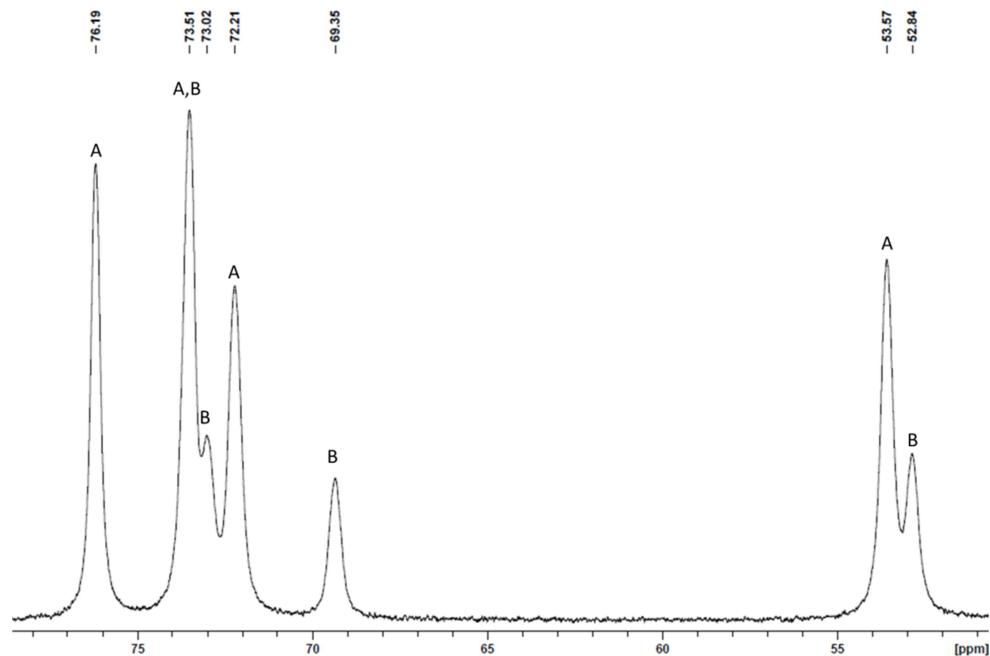


Figure A.34: $^{31}\text{P}\{^1\text{H}\}$ NMR spectrum of $[(\text{dmpe})_2\text{Mn}\{\kappa^2\text{-SiH}^n\text{Bu}(\text{N}^i\text{PrCHN}^i\text{Pr})\}]$ ($25^{\text{Bu,H}}$) in C_6D_6 (243 MHz, 298 K). A and B represent peaks from the dominant and minor isomers, respectively.

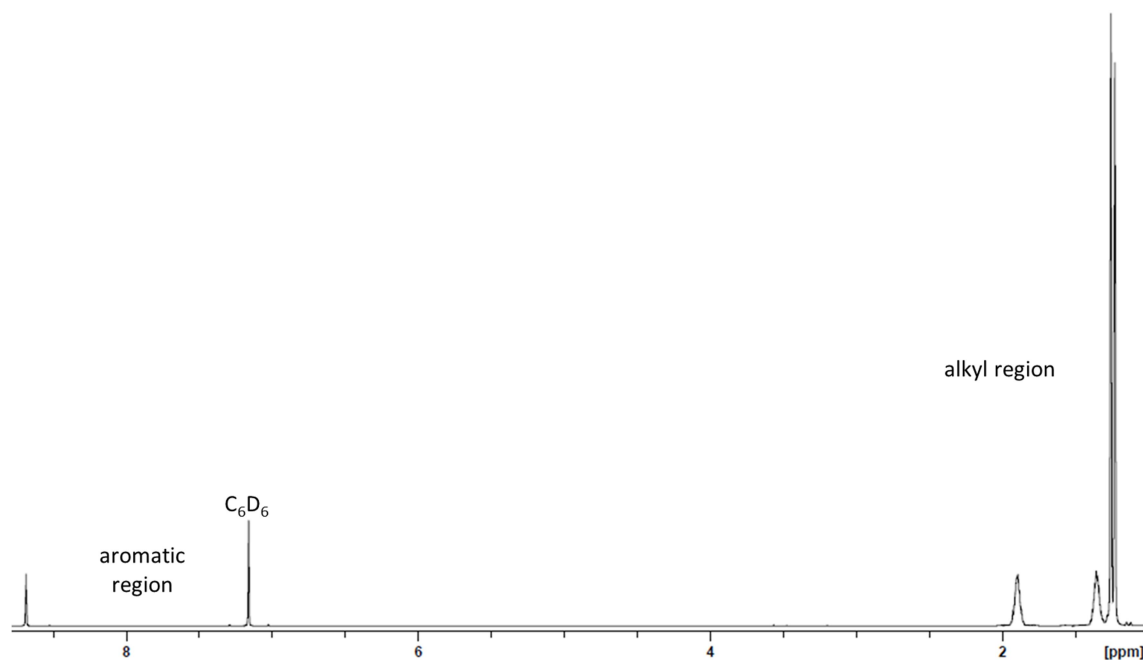


Figure A.35: ^1H NMR spectrum of *trans*- $[(\text{dmpe})_2\text{Mn}(\text{CO})(\kappa^1\text{-O}_2\text{CH})]$ (**26**) in C_6D_6 (600 MHz, 298 K).

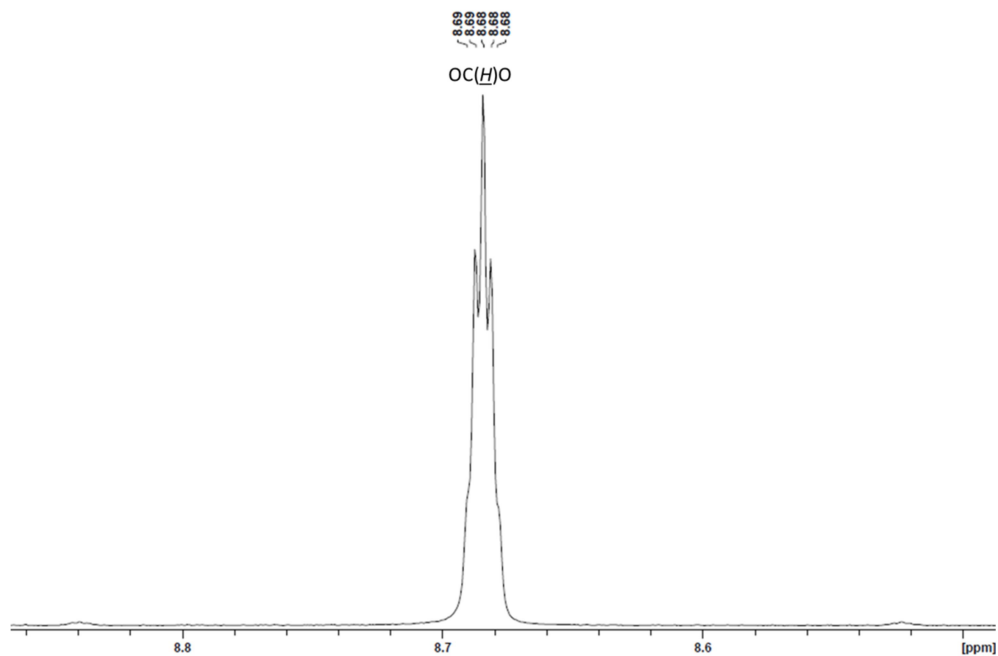


Figure A.36: Expanded formyl region of the ^1H NMR spectrum of *trans*- $[(\text{dmpe})_2\text{Mn}(\text{CO})(\kappa^1\text{-O}_2\text{CH})]$ (**26**) in C_6D_6 (600 MHz, 298 K).

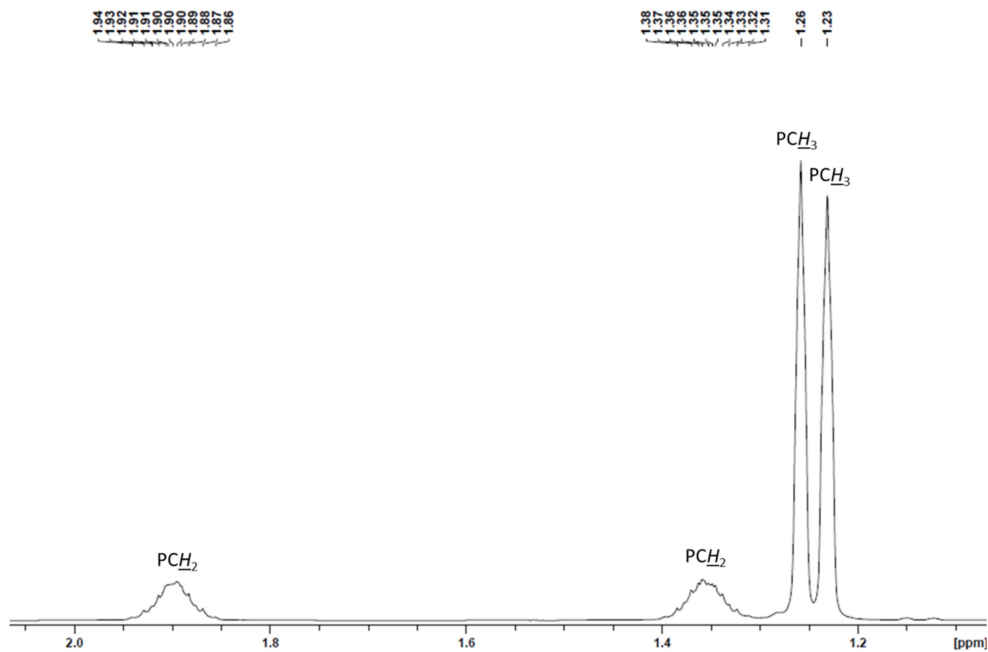


Figure A.37: Expanded alkyl region of the ^1H NMR spectrum of *trans*- $[(\text{dmpe})_2\text{Mn}(\text{CO})(\kappa^1\text{-O}_2\text{CH})]$ (**26**) in C_6D_6 (600 MHz, 298 K).

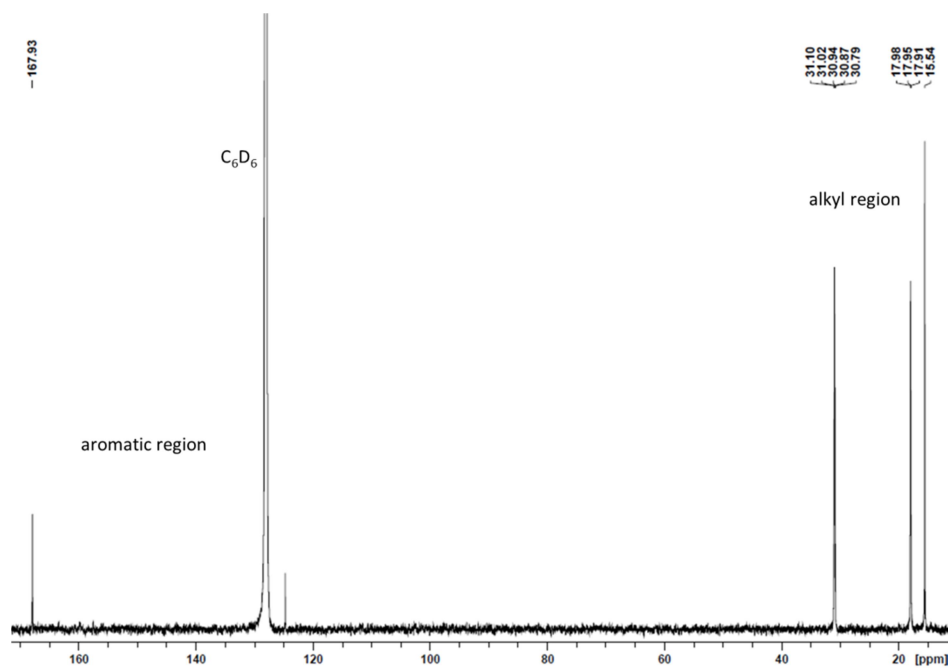


Figure A.38: $^{13}\text{C}\{^1\text{H}\}$ NMR spectrum of *trans*-[(dmpe) $_2$ Mn(CO)(κ^1 -O $_2$ CH)] (**26**) in C $_6$ D $_6$ (151 MHz, 298 K).

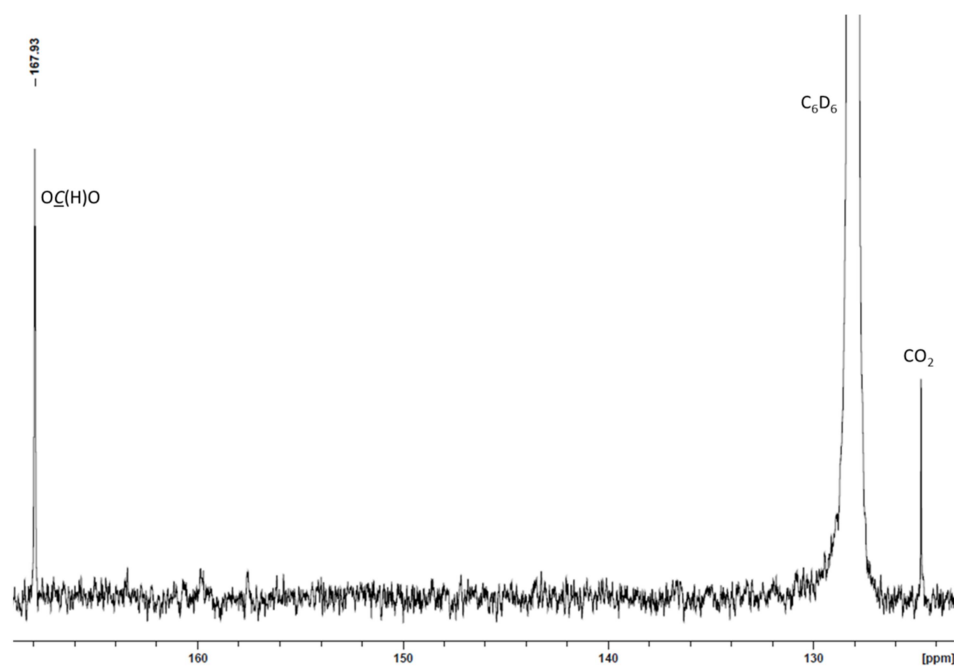


Figure A.39: Expanded formyl region of the $^{13}\text{C}\{^1\text{H}\}$ NMR spectrum of *trans*-[(dmpe) $_2$ Mn(CO)(κ^1 -O $_2$ CH)] (**26**) in C $_6$ D $_6$ (151 MHz, 298 K).

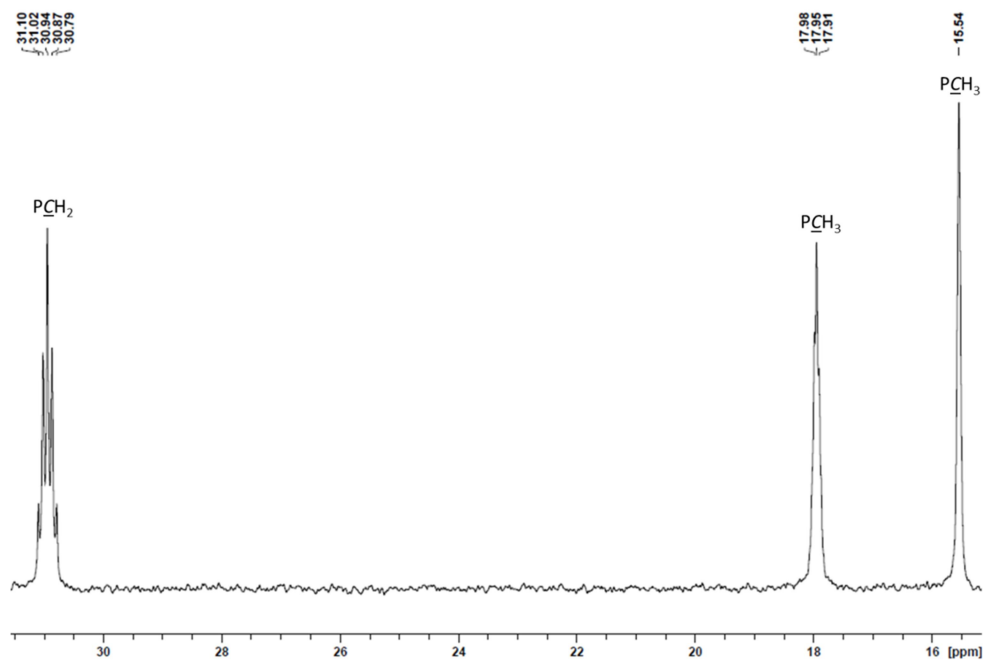


Figure A.40: Expanded alkyl region of the $^{13}\text{C}\{^1\text{H}\}$ NMR spectrum of *trans*- $[(\text{dmpe})_2\text{Mn}(\text{CO})(\kappa^1\text{-O}_2\text{CH})]$ (**26**) in C_6D_6 (151 MHz, 298 K).

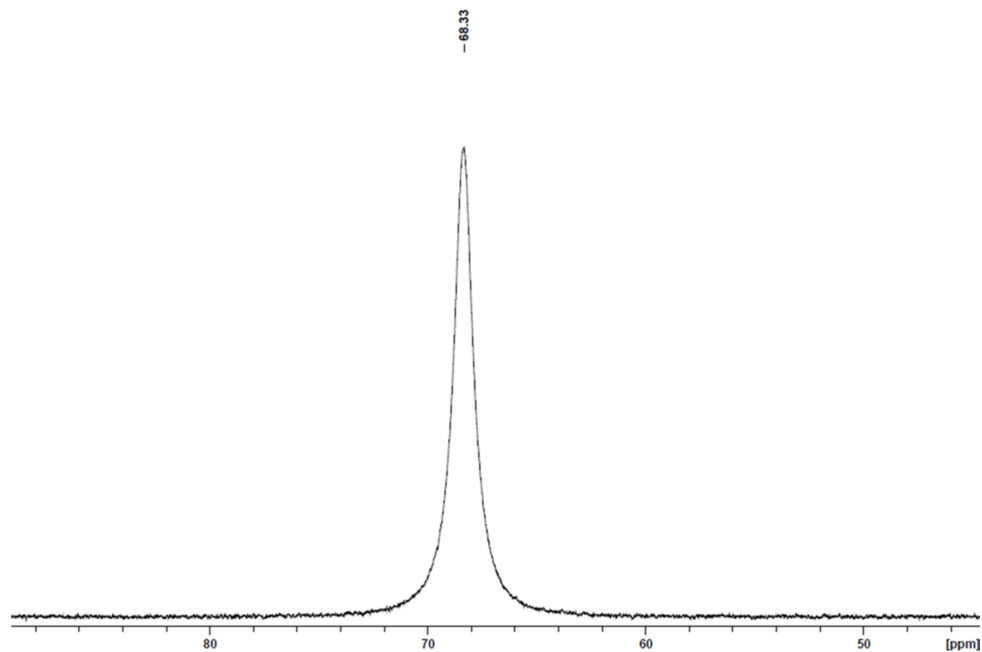


Figure A.41: $^{31}\text{P}\{^1\text{H}\}$ NMR spectrum of *trans*- $[(\text{dmpe})_2\text{Mn}(\text{CO})(\kappa^1\text{-O}_2\text{CH})]$ (**26**) in C_6D_6 (243 MHz, 298 K).

Appendix 2

Supplementary Information Related to Chapter 8

Figures in this chapter have been reprinted (adapted) from Price, J. S.; Emslie, D. J. H. Interconversion and reactivity of manganese silyl, silylene, and silene complexes, *Chem. Sci.* **2019**, Advance Articles, DOI: 10.1039/C9SC04513A. Published by The Royal Society of Chemistry.

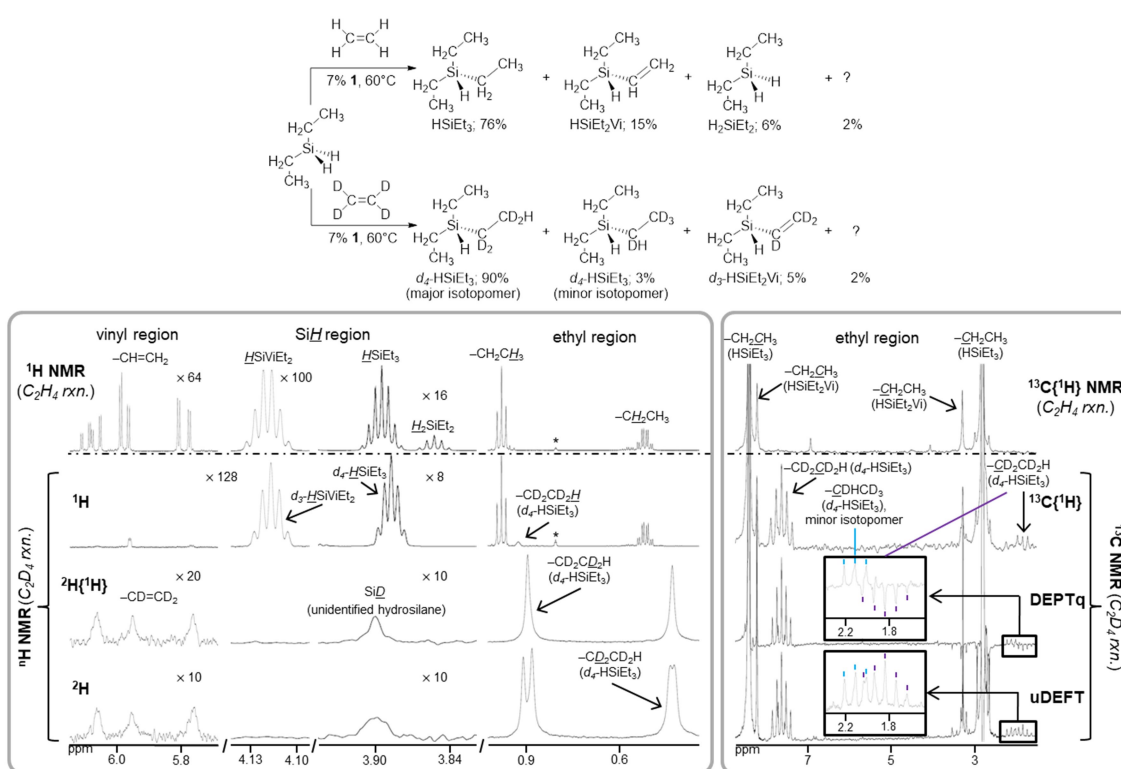


Figure B.1: NMR spectra {298 K, C_6D_6 , 600 (1H), 77 (2H), 151 ($^{13}C\{^1H\}$), or 175 ($^{13}C\{^1H\}$ -uDEFT and DEPTq) MHz} for reaction mixtures from catalytic hydrosilylation of H_2SiEt_2 by ethylene or d_4 -ethylene using $[(dmpe)_2MnH(C_2H_4)]$ (**10**) as a precatalyst (7 mol% catalyst load, 4 days at $60^\circ C$, $n_{ethylene} \approx 40 \times n_{H_2SiEt_2}$, initial pressure of C_2H_4 and C_2D_4 are c. 1.7 and 1.0 atm, respectively). Left: various regions of, from bottom to top, the 2H , $^2H\{^1H\}$, and 1H NMR spectra of the reaction involving d_4 -ethylene, and the 1H NMR spectrum of the reaction involving protonated ethylene (unknown hydrosilane

byproduct not shown). Right: the ethyl region of, from bottom to top, the uDEFT $^{13}\text{C}\{^1\text{H}\}$, DEPTq $^{13}\text{C}\{^1\text{H}\}$, and $^{13}\text{C}\{^1\text{H}\}$ NMR spectra of the reaction involving d_4 -ethylene, and the $^{13}\text{C}\{^1\text{H}\}$ NMR spectrum of the reaction involving protonated ethylene. * represents peaks tentatively assigned to the ethyl environments of HSiViEt_2 . In all cases (except the $^{13}\text{C}\{^1\text{H}\}$ NMR spectrum of the reaction involving protonated ethylene), NMR spectra were collected after vacuum distillation to remove manganese-containing species. Top: hydrosilane product distribution from hydrosilylation of ethylene (1st row) or d_4 -ethylene (2nd row) by H_2SiEt_2 .

Analysis of Figure B.1 (Hydrosilylation of d_4 -ethylene with H_2SiEt_2)

The ^2H NMR spectrum of d_4 - HSiEt_3 included 2 peaks at 0.90 ($-\text{CD}_2\text{CD}_2\text{H}$) and 0.46 ($-\text{CD}_2\text{CD}_2\text{H}$) ppm in a 2 : 1.9 ratio, with coupling constants to a single ^1H environment of 2.0 Hz (2-bond) and 0.8 Hz (3-bond), respectively. The slight deviation from the expected 2 : 2 ratio is presumably do to the presence of a small amount of the minor (3%) isotopomer $\text{HSiEt}_2(-\text{CDHCD}_3)$ {the major (97%) isotopomer is $\text{HSiEt}_2(-\text{CD}_2\text{CD}_2\text{H})$ }. Furthermore, the ^1H NMR spectrum contained a pentet at 3.89 ppm ($^3J_{\text{H,H}} = 3.2$ Hz) due to the SiH environment (from coupling to four Et_α protons, isotopically shifted 0.005 ppm upfield) and a broad singlet at 0.93 ppm due to the $-\text{CD}_2\text{CD}_2\text{H}$ environment (isotopically shifted by 0.05 ppm upfield relative to the fully protonated Et_β protons), along with two signals from the two environments in the fully protonated $-\text{CH}_2\text{CH}_3$ substituents. The $^{13}\text{C}\{^1\text{H}\}$ NMR spectrum features an isotopically shifted 1:2:3:2:1 pentet ($^1J_{\text{C,D}} = 19$ Hz) for the $-\text{CD}_2\text{CD}_2\text{H}$ environment, with 1-bond coupling to two deuterium atoms (at 7.64 ppm relative to 8.43 ppm for the analogous singlet from the $-\text{CH}_2\text{CH}_3$ environment). Furthermore, an isotopically shifted $-\text{CD}_2\text{CD}_2\text{H}$ environment was observed as a 1:2:3:2:1 pentet ($^1J_{\text{C,D}} = 18$ Hz) in the $^{13}\text{C}\{^1\text{H}\}$ DEPTq and uDEFT NMR spectra (at 1.83 ppm relative to 2.79 ppm for the analogous $-\text{CH}_2\text{CH}_3$ environment). Also present in the $^{13}\text{C}\{^1\text{H}\}$ -uDEFT NMR spectrum was a 1:1:1 triplet ($^1J_{\text{C,D}} = 18$ Hz) at 2.11 ppm from the $-\text{CDHCD}_3$ environment of the minor isotopomer; the similar intensity of the 1:1:1 triplet from a small amount of $\text{HSiEt}_2(-\text{CDHCD}_3)$ to the

1:2:3:2:1 pentet from the dominant isotopomer $\text{HSiEt}_2(-\text{CD}_2\text{CD}_2\text{H})$ is due to a combination of (for the former environment) a more concentrated signal (triplet vs. pentet), shorter relaxation time, and presence of NOE signal enhancement due to the adjacent ^1H environment. No signal was observed for the $-\text{CDHCD}_3$ environment in the minor isotopomer, presumably because it would be spread into a septet, have longer relaxation time, and no NOE signal enhancement due to no adjacent ^1H environments.

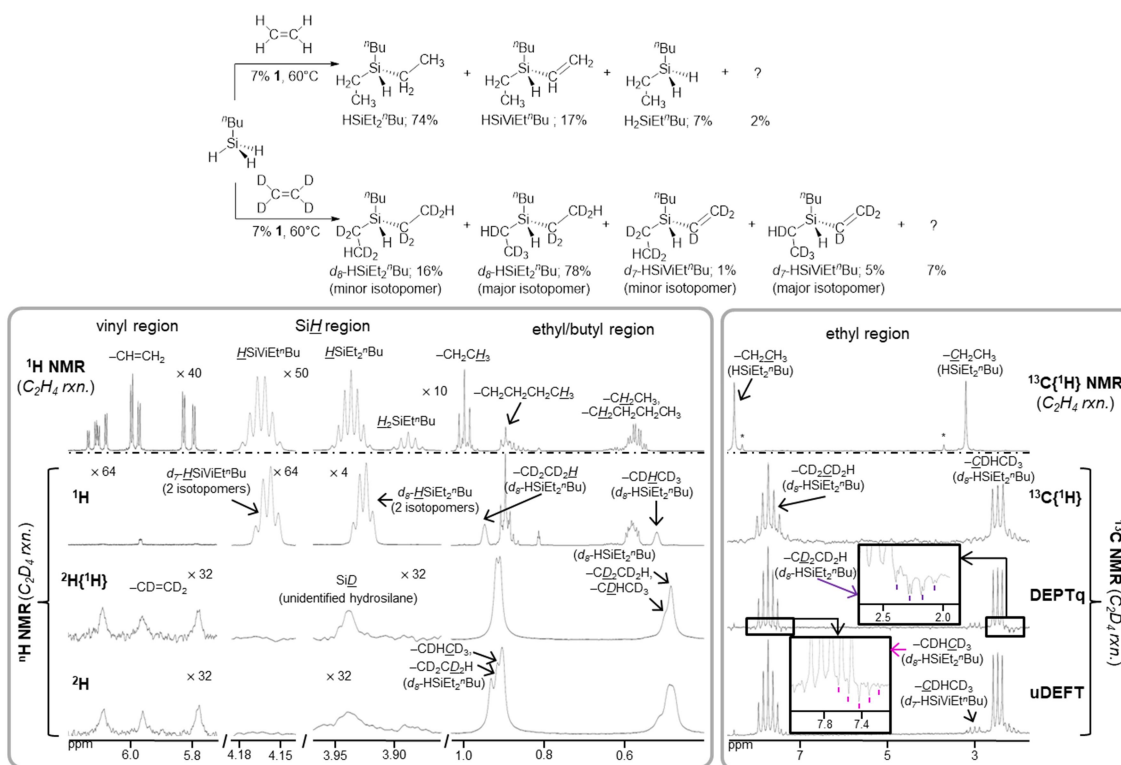


Figure B.2: NMR spectra {298 K, C_6D_6 , 600 (^1H), 77 (^2H), 151 ($^{13}\text{C}\{^1\text{H}\}$), or 175 ($^{13}\text{C}\{^1\text{H}\}$ -uDEPT and DEPTq) MHz} for reaction mixtures from catalytic hydrosilylation of $\text{H}_3\text{Si}^n\text{Bu}$ by ethylene or d_4 -ethylene using $[(\text{dmpe})_2\text{MnH}(\text{C}_2\text{H}_4)]$ (**10**) as a precatalyst (7 mol% catalyst load, 4 days at 60 °C, $n_{\text{ethylene}} \approx 40 \times n_{\text{H}_3\text{Si}^n\text{Bu}}$, initial pressure of C_2H_4 and C_2D_4 are c. 1.7 and 1.0 atm, respectively). Left: various regions of, from bottom to top, the ^2H , $^2\text{H}\{^1\text{H}\}$, and ^1H NMR spectra of the reaction involving d_4 -ethylene, and ^1H NMR spectrum of the reaction involving ethylene (unknown hydrosilane byproduct not shown). Right: the ethyl region of, from bottom to top, the uDEFT $^{13}\text{C}\{^1\text{H}\}$, DEPTq

$^{13}\text{C}\{^1\text{H}\}$, and $^{13}\text{C}\{^1\text{H}\}$ NMR spectra of the reaction involving d_4 -ethylene, and the $^{13}\text{C}\{^1\text{H}\}$ NMR spectrum of the reaction involving protonated ethylene. * indicate peaks tentatively assigned to the ethyl environments of $\text{HSiViEt}^n\text{Bu}$. NMR spectra were collected after Vacuum distillation removed manganese-containing species. Top: hydrosilane product distribution from hydrosilylation of ethylene (1st row) or d_4 -ethylene (2nd row) by $\text{H}_3\text{Si}^n\text{Bu}$. The $^{13}\text{C}\{^1\text{H}\}$ NMR spectrum of the reaction involving protonated ethylene was from a reaction mixture allowed to react for 8 days.

Analysis of Figure B.2 (Hydrosilylation of d_4 -ethylene with $\text{H}_3\text{Si}^n\text{Bu}$)

The ^2H NMR spectrum included multiplets at 0.91-0.92 ppm and 0.48-0.50 ppm in a 3 : 2 ratio for the beta and alpha ethyl environments, respectively, of the deuterated ethyl substituents in $d_8\text{-HSiEt}_2^n\text{Bu}$. Both multiplets were formed from two overlapping signals from the two potential isotope distributions. The two peaks, at 0.92 and 0.91 ppm, which compose the β multiplet, were both doublets with coupling of 2 and 0.8 Hz, to a single proton environment in a $-\text{CD}_2\text{CD}_2\text{H}$ (2-bond coupling) or $-\text{CDHCD}_3$ (3-bond coupling) substituent, respectively. The multiplet for the alpha environment appears to be an overlapping singlet (from the $-\text{CD}_2\text{CD}_2\text{H}$ environment) and doublet (from the $-\text{CDHCD}_3$ environment, due to 2-bond coupling to ^1H), though a coupling constant for the latter could not be accurately determined. Given that one ethyl environment is nearly exclusively $-\text{CD}_2\text{CD}_2\text{H}$, the observed relative integrations are consistent with a 1 : 5 ratio of $-\text{CD}_2\text{CD}_2\text{H}$: $-\text{CDHCD}_3$ isotope distributions in the other ethyl group. The ^1H NMR spectrum contained an apparent quartet from the SiH environment in $d_8\text{-HSiEt}_2^n\text{Bu}$, with a 1:3.4:4.1:1.7 pattern ($^2J_{\text{H,H}} = 3.2$ Hz). This is consistent with overlapping 1:3:3:1 quartet (3.93 ppm) and 1:2:1 triplet (3.92 ppm) signals from the SiH environments of the two isotopomers $\text{HSi}(-\text{CD}_2\text{CD}_2\text{H})(-\text{CDHCD}_3)^n\text{Bu}$ (with three alpha protons) and $\text{HSi}(-\text{CD}_2\text{CD}_2\text{H})_2^n\text{Bu}$ (with two alpha protons) in a 5 : 1 ratio (which would theoretically yield an apparent quartet with a 1:3.5:4.0:1.5 coupling pattern), which is also consistent with the ^2H NMR integrations (and isotopically shifted upfield from the analogous signal in fully protonated $\text{HSiEt}_2^n\text{Bu}$ by 0.01 and 0.02 ppm, respectively). Also present in the ^1H

NMR spectrum were two broad singlets at 0.95 and 0.52 ppm from the proton environments in the $-\text{CD}_2\text{CD}_2\text{H}$ and $-\text{CDHCD}_3$ environments, respectively, in both cases isotopically shifted upfield from the respective fully protonated ethyl environments by 0.05 ppm. Signals from both isotopomers were observed in the $^{13}\text{C}\{^1\text{H}\}$ NMR spectrum. The major signal in the β ethyl region was a 1:2:3:2:1 pentet at 7.73 ppm ($^1J_{\text{D,C}} = 19$ Hz, isotopically shifted upfield by 0.77 ppm from the fully protonated ethyl environment in $\text{HSiEt}_2^{\text{''}}\text{Bu}$) due to the $-\text{CD}_2\text{CD}_2\text{H}$ environment, and in the uDEFT $^{13}\text{C}\{^1\text{H}\}$ spectrum, small spikes in the noise just to the right of this peak (and overlapping with the right portion of the peak) were observed which could be from the $-\text{CDHCD}_3$ environment, though it is small due to being more spread out (a septet) and lacking an adjacent ^1H environment (meaning that in addition to having a longer relaxation time, no NOE enhancement would be observed). The alpha ethyl environment is dominated by a 1:1:1 triplet ($^1J_{\text{C,D}} = 18$ Hz) at 2.47 ppm from the $-\text{CDHCD}_3$ environment (isotopically shifted upfield by 0.73 ppm from the fully protonated ethyl environment in $\text{HSiEt}_2^{\text{''}}\text{Bu}$), with a multiplet just to the right which is consistent with two nearly-overlapping pentets at 2.22 and 2.20 ppm ($^1J_{\text{C,D}} = 19$ Hz) from the $-\text{CD}_2\text{CD}_2\text{H}$ environments in the two isotopomers (isotopically shifted by 0.98 and 1.0 ppm, respectively, from the fully protonated ethyl environment in $\text{HSiEt}_2^{\text{''}}\text{Bu}$). An additional 1:1:1 triplet at 3.00 ppm is from the $-\text{CDHCD}_3$ environment in the partially deuterated $\text{HSiEtVi}^{\text{''}}\text{Bu}$ byproduct.

References

1. (a) Jairath, R.; Jain, A.; Tolles, R.; Hampden-Smith, M.; Kodas, T., Chapter 1: Introduction. In *The Chemistry of Metal CVD*, Kodas, T.; Hampden-Smith, M., Eds. VCH: New York, 1994; pp 1-38; (b) Hampden-Smith, M. J.; Kodas, T. T. Chemical vapor deposition of metals: Part 1. An overview of CVD processes, *Chemical Vapor Deposition* **1995**, *1*, 8-23.
2. Lang, H.; Dietrich, S., Metals-gas-phase deposition and applications In *Comprehensive Inorganic Chemistry II*, Elsevier B.V. 2013; Vol. 4, pp 211-269.
3. Koponen, S. E.; Gordon, P. G.; Barry, S. T. Principles of precursor design for vapour deposition methods, *Polyhedron* **2016**, *108*, 59-66.
4. Hitchman, M.; Jensen, K., *Chemical Vapor Deposition; Principles and Applications*. Academic Press: London, 1993.
5. Choy, K. L. Chemical vapor deposition of coatings, *Prog. Mater. Sci.* **2003**, *48*, 57-170.
6. Hampden-Smith, M.; Kodas, T., Chapter 8: Chemical Vapor Deposition of Assorted Metals. In *The Chemistry of Metal CVD*, Kodas, T.; Hampden-Smith, M., Eds. VCH: New York, 1994; pp 357-428.
7. Jegier, J. A.; Gladfelter, W. L. The use of aluminum and gallium hydrides in materials science, *Coord. Chem. Rev.* **2000**, *206-207*, 631-650.
8. (a) Gladfelter, W. L.; Boyd, D. C.; Jensen, K. F. Trimethylamine Complexes of Alane as Precursors for the Low-Pressure Chemical Vapor Deposition of Aluminum, *Chem. Mater.* **1989**, *1*, 339-343; Beach, D. B.; (b) Blum, S. E.; LeGoues, F. K. Chemical vapor deposition of aluminum from trimethylamine-alane, *J. Vac. Sci. Technol., A* **1989**, *7*, 3117-3118; (c) Wee, A. T. S.; Murrell, A. J.; Singh, N. K.; O'Hare, D.; Foord, J. S. Aluminum Film Growth by Chemical Vapor Deposition of $\text{AlH}_3(\text{NMe}_3)_2$, *J. Chem. Soc., Chem. Commun.* **1990**, 11-13; (d) Gross, M. E.; Fleming, C. G.; Cheung, K. P.; Heimbrook, L. A. Liquid source metalorganic chemical vapor deposition of aluminum from triethylamine alane, *J. Appl. Phys.* **1991**, *69*, 2589-2592; (e) Dubois, L. H.; Zegarski, B. R.; Gross, M. E.; Nuzzo, R. G. Aluminum thin film growth by the thermal

Ph.D. Thesis — Jeffrey S. Price; McMaster University – Chemistry

decomposition of triethylamine alane, *Surf. Sci.* **1991**, *244*, 89-95; (f) Simmonds, M. G.; Phillips, E. C.; Hwang, J. W.; Gladfelter, W. L. A stable, liquid precursor for aluminum, *Chemtronics* **1991**, *5*, 155-158.

9. (a) Glass, J. A., Jr.; Kher, S.; Spencer, J. T. Chemical vapor deposition precursor chemistry. I. The deposition of pure aluminum thin films from an aluminaborane precursor compound by chemical vapor deposition, *Thin Solid Films* **1992**, *207*, 15-18;

(b) Glass, J. A., Jr.; Kher, S. S.; Spencer, J. T. Chemical Vapor Deposition Precursor Chemistry. 2. Formation of Pure Aluminum, Alumina, and Aluminum Boride Thin Films from Boron-Containing Precursor Compounds by Chemical Vapor Deposition, *Chem. Mater.* **1992**, *4*, 530-538.

10. (a) Bhat, R.; Koza, M. A.; Chang, C. C.; Schwarz, S. A.; Harris, T. D. The Growth and Characterization of AlGaAs using Dimethyl Aluminum Hydride, *J. Cryst. Growth* **1986**, *77*, 7-10; (b) Tsubouchi, K.; Masu, K.; Shigeeda, N.; Matano, T.; Hiura, Y.; Mikoshiba, N. Complete planarization of via holes with aluminum by selective and nonselective chemical vapor deposition, *Appl. Phys. Lett.* **1990**, *57*, 1221-1223; (c) Tsubouchi, K.; Masu, K. Selective aluminum chemical vapor deposition, *J. Vac. Sci. Technol., A* **1992**, *10*, 856-862.

11. Niemer, B.; Zinn, A. A.; Stovall, W. K.; Gee, P. E.; Hicks, R. F.; Kaesz, H. D. Organometallic chemical vapor deposition of tungsten metal, and suppression of carbon incorporation by codeposition of platinum, *Appl. Phys. Lett.* **1992**, *61*, 1793-1795.

12. Zinn, A. A., Chapter 3: Chemical Vapor Deposition of Tungsten. In *The Chemistry of Metal CVD*, Kodas, T.; Hampden-Smith, M., Eds. VCH: New York, 1994; pp 105-174.

13. Jones, A. C.; Hitchman, M., *Chemical Vapour Deposition: Precursors, Processes and Applications*. RSC Publishing: Cambridge, 2009.

14. Kim, H. Atomic layer deposition of metal and nitride thin films: Current research efforts and applications for semiconductor device processing, *J. Vac. Sci. Technol., B: Microelectron. Nanometer Struct.--Process., Meas., Phenom.* **2003**, *21*, 2231-2261.

15. Zaera, F. The Surface Chemistry of Atomic Layer Depositions of Solid Thin Films, *J. Phys. Chem. Lett.* **2012**, *3*, 1301-1309.
16. (a) Bahlawane, N.; Kohse-Höinghaus, K.; Premkumar, P. A.; Lenoble, D. Advances in the deposition chemistry of metal-containing thin films using gas phase processes, *Chem. Sci.* **2012**, *3*, 929-941; (b) Knez, M.; Nielsch, K.; Niinistö, L. Synthesis and Surface Engineering of Complex Nanostructures by Atomic Layer Deposition, *Adv. Mater.* **2007**, *19*, 3425-3438; (c) George, S. M. Atomic Layer Deposition: An Overview, *Chem. Rev.* **2010**, *110*, 111-131; (d) Zaera, F. The surface chemistry of thin film atomic layer deposition (ALD) processes for electronic device manufacturing, *J. Mater. Chem.* **2008**, *18*, 3521-3526; (e) Puurunen, R. L. Surface chemistry of atomic layer deposition: A case study for the trimethylaluminum/water process, *J. Appl. Phys.* **2005**, *97*, 121301/121301-121301/121352; (f) Leskelä, M.; Ritala, M. Atomic Layer Deposition Chemistry: Recent Developments and Future Challenges, *Angew. Chem., Int. Ed.* **2003**, *42*, 5548-5554.
17. Kim, H.; Lee, H.-B.-R.; Maeng, W. J. Applications of atomic layer deposition to nanofabrication and emerging nanodevices, *Thin Solid Films* **2009**, *517*, 2563-2580.
18. (a) Profijt, H. B.; Potts, S. E.; van de Sanden, M. C. M.; Kessels, W. M. M. Plasma-Assisted Atomic Layer Deposition: Basics, Opportunities, and Challenges, *J. Vac. Sci. Technol., A* **2011**, *29*, 050801/050801-050801/050826; (b) Kariniemi, M.; Niinistö, J.; Vehkamäki, M.; Kemell, M.; Ritala, M.; Leskelä, M.; Putkonen, M. Conformality of remote plasma-enhanced atomic layer deposition processes: An experimental study, *J. Vac. Sci. Technol., A* **2012**, *30*, 01A115/111-101A115/115.
19. (a) Emslie, D. J. H.; Chadha, P.; Price, J. S. Metal ALD and pulsed CVD: Fundamental reactions and links with solution chemistry, *Coord. Chem. Rev.* **2013**, *257*, 3282-3296; (b) Blakeney, K. J.; Winter, C. H. Atomic Layer Deposition of Aluminum Metal Films Using a Thermally Stable Aluminum Hydride Reducing Agent, *Chem. Mater.* **2018**, *30*, 1844-1848; (c) Klesko, J. P.; Thrush, C. M.; Winter, C. H. Thermal Atomic Layer Deposition of Titanium Films Using Titanium Tetrachloride and 2-Methyl-1,4-bis(trimethylsilyl)-2,5-cyclohexadiene or 1,4-Bis(trimethylsilyl)-1,4-dihydropyrazine,

Ph.D. Thesis — Jeffrey S. Price; McMaster University – Chemistry

- Chem. Mater.* **2015**, *27*, 4918-4921; (d) Hämäläinen, J.; Mizohata, K.; Meinander, K.; Mattinen, M.; Vehkamaeki, M.; Räisänen, J.; Ritala, M.; Leskelä, M. Rhenium Metal and Rhenium Nitride Thin Films Grown by Atomic Layer Deposition, *Angew. Chem., Int. Ed.* **2018**, *57*, 14538-14542; (e) Mäkelä, M.; Hatanpää, T.; Mizohata, K.; Meinander, K.; Niinistö, J.; Räisänen, J.; Ritala, M.; Leskelä, M. Studies on Thermal Atomic Layer Deposition of Silver Thin Films, *Chem. Mater.* **2017**, *29*, 2040-2045; (f) Mäkelä, M.; Hatanpää, T.; Mizohata, K.; Räisänen, J.; Ritala, M.; Leskelä, M. Thermal Atomic Layer Deposition of Continuous and Highly Conducting Gold Thin Films, *Chem. Mater.* **2017**, *29*, 6130-6136; (g) Stevens, E. C.; Mousa, M. B. M.; Parsons, G. N. Thermal atomic layer deposition of Sn metal using SnCl₄ and a vapor phase silyl dihydropyrazine reducing agent, *J. Vac. Sci. Technol., A* **2018**, *36*, 06A106/101-106A106/110.
20. Kalutarage, L. C.; Martin, P. D.; Heeg, M. J.; Winter, C. H. Volatile and Thermally Stable Mid to Late Transition Metal Complexes Containing α -Imino Alkoxide Ligands, a New Strongly Reducing Coreagent, and Thermal Atomic Layer Deposition of Ni, Co, Fe, and Cr Metal Films, *J. Am. Chem. Soc.* **2013**, *135*, 12588-12591.
21. Values to 2 decimal places are from: (a) Huheey, J.E.; Keiter, E.A.; Keiter, R.L. *Inorganic Chemistry: Principles of Structure and Reactivity*, fourth ed.; HarperCollins College Publishers, New York, 1993. Values to 1 decimal place are from: (b) Pauling, L. *The Nature of the Chemical Bond*, third ed.; Cornell University Press, New York, 1960.
22. (a) Gadkari, P. R.; Warren, A. P.; Todi, R. M.; Petrova, R. V.; Coffey, K. R. Comparison of the agglomeration behavior of thin metallic films on SiO₂, *J. Vac. Sci. Technol., A* **2005**, *23*, 1152-1161; (b) Boragno, C.; Buatier de Mongeot, F.; Felici, R.; Robinson, I. K. Critical thickness for the agglomeration of thin metal films, *Phys. Rev. B: Condens. Matter Mater. Phys.* **2009**, *79*, 155443/155441-155443/155447.
23. Mårtensson, P.; Carlsson, J.-O. Atomic Layer Epitaxy of Copper Growth and Selectivity in the Cu(II)-2,2,6,6-tetramethyl-3,5-heptanedionate/H₂ Process, *J. Electrochem. Soc.* **1998**, *145*, 2926-2931.

24. Hierso, J.-C.; Feurer, R.; Poujardieu, J.; Kihn, Y.; Kalck, P. Metal-organic chemical vapor deposition in a fluidized bed as a versatile method to prepare layered bimetallic nanoparticles, *J. Mol. Catal. A: Chem.* **1998**, *135*, 321-325.
25. Kwon, J.; Saly, M.; Halls, M. D.; Kanjolia, R. K.; Chabal, Y. J. Substrate Selectivity of (^tBu-Allyl)Co(CO)₃ during Thermal Atomic Layer Deposition of Cobalt, *Chem. Mater.* **2012**, *24*, 1025-1030.
26. (a) Jiang, X.; Bent, S. F. Area-Selective ALD with Soft Lithographic Methods: Using Self-Assembled Monolayers to Direct Film Deposition, *J. Phys. Chem. C* **2009**, *113*, 17613-17625; (b) Färm, E.; Kemell, M.; Ritala, M.; Leskelä, M. Self-Assembled Octadecyltrimethoxysilane Monolayers Enabling Selective-Area Atomic Layer Deposition of Iridium, *Chem. Vap. Deposition* **2006**, *12*, 415-417; (c) Park, K. J.; Doub, J. M.; Gougousi, T.; Parsons, G. N. Microcontact patterning of ruthenium gate electrodes by selective area atomic layer deposition, *Appl. Phys. Lett.* **2005**, *86*, 051903/051901-051903/051903; (d) Seitz, O.; Dai, M.; Aguirre-Tostado, F. S.; Wallace, R. M.; Chabal, Y. J. Copper–Metal Deposition on Self Assembled Monolayer for Making Top Contacts in Molecular Electronic Devices, *J. Am. Chem. Soc.* **2009**, *131*, 18159-18167; (e) Färm, E.; Kemell, M.; Ritala, M.; Leskelä, M. Selective-Area Atomic Layer Deposition Using Poly(methyl methacrylate) Films as Mask Layers, *J. Phys. Chem. C* **2008**, *112*, 15791-15795; (g) Lee, H.-B.-R.; Kim, W.-H.; Lee, J. W.; Kim, J.-M.; Heo, K.; Hwang, I. C.; Park, Y.; Hong, S.; Kim, H. High Quality Area-Selective Atomic Layer Deposition Co Using Ammonia Gas as a Reactant, *J. Electrochem. Soc.* **2010**, *157*, D10-D15; (g) Kim, W.-H.; Lee, H.-B.-R.; Heo, K.; Lee, Y. K.; Chung, T.-M.; Kim, C. G.; Hong, S.; Heo, J.; Kim, H. Atomic Layer Deposition of Ni Thin Films and Application to Area-Selective Deposition, *J. Electrochem. Soc.* **2011**, *158*, D1-D5.
27. Park, K. J.; Parsons, G. N. Selective area atomic layer deposition of rhodium and effective work function characterization in capacitor structures, *Appl. Phys. Lett.* **2006**, *89*, 043111/043111-043111/043113.
28. Lee, B. H.; Hwang, J. K.; Nam, J. W.; Lee, S. U.; Kim, J. T.; Koo, S.-M.; Baunemann, A.; Fischer, R. A.; Sung, M. M. Low-Temperature Atomic Layer Deposition

of Copper Metal Thin Films: Self-Limiting Surface Reaction of Copper Dimethylamino-2-propoxide with Diethylzinc, *Angew. Chem., Int. Ed.* **2009**, *48*, 4536-4539.

29. (a) Juppo, M.; Vehkamäki, M.; Ritala, M.; Leskelä, M. Deposition of molybdenum thin films by an alternate supply of MoCl₅ and Zn, *J. Vac. Sci. Technol., A* **1998**, *16*, 2845-2850; (b) Kim, S.-H.; Kwak, N.; Kim, J.; Sohn, H. A Comparative Study of the Atomic-Layer-Deposited Tungsten Thin Films as Nucleation Layers for W-Plug Deposition, *J. Electrochem. Soc.* **2006**, *153*, G887-G893.

30. (a) Knaut, M.; Junige, M.; Albert, M.; Bartha, J. W. *In-situ* real-time ellipsometric investigations during the atomic layer deposition of ruthenium: A process development from [(ethylcyclopentadienyl)(pyrrolyl)ruthenium] and molecular oxygen, *J. Vac. Sci. Technol., A* **2012**, *30*, 01A151/151-101A151/159; (b) Choi, S.-H.; Cheon, T.; Kim, S.-H.; Kang, D.-H.; Park, G.-S.; Kim, S. Thermal Atomic Layer Deposition (ALD) of Ru Films for Cu Direct Plating, *J. Electrochem. Soc.* **2011**, *158*, D351-D356; (c) Leick, N.; Verkuijlen, R. O. F.; Lamagna, L.; Langereis, E.; Rushworth, S.; Roozeboom, F.; van de Sanden, M. C. M.; Kessels, W. M. M. Atomic layer deposition of Ru from CpRu(CO)₂Et using O₂ gas and O₂ plasma, *J. Vac. Sci. Technol., A* **2011**, *29*, 021016/021011-021016/021017.

31. (a) Hämäläinen, J.; Sajavaara, T.; Puukilainen, E.; Ritala, M.; Leskelä, M. Atomic Layer Deposition of Osmium, *Chem. Mater.* **2012**, *24*, 55-60; (b) Aaltonen, T.; Ritala, M.; Leskela, M. ALD of rhodium thin films from Rh(acac)₃ and oxygen, *Electrochem. Solid-State Lett.* **2005**, *8*, C99-C101.

32. (a) Lee, H.-B.-R.; Kim, H. High-Quality Cobalt Thin Films by Plasma-Enhanced Atomic Layer Deposition, *Electrochem. Solid-State Lett.* **2006**, *9*, G323-G325; (b) Yang, C.-M.; Yun, S.-W.; Ha, J.-B.; Na, K.-I.; Cho, H.-I.; Lee, H.-B.; Jeong, J.-H.; Kong, S.-H.; Hahm, S.-H.; Lee, J.-H. Effectiveness of Self-Carbon and Titanium Capping Layers in NiSi Formation with Ni Film Deposited by Atomic Layer Deposition, *Jpn. J. Appl. Phys., Part 1* **2007**, *46*, 1981-1983; (c) Deng, F.; Johnson, R. A.; Asbeck, P. M.; Lau, S. S.; Dubbelday, W. B.; Hsiao, T.; Woo, J. Salicidation process using NiSi and its device application, *J. Appl. Phys.* **1997**, *81*, 8047-8051; (d) Łaszcz, A.; Ratajczak, J.;

Czerwinski, A.; Kącki, J.; Breil, N.; Larrieu, G.; Dubois, E. TEM studies of PtSi low Schottky-barrier contacts for source/drain in MOS transistors, *Cent. Eur. J. Phys.* **2011**, *9*, 423-427.

33. Henkel, C.; Abermann, S.; Bethge, O.; Bertagnolli, E. Atomic layer-deposited platinum in high-*k*/metal gate stacks, *Semicond. Sci. Technol.* **2009**, *24*, 125013/125011-125013/125016.

34. (a) Kariniemi, M.; Niinistö, J.; Hatanpää, T.; Kemell, M.; Sajavaara, T.; Ritala, M.; Leskelä, M. Plasma-Enhanced Atomic Layer Deposition of Silver Thin Films, *Chem. Mater.* **2011**, *23*, 2901-2907; (b) Dai, M.; Kwon, J.; Halls, M. D.; Gordon, R. G.; Chabal, Y. J. Surface and Interface Processes during Atomic Layer Deposition of Copper on Silicon Oxide, *Langmuir* **2010**, *26*, 3911-3917.

35. Neishi, K.; Aki, S.; Matsumoto, K.; Sato, H.; Itoh, H.; Hosaka, S.; Koike, J. Formation of a manganese oxide barrier layer with thermal chemical vapor deposition for advanced large-scale integrated interconnect structure, *Appl. Phys. Lett.* **2008**, *93*, 032106/032101-032106/032103.

36. (a) Koike, J.; Wada, M. Self-forming diffusion barrier layer in Cu–Mn alloy metalization, *Appl. Phys. Lett.* **2005**, *87*, 041911/041911-041911/041913; (b) Usui, T.; Nasu, H.; Takahashi, S.; Shimizu, N.; Nishikawa, T.; Yoshimaru, M.; Shibata, H.; Wada, M.; Koike, J. Highly Reliable Copper Dual-Damascene Interconnects with Self-Formed MnSi_xO_y Barrier Layer, *IEEE Trans. Electron Devices* **2006**, *53*, 2492-2499; (c) Koike, J.; Haneda, M.; Iijima, J.; Otsuka, Y.; Sako, H.; Neishi, K. Growth kinetics and thermal stability of a self-formed barrier layer at Cu–Mn/SiO₂ interface, *J. Appl. Phys.* **2007**, *102*, 043527/043521-043527/043527; (d) Haneda, M.; Iijima, J.; Koike, J. Growth behavior of self-formed barrier at Cu–Mn/SiO₂ interface at 250–450 °C, *Appl. Phys. Lett.* **2007**, *90*, 252107/252101-252107/252103; (e) Iijima, J.; Fujii, Y.; Neishi, K.; Koike, J. Resistivity reduction by external oxidation of Cu–Mn alloy films for semiconductor interconnect application, *J. Vac. Sci. Technol., B: Microelectron. Nanometer Struct.--Process., Meas., Phenom.* **2009**, *27*, 1963-1968.

Ph.D. Thesis — Jeffrey S. Price; McMaster University – Chemistry

37. Sun, H.; Qin, X.; Zaera, F. Chemical Nature of the Thin Films that Form on SiO₂/Si(100) Surfaces Upon Manganese Deposition, *J. Phys. Chem. Lett.* **2011**, *2*, 2525-2530.
38. Waterman, R. σ -Bond Metathesis: A 30-Year Retrospective, *Organometallics* **2013**, *32*, 7249-7263.
39. Hierso, J.-C.; Feurer, R.; Kalck, P. Platinum and Palladium Films Obtained by Low-Temperature MOCVD for the Formation of Small Particles on Divided Supports as Catalytic Materials, *Chem. Mater.* **2000**, *12*, 390-399.
40. (a) Aaltonen, T.; Ritala, M.; Sajavaara, T.; Keinonen, J.; Leskelä, M. Atomic Layer Deposition of Platinum Thin Films, *Chem. Mater.* **2003**, *15*, 1924-1928; (b) Aaltonen, T.; Ritala, M.; Tung, Y.-L.; Chi, Y.; Arstila, K.; Meinander, K.; Leskelä, M. Atomic layer deposition of noble metals: Exploration of the low limit of the deposition temperature, *J. Mater. Res.* **2004**, *19*, 3353-3358.
41. Aylett, B. J.; Colquhoun, H. M. Chemical vapor deposition of transition-metal silicides by pyrolysis of silyl transition-metal carbonyl compounds, *J. Chem. Soc., Dalton Trans.* **1977**, 2058-2061.
42. Stauf, G. T.; Dowben, P. A.; Boag, N. M.; Morales de la Garza, L.; Dowben, S. L. Organometallic Chemical Vapor Phase Deposition of "Mn₂Si", *Thin Solid Films* **1988**, *156*, 327-336.
43. Higgins, J. M.; Schmitt, A. L.; Guzei, I. A.; Jin, S. Higher Manganese Silicide Nanowires of Nowotny Chimney Ladder Phase, *J. Am. Chem. Soc.* **2008**, *130*, 16086-16094.
44. Guan, J.; Jin, J.; Chen, X.; Zhang, B.; Su, D.; Liang, C. Preparation and Formation Mechanism of Highly Dispersed Manganese Silicide on Silica by MOCVD of Mn(CO)₅SiCl₃, *Chem. Vap. Deposition* **2013**, *19*, 68-73.
45. Hampden-Smith, M. J.; Garvey, J.; Lei, D.; Huffman, J. C. Chemical Vapor Deposition of Binary Metal Germanides, *Mater. Res. Soc. Symp. Proc.* **1990**, *187*, 187-192.

Ph.D. Thesis — Jeffrey S. Price; McMaster University – Chemistry

46. Fischer, R. A. Organometallic CVD of CoGa and related bimetallic thin films from novel single source precursors, *Mater. Res. Soc. Symp. Proc.* **1993**, 282, 267-273.
47. Malandrino, G.; Toro, R. G.; Catalano, M. R.; Fragalà, M. E.; Rossi, P.; Paoli, P. Pompon-Like MnF₂ Nanostructures from a Single-Source Precursor through Atmospheric Pressure Chemical Vapor Deposition, *Eur. J. Inorg. Chem.* **2012**, 2012, 1021-1024.
48. Tomasini, P.; Haidoux, A.; Tedenac, J. C.; Maurin, M. Methylpentacarbonylmanganese as organometallic precursor for the epitaxial growth of manganese selenide heterostructures, *J. Cryst. Growth* **1998**, 193, 572-576.
49. (a) Nouhi, A.; Stirn, R. J. Heteroepitaxial growth of Cd_{1-x}Mn_xTe on GaAs by metalorganic chemical vapor deposition, *Appl. Phys. Lett.* **1987**, 51, 2251-2253; (b) Feng, Z. C.; Sudharsanan, R.; Perkowitz, S.; Erbil, A.; Pollard, K. T.; Rohatgi, A. Raman scattering characterization of high-quality Cd_{1-x}Mn_xTe films grown by metalorganic chemical vapor deposition, *J. Appl. Phys.* **1988**, 64, 6861-6863; (c) Mazur, J. H.; Grodzinski, P.; Nouhi, A.; Stirn, R. J. High resolution transmission electron microscopy investigation of the defect structure in cadmium manganese telluride layers grown on gallium arsenide by MOCVD, *Mater. Res. Soc. Symp. Proc.* **1988**, 102, 337-340.
50. Pain, G. N.; Bharatula, N.; Christiansz, G. I.; Kibel, M. H.; Kwietniak, M. S.; Sandford, C.; Warminski, T.; Dickson, R. S.; Rowe, R. S.; McGregor, K.; Deacon, G. B.; West, B. O.; Glanvill, S. R.; Hay, D. G.; Rossouw, C. J.; Stevenson, A. W. Use of MeMn(CO)₅ in the Low Temperature MOCVD Growth of Mn Containing Alloys, *J. Cryst. Growth* **1990**, 101, 208-210.
51. Lane, P. A.; Cockayne, B.; Wright, P. J.; Oliver, P. E.; Tilsley, M. E. G.; Smith, N. A.; Harris, I. R. Metalorganic chemical vapor deposition of manganese arsenide for thin film magnetic applications, *J. Cryst. Growth* **1994**, 143, 237-242.
52. Almond, M. J.; Redman, H.; Rice, D. A. Growth of thin layers of metal sulfides by chemical vapor deposition using dual source and single source precursors: routes to Cr₂S₃, α-MnS and FeS, *J. Mater. Chem.* **2000**, 10, 2842-2846.

53. Itoh, H.; Yamaguchi, H.; Naka, S. Preparation of (Mn, Zn)Fe₂O₄ Films by Pyrolytic CVD of Acetylacetonatocomplexes, *Nippon Kagaku Kaishi* **1987**, 1987, 2004-2005.
54. Nakamura, T. Intermolecular interaction between rare earth and manganese precursors in metalorganic chemical vapor deposition of perovskite manganite films, *Phys. Status Solidi C* **2015**, 12, 958-963.
55. Au, Y.; Wang, Q. M.; Li, H.; Lehn, J.-S. M.; Shenai, D. V.; Gordon, R. G. Vapor Deposition of Highly Conformal Copper Seed Layers for Plating Through-Silicon Vias (TSVs), *J. Electrochem. Soc.* **2012**, 159, D382-D385.
56. Wright, P. J.; Cockayne, B.; Cattell, A. F.; Dean, P. J.; Pitt, A. D.; Blackmore, G. W. Manganese Doping of ZnS and ZnSe Epitaxial Layers Grown by Organometallic Chemical Vapor Deposition, *J. Cryst. Growth* **1982**, 59, 155-160.
57. (a) Su, S. H.; Tsai, P. R.; Yokoyama, M.; Su, Y. K. Use of di- π -cyclopentadienyl manganese as a dopant source for ZnS in metalorganic chemical vapor deposition, *J. Electrochem. Soc.* **1996**, 143, 4116-4118; (b) Topol, A. W.; Dunn, K. A.; Barth, K. W.; Nuesca, G. M.; Taylor, B. K.; Dovidenko, K.; Kaloyeros, A. E.; Tuenge, R. T.; King, C. N. Chemical vapor deposition of ZnS:Mn for thin-film electroluminescent display applications, *J. Mater. Res.* **2004**, 19, 697-706.
58. Hara, K.; Sato, A.; Azumada, K.; Atsumori, T.; Shiratori, M. Preparation of AlN:Mn films by metalorganic chemical vapor deposition for thin film electroluminescent devices, *Phys. Status Solidi C* **2003**, 0, 2274-2277.
59. Rizzi, G. A.; Zanoni, R.; Di Siro, S.; Perriello, L.; Granozzi, G. Epitaxial growth of MnO nanoparticles on Pt(111) by reactive deposition of Mn₂(CO)₁₀, *Surf. Sci.* **2000**, 462, 187-194.
60. Assim, K.; Jeschke, J.; Jakob, A.; Dhakal, D.; Melzer, M.; Georgi, C.; Schulz, S. E.; Gessner, T.; Lang, H. Manganese half-sandwich complexes as metal-organic chemical vapor deposition precursors for manganese-based thin films, *Thin Solid Films* **2016**, 619, 265-272.

61. Maruyama, T.; Osaki, Y. Electrochromic Properties of Manganese Oxide Thin Films Prepared by Chemical Vapor Deposition, *J. Electrochem. Soc.* **1995**, *142*, 3137-3141.
62. Gorbenko, O. Y.; Graboy, I. E.; Amelichev, V. A.; Bosak, A. A.; Kaul, A. R.; Guttler, B.; Svetchnikov, V. L.; Zandbergen, H. W. The structure and properties of Mn₃O₄ thin films grown by MOCVD, *Solid State Commun.* **2002**, *124*, 15-20.
63. Nakamura, T.; Tai, R.; Nishimura, T.; Tachibana, K. Spectroscopic Study on Metalloorganic Chemical Vapor Deposition of Manganese Oxide Films, *J. Electrochem. Soc.* **2005**, *152*, C584-C587.
64. Lipani, Z.; Catalano, M. R.; Rossi, P.; Paoli, P.; Malandrino, G. A Novel Manganese(II) MOCVD Precursor: Synthesis, Characterization, and Mass Transport Properties of Mn(hfa)₂·tmeda, *Chem. Vap. Deposition* **2013**, *19*, 22-28.
65. Maccato, C.; Bigiani, L.; Carraro, G.; Gasparotto, A.; Seraglia, R.; Kim, J.; Devi, A.; Tabacchi, G.; Fois, E.; Pace, G.; Di Noto, V.; Barreca, D. Molecular Engineering of Mn^{II} Diamine Diketonate Precursors for the Vapor Deposition of Manganese Oxide Nanostructures, *Chem. - Eur. J.* **2017**, *23*, 17954-17963.
66. Bigiani, L.; Barreca, D.; Gasparotto, A.; Sada, C.; Marti-Sanchez, S.; Arbiol, J.; Maccato, C. Controllable vapor phase fabrication of F:Mn₃O₄ thin films functionalized with Ag and TiO₂, *CrystEngComm* **2018**, *20*, 3016-3024.
67. Du, L.; Yu, S.; Liu, X.; Ding, Y. An aminopyridinato Mn(II) compound as a novel CVD precursor for manganese-containing films, *New J. Chem.* **2018**, *42*, 4553-4558.
68. Sang, W.-b.; Durose, K.; Brinkman, A. W.; Tanner, B. K. Growth and characterization of magnetic metal Mn film by MOCVD, *Mater. Chem. Phys.* **1997**, *47*, 75-77.
69. Sun, H.; Zaera, F. Chemical Vapor Deposition of Manganese Metallic Films on Silicon Oxide Substrates, *J. Phys. Chem. C* **2012**, *116*, 23585-23595.

Ph.D. Thesis — Jeffrey S. Price; McMaster University – Chemistry

70. Au, Y.; Lin, Y.; Kim, H.; Beh, E.; Liu, Y.; Gordon, R. G. Selective chemical vapor deposition of manganese self-aligned capping layer for Cu interconnections in microelectronics, *J. Electrochem. Soc.* **2010**, *157*, D341-D345.
71. (a) Kurokawa, A.; Sutou, Y.; Koike, J.; Hamada, T.; Matsumoto, K.; Nagai, H.; Maekawa, K.; Kanato, H. Simultaneous Formation of a Metallic Mn Layer and a $\text{MnO}_x/\text{MnSi}_x\text{O}_y$ Barrier Layer by Chemical Vapor Deposition at 250 °C, *Jpn. J. Appl. Phys.* **2013**, *52*, 05FA02/01-05FA02/03; (b) Tsuchiya, Y.; Ando, D.; Sutou, Y.; Koike, J. Formation behavior and adhesion property of metallic Mn layer on porous SiOC by chemical vapor deposition, *Jpn. J. Appl. Phys.* **2014**, *53*, 05GA10/01-05GA10/05.
72. Qin, X.; Sun, H.; Zaera, F. Thermal chemistry of $\text{Mn}_2(\text{CO})_{10}$ during deposition of thin manganese films on silicon oxide and on copper surfaces, *J. Vac. Sci. Technol., A* **2012**, *30*, 01A112/111-101A112/110.
73. (a) Matsumoto, K.; Neishi, K.; Itoh, H.; Sato, H.; Hosaka, S.; Koike, J. Chemical vapor deposition of Mn and Mn oxide and their step coverage and diffusion barrier properties on patterned interconnect structures, *Appl. Phys. Express* **2009**, *2*, 036503/036501-036503/036503; (b) Dixit, V. K.; Neishi, K.; Akao, N.; Koike, J. Structural and Electronic Properties of a Mn Oxide Diffusion Barrier Layer Formed by Chemical Vapor Deposition, *IEEE Trans. Device Mater. Reliab.* **2011**, *11*, 295-302.
74. Dossi, C.; Recchia, S.; Fusi, A.; Psaro, R., Intrazeolitic redox chemistry of manganese prepared from Chemical vapor desposition of $\text{Mn}_2(\text{CO})_{10}$ on NaY. In *Studies in Surface Science and Catalysis*, Karge, H. G.; Weitkamp, J., Eds. Elsevier 1995; Vol. 98, pp 126-128.
75. Nilsen, O.; Fjellvåg, H.; Kjekshus, A. Growth of manganese oxide thin films by atomic layer deposition, *Thin Solid Films* **2003**, *444*, 44-51.
76. (a) Nilsen, O.; Foss, S.; Fjellvåg, H.; Kjekshus, A. Effect of substrate on the characteristics of manganese(IV) oxide thin films prepared by atomic layer deposition, *Thin Solid Films* **2004**, *468*, 65-74; (b) Nilsen, O.; Foss, S.; Kjekshus, A.; Fjellvåg, H. Growth of Nano-Needles of Manganese(IV) Oxide by Atomic Layer Deposition, *J. Nanosci. Nanotechnol.* **2008**, *8*, 1003-1011; Li, Y. W.; (c) Qiao, Q.; Zhang, J. Z.; Hu, Z.

- G.; Chu, J. H. Influence of post-annealing on structural, electrical and optical properties of manganese oxide thin films grown by atomic layer deposition, *Thin Solid Films* **2015**, *574*, 115-119; (d) Mattelaer, F.; Bosserez, T.; Rongé, J.; Martens, J. A.; Dendooven, J.; Detavernier, C. Manganese oxide films with controlled oxidation state for water splitting devices through a combination of atomic layer deposition and post-deposition annealing, *RSC Adv.* **2016**, *6*, 98337-98343; (e) Nieminen, H.-E.; Miikkulainen, V.; Settipani, D.; Simonelli, L.; Hönicke, P.; Zech, C.; Kayser, Y.; Beckhoff, B.; Honkanen, A.-P.; Heikkilä, M. J.; Mizohata, K.; Meinander, K.; Ylivaara, O. M. E.; Huotari, S.; Ritala, M. Intercalation of Lithium Ions from Gaseous Precursors into β -MnO₂ Thin Films Deposited by Atomic Layer Deposition, *J. Phys. Chem. C* **2019**, *123*, 15802-15814.
77. Silva, R. M.; Clavel, G.; Fan, Y.; Amsalem, P.; Koch, N.; Silva, R. F.; Pinna, N. Coating of Vertically Aligned Carbon Nanotubes by a Novel Manganese Oxide Atomic Layer Deposition Process for Binder-Free Hybrid Capacitors, *Adv. Mater. Interfaces* **2016**, *3*, 1600313/1600311-1600313/1600318.
78. Jin, H.; Hagen, D.; Karppinen, M. Low-temperature atomic layer deposition of crystalline manganese oxide thin films, *Dalton Trans.* **2016**, *45*, 18737-18741.
79. (a) Burton, B. B.; Fabreguette, F. H.; George, S. M. Atomic layer deposition of MnO using Bis(ethylcyclopentadienyl)manganese and H₂O, *Thin Solid Films* **2009**, *517*, 5658-5665; (b) Pickrahn, K. L.; Park, S. W.; Gorlin, Y.; Lee, H.-B.-R.; Jaramillo, T. F.; Bent, S. F. Active MnO_x Electrocatalysts Prepared by Atomic Layer Deposition for Oxygen Evolution and Oxygen Reduction Reactions, *Adv. Energy Mater.* **2012**, *2*, 1269-1277; (c) Strandwitz, N. C.; Comstock, D. J.; Grimm, R. L.; Nichols-Nieler, A. C.; Elam, J.; Lewis, N. S. Photoelectrochemical Behavior of n-type Si(100) Electrodes Coated with Thin Films of Manganese Oxide Grown by Atomic Layer Deposition, *J. Phys. Chem. C* **2013**, *117*, 4931-4936; (d) Pickrahn, K. L.; Gorlin, Y.; Seitz, L. C.; Garg, A.; Nordlund, D.; Jaramillo, T. F.; Bent, S. F. Applications of ALD MnO to electrochemical water splitting, *Phys. Chem. Chem. Phys.* **2015**, *17*, 14003-14011.

80. Du, L.; Yu, S.; Liu, X.; Ding, Y. An efficient atomic layer deposition process of MnO_x films using bis(*N,N'*-di-*tert*-butylacetamidinato)manganese-(II) and H_2O as reactants, *Appl. Surf. Sci.* **2019**, *486*, 460-465.
81. Qin, X.; Zaera, F. Oxidizing versus Reducing Co-reactants in Manganese Atomic Layer Deposition (ALD) on Silicon Oxide Surfaces, *ECS J. Solid State Sci. Technol.* **2014**, *3*, Q89-Q94.
82. Uusi-Esko, K.; Malm, J.; Karppinen, M. Atomic Layer Deposition of Hexagonal and Orthorhombic YMnO_3 Thin Films, *Chem. Mater.* **2009**, *21*, 5691-5694.
83. Uusi-Esko, K.; Karppinen, M. Extensive Series of Hexagonal and Orthorhombic RMnO_3 (R = Y, La, Sm, Tb, Yb, Lu) Thin Films by Atomic Layer Deposition, *Chem. Mater.* **2011**, *23*, 1835-1840.
84. Uusi-Esko, K.; Rautama, E. L.; Laitinen, M.; Sajavaara, T.; Karppinen, M. Control of Oxygen Nonstoichiometry and Magnetic Property of MnCo_2O_4 Thin Films Grown by Atomic Layer Deposition, *Chem. Mater.* **2010**, *22*, 6297-6300.
85. Miikkulainen, V.; Ruud, A.; Østreng, E.; Nilsen, O.; Laitinen, M.; Sajavaara, T.; Fjellvåg, H. Atomic Layer Deposition of Spinel Lithium Manganese Oxide by Film-Body-Controlled Lithium Incorporation for Thin-Film Lithium-Ion Batteries, *J. Phys. Chem. C* **2014**, *118*, 1258-1268.
86. Pickrahn, K. L.; Garg, A.; Bent, S. F. ALD of Ultrathin Ternary Oxide Electrocatalysts for Water Splitting, *ACS Catal.* **2015**, *5*, 1609-1616.
87. Kalutarage, L. C.; Clendenning, S. B.; Winter, C. H. Manganese Precursor Selection and the Thermal Atomic Layer Deposition of Copper/Manganese Alloy Films, *ECS Trans.* **2014**, *64*, 147-157.
88. Ahvenniemi, E.; Karppinen, M. ALD/MLD processes for Mn and Co based hybrid thin films, *Dalton Trans.* **2016**, *45*, 10730-10735.
89. Klesko, J. P.; Bellow, J. A.; Saly, M. J.; Winter, C. H.; Julin, J.; Sajavaara, T. Unusual stoichiometry control in the atomic layer deposition of manganese borate films from manganese bis(tris(pyrazolyl)borate) and ozone, *J. Vac. Sci. Technol., A* **2016**, *34*, 051515/051511-051515/051516.

Ph.D. Thesis — Jeffrey S. Price; McMaster University – Chemistry

90. Lee, Y.; Sun, H.; Young, M. J.; George, S. M. Atomic Layer Deposition of Metal Fluorides Using HF–Pyridine as the Fluorine Precursor, *Chem. Mater.* **2016**, *28*, 2022-2032.
91. Davidson, P. J.; Lappert, M. F.; Pearce, R. Stable Homoleptic Metal Alkyls, *Accounts Chem. Res.* **1974**, *7*, 209-217.
92. Eisch, J. J.; Adeosun, A. A.; Dutta, S.; Fregene, P. O. The Decomposition of Transition Metal Alkyls Revisited: Surprising Wellspring of Novel Reagents for Organic Synthesis, *Eur. J. Org. Chem.* **2005**, 2657-2670.
93. Hartwig, J., *Organotransition Metal Chemistry: From Bonding to Catalysis*. University Science Books: Sausalito, Cal., 2010.
94. Beerman, D. v. C., K. Organische Mangan-Verbindungen, *Angew. Chem.* **1959**, *71*, 627.
95. Anderson, R. A.; Carmona-Guzman, E.; Mertis, K.; Sigurdson, E.; Wilkinson, G. Trimethylsilylmethyl and Methyl Complexes of Manganese, Cobalt and Uranium, *J. Organomet. Chem.* **1975**, *99*, C19-C20.
96. Anderson, R. A.; Carmona-Guzman, E.; Gibson, J. F.; Wilkinson, G. Neopentyl, Neophyl, and Trimethylsilylmethyl Compounds of Manganese. Manganese(II) Dialkyls; Manganese(II) Dialkyl Amine Adducts; Tetra-alkylmanganate(II) Ions and Lithium Salts; Manganese(IV) Tetraalkyls, *J. Chem. Soc., Dalton Trans.* **1976**, 2204-2211.
97. Bochman, M.; Wilkinson, G.; Young, G. B. Preparation and Properties of 1-Adamantylmethyl and Adamantyl Complexes of Transition Metals, *J. Chem. Soc., Dalton Trans.* **1980**, 1879-1887.
98. Personal communication (ref 6) within ref 96.
99. Alberola, A.; Blair, V. L.; Carrella, L. M.; Clegg, W.; Kennedy, A. R.; Klett, J.; Mulvey, R. E.; Newton, S.; Rentschler, E.; Russo, L. Bis[(trimethylsilyl)methyl]manganese: Structural Variations of Its Solvent-Free and TMEDA-, Pyridine-, and Dioxane-Complexed Forms, *Organometallics* **2009**, *28*, 2112-2118.

Ph.D. Thesis — Jeffrey S. Price; McMaster University – Chemistry

100. Cámpora, J.; Palma, P.; Pérez, C. M.; Rodríguez-Delgado, A.; Alvarez, E.; Gutiérrez-Puebla, E. Synthesis and Reactions of Manganese(II) Dialkyl Complexes Containing Monodentate and Bidentate Nitrogen Ligands, *Organometallics* **2010**, *29*, 2960-2970.
101. Raithby, P. R.; Hursthouse, M. B.; Anderson, R. A.; Carmona-Guzman, E.; Wilkinson, G. *CSD Communication* **2012**.
102. Andersen, R. A.; Haaland, A.; Rypdal, K.; Volden, H. V. The Molecular Structure of Monomeric Base-free Bis(neopentyl)manganese by Gas Electron Diffraction, *J. Chem. Soc., Chem. Commun.* **1985**, 1807-1808.
103. Buttrus, N. H.; Eaborn, C.; Hitchcock, P. B.; Smith, J. D.; Sullivan, A. C. Preparation and Crystal Structure of a Two-coordinate Manganese Compound, Bis[tris(trimethylsilyl)methyl]manganese, *J. Chem. Soc., Chem. Commun.* **1985**, 1380-1381.
104. Samuel, P. P.; Mondal, K. C.; Roesky, H. W.; Hermann, M.; Frenking, G.; Demeshko, S.; Meyer, F.; Stückl, A. C.; Christian, J. H.; Dalal, N. S.; Ungur, L.; Chibotaru, L. F.; Pröpper, K.; Meents, A.; Dittrich, B. Synthesis and Characterization of a Two-Coordinate Manganese Complex and its Reaction with Molecular Hydrogen at Room Temperature, *Angew. Chem., Int. Ed.* **2013**, *52*, 11817-11821.
105. Andersen, R. A.; Berg, D. J.; Fernholt, L.; Faegri, K., Jr.; Green, J. C.; Haaland, A.; Lappert, M. F.; Leung, W. P.; Rypdal, K. Monomeric, Base-Free Manganese(II) Dialkyls; Synthesis, Magnetic Properties and Molecular Structure of MnR_2 [$R = CH(SiMe_3)_2$], SCF MO calculations on $Mn(CH_3)_2$ and photoelectron spectra of $Mn(CH_2CMe_3)_2$, *Acta Chem. Scand., Ser. A* **1988**, *A42*, 554-562.
106. Al-Juaid, S. S.; Eaborn, C.; El-Hamruni, S. M.; Hitchcock, P. B.; Smith, J. D.; Sozerli Can, S. E. Attachment to manganese or cobalt of a bulky tri(organosilyl)methyl ligand containing an NMe_2 or an OMe donor group, *J. Organomet. Chem.* **2002**, *649*, 121-127.

Ph.D. Thesis — Jeffrey S. Price; McMaster University – Chemistry

107. Manzer, L. E.; Guggenberger, L. J. Syntheses and structures of novel paramagnetic organometallic complexes of manganese(II) and chromium(II), *J. Organomet. Chem.* **1977**, *139*, C34-C38.
108. Tong, H.; Liu, D. Synthesis and Structural Characterization of Bis[2-dimethylamino- α -trimethylsilylbenzyl]Mn(II), *Anal. Sci.: X-Ray Struct. Anal. Online* **2008**, *24*, x67-x68.
109. Rankin, D. W. H.; Mitzel, N. W.; Morrison, C. A., *Structural Methods in Molecular Inorganic Chemistry*. 1 ed.; John Wiley & Sons: Chichester, UK, 2013.
110. Davies, J. I.; Howard, C. G.; Skapski, A. C.; Wilkinson, G. Tertiary Phosphine Adducts of Manganese(II) Dialkyls: Synthesis and X-Ray Crystal Structure of Bis(trimethylphosphine)bis(trimethylsilylmethyl)bis(μ -trimethylsilylmethyl)dimanganese(II), *J. Chem. Soc., Chem. Commun.* **1982**, 1077-1078.
111. Howard, C. G.; Girolami, G. S.; Wilkinson, G.; Thornton-Pett, M.; Hursthouse, M. B. Tertiary Phosphine Adducts of Manganese(II) Dialkyls. Part 2. Synthesis, Properties, and Structures of Monomeric Complexes, *J. Chem. Soc., Dalton Trans.* **1983**, 2631-2637.
112. Howard, C. G.; Wilkinson, G.; Thornton-Pett, M.; Hursthouse, M. B. Tertiary Phosphine Adducts of Manganese(II) Dialkyls. Part 1. Synthesis, Properties, and Structures of Alkyl-bridged Dimers, *J. Chem. Soc., Dalton Trans.* **1983**, 2025-2030.
113. Girolami, G. S.; Wilkinson, G.; Galas, A. M. R.; Thornton-Pett, M.; Hursthouse, M. B. Synthesis and Properties of the Divalent 1,2-Bis(dimethylphosphino)ethane (dmpe) Complexes $MCl_2(dmpe)_2$ and $MMe_2(dmpe)_2$ ($M = Ti, V, Cr, Mn, \text{ or } Fe$). X-Ray Crystal Structures of $MCl_2(dmpe)_2$ ($M = Ti, V, \text{ or } Cr$), $MnBr_2(dmpe)_2$, $TiMe_{1.3}Cl_{0.7}(dmpe)_2$, and $CrMe_2(dmpe)_2$, *J. Chem. Soc., Dalton Trans.* **1985**, 1339-1348.
114. Hitchcock, P. B.; Lappert, M. F.; Leung, W. P.; Buttrus, N. H. Silylmethyl and related complexes. VIII. Bis[bis(trimethylsilyl)methyl]manganese(II): its synthesis, properties, and crystal structures of its tetrahydrofuran and bis(dimethylphosphino)ethane adducts, *J. Organomet. Chem.* **1990**, *394*, 57-67.

115. Riollet, V.; Copéret, C.; Basset, J.-M.; Rousset, L.; Bouchu, D.; Grosvalet, L.; Perrin, M. Reaction of "[Mn^{II}(CH₂*t*Bu)₂]" with Bidentate Diimine Ligands: From Simple Base Adducts to C–C Activation of the Ligand, *Angew. Chem., Int. Ed.* **2002**, *41*, 3025-3027.
116. Bart, S. C.; Hawrelak, E. J.; Schmisser, A. K.; Lobkovsky, E.; Chirik, P. J. Synthesis, Reactivity, and Solid State Structures of Four-Coordinate Iron(II) and Manganese(II) Alkyl Complexes, *Organometallics* **2004**, *23*, 237-246.
117. Crewdson, P.; Gambarotta, S.; Yap, G. P. A.; Thompson, L. K. Dinuclear and Octanuclear Mn(II) Complexes with μ^2 -C, μ^2 -N(Pyrrolide), and μ - η^1 : η^5 -(Pyrrolide) Bridges: A Structural and Magnetic Study, *Inorg. Chem.* **2003**, *42*, 8579-8584.
118. Blair, V. L.; Clegg, W.; Conway, B.; Hevia, E.; Kennedy, A.; Klett, J.; Mulvey, R. E.; Russo, L. Alkali-Metal-Mediated Manganation(II) of Functionalized Arenes and Applications of *ortho*-Manganated Products in Pd-Catalyzed Cross-Coupling Reactions with Iodobenzene, *Chem. - Eur. J.* **2008**, *14*, 65-72.
119. Kennedy, A. R.; Klett, J.; Mulvey, R. E.; Robertson, S. D. N-Heterocyclic-Carbene-Induced Monomerization of Sterically Encumbered Dialkylmagnesium and Dialkylmanganese Polymers, *Eur. J. Inorg. Chem.* **2011**, *2011*, 4675-4679.
120. Girolami, G. S.; Howard, C. G.; Wilkinson, G.; Dawes, H. M.; Thornton-Pett, M.; Motevalli, M.; Hursthouse, M. B. Alkyl, Hydrido, and Tetrahydroaluminato Complexes of Manganese with 1,2-Bis(dimethylphosphino)ethane (dmpe). X-Ray Crystal Structures of Mn₂(μ -C₆H₁₁)₂(C₆H₁₁)₂(μ -dmpe), (dmpe)₂Mn(μ -H)₂AlH(μ -H)₂AlH(μ -H₂)Mn(dmpe)₂, and Li₄{MnH(C₂H₄)[CH₂(Me)PCH₂CH₂PMe₂]₂}₂·2Et₂O, *J. Chem. Soc., Dalton Trans.* **1985**, 921-929.
121. (a) Al-Afyouni, M. H.; Krishnan, V. M.; Arman, H. D.; Tonzetich, Z. J. Synthesis and Reactivity of Manganese(II) Complexes Containing N-Heterocyclic Carbene Ligands, *Organometallics* **2015**, *34*, 5088-5094; (b) Hashimoto, T.; Kawato, Y.; Nakajima, Y.; Ohki, Y.; Tatsumi, K.; Ando, W.; Sato, K.; Shimada, S. Synthesis of dimethylmanganese(II) complexes bearing *N*-heterocyclic carbenes and nucleophilic

substitution reaction of tetraalkoxysilanes by diorganomanganese(II) complexes, *J. Organomet. Chem.* **2016**, *820*, 14-19.

122. Stalzer, M. M.; Telser, J.; Krzystek, J.; Motta, A.; Delferro, M.; Marks, T. J. A Neutrally Charged Trimethylmanganese(III) Complex: Synthesis, Characterization, and Disproportionation Chemistry, *Organometallics* **2016**, *35*, 2683-2688.

123. Pérez, C. M.; Rodríguez-Delgado, A.; Palma, P.; Álvarez, E.; Gutiérrez-Puebla, E.; Cámpora, J. Neutral and Cationic Alkylmanganese(II) Complexes Containing 2,6-Bisiminopyridine Ligands, *Chem. - Eur. J.* **2010**, *16*, 13834-13842.

124. Zhang, G.; Zeng, H.; Wu, J.; Yin, Z.; Zheng, S.; Fettinger, J. C. Highly Selective Hydroboration of Alkenes, Ketones and Aldehydes Catalyzed by a Well-Defined Manganese Complex, *Angew. Chem., Int. Ed.* **2016**, *55*, 14369-14372.

125. Engerer, L. K.; Carlson, C. N.; Hanusa, T. P.; Brennessel, W. W.; Young, V. G., Jr. σ - vs π -Bonding in Manganese(II) Allyl Complexes, *Organometallics* **2012**, *31*, 6131-6138.

126. Koschmieder, S. U.; Wilkinson, G.; Hussain-Bates, B.; Hursthouse, M. B. Reactions of Organic Isocyanates and *tert*-Butyl Isocyanide with Manganese(II) Alkyls and Trimesitylchromium, *J. Chem. Soc., Dalton Trans.* **1992**, 19-24.

127. Bower, B. K.; Tennent, H. G. Transition Metal Bicyclo[2.2.1]hept-1-yls, *J. Am. Chem. Soc.* **1972**, *94*, 2512-2514.

128. March, J., *Advanced Organic Chemistry: Reactions, Mechanisms, and Structure*. 4 ed.; Wiley: New York, 1992.

129. Howard, C. G.; Girolami, G. S.; Wilkinson, G.; Thornton-Pett, M.; Hursthouse, M. B. Manganese(IV) Alkyl Complexes. Synthesis and Structure of Tetramethyl[1,2-bis(dimethylphosphino)ethane]manganese(IV), *J. Chem. Soc., Chem. Commun.* **1983**, 1163-1164.

130. (a) Heimer, T. The band spectrum of MnH, *Naturwissenschaften* **1936**, *24*, 521-522; (b) Pearse, R. W. B.; Gaydon, A. G. Band spectrum of manganese hydride, *Nature* **1937**, *139*, 590; (c) Stalinski, B. The structure and magnetic properties of hydrides of transition metals, *Zeszyty Nauk. Politech. Wroclaw-Chem.* **1957**, No. 4, 25-78.

Ph.D. Thesis — Jeffrey S. Price; McMaster University – Chemistry

131. Hieber, W.; Wagner, G. Zur Kenntnis des Mangancarbonyls, *Z. Naturforsch.* **1957**, *12b*, 478-479.
132. LaPlaca, S. J.; Hamilton, W. C.; Ibers, J. A. Crystal and Molecular Structure of Manganese Pentacarbonyl Hydride, *Inorg. Chem.* **1964**, *3*, 1491-1495.
133. La Placa, S. J.; Hamilton, W. C.; Ibers, J. A.; Davison, A. Nature of the Metal–Hydrogen Bond in Transition Metal–Hydrogen Complexes. Neutron and X-Ray Diffraction Studies of β -Pentacarbonylmanganese Hydride, *Inorg. Chem.* **1969**, *8*, 1928-1935.
134. Booth, B. L.; Haszeldine, R. N. Metal Carbonyl Chemistry. Part 1. Reactions of Phosphorus-containing Ligands with Hydridopentacarbonylmanganese, *J. Chem. Soc., Inorg., Phys., Theoret.* **1966**, 157-160.
135. Laing, M.; Singleton, E.; Kruger, G. Crystal and molecular structure of *trans*-bis(diphenylmethylphosphine)tricarbonylmanganese hydride, *J. Organometal. Chem.* **1973**, *54*, C30-C32.
136. Hayakawa, H.; Nakayama, H.; Kobayashi, A.; Sasaki, Y. Molecular and Crystal Structure of Hydrido(tricarbonyl) bis(triphenylphosphine)manganese(I), $\text{HMn}(\text{CO})_3[\text{P}(\text{C}_6\text{H}_5)_3]_2$, *Bull. Chem. Soc. Jpn.* **1978**, *51*, 2041-2045.
137. Weiler, G.; Huttner, G.; Zsolnai, L.; Berke, H. Phosphordonor-substituierte Formylmangan-Komplexe, *Z. Naturforsch., B: Chem. Sci.* **1987**, *42*, 203-209.
138. (a) Rausch, M. D.; Ogasa, M.; Ayers, M. A.; Rogers, R. D.; Rollins, A. N. Formation and Molecular Structure of Hydridotricarbonyl $\{[\eta^5$ - (diphenylphosphino)cyclopentadienyl] $[\eta^7$ - (diphenylphosphino)cycloheptatrienyl]titanium-*P,P'*\}manganese: A New Chelated Titanium–Manganese Heterobimetallic Compound, *Organometallics* **1991**, *10*, 2481-2484; (b) Onaka, S.; Haga, M.-a.; Takagi, S.; Otsuka, M.; Mizuno, K. Synthesis, X-Ray Analysis, and Electrochemical Study of Some Manganese Carbonyl Derivatives with 1,1'-Bis(diphenylphosphino)ferrocene, dppfe, *Bull. Chem. Soc. Jpn.* **1994**, *67*, 2440-2446; (c) O'Keiffe, L. S.; Mitchell, A. C.; Becker, T. M.; Ho, D. M.; Mandal, S. K. Reactions of $[(\text{CO})_3(\text{P-P})\text{Mn}]_2$ with primary alcohols, where, P-P is dppe $\{\text{Ph}_2\text{P}(\text{CH}_2)_2\text{PPh}_2\}$, dppp

{Ph₂P(CH₂)₃PPh₂}, dppb {Ph₂P(CH₂)₄PPh₂}, dpppe {Ph₂P(CH₂)₅PPh₂}, dtpe {(*p*-tol)₂P(CH₂)₂P(*p*-tol)₂}, or dcpe {(^chex)₂P(CH₂)₂P(^chex)₂}. Synthesis of *fac*-(CO)₃(P-P)MnH and the X-ray structure of *fac*-(CO)₃(dtpe)MnH, *J. Organomet. Chem.* **2000**, *613*, 13-18.

139. Darensbourg, D. J.; Ganguly, P.; Billodeaux, D. R. Structural Characterization of Several (CO)₃(dppp)MnX Derivatives, dppp = 1,3-Bis(diphenylphosphino)propane and X = H, OTs, OC₂H₅, Cl, Br, or N₃. An Assessment of Their Efficacy for Catalyzing the Coupling of Carbon Dioxide and Epoxides, *Organometallics* **2004**, *23*, 6025-6030.

140. Bolaño, S.; Bravo, J.; Castro, J.; García-Fontán, S.; Lamas, E.; Rodríguez Seoane, P. Synthesis and Characterization of Di- and Tricarbonylhydridomanganese(I) Complexes, *Z. Anorg. Allg. Chem.* **2009**, *635*, 2503-2510.

141. Welch, K. D.; Dougherty, W. G.; Kassel, W. S.; DuBois, D. L.; Bullock, R. M. Synthesis, Structures, and Reactions of Manganese Complexes Containing Diphosphine Ligands with Pendant Amines, *Organometallics* **2010**, *29*, 4532-4540.

142. Jana, R.; Chakraborty, S.; Blacque, O.; Berke, H. Manganese and Rhenium Formyl Complexes of Diphosphinylborane Ligands: Stabilization of the Formyl Unit from Intramolecular B–O Bond Formation, *Eur. J. Inorg. Chem.* **2013**, *2013*, 4574-4584.

143. Hulley, E. B.; Helm, M. L.; Bullock, R. M. Heterolytic cleavage of H₂ by bifunctional manganese(I) complexes: impact of ligand dynamics, electrophilicity, and base positioning, *Chem. Sci.* **2014**, *5*, 4729-4741.

144. Kallmeier, F.; Dudzic, B.; Irrgang, T.; Kempe, R. Manganese-Catalyzed Sustainable Synthesis of Pyrroles from Alcohols and Amino Alcohols, *Angew. Chem., Int. Ed.* **2017**, *56*, 7261-7265.

145. Stewart, M. A.; Moore, C. E.; Ditri, T. B.; Labios, L. A.; Rheingold, A. L.; Figueroa, J. S. Electrophilic functionalization of well-behaved manganese monoanions supported by *m*-terphenyl isocyanides, *Chem. Commun.* **2011**, *47*, 406-408.

146. Turner, J.; Abdalla, J. A. B.; Bates, J. I.; Tirfoin, R.; Kelly, M. J.; Phillips, N.; Aldridge, S. Formation of sub-valent carbenoid ligands by metal-mediated

dehydrogenation chemistry: coordination and activation of $\text{H}_2\text{Ga}\{\text{NDippCMe}_2\text{CH}\}$, *Chem. Sci.* **2013**, *4*, 4245-4250.

147. Buhaibeh, R.; Filippov, O. A.; Bruneau-Voisine, A.; Willot, J.; Duhayon, C.; Valyaev, D. A.; Lugan, N.; Canac, Y.; Sortais, J.-B. Phosphine-NHC Manganese Hydrogenation Catalyst Exhibiting a Non-Classical Metal-Ligand Cooperative H_2 Activation Mode, *Angew. Chem., Int. Ed.* **2019**, *58*, 6727-6731.

148. Mukherjee, A.; Nerush, A.; Leitius, G.; Shimon, L. J. W.; Ben David, Y.; Espinosa Jalapa, N. A.; Milstein, D. Manganese-Catalyzed Environmentally Benign Dehydrogenative Coupling of Alcohols and Amines to Form Aldimines and H_2 : A Catalytic and Mechanistic Study, *J. Am. Chem. Soc.* **2016**, *138*, 4298-4301.

149. Mastalir, M.; Glatz, M.; Gorgas, N.; Stöger, B.; Pittenauer, E.; Allmaier, G.; Veiros, L. F.; Kirchner, K. Divergent Coupling of Alcohols and Amines Catalyzed by Isoelectronic Hydride Mn^{I} and Fe^{II} PNP Pincer Complexes, *Chem. - Eur. J.* **2016**, *22*, 12316-12320.

150. Bertini, F.; Glatz, M.; Gorgas, N.; Stöger, B.; Peruzzini, M.; Veiros, L. F.; Kirchner, K.; Gonsalvi, L. Carbon dioxide hydrogenation catalysed by well-defined $\text{Mn}(\text{I})$ PNP pincer hydride complexes, *Chem. Sci.* **2017**, *8*, 5024-5029.

151. Nguyen, D. H.; Trivelli, X.; Capet, F.; Paul, J.-F.; Dumeignil, F.; Gauvin, R. M. Manganese Pincer Complexes for the Base-Free, Acceptorless Dehydrogenative Coupling of Alcohols to Esters: Development, Scope, and Understanding, *ACS Catal.* **2017**, *7*, 2022-2032; Liu, Q. *CSD Communication* **2017**.

152. Kumar, A.; Daw, P.; Espinosa-Jalapa, N. A.; Leitius, G.; Shimon, L. J. W.; Ben-David, Y.; Milstein, D. CO_2 activation by manganese pincer complexes through different modes of metal–ligand cooperation, *Dalton Trans.* **2019**, *48*, 14580-14584.

153. Bernhardt, R. J.; Eyman, D. P. Synthesis and Characterization of (Arene)manganese Dicarbonyl Halides and Hydride, *Organometallics* **1984**, *3*, 1445-1446.

154. Schlom, P. J.; Morken, A. M.; Eyman, D. P.; Baenziger, N. C.; Schauer, S. J. Reactivity and Structure of Manganese Complex (η^6 -C₆(CH₃)₆)Mn(CO)₂H: Stable Alkylrhenium Analog, *Organometallics* **1993**, *12*, 3461-3467.
155. Hieber, W.; Höfler, M.; Muschi, J. Bis-phosphinsubstituierte Carbonylmanganate(-I) und ihre Derivate, *Chem. Ber.* **1965**, *98*, 311-320.
156. Ugo, R.; Bonati, F. Production of the species HMn(CO)₃(ligand)₂ from dimanganese decacarbonyl and triphenylphosphine or triphenyl phosphite, *J. Organomet. Chem.* **1967**, *8*, 189-192.
157. Reimann, R. H.; Singleton, E. Reactions of metal carbonyls. Part 7. Substitution reactions of decacarbonyldimanganese with tertiary phosphorus and arsenic ligands, *J. Chem. Soc., Dalton Trans.* **1976**, 2109-2114.
158. Mandal, S. K.; Ho, D. M.; Orchin, M. Reaction of Electrophiles with Manganese(I) and Rhenium(I) Alkoxide Complexes: Reversible Absorption of Atmospheric Carbon Dioxide, *Organometallics* **1993**, *12*, 1714-1719.
159. Elangovan, S.; Topf, C.; Fischer, S.; Jiao, H.; Spannenberg, A.; Baumann, W.; Ludwig, R.; Junge, K.; Beller, M. Selective Catalytic Hydrogenations of Nitriles, Ketones, and Aldehydes by Well-Defined Manganese Pincer Complexes, *J. Am. Chem. Soc.* **2016**, *138*, 8809-8814.
160. Chatterton, N. P.; Guilera, G.; McGrady, G. S. Structure of the Elusive Hydrido(methylcyclopentadienyl)dicarbonylmanganate(I) Anion, $[(\eta^5$ -C₅H₄Me)Mn(CO)₂H]⁻, as Determined by Single-Crystal X-ray Diffraction, *Organometallics* **2004**, *23*, 1165-1167.
161. Mock, S.; Schubert, U. Substitutions-Reaktionen der anionischen Hydrid-Komplexe $[(\pi$ -MeC₅H₄)(CO)₂MnH]⁻ and $[(\pi$ -Aromat)(CO)₂CrH]⁻, *Chem. Ber.* **1993**, *126*, 2591-2599.
162. Leong, V. S.; Cooper, N. J. Synthesis and Chemical Characterization of [Mn(η -C₅H₅)(CO)₂]²⁻, *Organometallics* **1988**, *7*, 2080-2081.

Ph.D. Thesis — Jeffrey S. Price; McMaster University – Chemistry

163. Hulley, E. B.; Welch, K. D.; Appel, A. M.; DuBois, D. L.; Bullock, R. M. Rapid, Reversible Heterolytic Cleavage of Bound H₂, *J. Am. Chem. Soc.* **2013**, *135*, 11736-11739.
164. Miles, W. J., Jr.; Clark, R. J. Metal Carbonyl-Phosphorus Trifluoride Systems. VI. Manganese Pentacarbonyl Hydrides and Perfluoroalkyls, *Inorg. Chem.* **1968**, *7*, 1801-1806.
165. (a) Miles, W. J., Jr.; Garrett, B. B.; Clark, R. J. Manganese Nuclear Magnetic Resonance of the Phosphorus Trifluoride Derivatives of Manganese Pentacarbonyl Hydride, *Inorg. Chem.* **1969**, *8*, 2817-2818; (b) Head, R. A.; Nixon, J. F.; Sharp, G. J.; Clark, R. J. Photoelectron Spectroscopic Study of Metal Trifluorophosphine and Hydridotrifluorophosphine Complexes, *J. Chem. Soc., Dalton Trans.* **1975**, 2054-2059.
166. Das, A. K.; Rao, D. V. R. Halogenation of Dihalo Complexes of Manganese(II) Containing Nitrogen Donor Ligands, *Z. Anorg. Allg. Chem.* **1970**, *379*, 213-217.
167. Hames, B. W.; Legzdins, P.; Oxley, J. C. Organometallic Nitrosyl Chemistry. 13. Reactions of Sodium Dihydridobis(2-methoxyethoxy)aluminate with Some Cationic and Neutral Nitrosyl Complexes, *Inorg. Chem.* **1980**, *19*, 1565-1571.
168. (a) Green, M. L. H.; O'Hare, D.; Wallis, J. M. Synthesis of Mono- η -benzenebis(trimethylphosphine)manganese and -rhenium Compounds Using the Metal Atoms, *J. Chem. Soc., Chem. Commun.* **1984**, 233-234; (b) Green, M. L. H.; O'Hare, D.; Wallis, J. M. Mono- η -arenebis(trimethylphosphine)rhenium Chemistry: Alkyl, Hydrido, Halo and Olefin Derivatives, *Polyhedron* **1986**, *5*, 1363-1370.
169. Gusev, D. G.; Nietlispach, D.; Vymenits, A. B.; Bakhmutov, V. I.; Berke, H. Synthesis and NMR T_1 Relaxation Study of Rhenium and Manganese Hydride Complexes, *Inorg. Chem.* **1993**, *32*, 3270-3276.
170. Nietlispach, D.; Bosch, H. W.; Berke, H. A Comparative Study of the Reactivity of Mn(NO)₂L₂H and Mn(CO)₃L₂H Complexes (L = Phosphorus Donor), *Chem. Ber.* **1994**, *127*, 2403-2415.
171. Merwin, R. K.; Ontko, A. C.; Houllis, J. F.; Roddick, D. M. Synthesis and characterization of CpMn(dfepe)(L) complexes (dfepe = (C₂F₅)₂PCH₂CH₂P(C₂F₅)₂; L =

CO, H₂, N₂): an unusual example of a dihydride to dihydrogen photochemical conversion, *Polyhedron* **2004**, *23*, 2873-2878.

172. Girolami, G. S.; Wilkinson, G.; Thornton-Pett, M.; Hursthouse, M. B. Hydrido, Alkyl, and Ethylene 1,2-Bis(dimethylphosphino)ethane Complexes of Manganese and the Crystal Structures of MnBr₂(dmpe)₂, [Mn(AlH₄)(dmpe)₂]₂ and MnMe₂(dmpe)₂, *J. Am. Chem. Soc.* **1983**, *105*, 6752-6753.

173. Perthuisot, C.; Fan, M.; Jones, W. D. Catalytic Thermal C–H Activation with Manganese Complexes: Evidence for η^2 -H₂ Coordination in a Neutral Manganese Complex and Its Role in C–H Activation, *Organometallics* **1992**, *11*, 3622-3629.

174. Filippou, A. C.; Ghana, P.; Chakraborty, U.; Schnakenburg, G. Manganese–Tin Triple Bonds: A New Synthetic Route to the Manganese Stannylidyne Complex Cation *trans*-[H(dmpe)₂Mn≡Sn(C₆H₃-2,6-Mes₂)]⁺ (dmpe = Me₂PCH₂CH₂PMe₂, Mes = 2,4,6-Trimethylphenyl), *J. Am. Chem. Soc.* **2013**, *135*, 11525-11528.

175. Maekawa, M.; Römel, M.; Daniliuc, C. G.; Jones, P. G.; White, P. S.; Neese, F.; Walter, M. D. Reactivity studies on [Cp'MnX(thf)]₂: manganese amide and polyhydride synthesis, *Chem. Sci.* **2012**, *3*, 2972-2979.

176. Mukhopadhyay, T. K.; Rock, C. L.; Hong, M.; Ashley, D. C.; Groy, T. L.; Baik, M.-H.; Trovitch, R. J. Mechanistic Investigation of Bis(imino)pyridine Manganese Catalyzed Carbonyl and Carboxylate Hydrosilylation, *J. Am. Chem. Soc.* **2017**, *139*, 4901-4915.

177. Spessard, G.; Miessler, G., *Organometallic Chemistry*. 2 ed.; Oxford University Press: New York, 2010; p 152.

178. Koetzle, T. F. Neutron Diffraction Studies of Metal Hydride and Dihydrogen Complexes, *Trans. Am. Crystallogr. Assoc.* **1997**, *31*, 57-68.

179. Abramov, Y. A.; Brammer, L.; Klooster, W. T.; Bullock, R. M. Experimental Charge Density and Neutron Structural Study of *cis*-HMn(CO)₄PPh₃: Comprehensive Analysis of Chemical Bonding and Evidence for a C–H···H–Mn Hydrogen Bond, *Inorg. Chem.* **1998**, *37*, 6317-6328.

Ph.D. Thesis — Jeffrey S. Price; McMaster University – Chemistry

180. Morris, R. H. Brønsted-Lowry Acid Strength of Metal Hydride and Dihydrogen Complexes, *Chem. Rev.* **2016**, *116*, 8588-8654.
181. Richmond, T. G.; Basolo, F.; Shriver, D. F. Interaction of Metal Carbonyl Hydrides with Lewis Acids, *Organometallics* **1982**, *1*, 1624-1628.
182. Hieber, W.; Wagner, G. Über "Manganpentacarbonylwasserstoff", $\text{HMn}(\text{CO})_6$, *Z. Naturforsch.* **1958**, *13b*, 339-347.
183. Moore, E. J.; Sullivan, J. M.; Norton, J. R. Kinetic and Thermodynamic Acidity of Hydrido Transition-Metal Complexes. 3. Thermodynamic Acidity of Common Mononuclear Carbonyl Hydrides, *J. Am. Chem. Soc.* **1986**, *108*, 2257-2263.
184. (a) Bernhardt, R. J.; Wilmoth, M. A.; Weers, J. J.; LaBrush, D. M.; Eyman, D. P.; Huffman, J. C. Derivatives of the (Arene) $\text{M}(\text{CO})_2$ (M = Mn or Re) Fragment. The Molecular Structure of $(\eta^6\text{-C}_6\text{Me}_6)\text{Mn}(\text{CO})_2\text{Cl}$, *Organometallics* **1986**, *5*, 883-888; (b) Wilmoth, M. A.; Bernhardt, R. J.; Eyman, D. P.; Huffman, J. C. Carbonylation of $[\eta^6\text{-C}_6(\text{CH}_3)_6]\text{Mn}(\text{CO})_2\text{H}$, *Organometallics* **1986**, *5*, 2559-2561.
185. Bullock, R. M.; Rappoli, B. J. Preparation and Reactions of $\text{Mn}_2(\text{CO})_9(\eta^1\text{-aldehyde})$ Complexes, *J. Am. Chem. Soc.* **1991**, *113*, 1659-1669.
186. Paprott, G.; Lehmann, S.; Seppelt, K. Reaktionen des 1,2,3,4,5-Pentafluorocyclopentadiens, *Chem. Ber.* **1988**, *121*, 727-733.
187. Schunn, R. A. Interaction of Transition Metal Hydride Complexes with Deuterium, Ethylene- d_4 , and 1-Butene, *Inorg. Chem.* **1970**, *9*, 2567-2572.
188. Beck, W.; Danzer, W.; Höfer, R. Reactions of Carbonylmetal Hydrides with Aziridine and Propylene Sulfide (2-Methylthiirane), *Angew. Chem., Int. Ed. Engl.* **1973**, *12*, 77-78.
189. Dobbie, R. C. Action of Bistrifluoromethylphosphino Compounds on Pentacarbonylmanganese Hydride, *J. Chem. Soc. A* **1971**, 230-233.
190. (a) Nappa, M. J.; Santi, R.; Halpern, J. Mechanisms of the Carbon-Hydrogen Bond-Forming Binuclear Reductive Elimination Reactions of Benzyl- and Hydridomanganese Carbonyls, *Organometallics* **1985**, *4*, 34-41; (b) Warner, K. E.; Norton, J. R. Intermolecular Formation of C-H Bonds: Application to the Synthesis of

Heterobimetallic Complexes, *Organometallics* **1985**, *4*, 2150-2160; (c) Kovács, I.; Hoff, C. D.; Ungváry, F.; Markó, L. Kinetic Investigation of the Mixed-Metal Bimolecular Reductive Eliminations in the Reactions of $\text{EtOC(O)CH}_2\text{M(CO)}_n$ or EtOC(O)M(CO)_n ($\text{M} = \text{Co}$, $n = 4$; $\text{M} = \text{Mn}$, $n = 5$) with HCo(CO)_4 or HMn(CO)_5 , *Organometallics* **1985**, *4*, 1347-1350.

191. Kubas, G. J., *Metal Dihydrogen and σ -Bond Complexes: Structure, Theory, and Reactivity*. Kluwer Academic/Plenum: New York, 2001.

192. Kubas, G. J., Chapter 24: Dihydrogen and Other σ Bond Complexes. In *Comprehensive Organometallic Chemistry III*, Mingos, D. M. P.; Crabtree, R. H., Eds. Elsevier: Boston, 2007; Vol. 1, pp 671-698.

193. Kubas, G. J.; Ryan, R. R.; Swanson, B. I.; Vergamini, P. J.; Wasserman, H. J. Characterization of the First Examples of Isolable Molecular Hydrogen Complexes, $\text{M(CO)}_3(\text{PR}_3)_2(\text{H}_2)$ ($\text{M} = \text{Mo}$, W ; $\text{R} = \text{Cy}$, *i*-Pr). Evidence for a Side-on Bonded H_2 Ligand, *J. Am. Chem. Soc.* **1984**, *106*, 451-452.

194. (a) Zilm, K. W.; Merrill, R. A.; Kummer, M. W.; Kubas, G. J. Characterization of transition-metal molecular hydrogen complexes by solid-state proton NMR, *J. Am. Chem. Soc.* **1986**, *108*, 7837-7839; (b) Zilm, K. W.; Millar, J. M. Solid State and Solution NMR of Nonclassical Transition-Metal Polyhydrides, *Adv. Magn. Opt. Reson.* **1990**, *15*, 163-200.

195. Morris, R. H. Dihydrogen, dihydride and in between: NMR and structural properties of iron group complexes, *Coord. Chem. Rev.* **2008**, *252*, 2381-2394.

196. (a) Howdle, S. M.; Poliakoff, M. Organometallic Photochemistry in Supercritical Fluids: the Reaction of H_2 with $[(\eta^5\text{-C}_5\text{H}_5)\text{M(CO)}_3]$ ($\text{M} = \text{Re}$ and Mn) and the Formation of a 'Non-classical' Dihydrogen Complex of Manganese(I), *J. Chem. Soc., Chem. Commun.* **1989**, 1099-1101; (b) Howdle, S. M.; Healy, M. A.; Poliakoff, M. Organometallic Chemistry in Supercritical Fluids. The Generation and Detection of Dinitrogen and Nonclassical Dihydrogen Complexes of Group 6, 7, and 8 Transition Metals at Room Temperature, *J. Am. Chem. Soc.* **1990**, *112*, 4804-4813.

Ph.D. Thesis — Jeffrey S. Price; McMaster University – Chemistry

197. Johnson, F. P. A.; George, M. W.; Bagratashvili, V. N.; Vereshchagina, L. N.; Poliakoff, M. Steric Effects in the Kinetics of Organometallic Reactions: A Time-Resolved Infrared Study of $[(\eta^5\text{-C}_5\text{R}_5)\text{Mn}(\text{CO})_2]$ (R = H, Me, Et) in n-heptane solution, *Mendeleev Commun.* **1991**, 26-28.
198. Sweany, R. L.; Watzke, D. Synthesis and Characterization of Dihydrogen Complexes of Tetracarbonylbromomanganese(I) and Tetracarbonylchloromanganese(I) in Argon Matrixes, *Organometallics* **1997**, *16*, 1037-1042.
199. (a) Albertin, G.; Antoniutti, S.; Bettioli, M.; Bordignon, E.; Busatto, F. Synthesis, Characterization, and Reactivity of Cationic Molecular Hydrogen Complexes of Manganese(I), *Organometallics* **1997**, *16*, 4959-4969; (b) Toupadakis, A.; Kubas, G. J.; King, W. A.; Scott, B. L.; Huhmann-Vincent, J. Comparative Binding of H₂, N₂, and Related Ligands to $[\text{Mn}(\text{CO})_3(\text{PCy}_3)_2]^+$ and Other 16e Electrophiles. N₂ Does Not Coordinate, and H₂ Is the Most Versatile Weak Ligand, *Organometallics* **1998**, *17*, 5315-5323.
200. Fang, X.; Huhmann-Vincent, J.; Scott, B. L.; Kubas, G. J. H₂ binding to and silane alcoholysis on an electrophilic Mn(I) fragment with tied-back phosphite ligands. X-ray structure of a Mn-CH₂Cl₂ complex, *J. Organomet. Chem.* **2000**, *609*, 95-103.
201. (a) King, W. A.; Luo, X.-L.; Scott, B. L.; Kubas, G. J.; Zilm, K. W. Cationic Manganese(I) Dihydrogen and Dinitrogen Complexes Derived from a Formally 16-Electron Complex with a Bis-Agostic Interaction, $[\text{Mn}(\text{CO})(\text{Ph}_2\text{PC}_2\text{H}_4\text{PPh}_2)_2]^+$, *J. Am. Chem. Soc.* **1996**, *118*, 6782-6783; (b) King, W. A.; Scott, B. L.; Eckert, J.; Kubas, G. J. Reversible Displacement of Polyagostic Interactions in 16e $[\text{Mn}(\text{CO})(\text{R}_2\text{PC}_2\text{H}_4\text{PR}_2)_2]^+$ by H₂, N₂, and SO₂. Binding and Activation of $\eta^2\text{-H}_2$ trans to CO Is Nearly Invariant to Changes in Charge and cis Ligands, *Inorg. Chem.* **1999**, *38*, 1069-1084.
202. Hartwig, J.; Boebel, T., *Organotransition Metal Chemistry: From Bonding to Catalysis*. University Science Books: Sausalito, Cal., 2010.
203. Jetz, W.; Simons, P. B.; Thompson, J. A. J.; Graham, W. A. G. Organometallic Compounds with Metal-Metal Bonds. IV. Pentacarbonylmanganese and

Ph.D. Thesis — Jeffrey S. Price; McMaster University – Chemistry

- Pentacarbonylrhenium Derivatives of Silicon, Germanium, Tin, and Lead. Preparation and Infrared and Nuclear Magnetic Resonance Studies, *Inorg. Chem.* **1966**, *5*, 2217-2222.
204. Lebuis, A.-M.; Christendat, D.; Gilson, D. F. R.; Butler, I. S. Pentacarbonyl(triphenylsilyl)manganese(I), *Acta Crystallogr., Sect. C: Cryst. Struct. Commun.* **1997**, *C53*, 1206-1208.
205. Hamilton, R. S.; Corey, E. R. *Abstr. Inorg. Div. 156th Nat. Meeting Amer. Chem. Soc.*, Atlantic City, N.J., Sept., 1968, No. 025.
206. Graham, W. A. G.; Jetz, W. Silicon-Transition Metal Chemistry. I. Photochemical Preparation of Silyl(transition metal) Hydrides, *Inorg. Chem.* **1971**, *10*, 4-9.
207. Graham, W. A. G.; Hart-Davis, A. J. Silicon-Transition Metal Chemistry. VI. Kinetics and Mechanism of the Replacement of Triphenylsilane by Triphenylphosphine in Hydridotriphenylsilyl (π -cyclopentadienyl)dicarbonylmanganese, *J. Am. Chem. Soc.* **1971**, *93*, 4388-4393.
208. Schubert, U.; Ackermann, K.; Wörle, B. A Long Si-H Bond or a Short Si-H Nonbond? Neutron Diffraction Study of $(\eta^5\text{-CH}_3\text{C}_5\text{H}_4)(\text{CO})_2(\text{H})\text{MnSiF}(\text{C}_6\text{H}_5)_2$, *J. Am. Chem. Soc.* **1982**, *104*, 7378-7380.
209. Colomer, E.; Corriu, R. J. P.; Marzin, C.; Vioux, A. Study of the Insertion Products of Manganese in the Silicon-Hydrogen Bond. Nature of the Bond and Proton Exchange in the H-Mn-Si-H system, *Inorg. Chem.* **1982**, *21*, 368-373.
210. Holleman, A. F.; Wiberg, E., Chapter XXVIII: The Manganese Group, 1 Manganese [1]. In *Inorganic Chemistry*, 34 ed.; Academic Press: San Diego, 2001; pp 1405-1415.
211. Groom, C. R.; Bruno, I. J.; Lightfoot, M. P.; Ward, S. C. The Cambridge Structural Database, *Acta Cryst.* **2016**, *B72*, 171-179.
212. Berry, A. D.; MacDiarmid, A. G. Synthesis and Properties of Trimethylsilylmanganese Pentacarbonyl, *Inorg. Nucl. Chem. Lett.* **1969**, *5*, 601-605.
213. Nicholson, B. K.; Simpson, J. Polysilane derivatives of the transition metals. I. Synthesis of $(\text{Me}_3\text{Si})_3\text{SiMn}(\text{CO})_5$ and related compounds, *J. Organometal. Chem.* **1971**, *32*, C29-C30.

Ph.D. Thesis — Jeffrey S. Price; McMaster University – Chemistry

214. Couldwell, M. C.; Simpson, J. Crystal and Molecular Structure of Tetracarbonyl(trimethylsilyl)(tri-phenyl-phosphine)manganese(I), *J. Chem. Soc., Dalton Trans.* **1976**, 714-719.
215. Yang, X.; Wang, C. Dichotomy of Manganese Catalysis via Organometallic or Radical Mechanism: Stereodivergent Hydrosilylation of Alkynes, *Angew. Chem., Int. Ed.* **2018**, *57*, 923-928.
216. (a) Malisch, W.; Kuhn, M. Die modifizierte Alkalisalz-Eliminierungsmethode – ein genereller Weg zu Komplexen mit Silicium-Übergangsmetall-Struktureinheiten, *Chem. Ber.* **1974**, *107*, 979-995; Gladysz, J. A.; (b) Williams, G. M.; Tam, W.; Johnson, D. L.; Parker, D. W.; Selover, J. C. Synthesis of Metal Carbonyl Monoanions by Trialkylborohydride Cleavage of Metal Carbonyl Dimers: A Convenient One-Flask Preparation of Metal Alkyls, Metal Acyls, and Mixed-Metal Compounds, *Inorg. Chem.* **1979**, *18*, 553-558.
217. Hengge, E.; Pinter, E.; Eibl, M.; Uhlig, F. Undecamethylcyclohexasilane derivatives of Group IV elements and manganese, *Bull. Soc. Chim. Fr.* **1995**, *132*, 509-512.
218. Hoffmann, F.; Wagler, J.; Böhme, U.; Roewer, G. The molecular structures of $M(\text{CO})_5\text{Si}_6\text{Me}_{11} \cdot 0.5 n\text{-C}_5\text{H}_{12}$ ($M = \text{Mn, Re}$), *J. Organomet. Chem.* **2017**, *835*, 12-16.
219. Li, S.; Johnson, D. L.; Gladysz, J. A.; Servis, K. L. ^{29}Si NMR Spectra of Metal Carbonyl Silanes by the Selective Population Transfer Method, *J. Organomet. Chem.* **1979**, *166*, 317-321.
220. Nicholson, B. K.; Simpson, J.; Robinson, W. T. Polysilane Derivatives of the Transition Metals II. The Crystal and Molecular Structure of [Tris(trimethylsilyl)silyl]pentacarbonylmanganese, $(\text{Me}_3\text{Si})_3\text{SiMn}(\text{CO})_5$, *J. Organometal. Chem.* **1973**, *47*, 403-412.
221. Christendat, D.; Butler, I. S.; Gilson, D. F. R.; Morin, F. G. Solid-state nuclear magnetic resonance studies of triphenylsilyl-, triphenyltin-, and triphenyllead(pentacarbonyl)manganese(I) complexes, *Can. J. Chem.* **1999**, *77*, 1892-1898.

222. Heyn, R. H.; Tilley, T. D. Coordinatively and electronically unsaturated tris(trimethylsilyl)silyl complexes of manganese and iron, *Inorg. Chim. Acta* **2002**, *341*, 91-98.
223. Schubert, U.; Ackermann, K.; Kraft, G.; Wörle, B. Hydrido Silyl Complexes. IV. Structural Changes in Hydrido Silyl Complexes Due to Si–H Interaction; Comparison of the Structures of $(\pi\text{-CH}_3\text{C}_5\text{H}_4)(\text{CO})_2\text{Mn}(\text{H})\text{SiCl}_3$ and *trans*- $(\pi\text{-CH}_3\text{C}_5\text{H}_4)(\text{CO})_2\text{Mn}(\text{SiCl}_3)_2$, *Z. Naturforsch., B: Anorg. Chem., Org. Chem.* **1983**, *38B*, 1488-1492.
224. Schubert, U. η^2 Coordination of Si–H σ Bonds to Transition Metals, *Adv. Organomet. Chem.* **1990**, *30*, 151-187.
225. For general reviews of this field, see refs. 226-229 and Lin, Z. Structural and bonding characteristics in transition metal–silane complexes, *Chem. Soc. Rev.* **2002**, *31*, 239-245.
226. Crabtree, R. H. Transition Metal Complexation of σ Bonds, *Angew. Chem., Int. Ed. Engl.* **1993**, *32*, 789-805.
227. Corey, J. Y.; Braddock-Wilking, J. Reactions of Hydrosilanes with Transition-Metal Complexes: Formation of Stable Transition-Metal Silyl Compounds, *Chem. Rev.* **1999**, *99*, 175-292.
228. Corey, J. Y. Reactions of Hydrosilanes with Transition Metal Complexes and Characterization of the Products, *Chem. Rev.* **2011**, *111*, 863-1071.
229. Corey, J. Y. Reactions of Hydrosilanes with Transition Metal Complexes, *Chem. Rev.* **2016**, *116*, 11291-11435.
230. Selected early contributions to this field include ref. 208 and (a) Raba , H.; Saillard, J. Y.; Schubert, U. Interaction between a σ bond and a d^n ML_n fragment: an MO analysis of the MnSiH three-center interaction in $\text{CpMnL}_2\text{HSiR}_3$ complexes, *J. Organomet. Chem.* **1987**, *330*, 397-413; (b) Schubert, U.; Schwarz, M.; M ller, F. Silicon-Containing Carbene Complexes. 15. A Strong $\text{W}\cdots\text{H}\cdots\text{Si}$ Interaction in the 16-Electron Carbene Complex $(\text{CO})_4\text{WC}(\text{NMe}_2)\text{SiHMes}_2$, *Organometallics* **1994**, *13*, 1554-1555; (c) Schubert, U.; Gilges, H. Transition Metal Silyl Complexes. 53. Magnitude of

Ph.D. Thesis — Jeffrey S. Price; McMaster University – Chemistry

the Chelate Effect in the Oxidative Addition of Si–H Bonds, *Organometallics* **1996**, *15*, 2373-2375.

231. Hoyano, J.; Elder, M.; Graham, W. A. G. Hydrogen-Bridged Silicon-Rhenium Bonds. A Diphenylsilane Complex of Rhenium Carbonyl, *J. Am. Chem. Soc.* **1969**, *91*, 4568-4569.

232. Nikonov, G. I. New types of non-classical interligand interactions involving silicon based ligands, *J. Organomet. Chem.* **2001**, *635*, 24-36.

233. Nikonov, G. I. Recent Advances in Nonclassical Interligand Si···H Interactions, *Adv. Organomet. Chem.* **2005**, *53*, 217-309.

234. Lachaize, S.; Sabo-Etienne, S. σ -Silane Ruthenium Complexes: The Crucial Role of Secondary Interactions, *Eur. J. Inorg. Chem.* **2006**, 2115-2127.

235. Spencer, M. D.; Shelby, Q. D.; Girolami, G. S. Titanium-Catalyzed Dehydrocoupling of Silanes: Direct Conversion of Primary Monosilanes to Titanium(0) Oligosilane Complexes with Agostic α -Si–H···Ti Interactions, *J. Am. Chem. Soc.* **2007**, *129*, 1860-1861.

236. Nikonov, G. I.; Kuzmina, L. G.; Lemenovskii, D. A.; Kotov, V. V. Interligand Hypervalent Interaction in the Bis(silyl) Hydride Derivatives of Niobocene, *J. Am. Chem. Soc.* **1995**, *117*, 10133-10134.

237. Nikonov, G. I.; Kuzmina, L. G.; Vyboishchikov, S. F.; Lemenovskii, D. A.; Howard, J. A. K. Niobocene Silyl Hydride Complexes with Nonclassical Interligand Hypervalent Interactions, *Chem. - Eur. J.* **1999**, *5*, 2947-2964.

238. Spaltenstein, E.; Palma, P.; Kreutzer, K. A.; Willoughby, C. A.; Davis, W. M.; Buchwald, S. L. Preparation and X-ray Structure of $\text{Cp}_2\text{Ti}(\text{Ph}_2\text{SiH}_2)(\text{PMe}_3)$, *J. Am. Chem. Soc.* **1994**, *116*, 10308-10309.

239. Scherer, W.; Eickerling, G.; Tafipolsky, M.; McGrady, G. S.; Sirsch, P.; Chatterton, N. P. Elucidation of the bonding in $\text{Mn}(\eta^2\text{-SiH})$ complexes by charge density analysis and T_1 NMR measurements: asymmetric oxidative addition and anomeric effects at silicon, *Chem. Commun.* **2006**, 2986-2988.

240. Hauf, C.; Barquera-Lozada, J. E.; Meixner, P.; Eickerling, G.; Altmannshofer, S.; Stalke, D.; Zell, T.; Schmidt, D.; Radius, U.; Scherer, W. Remanent Si–H Interactions in Late Transition Metal Silane Complexes, *Z. Anorg. Allg. Chem.* **2013**, *639*, 1996-2004.
241. Meixner, P.; Batke, K.; Fischer, A.; Schmitz, D.; Eickerling, G.; Kalter, M.; Ruhland, K.; Eichele, K.; Barquera-Lozada, J. E.; Casati, N. P. M.; Montisci, F.; Macchi, P.; Scherer, W. $J(\text{Si,H})$ Coupling Constants of Activated Si–H Bonds, *J. Phys. Chem. A* **2017**, *121*, 7219-7235.
242. (a) Nikonov, G. I.; Mountford, P.; Ignatov, S. K.; Green, J. C.; Leech, M. A.; Kuzmina, L. G.; Razuvaev, A. G.; Rees, N. H.; Blake, A. J.; Howard, J. A. K.; Lemenovskii, D. A. Surprising diversity of non-classical silicon-hydrogen interactions in half-sandwich complexes of Nb and Ta: M–H \cdots Si–Cl interligand hypervalent interaction (IHI) versus stretched and unstretched β -Si–H \cdots M agostic bonding, *J. Chem. Soc., Dalton Trans.* **2001**, 2903-2915; (b) Dubberley, S. R.; Ignatov, S. K.; Rees, N. H.; Razuvaev, A. G.; Mountford, P.; Nikonov, G. I. Are $J(\text{Si–H})$ NMR Coupling Constants Really a Probe for the Existence of Nonclassical H–Si Interactions?, *J. Am. Chem. Soc.* **2003**, *125*, 642-643; (c) Nikonov, G. I.; Mountford, P.; Dubberley, S. R. Tantalizing Chemistry of the Half-Sandwich Silylhydride Complexes of Niobium: Identification of Likely Intermediates on the Way to Agostic Complexes, *Inorg. Chem.* **2003**, *42*, 258-260; (d) Dorogov, K. Y.; Yousufuddin, M.; Ho, N.-N.; Churakov, A. V.; Kuzmina, L. G.; Schultz, A. J.; Mason, S. A.; Howard, J. A. K.; Lemenovskii, D. A.; Bau, R.; Nikonov, G. I. Syntheses and Structures of Asymmetric Bis(silyl) Niobocene Hydrides, *Inorg. Chem.* **2007**, *46*, 147-160; (e) Gutsulyak, D. V.; Churakov, A. V.; Kuzmina, L. G.; Howard, J. A. K.; Nikonov, G. I. Steric and Electronic Effects in Half-Sandwich Ruthenium Silane σ -Complexes with Si–H and Si–Cl Interligand Interactions, *Organometallics* **2009**, *28*, 2655-2657; (f) Gutsulyak, D. V.; Vyboishchikov, S. F.; Nikonov, G. I. Cationic Silane σ -complexes of Ruthenium with Relevance to Catalysis, *J. Am. Chem. Soc.* **2010**, *132*, 5950-5951; (g) Khalimon, A. Y.; Ignatov, S. K.; Okhapkin, A. I.; Simionescu, R.; Kuzmina, L. G.; Howard, J. A. K.; Nikonov, G. I. Unusual Structure, Fluxionality, and Reaction Mechanism of Carbonyl Hydrosilylation by Silyl Hydride Complex

Ph.D. Thesis — Jeffrey S. Price; McMaster University – Chemistry

- [(ArN=)Mo(H)(SiH₂Ph)(PMe₃)₃], *Chem. - Eur. J.* **2013**, *19*, 8573-8590; (h) Khalimon, A. Y.; McLeod, N. A.; Ignatov, S. K.; Okhapkin, A. I.; Kuzmina, L. G.; Howard, J. A. K.; Nikonov, G. I. Multiple coupling of silanes with imido complexes of Mo, *Dalton Trans* **2014**, *43*, 8446-8453; (i) Mai, V. H.; Korobkov, I.; Nikonov, G. I. Half-Sandwich Silane σ -Complexes of Ruthenium Supported by NHC Carbene, *Organometallics* **2016**, *35*, 936-942.
243. Duckett, S. B.; Kuzmina, L. G.; Nikonov, G. I. Fine tuning of Si–H interligand hypervalent interactions (IHI) in half-sandwich silyl hydrido complexes of ruthenium, *Inorg. Chem. Commun.* **2000**, *3*, 126-128.
244. Osipov, A. L.; Gerdov, S. M.; Kuzmina, L. G.; Howard, J. A. K.; Nikonov, G. I. Syntheses and X-ray Diffraction Studies of Half-Sandwich Hydridosilyl Complexes of Ruthenium, *Organometallics* **2005**, *24*, 587-602.
245. Vyboishchikov, S. F.; Nikonov, G. I. Unique {H(SiR₃)₂}, (H₂SiR₃), H(HSiR₃), and (H₂)SiR₃ Ligand Sets Supported by the {Fe(Cp)(L)} Platform (L = CO, PR₃), *Chem. - Eur. J.* **2006**, *12*, 8518-8533.
246. Vyboishchikov, S. F.; Nikonov, G. I. Rhodium Silyl Hydrides in Oxidation State +5: Classical or Nonclassical?, *Organometallics* **2007**, *26*, 4160-4169.
247. Gutsulyak, D. V.; Kuzmina, L. G.; Howard, J. A. K.; Vyboishchikov, S. F.; Nikonov, G. I. Cp(PrⁱMeP)FeH₂SiR₃: Nonclassical Iron Silyl Dihydride, *J. Am. Chem. Soc.* **2008**, *130*, 3732-3733.
248. Mai, V. H.; Kuzmina, L. G.; Churakov, A. V.; Korobkov, I.; Howard, J. A. K.; Nikonov, G. I. NHC carbene supported half-sandwich hydridosilyl complexes of ruthenium: the impact of supporting ligands on Si···H interligand interactions, *Dalton Trans.* **2016**, *45*, 208-215.
249. Delpech, F.; Sabo-Etienne, S.; Donnadieu, B.; Chaudret, B. Stoichiometric and Catalytic Activation of Allyldimethylsilane. Synthesis of [RuH₂{ η^4 -HSiMe₂(CH=CHMe)}(PCy₃)₂], *Organometallics* **1998**, *17*, 4926-4928.
250. Atheaux, I.; Delpech, F.; Donnadieu, B.; Sabo-Etienne, S.; Chaudret, B.; Hussein, K.; Barthelat, J.-C.; Braun, T.; Duckett, S. B.; Perutz, R. N. Exchange Processes in

Ph.D. Thesis — Jeffrey S. Price; McMaster University – Chemistry

Complexes with Two Ruthenium (η^2 -Silane) Linkages: Role of the Secondary Interactions between Silicon and Hydrogen Atoms, *Organometallics* **2002**, *21*, 5347-5357.

251. Lachaize, S.; Sabo-Etienne, S.; Donnadiu, B.; Chaudret, B. Mechanistic studies on ethylene silylation with chlorosilanes catalyzed by ruthenium complexes, *Chem. Commun.* **2003**, 214-215.

252. (a) Montiel-Palma, V.; Piechaczyk, O.; Picot, A.; Auffrant, A.; Vendier, L.; Le Floch, P.; Sabo-Etienne, S. Bonding Mode of a Bifunctional P~Si-H Ligand in the Ruthenium Complex "Ru(PPh₂CH₂OSiMe₂H)₃", *Inorg. Chem.* **2008**, *47*, 8601-8603; (b) Montiel-Palma, V.; Muñoz-Hernández, M. A.; Cuevas-Chávez, C. A.; Vendier, L.; Grellier, M.; Sabo-Etienne, S. Phosphinodi(benzylsilane) PhP{(o-C₆H₄CH₂)SiMe₂H}₂: A Versatile "PSi₂H_x" Pincer-Type Ligand at Ruthenium, *Inorg. Chem.* **2013**, *52*, 9798-9806.

253. Grellier, M.; Ayed, T.; Barthelat, J.-C.; Albinati, A.; Mason, S.; Vendier, L.; Coppel, Y.; Sabo-Etienne, S. Versatile Coordination of 2-Pyridinetetramethyldisilazane at Ruthenium: Ru(II) vs Ru(IV) As Evidenced by NMR, X-ray, Neutron, and DFT Studies, *J. Am. Chem. Soc.* **2009**, *131*, 7633-7640.

254. (a) Smart, K. A.; Grellier, M.; Vendier, L.; Mason, S. A.; Capelli, S. C.; Albinati, A.; Sabo-Etienne, S. Step-by-Step Introduction of Silazane Moieties at Ruthenium: Different Extents of Ru-H-Si Bond Activation, *Inorg. Chem.* **2013**, *52*, 2654-2661; (b) Smart, K. A.; Grellier, M.; Coppel, Y.; Vendier, L.; Mason, S. A.; Capelli, S. C.; Albinati, A.; Montiel-Palma, V.; Muñoz-Hernández, M. A.; Sabo-Etienne, S. Nature of Si-H Interactions in a Series of Ruthenium Silazane Complexes Using Multinuclear Solid-State NMR and Neutron Diffraction, *Inorg. Chem.* **2014**, *53*, 1156-1165.

255. Scherer, W.; Meixner, P.; Barquera-Lozada, J. E.; Hauf, C.; Obenhuber, A.; Brück, A.; Wolstenholme, D. J.; Ruhland, K.; Leusser, D.; Stalke, D. A Unifying Bonding Concept for Metal Hydrosilane Complexes, *Angew. Chem., Int. Ed.* **2013**, *52*, 6092-6096.

Ph.D. Thesis — Jeffrey S. Price; McMaster University – Chemistry

256. Scherer, W.; Meixner, P.; Batke, K.; Barquera-Lozada, J. E.; Ruhland, K.; Fischer, A.; Eickerling, G.; Eichele, K. $J(\text{Si},\text{H})$ Coupling Constants in Nonclassical Transition-Metal Silane Complexes, *Angew. Chem., Int. Ed.* **2016**, *55*, 11673-11677.
257. Examples include ref. 258 and (a) Fan, M.-F.; Jia, G.; Lin, Z. Metal–Silane Interaction in the Novel Pseudooctahedral Silane Complex *cis*- $\text{Mo}(\text{CO})(\text{PH}_3)_4(\text{H}\cdots\text{SiH}_3)$ and Some Related Isomers: An *ab Initio* Study, *J. Am. Chem. Soc.* **1996**, *118*, 9915-9921; (b) Fan, M.-F.; Lin, Z. Peculiar Hydride–Silyl Interactions in Group 5 Bent Metallocene Complexes, Studied by *ab Initio* Calculations, *Organometallics* **1998**, *17*, 1092-1100; (c) Bader, R. F. W.; Matta, C. F.; Cortés-Guzmán, F. Where To Draw the Line in Defining a Molecular Structure, *Organometallics* **2004**, *23*, 6253-6263.
258. Lichtenberger, D. L. Electron Distribution, Bonding, and $J(\text{Si}-\text{H})$ NMR Coupling Constant in $(\eta^5\text{-C}_5\text{H}_5)(\text{CO})_2\text{MnHSiCl}_3$: The Molecular Orbital View, *Organometallics* **2003**, *22*, 1599-1602.
259. McGrady, G. S.; Sirsch, P.; Chatterton, N. P.; Ostermann, A.; Gatti, C.; Altmannshofer, S.; Herz, V.; Eickerling, G.; Scherer, W. Nature of the Bonding in Metal-Silane σ -Complexes, *Inorg. Chem.* **2009**, *48*, 1588-1598.
260. Ignatov, S. K.; Rees, N. H.; Tyrrell, B. R.; Dubberley, S. R.; Razuvaev, A. G.; Mountford, P.; Nikonov, G. I. Nonclassical Titanocene Silyl Hydrides, *Chem. - Eur. J.* **2004**, *10*, 4991-4999.
261. Alcaraz, G.; Sabo-Etienne, S. NMR: A good tool to ascertain σ -silane or σ -borane formulations?, *Coord. Chem. Rev.* **2008**, *252*, 2395-2409.
262. For pioneering early work using $J_{\text{Si},\text{H}}$ to analyze interligand Si–H interactions from magnitude alone see ref. 209.
263. Berger, S.; Braun, S., *200 and More NMR Experiments: A Practical Course*. Wiley-VCH: Weinheim, 2004.
264. (a) Schraml, J.; Bellama, J., ^{29}Si Nuclear Magnetic Resonance. In *Determination of Organic Structures by Physical Methods*, Nachod, F.; Zuckerman, J.; Randall, E., Eds. Academic Press: New York, 1976; Vol. 6, pp 203-270; (b) Harris, R. K.; Kennedy, J. D.; McFarlane, W., Group IV-Silicon, Germanium, Tin and Lead. In *NMR and the Periodic*

Table, Harris, R. K.; Mann, B. E., Eds. Academic Press: New York, USA, 1978; pp 309-377.

265. For a review of complexes with multiple nonclassical Si–H interactions involving a single Si atom, see Nikonov, G. I. Going Beyond σ Complexation: Nonclassical Interligand Interactions of Silyl Groups with Two and More Hydrides, *Angew. Chem., Int. Ed.* **2001**, *40*, 3353-3355.

266. For examples of computational reports on complexes with multiple nonclassical Si–H interactions involving a single Si, see (a) Lin, Z.; Hall, M. B. Hydride Locations and Bonding Studies in Some Silyl Polyhydride Rhenium Complexes, *Inorg. Chem.* **1991**, *30*, 2569-2572; (b) Ray, M.; Nakao, Y.; Sato, H.; Sakaki, S.; Watanabe, T.; Hashimoto, H.; Tobita, H. Experimental and Theoretical Study of a Tungsten Dihydride Silyl Complex: New Insight into Its Bonding Nature and Fluxional Behavior, *Organometallics* **2010**, *29*, 6267-6281.

267. Luo, X. L.; Crabtree, R. H. Homogeneous Catalysis of Silane Alcoholysis via Nucleophilic Attack by the Alcohol on an $\text{Ir}(\eta^2\text{-HSiR}_3)$ intermediate catalyzed by $[\text{IrH}_2\text{S}_2(\text{PPh}_3)_2]\text{SbF}_6$ (S = Solvent), *J. Am. Chem. Soc.* **1989**, *111*, 2527-2535.

268. (a) Luo, X. L.; Baudry, D.; Boydell, P.; Charpin, P.; Nierlich, M.; Ephritikhine, M.; Crabtree, R. H. Reaction of $\text{ReH}_7(\text{PPh}_3)_2$ with Silanes: Preparation and Characterization of the First Silyl Polyhydride Complexes, $\text{ReH}_6(\text{SiR}_3)(\text{PPh}_3)_2$ ($\text{SiR}_3 = \text{SiPh}_3, \text{SiEt}_3, \text{SiHEt}_2$), *Inorg. Chem.* **1990**, *29*, 1511-1517; (b) Luo, X. L.; Schulte, G. K.; Demou, P.; Crabtree, R. H. Unusual Stereochemical Rigidity in Seven-Coordination. Synthesis and Structural Characterization of $\text{ReH}_2(\text{EPh}_3)(\text{CO})(\text{PMe}_2\text{Ph})_3$ (E = Si, Sn), *Inorg. Chem.* **1990**, *29*, 4268-4273.

269. Jagirdar, B. R.; Palmer, R.; Klabunde, K. J.; Radonovich, L. J. Metal Hydride vs Side-on σ -Bonded Trichlorosilane Complexes of Arene–Chromium Derivatives: $(\eta^6\text{-arene})\text{Cr}(\text{CO})(\text{H})_2(\text{SiCl}_3)_2$, *Inorg. Chem.* **1995**, *34*, 278-283.

270. Hussein, K.; Marsden, C. J.; Barthelat, J.-C.; Rodriguez, V.; Conejero, S.; Sabo-Etienne, S.; Donnadieu, B.; Chaudret, B. X-Ray structure and theoretical studies of

Ph.D. Thesis — Jeffrey S. Price; McMaster University – Chemistry

$\text{RuH}_2(\eta^2\text{-H}_2)(\eta^2\text{-H-SiPh}_3)(\text{PCy}_3)_2$, a complex with two different η^2 -coordinated σ bonds, *Chem. Commun.* **1999**, 1315-1316.

271. Mautz, J.; Heinze, K.; Wadepohl, H.; Huttner, G. Reductive Activation of *tripod* Metal Compounds: Identification of Intermediates and Preparative Application, *Eur. J. Inorg. Chem.* **2008**, 1413-1422.

272. Lee, T. Y.; Dang, L.; Zhou, Z.; Yeung, C. H.; Lin, Z.; Lau, C. P. Nonclassical Ruthenium Silyl Dihydride Complexes $\text{TpRu}(\text{PPh}_3)(\eta^3\text{-HSiR}_3\text{H})$ [Tp = Hydridotris(pyrazolyl)borate]: Catalytic Hydrolytic Oxidation of Organosilanes to Silanols with $\text{TpRu}(\text{PPh}_3)(\eta^3\text{-HSiR}_3\text{H})$, *Eur. J. Inorg. Chem.* **2010**, 5675-5684.

273. Fasulo, M. E.; Calimano, E.; Buchanan, J. M.; Tilley, T. D. Multiple Si-H Bond Activations by ${}^t\text{Bu}_2\text{PCH}_2\text{CH}_2\text{P}{}^t\text{Bu}_2$ and ${}^t\text{Bu}_2\text{PCH}_2\text{P}{}^t\text{Bu}_2$ Di(phosphine) Complexes of Rhodium and Iridium, *Organometallics* **2013**, 32, 1016-1028.

274. Zuzek, A. A.; Parkin, G. Si-H and Si-C Bond Cleavage Reactions of Silane and Phenylsilanes with $\text{Mo}(\text{PMe}_3)_6$: Silyl, Hypervalent Silyl, Silane, and Disilane Complexes, *J. Am. Chem. Soc.* **2014**, 136, 8177-8180.

275. Liu, H.-J.; Landis, C.; Raynaud, C.; Eisenstein, O.; Tilley, T. D. Donor-Promoted 1,2-Hydrogen Migration from Silicon to a Saturated Ruthenium Center and Access to Silaoxiranyl and Silaiminyl Complexes, *J. Am. Chem. Soc.* **2015**, 137, 9186-9194.

276. (a) Lichtenberger, D. L.; Rai-Chaudhuri, A. Electronic Structure Factors of Si-H Bond Activation by Transition Metals. The Valence Photoelectron Spectrum of Silylmanganese Complex $(\eta^5\text{-C}_5\text{H}_5)\text{Mn}(\text{CO})_2\text{HSiCl}_3$, *J. Am. Chem. Soc.* **1989**, 111, 3583-3591; (b) Lichtenberger, D. L.; Rai-Chaudhuri, A. Electronic Structure Factors of Si-H Bond Activation by Transition Metals. Valence Photoelectron Spectra of $(\eta^5\text{-C}_5\text{H}_4\text{CH}_3)\text{Mn}(\text{CO})(\text{PMe}_3)\text{HSiCl}_3$ and $(\eta^5\text{-C}_5\text{H}_4\text{CH}_3)\text{Mn}(\text{CO})(\text{PMe}_3)\text{HSiHPh}_2$ (Me = CH₃, Ph = C₆H₅), *Inorg. Chem.* **1990**, 29, 975-981; (c) Lichtenberger, D. L.; Rai-Chaudhuri, A. Electronic Structure Control of Si-H Bond Activation by Transition Metals. 2. Valence Photoelectron Spectra of $(\eta^5\text{-C}_5\text{H}_4\text{CH}_3)\text{Mn}(\text{CO})_2\text{HSiPh}_3$, $(\eta^5\text{-C}_5\text{H}_4\text{CH}_3)\text{Mn}(\text{CO})_2\text{HSiHPh}_2$ and $(\eta^5\text{-C}_5\text{H}_4\text{CH}_3)\text{Mn}(\text{CO})_2\text{HSiFPh}_2$ (Ph = C₆H₅), *J. Am. Chem. Soc.* **1990**, 112, 2492-2497.

277. Lichtenberger, D. L.; Rai-Chaudhuri, A. Cyclopentadienyl Ring Methylation and its Effect on Si–H Bond Activation in $(\eta^5\text{-C}_5\text{H}_{5-n}(\text{CH}_3)_n)\text{Mn}(\text{CO})_2\text{HSiH}(\text{C}_6\text{H}_5)_2$ ($n = 0, 1, 5$) Complexes, *Organometallics* **1990**, *9*, 1686-1690.
278. (a) Paterson, M. J.; Chatterton, N. P.; McGrady, G. S. View from the bridge: a pseudo-Jahn-Teller approach to transition metal hydrosilane complexes, *New J. Chem.* **2004**, *28*, 1434-1436; (b) Jabłoński, M. Geometry- and QTAIM-Based Comparison of Intramolecular Charge-Inverted Hydrogen Bonds, $\text{M}\cdots(\text{H-Si})$ "Agostic Bond", and $\text{M}\cdots(\eta^2\text{-SiH}) \sigma$ Interactions, *J. Phys. Chem. A* **2015**, *119*, 11384-11396; (c) Jabłoński, M. Systematic studies of the influence of electronegative X (X = F and Cl) substituents on the structure of the Mn–H–Si unit and the strength of the $\text{Mn}\cdots(\eta^2\text{-SiH}) \sigma$ interaction in $\text{Cp}(\text{OC})_2\text{Mn}[\eta^2\text{-H}(\text{SiH}_{3-n}\text{X}_n)]$ ($n = 0-3$) complexes, *Comput. Theor. Chem.* **2016**, *1076*, 51-56; (d) Jabłoński, M. Conciliatory Inductive Model Explaining the Origin of Changes in the $\eta^2\text{-SiH}$ Bond Length Caused by Presence of Strongly Electronegative Atoms X (X = F, Cl) in $\text{Cp}(\text{OC})_2\text{Mn}[\eta^2\text{-H}(\text{SiH}_{3-n}\text{X}_n)]$ ($n = 0-3$) Complexes, *J. Phys. Chem. A* **2016**, *120*, 4211-4222.
279. Faltynek, R. A.; Wrighton, M. S. Photoinduced Substitution and Oxidative Addition Reactions of Pentacarbonylmanganese(–1) and Tetracarbonyl(triphenylphosphine)manganese(–1), *J. Am. Chem. Soc.* **1978**, *100*, 2701-2705.
280. Schubert, U.; Wörle, B.; Jandik, P. The $(\eta^5\text{-CH}_3\text{C}_5\text{H}_4)\text{Mn}(\text{CO})_2$ Moiety as Protecting Group in the Monohalogenation of Diphenylsilane, *Angew. Chem., Int. Ed. Engl.* **1981**, *20*, 695-696.
281. Braunschweig, H.; Ganter, B. Convenient synthesis of $\text{K}[(\text{C}_5\text{H}_4\text{Me})\text{MnH}(\text{CO})_2]$ and reactions with $\text{Cl}_2\text{B}[\text{N}(\text{SiMe}_3)_2]$ and $\text{B}_2\text{R}_2\text{Cl}_2$ ($R = \text{Me}_2\text{N}, \text{Me}_3\text{C}$), *J. Organomet. Chem.* **1997**, *545-546*, 163-167.
282. Swennenhuis, B. H. G.; Poland, R.; DeYonker, N. J.; Webster, C. E.; Darendbourg, D. J.; Bengali, A. A. Ligand Displacement from $\text{TpMn}(\text{CO})_2\text{L}$ Complexes: A Large Rate Enhancement in Comparison to the $\text{CpMn}(\text{CO})_2\text{L}$ Analogues, *Organometallics* **2011**, *30*, 3054-3063.

Ph.D. Thesis — Jeffrey S. Price; McMaster University – Chemistry

283. Colomer, E.; Corriu, R. J. P.; Vioux, A. Synthesis and Properties of Manganese Hydrides Having a Functional Silicon, *Inorg. Chem.* **1979**, *18*, 695-700.
284. Schubert, U.; Kraft, G.; Kalbas, C. Hydrido Silyl Complexes. Part III. Steric Effects of Phosphorus Ligands on the Preparation of Chiral Hydrido Silyl Complexes of Manganese, *Transition Met. Chem.* **1984**, *9*, 161-162.
285. (a) Colomer, E.; Corriu, R.; Vioux, A. Preparation and Reactivity of the Optically Active Silicon-Manganese Compound $(-)-[(\pi\text{-Methylcyclopentadienyl})\text{Mn}(\text{CO})_2(\text{H})\text{SiMePh}(\alpha\text{-naphthyl})]$, *J. Chem. Soc., Chem. Commun.* **1976**, 175-176; (b) Colomer, E.; Corriu, R.; Vioux, A. Preparation and Reactivity of the Optically Active Silicon-Manganese Compound $(-)-(\eta^5\text{-Methylcyclopentadienyl})\text{Mn}(\text{CO})_2(\text{H})\text{SiMePh}(1\text{-naphthyl})$, *J. Chem. Res. S (Synopses)* **1977**, 168-169.
286. Kraft, G.; Kalbas, C.; Schubert, U. Hydrido-silyl-komplexe VI. Elektronische und Sterische Einflüsse von Phosphin-liganden auf die Aktivierungsparameter der Reduktiven Eliminierung von Diphenylsilan aus $(\eta^5\text{-CH}_3\text{C}_5\text{H}_4)(\text{CO})(\text{PR}_3)\text{Mn}(\text{H})\text{SiHPh}_2$ -komplexen, *J. Organomet. Chem.* **1985**, *289*, 247-256.
287. Schubert, U.; Scholz, G.; Müller, J.; Ackermann, K.; Wörle, B.; Stansfield, R. F. D. Hydrido-silyl-komplexe VII. Strukturchemische und ^{29}Si -NMR-spektroskopische Untersuchungen an $\text{C}_5\text{R}'_5(\text{CO})(\text{L})\text{Mn}(\text{H})\text{SiR}_3$. Einfluss der Substituenten R und R' sowie des Liganden L auf die Mn,H,Si-Dreizentrenbindung, *J. Organomet. Chem.* **1986**, *306*, 303-326.
288. Hill, R. H.; Wrighton, M. S. Oxidative Addition of Trisubstituted Silanes to Photochemically Generated Coordinatively Unsaturated Species $(\eta^4\text{-C}_4\text{H}_4)\text{Fe}(\text{CO})_2$, $(\eta^5\text{-C}_5\text{H}_5)\text{Mn}(\text{CO})_2$, and $(\eta^6\text{-C}_6\text{H}_6)\text{Cr}(\text{CO})_2$ and Related Molecules, *Organometallics* **1987**, *6*, 632-638.
289. Schubert, U.; Bahr, K.; Müller, J. Übergangsmetall-silyl-komplexe XIX. Mn,H,Si-Dreizentrenbindung in Komplexen mit Phosphinoethylsilyl-chelatliganden, *J. Organomet. Chem.* **1987**, *327*, 357-363.

290. Young, K. M.; Wrighton, M. S. Temperature Dependence of the Oxidative Addition of Triethylsilane to Photochemically Generated $(\eta^5\text{-C}_5\text{Cl}_5)\text{Mn}(\text{CO})_2$, *Organometallics* **1989**, *8*, 1063-1066.
291. Sun, J.; Lu, R. S.; Bau, R.; Yang, G. K. Oxidative Addition of Silanes to Cyclopentadienylbis(phosphine)carbonylmanganese. Fluxional Behavior of Manganese Silyl Hydride Complexes, *Organometallics* **1994**, *13*, 1317-1325.
292. Palmer, B. J.; Hill, R. H. The Energetics of the Oxidative Addition of Trisubstituted Silanes to Photochemically Generated $(\eta^5\text{-C}_5\text{R}_5)\text{Mn}(\text{CO})_2$, *Can. J. Chem.* **1996**, *74*, 1959-1967.
293. Karch, R.; Schubert, U. Transition metal silyl complexes. Part 54. Hydrido disilanyl complexes $\text{L}_n\text{M}(\text{H})\text{SiR}_2\text{SiR}_2\text{H}$ ($\text{L}_n\text{M} = (\text{MeCp})(\text{CO})_2\text{Mn}$, $\text{Cp}(\text{CO})_2\text{Re}$, $(\text{CO})_3(\text{PPh}_3)\text{Fe}$), *Inorg. Chim. Acta* **1997**, *259*, 151-160.
294. Schubert, U.; Grubert, S. Transition Metal Silyl Complexes. Part 57. Photochemical Reaction of $(\pi\text{-MeC}_5\text{H}_4)\text{Mn}(\text{CO})_2\text{L}$ with $\text{HMe}_2\text{Si-X-SiMe}_2\text{H}$, *Monatsh. Chem.* **1998**, *129*, 437-443.
295. Komuro, T.; Okawara, S.; Furuyama, K.; Tobita, H. Silane(silyl) and Bis(silyl)hydrido Manganese Complexes with Different $\text{Mn}\cdots\text{H}\cdots\text{Si}$ Interaction: Observation of Gradual Si-H Bond Activation on the Metal Center, *Chem. Lett.* **2012**, *41*, 774-776.
296. Valyaev, D. A.; Wei, D.; Elangovan, S.; Cavailles, M.; Dorcet, V.; Sortais, J.-B.; Darcel, C.; Lugan, N. Half-Sandwich Manganese Complexes Bearing Cp Tethered *N*-Heterocyclic Carbene Ligands: Synthesis and Mechanistic Insights into the Catalytic Ketone Hydrosilylation, *Organometallics* **2016**, *35*, 4090-4098.
297. Carré, F.; Colomer, E.; Corriu, R. J. P.; Vioux, A. Stereochemistry of the Insertion of Manganese into Si-H and Ge-H Bonds. Complexes Containing a Two-Electron, Three-Center $\text{Mn}\cdots\text{H}\cdots\text{Si}$ (or Ge) Interaction, *Organometallics* **1984**, *3*, 1272-1278.
298. (a) Schlecht, S.; Hartwig, J. F. σ -Borane Complexes of Manganese and Rhenium, *J. Am. Chem. Soc.* **2000**, *122*, 9435-9443; (b) Al-Fawaz, A.; Aldridge, S.; Coombs, D. L.;

Dickinson, A. A.; Willock, D. J.; Ooi, L.-I.; Light, M. E.; Coles, S. J.; Hursthouse, M. B. Reactivity of the bis(pentafluorophenyl)boranes $\text{ClB}(\text{C}_6\text{F}_5)_2$ and $[\text{HB}(\text{C}_6\text{F}_5)_2]_n$ towards late transition metal reagents, *Dalton Trans.* **2004**, 4030-4037.

299. (a) Weidenbruch, M. Silylenes and disilenes: examples of low coordinated silicon compounds, *Coord. Chem. Rev.* **1994**, *130*, 275-300; (b) Gaspar, P.; West, R., Chapter 43: Silylenes. In *The Chemistry of Organic Silicon Compounds*, Rappoport, Z.; Apeloig, Y., Eds. John Wiley & Sons: Chichester, UK, 1998; Vol. 2, pp 2463-2568.

300. Brook, M., Silicon-Based Reactive Intermediates. In *Silicon in Organic, Organometallics, and Polymer Chemistry*, John Wiley & Sons: New York, 2000; pp 39-96.

301. (a) Haaf, M.; Schmedake, T. A.; West, R. Stable Silylenes, *Acc. Chem. Res.* **2000**, *33*, 704-714; Gehrhus, B.; Lappert, M. F. Chemistry of thermally stable bis(amino)silylenes, *J. Organomet. Chem.* **2001**, *617-618*, 209-223; (b) Hill, N. J.; West, R. Recent developments in the chemistry of stable silylenes, *J. Organomet. Chem.* **2004**, *689*, 4165-4183; (c) Mizuhata, Y.; Sasamori, T.; Tokitoh, N. Stable Heavier Carbene Analogs, *Chem. Rev.* **2009**, *109*, 3479-3511; (d) Iwamoto, T.; Ishida, S., Chapter 8: Stable Silylenes and Their Transition Metal Complexes. In *Organosilicon Compounds: Theory and Experiment (Synthesis)*, Lee, V. Y., Ed. Academic Press: London, 2017; Vol. 1, pp 361-532.

302. Ogino, H. Synthesis of Silylene and Silyl(silylene)metal Complexes, *Chem. Rec.* **2002**, *2*, 291-306.

303. Okazaki, M.; Tobita, H.; Ogino, H. Reactivity of silylene complexes, *Dalton Trans.* **2003**, 493-506.

304. Waterman, R.; Hayes, P. G.; Tilley, T. D. Synthetic Development and Chemical Reactivity of Transition-Metal Silylene Complexes, *Acc. Chem. Res.* **2007**, *40*, 712-719.

305. Yamamoto, K.; Okinoshima, H.; Kumada, M. Evidence for "silylenoid" species in disproportionation of pentamethyldisilane catalyzed by trans-dichlorobis(triethylphosphine)platinum, *J. Organometal. Chem.* **1971**, *27*, C31-C32.

Ph.D. Thesis — Jeffrey S. Price; McMaster University – Chemistry

306. Schmid, G.; Welz, E. Base-Stabilized Silyleneiron Complexes, *Angew. Chem. Int. Ed. Engl.* **1977**, *16*, 785-786.
307. Straus, D. A.; Tilley, T. D.; Rheingold, A. L.; Geib, S. J. Preparation, Characterization, and X-ray Crystal Structure of an Acetonitrile-Complexed Ruthenium Silylene, *J. Am. Chem. Soc.* **1987**, *109*, 5872-5873.
308. Zybill, C.; Müller, G. Synthesis and Structure of $[(OC)_4Fe=Si(OtBu)_2\cdot HMPT]$, a Donor-Stabilized Silanediyl (“Silylene”) Complex, *Angew. Chem. Int. Ed. Engl.* **1987**, *26*, 669-670.
309. Straus, D. A.; Grumbine, S. D.; Tilley, T. D. Base-Free Silylene Complexes $[(\eta^5-C_5Me_5)(PMe_3)_2Ru=Si(SR)_2]BPh_4$ (R = Et, *p*-MeC₆H₄), *J. Am. Chem. Soc.* **1990**, *112*, 7801-7802.
310. Grumbine, S. D.; Tilley, T. D.; Rheingold, A. L. Synthesis and Structure of a Transition-Metal-Substituted Silylene Complex, $(CO)_4OsSi(STol-p)[Ru(\eta^5-C_5Me_5)(PMe_3)_2]$, *J. Am. Chem. Soc.* **1993**, *115*, 358-360.
311. Grumbine, S.; Tilley, T. D., Synthesis and Characterization of Transition Metal Silylene and Silylyne Complexes. In *Progress in Organosilicon Chemistry*, Marciniak, B.; Chojnowski, J., Eds. Gordon and Breach: Amsterdam, 1995; pp 133-146.
312. (a) Nakatsuji, H.; Ushio, J.; Yonezawa, T. Does a Silylene-Metal Complex Exist?, *J. Organomet. Chem.* **1983**, *258*, C1-C4; (b) Cundari, T. R.; Gordon, M. S. Nature of the Transition Metal–Silicon Double Bond, *J. Phys. Chem.* **1992**, *96*, 631-636; (c) Márquez, A.; Fernández Sanz, J. Electronic Structure of the Transition-Metal–Carbene-like Complexes $(CO)_5Mo-M'H_2$ (M' = C, Si, Ge and Sn). A Theoretical Study Based on ab initio CASSCF Calculations, *J. Am. Chem. Soc.* **1992**, *114*, 2903-2909; Jacobsen, H.; (d) Ziegler, T. Trends in Structure and Bonding of Fischer Type Chromium Carbenes and Silylenes. A Density Functional Study, *Organometallics* **1995**, *14*, 224-230.
313. (a) Kasdan, A.; Herbst, E.; Lineberger, W. C. Laser photoelectron spectrometry of the negative ions of silicon and its hydrides, *J. Chem. Phys.* **1975**, *62*, 541-548; (b) Berkowitz, J.; Greene, J. P.; Cho, H.; Ruščić, B. Photoionization mass spectrometric

Ph.D. Thesis — Jeffrey S. Price; McMaster University – Chemistry

studies of silyldiyne, silylene, silyl, and silane (SiH_n ($n = 1-4$)), *J. Chem. Phys.* **1987**, *86*, 1235-1248.

314. Schmedake, T. A.; Haaf, M.; Paradise, B. J.; Millevolte, A. J.; Powell, D. R.; West, R. Electronic and steric properties of stable silylene ligands in metal(0) carbonyl complexes, *J. Organomet. Chem.* **2001**, *636*, 17-25.

315. Blom, B.; Stoelzel, M.; Driess, M. New Vistas in N-Heterocyclic Silylene (NHSi) Transition-Metal Coordination Chemistry: Syntheses, Structures and Reactivity towards Activation of Small Molecules, *Chem. - Eur. J.* **2013**, *19*, 40-62.

316. Álvarez-Rodríguez, L.; Cabeza, J. A.; García-Álvarez, P.; Polo, D. The transition-metal chemistry of amidinatosilylenes, -germylenes and -stannylenes, *Coord. Chem. Rev.* **2015**, *300*, 1-28.

317. (a) Azhakar, R.; Ghadwal, R. S.; Roesky, H. W.; Wolf, H.; Stalke, D. Stabilization of Low Valent Silicon Fluorides in the Coordination Sphere of Transition Metals, *J. Am. Chem. Soc.* **2012**, *134*, 2423-2428; (b) Meltzer, A.; Präsang, C.; Milsman, C.; Driess, M. The Striking Stabilization of $\text{Ni}^0(\eta^6\text{-Arene})$ Complexes by an Ylide-Like Silylene Ligand, *Angew. Chem., Int. Ed.* **2009**, *48*, 3170-3173; (c) Meltzer, A.; Inoue, S.; Präsang, C.; Driess, M. Steering S–H and N–H Bond Activation by a Stable N-Heterocyclic Silylene: Different Addition of H_2S , NH_3 , and Organoamines on a Silicon(II) Ligand versus Its $\text{Si(II)} \rightarrow \text{Ni(CO)}_3$ Complex, *J. Am. Chem. Soc.* **2010**, *132*, 3038-3046.

318. Thomas, C. M.; Peters, J. C. An $\eta^3\text{-H}_2\text{SiR}_2$ adduct of $[\{\text{PhB}(\text{CH}_2\text{P}i\text{Pr}_2)_3\}\text{Fe}^{\text{II}}\text{H}]$, *Angew. Chem., Int. Ed.* **2006**, *45*, 776-780.

319. (a) Ruddy, A. J.; Mitton, S. J.; McDonald, R.; Turculet, L. Hemilabile silyl pincer ligation: platinum group PSiN complexes and triple C-H activation to form a (PSiC)Ru carbene complex, *Chem. Commun.* **2012**, *48*, 1159-1161; Suh, H.-W.; (b) Schmeier, T. J.; Hazari, N.; Kemp, R. A.; Takase, M. K. Experimental and Computational Studies of the Reaction of Carbon Dioxide with Pincer-Supported Nickel and Palladium Hydrides, *Organometallics* **2012**, *31*, 8225-8236.

320. Zhang, J.; Foley, B. J.; Bhuvanesh, N.; Zhou, J.; Janzen, D. E.; Whited, M. T.; Ozerov, O. V. Synthesis and Reactivity of Pincer-Type Cobalt Silyl and Silylene Complexes, *Organometallics* **2018**, *37*, 3956-3962.
321. Herrmann, W. A. The methylene bridge, *Adv. Organomet. Chem.* **1982**, *20*, 159-263.
322. Ueno, K.; Asami, S.; Watanabe, N.; Ogino, H. Synthesis of Self-Stabilized and Donor-Free Silyl(silylene)tungsten Complexes, *Organometallics* **2002**, *21*, 1326-1328.
323. Grubine, S. D.; Tilley, T. D.; Arnold, F. P.; Rheingold, A. L. A Fischer-Type Silylene Complex of Platinum: [*trans*-(Cy₃P)₂(H)Pt=Si(SEt)₂]BPh₄, *J. Am. Chem. Soc.* **1993**, *115*, 7884-7885.
324. (a) Besora, M.; Maseras, F.; Lledós, A.; Eisenstein, O. Silyl, Hydrido-Silylene, or Other Bonding Modes: Some Unusual Structures of [(dhpe)Pt(SiHR₂)]⁺ (dhpe = H₂P-CH₂-CH₂-PH₂; R = H, Me, SiH₃, Cl, OMe, NMe₂) and [(dhpe)Pt(SiR₃)]⁺ (R = Me, Cl) from DFT Calculations, *Inorg. Chem.* **2002**, *41*, 7105-7112; (b) Besora, M.; Maseras, F.; Lledós, A.; Eisenstein, O. Silyl, Hydrido Silylene or Alternative Bonding Modes: The Many Possible Structures of [(C₅H₅)(PH₃)IrX]⁺ (X = SiHR₂ and SiR₃; R = H, CH₃, SiH₃, and Cl), *Organometallics* **2006**, *25*, 4748-4755.
325. Watanabe, T.; Hashimoto, H.; Tobita, H. Hydrido(hydrosilylene)tungsten Complexes with Strong Interactions between the Silylene and Hydrido Ligands, *Angew. Chem., Int. Ed.* **2004**, *43*, 218-221.
326. Mork, B. V.; Tilley, T. D.; Schultz, A. J.; Cowan, J. A. Silylene Hydride Complexes of Molybdenum with Silicon-Hydrogen Interactions: Neutron Structure of (η^5 -C₅Me₅)(Me₂PCH₂CH₂PMe₂)Mo(H)(SiEt₂), *J. Am. Chem. Soc.* **2004**, *126*, 10428-10440.
327. Watanabe, T.; Hashimoto, H.; Tobita, H. Hydrido(hydrosilylene)tungsten Complexes: Dynamic Behavior and Reactivity Toward Acetone, *Chem. - Asian J.* **2012**, *7*, 1408-1416.
328. Yoshimoto, T.; Hashimoto, H.; Hayakawa, N.; Matsuo, T.; Tobita, H. A Silylyne Tungsten Complex Having an Eind Group on Silicon: Its Dimer-Monomer Equilibrium

and Cycloaddition Reactions with Carbodiimide and Diaryl Ketones, *Organometallics* **2016**, *35*, 3444-3447.

329. Smith, P. W.; Tilley, T. D. Base-Free Iron Hydrosilylene Complexes via an α -Hydride Migration that Induces Spin Pairing, *J. Am. Chem. Soc.* **2018**, *140*, 3880-3883.

330. Fasulo, M. E.; Lipke, M. C.; Tilley, T. D. Structural and mechanistic investigation of a cationic hydrogen-substituted ruthenium silylene catalyst for alkene hydrosilation, *Chem. Sci.* **2013**, *4*, 3882-3887.

331. Lipke, M. C.; Neumeier, F.; Tilley, T. D. Interconversion of η^3 -H₂SiRR' σ -Complexes and 16-Electron Silylene Complexes via Reversible H-H or C-H Elimination, *J. Am. Chem. Soc.* **2014**, *136*, 6092-6102.

332. Liu, H.-J.; Raynaud, C.; Eisenstein, O.; Tilley, T. D. Cyclometalated N-Heterocyclic Carbene Complexes of Ruthenium for Access to Electron-Rich Silylene Complexes That Bind the Lewis Acids CuOTf and AgOTf, *J. Am. Chem. Soc.* **2014**, *136*, 11473-11482.

333. Iluc, V. M.; Hillhouse, G. L. Arrested 1,2-Hydrogen Migration from Silicon to Nickel upon Oxidation of a Three-Coordinate Ni(I) Silyl Complex, *J. Am. Chem. Soc.* **2010**, *132*, 11890-11892.

334. Simons, R. S.; Gallucci, J. C.; Tessier, C. A.; Youngs, W. J. Synthesis and characterization of the sterically hindered iridium(III)-silyl complex: (Et₃P)₃(H)₂Ir[Si(H)Cl(C₆H₃-Mes₂-2,6)] and the generation of the cationic iridium(III)-silylene complex: [(Et₃P)₃(H)₂Ir=Si(H)(C₆H₃-Mes₂-2,6)][B(C₆F₅)₄], *J. Organomet. Chem.* **2002**, *654*, 224-228.

335. Feldman, J. D.; Peters, J. C.; Tilley, T. D. Activations of Silanes with [PhB(CH₂PPh₂)₃]Ir(H)(η^3 -C₈H₁₃). Formation of Iridium Silylene Complexes via the Extrusion of Silylenes from Secondary Silanes R₂SiH₂, *Organometallics* **2002**, *21*, 4065-4075.

336. (a) Calimano, E.; Tilley, T. D. Alkene Hydrosilation by a Cationic Hydrogen-Substituted Iridium Silylene Complex, *J. Am. Chem. Soc.* **2008**, *130*, 9226-9227; (b) Calimano, E.; Tilley, T. D. Synthesis and Structure of PNP-Supported Iridium Silyl and

Silylene Complexes: Catalytic Hydrosilylation of Alkenes, *J. Am. Chem. Soc.* **2009**, *131*, 11161-11173.

337. Mork, B. V.; Tilley, T. D. Synthons for Coordinatively Unsaturated Complexes of Tungsten, and Their Use for the Synthesis of High Oxidation-State Silylene Complexes, *J. Am. Chem. Soc.* **2004**, *126*, 4375-4385.

338. Fukuda, T.; Hashimoto, H.; Sakaki, S.; Tobita, H. Stabilization of a Silaldehyde by its η^2 Coordination to Tungsten, *Angew. Chem., Int. Ed.* **2016**, *55*, 188-192.

339. Fukuda, T.; Yoshimoto, T.; Hashimoto, H.; Tobita, H. Synthesis of a Tungsten–Silylyne Complex via Stepwise Proton and Hydride Abstraction from a Hydrido Hydrosilylene Complex, *Organometallics* **2016**, *35*, 921-924.

340. Glaser, P. B.; Tilley, T. D. Catalytic Hydrosilylation of Alkenes by a Ruthenium Silylene Complex. Evidence for a New Hydrosilylation Mechanism, *J. Am. Chem. Soc.* **2003**, *125*, 13640-13641.

341. (a) Glaser, P. B.; Tilley, T. D. Synthesis and Reactivity of Silyl and Silylene Ligands in the Coordination Sphere of the 14-Electron Fragment $\text{Cp}^*(\text{iPr}_3\text{P})\text{Os}^+$, *Organometallics* **2004**, *23*, 5799-5812; (b) Hayes, P. G.; Waterman, R.; Glaser, P. B.; Tilley, T. D. Synthesis, Structure, and Reactivity of Neutral Hydrogen-Substituted Ruthenium Silylene and Germylene Complexes, *Organometallics* **2009**, *28*, 5082-5089; (c) Fasulo, M. E.; Glaser, P. B.; Tilley, T. D. $\text{Cp}^*(\text{PiPr}_3)\text{RuOTf}$: A Reagent for Access to Ruthenium Silylene Complexes, *Organometallics* **2011**, *30*, 5524-5531.

342. Hayes, P. G.; Beddie, C.; Hall, M. B.; Waterman, R.; Tilley, T. D. Hydrogen-Substituted Osmium Silylene Complexes: Effect of Charge Localization on Catalytic Hydrosilylation, *J. Am. Chem. Soc.* **2006**, *128*, 428-429.

343. Ochiai, M.; Hashimoto, H.; Tobita, H. Synthesis and Structure of a Hydrido(hydrosilylene)ruthenium Complex and Its Reactions with Nitriles, *Angew. Chem., Int. Ed.* **2007**, *46*, 8192-8194.

344. Boesveld, W. M.; Gehrhus, B.; Hitchcock, P. B.; Lappert, M. F.; Schleyer, P. v. R. A crystalline carbene-silylene adduct 1,2- $\text{C}_6\text{H}_4[\text{N}(\text{R})]_2\text{C}-\text{Si}[\text{N}(\text{R})]_2\text{C}_6\text{H}_4-1,2$ (R =

- CH₂Bu[†]); synthesis, structure and bonding in model compounds, *Chem. Commun.* **1999**, 755-756.
345. Ghadwal, R. S.; Roesky, H. W.; Merkel, S.; Henn, J.; Stalke, D. Lewis Base Stabilized Dichlorosilylene, *Angew. Chem., Int. Ed.* **2009**, *48*, 5683-5686.
346. Filippou, A. C.; Chernov, O.; Schnakenburg, G. SiBr₂(Idipp): A Stable N-Heterocyclic Carbene Adduct of Dibromosilylene, *Angew. Chem., Int. Ed.* **2009**, *48*, 5687-5690.
347. Li, J.; Merkel, S.; Henn, J.; Meindl, K.; Döring, A.; Roesky, H. W.; Ghadwal, R. S.; Stalke, D. Lewis-Base-Stabilized Dichlorosilylene: A Two-Electron σ -Donor Ligand, *Inorg. Chem.* **2010**, *49*, 775-777.
348. Tavčar, G.; Sen, S. S.; Azhakar, R.; Thorn, A.; Roesky, H. W. Facile Syntheses of Silylene Nickel Carbonyl Complexes from Lewis Base Stabilized Chlorosilylenes, *Inorg. Chem.* **2010**, *49*, 10199-10202.
349. Filippou, A. C.; Chernov, O.; Stumpf, K. W.; Schnakenburg, G. Metal–Silicon Triple Bonds: The Molybdenum Silylidyne Complex [Cp(CO)₂Mo≡Si-R], *Angew. Chem., Int. Ed.* **2010**, *49*, 3296-3300.
350. Ghadwal, R. S.; Azhakar, R.; Pröpper, K.; Holstein, J. J.; Dittrich, B.; Roesky, H. W. N-Heterocyclic Carbene Stabilized Dichlorosilylene Transition-Metal Complexes of V(I), Co(I), and Fe(0), *Inorg. Chem.* **2011**, *50*, 8502-8508.
351. Filippou, A. C.; Baars, B.; Chernov, O.; Lebedev, Y. N.; Schnakenburg, G. Silicon–Oxygen Double Bonds: A Stable Silanone with a Trigonal-Planar Coordinated Silicon Center, *Angew. Chem., Int. Ed.* **2014**, *53*, 565-570.
352. Ghadwal, R. S.; Rottschäfer, D.; Andrada, D. M.; Frenking, G.; Schürmann, C. J.; Stammler, H.-G. Normal-to-abnormal rearrangement of an N-heterocyclic carbene with a silylene transition metal complex, *Dalton Trans.* **2017**, *46*, 7791-7799.
353. Majumdar, M.; Omlor, I.; Yildiz, C. B.; Azizoglu, A.; Huch, V.; Scheschkewitz, D. Reductive Cleavage of Carbon Monoxide by a Disilenide, *Angew. Chem., Int. Ed.* **2015**, *54*, 8746-8750.

354. Al-Rafia, S. M. I.; Malcolm, A. C.; McDonald, R.; Ferguson, M. J.; Rivard, E. Efficient generation of stable adducts of Si(II) dihydride using a donor-acceptor approach, *Chem. Commun.* **2012**, *48*, 1308-1310.
355. Eisenhut, C.; Szilvási, T.; Dübek, G.; Breit, N. C.; Inoue, S. Systematic Study of N-Heterocyclic Carbene Coordinate Hydrosilylene Transition-Metal Complexes, *Inorg. Chem.* **2017**, *56*, 10061-10069.
356. Fukuda, T.; Hashimoto, H.; Tobita, H. Unexpected Formation of NHC-Stabilized Hydrosilylyne Complexes via Alkane Elimination from NHC-Stabilized Hydrido(alkylsilylene) Complexes, *J. Am. Chem. Soc.* **2015**, *137*, 10906-10909.
357. Lutters, D.; Severin, C.; Schmidtman, M.; Müller, T. Activation of 7-Silanorbornadienes by N-Heterocyclic Carbenes: A Selective Way to N-Heterocyclic-Carbene-Stabilized Silylenes, *J. Am. Chem. Soc.* **2016**, *138*, 6061-6067.
358. Hickox, H. P.; Wang, Y.; Xie, Y.; Wei, P.; Schaefer III, H. F.; Robinson, G. H. Push–Pull Stabilization of Parent Monochlorosilylenes, *J. Am. Chem. Soc.* **2016**, *138*, 9799-9802.
359. Zhang, H.; Ouyang, Z.; Liu, Y.; Zhang, Q.; Wang, L.; Deng, L. (Aminocarbene)(Divinyltetramethyldisiloxane)Iron(0) Compounds: A Class of Low-Coordinate Iron(0) Reagents, *Angew. Chem., Int. Ed.* **2014**, *53*, 8432-8436.
360. Schneider, H.; Schmidt, D.; Eichhöfer, A.; Radius, M.; Weigend, F.; Radius, U. Synthesis and Reactivity of NHC-Stabilized Iron(II)-Mesityl Complexes, *Eur. J. Inorg. Chem.* **2017**, *2017*, 2600-2616.
361. Maiti, A.; Mandal, D.; Omlor, I.; Dhara, D.; Klemmer, L.; Huch, V.; Zimmer, M.; Scheschkewitz, D.; Jana, A. Equilibrium Coordination of NHCs to Si(IV) Species and Donor Exchange in Donor-Acceptor Stabilized Si(II) and Ge(II) Compounds, *Inorg. Chem.* **2019**, *58*, 4071-4075.
362. Witzke, R. J.; Tilley, T. D. A two-coordinate Ni(I) silyl complex: CO₂ insertion and oxidatively-induced silyl migrations, *Chem. Commun.* **2019**, *55*, 6559-6562.
363. Cai, X.; Gehrhus, B.; Hitchcock, P. B.; Lappert, M. F. Reactions of the stable bis(amino)silylene Si[$\{N(CH_2tBu)\}_2C_6H_4-1,2$] with Group 3 or lanthanide metal organic

Ph.D. Thesis — Jeffrey S. Price; McMaster University – Chemistry

compounds. Crystal structures of $[\text{Ln}(\eta^5\text{-C}_5\text{H}_5)_3\text{Si}\{\text{N}(\text{CH}_2t\text{Bu})\}_2\text{C}_6\text{H}_4\text{-1,2}\}] \cdot \text{C}_7\text{H}_8$ (Ln = Y or Yb), *Can. J. Chem.* **2000**, *78*, 1484-1490.

364. Blom, B.; Driess, M.; Gallego, D.; Inoue, S. Facile Access to Silicon-Functionalized Bis-Silylene Titanium(II) Complexes, *Chem. - Eur. J.* **2012**, *18*, 13355-13360.

365. Lee, V. Y.; Aoki, S.; Yokoyama, T.; Horiguchi, S.; Sekiguchi, A.; Gornitzka, H.; Guo, J.-D.; Nagase, S. Toward a Silicon Version of Metathesis: From Schrock-Type Titanium Silylidenes to Silatitanacyclobutenes, *J. Am. Chem. Soc.* **2013**, *135*, 2987-2990.

366. Nakata, N.; Fujita, T.; Sekiguchi, A. A Stable Schrock-Type Hafnium–Silylene Complex, *J. Am. Chem. Soc.* **2006**, *128*, 16024-16025.

367. Dong, Z.; Reinhold, C. R. W.; Schmidtman, M.; Müller, T. A Stable Silylene with a σ^2 , π -Butadiene Ligand, *J. Am. Chem. Soc.* **2017**, *139*, 7117-7123.

368. Azhakar, R.; Ghadwal, R. S.; Roesky, H. W.; Hey, J.; Stalke, D. Facile Access to Transition-Metal–Carbonyl Complexes with an Amidinate-Stabilized Chlorosilylene Ligand, *Chem. - Asian J.* **2012**, *7*, 528-533.

369. Lalov, A. V.; Egorov, M. P.; Nefedov, O. M.; Cherkasov, V. K.; Ermolaev, N. L.; Piskunov, A. V. Generation of the first representatives of the Schrock complexes of heavy carbene analogs, *Russ. Chem. Bull.* **2005**, *54*, 807-810.

370. Shinohara, A.; McBee, J.; Waterman, R.; Tilley, T. D. Paramagnetic Vanadium Silyl Complexes: Synthesis, Structure, and Reactivity, *Organometallics* **2008**, *27*, 5717-5722.

371. Koshikawa, H.; Okazaki, M.; Matsumoto, S.-i.; Ueno, K.; Tobita, H.; Ogino, H. Synthesis and Structure of a Base-Stabilized Silyl(silylene)tantalum Complex, *Chem. Lett.* **2005**, *34*, 1412-1413.

372. (a) Azhakar, R.; Sarish, S. P.; Roesky, H. W.; Hey, J.; Stalke, D. Syntheses of Group 7 Metal Carbonyl Complexes with a Stable N-Heterocyclic Chlorosilylene, *Inorg. Chem.* **2011**, *50*, 5039-5043; (b) Azhakar, R.; Roesky, H. W.; Holstein, J. J.; Dittrich, B. The group 7 metal carbonyl complexes from a stable heteroleptic silylene $\text{PhC}(\text{N}t\text{Bu})_2\text{SiNPh}_2$, *Dalton Trans.* **2012**, *41*, 12096-12100.

373. Lee, K. E.; Arif, A. M.; Gladysz, J. A. Synthesis and Reactivity of Functionalized Dimethylsilyl Complexes of the Formula $(\eta^5\text{-C}_5\text{H}_5)\text{Re}(\text{NO})(\text{PPh}_3)(\text{SiMe}_2\text{X})$; New Base-Stabilized Silylene Complexes, Novel Lewis Acid Adducts, and Evidence for Base-Free Silylene Complexes, *Chem. Ber.* **1991**, *124*, 309-320.
374. (a) Tumanskii, B.; Pine, P.; Apeloig, Y.; Hill, N. J.; West, R. Radical Reactions of a Stable N-Heterocyclic Silylene: EPR Study and DFT Calculation, *J. Am. Chem. Soc.* **2004**, *126*, 7786-7787; (b) Sheberla, D.; Tumanskii, B.; Bravo-Zhivotovskii, D.; Molev, G.; Molev, V.; Lee, V. Y.; Takanashi, K.; Sekiguchi, A.; Apeloig, Y. Electronic Structure of Bis(silyl)carbon-, Bis(silyl)silicon-, and Bis(silyl)germanium-Centered Radicals $(\text{R}_3\text{Si})_2\text{XE}^\cdot$ (E = C, Si, Ge; X = H, $\text{Re}(\text{CO})_5$, F): EPR and DFT Studies, *Organometallics* **2010**, *29*, 5596-5606.
375. Simon, G. L.; Dahl, L. F. Structural Characterization of Di- μ -diphenylsilyl-bis(tetracarbonylmanganese), $\text{Mn}_2(\text{CO})_8(\mu\text{-Si}(\text{C}_6\text{H}_5)_2)_2$. Stereochemical Analysis of an Organosilyl-Bridged Dimer Containing a Metal–Metal Interaction, *J. Amer. Chem. Soc.* **1973**, *95*, 783-789.
376. Herrmann, W. A.; Weichmann, J.; Küsthardt, U.; Schäfer, A.; Hörlein, R.; Hecht, C.; Voss, E.; Serrano, R. Methylene Addition to Multiple Bonds Between Ligand-Free Main Group Elements and Transition Metals — A General Reaction, *Angew. Chem., Int. Ed. Engl.* **1983**, *22*, 1543-1557.
377. Herrmann, W. A.; Voss, E.; Guggolz, E.; Ziegler, M. L. Multiple bonds between Main Group elements and transition metals. XVI. Double oxidative addition of monosilane to the coordinatively unsaturated organometallic fragment $(\eta^5\text{-C}_5\text{Me}_5)\text{Mn}(\text{CO})_2$: preparation and molecular structure of μ -silylenebis[dicarbonyl(hydrido)(η^5 -pentamethylcyclopentadienyl)manganese], *J. Organomet. Chem.* **1985**, *284*, 47-57.
378. Corriu, R.; Lanneau, G.; Priou, C. Intramolecular Base Stabilization of Si=N and Si=P Compounds and Related Transition-Metal Silanediyl Complexes, *Angew. Chem., Int. Ed. Engl.* **1991**, *30*, 1130-1132.

379. Takeuchi, T.; Tobita, H.; Ogino, H. Synthesis and Structure of the First Donor-Stabilized Bis(silylene)manganese Complex, *Organometallics* **1991**, *10*, 835-836.
380. Zhou, Y.-P.; Mo, Z.; Luecke, M.-P.; Driess, M. Stereoselective Transfer Semi-Hydrogenation of Alkynes to *E*-Olefins with *N*-Heterocyclic Silylene–Manganese Catalysts, *Chem. - Eur. J.* **2018**, *24*, 4780-4784.
381. (a) Brook, M., Chapter 12.8: Hydrosilylation. In *Silicon in Organic, Organometallics, and Polymer Chemistry*, John Wiley & Sons: New York, 2000; pp 401-422; (b) Nakajima, Y.; Shimada, S. Hydrosilylation reaction of olefins: recent advances and perspectives, *RSC Adv.* **2015**, *5*, 20603-20616.
382. Roy, A. K. A Review of Recent Progress in Catalyzed Homogeneous Hydrosilation (Hydrosilylation), *Adv. Organomet. Chem.* **2008**, *55*, 1-59.
383. Marciniak, B.; Maciejewski, H.; Pietraszuk, C.; Pawluć, P., *Hydrosilylation: A Comprehensive Review on Recent Advances*. Springer: Netherlands, 2009; Vol. 1.
384. Troegel, D.; Stohrer, J. Recent advances and actual challenges in late transition metal catalyzed hydrosilylation of olefins from an industrial point of view, *Coord. Chem. Rev.* **2011**, *255*, 1440-1459.
385. Lipke, M. C.; Liberman-Martin, A. L.; Tilley, T. D. Electrophilic Activation of Silicon–Hydrogen Bonds in Catalytic Hydrosilations, *Angew. Chem., Int. Ed.* **2017**, *56*, 2260-2294.
386. Brunner, H. A New Hydrosilylation Mechanism–New preparative opportunities, *Angew. Chem., Int. Ed.* **2004**, *43*, 2749-2750.
387. Fasulo, M. E.; Tilley, T. D. Stoichiometric Reaction Chemistry of Cationic Ruthenium Silylene Complexes toward Polar and Nonpolar Organic Substrates, *Organometallics* **2012**, *31*, 5049-5057.
388. (a) Beddie, C.; Hall, M. B. A Theoretical Investigation of Ruthenium-Catalyzed Alkene Hydrosilation: Evidence To Support an Exciting New Mechanistic Proposal, *J. Am. Chem. Soc.* **2004**, *126*, 13564-13565; (b) Beddie, C.; Hall, M. B. Do B3LYP and CCSD(T) Predict Different Hydrosilylation Mechanisms? Influences of Theoretical

Ph.D. Thesis — Jeffrey S. Price; McMaster University – Chemistry

Methods and Basis Sets on Relative Energies in Ruthenium–Silylene-Catalyzed Ethylene Hydrosilylation, *J. Phys. Chem. A* **2006**, *110*, 1416-1425.

389. Klei, S. R.; Tilley, T. D.; Bergman, R. G. Stoichiometric and Catalytic Behavior of Cationic Silyl and Silylene Complexes, *Organometallics* **2002**, *21*, 4648-4661.

390. Lee, V. Y.; Gapurenko, O. A.; Minkin, V. I.; Horiguchi, S.; Sekiguchi, A. [2+2] Cycloaddition of the Schrock titanium silylidene and acetylene, *Russian Chemical Bulletin* **2016**, *65*, 1139-1141.

391. Stoelzel, M.; Präsang, C.; Inoue, S.; Enthaler, S.; Driess, M. Hydrosilylation of Alkynes by Ni(CO)₃-Stabilized Silicon(II) Hydride, *Angew. Chem., Int. Ed.* **2012**, *51*, 399-403.

392. Feldman, J. D.; Mitchell, G. P.; Nolte, J.-o.; Tilley, T. D. Synthesis and study of platinum silylene complexes of the type (R₃P)₂Pt=SiMes₂ (Mes = 2,4,6-trimethylphenyl), *Can. J. Chem.* **2003**, *81*, 1127-1136.

393. Atheaux, I.; Donnadiou, B.; Rodriguez, V.; Sabo-Etienne, S.; Chaudret, B.; Hussein, K.; Barthelat, J.-C. A Unique Coordination of SiH₄: Isolation, Characterization, and Theoretical Study of (PR₃)₂H₂Ru(SiH₄)RuH₂(PR₃)₂, *J. Am. Chem. Soc.* **2000**, *122*, 5664-5665.

394. Lipke, M. C.; Tilley, T. D. High Electrophilicity at Silicon in η^3 -Silane σ -Complexes: Lewis Base Adducts of a Silane Ligand, Featuring Octahedral Silicon and Three Ru–H–Si Interactions, *J. Am. Chem. Soc.* **2011**, *133*, 16374-16377.

395. Lipke, M. C.; Poradowski, M.-N.; Raynaud, C.; Eisenstein, O.; Tilley, T. D. Catalytic Olefin Hydrosilations Mediated by Ruthenium η^3 -H₂Si σ Complexes of Primary and Secondary Silanes, *ACS Catal.* **2018**, *8*, 11513-11523.

396. Mork, B. V.; Tilley, T. D. Multiple Bonding Between Silicon and Molybdenum: A Transition-Metal Complex with Considerable Silylyne Character, *Angew. Chem., Int. Ed.* **2003**, *42*, 357-360.

397. Hashimoto, H.; Tobita, H. Recent advances in the chemistry of transition metal-silicon/germanium triple-bonded complexes, *Coord. Chem. Rev.* **2018**, *355*, 362-379.

Ph.D. Thesis — Jeffrey S. Price; McMaster University – Chemistry

398. Grumbine, S. D.; Chadha, R. K.; Tilley, T. D. Transition Metal Complexes Containing Donor-Stabilized Silylyne Ligands. Reductive Dimerization to a Silylene Complex, *J. Am. Chem. Soc.* **1992**, *114*, 1518-1520.
399. Filippou, A. C.; Chernov, O.; Schnakenburg, G. Chromium–Silicon Multiple Bonds: The Chemistry of Terminal N-Heterocyclic Carbene-Stabilized Halosilylydyne Ligands, *Chem. - Eur. J.* **2011**, *17*, 13574-13583.
400. Gusel'nikov, L. E.; Flowers, M. C. Thermal decomposition of 1,1-dimethyl-1-silacyclobutane and some reactions of an unstable intermediate containing a silicon-carbon double bond, *Chem. Commun.* **1967**, 864-865.
401. Brook, A. G.; Harris, J. W.; Lennon, J.; El Sheikh, M. Relatively stable silaethylenes. Photolysis of acylpolysilanes, *J. Am. Chem. Soc.* **1979**, *101*, 83-95.
402. Brook, A. G.; Abdesaken, F.; Gutekunst, B.; Gutekunst, G.; Kallury, R. K. A solid silaethene: isolation and characterization, *J. Chem. Soc., Chem. Commun.* **1981**, 191-192.
403. Brook, A. G.; Nyburg, S. C.; Abdesaken, F.; Gutekunst, B.; Gutekunst, G.; Krishna, R.; Kallury, M. R.; Poon, Y. C.; Chang, Y. M.; Winnie, W. N. Stable solid silaethylenes, *J. Am. Chem. Soc.* **1982**, *104*, 5667-5672.
404. Baines, K. M. Brook silenes: inspiration for a generation, *Chem. Commun.* **2013**, *49*, 6366-6369.
405. Schmidt, M. W.; Truong, P. N.; Gordon, M. S. π -Bond Strengths in the Second and Third Periods, *J. Am. Chem. Soc.* **1987**, *109*, 5217-5227.
406. Walsh, R. The π -Bond Energy in Silicoolefins, *J. Organometal. Chem.* **1972**, *38*, 245-248; Gusel'nikov, L. E.; Nametkin, N. S.; Vdovin, V. M. Unstable Silicon Analogs of Unsaturated Compounds, *Acc. Chem. Res.* **1975**, *8*, 18-25.
407. Brook, A. G.; Brook, M. A. The Chemistry of Silenes, *Adv. Organomet. Chem.* **1996**, *39*, 71-158.
408. (a) Müller, T.; Ziche, W.; Auner, N. In *Silicon-carbon and silicon-nitrogen multiply bonded compounds* 1998 Wiley; pp 857-1062; (b) Baines, K. M.; Samuel, M. S. 4.4.2 Product Subclass 2: Silenes, *Sci. Synth.* **2002**, *4*, 125-134; (c) Lerner, H.-W. Silenes

Ph.D. Thesis — Jeffrey S. Price; McMaster University – Chemistry

- the silicon carbon double bond, *Recent Res. Dev. Org. Chem.* **2004**, *8*, 159-196; (d) Ottosson, H.; Steel, P. G. Silylenes, Silenes, and Disilenes: Novel Silicon-Based Reagents for Organic Synthesis?, *Chem. - Eur. J.* **2006**, *12*, 1576-1585; (e) Ottosson, H.; Rouf, A. M. Silenes (update 1, 2011), *Sci. Synth., Knowl. Updates* **2011**, 37-46; (f) Raabe, G.; Michl, J. Multiple Bonding to Silicon, *Chem. Rev.* **1985**, *85*, 419-509.
409. Pannell, K. H. Rearrangements of silylmethyl- and silylacetyl-iron complexes, *J. Organometal. Chem.* **1970**, *21*, P17-P18.
410. Lickiss, P. D. Transition Metal Complexes of Silylenes, Silenes, Disilenes, and Related Species, *Chem. Soc. Rev.* **1992**, *21*, 271-279; Ishida, S.; Iwamoto, T. Recent advances in η^2 -disilene and η^2 -disilyne mononuclear transition metal complexes and related compounds, *Coord. Chem. Rev.* **2016**, *314*, 34-63.
411. Bravo-Zhivotovskii, D.; Peleg-Vasserman, H.; Kosa, M.; Molev, G.; Botoshanskii, M.; Apeloig, Y. The Direct Synthesis of a Silene–Organometallic Complex, *Angew. Chem., Int. Ed.* **2004**, *43*, 745-748.
412. Sakaki, S.; Ieki, M. Ethylene, silene, and disilene coordinate bonds with platinum(0) and platinum(II). An ab initio MO/MP4 and SD-CI study, *Inorg. Chem.* **1991**, *30*, 4218-4224.
413. Campion, B. K.; Heyn, R. H.; Tilley, T. D. A Stable η^2 -Silene Complex of Iridium: $(\eta^5\text{-C}_5\text{Me}_5)(\text{PMe}_3)\text{Ir}(\eta^2\text{-CH}_2=\text{SiPh}_2)$, *J. Am. Chem. Soc.* **1990**, *112*, 4079-4081.
414. Klei, S. R.; Tilley, T. D.; Bergman, R. G. An Observable Silene/Silylene Rearrangement in a Cationic Iridium Complex, *Organometallics* **2001**, *20*, 3220-3222.
415. (a) Campion, B. K.; Heyn, R. H.; Tilley, T. D. Preparation, Isolation, and Characterization of Transition-Metal η^2 -Silene Complexes. X-ray Crystal Structure of $(\eta^5\text{-C}_5\text{Me}_5)[\text{P}(i\text{-Pr})_3]\text{Ru}(\text{H})(\eta^2\text{-CH}_2\text{SiPh}_2)$, *J. Am. Chem. Soc.* **1988**, *110*, 7558-7560; (b) Campion, B. K.; Heyn, R. H.; Tilley, T. D.; Rheingold, A. L. Synthesis and Study of the Ruthenium–Silene Complexes $(\eta^5\text{-C}_5\text{Me}_5)(\text{PR}_3)\text{RuH}(\eta^2\text{-CH}_2=\text{SiR}'_2)$ (R = $i\text{Pr}$, Cy; R' = Me, Ph), *J. Am. Chem. Soc.* **1993**, *115*, 5527-5537.

Ph.D. Thesis — Jeffrey S. Price; McMaster University – Chemistry

416. Dioumaev, V. K.; Carroll, P. J.; Berry, D. H. Tandem β -C–H Activation/Si–H Elimination Reactions: Stabilization of C–H Activation Products by β -Agostic Si–H Interactions, *Angew. Chem., Int. Ed.* **2003**, *42*, 3947-3949.
417. Koloski, T. S.; Carroll, P. J.; Berry, D. H. Structure and Reactivity of $\text{Cp}_2\text{W}(\eta^2\text{-Me}_2\text{Si=CH}_2)$, a Tungsten Silene Complex, *J. Am. Chem. Soc.* **1990**, *112*, 6405-6406.
418. Nakata, N.; Rodriguez, R.; Troadec, T.; Saffon-Merceron, N.; Sotiropoulos, J.-M.; Baccaredo, A.; Kato, T. A Stable Silene Substituted by Strong π -Donors at the Silicon Center, *Angew. Chem., Int. Ed.* **2013**, *52*, 10840-10844.
419. (a) Dioumaev, V. K.; Plössl, K.; Carroll, P. J.; Berry, D. H. Formation and Interconversion of Ruthenium–Silene and 16-Electron Ruthenium Silyl Complexes, *J. Am. Chem. Soc.* **1999**, *121*, 8391-8392; (b) Dioumaev, V. K.; Plössl, K.; Carroll, P. J.; Berry, D. H. Access to Unsaturated Ruthenium Complexes via Phosphine Complexation with Triphenylborane: Synthesis and Structure of a Zwitterionic Arene Complex, $(\eta^6\text{-Ph-BPh}_2\text{H})\text{Ru}(\text{PMe}_3)_2(\text{SiMe}_3)$, *Organometallics* **2000**, *19*, 3374-3378.
420. Lewis, C.; Wrighton, M. S. Low-Temperature Photochemistry of $(\eta^5\text{-C}_5\text{R}_5)\text{W}(\text{CO})_3\text{CH}_2\text{SiMe}_2\text{H}$: Loss of Carbon Monoxide Followed by β -Hydrogen Transfer, *J. Am. Chem. Soc.* **1983**, *105*, 7768-7770.
421. Randolph, C. L.; Wrighton, M. S. Low-Temperature Photochemistry of $(\eta^5\text{-C}_5\text{Me}_5)\text{Fe}(\text{CO})_2\text{CH}_2\text{SiHMe}_2$: Establishment of $(\eta^5\text{-C}_5\text{Me}_5)\text{Fe}(\text{CO})(\text{CH}_2\text{SiMe}_2)\text{H}$ as the Intermediate in the Rearrangement of $(\eta^5\text{-C}_5\text{Me}_5)\text{Fe}(\text{CO})_2\text{CH}_2\text{SiHMe}_2$ to $(\eta^5\text{-C}_5\text{Me}_5)\text{Fe}(\text{CO})_2\text{SiMe}_3$, *Organometallics* **1987**, *6*, 365-371.
422. "Characteristic Bond Lengths in Free Molecules" in CRC Handbook of Chemistry and Physics, 100th Edition (Internet Version 2019), Rumble, J. R. ed., CRC Press/Taylor & Francis, Boca Raton, Fl.
423. (a) Wiberg, N.; Wagner, G.; Müller, G. Isolation and Structure of a Stable Molecule Containing a Silicon-Carbon Double Bond, *Angew. Chem., Int. Ed. Engl.* **1985**, *24*, 229-230; (b) Wiberg, N.; Wagner, G.; Riede, J.; Müller, G. Structure of the Stable Silaethene $\text{Me}_2\text{Si=C}(\text{SiMe}_3)(\text{SiMe-}t\text{-Bu}_2)$, *Organometallics* **1987**, *6*, 32-35; (c) Apeloig, Y.; Bendikov, M.; Yuzefovich, M.; Nakash, M.; Bravo-Zhivotovskii, D.; Blaser, D.;

Ph.D. Thesis — Jeffrey S. Price; McMaster University – Chemistry

Boese, R. Novel Stable Silenes via a Sila-Peterson-type Reaction. Molecular Structure and Reactivity, *J. Am. Chem. Soc.* **1996**, *118*, 12228-12229.

424. "Van der Waals and Covalent Radii of the Elements" in CRC Handbook of Chemistry and Physics, 100th Edition (Internet Version 2019), Rumble, J. R. ed., CRC Press/Taylor & Francis, Boca Raton, Fl.

425. Breitmaier, E.; Voelter, W., *¹³C NMR Spectroscopy*. Verlag Chemie: New York, 1978.

426. Brookhart, M.; Green, M. L. H.; Wong, L. L. Carbon-hydrogen-transition metal bonds, *Prog. Inorg. Chem.* **1988**, *36*, 1-124.

427. Man, B. E.; Taylor, B. F., *¹³C NMR Data for Organometallic Compounds*. Academic Press: New York, 1981.

428. Berry, D. H.; Chey, J. H.; Zipin, H. S.; Carroll, P. J. Disilene Complexes of Molybdenum and Tungsten, *J. Am. Chem. Soc.* **1990**, *112*, 452-453.

429. (a) Jacobson, D. B.; Bakhtiar, R. Generation, Characterization, and Properties of Iron–Silylene and Iron–Silene Cationic Complexes in the Gas Phase, *J. Am. Chem. Soc.* **1993**, *115*, 10830-10844; (b) Bakhtiar, R.; Holznagel, C. M.; Jacobson, D. B. Generation and Characterization of Isomeric Iron–Silylene and Iron–Silene Cationic Complexes in the Gas Phase, *J. Am. Chem. Soc.* **1993**, *115*, 345-347; (c) Bärsch, S.; Böhme, T.; Schröder, D.; Schwarz, H. Theoretical and experimental studies on the activation of ethylsilane by bare Co⁺ cations, *Int. J. Mass Spectrom.* **2000**, *199*, 107-125.

430. (a) Mori, M.; Kuroda, S.; Dekura, F. Formation of Silazirconacyclopentene via Zirconium-Silene Complex and Alkyne, *J. Am. Chem. Soc.* **1999**, *121*, 5591-5592; (b) Kuroda, S.; Sato, Y.; Mori, M. Reaction of silazirconacyclopentene formed from zirconium–silene complex and alkyne with isocyanide, *J. Organomet. Chem.* **2000**, *611*, 304-307; (c) Kuroda, S.; Dekura, F.; Sato, Y.; Mori, M. Formation of Silazirconacyclopentenenes from Zirconium-Silene Complex and Alkynes and Their Reactivities, *J. Am. Chem. Soc.* **2001**, *123*, 4139-4146.

431. Montiel-Palma, V.; Muñoz-Hernández, M. A.; Ayed, T.; Barthelat, J.-C.; Grellier, M.; Vendier, L.; Sabo-Etienne, S. Agostic Si–H bond coordination assists C–H bond

activation at ruthenium in bis(phosphinobenzylsilane) complexes, *Chem. Commun.* **2007**, 3963-3965.

432. Kon, Y.; Sakamoto, K.; Kabuto, C.; Kira, M. A Cobalt Silacyclobutadiene Complex, *Organometallics* **2005**, *24*, 1407-1409.

433. (a) Freeman, W. P.; Tilley, T. D.; Rheingold, A. L. Stable Silacyclopentadienyl Complexes of Ruthenium: (η^5 -C₅Me₅)Ru[η^5 -Me₄C₄SiSi(SiMe₃)₃] and X-ray Structure of Its Protonated Form, *J. Am. Chem. Soc.* **1994**, *116*, 8428-8429; (b) Dysard, J. M.; Tilley, T. D. η^5 -Silolyl and η^5 -Germolyl Complexes of d⁰ Hafnium. Structural Characterization of an η^5 -Silolyl Complex, *J. Am. Chem. Soc.* **1998**, *120*, 8245-8246; (c) Dysard, J. M.; Tilley, T. D. Synthesis and Reactivity of η^5 -Silolyl, η^5 -Germolyl, and η^5 -Germole Dianion Complexes of Zirconium and Hafnium, *J. Am. Chem. Soc.* **2000**, *122*, 3097-3105; (d) Lee, V. Y.; Kato, R.; Sekiguchi, A.; Krapp, A.; Frenking, G. Heavy Ferrocene: A Sandwich Complex Containing Si and Ge Atoms, *J. Am. Chem. Soc.* **2007**, *129*, 10340-10341; (e) Yasuda, H.; Lee, V. Y.; Sekiguchi, A. η^5 -1,2,3-Trisilacyclopentadienyl - A Ligand for Transition Metal Complexes: Rhodium Half-Sandwich and Ruthenium Sandwich, *J. Am. Chem. Soc.* **2009**, *131*, 9902-9903; (f) Lee, V. Y.; Kato, R.; Sekiguchi, A. Heavy Metallocenes of the Group 8 Metals: Ferrocene and Ruthenocene Derivatives, *Bull. Chem. Soc. Jpn.* **2013**, *86*, 1466-1471.

434. (a) Dysard, J. M.; Tilley, T. D.; Woo, T. K. Silabenzene and Disilabenzene Complexes of Ruthenium, *Organometallics* **2001**, *20*, 1195-1203; (b) Shinohara, A.; Takeda, N.; Sasamori, T.; Matsumoto, T.; Tokitoh, N. Synthesis and Properties of η^6 -Silabenzene-M(CO)₃ Complexes (M = Cr, Mo), *Organometallics* **2005**, *24*, 6141-6146.

435. Yin, J.; Klosin, J.; Abboud, K. A.; Jones, W. M. Preparation and Properties of a Ruthenium Complex of a "1-Silaallene", *J. Am. Chem. Soc.* **1995**, *117*, 3298-3299.

436. (a) Sakaba, H.; Watanabe, S.; Kabuto, C.; Kabuto, K. Novel η^3 -1-Silaallyl Tungsten Complexes via Si-H Bond Activation of Hydrovinyllsilanes: Structure and Reactivity toward Methanol, *J. Am. Chem. Soc.* **2003**, *125*, 2842-2843; (b) Sakaba, H.; Tonosaki, H.; Isozaki, K.; Kwon, E. η^3 -Silaallyl/Alkenylsilyl Molybdenum Complex:

Synthesis, Structure, and Reactivity toward Primary Amines To Form Mo–N–Si Three-Membered Cyclic Complexes, *Organometallics* **2015**, *34*, 1029-1037.

437. (a) Ray, M.; Nakao, Y.; Sato, H.; Sakaki, S. Theoretical Study of Tungsten η^3 -Silaallyl/ η^3 -Vinylsilyl and Vinyl Silylene Complexes: Interesting Bonding Nature and Relative Stability, *Organometallics* **2007**, *26*, 4413-4423; (b) Ray, M.; Nakao, Y.; Sato, H.; Sakaba, H.; Sakaki, S. How to Stabilize η^3 -Silapropargyl/Alkynylsilyl Complex of $[\text{CpL}_2\text{M}]^+$ ($L = \text{CO}$, PMe_3 , or PF_3 and $\text{M} = \text{W}$ or Mo): Theoretical Prediction, *Organometallics* **2009**, *28*, 65-73.

438. (a) Ohff, A.; Kosse, P.; Baumann, W.; Tillack, A.; Kempe, R.; Görls, H.; Burlakov, V. V.; Rosenthal, U. Novel *trans*- η^2 -Alkyne Complexes of Titanocene with Strong Si–H–Ti Interactions. Synthesis, Spectral Characteristics, and X-ray Crystal Structure, *J. Am. Chem. Soc.* **1995**, *117*, 10399-10400; (b) Peulecke, N.; Ohff, A.; Kosse, P.; Tillack, A.; Spannenberg, A.; Kempe, R.; Baumann, W.; Burlakov, V. V.; Rosenthal, U. Si–H Activation in Titanocene and Zirconocene Complexes of Alkynylsilanes $\text{RC}\equiv\text{CSiMe}_2\text{H}$ ($\text{R} = t\text{Bu}$, Ph , SiMe_3 , SiMe_2H): A Model To Understand Catalytic Reactions of Hydrosilanes, *Chem. - Eur. J.* **1998**, *4*, 1852-1861.

439. Yabe-Yoshida, M.; Kabuto, C.; Kabuto, K.; Kwon, E.; Sakaba, H. η^3 -Silapropargyl/Alkynylsilyl Molybdenum Complexes: Synthesis, Structure, and Reactivity toward Methanol, *J. Am. Chem. Soc.* **2009**, *131*, 9138-9139.

440. Gunale, A.; Steiner, D.; Schweikart, D.; Pritzkow, H.; Berndt, A.; Siebert, W. Unusual Mono- and Dinuclear Cobalt and Platinum Complexes of Rearranged Boriranylideneborane and Diboretanylideneborane Ligands: Dicobalt- μ -diborylcarbene Complexes as Derivatives of Planar Methane, *Chem. - Eur. J.* **1998**, *4*, 44-52.

441. Tanabe, Y.; Mizuhata, Y.; Tokitoh, N. Novel silacyclohexadienyl chromium and iron complexes bearing a bulky substituent on the central silicon atom, *Pure Appl. Chem.* **2010**, *82*, 879-890.

442. Suzuki, E.; Komuro, T.; Kanno, Y.; Tobita, H. (η^3 - α -Silabenzyl)tungsten Complexes: An Isolable Intermediate for Interconversion between a Silylene Complex and a Silyl Complex through 1,2-Aryl Migration, *Organometallics* **2013**, *32*, 748-751.

443. Komuro, T.; Kanno, Y.; Tobita, H. Synthesis, Structure, and Reactions of a (η^3 - α -silylbenzyl)molybdenum Complex: A Synthetic Equivalent of a Coordinatively Unsaturated Silyl Complex, *Organometallics* **2013**, *32*, 2795-2803.
444. Sakaba, H.; Oike, H.; Kawai, M.; Takami, M.; Kabuto, C.; Ray, M.; Nakao, Y.; Sato, H.; Sakaki, S. Synthesis, Structure, and Bonding Nature of Ethynediyl-Bridged Bis(silylene) Dinuclear Complexes of Tungsten and Molybdenum, *Organometallics* **2011**, *30*, 4515-4531.
445. Lamač, M.; Spannenberg, A.; Jiao, H.; Hansen, S.; Baumann, W.; Arndt, P.; Rosenthal, U. Formation of a 1-Zircona-2,5-disilacyclopent-3-yne: Coordination of 1,4-Disilabutatriene to Zirconocene?, *Angew. Chem., Int. Ed.* **2010**, *49*, 2937-2940.
446. Mizuhata, Y.; Inamura, K.; Tokitoh, N. Coordination chemistry of 9-sila- and 9-germa-phenanthrenes – unique coordination modes in their metallene complexes, *Can. J. Chem.* **2014**, *92*, 441-446.
447. (a) Vidjayacoumar, B.; Emslie, D. J. H.; Clendenning, S. B.; Blackwell, J. M.; Britten, J. F.; Rheingold, A. Investigation of AlMe₃, BEt₃, and ZnEt₂ as Co-Reagents for Low-Temperature Copper Metal ALD/Pulsed-CVD, *Chem. Mater.* **2010**, *22*, 4844-4853; (b) Vidjayacoumar, B.; Ramalingam, V.; Emslie, D. J. H.; Blackwell, J.; Clendenning, S. Solution Reactivity Studies for Identification of Promising New ALD and Pulsed CVD Reaction Chemistries, *ECS Transactions* **2013**, *50*, 53-66.
448. (a) Lim, B. S.; Rahtu, A.; Gordon, R. G. Atomic layer deposition of transition metals, *Nat. Mater.* **2003**, *2*, 749-754; (b) Lim, B. S.; Rahtu, A.; Park, J.-S.; Gordon, R. G. Synthesis and Characterization of Volatile, Thermally Stable, Reactive Transition Metal Amidinates, *Inorg. Chem.* **2003**, *42*, 7951-7958.
449. Igumenov, I. K.; Semyannikov, P. P.; Trubin, S. V.; Morozova, N. B.; Gelfond, N. V.; Mischenko, A. V.; Norman, J. A. Approach to control deposition of ultra thin films from metal organic precursors: Ru deposition, *Surf. Coat. Technol.* **2007**, *201*, 9003-9008.
450. Dussarrat, C.; Gatineau, J. High Purity Iridium Thin Films Depositions Using the Inorganic IrF₆, *Proc. - Electrochem. Soc.* **2005**, *2005-05*, 354-359.

Ph.D. Thesis — Jeffrey S. Price; McMaster University – Chemistry

451. Utriainen, M.; Kroger-Laukkanen, M.; Johansson, L. S.; Niinisto, L. Studies of metallic thin film growth in an atomic layer epitaxy reactor using $M(\text{acac})_2$ ($M = \text{Ni}, \text{Cu}, \text{Pt}$) precursors, *Appl. Surf. Sci.* **2000**, *157*, 151-158.
452. (a) Senkevich, J. J.; Tang, F.; Rogers, D.; Drotar, J. T.; Jezewski, C.; Lanford, W. A.; Wang, G.-c.; Lu, T.-m. Substrate-independent palladium atomic layer deposition, *Chem. Vap. Deposition* **2003**, *9*, 258-264; (b) Ten Eyck, G. A.; Pimanpang, S.; Bakhru, H.; Lu, T.-M.; Wang, G.-C. Atomic layer deposition of Pd on an oxidized metal substrate, *Chem. Vap. Deposition* **2006**, *12*, 290-294.
453. (a) Maartensson, P.; Carlsson, J. O. Atomic layer epitaxy of copper on tantalum, *Chem. Vap. Deposition* **1997**, *3*, 45-50; (b) Li, Z.; Barry, S. T.; Gordon, R. G. Synthesis and Characterization of Copper(I) Amidinates as Precursors for Atomic Layer Deposition (ALD) of Copper Metal, *Inorg. Chem.* **2005**, *44*, 1728-1735; (c) Li, Z.; Rahtu, A.; Gordon, R. G. Atomic Layer Deposition of Ultrathin Copper Metal Films from a Liquid Copper(I) Amidinate Precursor, *J. Electrochem. Soc.* **2006**, *153*, C787-C794.
454. (a) Ozin, G. A.; McCaffrey, J. G. Synthesis of ligand-free transition-metal dihydrides in low-temperature matrixes: manganese dihydride, MnH_2 , *J. Am. Chem. Soc.* **1984**, *106*, 807-809; (b) Wang, X.; Andrews, L. Matrix Infrared Spectra and Density Functional Theory Calculations of Manganese and Rhenium Hydrides, *J. Phys. Chem. A* **2003**, *107*, 4081-4091.
455. Meier, R. M.; Hanusa, T. P., Structural organomanganese chemistry. John Wiley & Sons Ltd.: New York, 2011; pp 43-169.
456. Section 9: Molecular Structure and Spectroscopy-Atomic Radii of the Elements. In *CRC Handbook of Chemistry and Physics*, 95 ed. Taylor and Francis Group LLC2014-2015.
457. (a) Oberteuffer, J. A.; Ibers, J. A. Refinement of the atomic and thermal parameters of α -manganese from a single crystal, *Acta Crystallogr., Sect. B* **1970**, *26*, 1499-1504; (b) Preston, G. D. Crystal structure of β -manganese, *Philos. Mag. (1798-1977)* **1928**, *5*, 1207-1225; (c) Haglund, J.; Fernandez Guillermet, F.; Grimvall, G.;

Ph.D. Thesis — Jeffrey S. Price; McMaster University – Chemistry

Koring, M. Theory of bonding in transition-metal carbides and nitrides, *Phys. Rev. B.* **1993**, *48*, 11685-11691.

458. (a) Dunitz, J. D., *Perspectives in Structural Chemistry*. John Wiley and Sons: New York, 1968; Vol. II; (b) Hilderbrandt, R. L.; Wieser, J. D.; Montgomery, L. K. Conformations and Structures of Cyclodecane as Determined by Electron Diffraction and Molecular Mechanics Calculations, *J. Am. Chem. Soc.* **1973**, *95*, 8598.

459. Dumke, A. C.; Pape, T.; Kösters, J.; Feldmann, K.-O.; Schulte to Brinke, C.; Hahn, F. E. Metal-Template-Controlled Stabilization of β -Functionalized Isocyanides, *Organometallics* **2013**, *32*, 289-299.

460. Xu, Z.; Thompson, L. K.; Waldmann, O. *MAGMUN4.1*.

461. (a) Evans, D. F. The Determination of the Paramagnetic Susceptibility of Substances in Solution by Nuclear Magnetic Resonance, *J. Chem. Soc.* **1959**, 2003-2005; (b) Schubert, E. M. Utilizing the Evans Method with a Superconducting NMR Spectrometer in the Undergraduate Laboratory, *J. Chem. Educ.* **1992**, *69*, 62.

462. Nakagawa, Y.; Hori, T. Phase diagram of the manganese-zinc system, *Transactions of the Japan Institute of Metals* **1972**, *13*, 165-170.

463. (a) Zhu, Z.; Wright, R. J.; Olmstead, M. M.; Rivard, E.; Brynda, M.; Power, P. P. A Zinc–Zinc-Bonded Compound and its Derivatives Bridged by One or Two Hydrogen Atoms: a New Type of Zn–Zn Bonding, *Angew. Chem., Int. Ed.* **2006**, *45*, 5807-5810; (b) Zhu, Z.; Brynda, M.; Wright, R. J.; Fischer, R. C.; Merrill, W. A.; Rivard, E.; Wolf, R.; Fettinger, J. C.; Olmstead, M. M.; Power, P. P. Synthesis and Characterization of the Homologous M–M Bonded Series Ar⁺MMAr⁺ (M = Zn, Cd, or Hg; Ar⁺ = C₆H₃-2,6-(C₆H₃-2,6-Prⁱ)₂) and Related Arylmetal Halides and Hydride Species, *J. Am. Chem. Soc.* **2007**, *129*, 10847-10857.

464. Zhu, Z.; Fettinger, J. C.; Olmstead, M. M.; Power, P. P. Steric Enhancement of Group 12 Metal Hydride Stability and the Reaction of an Arylzinc Hydride with Tetramethylpiperidinyl Oxide (TEMPO), *Organometallics* **2009**, *28*, 2091-2095.

Ph.D. Thesis — Jeffrey S. Price; McMaster University – Chemistry

465. Greene, T. M.; Andrews, L.; Downs, A. J. The Reaction of Zinc, Cadmium, and Mercury Atoms with Methane: Infrared Spectra of the Matrix-Isolated Methylmetal Hydrides, *J. Am. Chem. Soc.* **1995**, *117*, 8180-8187.
466. Flory, M. A.; Apponi, A. J.; Zack, L. N.; Ziurys, L. M. Activation of Methane by Zinc: Gas-Phase Synthesis, Structure, and Bonding of HZnCH₃, *J. Am. Chem. Soc.* **2010**, *132*, 17186-17192.
467. Ashby, E. C.; Watkins, J. J. Zinc Dihydride, *Inorg. Synth.* **1977**, *17*, 6-9.
468. Lide, D., Structure of Free Molecules in the Gas Phase. In *CRC Handbook of Chemistry and Physics*, 98 ed.; Rumble, J. R., Ed. CRC Press 2018.
469. Jonas, K.; Häselhoff, C. C.; Goddard, R.; Krüger, C. Manganese(II) cyclopentadienide and (cyclopentadienyl)manganese(biphenyl) as starting materials for the synthesis of carbonyl free organomanganese complexes, *Inorg. Chim. Acta* **1992**, *198-200*, 533-541.
470. Doherty, N. M.; Bercaw, J. E. Kinetics and Mechanism of the Insertion of Olefins into Transition Metal–Hydride Bonds, *J. Am. Chem. Soc.* **1985**, *107*, 2670-2682.
471. Yasuda, H.; Yamamoto, H.; Arai, T.; Nakamura, A.; Chen, J.; Kai, Y.; Kasai, N. Facile Synthesis and Stereochemistry of Alkyne Complexes from Cp₂MH and Cp₂MCH₂CH₂R (M = Nb, Ta), *Organometallics* **1991**, *10*, 4058-4066.
472. van Asselt, A.; Trimmer, M. S.; Henling, L. M.; Bercaw, J. E. Dioxygen-Derived Peroxo-Alkyl Complexes of Permethyltantalocene. Structural Characterization of (h⁵-C₅Me₅)₂Ta(h²-O₂)(CH₂C₆H₅) and Acid-Catalyzed Rearrangement to Oxo-Alkoxide Derivatives, *J. Am. Chem. Soc.* **1988**, *110*, 8254-8255.
473. (a) Carmichael, A. J.; McCamley, A. Synthesis and Characterization of Cationic Bis(cyclopentadienyl)tungsten(IV) Complexes Containing Alkyl, Chloride and Hydride Ligands, *J. Chem. Soc., Dalton Trans.* **1995**, 3125-3129; (b) Chernega, A.; Cook, J.; Green, M. L. H.; Labella, L.; Simpson, S. J.; Souter, J.; Stephens, A. H. H. New *ansa*-2,2-bis(h-cyclopentadienyl)propane molybdenum and tungsten compounds and intramolecular hydrogen-deuterium exchange in methyl-hydride and ethyl-hydride derivatives, *J. Chem. Soc., Dalton Trans.* **1997**, 3225-3243.

Ph.D. Thesis — Jeffrey S. Price; McMaster University – Chemistry

474. Dudle, B.; Rajesh, K.; Blacque, O.; Berke, H. Rhenium in Homogeneous Catalysis: [ReBrH(NO)(labile ligand)(large-bite-angle diphosphine)] Complexes as Highly Active Catalysts in Olefin Hydrogenations, *J. Am. Chem. Soc.* **2011**, *133*, 8168-8178.
475. Bennett, M. A.; McMahon, I. J.; Pelling, S. The Protonation of Arene-Bis(ethylene) Complexes of Ruthenium and Osmium, *J. Organomet. Chem.* **1990**, *382*, 175-184.
476. (a) Brookhart, M.; Lincoln, D. M. Comparison of Migratory Aptitudes of Hydride and Alkyl Groups in β -Migratory Insertion Reactions of $\text{Cp}^*(\text{P}(\text{OMe})_3)\text{Rh}(\text{C}_2\text{H}_4)\text{R}^+$ (R = H, CH_2CH_3), *J. Am. Chem. Soc.* **1988**, *110*, 8719-8720; (b) Bianchini, C.; Meli, A.; Peruzzini, M.; Vizza, F.; Frediani, P.; Ramirez, J. A. Tripodal Polyphosphine Ligands in Homogeneous Catalysis. 1. Hydrogenation and Hydroformylation of Alkynes and Alkenes assisted by Organorhodium Complexes with $\text{Me}(\text{CH}_2\text{PPh}_2)_3$, *Organometallics* **1990**, *9*, 226-240.
477. (a) Padilla-Martínez, I. I.; Poveda, M. L.; Carmona, E.; Monge, M. A.; Ruiz-Valero, C. Synthesis and Reactivity of $[\text{Ir}(\text{C}_2\text{H}_4)_2\text{Tpm}^{\text{Me}_2}]\text{PF}_6$ (Tpm^{Me_2} = Tris(3,5-dimethylpyrazolyl)methane): Comparison with the Analogous Tp^{Me_2} Derivatives (Tp^{Me_2} = Hydrotris(3,5-dimethylpyrazolyl)borate), *Organometallics* **2002**, *21*, 93-104; (b) García-Camprubí, A.; Martín, M.; Sola, E. Addition of Water Across Si-Ir Bonds in Iridium Complexes with *k-P,P,Si* (biPSi) Pincer Ligands, *Inorg. Chem.* **2010**, *49*, 10649-10657.
478. Shultz, L. H.; Tempel, D. J.; Brookhart, M. Palladium(II) η -Agostic Alkyl Cations and Alkyl Ethylene Complexes: Investigation of Polymer Chain Isomerization Mechanisms, *J. Am. Chem. Soc.* **2001**, *123*, 11539-11555.
479. Shiotsuki, M.; White, P. S.; Brookhart, M.; Templeton, J. L. Mechanistic Studies of Platinum(II)-Catalyzed Ethylene Dimerization: Determination of Barriers to Migratory Insertion in Diimine Pt(II) Hydrido Ethylene and Ethyl Ethylene Intermediates, *J. Am. Chem. Soc.* **2007**, *129*, 4058-4067.

480. Green, M. L. H.; Wong, L. L. Is a 16-Electron, *s*-Ethyl Intermediate Necessary for Hydrogen Scrambling in Ethylene-Hydride Complexes?, *J. Chem. Soc., Chem. Commun.* **1988**, 677-679.
481. Faller, J. W.; Fontaine, P. P. Stereoselectivity in a Chiral Ruthenium Ethylene Hydride Complex: Evidence of an Agostic Intermediate, *Organometallics* **2007**, *26*, 1738-1743.
482. Findlater, M.; Cartwright-Sykes, A.; White, P. S.; Schauer, C. K.; Brookhart, M. Role of Coordination Geometry in Dictating the Barrier to Hydride Migration in d^6 Square-Pyramidal Iridium and Rhodium Pincer Complexes, *J. Am. Chem. Soc.* **2011**, *133*, 12274-12284.
483. (a) Tempel, D. J.; Brookhart, M. The Dynamics of the *b*-Agostic Isopropyl Complex $(\text{ArN}=\text{C}(\text{R})-\text{C}(\text{R})=\text{NAr})\text{Pd}(\text{CH}(\text{CH}_2\text{-}m\text{-H})(\text{CH}_3))^+\text{BAR}'_4^-$ ($\text{Ar} = 2,6\text{-C}_6\text{H}_3(i\text{-Pr})_2$): Evidence for In-Place Rotation versus Dissociation of the Agostic Methyl Group, *Organometallics* **1998**, *17*, 2290-2296; (b) McNally, J. P.; Cooper, N. J. Mechanism of the Conversion of Intermediate 16-Electron Tungstenocene Alkyls into Alkene Hydrides and Fluxionality within $[\text{W}(\text{h-C}_5\text{H}_5)_2(\text{CH}_2=\text{CHCH}_3)\text{H}][\text{PF}_6]$, *Organometallics* **1988**, *7*, 1704-1715; (c) Casey, C. P.; Yi, C. S. Acid-Catalyzed Isomerization and Deuterium Exchange of Rhenium Alkene Complexes Via In-Place Rotation of an Agostic Alkylrhenium Cation, *Organometallics* **1991**, *10*, 33-35; (d) Bercaw, J. E.; Burger, B. J.; Green, M. L. H.; Santarsiero, B. D.; Sella, A.; Trimmer, M. S.; Wong, L. L. A New Mechanism for Exchange Processes observed in the Compounds $[\text{M}(\text{h-C}_5\text{H}_5)_2(\text{exo-h-RCH}=\text{CH}_2)\text{H}]$, $\text{M} = \text{Nb}$ and Ta , *J. Chem. Soc., Chem. Commun.* **1989**, 734-736.
484. (a) Green, M. L. H.; Wong, L.-L. η -Benzenebis(trimethylphosphine)iron as a Precursor to $\text{Fe}(\eta\text{-C}_5\text{R}_5)(\text{PMe}_3)_2$ Derivatives, $\text{R} = \text{H, Me}$: the Equilibrium $[\text{Fe}](\text{PMe}_3)\text{Et} \rightleftharpoons [\text{Fe}](\eta\text{-C}_2\text{H}_4)\text{H} + \text{PMe}_3$, where $[\text{Fe}] = \text{Fe}(\eta\text{-C}_5\text{Me}_5)(\text{PMe}_3)$, *J. Chem. Soc., Chem. Commun.* **1984**, 1442-1443; (b) Green, M. L. H.; Wong, L.-L. η -Benzenebis(trimethylphosphine)iron as a Precursor to $[\text{Fe}(\eta\text{-C}_5\text{R}_5)(\text{PMe}_3)_2]$ ($\text{R} = \text{H}$ or Me) Derivatives: the Equilibrium $[\text{Fe}](\text{PMe}_3)\text{Et} \rightleftharpoons [\text{Fe}](\eta\text{-C}_2\text{H}_4)\text{H} + \text{PMe}_3$, where $[\text{Fe}] = \text{Fe}(\eta\text{-C}_5\text{Me}_5)(\text{PMe}_3)$, *J. Chem. Soc., Dalton Trans.* **1987**, 411-416.

485. (a) Bianchini, C.; Meli, A.; Peruzzini, M.; Frediani, P.; Bohanna, C.; Esteruelas, M. A.; Oro, L. A. Selective Hydrogenation of 1-Alkynes to Alkenes Catalyzed by an Iron(II) *cis*-Hydride η^2 -Dihydrogen Complex. A Case of Intramolecular Reaction between η^2 -H₂ and σ -Vinyl Ligands, *Organometallics* **1992**, *11*, 138-145; (b) Hills, A.; Hughes, D. L.; Jimenez-Tenorio, M.; Leigh, G. J.; Rowley, A. T. Bis[1,2-bis(dimethylphosphino)ethane]dihydrogenhydridoiron(II) Tetraphenylborate as a Model for the Function of Nitrogenases, *J. Chem. Soc., Dalton Trans.* **1993**, 3041-3049; (c) Gao, Y.; Holah, D. G.; Hughes, A. N.; Spivak, G. J.; Havighurst, M. D.; Magnuson, V. R. Some reaction chemistry of *trans*-[Fe(H)(η^2 -H₂)(η^2 -dppm)₂][BF₄]. The crystal and molecular structure of *trans*-[Fe(H)(CH₃CN)(η^2 -dppm)₂][BF₄], dppm = bis(diphenylphosphino)methane, *Polyhedron* **1998**, *17*, 3881-3888.
486. (a) Kempter, A.; Gemel, C.; Cadenbach, T.; Fischer, R. A. Nickel Olefin Complexes Supported by GaI(DDP), *Organometallics* **2007**, *26*, 4257-4264; (b) Goddard, R.; Krüger, C.; Pörschke, K. R.; Wilke, G. Elektronendichte-Verteilungen in Metallorganischen Verbindungen. Wechselnde Struktur-Und Bindungsverhältnisse in Dimeren Metallorganischen Nickel-Hydriden Mit Ionenpaar-Beziehungen zu den Hauptgruppen-Metallen Natrium und Lithium, *J. Organomet. Chem.* **1986**, *308*, 85-103; (c) Pörschke, K. R.; Kleimann, W.; Wilke, G.; Claus, K. H.; Krüger, C. Synthesis and Structure of [Na(tmeda)₂]⁺[HNi₂(C₂H₄)₄]⁻, *Angew. Chem., Int. Ed. Engl.* **1983**, *22*, 991-992.
487. Klein, H. F.; Hammer, R.; Gross, J.; Schubert, U. Olefin-Insertion into Cobalt(d⁸) Complexes - Structure of Ethylene(phenyl)tris(trimethylphosphane)cobalt, *Angew. Chem., Int. Ed. Engl.* **1980**, *19*, 809-810.
488. Wadepohl, H.; Kohl, U.; Bittner, M.; Köppel, H. Experimental and Theoretical Study of the Hydride Migration to Ethylene in an Electron-Rich Cobalt Complex, *Organometallics* **2005**, *24*, 2097-2105.
489. Thompson, M. E.; Baxter, S. M.; Bulls, A. R.; Burger, B. J.; Nolan, M. C.; Santarsiero, B. D.; Schaefer, W. P.; Bercaw, J. E. "s-Bond Metathesis" for C-H Bonds of Hydrocarbons and Sc-R (R = H, alkyl, aryl) Bonds of Permethylscandocene Derivatives.

Ph.D. Thesis — Jeffrey S. Price; McMaster University – Chemistry

Evidence for Noninvolvement of the p System in Electrophilic Activation of Aromatic and Vinylic C-H Bonds, *J. Am. Chem. Soc.* **1987**, *109*, 203-219.

490. (a) Luinstra, G. A.; ten Cate, L. C.; Heeres, H. J.; Pattiasina, J. W.; Meetsma, A.; Teuben, J. H. Synthesis and Reactivity of Tervalent Paramagnetic Titanium Compounds (h^5 -C₅Me₅)₂TiR: Molecular Structure of (h^5 -C₅Me₅)₂TiCH₂CMe₃, *Organometallics* **1991**, *10*, 3227-3237; (b) Dawoodi, Z.; Green, M. L. H.; Mtetwa, V. S. B.; Prout, K. Evidence for a Direct Bonding Interaction between Titanium and a b-C-H Moiety in a Titanium-Ethyl Compound; X-Ray Crystal-Structure of [Ti(Me₂PCH₂CH₂PMe₂)EtCl₃], *J. Chem. Soc., Chem. Commun.* **1982**, 802-803; (c) Haaland, A.; Scherer, W.; Ruud, K.; McGrady, G. S.; Downs, A. J.; Swang, O. On the Nature and Incidence of b-Agostic Interactions in Ethyl Derivatives of Early Transition Metals: Ethyltitanium Trichloride and Related Compounds, *J. Am. Chem. Soc.* **1998**, *120*, 3762-3772; (d) Lukens, W. W.; Smith III, M. R.; Andersen, R. A. A p-Donor Spectrochemical Series for X in (Me₅C₅)₂TiX, and b-Agostic Interactions in X=Et and N(Me)Ph, *J. Am. Chem. Soc.* **1996**, *118*, 1719-1728.

491. Scherer, W.; Priermeier, T.; Haaland, A.; Volden, H. V.; McGrady, G. S.; Downs, A. J.; Boese, R.; Bläser, D. Molecular Structures of EtTiCl₃ and EtTiCl₃(dmpe) (dmpe = Me₂PCH₂CH₂PMe₂): New Insights into b-Agostic Bonding, *Organometallics* **1998**, *17*, 4406-4412.

492. (a) Conroy-Lewis, F. M.; Mole, L.; Redhouse, A. D.; Litster, S. A.; Spencer, J. L. Synthesis of Coordinatively Unsaturated Diphosphine Nickel(II) and Palladium(II) b-Agostic Ethyl Cations: X-ray Crystal Structure of [Ni(Bu^tP(CH₂)₂PBu^t)(C₂H₅)] [BF₄], *J. Chem. Soc., Chem. Commun.* **1991**, 1601-1603; (b) Wiencko, H. L.; Kogut, E.; Warren, T. H. Neutral β-diketiminato nickel(II) monoalkyl complexes, *Inorg. Chim. Acta* **2003**, *345*, 199-208.

493. Kogut, E.; Zeller, A.; Warren, T. H.; Strassner, T. Structure and Dynamics of Neutral b-H Agostic Nickel Alkyls: A Combined Experimental and Theoretical Study, *J. Am. Chem. Soc.* **2004**, *126*, 11984-11994.

494. (a) Leatherman, M. D.; Svejda, S. A.; Johnson, L. K.; Brookhart, M. Mechanistic Studies of Nickel(II) Alkyl Agostic Cations and Alkyl Ethylene Complexes:

Ph.D. Thesis — Jeffrey S. Price; McMaster University – Chemistry

Investigations of Chain Propagation and Isomerization in (a-diimine)Ni(II)-Catalyzed Ethylene Polymerization, *J. Am. Chem. Soc.* **2003**, *125*, 3068-3081; (b) Xu, H. W.; White, P. B.; Hu, C. H.; Diao, T. N. Structure and Isotope Effects of the β -H Agostic (a-Diimine)Nickel Cation as a Polymerization Intermediate, *Angew. Chem., Int. Ed.* **2017**, *56*, 1535-1538.

495. Brookhart, M.; Lincoln, D. M.; Volpe Jr., A. F.; Schmidt, G. F. Ligand and Substituent Effects on the Dynamics and Structure of Agostic Complexes of the Type $C_5R_5(L)Co(CH_2CHR'-m-H)^+BF_4^-$ (L = P(OMe)₃, PMe₃; R = H, Me; R' = H, Me), *Organometallics* **1989**, *8*, 1212-1218.

496. Brookhart, M.; Lincoln, D. M.; Bennett, M. A.; Pelling, S. Dynamics of Agostic Complexes of the Type $[C_5R_5(C_2H_4)M(CH_2CH_2-m-H)]^+$. Energy Differences between and Ancillary Ligand Control of Agostic and Terminal Hydride Structures, *J. Am. Chem. Soc.* **1990**, *112*, 2691-2694.

497. (a) Braga, D.; Grepioni, F.; Biradha, K.; Desiraju, G. R. Agostic interactions in organometallic compounds. A Cambridge Structural Database study, *J. Chem. Soc., Dalton Trans.* **1996**, 3925-3930; (b) Brookhart, M.; Green, M. L. H.; Parkin, G. Agostic interactions in transition metal compounds, *Proc. Natl. Acad. Sci. U. S. A.* **2007**, *104*, 6908-6914.

498. Bittner, M.; Köppel, H. Quantum Dynamical Study of β -Hydrogen Transfer in Two Selected Late-Transition-Metal Complexes, *J. Phys. Chem. A* **2004**, *108*, 11116-11126.

499. (a) Xu, R.; Bittner, M.; Klatt, G.; Köppel, H. Influence of Ligands on the Dynamics of Hydrogen Elimination in Cationic Complexes of Co and Rh, *J. Phys. Chem. A* **2008**, *112*, 13139-13148; (b) Xu, R.; Klatt, G.; Wadepohl, H.; Köppel, H. Hydrogen Scrambling in $[(C_5R_5)(L)M(H)(C_2H_4)]^+$ (M = Co, Rh). Relation of Experimental Kinetic Data to the Barriers of the Elementary Reaction Steps, *Inorg. Chem.* **2010**, *49*, 3289-3296.

500. Morris, R. J.; Girolami, G. S. Thirteen-Electron Manganese(II) Tetraalkyls. Synthesis, Characterization, and X-ray Crystal Structures of $[Li(tmed)]_2[MnMe_4]$ and the

Ph.D. Thesis — Jeffrey S. Price; McMaster University – Chemistry

" β -Unstable" Species $[\text{Li}(\text{tmed})]_2[\text{MnEt}_4]$ and $[\text{Li}(\text{tmed})]_2[\text{Mn}(\text{CH}_2\text{CH}_2-t\text{-Bu})_4]$, *Organometallics* **1989**, *8*, 1478-1485.

501. Treichel, P. M. Transition Metal-Isocyanide Complexes, *Adv. Organomet. Chem.* **1973**, *11*, 21-86; Singleton, E.; Oosthuizen, H. E. Metal isocyanide complexes, *Adv. Organomet. Chem.* **1983**, *22*, 209-310.

502. (a) Motz, P. L.; Alexander, J. J.; Ho, D. M. Isocyanide Insertion Reactions of Manganese(I) Alkyl and Iminoacyl Complexes, *Organometallics* **1989**, *8*, 2589-2601; (b) Motz, P. L.; Williams, J. P.; Alexander, J. J.; Ho, D. M.; Ricci, J. S.; Miller Jr., W. T. Coupling of Iminoacyl Groups to Diazabutadienes on Manganese Carbonyl Complexes, *Organometallics* **1989**, *8*, 1523-1533; (c) Utz, T. L.; Leach, P. A.; Geib, S. J.; Cooper, N. J. Formation of the 1,4-Diazabutadien-2-yl Complex $[\text{Mn}(\text{CNPh}^*)_4\{\text{C}(=\text{NPh}^*)\text{C}(\text{CH}_3)=\text{N}(\text{Ph}^*)\}]$ through Methylation of a Manganese(-I) Isonitrite, *Organometallics* **1997**, *16*, 4109-4114; (d) Becker, T. M.; Alexander, J. J.; Bauer, J. A. K.; Nauss, J. L.; Wireko, F. C. CNR and CO Insertion Reactions of 2,6-Xylyl Isocyanide with *p*-Chlorobenzylpentacarbonylmanganese, *Organometallics* **1999**, *18*, 5594-5605.

503. Tobita, H.; Matsuda, A.; Hashimoto, H.; Ueno, K.; Ogino, H. Direct Evidence for Extremely Facile 1,2- and 1,3-Group Migrations in an FeSi_2 System, *Angew. Chem., Int. Ed.* **2004**, *43*, 221-224.

504. Mitchell, G. P.; Tilley, T. D. Reversible Cycloaddition of Isocyanates to Ruthenium Silylene Complexes, *J. Am. Chem. Soc.* **1997**, *119*, 11236-11243.

505. Ochiai, M.; Hashimoto, H.; Tobita, H. Reactions of a Neutral Silylene Ruthenium Complex with Heterocumulenes: C=O Hydrosilylation of Isocyanates vs C=S Bond Cleavage of Isothiocyanate, *Organometallics* **2012**, *31*, 527-530.

506. Calimano, E.; Tilley, T. D. Reactions of Cationic PNP-Supported Iridium Silylene Complexes with Polar Organic Substrates, *Organometallics* **2010**, *29*, 1680-1692.

507. Price, J. S.; Emslie, D. J. H.; Britten, J. F. Manganese Silylene Hydride Complexes: Synthesis and Reactivity with Ethylene to Afford Silene Hydride Complexes, *Angew. Chem., Int. Ed.* **2017**, *56*, 6223-6227.

Ph.D. Thesis — Jeffrey S. Price; McMaster University – Chemistry

508. Lide, D., Characteristic Bond Lengths in Free Molecules. In *CRC Handbook of Chemistry and Physics*, 98 ed.; Rumble, J. R., Ed. CRC Press 2018.
509. Mantina, M.; Valero, R.; Cramer, C.; Truhlar, D., Atomic Radii of the Elements. In *CRC Handbook of Chemistry and Physics*, 98 ed.; Rumble, J. R., Ed. CRC Press 2018.
510. Price, J. S.; Emslie, D. J. H.; Berno, B. Manganese Silyl Dihydride Complexes: A Spectroscopic, Crystallographic, and Computational Study of Nonclassical Silicate and Hydrosilane Hydride Isomers, *Organometallics* **2019**, *38*, 2347-2362.
511. Schmidt, D.; Berthel, J. H. J.; Pietsch, S.; Radius, U. C-N Bond Cleavage and Ring Expansion of N-Heterocyclic Carbenes using Hydrosilanes, *Angew. Chem., Int. Ed.* **2012**, *51*, 8881-8885.
512. Delpech, F.; Sabo-Etienne, S.; Daran, J.-C.; Chaudret, B.; Hussein, K.; Marsden, C. J.; Barthelat, J.-C. Ruthenium Complexes Containing Two Ru-(η^2 -Si-H) Bonds: Synthesis, Spectroscopic Properties, Structural Data, Theoretical Calculations, and Reactivity Studies, *J. Am. Chem. Soc.* **1999**, *121*, 6668-6682.
513. Sakaba, H.; Hirata, T.; Kabuto, C.; Kabuto, K. Synthesis, Structure, and Dynamic Behavior of Tungsten Dihydride Silyl Complexes Cp*(CO)₂W(H)₂(SiHPhR) (R = Ph, H, Cl), *Organometallics* **2006**, *25*, 5145-5150.
514. Murphy, L. J.; Ferguson, M. J.; McDonald, R.; Lumsden, M. D.; Turculet, L. Synthesis of Bis(phosphino)silyl Pincer-Supported Iron Hydrides for the Catalytic Hydrogenation of Alkenes, *Organometallics* **2018**, *37*, 4814-4826.
515. Zuzek, A. A.; Neary, M. C.; Parkin, G. σ -Silane, Disilanyl, and [W(μ -H)Si(μ -H)W] Bridging Silylene Complexes *via* the Reactions of W(PMe₃)₄(η^2 -CH₂PMe₂)H with Phenylsilanes, *J. Am. Chem. Soc.* **2014**, *136*, 17934-17937.
516. (a) Delpech, F.; Sabo-Etienne, S.; Chaudret, B.; Daran, J.-C. Synthesis and Characterization of Chelating Bis(silane) Complexes [RuH₂{(η^2 -HSiMe₂)₂X}(PCy₃)₂] (X = C₆H₄, O) Containing Two Ru-(η^2 -Si-H) Bonds, *J. Am. Chem. Soc.* **1997**, *119*, 3167-3168; (b) Ayed, T.; Barthelat, J.-C.; Tangour, B.; Pradère, C.; Donnadiou, B.; Grellier, M.; Sabo-Etienne, S. Structure and Bonding in a Disilazane Ruthenium Complex. Catalytic Selective Deuteration of Disilazane, *Organometallics* **2005**, *24*, 3824-3826.

Ph.D. Thesis — Jeffrey S. Price; McMaster University – Chemistry

517. Ng, S. M.; Lau, C. P.; Fan, M.-F.; Lin, Z. Experimental and Theoretical Studies of Highly Fluxional $\text{TpRu}(\text{PPh}_3)_2\text{H}_2\text{SiR}_3$ Complexes (Tp = Hydridotris(pyrazolyl)borate), *Organometallics* **1999**, *18*, 2484-2490.
518. (a) Esteruelas, M. A.; Oro, L. A.; Valero, C. Hydrosilylation of Phenylacetylene via an $\text{Os}(\text{SiEt}_3)(\eta^2\text{-H}_2)$ Intermediate Catalyzed by $\text{OsHCl}(\text{CO})(\text{P}^i\text{Pr}_3)_2$, *Organometallics* **1991**, *10*, 462-466; (b) Lachaize, S.; Caballero, A.; Vendier, L.; Sabo-Etienne, S. Activation of Chlorosilanes at Ruthenium: A Route to Silyl σ -Dihydrogen Complexes, *Organometallics* **2007**, *26*, 3713-3721.
519. Luo, Y.-R., Bond Dissociation Energies. In *CRC Handbook of Chemistry and Physics*, 90 ed.; Lide, D., Ed. CRC Press 2010.
520. Keeler, J., *Understanding NMR Spectroscopy*. John Wiley & Sons: Chichester, 2010.
521. Kanno, Y.; Komuro, T.; Tobita, H. Direct Conversion of a Si–C(aryl) Bond to Si–Heteroatom Bonds in the Reactions of η^3 - α -Silabenzyl Molybdenum and Tungsten Complexes with 2-Substituted Pyridines, *Organometallics* **2015**, *34*, 3699-3705.
522. Okazaki, M.; Iwata, M.; Tobita, H.; Ogino, H. Reactions of $\text{M}[(\eta^5\text{-C}_5\text{Me}_5)\text{Fe}(\text{CO})_2]$ with $\text{ClSiMe}_2\text{NR}_2$ in THF, Et_2O and toluene (M = Li and K; R = Me, Et, i Pr and Ph), *Dalton Trans.* **2003**, 1114-1120.
523. "Characteristic Bond Lengths in Free Molecules" in *CRC Handbook of Chemistry and Physics*, 99th Edition (Internet Version 2018), Rumble, J. R. ed., CRC Press/Taylor & Francis, Boca Raton, Fl.
524. M. Kaftory, M. Kapon and M. Botoshansky, in *The Chemistry of Organic Silicon Compounds*, ed. Z. Rapport and Y. Apeloig, Wiley, New York, 1998, vol. 2, ch. 5.
525. (a) Kwok, W.-H.; Lu, G.-L.; Rickard, C. E. F.; Roper, W. R.; Wright, L. J. Tethered silyl complexes from nucleophilic substitution reactions at the Si–Cl bond of the chloro(diphenyl)silyl ligand in $\text{Ru}(\text{SiClPh}_2)(\kappa^2\text{-S}_2\text{CNMe}_2)(\text{CO})(\text{PPh}_3)_2$, *J. Organomet. Chem.* **2004**, *689*, 2979-2987; (b) Sato, T.; Okazaki, M.; Tobita, H.; Ogino, H. Synthesis, structure, and reactivity of novel iron(II) complexes with a five-membered chelate ligand $\kappa^2(\text{Si},\text{N})\text{-SiMe}_2\text{O}(2\text{-C}_5\text{H}_4\text{N})$, *J. Organomet. Chem.* **2003**, *669*, 189-199.

526. (a) Burger, C.; Kreuzer, F. H., Polysiloxanes and Polymers Containing Siloxane Groups. In *Silicon in Polymer Synthesis*, Kricheldorf, H. R., Ed. Springer: Berlin, 1996; pp 113-222; (b) Brook, M., Silicones. In *Silicon in Organic, Organometallic, and Polymer Chemistry*, John Wiley & Sons: New York, 2000; pp 256-308; (c) Brook, M., NMR Characterization of Silicon-Containing Species. In *Silicon in Organic, Organometallic, and Polymer Chemistry*, John Wiley & Sons: New York, 2000; pp 13-23.
527. Bertini, F.; Glatz, M.; Stöger, B.; Peruzzini, M.; Veiros, L. F.; Kirchner, K.; Gonsalvi, L. Carbon Dioxide Reduction to Methanol Catalyzed by Mn(I) PNP Pincer Complexes under Mild Reaction Conditions, *ACS Catal.* **2019**, *9*, 632-639.
528. Xie, H.; Lin, Z. Understanding the Reactivity Difference of Isocyanate and Isothiocyanate toward a Ruthenium Silylene Hydride Complex, *Organometallics* **2014**, *33*, 892-897.
529. Whited, M. T.; Zhang, J.; Ma, S.; Nguyen, B. D.; Janzen, D. E. Silylene-assisted hydride transfer to CO₂ and CS₂ at a [P₂Si]Ru pincer-type complex, *Dalton Trans.* **2017**, *46*, 14757-14761.
530. Zhang, X.-H.; Chung, L. W.; Lin, Z.; Wu, Y.-D. A DFT Study on the Mechanism of Hydrosilylation of Unsaturated Compounds with Neutral Hydrido(hydrosilylene)tungsten Complex, *J. Org. Chem.* **2008**, *73*, 820-829.
531. Sgro, M. J.; Piers, W. E. Synthesis, characterization and reactivity of yttrium and gadolinium silyl complexes, *Inorg. Chim. Acta* **2014**, *422*, 243-250.
532. Hayasaka, K.; Fukumoto, K.; Nakazawa, H. Dehydrogenative desulfurization of thiourea derivatives to give carbodiimides, using hydrosilane and an iron complex, *Dalton Trans.* **2013**, *42*, 10271-10276.
533. (a) Ochiai, M.; Hashimoto, H.; Tobita, H. Reactions of a hydrido(hydrosilylene)ruthenium complex with carbonyl compounds, *Dalton Trans.* **2009**, 1812-1814; Computational support for this proposal was subsequently provided by the Xie group; (b) Kuang, J.; Li, Y.; Wang, L.; Wu, Z.; Lei, Q.; Fang, W.; Xie, H. A substrate-dependent mechanism for the reactions of a hydrido(hydrosilylene)ruthenium

complex with carbonyl compounds: insights from quantum chemical calculations, *New J. Chem.* **2017**, *41*, 198-203.

534. (a) Goikhman, R.; Aizenberg, M.; Shimon, L. J. W.; Milstein, D. Transition Metal-Catalyzed Silanone Generation, *J. Am. Chem. Soc.* **1996**, *118*, 10894-10895; (b) Glaser, P. B.; Wanandi, P. W.; Tilley, T. D. Synthesis, Structure, and Reactivity of Osmium Silyl and Silylene Complexes $\text{Cp}^*(\text{Me}_3\text{P})_2\text{OsSiR}_2\text{X}$ and $[\text{Cp}^*(\text{Me}_3\text{P})_2\text{OsSiR}_2][\text{B}(\text{C}_6\text{F}_5)_4]$ (R = Me, ⁱPr; X = Cl, OTf), *Organometallics* **2004**, *23*, 693-704.

535. Veige, A. S.; Wolczanski, P. T.; Lobkovsky, E. B. $(\text{silox})_3\text{RePMe}_3$ (silox = ^tBu₃SiO) is carbonylated to the double insertion product $(\text{silox})(\text{Me}_3\text{P})\{\text{cis}-(\text{CO})_2\}\text{Re}\{\text{trans}-(\text{CO}_2\text{Si}^t\text{Bu}_3)_2\}$, *Chem. Commun.* **2001**, 2734-2735.

536. Curtis, M. D.; Greene, J. Small Ring Metallocycles. 4. Synthesis and Chemical Reactivity of *cyclo*-Metalladisiloxanes, $\text{MSiR}_2\text{OSiR}_2$, and *cyclo*-Metalladisilabutanes, $\text{MSiR}_2\text{CH}_2\text{SiR}_2$, *J. Am. Chem. Soc.* **1978**, *100*, 6362-6367.

537. Campion, B. K.; Heyn, R. H.; Tilley, T. D. Carbon Dioxide Activation by a Transition-metal–silicon Bond. Formation of Silanecarboxylate Complexes $[\text{Cp}_2\text{Sc}[\mu\text{-O}_2\text{CSiR}_3]_2]$, *Inorg. Chem.* **1990**, *29*, 4355-4356.

538. (a) Bhattacharyya, K. X.; Akana, J. A.; Laitar, D. S.; Berlin, J. M.; Sadighi, J. P. Carbon–Carbon Bond Formation on Reaction of a Copper(I) Stannyl Complex with Carbon Dioxide, *Organometallics* **2008**, *27*, 2682-2684; (b) Kleeberg, C.; Cheung, M. S.; Lin, Z.; Marder, T. B. Copper-Mediated Reduction of CO₂ with pinB–SiMe₂Ph via CO₂ Insertion into a Copper–Silicon Bond, *J. Am. Chem. Soc.* **2011**, *133*, 19060-19063.

539. Ariafard, A.; Brookes, N. J.; Stranger, R.; Yates, B. F. DFT Study on the Mechanism of the Activation and Cleavage of CO₂ by (NHC)CuEPh₃ (E = Si, Ge, Sn), *Organometallics* **2011**, *30*, 1340-1349.

540. Valyaev, D. A.; Lavigne, G.; Lugan, N. Manganese organometallic compounds in homogeneous catalysis: Past, present, and prospects, *Coord. Chem. Rev.* **2016**, *308*, 191-235.

541. Yang, X.; Wang, C. Manganese-Catalyzed Hydrosilylation Reactions, *Chem. - Asian J.* **2018**, *13*, 2307-2315.
542. (a) Pratt, S. L.; Faltynek, R. A. Hydrosilation Catalysis via Silylmanganese Carbonyl Complexes: Thermal vs. Photochemical Activation, *J. Organomet. Chem.* **1983**, *258*, C5-C8; (b) Hilal, H. S.; Abu-Eid, M.; Al-Subu, M.; Khalaf, S. Hydrosilylation Reactions Catalyzed by Decacarbonyldimanganese(0), *J. Mol. Catal.* **1987**, *39*, 1-11; (c) Hilal, H. S.; Suleiman, M. A.; Jondi, W. J.; Khalaf, S.; Masoud, M. M. Poly(siloxane)-supported decacarbonyldimanganese(0) catalyst for terminal olefin hydrosilylation reactions: the effect of the support on the catalyst selectivity, activity and stability, *J. Mol. Catal. A: Chem.* **1999**, *144*, 47-59; (d) Docherty, J. H.; Peng, J.; Dominey, A. P.; Thomas, S. P. Activation and discovery of earth-abundant metal catalysts using sodium *tert*-butoxide, *Nat. Chem.* **2017**, *9*, 595-600; (e) Carney, J. R.; Dillon, B. R.; Campbell, L.; Thomas, S. P. Manganese-Catalyzed Hydrofunctionalization of Alkenes, *Angew. Chem., Int. Ed.* **2018**, *57*, 10620-10624; (f) Mukhopadhyay, T. K.; Flores, M.; Groy, T. L.; Trovitch, R. J. A β -diketiminato manganese catalyst for alkene hydrosilylation: substrate scope, silicone preparation, and mechanistic insight, *Chem. Sci.* **2018**, *9*, 7673-7680; (g) Yang, X.; Wang, C. Diverse Fates of β -Silyl Radical under Manganese Catalysis: Hydrosilylation and Dehydrogenative Silylation of Alkenes, *Chin. J. Chem.* **2018**, *36*, 1047-1051.
543. Kong, C. J.; Gilliland III, S. E.; Clark, B. R.; Gupton, B. F. Highly-active, graphene-supported platinum catalyst for the solventless hydrosilylation of olefins, *Chem. Commun.* **2018**, *54*, 13343-13346.
544. Gountchev, T. I.; Tilley, T. D. Hydrosilylation Catalysis by C_2 -Symmetric Bis(silylamido) Complexes of Yttrium, *Organometallics* **1999**, *18*, 5661-5667.
545. (a) Oro, L. A.; Fernandez, M. J.; Esteruelas, M. A.; Jimenez, M. S. Hydrosilylation of Alkenes by Iridium Complexes, *J. Mol. Catal.* **1986**, *37*, 151-156; (b) Tanke, R. S.; Crabtree, R. H. Stabilization of Iridium(I), -(III), and -(V) in an Oxygen-Donor Ligand Environment and the Selective Dehydrogenative Silylation and Hydrosilylation of Ethylene with $\{C(Ph_2P=O)_3\}Ir(ol)_2$, *Organometallics* **1991**, *10*, 415-

- 418; (c) Chernyshev, E. A.; Belyakova, Z. V.; Knyazev, S. P.; Turkel'taub, G. N.; Parshina, E. V.; Serova, I. V.; Storozhenko, P. A. Hydrosilylation of Ethylene, *Russ. J. Gen. Chem.* **2006**, *76*, 225-228; (d) Adams, J. J.; Arulsamy, N.; Roddick, D. M. Acceptor Pincer Coordination Chemistry of Platinum: Reactivity Properties of $(^{CF_3}PCP)Pt(L)^+$ ($L = NC_3F_5, C_2H_4$), *Organometallics* **2009**, *28*, 1148-1157; (e) Lachaize, S.; Vendier, L.; Sabo-Etienne, S. Silyl and σ -silane ruthenium complexes: Chloride substituent effects on the catalysed silylation of ethylene, *Dalton Trans.* **2010**, *39*, 8492-8500.
546. Schroeder, M. A.; Wrighton, M. S. Pentacarbonyliron(0) Photocatalyzed Reactions of Trialkylsilanes with Alkenes, *J. Organomet. Chem.* **1977**, *128*, 345-358.
547. Price, J. S.; Emslie, D. J. H.; Vargas-Baca, I.; Britten, J. F. $[(dmpe)_2MnH(C_2H_4)]$ as a Source of a Low-Coordinate Ethyl Manganese(I) Species: Reactions with Primary Silanes, H_2 , and Isonitriles, *Organometallics* **2018**, *37*, 3010-3023.
548. Hartwig, J., *Organotransition Metal Chemistry From Bonding to Catalysis*. University Science Books: Sausalito, Cal., 2010.
549. Baker, R. T.; Ovenall, D. W.; Calabrese, J. C.; Westcott, S. A.; Taylor, N. J.; Williams, I. D.; Marder, T. B. Boryliridium and boraethyliridium complexes *fac*- $[IrH_2(PMe_3)_3(BRR')]$ and *fac*- $[IrH(PMe_3)_3(\eta^2-CH_2BHRR')]$, *J. Am. Chem. Soc.* **1990**, *112*, 9399-9400.
550. Hartwig, J. F.; De Gala, S. R. A Continuum Resulting from Equilibrium between Two Structural Extremes in Tungstenocene and Niobocene Boryl and Hydridoborate Complexes. π -Bonding in a d^2 Boryl System and the First d^0 Boryl Complex, *J. Am. Chem. Soc.* **1994**, *116*, 3661-3662.
551. Łodziana, Z.; Bloński, P.; Yan, Y.; Rentsch, D.; Remhof, A. NMR Chemical Shifts of ^{11}B in Metal Borohydrides from First-Principle Calculations, *J. Phys. Chem. C* **2014**, *118*, 6594-6603.
552. Agnew, D. W.; Moore, C. E.; Rheingold, A. L.; Figueroa, J. S. Controlled *cis* Labilization of CO from Manganese(I) Mixed Carbonyl/Isocyanide Complexes: An Entry

Point to Coordinatively Unsaturated Metallo-Lewis Acids, *Organometallics* **2017**, *36*, 363-371.

553. Besora, M.; Lledos, A., Coordination Modes and Hydride Exchange Dynamics in Transition Metal Tetrahydroborate Complexes. In *Contemporary Metal Boron Chemistry I*, Marder, T. B.; Lin, Z., Eds. Springer: Berlin, 2008; pp 149-202.

554. Carreño, R.; Riera, V.; Ruiz, M. A.; Bois, C.; Jeannin, Y. Reactivity of the Unsaturated Dihydrides $[\text{Mn}_2(\mu\text{-H})_2(\text{CO})_6(\mu\text{-L}_2)]$ ($\text{L}_2 = \text{Ph}_2\text{PCH}_2\text{PPh}_2$, $(\text{EtO})_2\text{POP}(\text{OEt})_2$) toward Boron Hydrides. X-ray Crystal Structure of $[\text{Mn}_2(\mu\text{-BH}_4)(\mu\text{-H})(\text{CO})_5(\mu\text{-Ph}_2\text{PCH}_2\text{PPh}_2)]$, a Molecule Displaying a Novel Coordination Mode of the Tetrahydroborate Ligand, *Organometallics* **1993**, *12*, 1946-1953.

555. Saha, K.; Ramalakshmi, R.; Gomosta, S.; Pathak, K.; Dorcet, V.; Roisnel, T.; Halet, J.-F.; Ghosh, S. Design, Synthesis, and Chemistry of Bis(σ)borate and Agostic Complexes of Group 7 Metals, *Chem. - Eur. J.* **2017**, *23*, 9812-9820.

556. Kruck, T.; Engelmann, A. Hydridopentakis(trifluorophosphine)rhenium, *Angew. Chem., Int. Ed. Engl.* **1966**, *5*, 836.

557. Schubert, U.; Kunz, E.; Harkers, B.; Willnecker, J.; Meyer, J. η^2 -Coordination of a Sn-H Bond to a Transition Metal. Molecular Structure of $(\eta^5\text{-MeC}_5\text{H}_4)(\text{CO})_2\text{Mn}(\text{H})\text{SnPh}_3$, *J. Am. Chem. Soc.* **1989**, *111*, 2572-2574.

558. Alvarez, M. A.; Alvarez, M. P.; Carreño, R.; Ruiz, M. A.; Bois, C. Reactivity of the unsaturated manganese dihydrides $[\text{Mn}_2(\mu\text{-H})_2(\text{CO})_6(\mu\text{-L}_2)]$ [$\text{L}_2 = (\text{EtO})_2\text{POP}(\text{OEt})_2$, $\text{Ph}_2\text{PCH}_2\text{PPh}_2$, $\text{Me}_2\text{PCH}_2\text{PMe}_2$] toward silicon and tin hydrides, *J. Organomet. Chem.* **2011**, *696*, 1736-1748.

559. Smith, A. L., *The Analytical Chemistry of Silicones*. John Wiley & Sons: New York, 1991.

560. Burger, B. J.; Bercaw, J. E., Vacuum Line Techniques for Handling Air-Sensitive Organometallic Compounds. In *Experimental Organometallic Chemistry - A Practicum in Synthesis and Characterization*, American Chemical Society: Washington, D.C., 1987; Vol. 357, pp 79-98.

Ph.D. Thesis — Jeffrey S. Price; McMaster University – Chemistry

561. Andersen, R. A.; Wilkinson, G. Bis[(trimethylsilyl)methyl]magnesium, *Inorg. Synth.* **1979**, *19*, 262-264.
562. Eisch, J. J.; Shafii, B.; Odom, J. D.; Rheingold, A. L. Aromatic Atabilization of the Triarylborirene Ring System by Tricoordinate Boron and Facile Ring Opening with Tetracoordinate Boron, *J. Am. Chem. Soc.* **1990**, *112*, 1847-1853.
563. Schaub, T.; Radius, U. Efficient C–F and C–C Activation by a Novel N-Heterocyclic Carbene–Nickel(0) Complex, *Chem. - Eur. J.* **2005**, *11*, 5024-5030.
564. Pelter, A.; Smith, K.; Brown, H., *Borane Reagents*. Academic Press: London, 1988.
565. Price, J. S.; Chadha, P.; Emslie, D. J. H. Base-Free and Bisphosphine Ligand Dialkylmanganese(II) Complexes as Precursors for Manganese Metal Deposition, *Organometallics* **2016**, *35*, 168-180.
566. Sheldrick, G. M. A short history of SHELX, *Acta Crystallogr., Sect. A: Found. Crystallogr.* **2008**, *64*, 112-122.
567. Sheldrick, G. M. Crystal structure refinement with SHELXL, *Acta Crystallogr., Sect. C: Struct. Chem.* **2015**, *71*, 3-8.
568. Dolomanov, O. V.; Bourhis, L. J.; Gildea, R. J.; Howard, J. A. K.; Puschmann, H. OLEX2: a complete structure solution, refinement and analysis program, *J. Appl. Crystallogr.* **2009**, *42*, 339-341.
569. (a) ADF2010, SCM, Theoretical Chemistry, Vrije Universiteit, Amsterdam, The Netherlands, <http://www.scm.com>; (b) Guerra, C. F.; Snijders, J. G.; te Velde, G.; Baerends, E. J. Towards an order-*N* DFT method, *Theor. Chem. Acc.* **1998**, *99*, 391-403; (c) te Velde, G.; Bickelhaupt, F. M.; Baerends, E. J.; Fonseca Guerra, C.; Van Gisbergen, S. J. A.; Snijders, J. G.; Ziegler, T. Chemistry with ADF, *J. Comput. Chem.* **2001**, *22*, 931-967.
570. Perdew, J. P.; Burke, K.; Ernzerhof, M. Generalized Gradient Approximation Made Simple, *Phys. Rev. Lett.* **1996**, *77*, 3865-3868.
571. (a) van Lenthe, E.; Baerends, E. J.; Snijders, J. G. Relativistic regular two-component Hamiltonians, *J. Chem. Phys.* **1993**, *99*, 4597-4610; (b) van Lenthe, E.;

Ph.D. Thesis — Jeffrey S. Price; McMaster University – Chemistry

Baerends, E. J.; Snijders, J. G. Relativistic total energy using regular approximations, *J. Chem. Phys.* **1994**, *101*, 9783-9792; (c) van Lenthe, E.; Snijders, J. G.; Baerends, E. J. The zero-order regular approximation for relativistic effects: The effect of spin-orbit coupling in closed shell molecules, *J. Chem. Phys.* **1996**, *105*, 6505-6516; (d) van Lenthe, E.; van Leeuwen, R.; Baerends, E. J.; Snijders, J. G. Relativistic Regular Two-Component Hamiltonians, *Int. J. Quantum Chem.* **1996**, *57*, 281-293; (e) van Lenthe, E.; Ehlers, A.; Baerends, E. J. Geometry optimizations in the zero order regular approximation for relativistic effects, *J. Chem. Phys.* **1999**, *110*, 8943-8953.

572. (a) Grimme, S.; Antony, J.; Ehrlich, S.; Krieg, H. A consistent and accurate ab initio parametrization of density functional dispersion correction (DFT-D) for the 94 elements H-Pu, *J. Chem. Phys.* **2010**, *132*, 154104; (b) Grimme, S.; Ehrlich, S.; Goerigk, L. Effect of the Damping Function in Dispersion Corrected Density Functional Theory, *J. Comput. Chem.* **2011**, *32*, 1456-1465.

573. (a) Becke, A. D. A multicenter numerical integration scheme for polyatomic molecules, *J. Chem. Phys.* **1988**, *88*, 2547-2553; (b) Franchini, M.; Philipsen, P. H. T.; Visscher, L. The Becke Fuzzy Cells Integration Scheme in the Amsterdam Density Functional Program Suite, *J. Comput. Chem.* **2013**, *34*, 1819-1827.

574. (a) Mayer, I. Charge, Bond Order and Valence in the Ab Initio SCF Theory, *Chem. Phys. Lett.* **1983**, *97*, 270-274; (b) Mayer, I. Charge, Bond Order and Valence in the Ab Initio SCF Theory (Addendum), *Chem. Phys. Lett.* **1985**, *117*, 396; (c) Mayer, I. On Bond Orders and Valences in the *Ab Initio* Quantum Chemical Theory, *Int. J. Quantum Chem.* **1986**, *29*, 73-84; (d) Sannigrahi, A. B.; Kar, T. Three-center bond index, *Chem. Phys. Lett.* **1990**, *173*, 569-572; (e) Bridgeman, A. J.; Cavigliasso, G.; Ireland, L. R.; Rothery, J. The Mayer bond order as a tool in inorganic chemistry, *J. Chem. Soc., Dalton Trans.* **2001**, 2095-2108.

575. Gopinathan, M. S.; Jug, K. Valency. I. A Quantum Chemical Definition and Properties, *Theor. Chim. Acta* **1983**, *63*, 497-509.

576. (a) Nalewajski, R. F.; Mrozek, J. Modified Valence Indices from the Two-Particle Density Matrix, *Int. J. Quantum Chem.* **1994**, *51*, 187-200; (b) Nalewajski, R. F.;

Ph.D. Thesis — Jeffrey S. Price; McMaster University – Chemistry

Mrozek, J.; Mazur, G. Quantum chemical valence indexes from the one-determinantal difference approach, *Can. J. Chem.* **1996**, *74*, 1121-1130; (c) Mrozek, J.; Nalewajski, R. F.; Michalak, A. Exploring Bonding Patterns of Molecular Systems using Quantum Mechanical Bond Multiplicities, *Pol. J. Chem.* **1998**, *72*, 1779-1791.

577. (a) Nalewajski, R. F.; Mrozek, J.; Michalak, A. Two-electron valence indices from the Kohn-Sham orbitals, *Int. J. Quantum Chem.* **1997**, *61*, 589-601; (b) Michalak, A.; DeKock, R. L.; Ziegler, T. Bond Multiplicity in Transition-Metal Complexes: Applications of Two-Electron Valence Indices, *J. Phys. Chem. A* **2008**, *112*, 7256-7263.

578. (a) Rodríguez, J. I.; Bader, R. F. W.; Ayers, P. W.; Michel, C.; Götz, A. W.; Bo, C. A high performance grid-based algorithm for computing QTAIM properties, *Chem. Phys. Lett.* **2009**, *472*, 149-152; (b) Rodríguez, J. I.; Köster, A. M.; Ayers, P. W.; Santos-Valle, A.; Vela, A.; Merino, G. An Efficient Grid-Based Scheme to Compute QTAIM Atomic Properties without Explicit Calculation of Zero-Flux Surfaces, *J. Comput. Chem.* **2009**, *30*, 1082-1092; (c) Rodríguez, J. I. An Efficient Method for Computing the QTAIM Topology of a Scalar Field: The Electron Density Case, *J. Comput. Chem.* **2013**, *34*, 681-686.

579. NBO 6.0: E. D. Glendening, J. K. Badenhoop, A. E. Reed, J. E. Carpenter, J. A. Bohmann, C. M. Morales, C. R. Landis, and F. Weinhold, Theoretical Chemistry Institute, University of Wisconsin, Madison, 2013; Weinhold, F. Natural Bond Orbital Analysis: A Critical Overview of Relationships to Alternative Bonding Perspectives, *J. Comput. Chem.* **2012**, *33*, 2363-2379.

580. (a) Ziegler, T.; Rauk, A. CO, CS, N₂, PF₃, and CNCH₃ as σ Donors and π Acceptors. A Theoretical Study by the Hartree-Fock-Slater Transition-State Method, *Inorg. Chem.* **1979**, *18*, 1755-1759; (b) Ziegler, T.; Rauk, A. A Theoretical Study of the Ethylene-Metal Bond in Complexes between Cu⁺, Ag⁺, Au⁺, Pt⁰, or Pt²⁺ and Ethylene, Based on the Hartree-Fock-Slater Transition-State Method, *Inorg. Chem.* **1979**, *18*, 1558-1565; (c) Bickelhaupt, F. M.; Baerends, E. J., Kohn-Sham DFT: Predicting and Understanding Chemistry. In *Reviews in Computational Chemistry*, Boyd, D. B.; Lipkowitz, K. B., Eds. Wiley-VCH: New York, 2000; pp 1-86.

Ph.D. Thesis — Jeffrey S. Price; McMaster University – Chemistry

581. (a) Mitoraj, M. P.; Michalak, A.; Ziegler, T. A Combined Charge and Energy Decomposition Scheme for Bond Analysis, *J. Chem. Theory Comput.* **2009**, *5*, 962-975; (b) Mitoraj, M. P.; Michalak, A.; Ziegler, T. On the Nature of the Agostic Bond between Metal Centers and β -Hydrogen Atoms in Alkyl Complexes. An Analysis Based on the Extended Transition State Method and the Natural Orbitals for Chemical Valence Scheme (ETS-NOCV), *Organometallics* **2009**, *28*, 3727-3733.
582. (a) Bérces, A.; Dickson, R. M.; Fan, L.; Jacobsen, H.; Swerhone, D.; Ziegler, T. An implementation of the coupled perturbed Kohn-Sham equations: perturbation due to nuclear displacements, *Comput. Phys. Commun.* **1997**, *100*, 247-262; (b) Jacobsen, H.; Bérces, A.; Swerhone, D. P.; Ziegler, T. Analytic second derivatives of molecular energies: a density functional implementation, *Comput. Phys. Commun.* **1997**, *100*, 263-276; (c) Wolff, S. K. Analytical Second Derivatives in the Amsterdam Density Functional Package, *Int. J. Quantum Chem.* **2005**, *104*, 645-659.
583. The SCANFREQ command rescans a specific range of frequencies along a normal mode numerically as described in the ADF manual: <https://www.scm.com/doc/ADF/Input/Frequencies.html#scanning-a-range-of-frequencies>. References for numeric frequency calculations are as follows; (a) Fan, L.; Ziegler, T. Application of density-functional theory to infrared absorption intensity calculations on main group molecules, *J. Chem. Phys.* **1992**, *96*, 9005-9012; (b) Fan, L.; Ziegler, T. Nonlocal Density Functional Theory as a Practical Tool in Calculations on Transition States and Activation Energies. Applications to Elementary Reaction Steps in organic Chemistry. *J. Am. Chem. Soc.* **1992**, *114*, 10890-10897.
584. (a) Autschbach, J.; Ziegler, T. Nuclear spin-spin coupling constants from regular approximate relativistic density functional calculations. I. Formalism and scalar relativistic results for heavy metal compounds, *J. Chem. Phys.* **2000**, *113*, 936-947; (b) Autschbach, J.; Ziegler, T. Nuclear spin-spin coupling constants from regular approximate relativistic density functional calculations. II. Spin-orbit coupling effects and anisotropies., *J. Chem. Phys.* **2000**, *113*, 9410-9418.

Ph.D. Thesis — Jeffrey S. Price; McMaster University – Chemistry

585. Grimme, S. Accurate Description of van der Waals Complexes by Density Functional Theory Including Empirical Corrections, *J. Comput. Chem.* **2004**, *25*, 1463-1473; Ernzerhof, M.; Scuseria, G. E. Assessment of the Perdew-Burke-Ernzerhof exchange-correlation functional, *J. Chem. Phys.* **1999**, *110*, 5029-5036.
586. (a) Note 29 in; Bulo, R.; Ehlers, A.; Grimme, S.; Lammertsma, K. Vinylphosphirane-Phospholene Rearrangements: pericyclic [1,3]-Sigmatropic Shifts or Not?, *J. Am. Chem. Soc.* **2002**, *124*, 13903-13910; (b) Pauncz, R., *Spin Eigenfunctions*. Plenum Press: New York, 1979; Szabo, A.; Ostlund, N., *Modern Quantum Chemistry*. 1st ed. revised ed. ed.; McGraw-Hill: New York, 1989.
587. Price, J. S.; Emslie, D. J. H. Interconversion and reactivity of manganese silyl, silylene, and silene complexes, *Chem. Sci.* **2019**, *10*, 10853-10869.